

# *New Technologies for Urban Safety of Mega Cities in Asia*

October 18-19, 2004  
Agra, India

*–Editor–*

**Junichi Susaki**

ICUS, IIS

The University of Tokyo, Japan

Organised By

*Department of Civil Engineering,  
Indian Institute of Technology Kanpur,  
Kanpur, India*

*International Center for Urban Safety Engineering (ICUS),  
Institute of Industrial Science, The University of Tokyo,  
Tokyo, Japan*

# **New Technologies for Urban Safety of Mega Cities in Asia**

**Taketo Uomoto**

Director and Professor of ICUS, IIS, University of Tokyo

## **ICUS Report No 6, December 2004**

### **Preface**

Over half of the world's population is concentrated in urban areas covering just four percent of the world's surface. Mega Cities (exceeding a population of ten millions) in particular are characterized by a high population density and high material demands. Rapid urbanization is a distinctive feature of Asia with a tremendous rate of population growth. It is estimated that by 2015, more than 50% of the Mega Cities are going to be in Asia. Due to rapid economic development, there has been a phenomenal growth of high-rise buildings and other infrastructure in Mega Cities. However, this growth of infrastructure is not adequately balanced by the appropriate measures for their maintenance and management and that has led to a deterioration of urban infrastructures and resulted in urban disasters in many cities. Moreover, dense concentration of population is leading to high rate of water-related illness from lack of safe drinking water or inadequate sanitation or environmental problems.

The recent developments of various advanced technologies have generated scopes and motivation to focus on devising appropriate methodologies for management and maintenance of urban buildings, infrastructures, mitigation of urban disasters and environmental problems for sustainable development of Asian Mega Cities with adequate safety and security. As a large percentage of population is under potential risk, safety and security of Asian Mega Cities deserve increased attention of various concerned groups including the researchers and decision makers. With this realization and recognition of the importance of advanced tools in urban safety, International Center for Urban Safety Engineering (ICUS) of the Institute of Industrial Science (IIS) and, organized a 2-day International symposium on October 18-19, 2004 on the use of advanced technologies towards development of methodologies for safety and security of Mega Cities in Asia. This symposium was also supported by 21<sup>st</sup> Century COE Program "Creation of New Science and Engineering for Sustainable Urban Regeneration", University of Tokyo.

The prime objective of the symposium is to bring together decision makers, practitioners and researchers involved in these fields to share their expertise, knowledge and experience for tackling the critical issues of urban safety with advanced technologies. A network of Asian researchers and practitioners was established for collaboration in various issues of urban safety of the Asian Mega Cities through the First and Second International Symposiums jointly organized by other institutions (Asian Institute of Technology (AIT), Thailand in 2002 and 21<sup>st</sup> Century COE Program, University of Tokyo, Japan in 2003). It is strongly expected that this symposium would be a platform for strengthening this network for future collaboration towards safety and security of the Asian Mega Cities.

I would like to thank the Steering Committee, Technical Committee and the Organizing Committee for their hard work, valuable suggestions and coordinating for the initiatives to make this symposium a success.

I wish all the distinguished guests and participants the very best and success

**International Center for Urban Safety Engineering**



# OPENING ADDRESS

SHIGEFUMI NISHIO

Director General of IIS, University of Tokyo, Japan

*Honorable Guest Professor Mehesh Tandon, President of the Indian Concrete Institute,*

*Honorable Guest Professor Samjay Dhande, Director of the Indian Institute of Technology, Kanpur*

*Distinguished Guests, Ladies and Gentlemen,*

*On behalf of the Institute of Industrial Science, University of Tokyo, I take pleasure in extending a warm welcome to Professor Tandon, Professor Dhande, and other distinguished guests and participants to the International SYMPOSIUM ON "NEW TECHNOLOGIES FOR URBAN SAFETY OF MEGA CITIES IN ASIA", being held here today.*

*At the outset, I would like to express my thanks to Professor M. C. Tandon, Professor Dhande who have taken time out of their busy schedules to be with us today, and agreeing to inaugurate the Symposium. I would also like to thank Professor Sudhir Misra, and their team for the hard work in co-organizing this symposium with the International Center for Urban Safety Engineering, or 'ICUS' of our Institute. I would also like to express my regret for my inability to attend in person.*

*ICUS was created about three year and a half ago in response to a growing need to deal with the various aspects of problems related to urban safety comprehensively, create greater social and academic awareness towards these issues, and, serve as an agency to collect and disseminate relevant information. Through this symposium, co-organized with the School of Civil Engineering, IIT, the center makes an effort to start a much-needed initiative towards greater collaboration between the professionals in India and Japan, and further our understanding of different aspects of urban safety.*

*The success of the symposium is evident by the overwhelming response it has generated, and will be judged by the initiatives that result in terms of exchange of information and ideas, sharing of resources, and generation of joint research and other projects. I take this opportunity to assure all help from my Institute and the University of Tokyo in this regard, and wish the symposium all success*

# CONTENTS

## Opening session

MAHESH TANDON	
Technical Hurdles of Implementing Infrastructure Projects.....	1
R.N. IYENGAR	
Seismic Hazard in Urban India with Delhi as a Case Study.....	9

## Technical sessions

### *Disaster Management*

TSO CHIEN PAN, B. LI, X. T. YOU AND C. L. LIM	
From Ground Shocks to Air Blasts– Multiple-Hazard Protections .....	25
TAWATCHAI TINGSANCHALI	
Optimal Improvement of Storm Sewer System for Inner Bangkok .....	37
MADHAV N. KULKARNI, NISHA RADHAKRISHNAN AND DEEPA RAI	
Techniques for Monitoring Deformation in Large Engineering Structures .....	47
AKIYUKI KAWASAKI AND SATORU SADOHARA	
Development of Slope Failure Disaster Management System in Urban Area -The Utilization of Existing Data Toward “E-Municipal Government” .....	59
SAID A. ELKHOLY AND KIMIRO MEGURO	
Numerical Modeling of Steel Structures in Fire Conditions using Improved Applied Element Method .....	69
REIKO AMANO, YOUICHI IZUSHI, HITOSHI KURIOKA, HIDEAKI KUWANA, TAKASHI TSURUDA, TAKESHI SUZUKI AND YOSHI OGAWA	
Water Screen Fire Disaster Prevention System Characteristics of Water Screen as Partitioning Technology .....	79

DUSHMANTA DUTTA, M. J. ALAM AND S. HIRONAKA Urban Flood Modeling in Lower Mekong Basin a physically based Distributed Modeling Approach .....	87
TRAN THUC AND NGUYEN HUU PHUC Hydraulics Computations to Study Flood Control for Hanoi City .....	97
AYSHA AKTER AND ROWSHAN MAMTAZ Sustainable Development of Water Supply, Sanitation and Waste Management: A Challenge to Dhaka Urban Slum Dwellers in Bangladesh. ....	104
DJILLALI BENOUEAR The need for an Integrated Disaster Management Strategy in North African Mega cities: A Case Study of Algiers .....	114

## ***Earthquake***

KIMIRO MEGURO AND YASUNORI HADA Application of Power Demand Changes to Evaluate Building and Dwelling damages due to Earthquake .....	124
HORI. M. AND OGUNI KENJI Integrated Earthquake Simulation using Simulation and Geographical Information System .....	134
KUSALA RAJENDRAN AND C. P. RAJENDRAN Understanding the Seismic Sources in India: Strategies for Seismic Hazard Reduction .....	142
SUDHIR K. JAIN AND C.V.R.MURTHY Capacity Building in India towards Earthquake Risk Reduction – Role of IIT Kanpur in Past Two Decades.....	156
JUNJI KIYONO AND KATSUMI NAGAI Casualty occurrence Mechanism Induced by Train Accident during an Earthquake .....	158
PHAN QUANG MINH Damage to Masonry Buildings in Dien Bien Phu Earthquake .....	168
SHAILESH KUMAR AGRAWAL AND AJAY CHOURASIA Seismic Vulnerability Analysis of Buildings in Jabalpur Urban Area.	172

PAOLA MAYORCA AND KIMIRO MEGURO An Innovative Seismic Strengthening Method for Unreinforced Masonry Structures using PP-Band Meshes .....	186
KRISHNAMOORTHY, KIRAN KUMAR SHETTY AND RAVI KUMAR Response of a Base Isolated Masonry Structure.....	194
N. H. M. KAMRUJJAMAN SERKER, PENNUNG WARNITCHAI AND DUSHMANTA DUTTA Urban Building Inventory from VHR Remote Sensing Imagery for Earthquake Risk Analysis in Bangkok .....	199
ROSHAN ALAYIL DIVAKARAN, PRABIR C. BASU AND AJAI S. PISHARADY Quantitative Approach for Seismic Retrofitting of Structures using Push Over Analysis.....	211
THURAICHAMY GUGANESAN SUNTHARAVADIVEL, YOZO FUJINO AND PING ZHU Evaluation of Earthquake Caused Damages using Non-Linear Dynamic Numerical Analysis.....	223
YUSUKE ONO, JUNJI KIYONO AND TATSUKI TAMAI Seismic Behavior of Urban Highway Tunnel in Vicinity of Embankment .....	230
KOJI TAKEWAKA AND GOVINDA RAJ PANDEY Seismic Behavior of Reinforced Concrete Piers deteriorated by Corrosion of Reinforcement .....	240
PENNUNG WARNITCHAI, SOMMAI PONGPORNUP, UNNOP PRAWATWONG AND AMORN PIMANMAS Seismic Performance of Post Tensioned Interior Flat Slab-Column Connections .....	250
N. CHANDRA SEKHAR, K. B. S. SUNIL BABU AND PRADEEP KUMAR RAMANCHARLA Equivalent Static Analysis as per 1893:2002: A Simple Software Tool.....	260

## ***Infrastructure Management***

TAKETO UOMOTO	
Introduction to JSCE Standard Specification for Concrete Structures	269
KEUN JOO BYUN	
Recent Advances in Assessment Technology of Infrastructures in Korea.....	279
PRASANTA KUMAR DEY AND STEPHEN O. OGUNLANA	
A Risk-Based Decision Support System for Inspection and Maintenance of Cross-Country Petroleum Pipelines.....	285
KIANG HWEE TAN	
Impact Resistance of FRP-Concrete Sandwich Panels.....	295
SOMNUK TANGTERMSIRIKUL	
Durability Design for Concrete Structures for Urban Safety in Thailand. ....	305
TOSHINOBU YAMAGUCHI, KOJI TAKEWAKA, JUNICHI MATSUMOTO AND YOSHIKAZU AKIRA	
An Experimental Study on complex deterioration of Concrete using Ground Granulated Blast-Furnace Slag.....	313
S. K. MANJREKAR	
Case Study of the Repair of a Major Bridge and Some Thoughts on Repair Materials.....	321
HISASHI KANADA Y. ISHIKAWA AND TAKETO UOMOTO	
Development of New Method to inspect deteriorated Concrete using NIR Spectroscopic Technique .....	331
M. A. ANSARY AND M. A. NOOR	
Vulnerability Assessment of Existing Engineered and Non Engineered Structures of Dhaka City using RVS and NDT Techniques.....	341
YOSHITAKA KATO	
Maintenance Management of Concrete Structures by using Repair-Risk .....	351
K. K. BAJPAI, C. V. R. MURTY AND DURGESH C. RAI	
Influence of Fiber Wrap Retrofitting on Gravity Designed RC Beam-Column Joints under Cyclic Loading.....	359

TAMON UEDA New Concept for Retrofitting Concrete Structures with Unconventional Materials.....	369
TIJO THOMAS AND PRADEEP KUMAR RAMANCHARLA Simulation of Plate Behavior under Non-Uniform Wind Loads .....	379
T. R. WARSI AND ANURAG KHANDELWAL Urban Safety and Security Issues, Constraints and Challenges ahead-Agra.....	389
MAHUA MUKHERJEE Urban Safety in Asian Cities: For the city dwellers, by the city dwellers.....	395

## ***Environment***

VIRENDRA PATHAK AND ONKAR DIKSHIT Per-Field Classification of Indian Urban Environment using IRS-1C Satellite Data.....	405
TRAN HUNG AND YOSHIFUMI YASUOKA Surface Climatic Impacts of Urbanization in the Ho Chi Minh City, Vietnam: An Integrated Study with Remote Sensing and Modeling	415
T. G. SITHARAM, C. S. VISWANATHA, M. S. SUDARSHAN AND P. S. R. NARASIMHA RAJU Subsurface Geotechnical Characterization Map of Bangalore City using 3-D Analyst in GIS.....	423
EKTA AMAR AND BHARAT LOHANI Registration of Laser Scanner Point Clouds for a large and complex Building .....	431
YOSHIFUMI YASUOKA, YOSUKE YAMAGISHI, TAO GUO, AND TAKAHIRO ENDO Extraction and 3-D Visualization of trees in Urban Environment.....	441
S. K. KATIYAR, ONKAR DIKSHIT AND KRISHNA KUMAR Ground Control for the Geometric Correction of Remotely Sensed Imagery: Requirements and Issues in India.....	447

SURENDER SINGH AND B. S. SOKHI Internet GIS based Municipal Information System: A Case Study of Dehradun Municipal Area .....	454
RYOZO OOKA, SHINSUKE KATO, HONG HUANG AND TAKEO TAKAHASHI Prediction of Atmospheric Pollutant Dispersion in an Urban Area by Wind Tunnel Experiment and Numerical Simulation .....	463
D. MOHAN Automobile Traffic Generated Atmospheric Pollution: Need for consideration in Urban Infrastructure Planning.....	469
K. VENKATESAN AND K. P. SUBRAMANIAN Road Safety Audit – Chennai .....	479
RAJIV GUPTA 2D-EA for Facility Allocation .....	488
K.W. FOONG AND H.C. CHIN Pedestrian Speed-Flow Model on Escalators and Staircases.....	498
JAYARAM H., VINOTH M. AND RAGHURAM P. Tele-Operated Surveillance Robot .....	508
DUSHMANTA DUTTA AND TAKETO UOMOTO ICUS and AIT Collaboration on Urban Safety Research.....	516
SHARAD VIMAL OBEROI AND NARINDER KUMAR THAKUR Safety Assessment of Existing Road in the Himalayas using Geographic Information System and Satellite Imagery.....	526



*Gate of Hotel*



*Symposium Hotel*



*Symposium Hotel*



*S. Misra*



*Opening Ceremony*





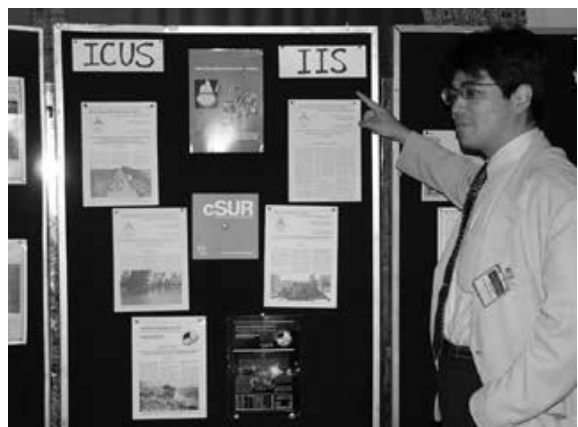
*M. Tandon*



*R. N. Iyengar*



*At Banquet*



*Poster of ICUS and IIS*



*T. C. Pan*



*T. Tingsanchali*



*T. Thuc*



*C. V. R. Murthy*



*P. Q. Minh*



*P. Wanitchai*



*K. J. Byun*



*At Presentation*



*K. H. Tan*



*S. Tangtermsirikul*



*M. A. Ansary*



*T. Ueda*



*T. Hung*



*At Presentation*



*End of the Symposium*

# *Opening Session*

# **TECHNICAL HURDLES OF IMPLEMENTING INFRASTRUCTURE PROJECTS**

MAHESH TANDON  
Tandon Consultants Pvt Ltd, New Delhi, INDIA

## **ABSTRACT**

*The current infrastructure scenario boasts of fast-track projects, many of which are in the process of being constructed with still others in the pipeline. While they are indicators of urban development and progress, they are not without their attendant ills: ugly dug-up trenches, diminished road-widths, crawling traffic, frequent bottle-necks, short-tempered commuters, etc.*

*More often than not the implant of an infrastructure project in an urban landscape is in the nature of a fire-fighting exercise facilitating pedestrian cross-over at one intersection or removing vehicular congestion at another or providing a signal-free stretch elsewhere. Symptomatic solutions such as these however, pose technical hurdles that include construction technology, land acquisition, traffic diversions and disturbances, effect on environment, to name a few.*

*This paper highlights the technical hurdles that challenge the implementation of infrastructure projects.*

## **1.0 INTRODUCTION**

Construction of transportation infrastructure structures like flyovers, viaducts, underpasses, tunnels, etc in urban situation poses many technical hurdles. Unfortunately, infrastructure requirements are or should be proportionate to the population residing in the area and hence more and more problems arise because of the existence of already built-up and congested areas where the structures have to be implemented.

## **2.0 DESIGN CONCEPTION AND CONSTRUCTION TECHNOLOGY**

Appropriateness of design conception and construction technology adopted for implementation of the structure is the most important consideration for urban transportation structures. Precast segmental construction technology, whereby small elements can be fabricated in a centralized casting yard and conveniently transported on the existing road network, is a popular choice, Fig 1. This also reduces site concreting with its attendant environmental issues like dust, noise, etc. Though the span arrangements can be fixed in advance the structure should be capable of



Low Bedded Trailer

*Figure 1: Transportation of Segment to Site*

absorbing minor changes in span lengths during construction. This is necessary because of the possibility of encountering un-chartered utilities which are discussed later in this chapter.

### **3.0 PROBLEMS OF LAND ACQUISITION**

The central verge of the road is ‘no-man’s land’ and presents the possibility of placing piers for long elevated viaducts without the necessity of acquisition of land or reducing the ground level carriageway, Fig 4. However, at points of take-off from ground level, large widths of the structure have to be accommodated, which results in a reduction of the carriageway width at such points.

For flyovers which are generally of small length, the ground level road becomes unusable for the whole width of the flyover.

### **4.0 FAST TRACK CONSTRUCTION**

The importance of fast-track construction cannot be over-emphasised for urban transportation projects. The design conception and methodology of construction must be geared for speed. Not only disturbance to life must be minimized but reverting back to improved version of ‘normalcy’ must be effected in the shortest possible time.

Detailed planning and constant monitoring by an experienced project management team hold the key to fast track construction.

Without incentives and disincentives, fast track construction has seldom been implemented successfully. Provisions for attractive bonus for early completion and strong penalties for delays must form an integral part

of the contract document. There are some very good examples where such provisions were made, viz the 50-odd flyovers on Mumbai city were completed in record time due to the innovative tender provisions introduced by the Maharashtra State Road Development Corporation (MSRDC), who were in charge of the implementation.

## **5.0 QUICK DISPUTE RESOLUTION**

Good unambiguous contract documentation is the key for reducing conflicts during implementation. However, differing interpretations and perceptions can still give rise to disputes. Also, no contract documentation can foresee all the problems that may surface during construction. However, in such circumstances, there should be no slowing down or shutting down of the construction activities.

When disputes do arise during project implementation, a previously identified and agreed-to transparent mechanism for its resolution should be activated. The decisions of this mechanism should be binding on all parties of the dispute at least as far as the construction speed is concerned.

## **6.0 TRAFFIC DISTURBANCE/DIVERSION DURING CONSTRUCTION**

There must be minimal disturbance to traffic during construction, Fig 2. To achieve this objective, the diversions have to be planned carefully at the conceptual design stage.



*Figure 2: Pitampura Cantilever Bridge no disturbance to Traffic  
(38.5m + 55m + 38.5m)*



The type and sequence of construction have a significant impact on the design. Hence, without a complete knowledge of how traffic would move on the arterial road during various stages of construction, the concept design itself may be initiated in the wrong direction.

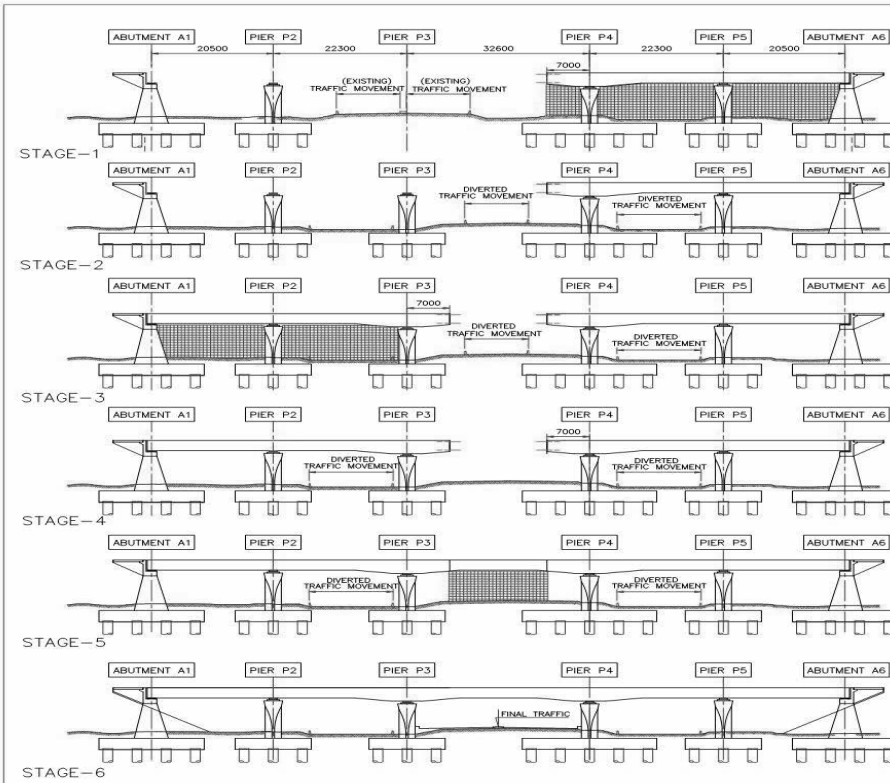


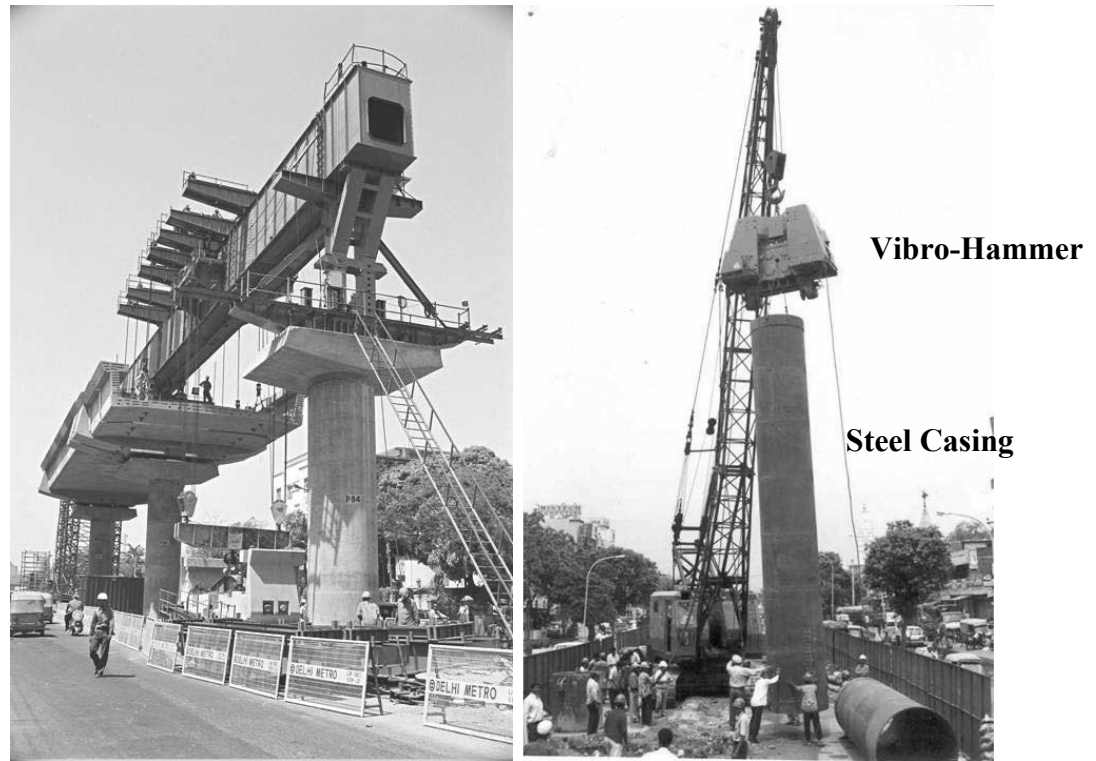
Figure 3: Construction Sequence of Substructure and Superstructure of Curved Over Bridge, AIIMS Crossing

A good example of the planning for traffic diversions and its effect on the design can be seen in Figure 3.

## 7.0 SAFETY DURING CONSTRUCTION

In urban transportation projects, the construction has not only to cater to workmen present on location, but also passers-by and habitants of the area. Apart from preventing physical injury to human beings who must receive the greatest attention, damage to existing infrastructure, especially utilities, must be avoided.

Proper barricading, signages and diversion are part of the process of ensuring safety during construction, given the heavy machinery and equipment that may be deployed on the project, Fig 4.



*Figure 4: Safety During Construction*

## 8.0 ENVIRONMENTAL IMPACT & AESTHETICS

How will an infrastructure project impact its environment? It is important to analyse and assess the potential impact of urban transportation projects on the natural, social and cultural environment of the area both during construction and in-service conditions.

Some of the issues can be identified as follows:

- Noise and dust pollution
- Replanting of trees which require to be displaced
- Rain water harvesting due to large built-up areas being created
- Landscaping to soften the visual impact
- Disposal of waste material , eg bentonite

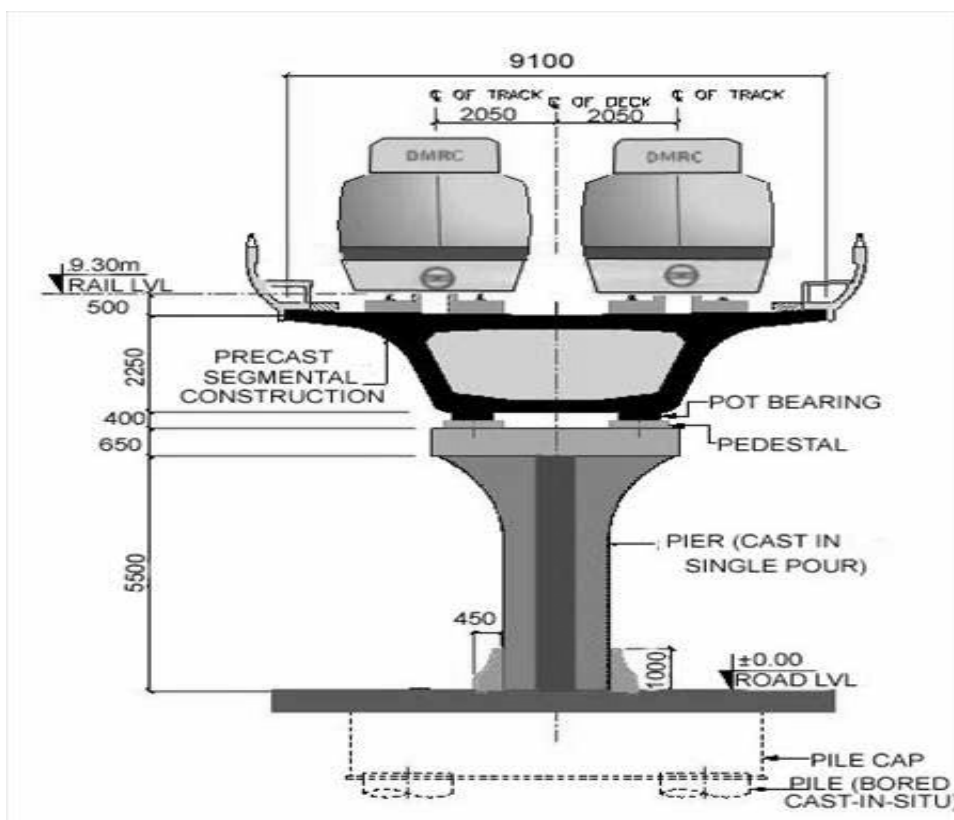
Due to its sheer size and importance in sociological terms, infrastructure projects loom prominently in the public consciousness. Disregarding its harmonious integration into the natural or built environment can have significant repercussions, the detrimental effects of which are always significant.

Graceful and aesthetic bridges elicit a sense of appreciation from lovers of natural beauty crowning majestic natural splendors. Smooth and elegant flyovers earn the unmitigated gratitude of millions of urban dwellers enhancing quality of life in the cities.

A good example of a project with a positive impact on the environment is shown in Fig 5. Aesthetics is a matter of good proportioning, shape and texture of the structure and reducing the visual impact of the bulky and heavy elements, Fig 6.

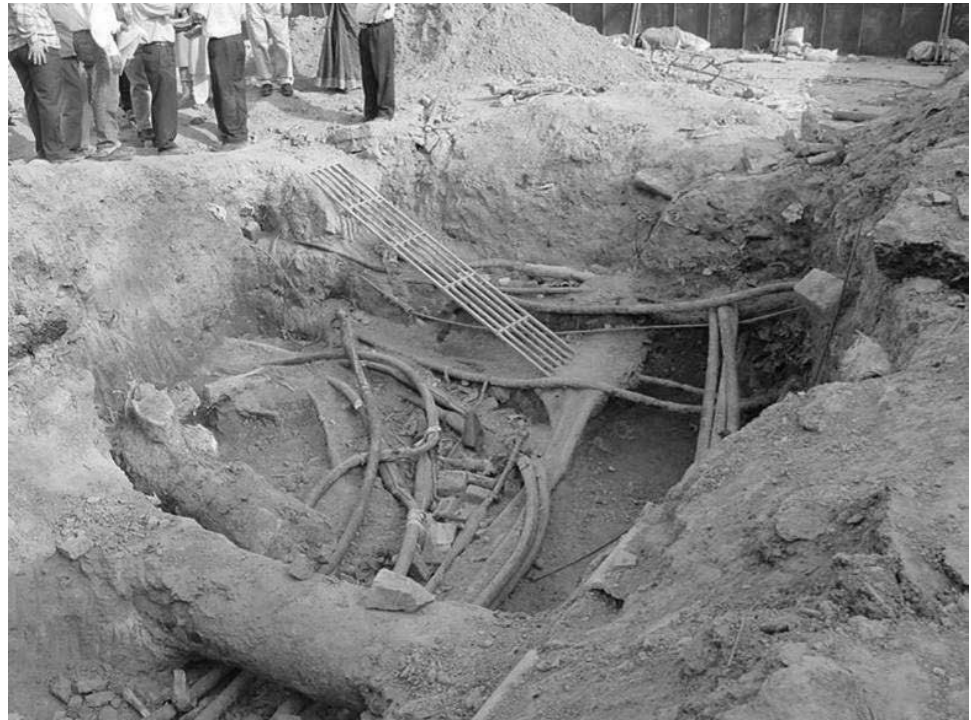


*Figure 5: Aerial View AIIMS-Safdarjung Crossing*



*Figure 6: Delhi Metro Viaduct Structural Engineer's Impression*

## 9.0 UNDERGROUND UTILITIES



*Figure 7: Example of Un-Chartered Utilities*



*Figure 8: Irregular Configuration of Piles for Straddling Across*

One of the most common reasons for delays in implementation of infrastructure projects can be attributed to the identification, removal and

diversion of underground utilities that comprise as diverse items as power cables, telephone lines, water and oil pipelines, sewage and storm water drains and latest inclusions like gas pipelines and optical fibre cables, Figs 7, 8.

Identification of the underground utilities poses a problem because not only are they 'hidden' but frequently 'un-chartered', implying complete ambiguity regarding their nature and location. Once identified, their removal and diversion often proves more difficult and time-consuming as different authorities responsible for them operate on un-coordinated time frames leading to great inconvenience to the public, not to mention significant cost and time over-runs.

## **10.0 HARDENED FACILITIES**

While protection of urban infrastructure from attacks by terrorist activity or vandalism is difficult, it is important to introduce features that would discourage such action due to difficulties imposed.

Some precautions which can be taken is to avoid external prestressing, introduce 'integral' bridges which can preclude bearings and thwart ingress or access to the structure except at a few designated points that can be specifically protected.

# ***SEISMIC HAZARD IN URBAN INDIA WITH DELHI AS A CASE STUDY***

R.N. IYENGAR

Department of Civil Engineering,  
Indian Institute of Science, Bangalore, INDIA

## **1.0 INTRODUCTION**

Strong earthquakes are rare events, rarer than cyclones, windstorms and tidal waves. Nevertheless, India has seen quite a few earthquakes in the recent past. It is not that the frequency has suddenly increased. Earthquakes have been known in this country from pre-historic times, more or less in the same regions, where they are presently felt. The present, apparent heightened awareness towards earthquake disaster mitigation in the country is attributable to large loss of life and property suffered during the Khillari (30<sup>th</sup> September 1993), Jabalpur (22<sup>nd</sup> May 1997) and Bhuj (26<sup>th</sup> January 2001) earthquakes. Post-event analysis of the regions affected by these earthquakes show that the pre-event seismic risk to structures was very high, and they were already in highly vulnerable conditions. It is well recognized that the seismic hazard of a city or a region is a natural property that cannot be altered. Human intervention in a habitat is possible to the extent the vulnerability of the built environment can be reduced leading to decreased risk levels and hence mitigation of a foreseen disaster.

Indian cities have grown unplanned and uncontrolled in recent years. In 1947 the population of the country was 33 Crores, of which 14% was urban. Presently, it is estimated that about 33-35% of the total population of 100 Crores (one billion) is concentrated in some 25-30 urban centers. Apart from the active migration of rural population to urban areas, it is observed that Indian cities have a tendency to expand and capture nearby villages into their territory. Thus, about 25% of urban population in the country lives in slums. In addition, there is always shortage in urban housing, which was estimated at 66.4 Lakh units in 2001. Hence, we have a situation where the quality of life shows dramatic spatial variation in a city than in a village. The same can be said about the vulnerability of constructions and infrastructures in big cities. With reference to residential buildings; Kutcha (informal), Semi-Pucca (semi-formal) and Pucca (formal) houses in our cities are roughly in the proportion 8:16:76, whereas this figure is 34:35:31 for rural areas. The above classification approximately corresponds to A-type, B-type and C-type buildings of the seismic code IS-1893. The 76% C-type houses in urban areas are not necessarily built to high standards of safety. They are particularly constrained by limits of affordability and acceptability. Thus, it is the social and economic rather than technological, issues that govern the safety of our cities during natural calamities. It is with these points in the background we have to discuss seismic hazard, vulnerability and risk to Indian cities. Success of disaster mitigation strategies depends on how well the stakeholders are sensitized to the

necessity for reducing the vulnerability of their structures. Since earthquakes are rare and unpredictable, there is always a tendency among the less informed persons, in the local administration, to deny the importance of risk mapping of cities as a pro-active step in the right direction. In recent years, it has been well recognized that national level seismic zone maps are at best preliminary estimates. They are useful as guides but cannot be substitutes for micro-zones of cities existing near active faults. Microzonation, which maps the hazard, vulnerability and risk to the built environment in a city, targets the building owners, local administrators and elected representatives responsible for the welfare of a ward of the size of approximately one square kilometer. The challenge one faces here, is to scientifically compute the basic hazard on small scales of the order of 1km x 1km, with faults that are hundreds of kilometers long at unknown depths, spread randomly in the contributing seismo-tectonic region of about 300,000 sq. km. Municipal engineers who like to evaluate the vulnerability or safety of existing buildings, need to know how the ground will vibrate in future at their sites within the city. This ground motion lasting for a few seconds is due to the release of energy stored for centuries at the fault level, but is nonetheless strongly influenced by the local soil conditions at the site. By superposing the building typology descriptions on the hazard map one can construct the vulnerability map, provided the damage probability matrices or motion-damage relationships are available. Damage statistics can be converted into financial loss estimates to create a risk map also for a city. Ultimately, seismic risk reduction achieved by a city habitat depends on how well the three key subjects namely engineering, earth sciences and social sciences are made to converge by the metropolitan administration.

In this article, the focus would be on how the seismo-tectonic knowledge of a region can be converted into a city level hazard map for engineering purposes. Delhi, the capital city of the country is taken as an example. In a city like Delhi founded on the banks of a river, that has brought several million tonnes of sediments from Himalayas, surface level ground motion can vary dramatically within short distances. A case study of mapping seismic hazard of Delhi through probabilistic seismic hazard analysis methods is presented with some limited and qualitative results on soil amplification.

## **2.0 SEISMIC HISTORY**

A general review of the seismic status of Delhi, has been previously presented by the author (Iyengar 2000). Varāha Mihira, who lived in 5<sup>th</sup> century A.D., has mentioned northern India including Delhi and its surroundings as the felt region of severe earthquakes. However, the first historically reported earthquake in Delhi city was on 17<sup>th</sup> July 1720. The MMI value of this event at Delhi (Old) has been estimated to be IX (Srivastav and Roy 1982). Even though the focus of this event has not been identified, from historical accounts it is surmised that the source should have been near Delhi city. It is known that Agra was affected severely by an earthquake on 6<sup>th</sup> July 1505. Another event of high intensity felt in the Agra-Mathura region on 25<sup>th</sup> August 1803 has been described by Nazir

Akbarabadi (1740-1830) in his Urdu poem *bhūcāl-nāma* (UPHS 1992). This event caused damage to Kutub Minar, one of the famous landmarks of Delhi. Again, the source of the shock has not been identified. However, it is gratifying to note that Taj Mahal withstood this event with no recognizable distress. In recent times an event of magnitude  $M_L=6$  occurred on 27<sup>th</sup> August 1960, having its epicentral tract in the Delhi-Gurgaon region. On 28<sup>th</sup> July 1994 an event of magnitude  $M_L=4$  caused minor damage to a few old buildings. While these events have had their sources in the Indo-gangetic plains nearer to Delhi city, distant events originating in the Himalayan plate boundary, such as Uttarakashi ( $M_L=6.4$ , 20<sup>th</sup> October 1991) and Chamoli ( $M_L=6.8$ , 29<sup>th</sup> March 1999) earthquakes have caused nonstructural damage in some parts of Delhi. Thus, the hazard at Delhi is controlled broadly by two different tectonic regimes with different recurrence characteristics.

### 3.0 REGIONAL SEISMICITY

From past investigations, it is known that a strong earthquake can induce severe ground vibrations up to distances of about 300 Km from its epicenter. It follows, for any site one has to consider all active faults within 300 Km radius of the site. Here, with India Gate in Delhi as the center, a seismo-tectonic map (Fig. 1) has been prepared, taking information from various sources (Valdiya 1976, GSI 2000, Srivastava and Roy 1982). Well-known geological features of Himalayas such as the Main Boundary Fault (MBF) and the Main Crustal Thrust (MCT) have several tributaries also. In the present study, all such branches have been merged with the parent fault. In Fig.1, twenty important faults are shown along with the known 278 past epicenters. This figure highlights Delhi's susceptibility to earthquakes originating either from the Himalayas or from local sources. The faults are numbered for further reference and some of their details are presented in Table 1. The magnitude  $M_u$  given in this table refers to the estimated maximum magnitude a particular fault may be able to produce. This value has been assigned based on past information, without excessive conservatism. The hazard at any point in Delhi is a function of the seismic activity of the region, which in turn is directly related to the individual recurrence property of the listed twenty faults. This amounts to stating that the quantified regional seismicity has to be accounted by the twenty faults in differing proportions. In the present case, this regional seismicity has to be understood for engineering purposes in terms of historical data, in the control region around Delhi city. Here we consider the historical period to be 1720-2001, during which there were 278 catalogued events of  $M_L \geq 3$  in the region. Aftershocks of large events have been omitted from this list. It is well known that catalogues contain more number of small magnitude events of recent dates detected with the help of instruments. On the other hand, larger earthquakes are rare but even without instruments their occurrence would be known from general regional history. This points to the limitation that any regional catalogue will be complete, at different magnitude levels, with differing periods of representative history. Quantification of completeness of a catalogue is essential to arrive at reliable ( $a$ ,  $b$ ) values in the Gutenberg-Richter recurrence relationship. Here, an additional



complication arises due to the control region being not seismically homogenous. To keep the work tractable, with the limited amount of reliable data available, the control region has been divided into two parts denoted as the Himalayan region (HR) and the Delhi region (DR) as shown in Fig.1. The maximum likelihood method proposed by Kijko and Sellvol (1989,1992), has been used for each of the two parts, with an upper bound on the maximum magnitude, to obtain the regional ( $a$ ,  $b$ ) values. This method can handle small errors and incompleteness in the data set. This leads to the expected values  $b=0.78\pm0.04$  for HR and  $b=0.87\pm0.04$  for DR. The recurrence relationships for the two sub-regions associated with Delhi, are shown in figure 2.

#### 4.0 FAULT DEAGGREGATION

A given point in the target region will be subject to ground motion from any of the twenty faults. However, each fault has different length, orientation and seismic activity rate. To compute the ground motion due to an event on a particular fault source  $s$  one needs to know the magnitude of the event and the site to source distance. The magnitude of a future event on any fault is a random variable since that fault has potential to produce an earthquake of magnitude  $m$  in the interval  $(m_0, m_u)$  as per its own recurrence properties, which is not known. To circumvent this difficulty, the heuristic principle of conservation of seismic activity is invoked. According to this principle, the number of earthquakes per year with  $m > m_0$  in the region, denoted as  $N_r(m_0)$ , should be equal to the sum of number of events  $N_s(m_0)$  ( $s=1,2,\dots,N_s$ ) possible on the different faults. For seismic hazard analysis,  $m_0$  can be fixed at 4.0 since events of still lower magnitudes are not of engineering importance. However, any fault longer than the rupture length required to cause an event with  $m_0=4$ , can generate ground vibration at the site in future. This observation leads one to recognize that  $N_s(m_0)$  may be taken to be proportional to the length of the fault. This gives the weighting factor  $\alpha_s = L_s / \sum L_s$  as an activity indicator for fault  $s$ . However this need not be the only factor influencing  $N_s(m_0)$ . For example, a shorter fault may be more active at the lower magnitude level  $m_0$ , than a longer fault that is capable of producing a higher magnitude. This property can be included if the slip rate of various faults in the region are known. Since this is not known, one has to proceed differently. All the past earthquakes are assigned to the twenty faults depending on the proximity of the respective epicenters to these faults. This way another weighing factor  $\delta_s$ , which is the ratio of the past earthquakes attributed to fault  $s$  to the total number of earthquakes in the region is obtained. This leads to the relation

$$N_s(m_0) = 0.5(\alpha_s + \delta_s) N_r(m_0) \quad (s=1,2,\dots,20) \quad (1)$$

The weight  $w_s = 0.5(\alpha_s + \delta_s)$  assigned to each fault is given in Table 1. With the help of the above expression, the regional recurrence is deaggregated into individual fault recurrence as shown in Fig. 3. Here it may be mentioned that the  $b$ -value of a fault has been taken to be equal to the regional  $b$ -value.

## 5.0 ATTENUATION OF PGA

The peak ground acceleration (PGA) at a site depends strongly on the magnitude of an event and the corresponding hypocentral distance. The pattern of decay of PGA with distance is a property of the region. The current practice is to obtain the attenuation relation by empirical methods, based on instrumental data. Sharma (1998) has proposed one such empirical relation, valid for mixed soft soil and rock sites in North India. However, he has not reported the standard deviation of the error in the regression. Hence, it is not applicable in probabilistic seismic hazard analysis (PSHA). With this in view, it is thought appropriate here to derive a relation valid for rock sites in northern India. By definition, such sites are expected to have a shear wave velocity of  $0.76 < V_s < 1.5$  km/s in the top layer of about 30 meters. Available strong motion data at such sites consists of 38 samples from Sharma's database plus 23 samples of new data. With the help of this data, the attenuation relation valid for rock sites in the Delhi region is obtained as

$$\log_{10}(y) = C_1 + C_2 M - B \log_{10}(r + e^{C_3 M}) + P\sigma \quad (2)$$

$$C_1 = -1.5232, C_2 = 0.3677, C_3 = 0.41, B = 1.0047, \sigma = 0.2632,$$

In the above equation  $P=0$ , stands for the median or 50 percentile (PGA/g) value and  $P=1$ , leads to the 84 percentile value of (PGA/g). A comparison between the present equation and the one given by Sharma, for mean PGA value, is shown in Fig. 4. The two relations are similar except for minor differences, which are attributable to mixed soil conditions retained by Sharma, in his database.

## 6.0 PROBABILISTIC SEISMIC HAZARD ANALYSIS (PSHA)

Probabilistic seismic hazard analysis has been discussed in the literature notably by Cornell and Merz (1975), Kiureghian and Ang (1977), Bullen and Bolt (1985) among others. Presently, international engineering standards and manuals such as USDOE-1024, IBC-2003, USNRG-1.165 and EM-1110 of US Army Corp of Engineers, specify hazard in terms of a given value being exceeded at a particular probability level in a time window of one or more years. If the number of earthquakes randomly occurring on a fault is taken to be a Poisson process, the probability of the random variable ( $Y=PGA/g$ ) exceeding the level  $a$  in the time period  $T$  at the site can be expressed in terms of the annual rate of exceedance  $\mu_a$  as,

$$P(Y > a) = 1 - \exp(-\mu_a T) \quad (3)$$

The basic expression for  $\mu_a$  is

$$\mu_a = \sum_{s=1}^{N_s} N_s(m_0) \int_m \int_r P(Y > a | m, r) p_{R|M}(r | m) p_M(m) dr dm \quad (4)$$

It is emphasized here that the above expression sums up all the individual contributions of twenty faults ( $s=1,2,\dots,20$ ) to obtain the annual probability of exceedance of PGA. As an example, for the central point (India Gate) of Delhi, the individual contribution of all the twenty faults to the mean annual hazard is presented in Fig.5, along with the total value. Details of the computations involved are presented elsewhere (Iyengar and Ghosh 2004). Once the value of  $\mu_a$  is found at a site, the probability of rock level PGA exceeding a design value  $a$  in a life period of  $T$  years is given by equation (3). By repeating the above computations at various points representing Delhi and its environs, one can construct a micro-zonation map to any required level of detail. Here, a rectangular region of 40 Km x 30 Km, with India Gate as the central point is taken as the target region. This region is divided into 1320 grid points at 1km x 1km distance apart. PSHA incorporates all known faults, epicenters, past data and local characteristics in a judicious manner to arrive at the site-level hazard. Here, this result is shown in Fig. 6, as (PGA/g) value, with 2% exceedance probability in 50 years. This corresponds to a return period of 2500 years as suggested by the International Building Code IBC-2003. At the rock level, it is seen that the hazard peaks up near the local Delhi fault at the center of the city. This effect is also seen from Fig.5, where the contribution of individual faults to hazard at the center point is shown. As one moves away from the center towards the corners, the distance from the Delhi fault increases and its contribution to the hazard decreases. The pattern of the contours in Fig.6 indicates that the hazard is strongly influenced by the southwest-northeast trending M-D fault. The PGA value shown at the center point of Delhi is of the order of 0.2g. This value compares with the value reported by Khattri (1992) at the probability level of 10% for a time window of 50 years. It has to be noted that the result of Fig.6 does not include the effect of soft soil deposits that are widely spread over Delhi. Further refinement of the micro-zonation map of Fig.6 is yet to be done by incorporating the effect of soft soil deposits.

## 7.0 LOCAL SITE EFFECTS

It is well established that structures on rock behave differently from those founded on soft soils. Delhi is a typical example of a city on the banks of a river that has left several paleo-channels over which presently human settlements exist. Delhi has also rock outcrops in its southern extensions, as seen from Fig.7. Besides the NNE-SSW trending ridge, the other parts of the city are overlain with alluvial sediments. These alluvial plains are flat except for a few interruptions by clusters of sand dunes or rock outcrops. The ridge, which is an extension of the Aravali hills into Delhi, seems to disappear below the western banks of River Yamuna north of Delhi. The land surface on the eastern side of the ridge is inclined towards River Yamuna with an average gradient of 3.5 m/km. Geological Survey of India (GSI 1978) summarizes the soils conditions in the Metropolitan area in the following manner: “The depths to bed rock.....vary from near surface in the Link Road, Pusa Road, Vijay Chowk, Daryaganj areas to as deep as 40 to 60 m in the Patel Road, Lal Quila, Rajghat areas,

80 to 100 m in the Aurobindo Marg- IIT area and 150 m in the Yamuna river bed area. The bedrock topography, in general, is undulating, characterized by several humps and depressions. In the North Delhi area, the depths to bedrock east of the ridge vary from near surface to 30 m, with a gradual easterly slope towards the river Yamuna. West of the ridge in the Mall Road- Imperial Avenue sections the depths vary from near surface to 30 m and more, with an abrupt deepening to 90 m in the north to as much as 200 m in the Roshanara garden area in the south. In the Sabzi Mandi, Rani-Jhansi Road area the bedrock occurs at shallow depths and at more than 20 m in the Chandni Chowk Sadar Bazar-Lal Quila areas. The bedrock is overlain mostly by clay in the North Delhi, Aurobindo Marg, and Yamuna river bed areas with indications of sand/silt with *kankar* and granular zones at several places. The overlying alluvium east of the ridge appears to be mostly sand/silt with *kankar*.” This is a qualitative, broad-brush picture of soil conditions in Delhi. Construction sites are of the size of a few ten meters. Thus, the local ground vibration transferred to the structure depends sensitively on the detailed vertical make up of the soil layers at the site. A proper study of the effect of local soils on the hazard calls for extensive investigations focusing on shear wave velocity and density profiles. Even though in engineering projects bore hole investigations are common, shear wave velocities are not routinely measured. Under these circumstances, what has been possible here is to estimate the transfer function of the ground at a few points. At construction sites borehole data up to 30-60 meter depth are acquired for purposes of foundation design. The geotechnical parameters obtained this way, can be used to estimate how the local soil modifies rock level PGA to the surface level PGA value. Seventeen borehole data from a construction project were available for further study (courtesy M/s Tandon Consultants Pvt.Ltd., New Delhi). The locations of these data are listed in Table 2 and shown in Fig.7. A typical profile of N value obtained by the Standard Penetration Test (SPT) is shown in Fig.8 to illustrate variation of engineering properties of soils with depth. The N value is widely used as a proxy for shear wave velocity through empirical correlations. One such relation proposed by Turnbull (2001) based on Australian and Japanese information is  $V_s = 3.9.N + 182.9$  m/s with a standard error of 70 m/s. In the absence of measured  $V_s$  values, they have been estimated from reported N values using the above equation. By repeating this exercise for all the seventeen stations, a picture of how  $V_s$  varies with depth can be obtained. The regression equation  $V_s = 173 D^{0.2}$  is found to be the average variation of  $V_s$  with depth D in meters (Iyengar and Ghosh 2004). Analytical representation of  $V_s$  has practical advantages when a large region overlain with alluvial soils has to be studied. In such a case, the rock level motion propagates vertically through the soil layers, as in a one-dimensional medium, to arrive at the surface in a modified fashion. This modification, incorporating nonlinear effects and layering properties can be carried out using the standard software SHAKE-91. Here, using this software, surface amplification function for unit amplitude Sinusoidal motion at the rock level is obtained for some stations and presented in Fig.9. The amplification will be a maximum corresponding to the natural frequency of the soil deposit. In Table 2, the first natural frequency of the local ground is listed along with some layering details. In the same table the engineering classification of the

sites as per international practice, using the average  $V_s$  value in the top 30 meters of the soil is also presented. Sites, where rock is not too deep, would correspond to site class B requiring no correction. This is the case for site no.3 and site no.5 with high natural frequency. At such places, the seismic hazard curve of Fig.6 can be directly used. For other sites, suitable correction for the PGA value would be necessary. The frequency response functions at C- and D-type sites (Fig.9) indicate that seismic waves, near the site resonant frequencies, are susceptible for amplification by as much as 1.5–2.5. Thus, notwithstanding the low PGA values at the rock level, surface acceleration values can be of the order of 0.3g and more in the Trans-Yamuna region. It has to be noted that Fig.9, refers to Sinusoidal motion at the rock level. In practice, one needs the surface level acceleration spectrum for real earthquake motion at the rock level. This calls for, more detailed work yet to be undertaken. Engineering properties of soil deposits can vary widely within short distances, particularly near riverbanks. Thus, it will be appropriate to compute surface level design basis accelerations from rock level values shown Fig.6, depending on the  $V_{30}$  value at the site. Amplification factors given by codes such as IBC-2003 can be used until results specific to Delhi region are obtained.

## 8.0 SUMMARY AND CONCLUSION

A planned natural disaster reduction strategy has to be built into the larger policy framework of sustainable development. The vulnerability of India's urban areas has been dramatically demonstrated by recent earthquakes; which did not originate in the more active Himalayan plate boundary. The looming risk to cities such as Delhi, Agra, Chandigarh, Gauhati and others can be perceived in the backdrop of severe earthquakes originating either in the Himalayan zone or in the Indo-Gangetic plains. As the cities expand, the potential for earthquake loss also increases. Repeatedly, India has had earthquakes turning into disasters without warning. While the loss in financial terms is a function of the state of development, initial investment and cost of living indices, the vulnerability of a city is dependent on the social and economic condition of the population. It is prudent to plan, develop and protect our vulnerable cities from possible future earthquake destruction. It is in this context, seismic micro-zonation of cities assumes great importance. If carried out properly, it is an excellent scientific tool for engineers and planners for involving all stakeholders in a city in land use planning and earthquake resistant construction practices. As an example, results are presented here in the form of a seismic hazard contour map covering Delhi city and its environs for an extent of 1200 sq. km on a grid of 1 sq. km. Engineers can use this map directly for rock sites and B-class soil sites in Delhi. For soft soil sites, amplification factors given in codes such as IBC-2003 can be used, till improved  $V_s$  values become available for Delhi. The present result should form a sound basis for future extensions to cover local soil effects, liquefaction susceptibility, and vulnerability analysis of buildings. It is hoped a national level effort will be forthcoming to map city level seismic hazard, followed by vulnerability analysis and risk estimation, as a step towards making our cities safer.

## REFERENCES

1. Bullen, K.E. and Bolt, B.A., (1985) *An introduction to the theory of seismology*. 4<sup>th</sup> edition. Cambridge University Press. Cambridge.
2. Cornell, C.A. and Merz, H.A., (1975), 'Seismic risk analysis of Boston', *J. of Struct. Div. ASCE*, **101**, ST10, pp. 2027-2043.
3. GSI, (2000), Seismo-tectonic Atlas of India and its Environs, *Geological Survey of India*, Calcutta, India.
4. Der Kiureghian, A. and Ang, A. H.-S., (1977), 'A fault rupture model for seismic risk analysis', *Bull. Seism. Soc. Am.*, **67**, 4, pp. 1173-1194.
5. DOE Std-1020 (2002), 'Natural phenomena hazards design and evaluation criteria for department of energy facilities', *U.S. Department of the Energy, Washington, D.C. U.S.A.*
6. EM 1110-2-6050, (1999), 'Response Spectra and Seismic Analysis for Concrete hydraulic Structures, Engineering Manual', US Army Corps of Engineers, Washington.
7. GSI, (1978) 'Urban Geology of Delhi' Miscellaneous Publications, No.42, Govt. of India.
8. Iyengar, R. N., (2000), 'Seismic Status of Delhi Megacity', *Current Science.*, **78**, 5, pp. 568-574.
9. Iyengar, R.N., and Ghosh, S., (2004) 'Microzonation of Earthquake Hazard in Greater Delhi Area' to appear in *Current Science, Bangalore*.
10. IMD (2002), India Meteorology Dept. 'Important earthquakes from the IMD Catalogue occurred in the region bounded by 25.5°- 31.5 °N and 74.5 °-80.5 °E', *personal communication*.
11. Khattri, K.N., (1992), 'Seismic hazard in Indian region', *Current Sc.*, **62**, 1, pp. 109-116,
12. Kijko, A., and Sellevoll, (1989), 'Estimation of Seismic Hazard Parameters from Incomplete Data Files. Part I: Utilization of extreme and complete catalogues with different threshold Magnitudes', *Bull. Seism. Soc. Am.*, **79**, pp. 645-654.
13. Kijko, A., and Sellevoll, M. A., (1992), 'Estimation of Earthquake Hazard Parameters from Incomplete Data Files. Part II: Incorporation of Magnitude Heterogeneity', *Bull. Seism. Soc. Am.*, **82**, pp. 120-134.
14. Sharma, M.L., (1998), 'Attenuation relationship for estimation of peak ground acceleration using data from strong-motion arrays in India', *Bull. Seism. Soc. Am.*, **88**, 4, pp. 1063-1069.
15. Srivastava, V.K. and Roy, A.K., (1982), 'Seismotectonics and seismic risk study in and around Delhi Region', *Proceedings IV Congress International Association of Engineering Geology*. **VIII**, pp. 77-82, New Delhi.
16. Turnbull M.L. (2001) 'Seismic Hazard Assessment and Microzonation of Bundaberg'. Masters Thesis, Central Queensland Univ. Australia.
17. UPHS:Uttar Pradesh Hindi Sansthan (1992) Nazir Granthavali, Collection of Poems of Nazir Akbarabadi.
18. Valdiya, K.S., (1976), 'Himalayan transverse faults and folds and their parallelism with subsurface structures of north Indian plains', *Tectonophysics*, **32**, pp. 353-386.

19. USNRG(1997): Regulatory Guide 1.165, 'Identification and characterization of seismic sources and determination of SSE ground motion', pp. 1-45.

*Table 1: Fault Characteristics*

No.	Fault Name	$M_u$	Length Km.	$w_s$	$M_{100}$
<b>Delhi Region</b>					
1	Great boundary fault (GBF)	7	320	0.1462	5.18
2	Mahendraghar-Dehradun (M-D)	7	300	0.2657	5.47
3	Moradabad	6.5	165	0.0790	4.87
4	Chahapoli	5.5	215	0.0872	4.81
5	Sabi Fracture	5.5	195	0.0796	4.78
6	Near Mathura	5	84	0.0371	4.40
7	Parallel fault to no. 6	5.5	115	0.0490	4.59
8	Fault left of Alwar	5	130	0.0547	4.53
9	Fault near Alwar	5	55	0.0260	4.27
10	Fault near Jaipur	5	117	0.0497	4.50
11	Mathura	6	100	0.0432	4.56
12	Sohna	6	105	0.0719	4.80
13	Delhi	4.5	7	0.0106	3.92
<b>Himalayan Region</b>					
14	Main Central Thrust (MCT)	8	350	0.5847	6.87
15	North Almora thrust (NAT)	6.9	280	0.1315	6.00
16	Main Boundary Thrust (MBT)	8	450	0.1647	6.22
17	Alaknanda	5.5	51	0.0454	5.15
18	Ropar	5	35	0.0144	4.61
19	Near Ramgarh	5	37	0.0149	4.62
20	South Almora Thrust (SAT)	6.5	130	0.0444	5.43

Table 2: Soil Site Location and Classification (Ref. Figure 6)

Site no.	Location	Grid coordinate s in km.	No. of layers above rock	Rock depth . m	Natural Freq. hz	$V_s^{30}$ m/s	Site Class as per IBC-2000
1	Sewanagar	20.9,20.0	10	55	1.00	235	D
2	Shahjahan Road	21.0,18.0	8	32	1.63	270	D
3	Boat Club	20.1,17.5	4	12	5.38	1009	B
4	N.D. Rly.Stn.	19.5,14.2	11	30	1.75	279	D
5	Chawri Bazar	20.6,13.5	4	09	6.00	1130	B
6	ISBT	20.9,10.6	8	30	2.00	317	D
7	Rohini	09.3,27.7	24	200	0.50	269	D
8	Punjabi Bagh	10.3,21.0	18	100	0.75	271	D
9	Kirti Nagar	12.5,19.2	19	40	1.63	318	D
10	Rama Road-Patel Road Jn.	13.0,19.0	18	27	2.00	296	D
11	Naraina Road-Patel Road Jn.	13.9,18.5	11	16	2.88	834	C
12	Patel Ngr.	14.8,18.0	9	14	2.74	910	B
13	Karol Bagh	17.0,17.5	18	27	1.88	420	C
14	Palika Place	19.2,17.2	16	24	2.13	524	C
15	Connaught Place	20.0,16.5	12	18	2.38	748	C
16	Mandi House	21.0,15.5	11	40	1.88	339	D
17	Tilak Bridge	22.8,16.2	11	40	1.75	257	D

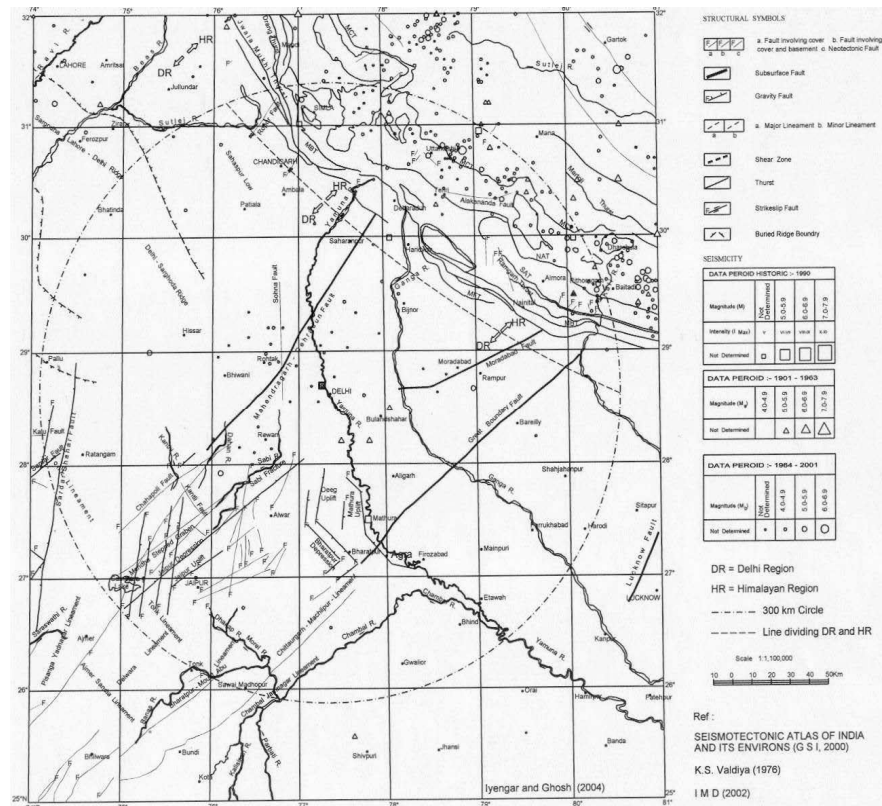


Figure 1: Seismo-tectonic map of Delhi Region



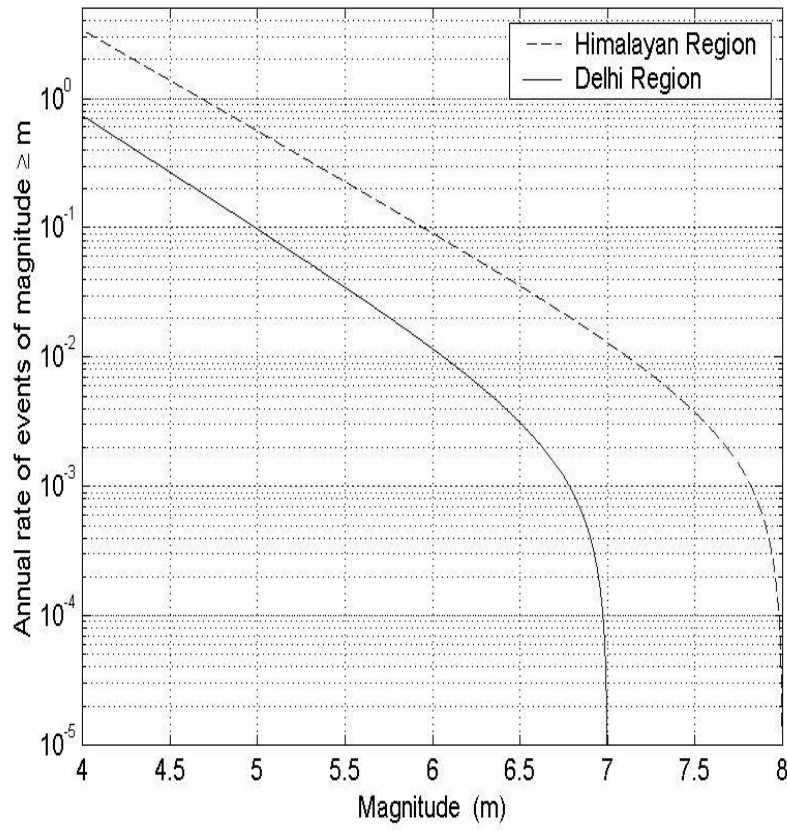


Figure 2: Regional Magnitude-Frequency Relationship

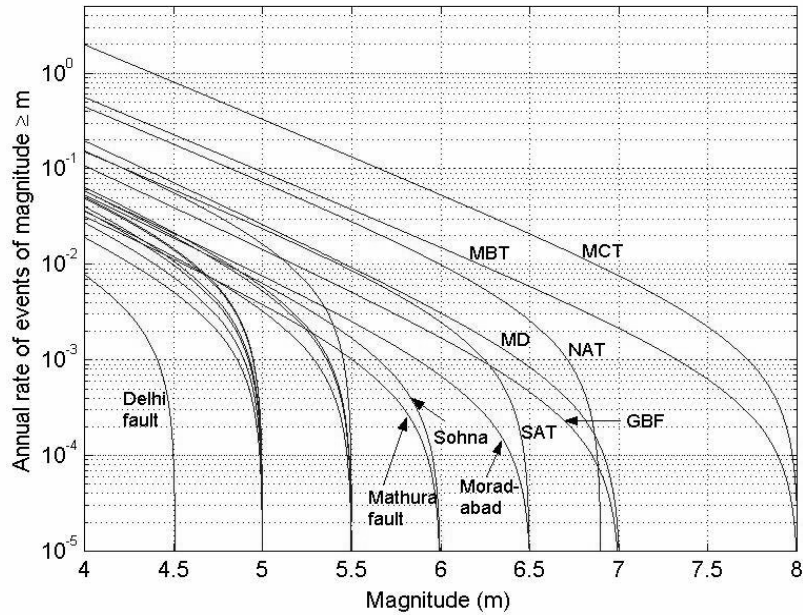


Figure 3: Deaggregation of regional hazard in terms of fault recurrence

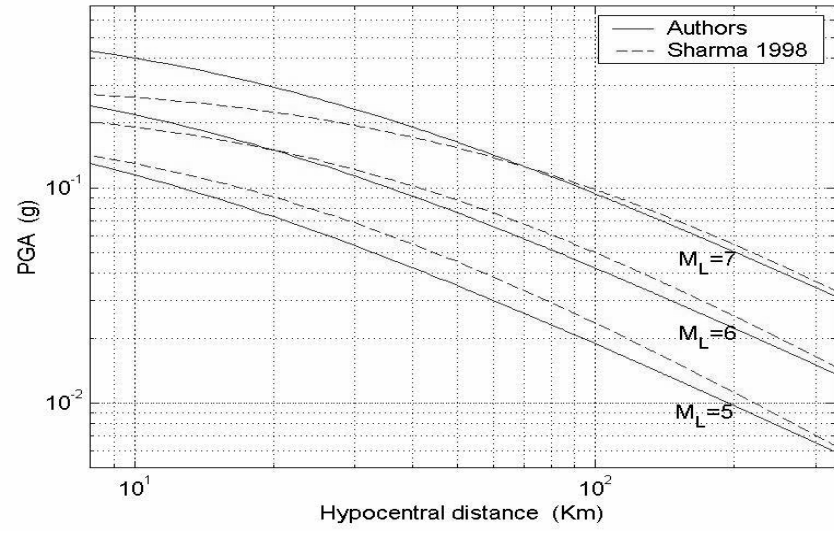


Figure 4: Attenuation of PGA in Northern India

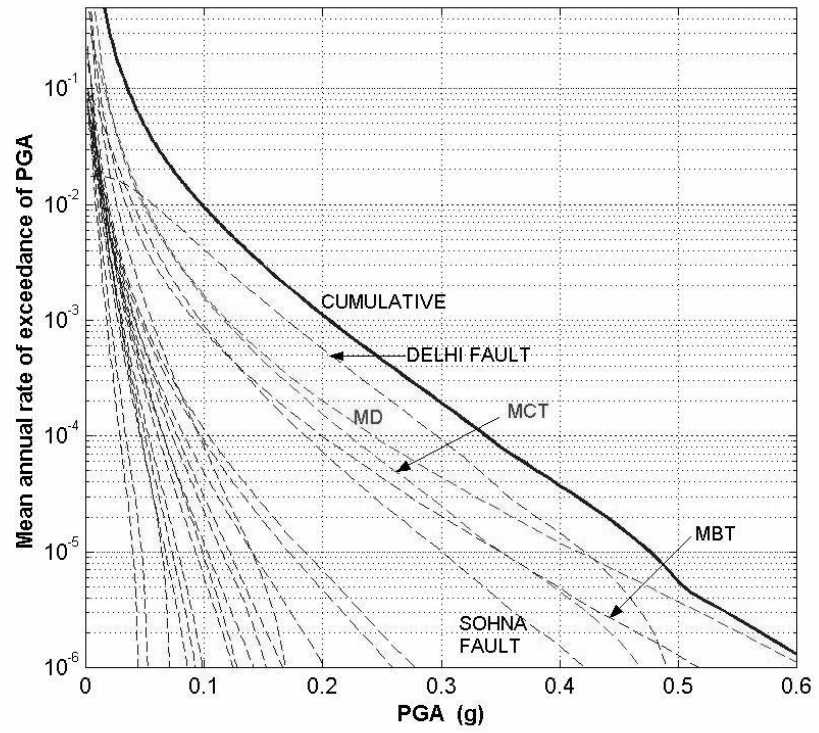


Figure 5: Hazard Deaggregation at India Gate due to Individual Faults

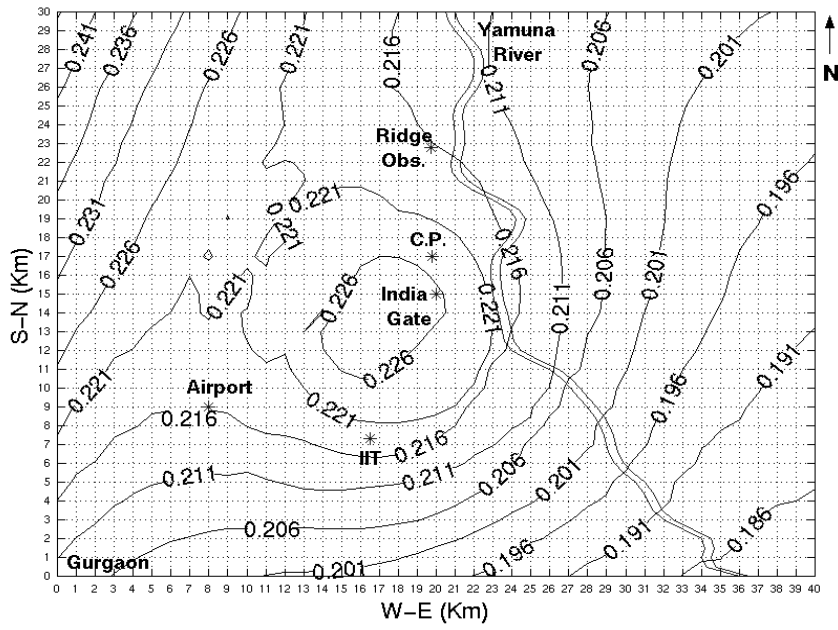


Figure 6: Microzonation of hazard at rock level. Contours of mean horizontal PGA( g) with 2% probability of exceedance in 50 years.

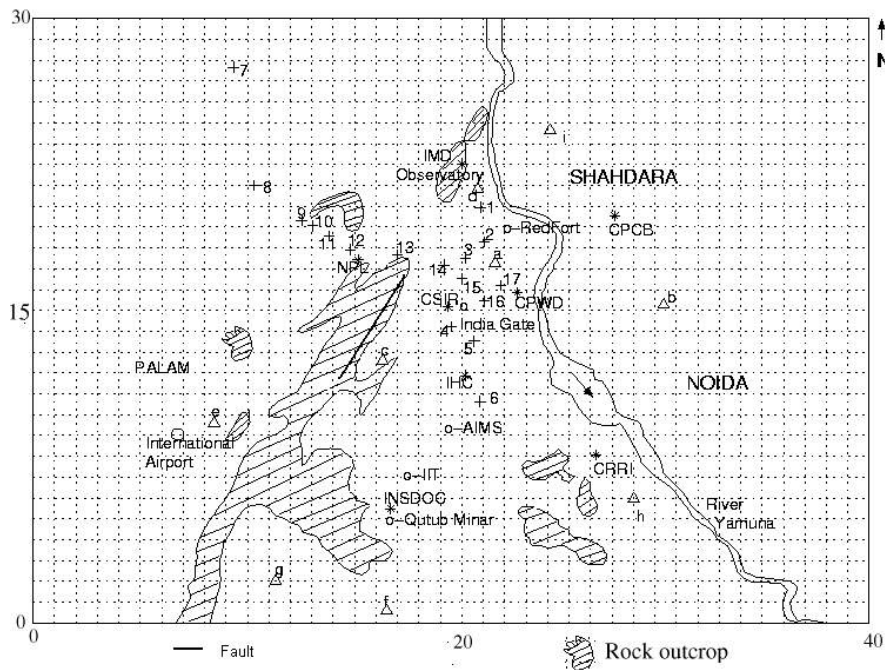


Figure 7: Rock Outcrops in Delhi City

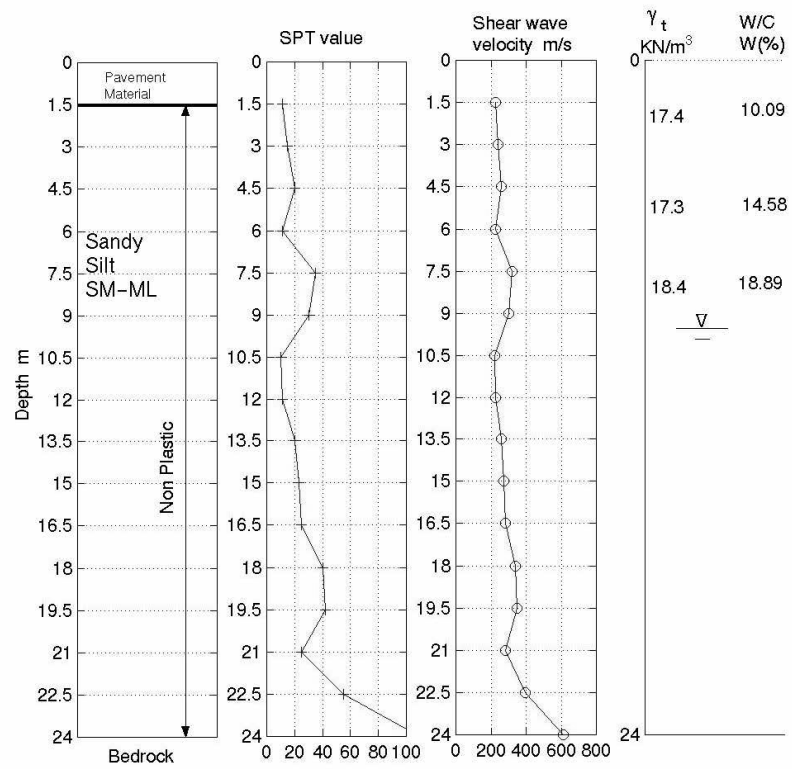
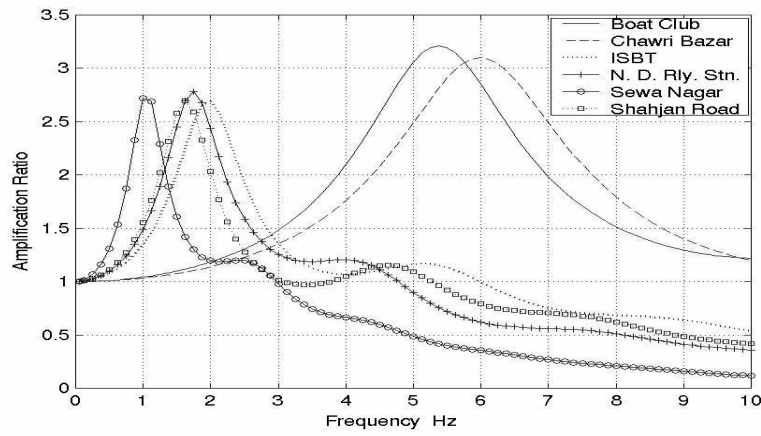
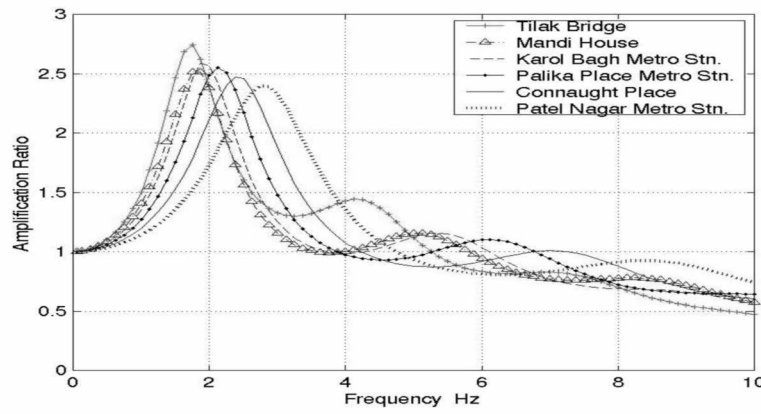


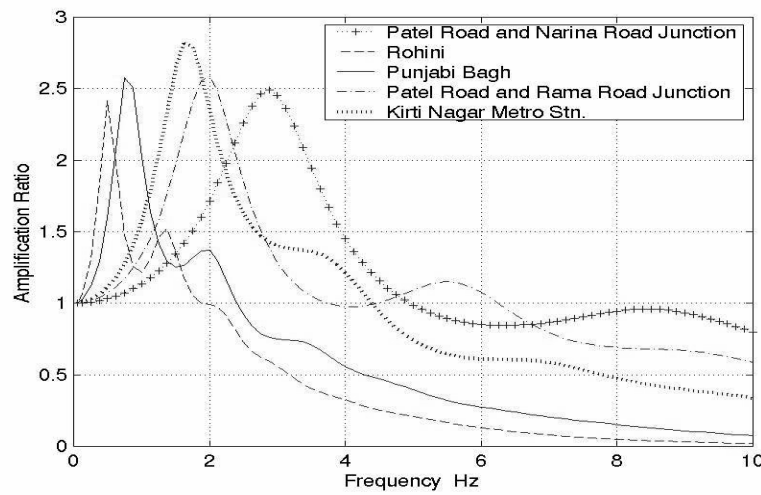
Figure 8: Bore-log at Palika Place.



(a)



(b)



(c)

Figure 9(a,b,c): Frequency Response Functions at the seventeen sites of Table 2.

# *Technical Sessions*

# **FROM GROUND SHOCKS TO AIR BLASTS – MULTIPLE-HAZARD PROTECTIONS**

T. C. PAN, B. LI, X. T. YOU AND C. L. LIM  
Protective Technology Research Centre, School of Civil and Environmental  
Engineering, Nanyang Technological University, Singapore  
*TCPan@pmail.ntu.edu.sg*

## **ABSTRACT**

*Singapore is an island city-state, located off the southern tip of Malay Peninsula. It has a land area of around 700 sq km and a population of about 3.5 millions of residents. Although small in size, the country's gross domestic product per capita was about US\$22,500 in 2003, among the highest in Asia. Most people live in high-rise residential buildings due to the land shortage. Being a metropolis with highly active trades and commerce, Singapore has also seen in recent years many modern high-rise commercial buildings constructed in her central business district.*

*This paper looks into the protective technologies for these modern high-rise residential and commercial buildings against multiple hazards. The hazards discussed here include both natural and man-made ones. They are the effects resulting from the long-distance major Sumatra earthquakes, ground shocks induced by underground explosions, and blast loading from terrorist bombings. The consequences from any extreme event of the multiple hazards could be devastating to the society at large due to the high concentration of population as well as the high-value commercial and financial activities housed in these modern high-rise building structures. This paper summarizes the experiences that have been gained in Singapore dealing with protection requirements against the multiple hazards.*

## **1.0 INTRODUCTION**

The most recent incident of terrorist car bombing occurred on Thursday, September 9, 2004, targeting the Australian Embassy in Jakarta, Indonesia. Many innocent people lost their lives in the tragic incident. In Singapore, the government has cautioned the general public that a terrorist attack against Singapore's interests remains a possibility. While both the security personnel and the general public have remained vigilant against any possible terrorist attacks in Singapore, the engineering community has been collectively looking into measures that may mitigate the effects of a terrorist attack on a major building and/or infrastructure. It has thus become clear that the adverse and fatal results of terrorism, which have become increasingly higher, should be reviewed at the same time whenever any additional measure to mitigate the risk of natural hazards is to be introduced. This should form the common first step towards a platform of integrated engineering methodologies to protect national interests against multiple hazards. This paper attempts to summarize the experiences that have been

gained in Singapore which deals with mitigating the effects of both natural and man-made hazards.

Located within the stable Sunda plate with mild winds, Singapore is believed to be in an aseismic area. It is about 350 km away from an active earthquake belt, comprising the Great Sumatra Fault and the subduction zone of Sunda Trench. Singapore has never experienced any earthquake damage, and hence buildings are generally not designed against the horizontal earthquake loadings. However, tremors caused by distant Sumatra earthquakes have been felt in Singapore for many years. The seismic response of typical Singapore buildings to the maximum credible earthquakes from Sumatra will be discussed.

As part of the national effort to intensify the land use of the land-scarce country, Singapore has explored the possibility of using underground facilities for various purposes. One of initiatives is to move the surface ammunition storages underground, which will reduce the precious land surrounding the surface storages that have been sterilized for safety reasons. As a result, the dynamic response of building structures to ground shocks that may result from underground explosions has been investigated. The results will be discussed in terms of the dynamic failure of RC buildings subjected to ground shocks, which in turn affects the minimum radial distance within which no residential buildings should be erected.

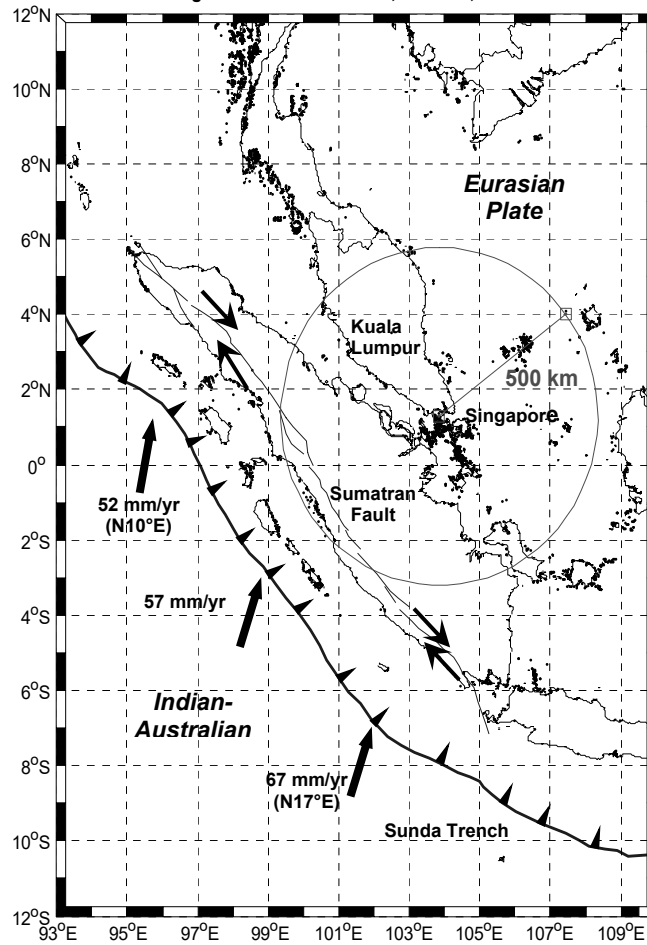
Recent terrorist bomb attacks around the world have demonstrated the ferocity, cruelty and unpredictability of the hazards posed by terrorism. Instead of trying to predict the next terror attack, it appears to be more important to protect critical assets like waterworks, seaports, airports, major buildings, etc. The transient dynamic response of a high-rise commercial building to a postulated external explosion load resulting from terrorist bombing will be discussed.

## **2.0 SEISMOTECTONICS OF SUMATRA AND THE MCE EVENT**

Sumatra is located adjacent to the Sunda trench, Figure 1, where the Indian-Australian plate subducts beneath the Eurasian plate at a rate of  $67 \pm 7$  mm per year towards  $N11^\circ E \pm 4^\circ$  (Tregoning et al, 1994). The islands of Sumatra and Java lie on the over-riding plate, one hundred some kilometres from the trench. Convergence is nearly orthogonal to the trench axis near Java, but it is highly oblique near Sumatra, where the strain is strongly partitioned between the dip slip on the subduction zone interface and the right-lateral slip on the Sumatran fault along the western coast of the island. Large earthquakes have thus been generated in the region. The largest subduction earthquake that has occurred in the Sunda trench is the great 1833 event with an estimated  $M_w$  between 8.8 and 9.2 (Zachariasen et al, 1999). The earthquake, with an average  $M_w$  of 9.0 with an epicentral distance of 723 km, is thus selected for this study to be the maximum credible earthquake (MCE) that the Sumatra subduction zone is capable of generating (Megawati and Pan, 2002). The larger of the two horizontal



components of the synthetic MCE ground motions is used in the convolution process to obtain the surface accelerations at a soft soil site.



*Figure 1: Seismotectonics of Sumatra region*

### 3.0 EFFECTS OF LONG-DISTANCE MAJOR EARTHQUAKES

One of the tallest buildings in Singapore that has been instrumented to monitor its seismic response has recorded 21 sets of seismic response data during the last decade. A detailed three dimensional finite element (FE) model of the building is constructed to simulate the seismic structural response. The correlation analyses of the recorded and the simulated seismic responses of the instrumented tall building to the major Bengkulu, Sumatra earthquake ( $M_s=8.0$ ) which happened on June 4, 2000, Figure 2, (Pan et al. 2001a) are presented in this paper.

A three dimensional mathematical model was constructed for numerical analyses. The FE model shown in Figure 3 contains 3,185 frame elements and 2,223 shell elements, and has 20,808 degrees of freedom. Besides the main structural elements, major openings, secondary openings and internal thin walls within the central core have all been considered in this model. The basement acceleration records of the earthquake occurred in

year 2000 at Bengkulu, 685 km away from Singapore are used as the input motions.

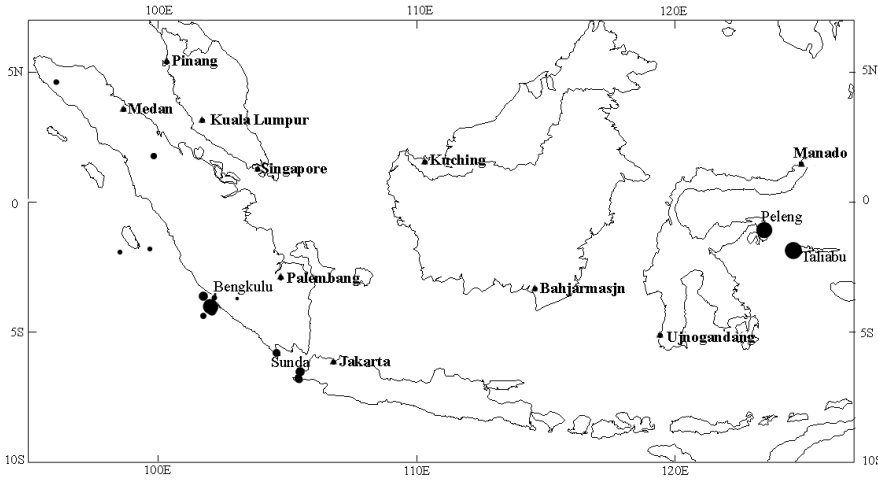


Figure 2: Epicentres of recorded earthquakes

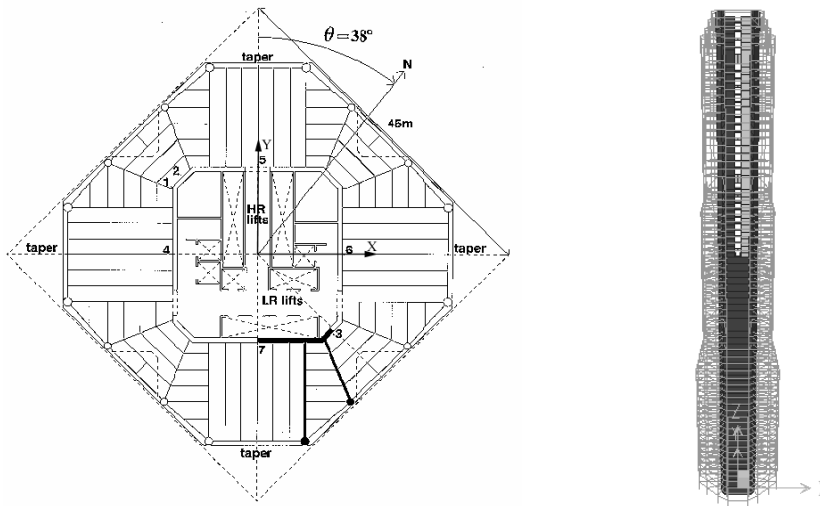
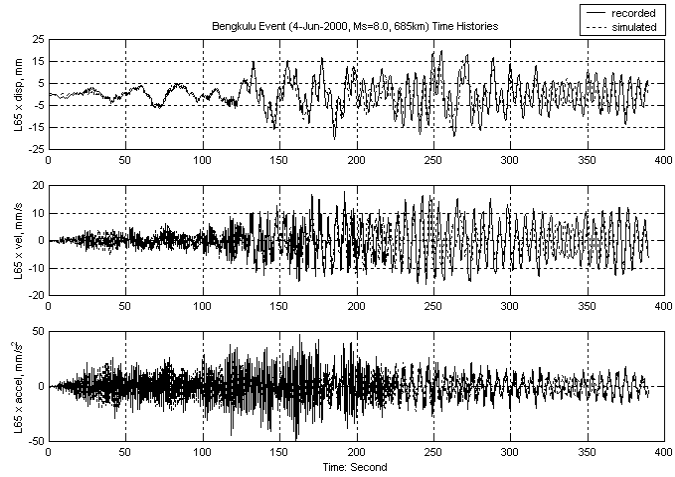


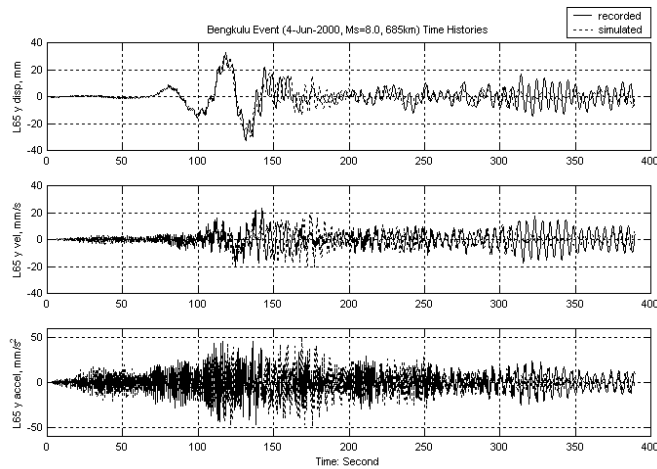
Figure 3: Floor plan and perspective view of the FE model

The simulated results and the recorded roof motions are shown in Figures 4a and 4b. The responses consist of mainly the first two natural modes in both directions and the rigid-body motions. The smaller spikes in the spectra of the simulated results at the first translational mode frequency in each direction, 0.19 Hz and 0.21 Hz for the x and y directions respectively, suggest that the FE model may be stiffer than the actual structure. This is also indicated by the measured fundamental frequencies which are higher than the simulated ones. The smaller spikes in the spectra may also be due to the consistently smaller magnitude of the simulated time histories when compared with the recorded ones. However, for this largest event recorded, the simulated and the recorded time histories match very well in both the displacement and velocity responses, except in the later

portion of the responses in the y direction, where the simulated results are smaller compared with the field records. Such phenomena were also observed in some other events, though sometimes in the other direction. They may have been caused by the sudden wind blows. The maximum values of the simulated roof displacements are 16 mm and 31 mm in the x and y directions, and those of the recorded roof displacements are 21 mm and 33 mm.



*Figure 4(a): Bengkulu event (2000.06.04): comparison of time histories at roof level in the x direction*



*Figure 4(b): Bengkulu event (2000.06.04): comparison of time histories at roof level in the y direction*

#### 4.0 EFFECTS OF EXPLOSION-INDUCED GROUND SHOCKS

Explosion-induced ground motions (EIGMs) or ground shocks could be one of the possible damaging ground motions to be faced in the lifetime of a structure owing to accidental or intentional explosions. However, since ground motions of earthquakes and EIGMs are inherently different, direct application of earthquake engineering principles to ground shock cases may be questionable. By subjecting a lightly-reinforced RC frame to a simulated

EIGM, the suitability of current earthquake design philosophies and damage assessment techniques for EIGMs is investigated in this section.

EIGM characteristics can be segmented into two parts: the major shock duration (Phase I) and the ensuing duration (Phase II). Dhakal and Pan (2003) showed that the high frequency nature of an EIGM led to a large shear force with small deformation during Phase I followed by significant deformation in Phase II. Other studies have shown that the EIGM produces significant local damages owing to the high frequency content of EIGMs (Ma et al, 2002). In this paper, impulse per unit mass of a ground motion is used as a gauge of the damaging potential of the ground input.

#### **4.1 Member and joint strengths**

Member strength includes flexural and shear strengths, respectively. While the predictive flexural strength equation stated in (Park and Pauley, 1974) has been widely accepted, there is less confidence on the existing shear strength predictive equations (ASCE-ACI, 1973, Karim, 1999, Priestley et al, 1994). Shear strength has been regarded to comprise contributions from concrete and steel reinforcement. With variations of the steel contribution, these predictive equations state a similar concrete contribution (Karim, 1999, Priestley et al, 1994). For the small deformation in Phase I, the contribution of the longitudinal reinforcement to the member shear strength may not be significant. Thus, the shear strength of members during Phase I would mainly be contributed by the concrete strength.

Observations of the buildings damaged during the strong Chilean earthquakes of the 1960's showed damage in the beam-column joints (i.e. joint panels). Joints act to transfer forces between beams and columns, and so their state reflects the extent of the load transfer mechanism. Joint performance has been observed to be dependent on joint shear strength (Paulay and Priestley 1978). When the joint shear strength is exceeded, member strengths will be compromised. For a non-seismically designed joint, joint cracking and joint failure were observed at a 0.5% and 3% inter-storey drift ratios, respectively (Pan et al 2001b, Li et al 2003).

#### **4.2 Post-elastic response and damage assessment**

Hysteretic models attempt to describe the post-elastic behaviour of RC members in terms of hysteretic energy dissipated. The advantage of using hysteretic model of members over material model is its lower computational effort. Park and Ang (1985) proposed a three-parameter post-elastic model where the post-elastic behaviour of members is described by stiffness degradation, strength deterioration and pinching parameter. In earthquake response analysis, damage assessment techniques provide qualitative information of structural performance under earthquake actions. Damage assessment techniques may be classified as strength-based, response-based or the hybrid of the two. Of the many damage assessment techniques, the hybrid damage assessment technique by Park and Ang (1985) is widely used.

The damage levels were categorized as moderate, severe and partial or total collapse.

### **4.3 Response to a simulated EIGM**

A non-seismically designed 6-storey RC frame was subjected to a simulated EIGM. The RC frame and the details are shown in Figure 5. The simulated EIGM is similar to that used in (Ma et al, 2002) for the horizontal ground motion at a distance from the explosion source. The simulated EIGM has a peak ground acceleration (PGA) of 124 g and a predominant frequency of about 200 Hz, Figure 6.

The IDARC software (Valles et al, 1996) with Park and Ang's three-parameter hysteretic model and damage assessment procedure was used for analysis. For a qualitative understanding of the generic damage assessment techniques, local mode responses described in Ma et al (2002) were not modelled, while 3% inter-storey drift ratio was used as the joint failure criterion. The shear failure occurs when the nominal shear stress exceeds the shear strength predicted in Priestley et al (1994).

The Phase I responses of different storey levels (ST) are: the maximum roof displacement 12 mm; the peak inter-storey drift ratio 0.29% reached at ST2, and the maximum storey acceleration 1.36 g at ST2. The largest nominal shear stress occurred at the base of interior column, which was below shear strength. The damage level was moderate according to Park and Ang's model. The Phase II response exhibited a much larger deformation. The largest roof displacement was 230 mm, and ST6 had the largest inter-storey drift ratio of 3.2% (i.e. joint failure). The maximum nominal shear stress occurred at the base of interior column without shear failure. For this column, there was flexural yielding. However, the damage level was identified as moderate. Therefore, such a damage level does not reflect the actual damage associated with the joint failure.

### **4.4 Failure analysis**

To understand the effects of the duration and the input impulse of EIGMs, duration multipliers (DM) and amplitude multipliers (AM) were applied on the above EIGM. The main parameters investigated are the predominant frequency and the amount of energy. Following this procedure, the response analysis and damage assessment of the 6-storey RC frame subjected to a family of scaled EIGMs were performed. Both shear failure and joint failure were investigated for the first storey interior column where the maximum shear stress occurred.

Combinations of DM and AM can lead to joint and/or failure in Phase I or Phase II. The damage level for the first storey column is presented in Figure 7. One bold line shows the boundary between the moderate and the severe damage levels for Phase I, Severe (I). The other bold line shows the boundary between the moderate and the severe damage levels for Phase II, Severe (II). Iso-impulse lines are shown as dotted lines in the background.

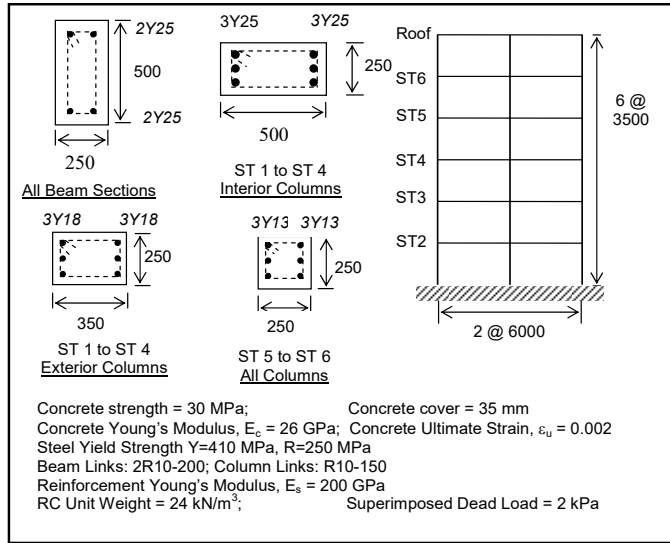


Figure 5: RC frame elevation and details

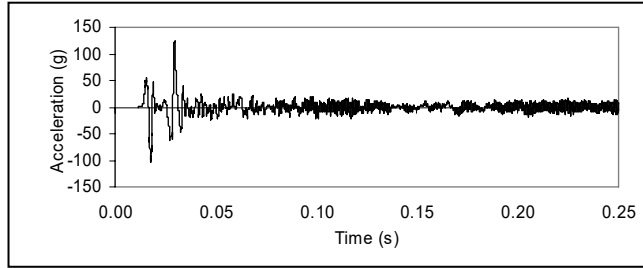


Figure 6: Horizontal acceleration time history of a simulated EIGM

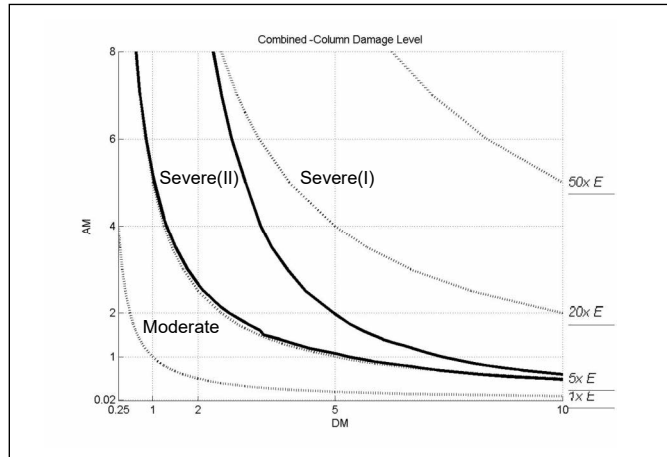


Figure 7: Zones of failure patterns for different response phases

The figure shows that the iso-impulse line of  $1xE$  produced moderate damage in both Phases I and II. A scaled EIGM with a  $DM=1$  and  $AM=2$  produced a moderate damage level. Therefore, it can be seen that the damage level as computed does not reflect adequately the shear failure and joint failure caused by this scaled EIGM.

## 5.0 EFFECTS OF EXTERNAL BLAST LOADING

Effects of an external explosion on a high-rise commercial RC building resulting from a vehicle bomb at the ground level near the building are investigated in this section. The standoff distance is qualitatively classified as long or short. The high-rise commercial building selected for the study is a 30-storey RC structure with frames and a shear wall core. The building structural system consists of one storey of basement, 9 storeys of shopping centres cum car park, one mechanical floor and 20 storeys of office space, Figure 8. It is about 146.5 m high, and the typical floor plan from the 10th storey upwards is 29 m x 44 m. Some beams and all floor slabs are post-tensioned RC members

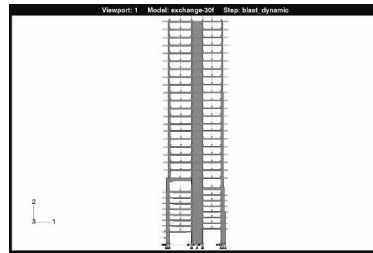


Figure 8: FEM model of the building

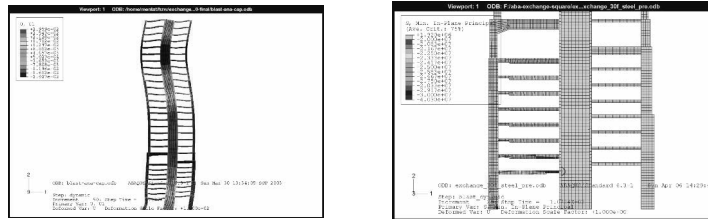


Figure 9: Deformation and stress distributions of the long standoff case

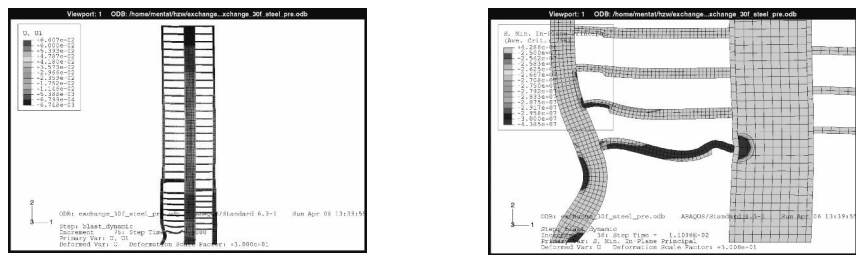


Figure 10: Deformation and stress distributions of the short standoff case

### 5.1 Blast load and FEM modelling

The parameters defining the blast loading characteristics are the peak pressure and loading duration, which can be determined using ConWep (Hyder, 1991). The distribution of the blast loading is non-uniform along the building height and varies with the explosive weight and the standoff distance. A typical plane frame of the building was analyzed. 2D solid

continuum element with 4 nodes was used to model the concrete, and rebar element was merged with the solid concrete element (ABAQUS, 2001). The cap plasticity model was used to represent the concrete behaviour under blast load, while the elasto-plastic model was used for rebars. The dead and the live load were first applied prior to the dynamic analysis of building response to surface blast load.

## **5.2 Blast response evaluations**

### **5.2.1 Long standoff case**

The building deformation at a representative time step of the long standoff distance case is shown in Figure 9. The lateral displacement of the blast-loaded bottom column reaches its peak at 13.4 ms. Plastic deformation was mainly concentrated at the bottom column and the beams of the second and the third storeys. Most severe damage appeared in the column around 13 ms and in the beam around 16 ms. The beam deformation was focused at its ends where local damages occurred. Shear wall played an important role in the global response and exhibited a lateral vibration beginning around 30 ms resulting from the force transferred from the beams. The lateral vibration propagated upwards and reached the roof level around 200 ms.

The maximum tensile and crushing stress of concrete are assumed to be 1.7 MPa and 25 MPa, respectively. The cracks would first occur in the shear wall and propagate towards the upper part of the building. At 3 ms, crushing of concrete first occurred at one corner of the fixed-end column and at the left ends of the second and the third storey beams. As the compressive wave propagated to the other end of the beams, the second storey beam was almost completely crushed. Crushing of concrete in the shear wall was confined to its connection with the second storey beam.

The local damage index based on curvature is used to evaluate the flexural performance of structural elements under blast load. The second and the third storey beams were nearly in complete failure. Sever damage appeared in columns on the first and the second storeys and in the beams at the fourth and the fifth storeys.

### **5.2.2 Short standoff case**

The building deformation at a representative time step of the short standoff distance case is shown in Figure 10. The lateral displacement reaches its peak value at 13.3 ms. The dynamic deformation was localized at the blast-loaded columns between the first and the third storeys. The beams connected with these columns might thus be damaged. Large residual deformations were observed for the blast-loaded columns and the beams connected to them. Compared with the long standoff case, the global response of the short standoff case hardly existed.

Extensive cracks first occurred in the blast-loaded bottom column. The cracks propagated sideways via the shear wall to the bottom column on the other side of the building as well as upwards in the wall. At 300 ms, the



crack reached the roof. In addition, cracks also appeared in the transfer girders located at the tenth storey as a large tensile stress propagated through them. Compared with the long standoff case, the cracks in the concrete columns in the short standoff case were more severe, while those in the shear wall were less severe. At 1.5 ms, concrete crushing first appeared at the right corner of the lower end of the bottom column. The crushing zone developed towards the central zone of the column. In addition, the concrete at the compressive zone of the second and the third storey beams was severely damaged.

Figure 10 shows that partial collapse or moderate damage may exist in the columns on the first and the second storeys. The beams at the second and the third storeys were destroyed completely. Compared with the long standoff case, damage in the short standoff case was more localized.

## 6.0 CONCLUSIONS

In summary, in protecting the building structures and infrastructural systems in Singapore, there is a need to investigate systematically the effects of multiple hazards which may include both natural and man-made events. The multiple hazards that have been investigated so far comprising the effects of long-distance major Sumatra earthquakes, explosion induced ground shocks, and blast-induced overpressures. The dynamic response of the non-seismically designed building structures in Singapore to these postulated multiple hazards has shown a variety of different characteristics. This will pose a challenge to the engineering community who must strike a balance between safety and economy in designing and constructing a building structure to resist the multiple hazards which may result from both natural and man-made events. The consequences from any extreme event of the multiple hazards could be devastating to the society at large due to the high concentration of population as well as the high-value commercial and financial activities housed in these modern high-rise building structures. However, it is important to realize that the dynamic effects of these events have drastically different loading characteristics as well as frequency of occurrence.

## REFERENCES

- ABAQUS, 2001. *Standard User's Manual*, Version 6.2, HKS, Inc.
- ASCE-ACI Joint Task Committee 426, 1973. *Shear Strength of Reinforced Concrete Members*. Journal of Structural Engineering, ASCE, Vol. 99, No. 6, pp. 1091-1187.
- Dhakal, R. P., and Pan, T.-C., 2003. *Response Characteristics of Structures Subjected to Blasting Induced Ground Motions*. Journal of Impact Engineering, Vol. 28, No. 8, pp. 813-828.
- Hyder, D. W., 1991. *ConWep: conventional weapons effects*. USAEWES / SS-R.
- Karim, S. R., 1999. *Shear Strength Prediction for Concrete Members*. Journal of Structural Engineering, ASCE, Vol. 125, No. 3, pp. 301- 308
- Li, B., Wu, Y. M., and Pan, T.-C., 2003. *Seismic Behavior of Non-*

- seismically Detailed Interior Beam-Wide Column Joints for Seismic Performance Part I: Experimental Results and Observed Behavior.* ACI Structural Journal, Vol. 31, No. 8, pp. 1501–1523.
- Ma, G., Hao, H., Lu, Y., and Zhou, Y. X., 2002. *Distributed Structural Damage Generated by High-Frequency Ground Motions.* Journal of Structural Engineering, ASCE, Vol. 128, No. 3, pp. 390–399.
- Megawati, K. and Pan, T.-C., 2002. *Prediction of the maximum credible ground motion in Singapore due to a great Sumatran subduction earthquake: the worst-case scenario.* J. Earthquake Engrg. Struct. Dyn, 31, 1501-1523
- Pan, T.-C., Dhakal, R. P., and Irawan, P., 2001a. *Dynamic and Pseudo-Dynamic tests of Lightly Reinforced Concrete Beam-Column Sub-Assemblies.* Technical Report No.2, Protective Technology Research Centre, School of Civil and Environmental Engineering, Nanyang Technological University.
- Pan, T.-C., Megawati, K., Brownjohn, J. M. W. and Lee, C. L., 2001b. *The Bengkulu, Southern Sumatra, Earthquake of 4 June 2000 (Mw=7.7): Another Warning to Remote Metropolitan Areas.* Seismological Research Letters, Seismological Society of America, Vol. 72, No. 2, 171 – 185.
- Park, R., and Paulay, T., 1974. *Reinforced Concrete Structures.* John Wiley and Sons.
- Park, Y. J., and Ang, A. H.-S., 1985. *Mechanistic Seismic Damage Model for Reinforced Concrete Structures.* Journal of Structural Engineering, ASCE, Vol. 111, No. 4, pp. 722-739.
- Paulay, T., Park, R., and Priestley, M. J. N., 1978. *Reinforced Concrete Beam-Column Joints under Seismic Action.* ACI Journal, Nov., pp. 585-593.
- Priestley, M. N. J, Verma, R., and Xiao, Y., 1994. *Seismic Shear Strength of Reinforced Concrete Columns.* Journal of Structural Engineering, ASCE, Vol. 120, No. 8, pp. 2310-2329.
- Tregoning, P., Brunner, F. K., Bock, Y., Puntodewo, S. S. O., McCaffrey, R., Genrich, J. F., Calais, E., Rais, J., Subarya, C., 1994. *First Geodetic measurement of convergence across the Java Trench.* Geophysical Research Letters, 21, 2135-2138.
- Valles, R. E., Reinhorn, A. M., Kunnath, S. K., Li, C., and Madan, A., 1996. *IDARC 2D Version 4.0: A Program for the Inelastic Damage Analysis of Buildings.* Technical Report NCEER-96-0010, National Center for Earthquake Engineering Research, State University of New York at Buffalo.
- Zachariasen, J., Sieh, K., Taylor, F. W., Edwards, R. L., and Hantoro, W. S., 1999. *Submergence and Uplift Associated with the Giant 1833 Sumatran Subduction Earthquake: evidence from coral micro atolls.* Journal of Geophysical Research, 104, 895-919.

# **OPTIMAL IMPROVEMENT OF STORM SEWER SYSTEM FOR INNER BANGKOK**

TAWATCHAI TINGSANCHALI

School of Civil Engineering, Asian Institute of Technology, Thailand

tawatch@ait.ac.th

## **ABSTRACT**

*A study area of 3.5 km<sup>2</sup> was selected in an inner part of Bangkok. The area is mostly residential consisting of buildings, pavements, grassland and unbuilt areas. The urban storm sewer system was investigated to find optimal improvement to alleviate frequent flooding problems due to its limited capacity. The MOUSE model developed by the Danish Hydraulic Institute was successfully calibrated and verified using two heaviest rainstorm data on 5 May 1990 and 7 June 1991. It was proposed to construct a flood retention pond in the center of the study area to receive drainage of surrounding floodwater by gravity and to pump it out to Klong Bang Sue, the main drain canal. The effects of replacement of some small sewer pipes by larger ones were determined.*

*The storm sewer system was analyzed for improvement by considering probabilistic rainfalls. Fourteen different sewer systems of different pipe diameters, pumping locations and capacities, and flood storage retention areas were considered. By considering Markov chain process, the transition probabilities of rainfall patterns and the steady state probabilities were calculated from past records. The MOUSE surface runoff model was run for seven different rainfall patterns. The computed runoff was used as input to the pipe flow model wherein hydrodynamic flood routing was performed to compute flooding depths and discharges. The water levels in the manholes and the discharges in the sewer pipes were calculated to determine the hydraulic effectiveness of each alternative. The expected annual flood damages were computed. Considering the objective function of maximum annual net benefit. A simulation model was used to determine the optimal improvement of the sewer system. Sensitivity analysis showed that the discount rate has a significant effect on optimal results while the Manning roughness coefficient has only a little effect.*

## **1.0 INTRODUCTION**

The study area is situated in the north of Bangkok and is delineated by Klong Bang Sue in the north, Klong Sam Sen in the south, Rama 6 road in west and Phahon Yothin road in the east. The study area is about 3.5 sq. km. in which 60% are residential areas and 40 % are commercial areas. The storm sewer system was consisted of a retention pond at the center of the study area, a number of pipes forming sewer networks, pumps and gates as shown in Figure 1. The surface area of retention pond is 14,500 m<sup>2</sup> and the average depth was 1.5 m. When rainfall occurs, runoffs are collected in the sewer system and discharged through the sewer pipes to the main open drain

channels - Klong Bang Sue and Klong Sam Sen. A part of runoff flows to the retention pond and water is pumped out to the main open drains. Frequent flooding occurs due to limited pipe sizes in the system to carry flow during high floods.

The main objective of this study is to determine an optimal improvement of the sewer system based on maximum net benefit. The MOUSE sewer system model developed by the DHI Water and Environment (2000) was used for determining the hydraulics of storm sewer flow.

## 2.0 MATHEMATICAL MODEL

### 2.1 MOUSE Model

The MOUSE model (DHI Water and Environment, 2000) is a software package for modeling urban storm sewer systems. The system consists of surface runoff model, pipe flow model, pollution model and routines for graphical presentation of input and output data.

#### *Surface runoff model*

The model applies the continuity equation and the kinematic wave equation in the surface runoff computation. The effective rainfall  $P_{eff}$  per unit area is expressed as

$$P_{eff}(t) = R(t) - Q_E(t) - Q_w(t) - Q_i(t) - Q_s(t) \quad (1)$$

where  $R$  = rainfall,  $Q_E$  = evaporation loss,  $Q_w$  = wetting loss,  $Q_i$  = infiltration loss and  $Q_s$  = storage loss and  $t$  is the time. The infiltration is calculated by using the Horton's equation with exponential decay with time. The hydraulic process routes the effective rainfall by using the kinematic wave equation assuming quasi-steady uniform flow of runoff over the surface without time delay. The runoff  $Q(t)$  is determined by

$$Q(t) = \frac{1}{n} \cdot B \cdot I_o^{1/2} \cdot y^{5/3} \quad (2)$$

where  $n$  = Manning  $n$ ,  $B$  = runoff width,  $I_o$  = bed slope,  $y$  = flow depth. Also,  $Q(t)$  can be expressed by the continuity equation

$$Q(t) = \frac{dy}{dt} A \quad (3)$$

where  $A$  = surface area,  $dt$  = time step and  $dy$  = change in depth. The water depth  $y$  and the runoff  $Q(t)$  can be determined implicitly by solving equations 1 and 2 simultaneously. The surface runoff model computes runoff

hydrographs at nodal points (manholes) in the sewer system for the pipe flow model computations.

### *Free surface and pipe flow model*

The governing equations for free surface flow are the following continuity and momentum equations

$$\frac{\partial Q}{\partial x} + \frac{\partial A}{\partial t} = 0 \quad (4)$$

$$\frac{\partial Q}{\partial t} + \frac{\partial}{\partial x} \left( \alpha \frac{Q^2}{A} \right) + g A \left( \frac{\partial y}{\partial x} \right) + g A I_f = g A I_0 \quad (5)$$

where  $Q$  = flow rate,  $A$  = cross sectional area,  $y$  = flow depth,  $g$  = gravitational acceleration,  $x$  = longitudinal axis,  $t$  = time,  $\alpha$  = velocity distribution factor,  $I_0$  = bottom slope,  $I_f$  = friction slope =  $Q|Q|/(n^2 A^2 R^{4/3})$ ,  $n$  = Manning roughness coefficient and  $R$  = hydraulic radius.

When full pipe flow occurs, equation 4 can be generalized by introducing a fictitious slot at the top of the pipe and can be written as:

$$\frac{\partial Q}{\partial x} + \frac{Q}{\rho} \frac{\partial \rho}{\partial x} + \frac{g A_0}{a^2} \frac{\partial y}{\partial t} = 0 \quad (6)$$

where the slot width  $T$  is defined as  $T = g A_0 / a^2$ ,  $A_0$  = full pipe cross sectional area and  $a$  = speed of sound in water ( $a \approx 1,000$  m/s for most pipes).

The outputs from the pipe flow model are discharge, velocity and depth hydrographs. Given the boundary and initial conditions, the discharge  $Q$  and depth  $h$  along pipes at different grid points and different time steps are computed using Abbott's six-point finite difference scheme. In order to obtain a stable numerical solution, the following Courant stability condition has to be satisfied, i.e.,  $\Delta t \leq \Delta x / V$ , where  $v$  = flow velocity (m/s),  $\Delta t$  = time step (seconds),  $\Delta x$  = distance between computation nodes in m.

## **2.2 Rainfall Probability**

The collected rainfall data at 10 minute interval during the heavy rainfall period (August, September and October) in 1983-2000 were categorized into rainfall patterns according to rainfall depth, time to peak of rainfall and maximum intensity of rainfall (Table 1). The rainfall process was assumed to constitute a Markov chain having a number of states  $m = 7$ . Using Markov chain process, the probability of rainfall at a certain time step depends on the probability of rainfall at the previous time step only. The transition probability of changing of rainfall state from  $i$  to  $j$ ,  $T_{ij}$  can be computed as

$$T_{ij} = N_{ij} / \sum_{i=1}^m N_{ij} \quad (7)$$

where  $N_{ij}$  = number of times that the rainfall data is changed from state  $i$  to state  $j$  in one time step and,

$$P_j = \sum_{i=1}^m P_i \cdot T_{ij} \quad (8)$$

$$\sum_{j=1}^m P_j = 1 \quad (9)$$

where  $P_i$  and  $P_j$  are the stationary probability of rainfall states  $i$  and  $j$ . The stationary probabilities are solved from equations 8 and 9 simultaneously and are equal to 0.956, 0.012, 0.011, 0.008, 0.005, 0.005 and 0.003 for the rainfall states 1 to 7 respectively.

*Table 1: States of rainfall patterns*

State	Rainfall Characteristics		
	Rainfall Depth (mm)	Time to Peak (min)	Max. Intensity (mm/min)
1	<20	$\geq 20$	<1
2	40-60	$\geq 10$	>1.5
3	40-60	$\geq 20$	1.0-1.5
4	60-80	$\geq 10$	>1.5
5	60-80	$\geq 20$	1.0-1.5
6	>80	$\geq 10$	>1.5
7	>80	$\geq 20$	1.0-1.5

The transition probability of changing of rainfall state from  $i$  to  $j$ ,  $T_{ij}$ , can be computed based on observed rainfall data, e.g.,  $T_{ij} = 0.96, 0.010, 0.010, 0.009, 0.006, 0.003$  and  $0.001$  for  $i=1$  and  $j=1$  to  $7$  respectively;  $T_{ij}=0.78, 0.11, 0.11, 0.0, 0.0, 0.0$  and  $0.0$  for  $i=2$  and  $j=1$  to  $7$  respectively, etc.

### 3.0 MODEL CALIBRATION AND VERIFICATION

System input data to MOUSE model are catchment characteristics and pipe data namely manholes, pump stations and retention basin. The existing sewer system has 88 sub-catchments, 94 manholes and 99 branches. For surface runoff model, hydrological input data are rainfall, evaporation, wetting, depression storage, initial filtration and exponential decay constant. The time step is 5 minutes. For the pipe flow model, input hydraulic parameters are head losses in manholes for various shapes of outlet. For numerical stability and convergence, a time step  $\Delta t = 30$  seconds and  $\Delta x = 100\sim 200$  m was used for hydrodynamic computation. The hourly water levels data at Klong Sam Sen and Klong Bang Sue were input as the

boundary conditions. The MOUSE model assumes initial pipe flow depth equal to 10% of the pipe diameter. The Manning roughness coefficient  $n$  is taken as 0.017 for rough concrete pipes. The value of Manning  $n$  was adjusted by trial and error in model calibration and verification based on observed storm data on 5 May 1990 and 7 June 1991 (Moe, 1992).

#### 4.0 ECONOMIC ANALYSIS

##### 4.1 Flood damage cost

From the field data analysis, Tang et al. (1991) proposed the following quadratic model:

$$FLD = 0.025 [a (D - D_m)^2 + b (D - D_m)] \quad (10)$$

where  $FLD_i$  = flood damage cost in US dollars per flooded establishment corresponding to rainfall state  $i$ ,  $D$  = maximum flooding depth above ground level in centimeters,  $D_m$  = minimum flooding depth in which there is no damage,  $a = 0.0482$ ,  $b = 80.26$ ,  $D_m = 1.63$  cm. The total expected flood damage cost was computed by,

$$\text{Expected Flood Damage Cost} = \sum_{i=1}^m P_i (FLD)_i E_i \quad (11)$$

where  $P_i$  = stationary probability of rainfall state  $i$ ,  $m$  = number of rainfall states and  $E_i$  = number of flooded establishments.

##### 4.2 Pipe cost

The pipe cost data includes cost of excavation and the cost of laying pipes, i.e.,  $C_p = 40.3 d^{1.717}$  where  $C_p$  = pipe cost per meter length in US dollars and  $d$  = diameter of pipe in meters. The pump cost function which includes the cost of construction and accessories was developed JICA (1985), i.e.  $C_{\text{pump}} = 0.1215 Q + 0.54$ , where  $C_{\text{pump}}$  = pump construction cost in million US dollars,  $Q$  = pump discharge ( $\text{m}^3/\text{sec}$ ). The operation and maintenance cost of pumping per year was estimated to be 7% of construction cost.

In the estimation of annual costs, the rate of discount and life of component was assumed as 10% and 30 years for pipes and 10% and 15 years respectively for pump costs.

##### 4.3 Cost of retention pond

A unit cost of US dollars 137.50 per square meter of additional retention area was used. The annual cost of retention for a planning period of 30 years and discount rate of 10% was taken. The optimization of sewer system improvement is based on the objective of maximizing the annual net benefit obtained from the flood protection, i.e.

$$\text{MAXIMIZE } Z = \text{MAX } (B - C) \quad (12)$$

where  $Z$  = annual net benefit,  $C$  = annual cost and  $B$  = annual benefit. The constraints are pipe diameter  $d_i \geq 0.2$  m,  $Q_i \geq 0$ ,  $D_m \leq 25$  cm.

$$C = \sum_{\text{Allnewpipes}} (C_p L)_i + \sum_{\text{Allpumps}} C_{\text{apump}} + C_R + \sum_{i=1}^m P_i (\text{FLD})_i \cdot E_i \quad (13)$$

$C$  = annual flood damage cost in existing sewer system,  $C_p$  = cost of pipe per m length,  $C_R$  = cost of retention basin,  $L$  = length of pipe in meter,  $C_{\text{apump}}$  = annual capital pump cost plus operation cost of pump,  $m$  = number of rainfall states. Other parameters were previously defined. The decision variables were the diameter  $d_i$  of pipes that need to be replaced, the capacity of the pumps  $Q_i$  and the surface area of the retention pond. The objective function is a non-linear function in which there are a large number of decision variables. As the sewer system is rather complicated, the optimization based on non-linear programming or dynamic programming may be very time consuming and even not possible. A simulation technique used by Fujiwara and Dayani (1991) was applied to the fourteen alternatives to find the maximum net benefit for optimal pipe sizes, the pump capacities and the retention area.

## 5.0 RESULTS AND DISCUSSIONS

Fourteen different sewer systems are considered by choosing different diameters of pipes, different locations and capacities of pumps, and retention area (Acharya, 1993). For each sewer system, the flooding depth and flooding area are calculated by running the pipe flow model. It was found that the effect of a rainfall pattern on inflow to sewers depends on the depth, duration of rainfall and the maximum intensity. The rainfall pattern R6 (Table 2) has the maximum runoff volume and its effect lasts for almost 6 hours. The rainfall pattern R2 (Table 2) produces the least volume of floodwater and time of runoff is also the least. The output from the runoff model was used as input to the pipe flow model. From the pipe flow model, the depth of flooding at manhole locations and volumes of floodwater were obtained for each rainfall pattern and each sewer system. The rainfall pattern R6 produces the maximum depth of flooding and also generates maximum volume of floodwater and hence the maximum flood damage cost. The simulation technique (Fujiwara and Dayani, 1991) was used to determine the optimal sewer system from fourteen cases. Only commercial sizes of pipes and box culverts were considered, i.e. diameters of 1.2 m, 1.5 m and 1.75 m, etc. From the results (Table 2) the sewer system no. 8 is the optimal sewer system because the net benefit is maximum. Also, the total cost in minimum and the benefit cost ratio is maximum compared to other sewer systems. The average flooding depth for the optimal sewer system is less than 25 cm. and the average flooding duration in less than one hour. The optimal sewer system (sewer system no. 8) has a maximum B/C ratio of 1.89 and a maximum annual net benefit of US \$ 340,000. Sensitivity analysis was carried out by changing the Manning  $n$  from 0.020 to 0.017



and 0.025 keeping other parameters fixed. It is found that the  $n$  value has very little effect on B/C ratio and the net benefit. Sensitivity analysis is also carried out by changing the discount rate  $i$  in calculating the annual costs. The effect of  $i$  value was found to be very significant. When the discount rate was decreased, the cost of sewer system decreased and hence the benefit cost ratio and the net benefit were increased.

## 6.0 CONCLUSIONS

By classifying observed rainfall by its depth, time to peak and maximum rainfall intensity, seven rainfall patterns were specified. The transition probability and steady state probability of rainfall were determined. By running the MOUSE model, it was found that the rainfall pattern R6 is the most severe one. A quadratic flood damage function and the cost models were applied in this study. The objective function is to maximize net benefit of the sewer system. Due to complicated sewer systems and nonlinear characteristic of the system benefit and cost, a simulation technique was applied to find the optimal sewer system with maximum net benefit. Fourteen different sewer systems were considered, the flooding depth and flooding area were calculated by the pipe flow model. The sewer system number 8 yields the maximum net benefit, the highest B/C ratio and the minimum total cost. Sensitivity analysis on the economic evaluation showed that the discount rate has a significant effect on the optimization results while the effect of Manning  $n$  is insignificant.

## REFERENCES

- Acharya, B.K., 1993. *A Probabilistic Model for the Design of an Urban Drainage System for an Inner Part of Bangkok*. Master Thesis, Asian Institute of Technology, Pathumthani, Thailand.
- DHI Water and Environment, 2000. *Modeling of Urban Sewer System*. Danish Hydraulic Institute, MOUSE Documentation, Horsholm, Denmark.
- JICA, 1985. *Master Plan For Flood Protection Drainage Project in Eastern Sub-urban Bangkok*. Project Report, Japan International Cooperation Agency, Japan
- Moe, M.M. 1992. *Computer Modeling of Urban Drainage System of an Inner Part of Bangkok*. Master Thesis, Asian Institute of Technology, Pathumthani, Thailand.
- Tang, J.C.S, Vongvisessomjai, S. and Kanchanarat, S., 1991. *Estimation of Flood Damage Cost for Bangkok*. Water Resources Management, 6(1), pp 47-50.
- Fujiwara, O. and Dayani, M.A., 1991. *A Semi-Markovian Analysis for Reliability of Water Distribution Networks*. Research Report, Industrial Engineering Division, Asian Institute of Technology, Pathumthani, Thailand.

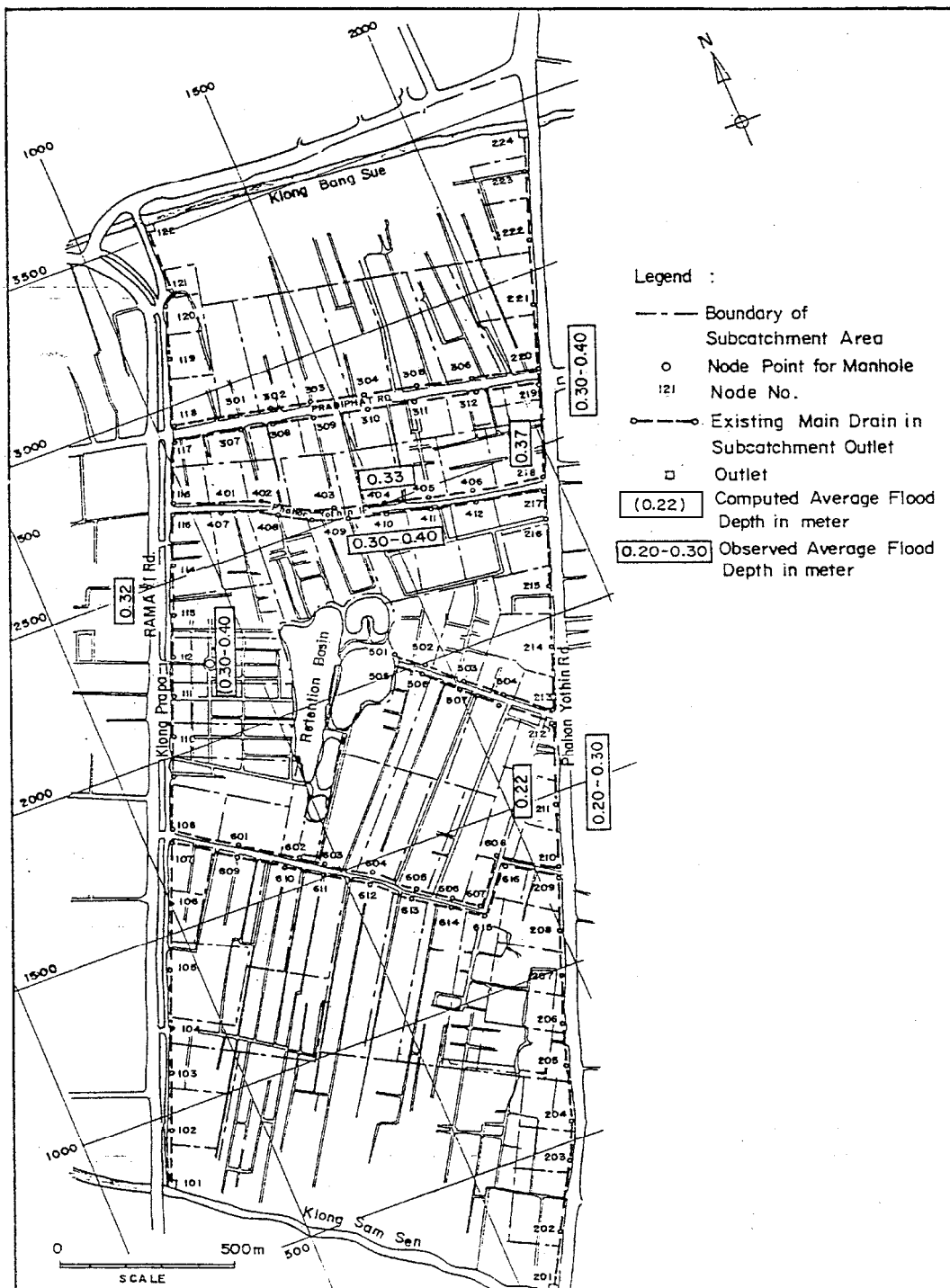


Figure 1: Sewer system of Inner Bangkok and verification of MOUSE model with observed flood depths, 7 June 1991

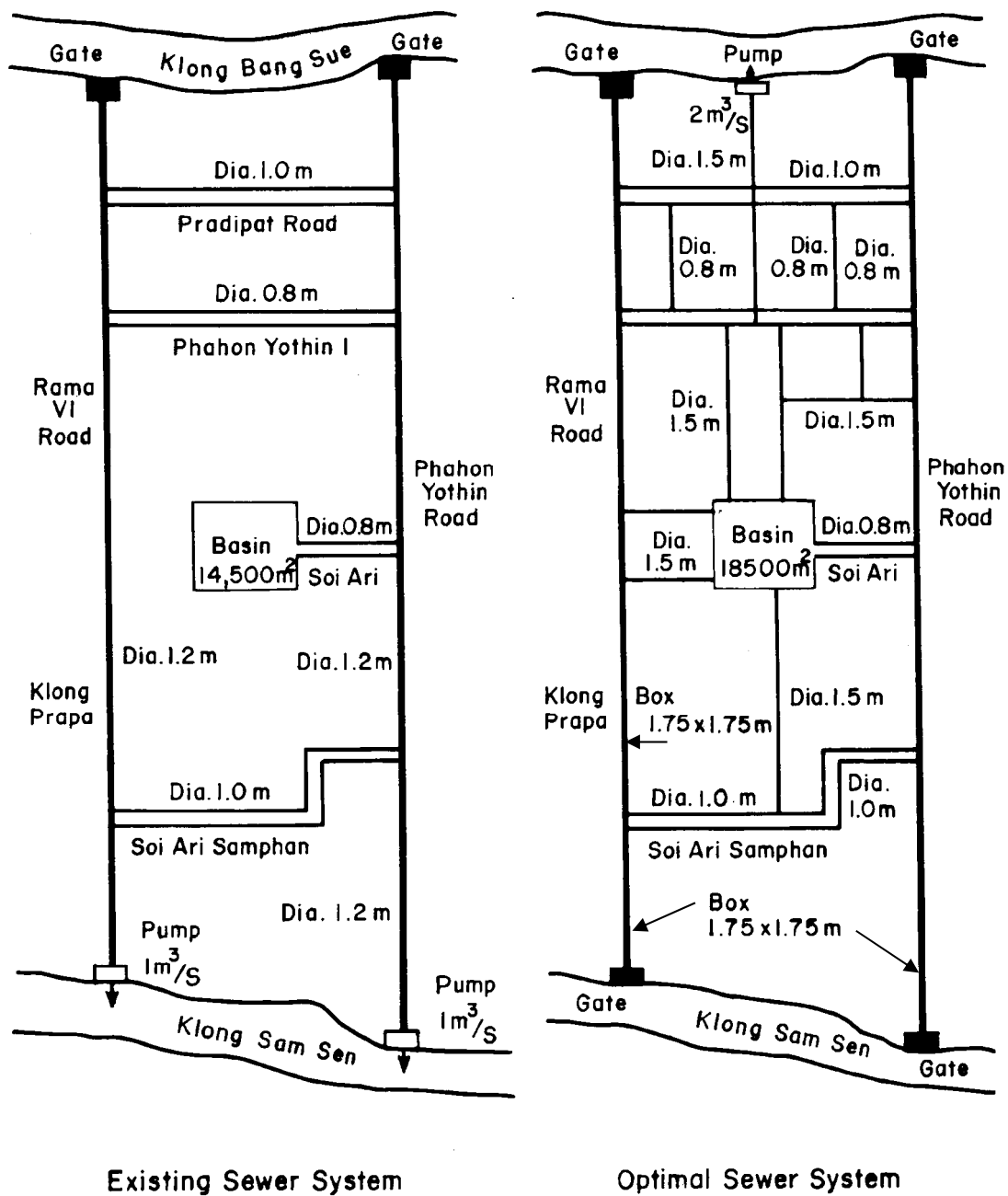


Figure 2: Existing and optimal storm sewer system in study area

Table 2: Results of sewer system optimization, discount rate  $i = 10\%$

System	Annual Cost (Million US\$)				Annual Benefit (Mil. US\$)	B/C Ratio	Annual Net Benefit (Mil. US\$)
	Construction	O&M	Flood Damage	Total			
1	-	-	0.76	0.76	-	-	-
2	0.17	0.012	0.28	0.46	0.48	1.04	0.02
5	0.58	0.010	0.02	0.61	0.75	1.23	0.14
12	0.31	0.007	0.14	0.46	0.62	1.33	0.16
14	0.31	0.007	0.14	0.46	0.62	1.34	0.16
3	0.30	0.019	0.14	0.46	0.62	1.36	0.16
11	0.53	0.019	0.01	0.57	0.75	1.32	0.18
13	0.32	0.007	0.13	0.45	0.64	1.43	0.19
6	0.52	0.022	0.01	0.56	0.75	1.35	0.20
10	0.34	0.022	0.10	0.46	0.66	1.44	0.20
9	0.41	0.011	0.05	0.47	0.72	1.54	0.25
7	0.42	0.025	0.02	0.46	0.74	1.60	0.28
4	0.38	0.008	0.05	0.43	0.72	1.65	0.28
8	0.32	0.007	0.05	0.37	0.71	1.89	0.34

# **TECHNIQUES FOR MONITORING DEFORMATION IN LARGE ENGINEERING STRUCTURES**

MADHAV N. KULKARNI, NISHA RADHAKRISHNAN  
AND DEEPA RAI

Department of Civil Engineering,  
Indian Institute of Technology Bombay, India  
*kulkarni@iitb.ac.in*

## **ABSTRACT**

*Construction of large engineering structures such as dams, bridges, high-rise buildings, etc., is essential for the urban development of a nation. However, under excessive loading, these structures are subjected to deformations, which may lead to their failures, thereby causing loss of lives and property. The safety of these structures demands their periodic monitoring. Results from the deformation monitoring measurements enable us to expand our existing knowledge of the correlation between the loading factors and the deformations. Thus, the safety control of such structures lies in the analysis of their structural behaviour, based on monitoring a large set of variables, which describes the actions (earthquakes, temperature variations, wind action etc) and the corresponding stresses.*

*For the purpose of monitoring and measuring deformation of dams, a number of methods have been developed. They have been broadly classified into physical and geodetic techniques. With the advancements in space technology, in the recent years, deformation monitoring and measurements are being done using Global Positioning System (GPS). With the advent of modern instruments, conventional geodetic surveying and physical methods have been replaced by use of instruments like tacheometers, fiber optic deformation sensors, GPS, etc.*

*This paper gives an overview of the physical methods and geodetic methods used in deformation monitoring and measurement. Deformation monitoring in bridges using tacheometers are described. The paper also gives a broad view of how GPS is used for deformation monitoring. A case study on Koyna dam deformation monitoring using GPS is presented, along with some recent results. The concept used here can also be used in deformation monitoring of the other structures.*

## **1.0 INTRODUCTION**

Large engineering structures such as dams, bridges, high-rise buildings, etc., are essential for the socio-economic development of a region. However, they need a careful safety control along their life span, since under excessive loading they might undergo failure, causing loss to lives and property. The monitoring of the actual state of existing structural buildings has a high

importance regarding to the assessment of the reliability and availability. The security and maintenance of bridges and tall buildings requires periodic monitoring, maintenance and restoration. Furthermore, accurate knowledge of the behaviour of the structures is becoming more important as new structures become lighter, new building techniques are introduced and an increasing number of existing bridges are required to remain in service beyond their theoretical service life. Hence, the safety of large engineering works demands periodic monitoring of the structure and in-depth analysis of its structural behaviour, based on the monitoring of a large set of variables contributing to deformation. Thus, the deformation forms the most relevant parameter to be monitored.

Deformation of large engineering structures is often measured in order to ensure that the structure is exhibiting safe structural behaviour. Deformation of a structure is the only single parameter affected by all the loads on the structural system and is an important critical parameter that would throw light in a significant measure on the structural behaviour of the structure (Narayana, 1982).

Several factors contribute to the deformation of these structures. The most important of all is the result of the varying stress and strains developed in the structure due to the effects of local crustal movements (Manake & Kulkarni, 2002). Other factors may include type of the material, wind actions, temperature variations, settlement of soil, and fluctuations in the load due to vehicular traffic. Deformation refers to the changes that a deformable body (natural or man-made objects) undergoes in its shape, dimension and position. Therefore, it is important to measure these movements for the purpose of safety assessment and as well as for preventing any disaster in the future. All deformations or movements are three-dimensional (3-D) and the several ways of measuring them can be broadly classified into Physical, Geodetic and Photogrammetric methods and more recently, the revolutionary space geodetic technique, the Global Positioning System (GPS) (Kulkarni, 1985) .

## **2.0 PHYSICAL METHODS**

The physical methods used for deformation studies involve the use of strain gauges, special thermometers, direct and indirect pendulum, plumbing equipment etc. Other kinds of instruments used are Carlson Stessmeters, Carlson Strainmeters, Coordimeters, Tiltmeters, Structural Response Recorders, Accelerometers and Uplift Pressure cells that are embedded in the body of the structure. Periodic observations with these instruments can yield some idea about the deformation of the structures. The main disadvantage of physical methods is that these instruments, deeply embedded in the body of the structure, are mostly inaccessible for maintenance and repair. These methods give only relative movement of points within the structure as no reference can be made to points outside the structure. Since they give only relative and not absolute measurements, these cannot be used for monitoring deformations due to crustal movements.

Thus they are useful only in estimating the structural deformations (Kulkarni, 1985).

### **3.0 GEODETIC METHODS**

Applications of geodetic technique to geodynamic, monitoring crustal movements for Earthquake studies and deformation measurements, have assumed great importance recently (Roy & Kulkarni, 1999). The classical and modern geodetic techniques being used to establish horizontal, vertical, gravimetric, geomagnetic, and tidal control networks can be classified as:

- Terrestrial Techniques includes Geodetic Triangulation, Electronic Distance Measuring instrument (EDM) Traverse, Astrogeodetic Methods, Precision Levelling.
- Space Techniques includes Doppler Satellite Surveying System, GPS, VLBI, SLR, LLR, Other Space Geodetic Techniques like LORAN, DORIS, etc.
- Geophysical Techniques in Geodes includes Gravimetric surveys, Geomagnetic surveys, Tidal observations and predictions.

High precision geodetic instruments including precision theodolites, precise levels, GPS receivers, EDMs, Gravimeters, Magnetometers, Tide gauges etc., are being used in India for such geodetic surveys.

### **4.0 PHOTOGRAMMETRIC METHODS**

These methods consist of periodic photography of large structures, targets and pillars, permanent pillars etc., to estimate the displacements. Photogrammetry provides a new perspective to monitoring work in the way that photographs are rich of information and can be analyzed at any time with high repeatability. This method has the advantage of depicting the entire ground surface whereas the conventional monitoring techniques can only handle discrete point measurements. But however, this method is still in experimental stage and not being used widely (Tsan-wing & Kin-Wah, 2001).

### **5.0 GPS FOR STRUCTURAL MONITORING**

Deformation of engineering structures is often measured in order to ensure that the structure is exhibiting safe deformation behaviour. Thereby, it is necessary to monitor structural deformation due to various factors like most importantly, seismic activity, wind forces, changes in the ground level, etc.

Physical instruments like Accelerometers, strain gauges and geodetic instruments like total stations are familiar tools for structural monitoring. However, relative displacements, which are the key to accessing drift and stress conditions, are very difficult to measure directly with the following instruments. This is because in order to compute displacements it is

necessary to perform suitable processing. Although acceleration measurements by accelerometers are useful for accessing design/analysis procedures and correlating the response of the structure they are inadequate for warning of potential failure or even recovering the permanent response of the event. Further limitations on monitoring are imposed by the high cost of equipment installation and maintenance. The regular monitoring of structures often require measurements of relative displacements, which may, in turn, be used to access the structure's stress and drift conditions during seismic events or wind forces (Tsakeri & Lekidis, 2001).

Recent advances in GPS technology have made it a cost-effective tool for monitoring the safety and performance of structures. It has the advantage of directly providing displacement information in absolute as well as in real time, making it a competitive alternative to the conventional surveying methods. GPS provides 3-D positions with reference to a fixed global coordinate system, simultaneously at all sites, with automated data collection and no line-of-sight requirement. It can provide continuous updating of positions of GPS receivers within few-mm accuracy with respect to stable points up to several km away. Furthermore, GPS satellites are not affected by earthquakes. The recent development in the field of structural monitoring applications is the advances in GPS receiver technology and data processing software. The collected information can be used to make decisions for further evaluation of the susceptibility to damage and future repair schemes for the dam. Hence, many dams worldwide are being monitored using this technique [Manake & Kulkarni (2002)].

## **6.0 BRIDGE DEFORMATION MONITORING**

The monitoring of a new or existing bridge can be approached either from the material or from the structural point of view. In the first case, monitoring will concentrate on the local properties of the materials used (e.g., concrete, steel, timber, composite materials) and observe their behaviour under load, temperature variations or aging.

In the structural approach, the structure is observed from a geometrical point of view. By using long gauge length deformation sensors with measurement bases much larger than the characteristic dimensions of the materials (for example a few m for a concrete bridge), it is possible to gain information about the deformation of the whole structure. Structural monitoring has usually been realized using external measuring methods like triangulation, dial gauges and invar wires. At present, geodetic methods like tacheometers have gained great importance in monitoring deformations in bridges (Inaudi et al. 1999).

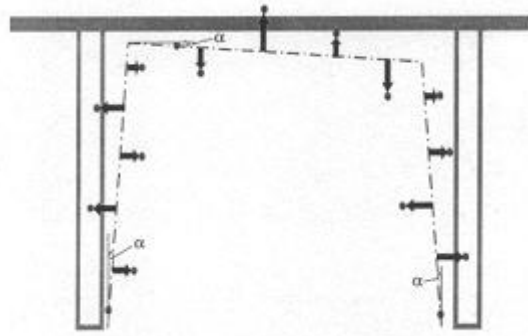
### **6.1 Tacheometers in bridge monitoring**

The use of Tacheometers for monitoring bridges is one among the many geodetic techniques. Currently, new tacheometers are being used to measure distances without a reflector up to a range of 200 m (TRIMBLE



5601). This instrument fulfills the following requirements. The requirements being the time of measurement should be less than 3 hours. Measurements should be possible under traffic load. No point marking should be involved and a reproductive accuracy of deformations of 5 – 10 mm within several years must be obtained. It should be suitable for monitoring bending of the superstructure and displacements of pillars and abutments. The technique should also involve automatic data processing. These tacheometers can scan and determine the building shape. With this information calculations of deformations are possible (Kuhlmann & Glaser, 1999).

Basic principle of the procedure is to derive the deformation of the building by comparison of shape and not by evaluation of movement of single points. For comparing of shape, the following Figure 1 has been considered.



*Figure 1: Deviation in a bridge zone  
(Kuhlmann & Glaser, 1999)*

For comparing the shape, geometrical objects are formed from the measured zone points. In detail the inclination and shape of the pillar and superstructure are studied.

This is done as follows:

- Inclination and shape of the pillar: They are described in the processing by angle  $\alpha$  of a fitting straight line in comparison to plumb line, and by deviations from this straight line.
- Inclination and shape of the superstructure: They are described in the processing by angle  $\alpha$  of a fitting straight line in comparison to a horizontal line, and by deviations from this straight line.

For calculation of the pillar inclinations every pillar side is considered separately. An average pillar inclination can be computed from the right and left side inclination.

## **7.0 HIGH-RISE BUILDING DEFORMATION MONITORING**

Due to the outcome of several severe earthquakes in the recent years, drift studies and assessment of susceptibility to damage of tall buildings have become important issues, particularly as many steel-framed buildings are damaged, some severely and some lightly.

Relative displacements, which are the key to assessing drift and stress conditions of structures, are difficult to measure directly. On the other hand, measuring acceleration response requires a double integration process to arrive at displacements. Accelerometer measurements cannot be used to recover the permanent displacements at the cm level. The level of accuracy of displacements calculated from accelerations has not been widely verified by observations. An alternative method to measure relative displacements while monitoring structural systems can be accomplished by using GPS technology. This has now advanced to 10 samples per second with an accuracy of  $\pm 1$  cm horizontally and  $\pm 2$  cm vertically (Celebi et al. 2001). This provides a great opportunity to reliably monitor long-period structures (tall buildings).

In the recent years, GPS has found to be highly significant in monitoring deformation of large engineering structures. A study on how GPS is used in monitoring the deformation of Koyna Dam is explained. The Indian Institute of Technology Bombay (IITB) has been working in the field of deformation measurements and analysis of Koyna Dam under a research project funded by the Department of Science and Technology (DST), Government of India. A GPS network has been established for this purpose, and observed over nine epochs, from December 2000 to April 2004, in order to investigate the potential of the GPS Technology in deformation measurement analysis. The study highlights methodology, analysis techniques and the results of the research work being carried. The analysis of results indicates a correlation between the change in the reservoir level and the deformation of the dam. Similarly, the same application and concept of measurement can also be used for estimating the degree of deformation in bridges and tall buildings.

## **8.0 CASE STUDY: KOYNA DAM, MAHARASHTRA**

Koyna Dam, a rubble concrete dam, located on the Krishna River, is an 85 m high and 800 m long rock-filled structure, with an 872 sq km of catchment area. The dam and the reservoir formed went under construction in 1962 and were completed in 1963. They are located on the Indian Peninsular shield, one of the oldest continental blocks on the earth's surface. Prior to the year 1962, this shield was referred to as a stable rock by geologists, which remained immune from any major seismic disturbance. But the December 11, 1967 earthquake at Koyna at approximately 4.21 am local time, with a magnitude of 6.6 – 7.5 on Richter Scale, contradicted this belief and evoked interest on the part of geologists, geodesists, dam experts and engineers. However, the dam in the region withstood this significant

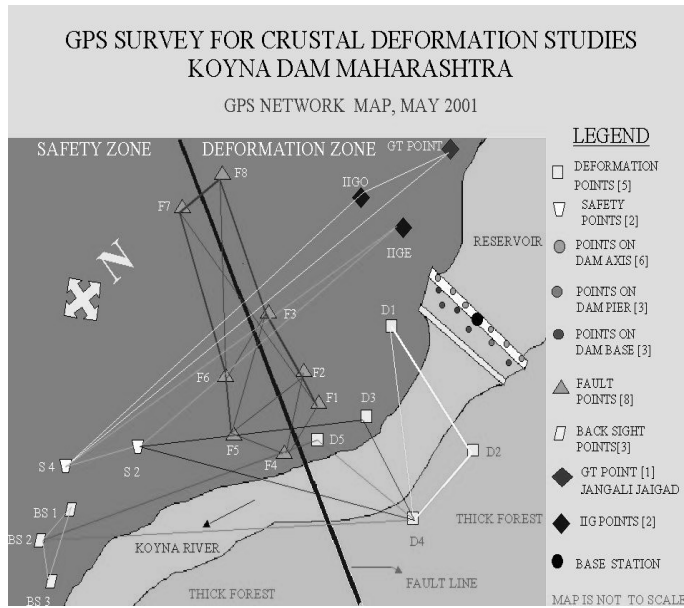
seismic activity without much damage. This occurrence in the Central Indian shield has led to serious introspection among geo-scientists and led to various studies dealing with the stability of the dam structure and the surrounding regions [Manake & Kulkarni (2002)].

Thus to study some of the factors that might be affecting the dam, it has been well instrumented for observations of structural behaviour, right from the design stage, and has proved to be significant. The instrumentation include physical instruments embedded in the dam structure or installed around the dam body like uplift pressure cells, thermometers, piezometers, stress and strain meters and coordimeters and these have been providing data since 1969. Apart from this, the advances in technology have evoked the use of GPS for carrying out dam and crustal deformation studies. The advantage of providing positions simultaneously at all sites, automated data collection, no line-of-sight requirement makes GPS more economical, efficient and convenient, as compared to the conventional surveying techniques. IITB in collaboration with DST has been working in the field of monitoring deformation of Koyna Dam from September 2000. The main objective of this work is to study the seismologically disturbed region of Koyna area and the behaviour of the dam body, using geodetic GPS technique. It includes establishing dense GPS network in the identified seismically active area, its repeat observations, detailed GPS data processing using scientific software and to estimate parameters responsible for deformations.

## **8.1 GPS network**

In order to carry out structural and crustal deformation studies, an extensive GPS network comprising 34 stations has been established in the vicinity of Koyna Dam, at the beginning of the project, in December 2000-January 2001. The GPS network set up in order to monitor the complete area is given in Figure 2.

The distribution of the GPS stations is One base station on the dam axis, established approximately at the centre and the top most point of the dam; Six stations on the dam axis (Three on either side of the base station); Three stations on the dam pier (Two on upstream (U/S) side & one on downstream (D/S) side); Three station on dam base (All on D/S side); One GT Station connected: Jangli Jaigad H. S situated approximately 8 km north of the dam; One at IIG (Indian Institute of Geo-magnetism) Observatory and one at Evaporation Lab; Eight GPS stations (fault points) along the fault line D/S of dam; Three back site stations (All on D/S side); Two safety stations (All on D/S side); Five deformation stations (All on D/S side)



*Figure 2: GPS Network established in the Koyna region.  
(Manake & Kulkarni (2002))*

The observations at the selected points were taken using dual frequency geodetic GPS receivers: 4000SSi with Choke Ring antenna and 5700 with Zephyr Geodetic antenna. The data is collected for a period of 6-8 hours with a sampling rate of 15 seconds, and satellite elevation mask of  $15^\circ$ . Repeat observations over the entire network have been carried out starting from Dec 2000. Till date, nine sets of observations have been taken (Dec. 2000, May 2001, Oct 2001, Sept 2002 and Dec. 2002, May 2003, Sept 2003, Dec 2003, April 2004), each fieldwork period spanning approximately three weeks.

## 8.2 Methodology for data processing and analysis

The objective of the work was to identify the factors responsible for deformation of the dam and their impact on the dam points and the surrounding region. The major factors that have been identified and studied in this project were the plate motion, varying reservoir water table. Other factors include seismic activity along fault zone, temperature, seepage, erosion, and settlement changes in the subsoil etc, which have not been included in this study.

The data is being processed using Bernese v4.2, which is a scientific software developed by the University of Bern. The processed data yield coordinates and baselines in both Cartesian Rectangular and Geodetic coordinate systems. All the changes in the coordinates and baseline lengths between the subsequent repeat observations (campaigns) have been established, and this gives the degree of global deformation between the campaigns. The global deformation includes the displacements caused due

to crustal (plate) motion, water level, seismic activity due to fault zone and other factors like subsidence etc.

In order to study the deformation of the dam due to continuously fluctuating water table, the base station on the dam axis was analysed. Continuous observations were taken for the base station throughout all the campaigns. The change in the coordinates of the point between the successive campaigns was estimated and the deformations thus obtained were studied to understand the pattern of deformation with respect to change in the water table.

### 8.3 GPS results and deformation analysis

The change in the coordinates obtained from GPS yield the global deformation of the points, which include two components, namely the local deformations and the plate deformation (of the Indian plate). In order to understand the deformation pattern of the dam, it is necessary to exclude the plate deformation from the global deformation to give the local deformation. For this purpose, the coordinates of IGS station IISc was used to compute the plate motion between the successive campaigns. Since IISc and Koyna are on the same plate (Indian plate), the deformation reflected in the Koyna points with respect to IISc would yield purely the local deformations. The local deformations of the base station for the successive campaigns were calculated and this is given in Table 1.

*Table 1: Local deformations of the Base Station  
(Global deformation – Plate motion)*

SL No	Campaigns	Global deformation (mm)	Plate motion (mm)	Local Deformation (mm)
1	Dec00-Oct01	92	97	-5
2	Oct01-Sept02	43	48	-5
3	Sept02-Dec02	18	13	5
4	Dec02-May03	12	22	-10
5	May03-Sept03	16	18	-2
6	Sept03-Dec03	10	08	2

(Negative sign indicates the point moves in the direction of plate motion, i.e., NNE; Positive sign indicates motion opposite to plate movement)

An attempt was made to correlate the global and local deformations of the base station with the water level for all the eight successive campaigns. This was done to understand the pattern of deformation of the dam with respect to change in water level. For this purpose, the standardized water level (z) for three years from 2000 – 2003 (the eight campaigns from Dec00 – Dec03) were computed.

The standardized water table is given by the formula

$$z = \frac{(Waterlevel - MDDL)}{(MWL - MDDL)}$$

where MDDL (minimum drawdown level) and MWL (mean water level). MWL is taken as 659.90 m, which is the mean of the water levels recorded since 1969 and MDDL so far recorded since 1969 is 609.60 m. The water table and the z values for 3 years are given in Table 2. The change in the z values ( $\Delta z$ ) between the successive campaigns are given in Table 3.

Table 2: Standardized Water table z

Campaigns	Water level (m)	z
Dec00	649.81	0.7994
May01	633.83	0.4817
Oct01	654.95	0.9016
Sept02	657.76	0.9575
Dec02	649.48	0.7928
May03	632.94	0.4640
Sept03	656.95	0.9414
Dec03	650.05	0.8042

Table 3: Change in z between successive campaigns

Campaigns	$\Delta z$
Dec00-Oct01	0.1022
Oct01-Sept02	0.0559
Sept02-Dec02	-0.1647
Dec02-May03	-0.288
May03-Sept03	0.4774
Sept03-Dec03	-0.1372

At Koyna, from earlier studies done by experts, it has been reported from physical instrumentation data analysis that the deflection of the dam increases very gradually for the water levels upto 625 m and increases rapidly for water levels beyond 625 m. Keeping this factor in mind, a polynomial in  $\Delta z$  was fit to the GPS local deformation data. It was found that polynomial in  $\Delta z$  of third degree fits well and this is shown in Figure 2.

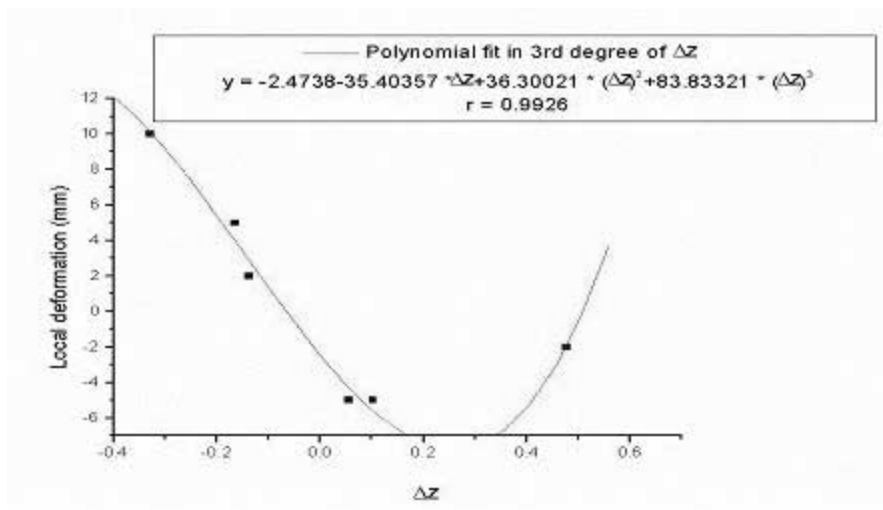


Figure 3: Deflection of Koyna Dam – Regression of deflection on water level

From the figure, a correlation of 0.9926 is observed. This clearly shows that the deformation of the dam is entirely due to the varying water table. This confirms the fact that the displacement of the structure may be solely because of the water table.

## 9.0 CONCLUSIONS

Several techniques have been developed for monitoring structural deformation of bridges, and high-rise buildings which from the stepping stone to urbanization. Since several years, physical and geodetic surveying methods have been widely used to monitor displacements of these structures. In the recent years, advancement in technology has led to the development of modern measurement methods like long gauge length deformation sensors, tacheometers with automatic reading and recording features to monitor deformations. The advancement in Space Geodesy has resulted in the use of GPS in structural deformation studies, since it overcomes the limitations of the terrestrial geodetic techniques. GPS has been widely used in monitoring of several types of structures, especially large dams, like Koyna Dam in India. The concept of monitoring deformation, as implemented by IITB GPS team for deformation analysis with respect to water level for the Koyna Dam, can also be applied to other type of structures.

## REFERENCES

- Celebi, M., Prescott, W., Hudnut, K., Behr, J., 2001. *GPS monitoring of structures: Recent Advances*. Proc. 30<sup>th</sup> Joint meeting of US-Japan co-operative Programme in Natural resources, August, San Francisco, U.S.A.
- Inaudi, D., Casanova, N., Vurpillot, S., 1999. *Bridge Deformation Monitoring with Fibre Optic sensors*. International Association for Bridge and Structural Engineering symposium, August 25-27, Rio de Janeiro, 475.
- Kuhlmann, H., Glaser, A., 1999. *Investigation of new measurement techniques for Bridge monitoring*, Institute of Application of Geodesy to Engineering, Germany.
- Kulkarni, M.N., 1985. Dam Deformation Studies by Geodetic method, *Indian Surveyor*, January, Journal of the Institution of Surveyors, India, 23.
- Manake, A., Kulkarni, M.N., 2002. Study of the Deformation of Koyna Dam using Global Positioning System, *Survey Review*, July **36(285)**, 497.
- Narayana, G.S., 1982. *Role of Geodetic Measurement in Surveillance of Dams*. Internal Report, Special Analysis & Instrumentation Directorate, Central Water commission, New Delhi.
- Roy, B.C., Kulkarni, M.N., 1999. *Geodetic and Geophysical aspects of Monitoring Seismotectonics in India*. *Indian Surveyor*, January, 15.
- Tsakiri, M., Lekidis, V., 2001. *The use of GPS for Monitoring Cable-stayed bridges in Seismic areas*. International Association of Geodesy symposia, **125**, 347.

Tsan-wing, N.G., Kin-Wah, L., 2001. *Application of Photogrammetry in Monitoring of Marine Rubble Structures*. The 10<sup>th</sup> FIG International Symposium on Deformation Measurements, Session II, Orange, California, U.S.A, March 19-22.



# **DEVELOPMENT OF SLOPE FAILURE DISASTER MANAGEMENT SYSTEM IN URBAN AREA THE UTILIZATION OF EXISTING DATA TOWARD “E-MUNICIPAL GOVERNMENT”**

AKIYUKI KAWASAKI AND SATORU SADOHARA  
Yokohama National University, Japan  
akiyuki@arc.ynu.ac.jp

## **ABSTRACT**

*Slope failure disaster management system in Yokohama, Japan, is under development using existing municipal government data and GIS, in order to improve steep slope management activities. Three basic methodologies for predicting dangerous slopes and sand covering areas are proposed in this study:*

- *Specifying steep slopes and sand covering areas in large city areas automatically using DEM (Digital Elevation Models) and LandUse data using GIS raster and vector analysis.*
- *Forecasting dangerous areas for slope failure with rainfall data using GIS. As a provoking cause for collapse, collapse records and rainfall data observed at 98 points in Yokohama every 15 minutes are analyzed.*
- *Statistical analysis of the possibility of slope failure disaster, using steep slope inventories by municipality, and multivariate analysis: Quantification Theory Type II. Relationships between collapse and the slope's factors (primary cause for collapse) are analyzed.*

*By combining these three methodologies, a “Real-time evaluation system against slope failure disaster” can be completed. As a conclusion of this paper, a prototype system was developed. This system consists of two components:*

- *A Slope Information Management System for effective daily support of steep slope management activities by integrating municipal data related to steep slope management (inventory, collapse record, and precipitation). All data are linked to the map. Searching, retrieving, and updating “Steep Slope data” are allowed, and can be shared by the Internet.*
- *Real-time Slope Failure Prediction System for response activities after a collapse by accumulation and analysis of slope failure records and precipitation data. The system development environment is as follows: OS: Windows XP; DB: Geodatabase (SQL Server2000 by MS ); GIS Engine: ArcObjects by ESRI;*

## 1.0 INTRODUCTION

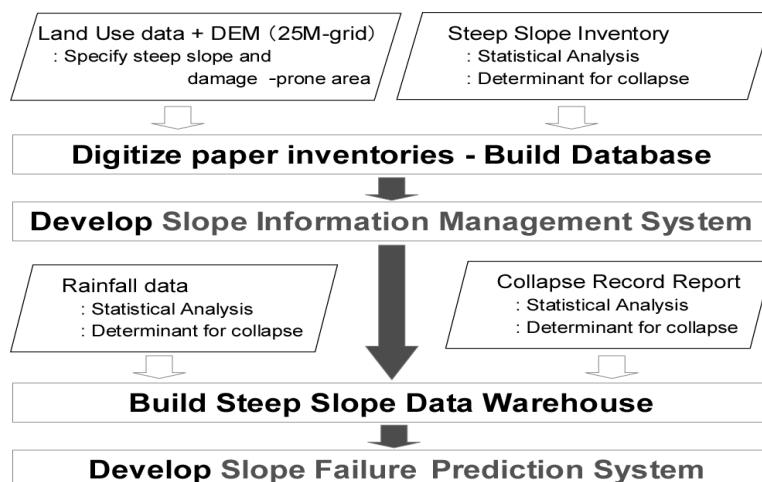
Slope failure disasters must be measured in Japan where they often occur. Recent efforts to develop soft-measures are underway because hard-measures, like covering hillsides with concrete, create economical and environmental problems. This paper demonstrates how to develop systems to manage slope failure disaster for municipal governments. Areas prone to slope failure disasters are predicted in real time using GIS and rainfall data. Also, a database system was developed to combine spatial data with existing paper data about potential slope failure disasters. This project provides an example of how existing hardcopy documents can be digitized and used to make "e-government" a reality.

## 2.0 OBJECTIVES

The purpose of this study is to create a "slope failure disaster management system" by existing data and documents in municipal government. We believe that making use of paper inventories are important to assist municipal slope failure disaster management and it will reduce the damage of slope failure disasters with a small budget and people. The objectives of the development are shown below:

- Link existing paper inventories with steep slope areas calculated by computer.
- Collect slope failure disasters record and analyze factors of collapse.
- Near real-time slope failure disaster prediction based on analysis and precipitation data.

The flowchart of the development is shown in figure 1.



*Figure 1: Flowchart of the development*

### 3.0 METHODOLOGIES

Three methodologies to develop a “real time slope failure disaster management system” are proposed in a series of our study. Details of each methodology are on papers of Kawasaki (2001) and Kawasaki (2003).

#### 3.1 Methodology of specifying “steep slope” and “predicted damage area”.

This method could be used in order to predict which buildings would be damaged by the collapse. Two GIS data: Land Use and 25m DEM, are used to specify steep slopes and damaged area. The model to specify “steep slopes” and “the predicted damage area” are shown in Figure 2. Spatial analysis functions by ESRI ArcGIS were combined in the model.

The result of the model was inspected in Minami-ku, Yokohama city (Figure 3): 191 areas specified by the model were matched with the areas specified by local governments out of 204. In other word, 93.6% of the areas specified by local governments were covered by the methodologies.

The predicted damaged area is calculated by the height of steep slope. It means that higher steep slope has longer damaged area. As a result of inspection, actual height of a slope was multiplied the calculated height by 0.87.

#### 3.2 Evaluate the primary cause, using “steep slope inventories” and “multivariate analysis; quantification theory type II”.

City of Yokohama inspected 3400 steep slopes in all around the city. Thirty detailed factors such as geology, height, vegetation, surface thickness, leaking water, etc., were inspected and ranked for its danger. In this study, nine important factors were quantified in order to multivariate analysis for each slope pattern. In Yokohama city, steep slopes were categorized to four patterns (Yokohama city steep slope evaluation committee, 2000)

Table 1 is the result of quantification theory type II for slope pattern No. 1. Each value means the contribution-ratio for the collapse. Higher value contributes to collapse strongly, while minus value is lower contribution. Regarding slope pattern No. 1, “Over-hang”, “Looseness relaxation”, and “Leaking water” are common strong factor for the collapse. On the other hand, “vegetation” tends to prevent slope collapse. Moreover, sum of values can be used to evaluate the possibility slope failure based on the past collapse record.

Figure 4 represent that most steep slopes which have value higher than around 0.2 were actually collapsed in the past. Therefore, if a slope had a value of higher than 0.08, it has strong potential of collapse in the future. As a result of our verification, the potential of collapse can be estimated in 87% of its accuracy.

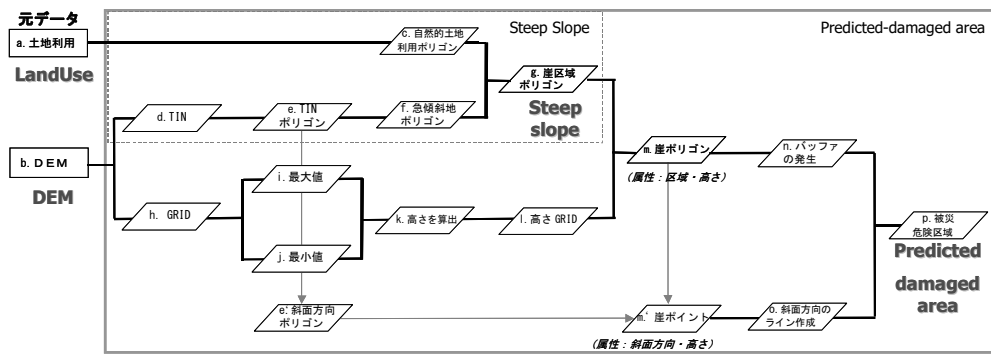


Figure 2: Process of extracting dangerous slopes and zones suffering from slope failures.

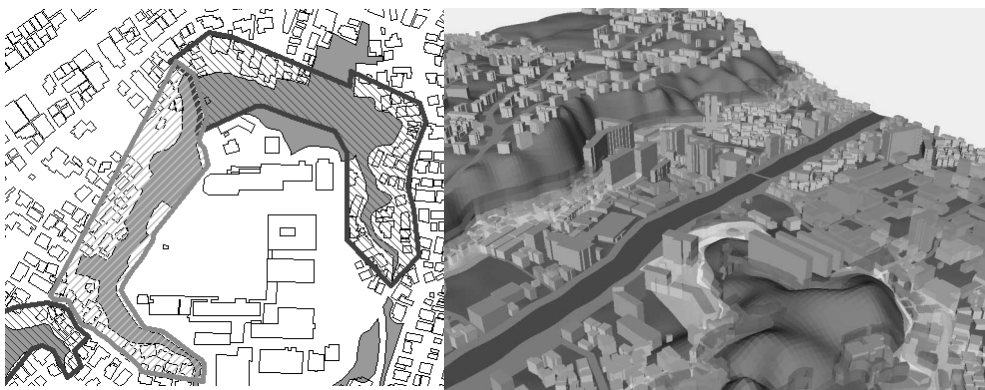


Figure 3: Left; Specified areas of this model (painted) and the areas by local governments (slashed), Right; Example of 3D visualization.

### 3.3 Forecasting the dangerous area for slope failure by rainfall data at the time using GIS spatial analysis.

In this step, a methodology to specify dangerous area for slope failure by one hour and three days accumulated rainfall using GIS raster analysis was proposed. Figure 5 shows relationships between collapses and rainfall (One hour rainfall and three days accumulated rainfall) in Yokohama city. As a trial, a approximate expression is calculated on the graph.

As Figure 6 shows, when one hour rainfall and three days rainfall data was put into ArcGIS spatial analyst with the approximate expression for slope failure, then ArcGIS calculate dangerous area for slope failure at the time. This methodology will allow specifying the dangerous area for slope failure every time the rainfall data is available. Red areas on figure 6 represent the area where rains exceeded that approximate expression. From the result of verification, about 75 % of actual collapse points were covered by the areas specified by this methodology. This relationship is important to make a real-time estimation, because rainfall data can be available every quarter hour in Yokohama.

Table 1: Results of Quantification Theory Type II

Item	Category	Num. of sample	Weightd coefficient	Range	partial correlation coefficient
Height of Slope (Hm)	10m -	24	-0.378	0.863	0.224
	5m - 10m	38	0.086		
	- 5m	12	0.485		
Slope (degree)	60° -	23	0.272	0.491	0.125
	40° - 60°	44	-0.107		
	- 40°	7	-0.219		
Thickness of Surface	50cm -	8	0.644	0.722	0.171
	- 50cm	66	-0.078		
Leaking Water	Exist	4	1.296	1.370	0.255
	No	70	-0.074		
Looseness Relaxation	Exist	8	1.207	1.353	0.311
	No	66	-0.146		
Vegetation	Bare ground	17	-0.346	0.624	0.159
	tree	5	0.151		
	grass/field	11	0.278		
	tree+grass/field	41	0.050		
Surface Water (above)	Exist	35	0.190	0.361	0.134
	No	39	-0.171		
Surface Water (slope)	Exist	42	0.160	0.369	0.158
	No	32	-0.209		
Drainage on top	Bad/Uncompleted	54	0.013	0.049	0.018
	Good	20	-0.036		
Over Hang	Exist	7	0.018	0.020	0.005
	No	67	-0.002		

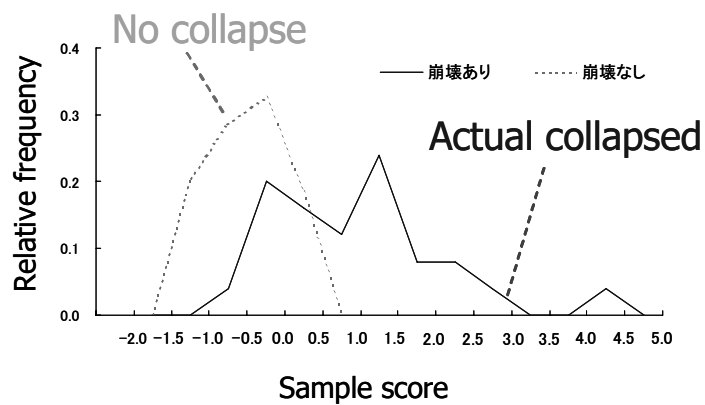


Figure 4: Frequency distribution of distinction result

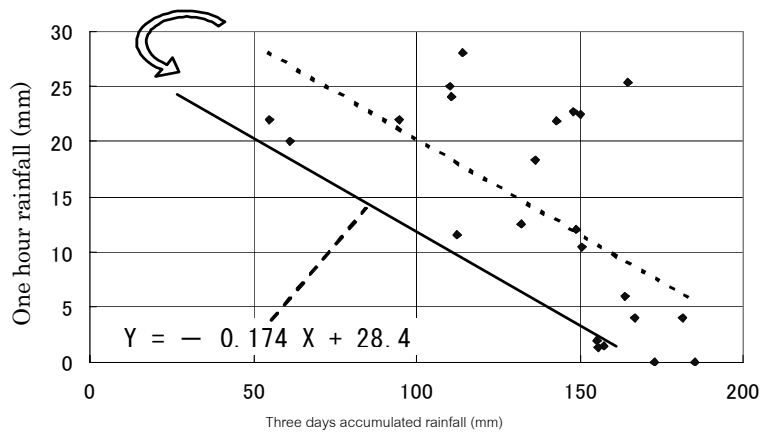


Figure 5: Relationship between rainfall and slope failure

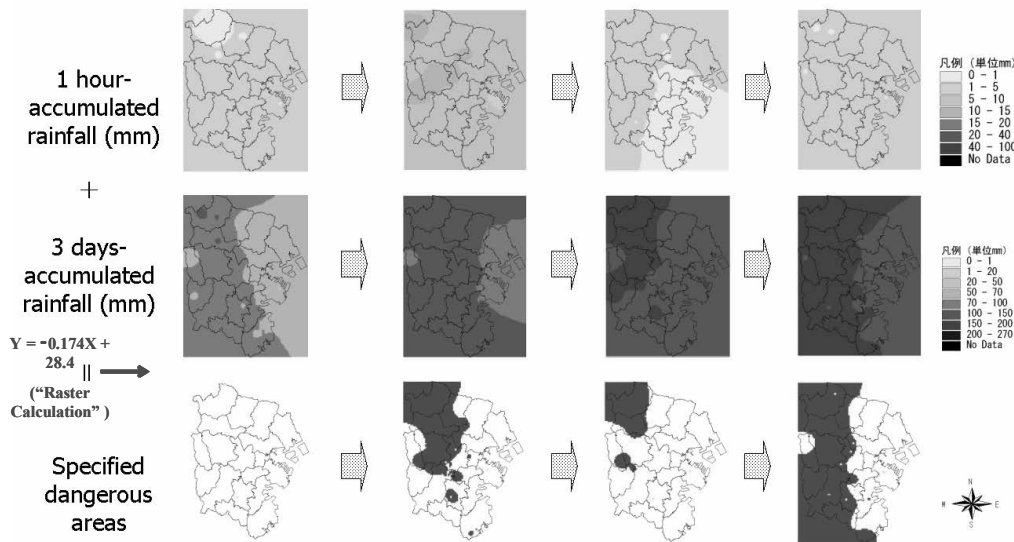


Figure 6: Dangerous area at the time by rainfall data (August/22/2001)

## 4.0 PROTO TYPED SYSTEM DEVELOPMENT

### 4.1 System design

The final objective of this study is to develop a slope failure disaster management system to support disaster management works in municipality. In this moment, two trial systems were developed. 1. “Slope Information Management System”, which is used for daily disaster management use. 2. “Real-time Slope Failure Prediction System”, which is for preparedness and emergency response work after disasters.

Municipality’s data related to slope failure (inventory, collapse record, and precipitation) were stored and managed using ArcGIS and ArcSDE (Spatial Database Engine), and three methodologies are integrated into the system for risk estimation and real time slope failure prediction. The system

flow is shown in Figure 7. The system is divided into four parts: “Management”, “Analysis”, “Prediction” and “Response”. Proto-typed system on two parts: “Management” and “Prediction” have been developed in this paper. The other two parts: “Analysis” with data ware house and “Response” for municipality, fire department, and local residents are under development. The system development environment is shown in Table 2.

Table 2: The system development environment

OS	Windows XP Professional
Database	ESRI Geodatabase (SQL Server2000 by Microsoft)
GIS Engine	ArcObjects by ESRI
Digital Map	Digital Mapping by Municipality of Yokohama
Analysis Software	Excel Statistics 2000 and SPSS 12.0

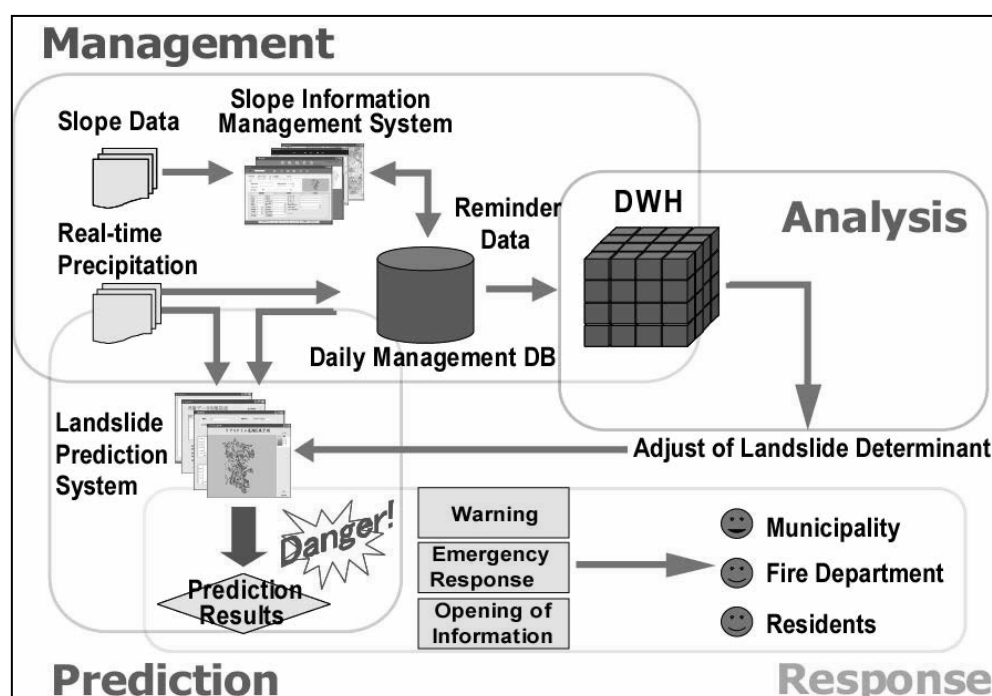


Figure 7: Flowchart of System design.

#### 4.2 Trial development of slope information management system

Slope information management system is designed for the daily disaster management use in municipality. Figure 8 shows interfaces of the system. Main functions in the system are: A. data input, and B. data searching and retrieving. Data input interfaces are based on the paper format of “Steep Slope Inventory”. The format of “Steep Slope Inventory” is based on the guidelines by Ministry of Land, Infrastructure and Transport. All of slope inventories have attached the linkage with digital map by municipality. It will allow searching a slope by the address list box or clicking on the map. Then, GIS data such as a boundary, road, evacuation area, buildings and

steep slopes could be overlaid on map window. Also, data related to neighborhood, and pictures are available.

Personnel in municipality can input detailed attribute data of a slope for inventory work. Then, pop up windows will help data input work. This kind of functions would reduce input misses; paper inventories had many of it though. These functions are required if a system has an analysis functions.

The searching and retrieving functions are required for querying a steep slope by its attribute. Then, system displays the place and attribute table of the slope.

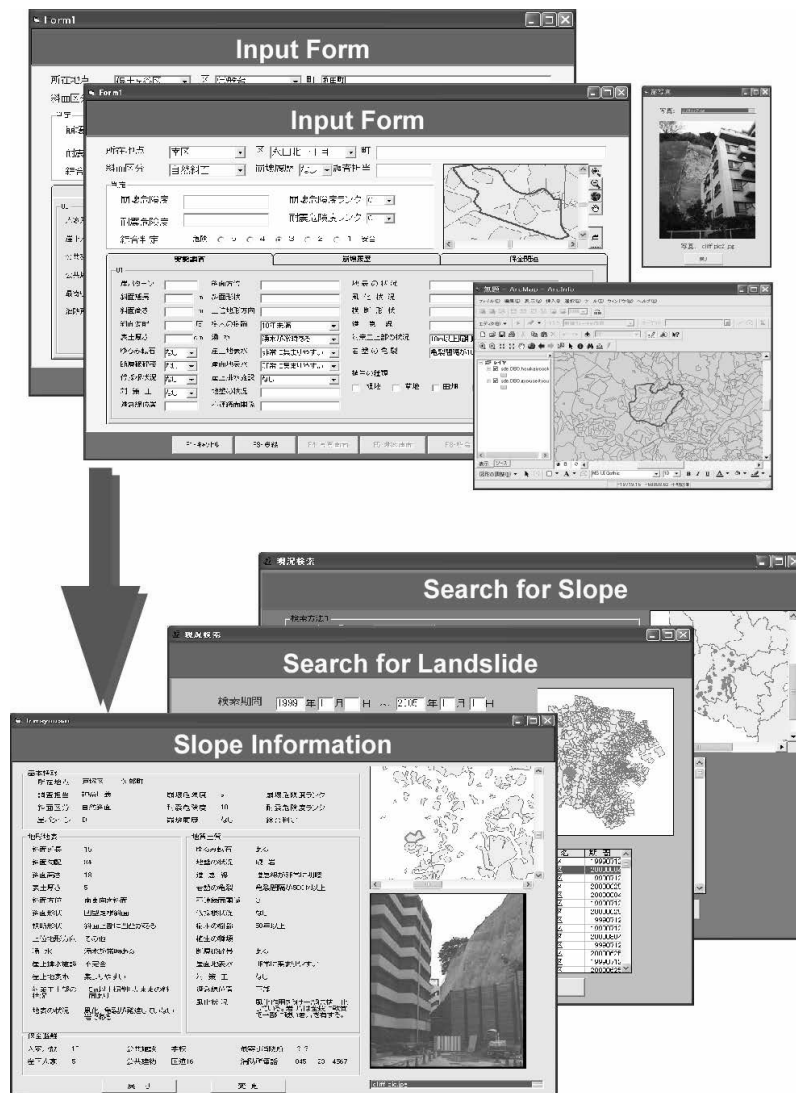


Figure 8: Interfaces of Slope Information Management System.

#### 4.3 Trial development of real-time slope failure prediction system

Proto-typed system of real-time slope failure prediction by accumulation and analysis of slope failure data, and precipitation data



updated every 15 minutes, was developed. In Yokohama, precipitation data at 97points around the city is available every 15 minutes. This system is receiving rainfall data automatically thorough the Internet, and processing the data to calculate. Information of observation points and the graphs of the short-time rainfall and the long term accumulated rainfall data at the time are shown in the interface (Figure 9). The result of the prediction will be shown on the window when rainfall exceeds a critical line. In addition, using the function of Data warehouse, all data can be stored and used for further analysis in order to improve prediction.

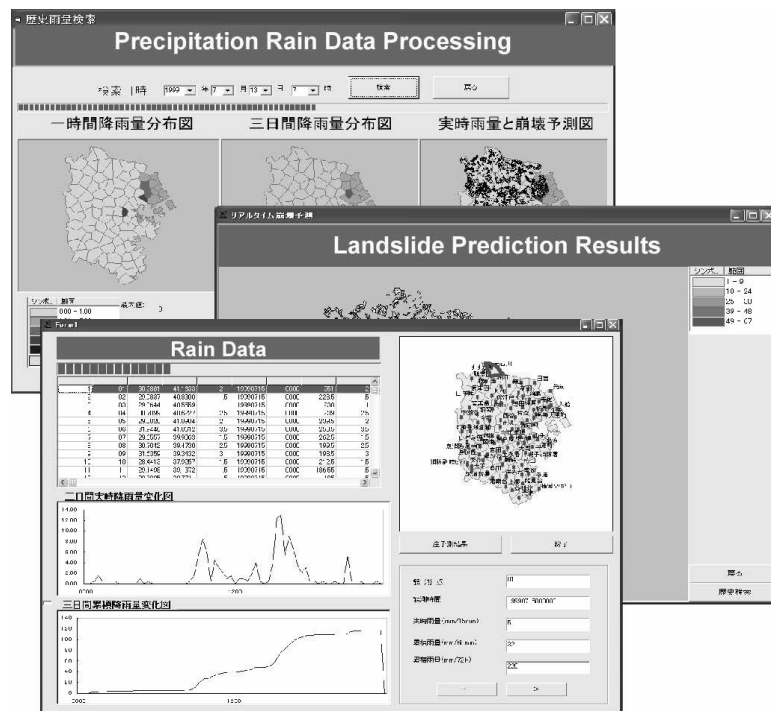


Figure 9: Interfaces of Real-time Slope Failure Prediction System.

## 5.0 CONCLUSIONS

Slope failure disaster management system in Yokohama, Japan, is under development using existing municipal government data and GIS. Three basic methodologies for predicting dangerous slopes and sand covering areas are proposed in this study:

- Specifying steep slopes and sand covering areas using DEM and LandUse data using GIS raster and vector analysis
- Forecasting dangerous areas for slope failure with rainfall data using GIS,
- Statistical analysis of the possibility of slope failure disaster, using steep slope inventories by municipality, and multivariate analysis: Quantification Theory Type II.

By combining these three methodologies, a prototype system of “Real-time evaluation system against slope failure disaster” was developed. This system consists of two components:

- Slope Information Management System for effective daily support of steep slope management activities by integrating municipal data related to steep slope management.
- Real-time Slope Failure Prediction System for response activities after a collapse by accumulation and analysis of slope failure records and precipitation data.

In next step, using advanced data such as high resolution remote sensing and laser profiler data, the precision of methodologies for evaluating and predicting slope failure disaster have to be improved. In addition, thorough a questionnaire and interview to users, system development needs further improvements as to be a decision-making support tool in practical disaster management work in municipality.

## ACKNOWLEDGEMENT

Special thanks to YNU Gake-team members for their dedicated work to this study: Mr. FANG Ji, Mr. IMAMASU Keisuke, Ms. INAGAKI Keiko, Ms. IRIBE Yoshimi, Mr. Li Long Ji, Mr. OKANISHI Yasushi, Ms. OKUMURA Mako, Ms. Rizka Oktora Ibrahim, Dr. YOSHIDA Satoshi, Mr. WANG Jin, and Ms. WANG Dongzhi.

This work is contribution to the 2004 Research and Development of Construction Technologies by the MLIT (The Ministry of Land, Infrastructure and Transport).

## REFERENCES

- Kawasaki, A., Sadohara, S., 2003. *The Utilization of GIS for the Measure against Slope Failure Disaster in Urban Area, Joint Workshop on US-Japan Cooperative Researches in Urban Earthquake Disaster Mitigation*. Unpublished report, Los Angels, California, USA.
- Kawasaki, A., Hattori, K., Urakawa, G., Nakajima T., And Sadohara, S. 2001. *The Utilization of GIS for the Measurement against Slope Failure Disaster*. Theory and Applications of GIS, Vol.9, No. 2, 25-32. (Japanese)
- Kawasaki, A., Yoshida, S., And Sadohara, S. 2003. *Statistical researches of the factors affecting slope failure in Yokohama*. J. Archit. Plann., AIJ, No. 569, 125-130. (Japanese)
- Yokohama City Steep Slope Evaluation Comitee, 2000. *Report of the evaluation of slope failure disaster in Yokohama City*. Unpublished report, Yokohama, JAPAN.

# **NUMERICAL MODELING OF STEEL STRUCTURES IN FIRE CONDITIONS USING IMPROVED APPLIED ELEMENT METHOD**

SAID A. ELKHOLY AND KIMIRO MEGURO  
Institute of Industrial Science, University of Tokyo  
*elkholy@prelude.iis.u-tokyo.ac.jp*

## **ABSTRACT**

*Steel structures are widely used for buildings due to the advantages of high strength, good ductility and fast fabrication and erection. However, unprotected steel structures suffer serious damage or even collapse in a fire disaster due to the progressive deterioration in both strength and stiffness of structural steel with increasing temperature. To protect life and reduce fire damage to property and financial loss, a steel structure must be designed to have the ability to sustain the applied design loads without the occurrence of excessive deflection or even failure in structural members for a specified period of time in the case of a fire.*

*In this paper, the Improved Applied Element Method (IAEM), which was originally developed as an effective analysis technique of large-scale structures up to complete failure under different hazard loads, has been progressively developed to carry out modeling the behavior of plane frame steel structures in fire. The paper presents the methodology of a new approach for thermal analysis of the large deflection behavior of steel structures at elevated temperatures. IAEM has been developed to cover both geometric and material nonlinearities, including the changes to material properties as temperatures increase. Rigorous treatments of thermal analysis in plane frame steel structures are illustrated. The effectiveness and validation of the proposed approach are demonstrated by comparison its results with those previously obtained by benchmark experiments or by other independent computer software.*

## **1.0 INTRODUCTION**

To obtain full knowledge of the total behavior of steel structures under fire, it is essential to simulate the collapsing process and the trace of yielding and deformation at each structural member. The reliable numerical models are highly required as a cost effective method of obtaining a comprehensive knowledge of the main parameters that affect response of structures under fire. The advanced analytical methods enable engineers to predict the type and range of possible collapse in both the design stage and after incidents to enhance the safety of people in structures subjected to fire.

In order to include nonlinear temperature distribution across the section and along the member, the effects of material and geometric nonlinearities, thermal strain and creep strain at elevated temperatures several techniques have been introduced during last four decades. These

techniques can be classified into two main categories depending on the formulation procedure of implementing the constitutive relations. The first category bases on the finite element method (FEM). Based on FEM, numerous researchers had developed a number of formulations or computer packages (such as: Cheng and Mak, 1975; Bailey, 1998). The accuracy of those formulations depended mainly on the adopted models for simulating the nonlinear material properties and the creep law.

The second category of the numerical approaches bases on plastic hinge technique (Wong et al. 1998; Vimonsatit et al. 2003). The plastic hinge approach is less computationally intensive and usually gives good predictive accuracy compared to the rigorous finite element approach (Vimonsatit et al. 2003).

None of the methods based on the discrete elements approach have yet been developed for carrying out the thermal analysis. Therefore, in this paper, the first implementation of the thermal analysis in the field of Discreet Element based approach is presented. This feature allows, not only to follow the total behavior of structures at elevated temperature, but also the analysis can extend up to complete failure.

## 2.0 IMPROVED APPLIED ELEMENT METHOD

IAEM is a newly developed method for structural analysis of large-scale plane-frame structures under hazardous loading conditions. It can follow total behavior of structures up to complete failure stage with high accuracy in reasonable CPU. In IAEM, each structural member is divided into a proper number of rigid elements connected by pairs of normal and shear springs uniformly distributed on the boundary line between elements. Two major extensions of the AEM (Meguro and Tagel-Den, 2001) have been implemented in IMEM: The first is improving the element type to use different thickness per each spring to be able to follow change of thickness in non-rectangular cross-sections. The second is using different thicknesses for calculating normal stiffness and shear stiffness in each pair of springs. The sort modifications allow modeling cross sectional geometric parameters of structural members using elements with large size. The value of normal and shear stiffness for each pair of springs can be determined as:

$$K_n^i = \frac{E * d * T_n^i}{a} \quad \text{and} \quad K_s^i = \frac{G * d * T_s^i}{a} \quad (1)$$

where:  $d$  is the distance between each spring;  $a$  is the length of the representative area;  $E$  and  $G$  are Young's and shear modules, respectively;  $T_n^i$  and  $T_s^i$  are the thickness represented by the pair of springs " $i$ " for normal and shear cases, respectively.

With these modifications, the total behavior of large-scale structures under different hazardous loading conditions can be simulated with a good accuracy and in a reasonable CPU time (Elkholy and Meguro, 2003;

Elkholy and Meguro, 2004). The IAEM has been progressively developed to carry out modeling the behavior of plane frame steel structures under fire.

### 3.0 CONSTITUTIVE MODEL OF STEEL UNDER FIRE

#### 3.1 Material model

A simplified uniaxial bilinear stress-strain model with kinematic strain hardening is adapted for representing the normal stiffness component of structural steel (Figure 1). In this model the plastic range remains constant throughout the various loading stages, and the hardening rule for the yield surface is assumed as a linear function of the increment of plastic strain. The model can be characterized by three parameters, the elastic modules ( $E$ ), yield strength ( $\sigma_y$ ), and straining of hardening parameter ( $\mu$ ). At increased temperature, the material properties degrade and its capacity to deform increases, which is measured by the reduction of the Young's modulus.

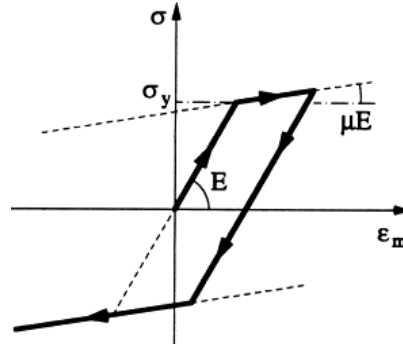


Figure 1: Bilinear material model

#### 3.2 Constitutive model

For heated and loaded steel, the constitutive model is described by assuming that the change in  $\Delta\epsilon$  is expressed as the sum of three components, as described in Equation (2) (Buchanan, 2001).

$$\Delta\epsilon = \epsilon_t - \epsilon_{\text{int}} = \epsilon_{\text{th}}(t) + \epsilon_{\sigma}(\sigma, T) + \epsilon_{\text{cr}}(\sigma, T, t) \quad (2)$$

where:

- $\epsilon_t$  is the total strain at time  $t$ ,
- $\epsilon_{\text{int}}$  is the initial strain at time  $t = 0$ ,
- $\epsilon_{\text{th}}(T)$  is the thermal strain being a function only of temperature “ $T$ ”,
- $\epsilon_{\sigma}(\sigma, T)$  is the stress-related strain, being a function of both the applied stress “ $\sigma$ ” and the temperature “ $T$ ”, and
- $\epsilon_{\text{cr}}(\sigma, T, t)$  is the creep strain, being a function of stress, temperature and time.

So far, the creep model for steel at elevated temperatures is not yet included in the proposed numerical model. It has been assumed that the variation of mechanical properties of steel with temperature takes into account the creep effects.

#### 4.0 THERMAL ANALYSIS BY USING IAEM

A step-by-step time integration procedure has been adopted to follow the response of the structure subjected to elevated temperature. The flow chart of the analysis in elastic loading condition is shown in Figure 2. For convenience of analysis, the following hypotheses are employed:

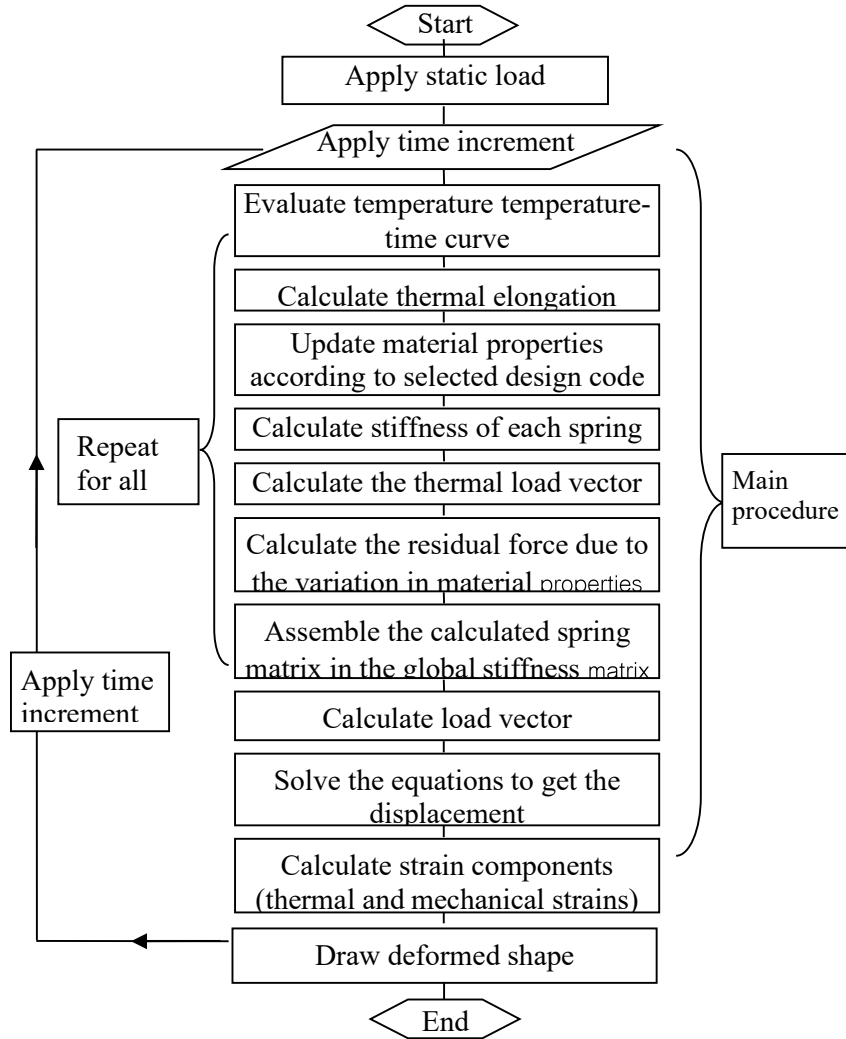


Figure 2: Flow chart of the program

Update the temperature profile through a given structure. The temperature  $\{T_i\}$  at time  $t_i$  is calculated at each spring location according to the selected fire scenario.

- Calculate the thermal elongation ( $\epsilon_{th}$ ) due to the temperature increment.
- Update the material properties (Young's modulus ( $E$ ), initial yield strength ( $\sigma_y$ ) and strain hardening parameter ( $\mu$ )) of all springs when the temperature of the structure is increased from  $\{T_{i-1}\}$  to  $\{T_i\}$ .
- Create the new stiffness matrix of the structure considering the variation of material parameters at each spring due to the rising of temperature.

- Calculate the thermal load vector of each element  $\{F_{Ti}\}$  due to the temperature increment  $\{\Delta T\} = \{T_i\} - \{T_{i-1}\}$ . For each spring, the thermal load is calculated according to Equation (3) and applied as a compression force applied at the elements' boundary.

$$F_n^i = K_n^i(\varepsilon_{th}(T_i) - \varepsilon_{th}(T_{i-1})) \quad (3)$$

- where  $K_n^i$  is the normal stiffness of spring  $i$ .
- After calculating the thermal load vector, the general equation of motion in case of thermal analysis is changed to be:

$$[M][\Delta\ddot{U}] + [C][\Delta\dot{U}] + [K][\Delta U] = \Delta f(t) + R_m + R_G + \Delta F(T) \quad (4)$$

- where:  $[M]$  is mass matrix;  $[C]$  is the damping matrix;  $[K]$  is the nonlinear stiffness matrix;  $\Delta F(T)$  is the incremental applied thermal load vector;  $\{\Delta\ddot{U}\}$ ,  $\{\Delta\dot{U}\}$ ,  $\{\Delta U\}$  and  $\{\Delta\ddot{U}_g\}$  are the incremental acceleration, velocity, acceleration, and gravity acceleration vectors, respectively.
- The value of the geometrical residuals around each element ( $R_G$ ) in case of dynamic load condition is calculated according to Equation (5) (Meguro and Tagel-din, 2002).

$$R_G = \Delta F(T) - [M] [\ddot{U}] - [C] [\dot{U}] - F_m \quad (5)$$

where  $F_m$  is the element force vector from the surrounding springs of each element

- Solve the equation of motion. Calculate the incremental and total displacement vectors and obtain the total strain at each spring.
- Subtract thermally induced strains ( $\varepsilon_{th}$ ) from total strains ( $\varepsilon_t$ ) to obtain the mechanical strains ( $\varepsilon_m$ ) at each spring.
- Assuming the stress-induced incremental strain is elastic, calculate the current stress.

$$\sigma = E(\varepsilon_t - \varepsilon_{th} - \varepsilon_{p0}) \quad (6)$$

- If the stress obtained in the above step exceeds the tensile or the compressive yield strength then recalculate the stress according to the inelastic rule given by:

$$\sigma = \mu E(\varepsilon_t - \varepsilon_{th}) \pm (1 - \mu)\sigma_y \quad (7)$$

- Calculate the geometrical residuals around each element from the equation below.
- Apply again a new time increment and repeat the whole procedure.

The most important feature in this technique is that it allows evaluated temperature analysis beyond instability. Moreover, it takes into account the dynamic effects, which can either add to destabilizing forces or delay them or both.

## 5.0 ILLUSTRATIVE EXAMPLES

To evaluate the capability of IAEM in modeling a steel structure under fire, a comparison was conducted between the numerical model and the results obtained experimental works.

A 5.50 m span beam of 305 x 165 UB 40 kg m<sup>-1</sup> cross-section and Grade 43 steel was loaded equally at the quarter points, as shown in Figure 3. The beam has flange slender ratio  $bf/tf = 16.18$  and a web slender ratio of  $h/tw = 50.5$ . Firstly, the beam was loaded with  $R = 0.6$  where  $R$  is the load ratios defined as the maximum bending moment of a simply supported beam to the plastic bending moment capacity of the beam at ambient temperature according to BS5950: Part 8. After fully applying the vertical loads, the beam is uniformly heated. Two support conditions had been considered in the analysis as shown in Figure3:

Case 1: Pin – Roller support conditions

Case 2: Fixed –Slide support conditions

To model the steel properties at elevated temperatures, the bilinear material model is employed with reduction factors shown in Figure 4. The straining of hardening is assumed to be zero at room temperature and increases gradually up to its maximum value of 0.05 at 400 °C and decreases again to be zero at 650 °C. Tri-linear models are assumed to represent the variation of modulus of elasticity and strength of steel with temperatures. These factors are chosen as a best fit the given moment-rotation curve given by (Bailey, 1998).

The mid span deflections, plotted against temperature, are shown in Figure 5 for the two boundary condition cases, together with the results illustrated by Bailey (1998). It can be seen from the figures the well agreement between the analytical modeling using IAEM and test results. The high capability of IAEM of evaluation the critical temperature and following the total behavior of the beam is demonstrated.

Figure 6 shows the failure mechanisms and the formation of the plastic zones for the heated beams. From the figure, In case of Pin – Roller support beam since the beam was free expand, the bending moment along the beam was only due to the imposed load and no axial load had been generated. The beam failed due to the formation of one plastic hinge at the mid-span. The figure shows the spread yielding sequences illustrated by the dark color. When the plastic zones develop, the beam has lost most of its strength and the deflection increases greatly, pulling the roller support closer to the pin support. This mode of failure is known as a runaway failure mode.

On the other hand, in case of Fixed –Slide support case the supports of the beam started to yield first. Subsequently, a third plastic hinge is formed at the mid span of the beam due to increasing deflection caused by formation of plastic hinges at the beam supports. Moreover, the critical temperature that produces failure of the beam is higher that the in pin- roller support case.



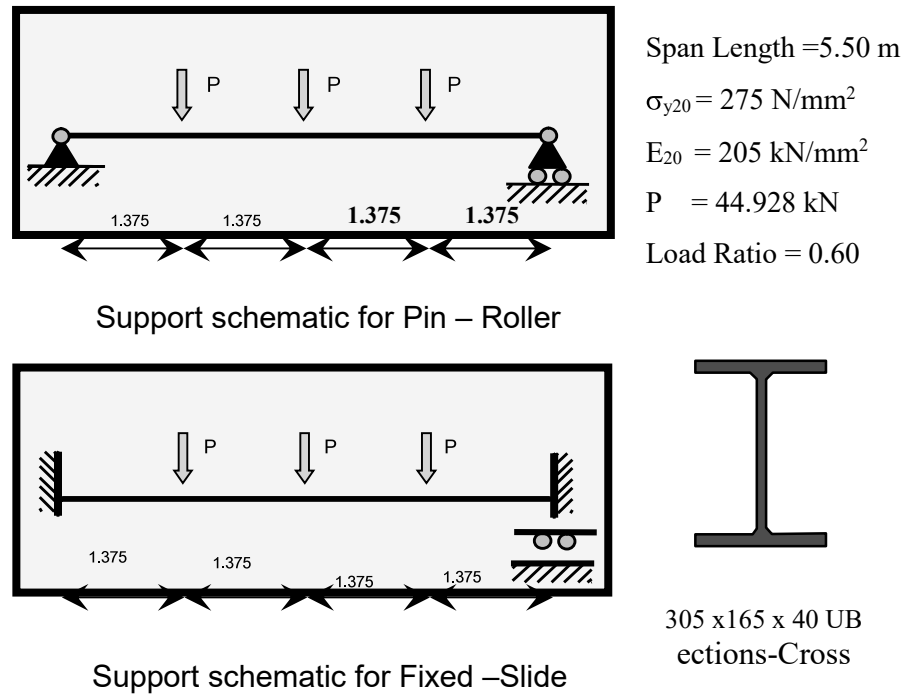


Figure 3: Beams configuration and loading

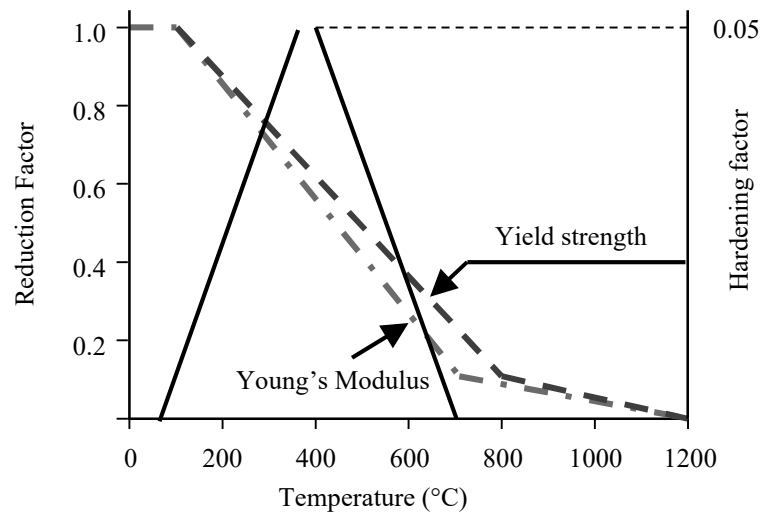


Figure 4: Material properties at elevated temperatures

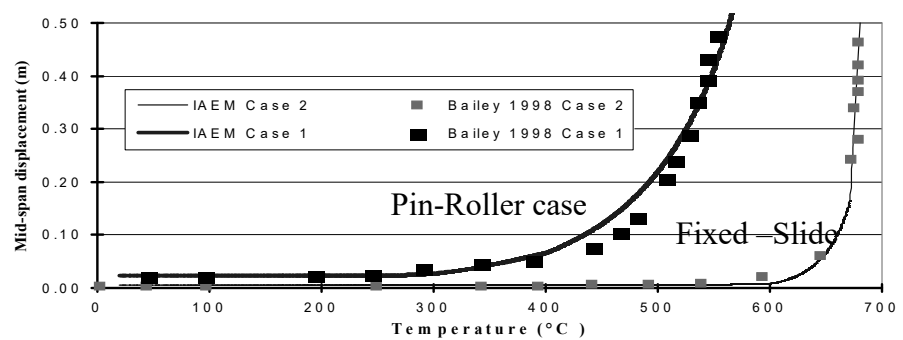
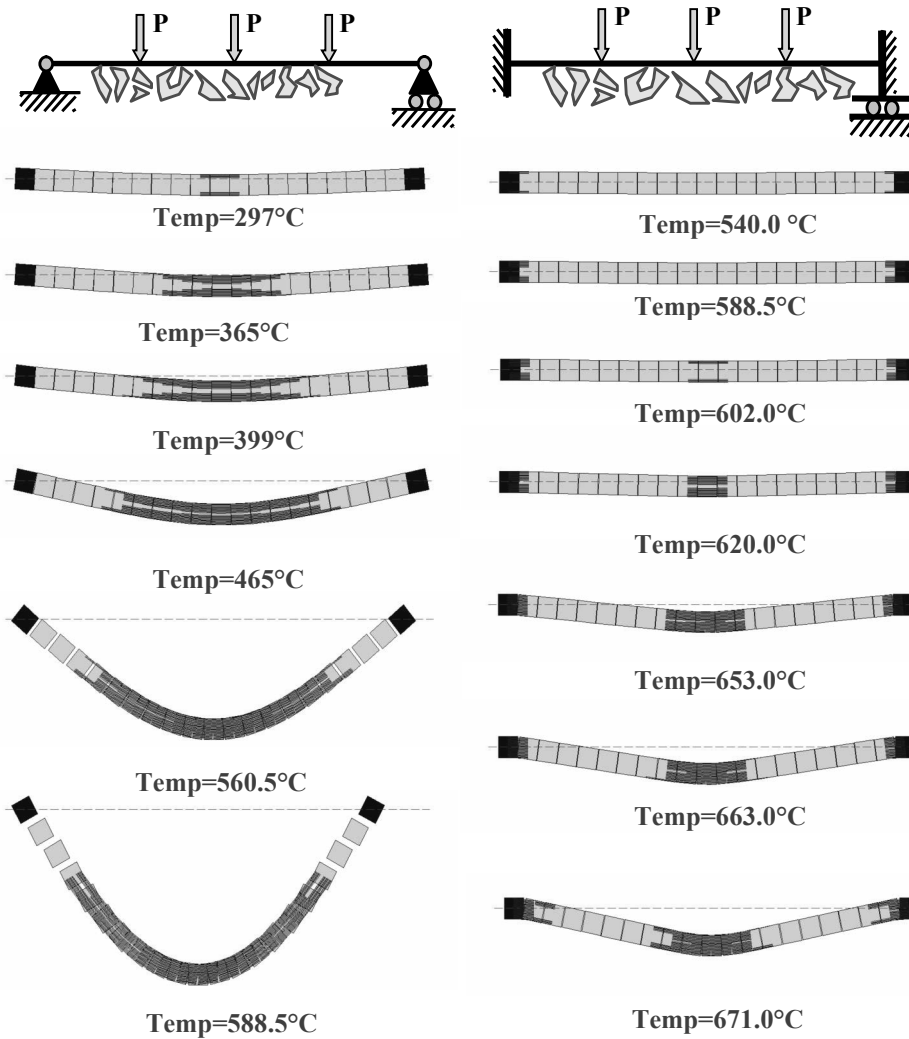


Figure 5: Behavior of heated beams



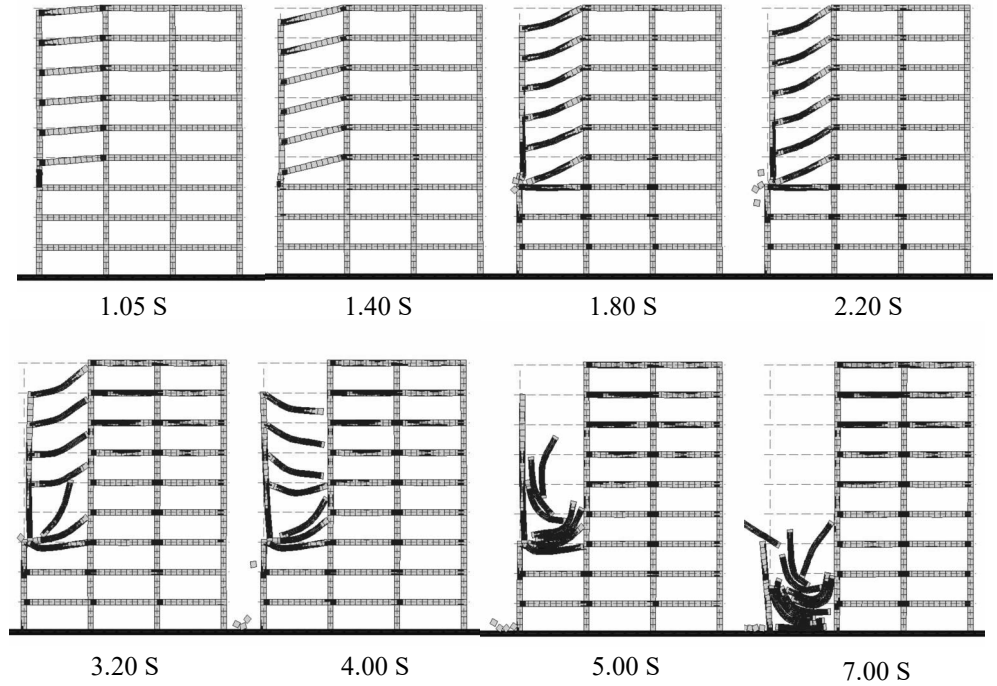
*Figure 6: Failure mechanism of the heated beams*

## 6.0 RESPONSE OF STEEL FRAME STRUCTURE TO A SUDDEN FAILURE OF A COLUMN

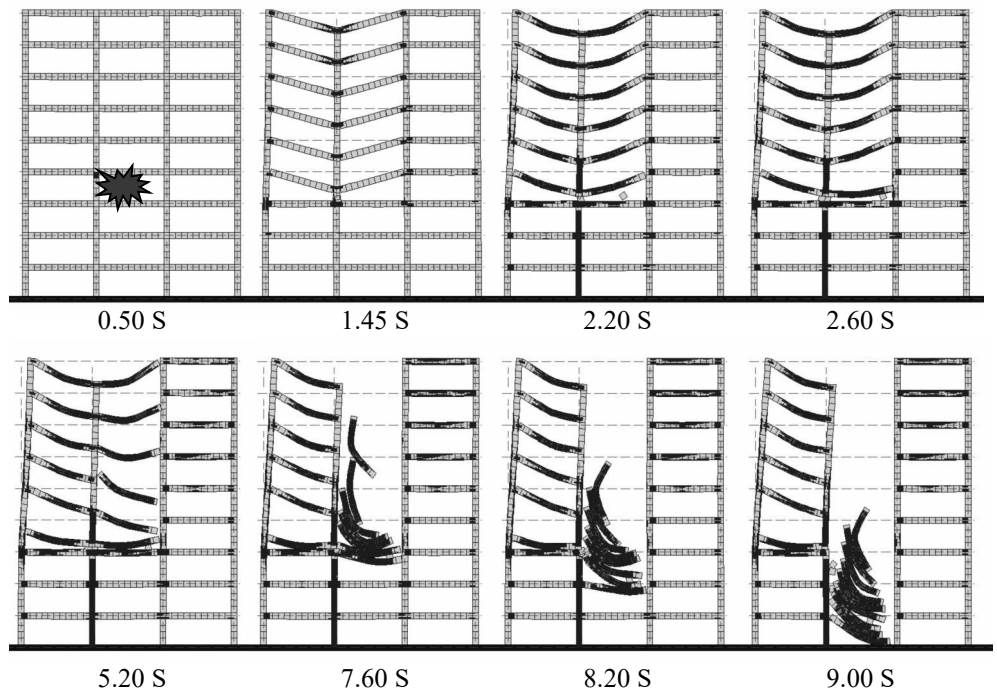
Progressive failure is a principal cause of injury and death in building failures regardless the source of the loading. Therefore, predicting and designing to prevent the progressive failure. By using IAEM with the same thermal analysis procedure, it is possible to evaluate the possibility of progressive collapse of multi-story steel frame structures due to a sudden failure in one of their supporting member.

The structure considered is a plane nine-story steel frame with three bays of 9.00m long. The typical story height is 3.75m. The dimensions of structure and that of structural members are illustrated in (Elkholy and Meguro, 2004). Using IAEM, only 477 elements are utilized for modeling the whole structure. In this paper, two cases of failure are introduced: failure due to exterior and interior columns (Figures 7 and 8). At first, the design load on the structure is applied as an initial load, while the sudden failure of one supporting structural element is applied as loading in time domain. The sudden failure of the structural members is modeled using a localized fire

scenario which produces reduction of the yield stress and Young's modulus to be 10% of their original values during a period of 0.10 second.



*Figure 7: Progressive collapse due to sudden failure of exterior column*



*Figure 8: Failure mechanism due to sudden failure of exterior column*

The figures show the entire collapse procedures and illustrate the high capability of following the trace of yielding and deformation at each structural member. The dark areas in the figures identify the zones that have plastic deformations. The sudden removal of the column causes also releasing of some of the potential energy and rapid alternation of internal

dynamic forces. The simulation shows that the lack of joint ductility may lead to a total collapse of the outer bay of the structure.

## 7.0 CONCLUSIONS

In this paper, a pioneering attempt to implement the thermal analysis in the field of Discrete Element based approaches is presented. The IAEM has been progressively developed to carry out modeling the behavior of plane frame steel structures under fire. The paper presents the methodology and basic formulations of a new approach for thermal analysis to analyze the large deflection behavior of steel structures at elevated temperatures. The most important feature in this technique is that it allows evaluated temperature analysis beyond instability. Moreover, it takes into account the dynamic effects, which can either add to destabilizing forces or delay them or both. The method can also follow the immediate geometric change in a structure due to sudden removal of any element in the structure. Releasing of potential energy and rapid alteration of internal forces can be simulated by using the direct step-by-step integration method technique used in IAEM.

## REFERENCES

- Bailey, C.G., 1998. *Development of Computer Software to Simulate the Structural Behavior of Steel-Framed Buildings in Fire*. Computer and Structures 67, 421-438.
- British Standard Institute, 1990. *BS 5950, Part 8, Code of Practice for the Fire Protection of Structural Steelwork*.
- Buchanan, A.H., 2001. *Structural Design for Fire Safety*. John Wiley & Sons, West Sussex, England.
- Cheng, W.C. and Mak, C.K., 1975. *Computer Analysis of Steel Frame in Fire*. Journal of the Structural Division 101, 855-867.
- Elkholy, S. and Meguro, K., 2003. *Structural Failure Simulation due to Fire by Applied Element Method*. JCROSSAR2003, The 5<sup>th</sup> Japan Conference on Structural Safety and Reliability, Tokyo, Japan.
- Elkholy, S. and Meguro, K., 2004. *Numerical Simulation of High-rise Steel Buildings using Improved Applied Element Method*. 13<sup>th</sup> World Conference on Earthquake Engineering, Vancouver, Paper No. 930.
- Meguro, k. and Tagel-Din, H., 2001. *Applied Element Simulation of RC Structures under Cyclic Loading*. Journal of Structural Engineering, ASCE 127 (11), 1295-1305.
- Meguro, K. and Tagel-din, H., 2002. *Applied Element Method used for Large Displacement Structural Analysis*. Journal of Natural Disaster Science 24(1), 25-34.
- Vimonsatit, V., Tan, K. and Ting, S., 2003. *Nonlinear Elastoplastic Analysis of Semirigid Steel Frames at Elevated Temperature: MP Approach*. Journal of Structural Engineering 129(5), 661-671.
- Wong, M. B., Ghojel, J. I., and Crozier, D. A., 1998. *Temperature-time Analysis for Steel Structures under Fire Conditions*. Struct. Eng. Mech. 6(3), 275-289.

# **WATER SCREEN FIRE DISASTER PREVENTION SYSTEM- CHARACTERISTICS OF WATER SCREEN AS PARTITIONING TECHNOLOGY**

REIKO AMANO<sup>1</sup>, YOUICHI IZUSHI<sup>2</sup>, HITOSHI KURIOKA<sup>2</sup>, HIDEAKI KUWANA<sup>2</sup>, TAKASHI TSURUDA<sup>3</sup>, TAKESHI SUZUKI<sup>3</sup>  
AND YOSHIO OGAWA<sup>3</sup>

<sup>1</sup>University of Tokyo Visiting Professor, Kajima Corporation, Tokyo, Japan

<sup>2</sup>Kajima Corporation, Tokyo, Japan

<sup>3</sup>National Research Institute of Fire and Disaster, Tokyo, Japan

amanor@kajima.com

## **ABSTRACT**

*With the enforcement of the Special Measures Act for Public Use of Deep Underground as well as with ongoing urban renewal, there is a need for fire disaster prevention technology to secure the occupants' safety in case of fire breaking-out in any underground space.*

*In this respect, a fire disaster prevention system using a water screen was developed for potential fires in underground spaces. This system is aimed at securing the occupants' integrity from the fire by partitioning the fire zone using a water screen and also at the safety of a structure by reducing damage due to the fire. It would correspond to the performance-based-design for providing refuge for the occupants.*

*In the paper to be prepared, results obtained from experiments on the characteristics of the water screen when used as partitioning technology will be described.*

## **1.0 INTRODUCTION**

With the enforcement of the Special Measures Act for Public Use of Deep Underground as well as with ongoing urban renewal, there is a need for fire disaster prevention technology in the case of a fire breaking out in any underground space or in tunnels.

With regard to this, a fire disaster prevention system using water screens was developed. The aim of this system is to secure the occupants' safety from the fire by partitioning the fire zone using water screens (hereafter referred to as WS). This technology creates water screens by spraying water with a droplet diameter of about 200  $\mu$  m out of nozzles arranged in a line for the partitioning.

In order to understand the partitioning effects of the WS in the case of a fire, fire tests were carried out in a road tunnel. The results of the first fire test using n-heptane mixed with 5% toluene as the origin of a fire have already been reported on.

In this paper, the details and results of a second test using gasoline as the origin of a fire are described.

## **2.0 TEST OUTLINE**

### **2.1 Aim of test**

This experiment aims at understanding the formation of the WS including their installation angle as well as the characteristics of the WS for isolating the origin of a fire in the case of the wind speed being controlled at 2m/sec by ventilators during a fire in a road tunnel with a vertical ventilation system. The other purpose is to investigate whether or not the partitioned environment can allow the occupants to survive in the case of a fire breaking out.

### **2.2 Experiment facility and model**

The experiments were carried out at the overall fire test facility. The large area used for the experiments was 25m high, 25m wide and 120m long. Smoke was introduced through 12 ports at a rate of 2000m<sup>3</sup>/min in total.

The model shown in Photo.1 was scaled down to 1/2 the size of a tunnel with the AA rank in the first class category for road standards. The model, composed of steel frames and fireproof panels, was a box with a height of 2.7m, a breadth of 5.4m and a length of 18.2m. On the sides of the model, fireproof glass windows were installed at 3 locations for the observation of the progress of the fire and the WS in operation.



*Photo 1: Entire view of the model*

Nozzles for the WS were arranged in two parallel lines which were about 1.6m apart from each other and formed the partition boundary in the vicinity of both of the end openings of the model. 5 or 6 nozzles were fixed

in a zigzag pattern in each line at 1.0m intervals. The total amount of water sprayed from the 11 nozzles installed on each side was 110L/min.

Smoke exhaust ducts and fans were installed at both of the end openings and in the center of the model.

### 2.3 Establishment of fire origin

Ordinary passenger cars were assumed as the origin of the fire in two cases, one of a single car and the other of 3 or 4, and the heat release rate for the combustion scale was set at 1.5MW and 5.0Mw respectively with consideration to the reduced scale ratio. A fire plate with a diameter of 1,000mm and a height of 200mm was placed at the center of the floor of the model in order to burn gasoline over a period of 10 minutes. The WS began to work 30 seconds after igniting the gasoline.

### 2.4 Measurement points

#### 2.4.1 Temperature distribution on the inside and outside of partitioned area

The atmospheric temperatures of the inside and outside of the fire zone which are partitioned from the fire using the WS were measured using sheath type thermocouples. The thermocouples were installed at 200mm intervals on the inside and outside of the partitioned area respectively and suspended 50mm below the surface of the ceiling. Fig.1 shows the measurement locations.

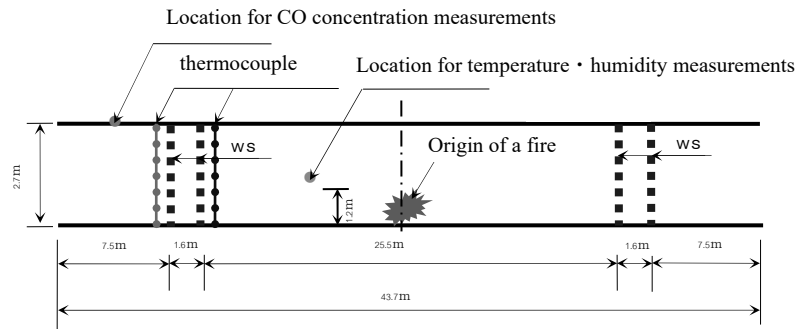
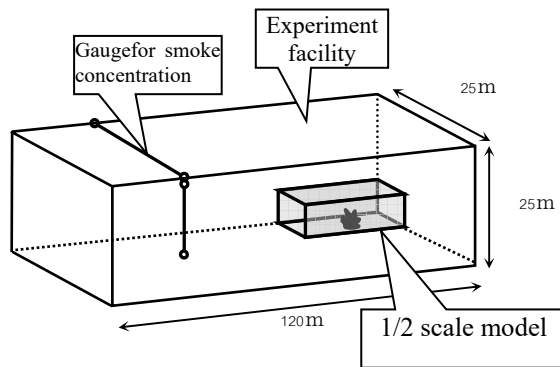


Figure 1: Measurement equipment installation in vertical section of the model

#### 2.4.2 Smoke concentration in the experiment facility

Figure 2 shows the locations where smoke concentration gauges were installed. The concentration of the smoke which filled the experiment area after rising up from the model was measured in the case of the WS being used and in the case when it was not used. The light concentration value was also measured using concentration gauges with photoelectric separating type sensors installed in vertical and horizontal directions (with a height of 9.9m~22.5m) at the ends of the experiment areas.



*Figure 2: Measurement equipment installation in vertical section of the experiment facility*

#### **2.4.3 CO concentration on the outside of the partitioned area**

The difference in the CO concentration of the smoke sampled by smoke exhaust ducts and fans installed at both openings of the model between in the case of the WS being used and in the case when it was not used was measured using CO concentration gauges. The measurement locations are shown in Fig.1.

#### **2.4.4 Temperature and humidity on the inside of the partitioned area**

The temperature and humidity with regard to the height of a human body (1.2m from the floor surface) in the case when the partitioned area was formed using the WS were measured using gauges for temperature and humidity installed halfway between the origin of the fire and the WS (6.3m from the center of the model). Fig.1 shows the locations of these gauges.

#### **2.4.5 Spray distribution of the WS**

Several fans for industrial use were installed at one opening of the model in order to create a wind in the tunnel. For the purpose of understanding the formation of the WS caused by the presence of wind speed, the water spray distribution was calculated from the amount of water collecting in each of 25cm square measuring devices which were spread all over the floor in the vicinity of the WS.

### **3.0 TEST RESULTS**

#### **3.1 Temperature distribution on the inside and outside of the WS**

Figs.3~6 illustrate the results of the atmospheric temperature measurements carried out on the inside and outside of the WS in the case of the WS being used. Figs.3 and 5 indicate the measurement results under a dead calm. Figs.4 and 6 indicate the results in the case of the wind speed



being 1.4m/s. The wind speed described in this paper is set with consideration to the reduced scale ratio and it corresponds to 2.0m/s in the case of converting it into the actual scale.

As can be seen in Figs.3 and 4, in the case of 1.5MW for the heat release rate, there was smoke in the proximity of the ceiling surface in the fire zone partitioned by the WS and the temperature in this area climbed up. The temperature in the vicinity of the ceiling on the outside of the WS fell. It can be seen from Fig.3 that under a dead calm the temperature on the outside of the WS dropped by 74% of the temperature in the vicinity of the ceiling surface. Fig.4 illustrates that the temperature under windy conditions dropped by 68% near the ceiling surface.

In the case of 5.0MW, it was discernible that the temperature fell by 79% under a dead calm as shown in Fig.5 and by 85% under windy conditions as shown in Fig.6 respectively.

It was confirmed from the above that the temperature of the air and smoke in the proximity of the ceiling surface was reduced by 70~80% due to the use of the WS regardless of the existence of wind.

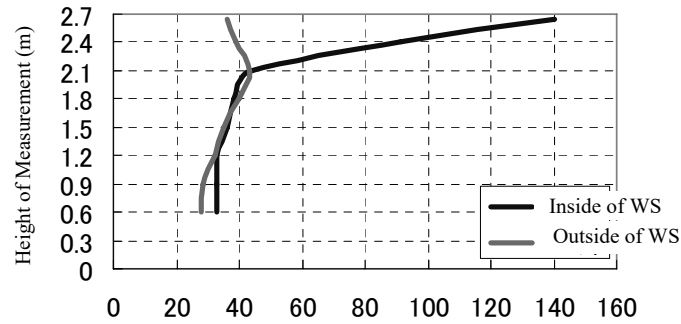


Figure 3: Temperature distribution on the inside and outside of WS  
(No wind 1.5MW)

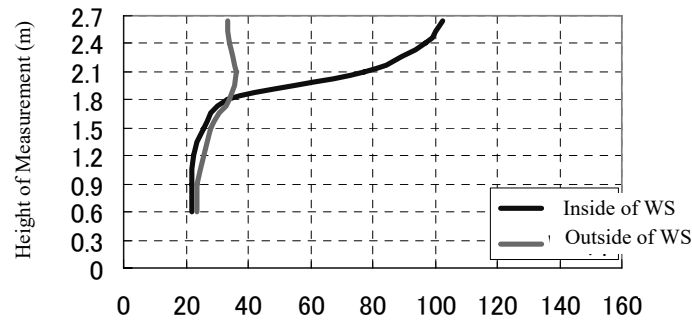


Figure 4: Temperature distribution on the inside and outside of WS  
(wind speed 1.4m/s, 1.5MW)

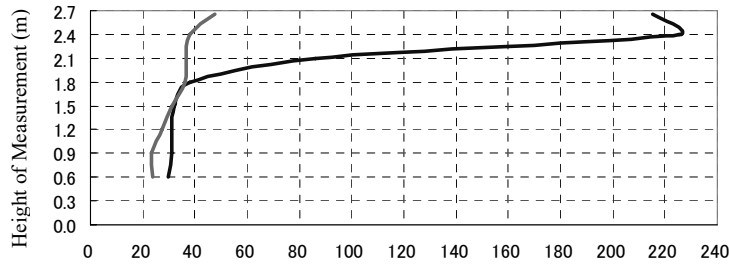


Figure 5: Temperature distribution on the inside and outside of WS  
(No wind 5.0MW)

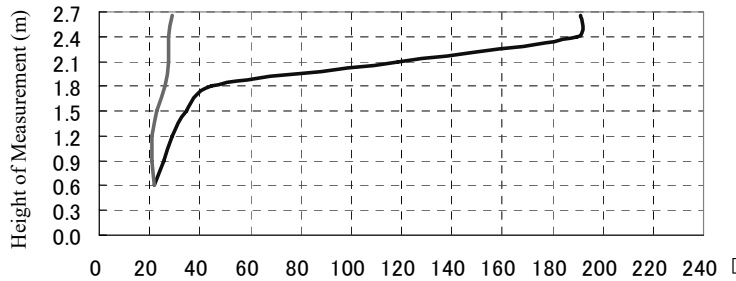


Figure 6: Temperature distribution on the inside and outside of WS  
(Wind speed 1.4m/s, 5.0MW)

### 3.2 Smoke concentration measurement results

Fig.7 illustrates the time history of the measured values for the smoke concentration obtained in the test facility in the case of 1.5MW. When assuming that the value obtained by integrating the measured value using the time axis corresponds to the total amount of the smoke flowing out of the model into the test facility, the temperature was reduced by 78% under a dead calm when the WS was used in the case of 1.5MW. When the wind speed was 1.4m/s, the temperature was reduced by 60% of the value in the case of the WS not being used. It was confirmed from the above that regardless of the existence of wind, 60~80% of the smoke rising from the origin of the fire was isolated by using the WS.

### 3.3 CO concentration measurement results on the outside of the partitioning area

The maximum value for CO concentration obtained by analyzing the smoke rising from the fire origin, collected at the ceiling of the opening of the model, in both cases of the WS being used and not being used was reduced by about 15% under a dead calm in the case of 1.5MW and was

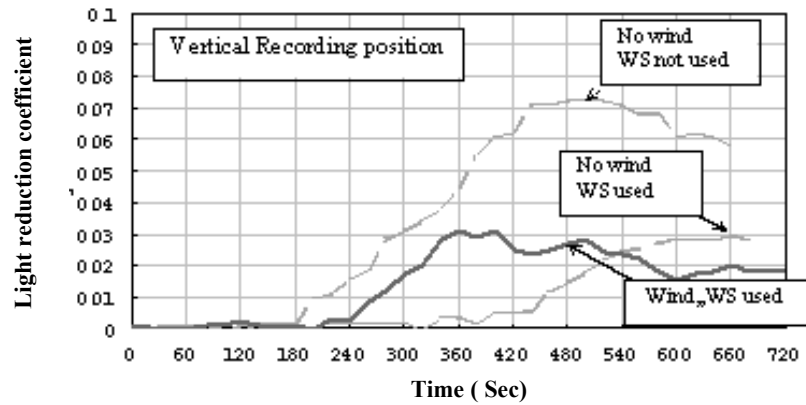


Figure 7: Time history graph of smoke concentration in the experiment Facility.

reduced by about 45% when the wind speed was 1.4m/s. It was thought that the fact that the temperature fell only 15% under a dead calm was caused by CO which is insoluble in water instead of the partitioning of the WS. It can be thought that the great decrease in the CO concentration in the case of 1.4m/s was caused by the incomplete collection of the smoke at the opening of the model due to the effects of the wind. Therefore, the reduction ratio of the CO concentration in the outside of the area partitioned using the WS was set at about 15%.

### 3.4 Temperature and humidity measurement results on the inside of the partitioned area

It was confirmed that the temperature as well as the humidity on the outside of the partitioned area while the WS was used did not reach the condition that is critical for human life. (Human bodies are exposed to the critical condition in 5 minutes when the humidity is 100% and the temperature is 50°C or more according to field guide to fires) the humidity rose to 100%, but the temperature was 20°C which was the exterior temperature. The maximum recorded temperature was 35°C.

### 3.5 WS Spray distribution measurement results

With regard to the water spray distribution of the WS under a dead calm, the maximum value for the spraying amount was seen at the center of the WS nozzle. (See Fig.8) In the case of the wind speed being 1.4m/s, the location for the maximum value of the spraying amount shifted to a point of 1.8m on the leeward from the center of the WS nozzle. (See Fig.9) It was confirmed from the above that the spraying angle was 33°. Furthermore, it was discernible from the eye measurement that in the case of 1.4m/s for the wind speed, the water screen was formed extending from the ceiling surface down to the floor surface.

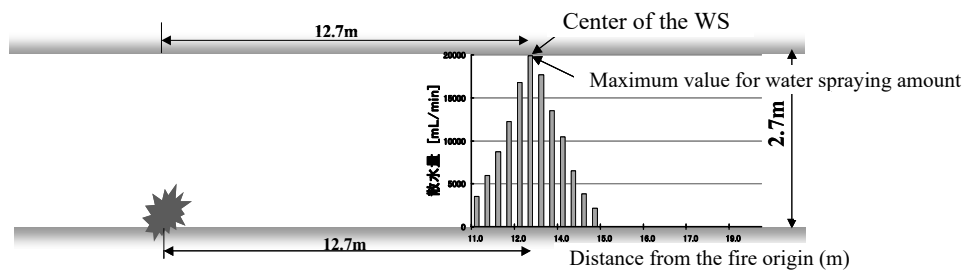


Figure 8: Water spraying graph (no wind)

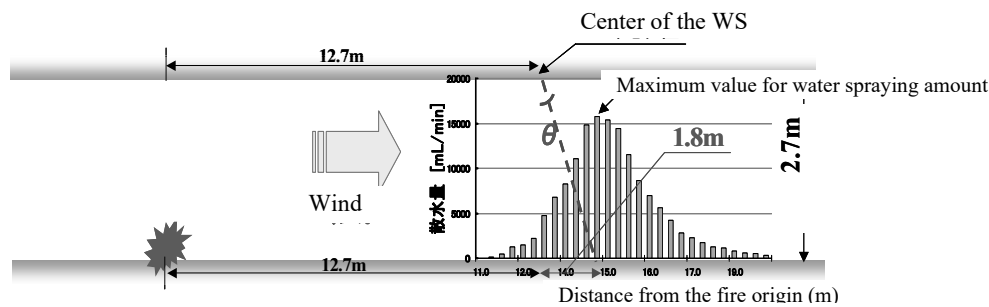


Figure 9: Water spraying graph (wind speed 1.4m/s)

#### 4.0 CONCLUSIONS

- As for the characteristics of the WS for the partitioning of a fire zone, it was confirmed that the isolation effects for heat, smoke and poisonous gas (CO) were 70~80%, 60~80% and 15% respectively.
- It was discernible that in the case of the wind speed being 1.4m/s (the wind speed converted to that on an actual scale: 2.0m/s), the WS was formed at an angle of 33° where the same effects were recognized.
- It was also confirmed that the occupants could survive in the fire zone partitioned using the WS and that activities for refuge and fire fighting could be effectively carried out.

As a result, the validity of the WS as partitioning technology for a fire was verified.

#### ACKNOWLEDGEMENT

We would like to express our thanks to the staff concerned of the HOCHIKI Corporation who gave us a great deal of cooperation for the experiments and analyses.

#### REFERENCES

Reiko Amano, Yoichi Izushi, Hitoshi Kurioka, Hiroomi Sato, Hideaki Kuwana, Takashi Tsuruda, Yoshio Ogawa, Takeshi, 2004. *Water Screen Fire Disaster Prevention System in Underground Space*. 6th Asia-Oceania Symposium on Fire Science and Technology, Soal [1].

# **URBAN FLOOD MODELING IN LOWER MEKONG BASIN: A PHYSICALLY BASED DISTRIBUTED MODELING APPROACH**

D. DUTTA<sup>1,2</sup>, M.J. ALAM<sup>1</sup> AND S. HIRONAKA<sup>3</sup>

<sup>1</sup>RNUS, SCE, Asian Institute of Technology, Thailand

<sup>2</sup>ICUS, IIS, University of Tokyo, Japan

<sup>3</sup>NEWJEC Inc., Tokyo, Japan

ddutta@ait.ac.th

## **ABSTRACT**

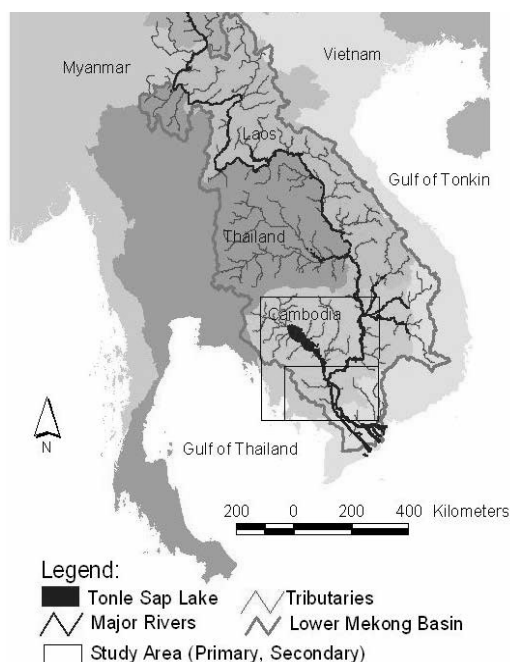
*This paper presents the results of an application of a distributed model in the lower Mekong River basin for flood inundation analysis. The distributed hydrological model is a combined surface-river flow model which solves the one-dimensional (1-D) unsteady flow equation for river channel flow and two-dimensional (2-D) flow equation for each grid of the floodplain simultaneously to calculate the flood inundation parameters in the basin. The calculations of flow from river channel to flood area caused by flood levee failure or overtopping of levee, flow from flood area to river channel such as sluice, pump etc., moreover, condition of basin or river channel, are done by using some suitable equations in conditions. The study area is the Cambodian floodplains of the Mekong River. In preliminary, the simulation has been carried out for the flooding condition of 2000. The simulated flow along the major rivers show close agreement with the observations. The results from the model application are presented here.*

## **1.0 INTRODUCTION**

The Mekong basin, one of the important and largest river basins in the world, originates in the highland of Tibet in China and ends in the South China Sea comprising the territories of six Southeast Asian countries- China, Myanmar, Lao PDR, Thailand, Cambodia and Vietnam. The drainage area of the basin is 795,000 km<sup>2</sup> with a total length of 4,620 km (Hori, 2000). The Lower Mekong basin covers 78% of the total basin area which includes four riparian countries of the region: Laos, Thailand, Cambodia and Vietnam (Figure 1).

The flooding in the Mekong basin, a very common phenomenon occurring several times a year, greatly varies in magnitude and extent in different parts due to spatial variability and local hydro meteorological characteristics including rainfall distribution. In the lower reaches of Cambodia, where the land is low and flat, a larger area is usually inundated. In 2000 during the period of August-November, the Lower Mekong region observed a record breaking flood in Cambodia and Vietnam estimating about 600 casualties, over 300,000 evacuated people and altogether with highest recorded water level in Phnom Penh since records began (Dutta, 2000). The reasons for the recent year's floods are reportedly due to

deforestation, reclaiming of land, urban expansion and the decrease of natural channels for the basin development (Kazama, et al., 2001). The frequency of flooding is also increased in the lower part.



*Figure 1: Location map of study area*

The flood modeling in the Mekong was first initiated in the decade of 1960 with a view to an establishment of a basin wide flood warning system for the alleviation of adverse effect of floods in the areas along the Mekong River and the Delta (Dutta and Herath, 2001). After the development of a flood forecasting system through UNDP program in 1970, the flood modeling has got a momentum to continue in different forms from simple black box or conceptual modeling to complex hydrodynamic system by various organizations. With the rapid progress in computational resources, there have been tremendous development in modeling approaches over the world, and some of these approaches have also been applied in Mekong Basin. A geomorphology based distributed hydrological model was applied to the upper central part of Mekong River basin, from Luong Prabang station at the boarder of China up to the Stung Treng gauging station in Cambodia, covering an extent of 402,636 km<sup>2</sup> as an initial study on distributed hydrological simulation in Mekong river basin (Herath et al., 2000). To evaluate multi-functional hydrologic role, a hydrologic model was applied to Tonle Sap and its vicinities (Masumoto, 2000). One-dimensional modeling along with 2-d model in Chaktomouk junction of Mekong River was carried out within the present study area in connection with morphological study (Olesen, 2000). Although, a great progress of flood modeling in Mekong River basin could be seen, there is still need of improvement in the existing approaches. Another limitation is that data availability and integration in the model development.

In this research, the Cambodian flood plain of the Mekong river, Tonle Sap Channel and Bassak river is selected as study area for modeling. These lower reaches of the Mekong River (below Kratie) have different hydrologic and hydraulic characteristics than the rest of the Mekong basin. The flow patterns in these portions of the basin are characterized by very low water surface slopes, inundation of a huge floodplain during and after the annual flood peak, and deposition of a fraction of the suspended sediment on the river dykes and adjacent floodplains (MRC, 2003).

## 2.0 MODELING APPROACH

### 2.1 Outline of the model

The distributed model used in this study is a coupled surface-river flow model, which has been designed to calculate the flow parameters in the river channel and floodplain simultaneously. The model was originally developed by the Public Work Research Institute (PWRI), Japan (Yoshimoto et al., 1992). The main characteristic of the model is the link between unsteady calculation in river channel and calculation of flood depth in river basin to reproduce the flood inundation phenomenon in large scale over the whole river system. The relation between stage in river channel and height of levee decides the points and scale of flood levee failure with unsteady calculation in river channel. A schematic diagram of the model is shown in Figure 2.

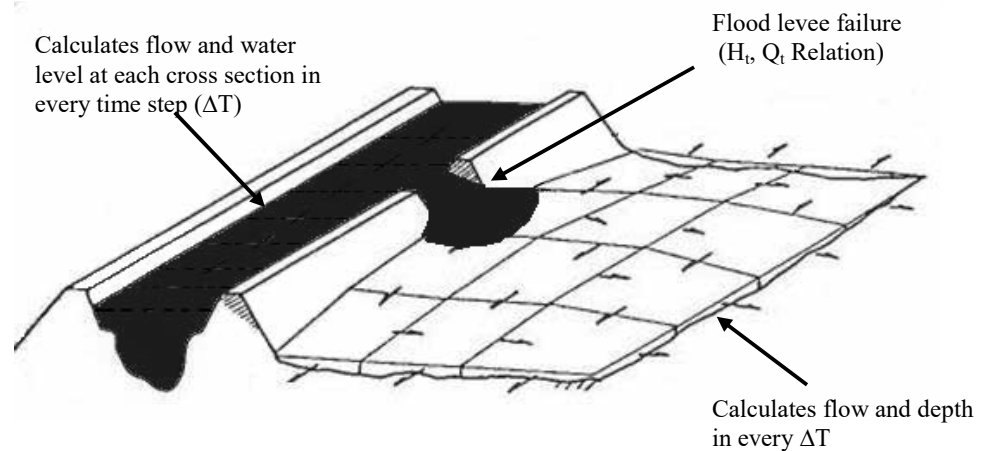


Figure 2: Outline of the model (adapted from Yoshimoto et al., 1992)

### 2.2 Governing equations

Basically, the model uses two dimensional unsteady flow equations for flood flow calculation in basin, and one dimensional unsteady equation for river flow. However, outside of these, flow from river channel to flood area caused by flood levee failure or over flow of levee, flow from flood area to river channel such as sluice, pump etc., moreover, condition of basin or river channel, in some cases these equations are not applicable, where some suitable equations are used in conditions. For example, in case of calculation about flood plain, local phenomena which is unable to solve with energy

equation as long as not using empirical coefficient occurred at the points where gradient of flood plain changes suddenly except the effects due to weir of bank, calculation is done using other equations as discussed in the sections below (Yoshimoto et al., 1992). Besides, model uses empirical equation for calculation of flow in box culvert or over banking flow when embankment exists on the flood plain. The unsteady equations are derived from continuity and momentum equations for one dimensional as well as for two dimensional flows.

## 2.3 Model setup

### 2.3.1 River system

For preliminary simulation, a small part of river system near Phnom Penh city has been considered which includes Mekong River (Below Kompong Cham), Bassak River and Tonle Sap Channel as shown in Figure 3 with hydrological gauging stations. The river setup has been assigned with cross sections. The raw cross sections data have been processed and given as H-B-A-R (Height-Width-Area- Hydraulic Radius) relation in the model. The details of cross-section of the the river system are given in Table 1.

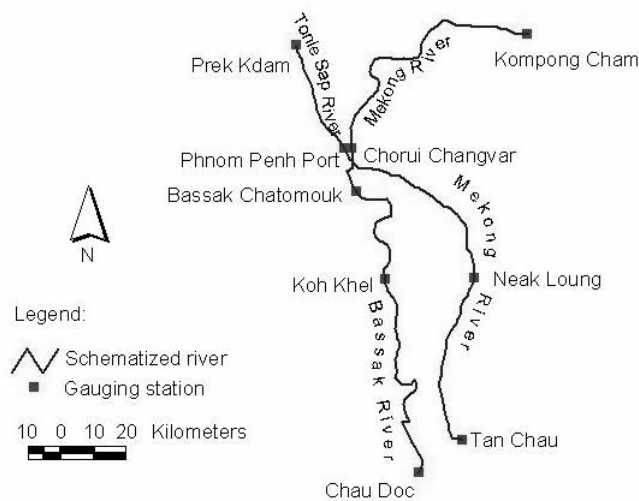


Figure 3: Model River Network

In river cross sections the link between the 2-D grids of the flood plain and the river channel is specified. The relation between stage in river channel and height of levee decide the points and scale of flood levee failure with unsteady calculation.

Table 1: Details of Model Rivers

Rivers	U/s locations	D/s location	No. of cross sections
Mekong	Kompong Cham	Tan Chau	84
Bassak	Mekong Ch.213.0 km	Chau Doc	32
Tonle Sap	Mekong Ch.213.0 km	Prek Kdam	38



### 2.3.2 Model grid

Rectangular grid of 1 km resolution has been used in this study. The total number of grids within the study area is 121113. The source of the Digital Elevation Model (DEM) is the Mekong River Commission Secretariat (MRCS), which has originally been derived from various sources data (Figure 4).

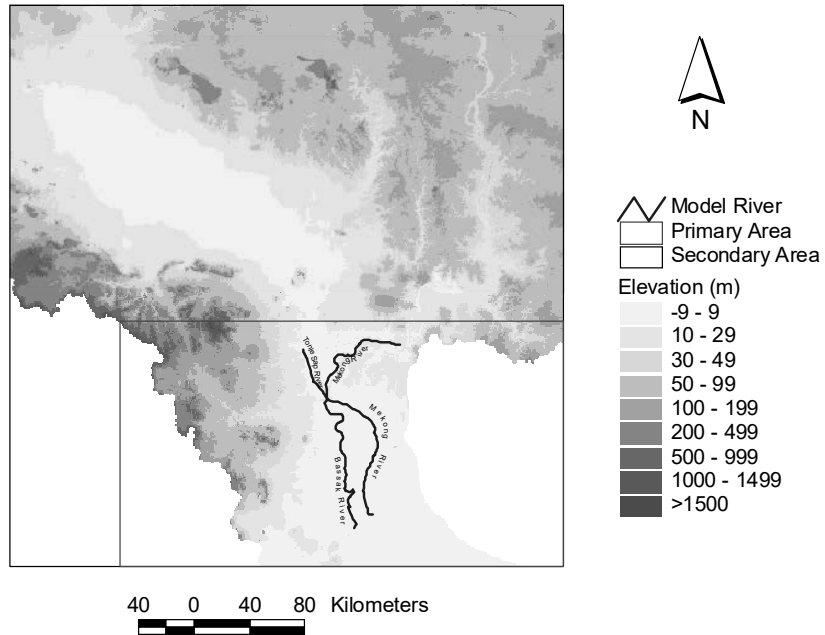


Figure 4: DEM of the Model Area (Source: MRCS)

### 2.3.3 Structures and other information

The model has the provision of incorporating hydraulic structures like weir, culvert and pumping options for drainage and retarding basin. The embankment or road alignment along with structures information gives the true description of the physical system. However, not all of these information are incorporated properly yet in this simulation, which are being updated from the available source for final calibration of the model.

### 2.4 Model application

The model has been applied for simulation of flooding during the period of 1<sup>st</sup> of July to 31<sup>st</sup> October of 2000. The stability of simulation is very much dependent on grid spacing and the time step used in computation. In use of 1 hour time step, stable simulation has been obtained. Rainfall has been specified as an internal runoff on the model grid. Evaporation value has been deducted from daily rainfall value to calculate the net rainfall. Based on the Thiessen polygon developed for the project area, rainfall has been distributed over the grid as internal runoff ( $\text{m}^3/\text{s}$ ). At 46 locations the rainfall data is available for 2000 and evaporation data available only in one station at the MRCS Headquarter. The average of daily rainfall of 46 stations is shown in Fig. 5.

### 2.4.1 Initial and boundary conditions

The initial water level in the river channels has been specified based on observed data. However, the flood plain has been considered dry at initial time step. The time series boundary data has mainly been obtained from the project of Consolidation of Hydro-Meteorological Data and Multi-Functional Hydrologic Roles of Tonle Sap Lake and Its Vicinities (Basinwide) (MRC, 2003). At the upstream of Mekong River a time series of daily discharge has been provided as an inflow. The discharge data has been generated based on a rating curve developed by 2002 observed data. The inflow boundary is shown in Fig. 6. At the down stream boundary locations daily observed time series water level data has been specified. Boundaries of the flood plain grid have been assumed closed, i.e. no flow is going out or coming into the basin through the boundary meshes.

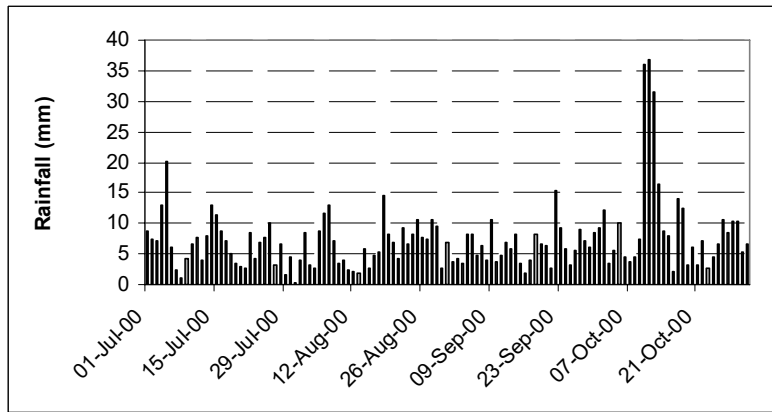


Figure 5: Average of daily rainfall of 46 stations around the study area

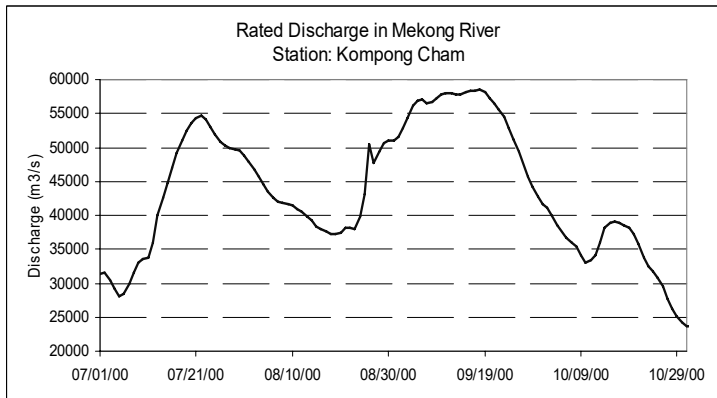


Figure 6: Inflow boundary to the upstream of Mekong River

#### **2.4.2 Roughness coefficient**

A fixed value of Manning roughness coefficient has been specified in each cross section of river channels. The roughness value for river channels is 0.03. For the flood plain grid the roughness value has been used based on the land use type. The landuse map of 1km resolution for the study area was obtained from Global mapping project. Besides, in roughness calculation, model also considers the occupied housing ratio in the each grid of the flood plain.

### **3.0 RESULTS AND DISCUSSIONS**

The simulation results of river water levels for the period of July 1<sup>st</sup> to October 31<sup>st</sup> of 2000 have been compared with the observed water levels at different gauging stations along the four river branches in the study area. In absence of any field observation, the simulated extents of flood inundation have been compared with satellite imagery. Fig. 7 shows the comparison of simulated and observed daily water levels at the gauging stations of Meklong river (Choroi Changvar and Neak Loung stations), Basak river (Koh Khel station) and Tonle Sap river (Phnom Penh Port station). The locations of these gauging stations are shown Fig. 3. It can be observed from the comparison that the simulated water levels match well with observed ones in Mekong and Basak Rivers. However, the simulated water level is much higher than observed water level at Phnom Penh Port in Tonle Sap river. The Tone Sap lake in the upstream of this river influences the flow characteristics greatly. For improvement of the simulated results, it will be important to incorporate this lake in the simulation.

The simulated maximum flood inundation extents and depths of September 20, 2000 are shown in Fig. 8. By comparing simulated inundation map with the flood extent observed from the LANDSAT TM image of September 26, 2000 (as shown Fig. 9), it can be noticed that the simulated flood pattern and locations agree well with the actual flooding. However, the simulated flood extent is much lesser than the observed flood extent from the remote sensing image along the Mekong and Tone Sap rivers. There are two major possible reasons for this. The first reason is that in simulation there no consideration of flood water entering to the study area from outside over the ground, only inflow along the river system is considered as the upstream boundary conditions. However in reality, there is a large amount of water entered to the study area as overland flow. The other possible reason is the low resolution of the DEM considered in the model. Flood modeling is very sensitive to DEM, it is required to consider high resolution topography dataset for obtaining better modeling outcomes.

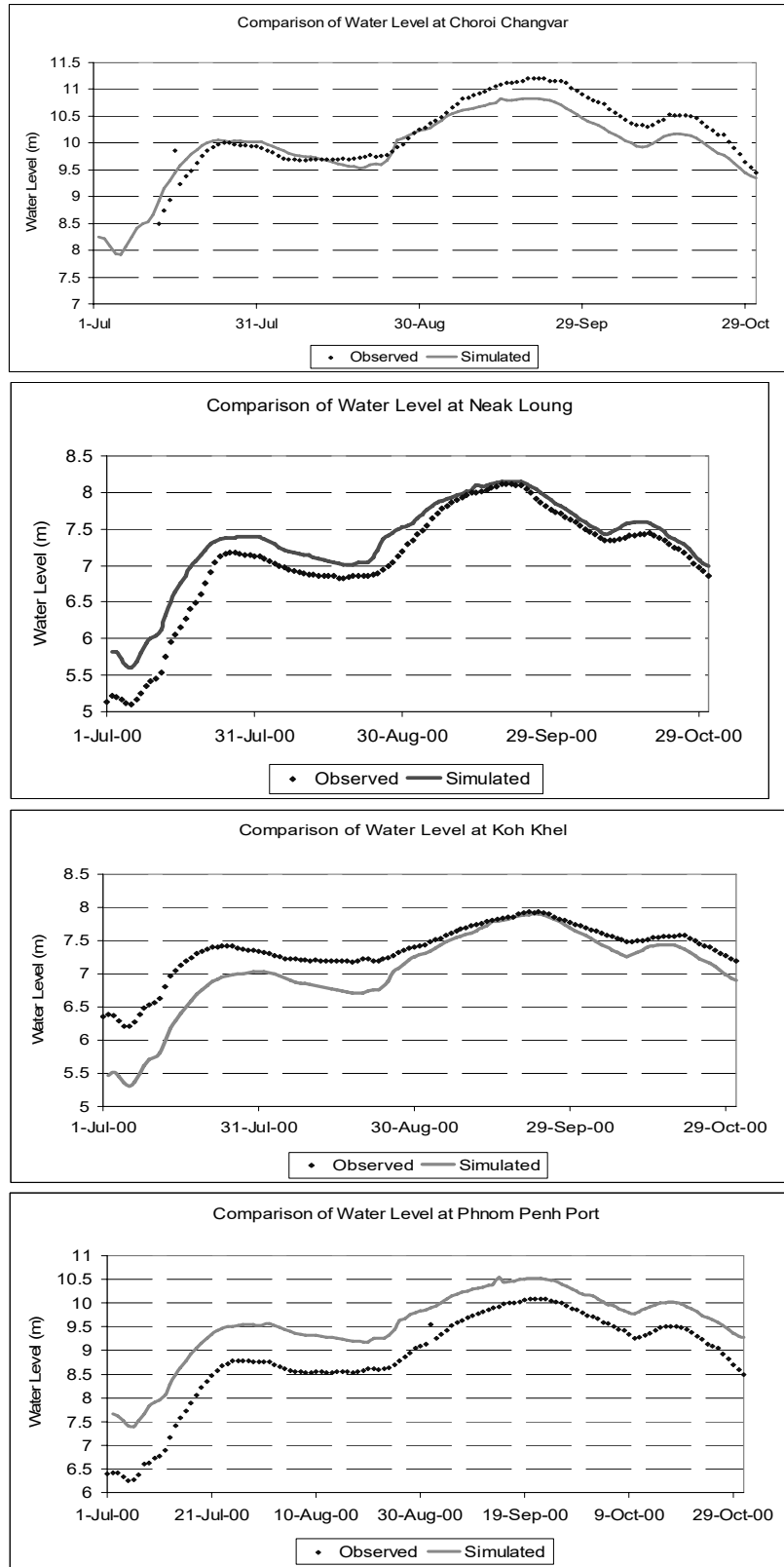
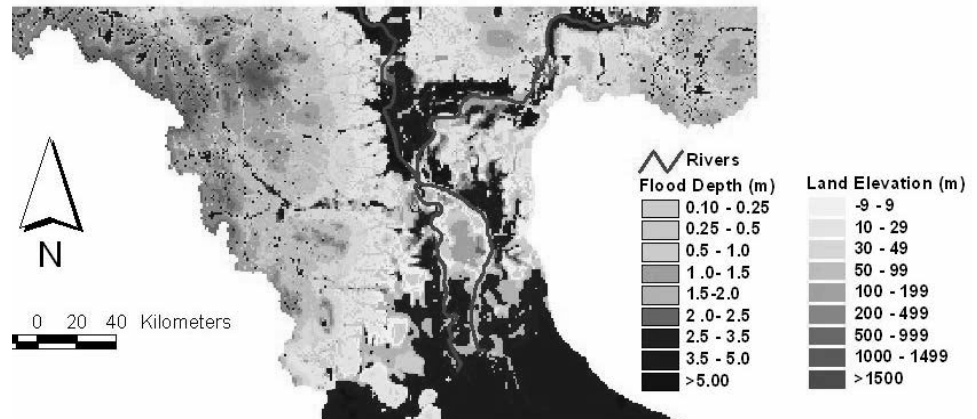
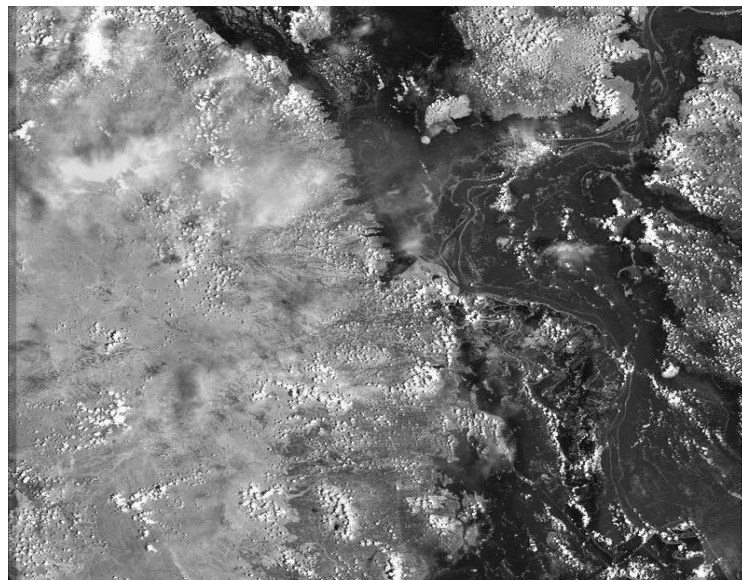


Figure 7: Comparison of simulated and observed water levels at the gauging stations Choroi Changvar, Neak Loung, Koh Khel, and Phnom Penh Port



*Figure 8: Simulated maximum flood depths and extents*



*Figure 9: LANDSAT image on flood of 26 September 200*

#### **4.0 CONCLUSION**

In this paper, a physically based distributed surface-river model has been introduced and the results of flood inundation simulation in an urban area in the lower Mekong basin have been presented. The simulated water levels along the Mekong and Basac rivers show close agreement with the observation. However, the extent of simulated flood inundation is lesser than that is observed from satellite data. It is required to improve the simulated inundation with realistic consideration of inflow from outside and higher resolution of DEM and the simulated flood inundation parameters in different locations should be thoroughly verified with the ground observation.

This is an on-going research project. In the next phase of simulation, the study area will be extended to cover the Tonle Sap Lake, which has a great influence in flood characteristics and flood inundation simulation will be carried out with updated details of topography and surface boundary conditions to consider the flow influx from outside of the study area.

## REFERENCES

- Chow, Ven Te, Maidment, David R., Mays, Larry W. 1988. *Applied Hydrology*. McGraw-Hill, Inc., pp35.
- Dutta, D. and S. Herath 2001. *Flood Modelling Experiences in Mekong River Basin*. Proceedings of the International Symposium on Achievements of IHP-V in Hydrological Research, Hanoi, Vietnam, IHP-V Technical Document in Hydrology No. 8, pp.51-52.
- Dutta, D. 2000. *Devastating Floods in Cambodia*, 2000. INCEDE Newsletter. Vol. 9, No. 1, pp. 1-4.
- Herath, S and Yang, D.2000. *Distributed Hydrologic Modeling in Mekong Basin*. Proceedings of the workshop on Hydrologic and Environmental Modelling in the Mekong Basin, 11-12 September 2000, Phnom Penh, pp30.
- Hori, H. 2000. *The Mekong: Environment and Development*. United Nations University Press, Japan, ISBN: 92-808-0986-5, pp1.
- Kazama, S., Hagiwara, T. and Sawamoto, M. 2001. *Temporal and Spatial Inundation Pattern Revealed by Numerical Simulation of the 2000 Flood in the Lower Mekong*. Proceedings of the International Symposium on Achievements of IHP in Hydrological Research, Hanoi, Viet Nam, 19-22 November 2001, IHP-V Technical Document in Hydrology No.8, International Hydrological Programme, UNESCO Jakarta Office.
- Masumoto, T. 2000. *Modelling of Multi-Functional Hydrologic Roles of Tonle Sap Lake and Its Vicinities*. Proceedings of the workshop on Hydrologic and Environmental Modelling in the Mekong Basin, 11-12 September 2000, Phnom Penh, pp181.
- Mekong River Commission (MRC). 2003. *Consolidation of Hydro-Meteorological Data and Multi-Functional Hydrologic Roles of Tonle Sap Lake and Its Vicinities (Basinwide)*. Draft Final, Main Report, pp1-1.
- Olesen, K. W. 2000. *Morphological Modelling of the Chaktomuk Junction*, Proceedings of the workshop on Hydrologic and Environmental Modelling in the Mekong Basin. 11-12 September 2000, Phnom Penh, pp289.
- Yoshimoto, T., Fueda, T., Ikeda, Y., Kawakami, T. 1992. *Technical Memorandum of Public Work Research Institute (PWRI)*. Flood Simulation of Two Dimensional Unsteady Flood Model, Public Works Research Institute, Japan , T. M. of PWRI No.3105, ISSN 0386-5878.
- Geographical Survey Institute. 1997. *Global Map'97 Dataset*. Secretariat of the International Steering Committee for Global Mapping, Kitasato 1, Tsukuba, Ibaraki, 305-0811, JAPAN.

# **HYDRAULICS COMPUTATIONS TO STUDY FLOOD CONTROL FOR HA NOI CITY, VIETNAM**

TRAN THUC<sup>1</sup> AND NGUYEN HUU PHUC<sup>2</sup>

<sup>1</sup>Institute of Meteorology and Hydrology, Viet Nam

<sup>2</sup> Department of Flood Control and Dike Management, Viet Nam

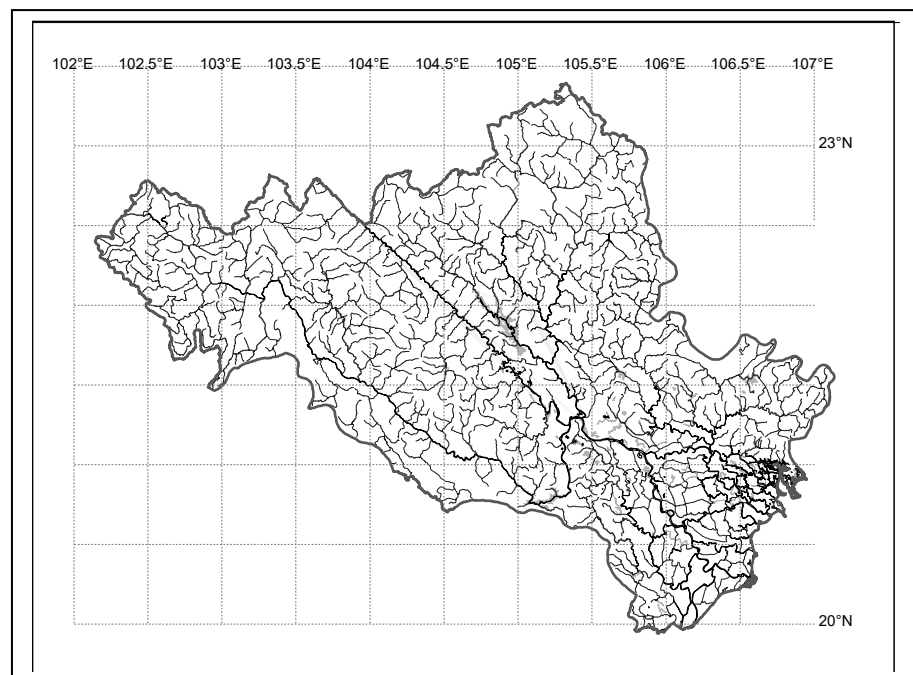
thuc@netnam.vn

## **ABSTRACT**

*Hydrodynamic model was applied for the Red River system, North Viet Nam to evaluate the effectiveness of the existing flood control measures in the river basin. Results of computations show that the current flood control structures of the Red River basin cannot cope with extreme flood, water level at Ha Noi is still higher than the designed value. Emergency spillways on the dike system were studied and it is found that they can significantly reduce water level at Ha Noi. With the use spillways, water level at Ha Noi can be kept lower than the designed value when a 2000-year return period flood occurred.*

## **1.0 INTRODUCTION**

The Red River system with a catchment area of about 143,000 km<sup>2</sup> is the biggest river system in North Vietnam. There are three main river tributaries, namely, Da River, Thao River and Lo River. The Red River system and its tributaries are shown in Fig. 1.



*Figure 1: Red river system*

Strategy for flood prevention in Red river Delta is “actively preparing for flooding”, including 6 basic measures: planting and protecting upstream forest, flood regulation by reservoirs, dyke system, flood drainage, flood diversion and detention.

*Reforestation and watershed protection:* The country has 19 million ha of forest land, but only about a half of the area is covered by forest, the remaining is covered by grass, bushes and scattering trees. Forest area is reduced very quickly due to shifting cultivation, irrational wood exploitation. The Viet Nam Government has been implementing activities of reforestation program in mountainous areas.

*Dyke system:* It is the main and most important measure. In the Red River delta, there is a river dike system of 2,000 km in length to protect the urban centers and the important economic zones. At present and in the future, dyke will remain the main and most effective flood prevention measure. In general, dyke systems in the Red River basin can stand against designed flood. However, it cannot cope with extreme flood, if a 1000-year return period flood happened, dyke might break.

*Flood regulation:* Hoa Binh Reservoir is a large-scale reservoir built in 1979 on the Da River, some 70 kilometers to the northwest of Ha Noi with a total storage capacity of 9.45 billion m<sup>3</sup>. In the Da River water resources development plan, a cascade of reservoirs will be built on the Da River, upstream of Hoa Binh reservoir.

*Flood diversion:* Day River flood diversion is responsible to divert flood of the Red River to Day River with a design discharge of 5,000 m<sup>3</sup>/s. However, due to flood plain encroachment, some calculations have shown that at present, only about 3,000 m<sup>3</sup>/s can be diverted. The most difficult problems for flood diversion in the Day River is that too many people (nearly 700,000) would now have to be resettled, and about 200 km of dykes need to be more frequently repaired.

*Flood detention:* Four areas are reserved for flood detention: Tam Thanh area (200 x 10<sup>3</sup> m<sup>3</sup>), Lap Thach area (100 x 10<sup>3</sup> m<sup>3</sup>), Luong Phu - Quang Oai area (600 x 10<sup>3</sup> m<sup>3</sup>).

*Flood drainage improvement:* After the historical flood in 1971, measures to improve flood drainage have been carried out. However, as dredging need a huge amount of money, difficulty in funding has limited the result of channel improvement.

A lot of experiences have been gained in flood prevention, preparedness. The Red River Delta still has a high potential threat of flooding. It is seen that current flood protection system is still insufficient to cope with extreme flood; more effective measures are needed for flood control and management for the North Viet Nam.





### 2.1.1 Boundary conditions

Upstream boundary conditions are flows at 4 hydrological stations: Hoa Binh, Yen Bai, Vu Quang, Thac Buoi, Cau Son, and Chu stations.

Downstream boundary conditions are tidal water levels at 12 hydrological stations: Nhu Tan on Day River, Truc Phuong on Ninh Co River, Ba Lat on Red River, Dinh Cu on Tra Ly River, Dong Xuyen on Thai Binh River, Kinh Khe on Van Uc River, Kien An on Lach Tray River, Cua Cam on Cam River, and Don Son on Da Bach River.

Cross section data measured in 2000 and hydrological data including water levels and discharges at hydrological stations are used in the computations.

### 2.1.2 Model calibration and verification

Flood data in the year of 1996 are used for model calibration and flood data in the year of 2000 are used for model verification.

From model calibration and verification, it is found that the computed results of water levels and discharges are in good agreement with the measured data, absolute error are small as shown in Table 1.

*Table 1: Results of Model Calibration and Verification*

Station	Absolute Error in Water Level (m)		Station	Absolute Error in Water Level (m)	
	Calib.	Verif.		Calib.	Verif.
Phu Tho	0.08	0.11	Nam Dinh	0.05	0.30
Trung Ha	0.28	0.28	Dap Cau	0.12	0.18
Viet Tri	0.19	0.27	Phu Lang Thuong	0.11	0.01
Son Tay	0.04	0.07	Pha Lai	0.05	0.25
Ha Noi	0.17	0.29	Ben Binh	0.04	0.20
Thuong Cat	0.02	0.28	Cat Khe	0.05	0.12
Ben Ho	0.08	0.29	Phu Luong	0.25	0.29
Hung Yen	0.18	0.08	Ba Nha	0.05	0.15
Trieu Duong	0.06	0.22	Trung Trang	0.25	0.26
Chanh Chu	0.20	0.03	An Phu	0.01	0.13
Tien Tien	0.24	0.00	Cao Kenh	0.15	0.05

## 2.2 Computation scenarios

Basing on the socio-economic, topographic, hydrological and hydraulic conditions of the Red River Delta, 36 emergency spillways on the dike system are identified with the concept of accepting certain damage but avoiding disaster due to dike break.

Characteristics of the spillway such as location, width and crest level, and storage capacity of the downstream area are used in the computations.

All the existing flood control measures in the Red River basin are applied, i.e., Hoa Binh Reservoir regulation, Day River flood diversion, and flood detentions areas.

Two cases are considered in the computations: (1) Case A: Natural flood in the Red River with 1000-year return period, and (2) Case B: Natural flood in the Red River with 2000-year return period.

**Case A:** Natural flow at Son Tay station is 53,000 m<sup>3</sup>/s (1000-year return period). Three scenarios are considered:

- Scenario A.1: Applied all existing flood control structures i.e., flood regulation, flood diversion, and flood detention, but without using emergency spillway. This is to study the capacity of the existing flood control structures in coping with extreme flood.
- Scenario A.2: Applied all existing flood control structures and all the identified spillways.
- Scenario A.3: Applied all existing flood control structures and only some of the identified spillways in the upper part of the river basin.

**Case B:** Natural flow at Son Tay station is 60,000 m<sup>3</sup>/s (2000-year return period). Three scenarios are considered:

- Scenario B.1: Applied all existing flood control structures, but without using emergency spillway.
- Scenario B.2: Applied all existing flood control structures and all the identified spillways.
- Scenario B.3: Applied all existing flood control structures and only some of the identified spillways in the upper part of the river basin.

## 2.3 Results and discussion:

Results of computations for Case A (flood with 1000-year return period) for different scenarios are shown in Table 2. From the results, it is found that:

- With the use of the existing flood control structures (Scenario A.1), maximum water level at Ha Noi reaches a value of 14.97 m, i.e., 0.77 m higher than the designed flood water level at Ha Noi. The existing flood control structures in the Red River basin cannot cope with 1000-year return period flood, emergency spillway is found necessary.
- With the use of the existing flood control structures and all the identified spillways (Scenario A.2), maximum water level at Ha Noi reaches a value of 13.46 m, i.e., 0.74 m lower than the designed flood water level at Ha Noi. The spillways together with the existing flood control structures in the Red River basin can cope with 1000-year return period flood.
- With the use of the existing flood control structures and some spillways upstream of Ha Noi (Scenario A.3), maximum water level at Ha Noi reaches a value of 13.58 m, i.e., 0.62 m lower than the designed flood water level at Ha Noi. The spillways upstream of Ha Noi together with the existing flood control structures in the Red River basin can cope with 1000-year return period flood.

*Table 2: Results of Computations for Case A (1000-year flood)*

Scenario	Water Level at Station				
	Son Tay	Ha Noi	T. Cat	Pha Lai	Hung Yen
A.1	18.09	14.97	14.44	9.16	9.36
A.2	17.07	13.46	13.05	7.57	7.91
A.3	17.12	13.58	13.15	7.58	8.04

*Note: Designed water level at Ha Noi is 14.20 m*

Results of computations for Case B (flood with 2000-year return period) for different scenarios are shown in Table 3. From the results, it is found that:

- With the use of the existing flood control structures (Scenario B.1), maximum water level at Ha Noi reaches a value of 15.86 m, i.e., 1.66 m higher than the designed flood water level at Ha Noi. The existing flood control structures in the Red River basin can not cope with 2000-year return period flood, emergency spillway is found necessary.
- With the use of the existing flood control structures and all the identified spillways (Scenario B.2), maximum water level at Ha Noi reaches a value of 13.95 m, i.e., 0.25 m lower than the designed flood water level at Ha Noi. The spillways together with the existing flood control structures in the Red River basin can cope with 2000-year return period flood.

- With the use of the existing flood control structures and some spillways upstream of Ha Noi (Scenario A.3), maximum water level at Ha Noi reaches a value of 14.09 m, i.e., 0.11 m lower than the designed flood water level at Ha Noi. The spillways upstream of Ha Noi together with the existing flood control structures in the Red River basin can cope with 2000-year return period flood.

*Table 3: Results of Computations for Case B (2000-year flood)*

Scenario	Water Level at Station				
	Son Tay	Ha Noi	Thuong Cat	Pha Lai	Hung Yen
B.1	19.01	15.86	15.28	9.49	10.04
B.2	17.96	13.95	13.55	7.6	8.012
B.3	18.04	14.09	13.69	7.61	8.29

*Note: Designed water level at Ha Noi is 14.20 m*

### 3.0 CONCLUSION

The existing flood control structures of the Red River basin cannot cope with extreme flood with 1000-year return period. Although, all the measures are taken, water level at Ha Noi is still higher than the designed value of 14.2 m.

Application of emergency spillways on the dike system can significantly reduce water level at Ha Noi. A number of scenarios are studied and it is found that spillways in the upstream of Ha Noi are more effective in reducing flood water level at Ha Noi. With the use of these spillways, water level at Ha Noi can be kept lower than the designed value for the case of 2000-year return period flood.

### REFERENCES

- Thuc T., Phuc N. H., 2003. *Hydraulic computations for determining emergency spillway for the Red River system.*
- ADB, 1995. *Red River Delta Master Plan.*
- US Army Corps of Engineers, Hydrologic Engineering Center, 2001. *UNET One Dimensional Unsteady Flow Through a Full Network of Open Channels, Version 4.0.*
- US Army Corps of Engineers, Hydrologic Engineering Center, 2001. *HECRAS Hydraulic Reference Manual.*

# **SUSTAINABLE DEVELOPMENT OF WATER SUPPLY, SANITATION AND WASTE MANAGEMENT: A CHALLENGE TO DHAKA URBAN SLUM DWELLERS IN BANGLADESH**

AYSHA AKTER<sup>1</sup> AND ROWSHAN MAMTAZ<sup>2</sup>

<sup>1</sup>School of Civil Engineering, AIT, Thailand

<sup>2</sup> Associate Professor, Dept. of C.E., Dhaka, Bangladesh

aysha\_akter@yahoo.com

## **ABSTRACT**

*The new ethic of ‘Sustainable Development’ in basic urban facility like water supply, sanitation and proper drainage system for waste disposal is now being supported by a number of technologies to achieve it in reality. Most of the developing countries’ urban slums receive few or no facility. Albeit there are several cost-effective basic infrastructures/services from the slum improvement providers (both public and private) but the poor situation of urban facilities still prevails in these settlements. That is because after providing these infrastructures/services, within a very short time most are either fully ruined or exist in a very shocking condition. The problem is particularly acute in the capital of Bangladesh - Dhaka, where about 33 percent out of total Dhaka’s population live in slum/squatter settlements within abject physical and environmental conditions like: out of total slum dwellers about 20 percent have land-access, 30 percent’s houses blessed of piped water supply, 20 percent have sanitation access and only 10 percent receives proper waste management facilities. There are lots of community based approaches which are positively influencing the long- run services but due to slum’s legality these facilities cover only one/two sector without any incorporation. Against this backdrop, an urgent ‘Sustainable Development’ is required to provide slum dwellers’ elementary needs through an integration of both technical and managerial. This paper focused narrow down at the existing facilities in context of non-slum area and identifies the responsible factors to achieve sustainability. The main discussion is devoted for improved Dhaka slum’s basic services through boost up the existing participatory approach to cope the challenges behind sustainability and finally come up with possible solution as an integrated ‘Rainwater Harvesting’ and ‘Bio-Gas Plant’ in corporation with the ‘Community Construction Contracts’. This paper concludes the proposed community-based cost-effective infrastructure can be accomplished the requirements of slums ‘Sustainable Development’.*

## 1.0 INTRODUCTION

The current slum population in the urbanizing world is about 928 million (UN-HABITAT, 2003) increases inevitably the needs for economic solution of water supply, sanitation and waste management. That is why the Sustainable Development took center point in worldwide development as a result of the Earth Summit (UNCED) held in Rio de Janeiro, Brazil, in 1992. However for proper realization recently the World Summit on Sustainable development, Rio+10, held in Johannesburg in 2002 has postulated the ‘Plan of Implementation’ stated that “...Integrate sanitation into water resources management strategies” (WSSD, 2002). The importance of sustainable development is already being aware by the developing countries but for successful implementation should be started from the most vulnerable part i.e. the urban slums. The fifth mega city of the world, Dhaka is in crying need to get rid from the inadequacy of water supply, sanitation and waste management services from its slum. So, in this circumstance how far Dhaka slums to achieve sustainability. For the exact answer just have a look back, in 1996 there were 3,007 slums and squatter settlements for 1.3 million people in the Metropolitan Area (the Centre for Urban Studies i.e. CUS survey, 1996). And the current estimated population for 2002 of the slums in and on the fringes of the Dhaka would be somewhere between 2.5 million and 3.0 million of the greater Dhaka Metropolitan Development Plan (DMDP) (1995-2015) (Figure 1).

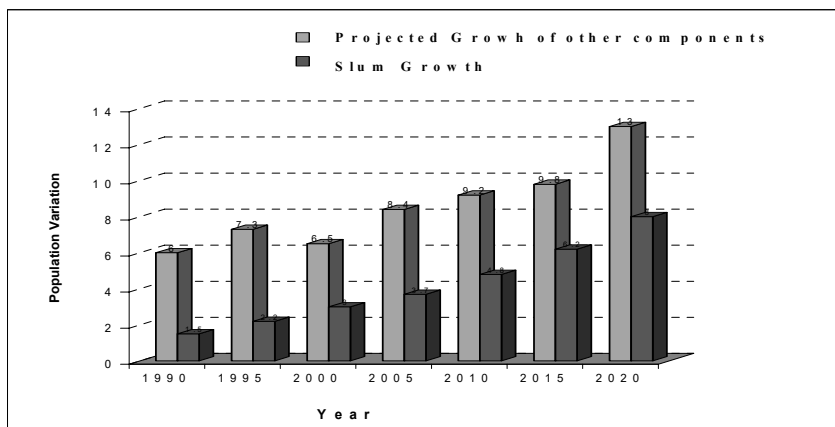


Figure1: Growth chart of city's population and slum population in DMDP area (Nawaz, 1999).

The current population of the same area under the above plan is around 10.0 million. According to the same plan by the year 2015, the total population of DMDP area would be in 17 million. The slum population unless corrective policies are adopted and implemented, would range between five and six million. In excess of thirty five percent of whole Dhaka would be living in unauthorized land and in miserable slum conditions. The living conditions of the city in general and that of the slums in particular while bad as they are today, it needs initiatives to be taken to decrease the miseries of the slum people. There may be difference in getting facility for the slum's situational condition like the slum situated in a

residential or commercial area might get special facilities rather than in a sub-urban area and vice versa. To get the exact picture eight slums have been selected from residential area (Kal-a-Wala Para Bastee, Nashimbag Bastee and Kallayanpur 4no. Pora Bastee), industrial area (Beg Rubber Industry Slum, Omor Sons Slum and Tiger Slum) and sub-urban area (West Vasantek Slum and West Vasantek 1 no. Slum). An intensive field survey on the prepared questionnaire has been conducted through door to door survey by random sampling and simulation with secondary information from different government and non government organization has been used for supporting primary information (Dhaka City Corporation i.e. DCC and Dhaka Water and Sewerage Authority, DWASA, Dusthaya Shathaya Kendra i.e. DSK, Waste Concern and others) (Akter, 2003).

## 2.0 EXISTING SITUATION

About half of the slum dwellers have no access to formal sources of water, very few of them have access to common sanitary latrine and slums have very poor garbage collection systems (Figure 2).



*(a) Water collection  
(gathering)*



*(b) Common latrine  
(discharging to water body)*



*(c) Solid waste (uncollected)*



*(d) Drain (jammed)*

*Figure 2: Existing overall Dhaka Slum situation*

In recent years, however, the Dhaka City Corporation has been continued supporting the slum communities' to access water supply, sanitation and primary solid wastes collection system through some innovative program by engaging the different private organizations but still it's a lengthy way towards the success through an integration between services as well as service providers.



## 2.1 Water supply

From the field survey it is observed that in the slums (Figure 3), the main source for drinking water is the supply water from Dhaka Water and Sewerage Authority (i.e. DWASA), which is of the same outlook with the findings of Coalition for the Urban Poor i.e. CUP which shows about 76.1% slum people use DWASA water for drinking purpose (CUP, 1998).

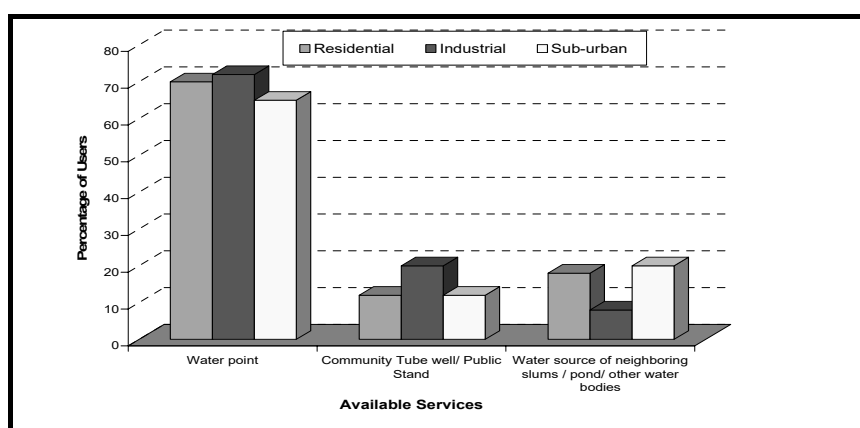


Figure 3: Use of water sources (percentage) in the study areas

The DWASA is charging Tk. 5 (1US\$=Tk 58) for 1,000 liters of water. In the slums of Dhaka the households are paying Tk.1 for 20 liters of water. This means that slum households are paying almost ten times more than the DWASA rate. However the system for storing DWASA water, the “Water Point” takes about Tk. 0.5 for 20 liters of water. Field survey shows the monthly income of the slum dwellers varying from Tk. 3,000 to 5,000. If it is consider their average monthly income Tk. 3,500 (As according to ADB 1996 study of Urban Poverty referred to the poverty line at Tk. 3,500/month/family in Bangladesh) and daily demand for water 500 liter per capita/family; then the total cost spends only for water will be  $[(500 \div 20) \times 0.5 \times 30 \text{ days}]$  i.e. Tk. 375 which is about 11% of their monthly income whereas for the city dwellers the investment is hardly 1.5% of their income.

One study from Asian Development Bank i.e. ADB showed many slums got illegal water connection (ADB, 1996); in this study illegal connection was also found in only one slum – West Vasantek no.1 slum, although the slum dwellers showed their interest to pay for better water supply. Among the study areas almost all but specially in two (Kallayanpur 4no. Pora Bastee and West Vasantek) slums have a quite large number inactive tube-well those are provided (by different GOs and NGOs projects) in the last 2/3 years due to lowering of ground water and lack of proper observation. For other cases different sources including stagnant rainwater pools serve them which are mostly unhygienic due to improper collection system the ‘first flush water’ of the rain has allowed for preservation and also inadequacy in cleanliness. So that some sever illness like diarrhea (due

to mixed dirty water from roof carry the epidemic germs) make them scare to use rain water.

## 2.2 Sanitation

It is revealed that the sanitation situation is worse than water supply situation in slums as well as in the full city area. Among the sanitary facility, 'Pit Latrine' is the main mode of sanitation for the slum people. It is estimated that about 20 percent of slum dwellers have access to such common sanitary toilets. The field survey showed that the Beg Rubber Industry slum has a better option for the slum dweller which is named 'Sanitation Block' with separate systems for male and female; it costs Tk.0.5/use of toilet. For emptying the pit 'Vacutag' machine is used to empty the human wastes and transport to an appropriate safer disposal or transfer site. On the other hand common pit latrine provision in residential area's (Kal-a-wala para and Nasimbag) slum has designed for 6 households /toilet and costs Tk.40/month/household (Figure 4).

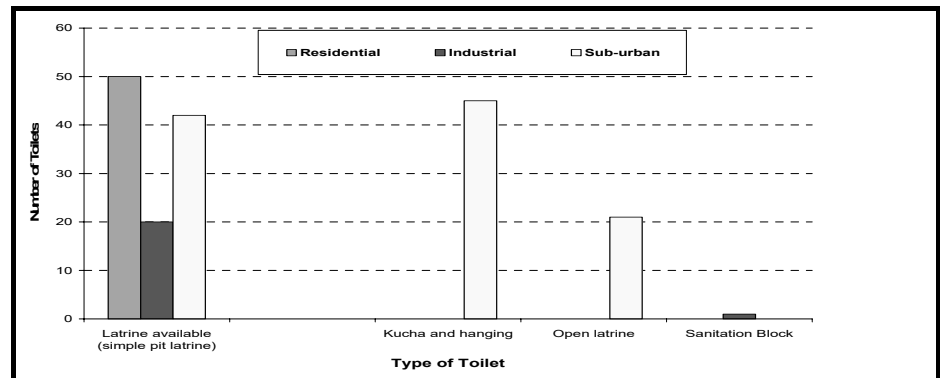


Figure 4: Variation in quality and availability of latrine facilities in the three study areas.

In West Vasantek slum the discharging pipe connected to adjacent water body although there is screen at the end of the pipe which protects the latrine to enter any wastes from outside (Figure 1c). The situation becomes noticeable in rainy season due to absence of drainage system. The overall situation of the West Vasantek 1.no slum is also worst as in this area has only one option which is the hanging toilet mostly on adjacent water body, facing a enormous problem like health problem due to contact with dirty water in every monsoon.

## 2.3 Waste management

According to a study of Center of Urban Studies i.e. CUS (1998), about 90% of the slums do not receive municipal solid waste collection services although the slum dwellers generate relatively small amount of waste per person. The solid waste from the slums are mostly disposed in nearby water body (Figure 1 d), low-lying areas and drainage ditches or

simply scattered in adjacent non-occupied areas. From the field study, it is observed that there are variations of the existing wastewater disposing practices in the three classified areas which is really alarming (Figure 5).

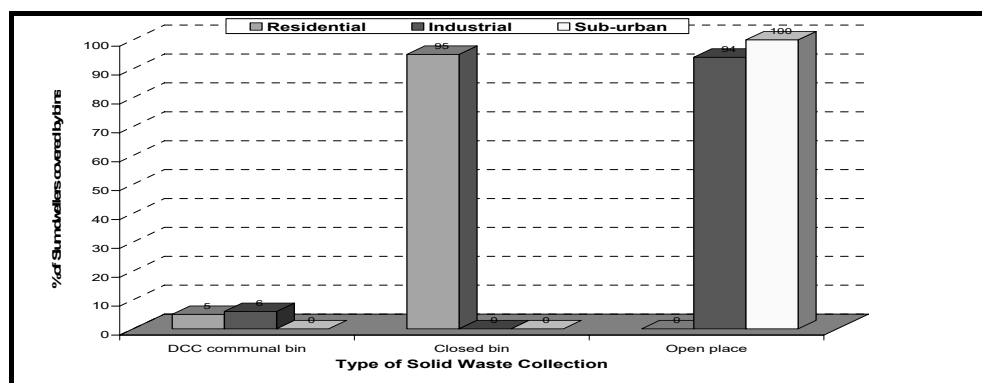


Figure 5: Drainage practices in the three areas (qualitative measure)

The two residential slums (Kal-a-wala para and Nasimbag slum) has got the practice of door-to-door collection of solid waste leading to community-based decentralized composting (namely ‘Barrel Composting’) program run by Waste Concern (Table 1) .

Table 1: Availability of Solid Waste Collecting Bins in the three areas

Indicator	Residential (%)	Industrial (%)	Sub-urban (%)
DCC communal bin	5	6	0
Closed bin (Barrel system)	95	0	0
Open place	0	94	100

The success comes from this ‘Barrel Composting’ program as the participant households are getting Tk. 2/kg of wastes from this facility provider. This program is sustainable due to its conversion process of organic (bio-degradable) portion of the waste to compost i.e. organic fertilizer. Although the carbon nitrogen ratio of solid waste is slightly higher like carbon 22.6% and nitrogen 0.41% in Dhaka, besides the optimum carbon nitrogen ratio 35 to 50 for aerobic composting, with some additional animal excreta the composting has finished within 40 days (Waste Concern, 2000). This excellent program attracts other slum dwellers due to its income generation opportunity.

### 3.0 RESPONSIBLE FACTORS

There are number of factors, which have significant roles in the development of slum’s overall situation. This study observed that the

situation of slums located in sub-urban area or periphery of the city area is worse in all basic services than those located in residential and industrial areas. The slums located at residential areas get relatively better facility than others slum area. So, the location is one of the responsible factors for slums that have a little effect on its overall development for service condition and quality. The sub-urban slums are not getting much attention from the slum dwellers development providers Government Organizations (GOs) and Non Government Organizations (NGOs) due to the gap in cooperative relationships between the service provider and slum leader. If local leader do not cooperate, the GOs and NGOs organization cannot implement any development activities successfully. The success rate of development activities like ‘Water Point’, ‘Tube-well’, ‘Common Latrine’, ‘Sanitation Block’ and ‘Barrel Composting’ by both GOs and NGOs proves if the slum community is properly aware, convinced, motivated and guided how the situation changed positively. So, for overall development the community participation can be taken as a prerequisite factor.

#### 4.0 POSSIBLE SOLUTION FOR SUSTAINABILITY

In context of above existing situation, the factors can be identified as challenge to cope with sustainability, are: first of all limited resources and their mismanagement then the contradictory behavior of existing policies of slum’s water supply and sanitation right, and the overall role of community. To ensure sustainable solution, the water sources should be taken care from further groundwater extraction and surface water pollution. Small scale recycling of wastewater like ‘Duck-weed Wastewater Treatment’ or any such type cost effective approach can be a great initiative. The slum which got quite large bare land (like West Vasantek no.1 of 48 acres for 2500 household can get effective supply by introducing a ‘Pond Sand Filtration’ i.e. PSF. But due to regular migratory place, initiatives for the wastewater treatment or PSF will not be a sustainable solution. Reinforcing of ‘Rainwater Harvesting’ can be achieved the target by proper plan and implementation as there is a considerable rainfall i.e. nearly 85% of the annual average rainfall observed in May to September of every year in Dhaka (Table 2).

*Table 2: Monthly average Rainfall for Dhaka city  
(source: Weather Center Dhaka Bangladesh, 2003).*

Jan	Feb	Mar	Apr	May	Jun	Jul	Aug	Sep	Oct	Nov	Dec	Annual
7.6	30.5	61.0	137.2	243.8	315.0	330.2	337.8	248.9	134.6	25.4	5.1	156.11

So, the choice of “**Rainwater Harvesting**” with local construction material for slum is sustainable solution. Only the supply side is not enough in the way of development, there is an urgent need for demand side management by establishment of existing law. This in turn, will allow investments in extending piped water coverage. Metering of water connection for non-slum area can be a great solution to overcome the

misuse both from Household connection and common pool connection, as there most of the consumer pays tariff in property tax basis.

At present the government has targeted to ensure sanitation for all by the year 2010 instead of 2015 which seems a grand offer for Dhaka slums. But for slum dwellers income generating low cost option rather than the separate toilet is far more attractive. For solid waste ‘Barrel Composting’ itself a sustainable solution although the integration manner with the latrine will diminish the slum drains blockage problem for every monsoon. Again integration is required with water supply to ensure hygiene as well as recycling or Waste Water Treatment to ensure sustainable slum environment. “**Bio-Gas Plant**” can bring a radical change in this perspective as an integration manner (Akter, 2004). For this circumstance, the outlet of the common toilet(s) incorporation with kitchen wastes as well as the other types of liquid/solid discharging outlet should be the main contributory part for the whole process. The main process which takes place in a digester is in an anaerobic form. In the biogas digester, small micro-organisms (bacteria) break down the human wastes and the organic kitchen wastes in the absence of oxygen into a mixture of methane gas (CH<sub>4</sub>), carbon dioxide (CO<sub>2</sub>) and small amount of other gasses. For successful operation first of all, there is a pre-requisite behavioural change required for using detergent in kitchen to promote the bacterial death in the reactor otherwise it will be an excellent integration approach to achieve the sustainability.

#### **For example West Vasantek no.1 Slum**

Population is 12,000 and households 2500 (secondary data DSK, 2002). According to Rahman (1996), potentiality of biogas generation consists:

#### **Gas generation**

Human excreta      0.4 kg / day/ person      0.074 m<sup>3</sup> / kg extra

Municipal waste      0.22 kg/head/day      0.06 m<sup>3</sup>/ kg waste

So, for West Vasantek no.1 slum the calculation shows a significant outcome (Table 3).

*Table 3: Bio-Gas generation for West Vasantek no.1 slum*

<b>Feed Materials</b>	<b>Total excreta (kg per day)</b>	<b>Gas may be obtained (m<sup>3</sup> per day )</b>
<b>Human Excreta</b>	4800	355.2
<b>Kitchen Wastes</b>	2640	158.2
<b>Total</b>		<b><u>513.4</u></b>

So, in small scale for a community toilet which is used by 6/7 families and with their kitchen wastes about three cubic meters of gas is produced in one such plant at a cost of Tk. 15,000 to 20,000. The produce gas is enough to meet up their cooking purpose as well as the output manure will be able to bring some financial solvency. Usually such type of plant's design period for 30 years, however it's totally depending upon the maintenance. The wastewater outlet in addition to the human excreta and kitchen wastes will meet the required water (normally to dilute wastes the required water is twice of the waste weight). And the collaboration of a pipe connection from rain harvested roof will be an immense pulse in the way of sustainability.

To upgrade the proposed solution i.e. 'Rainwater Harvesting' and 'Bio-Gas Plant', there is an enormous need for policy. So, in conjunction with these infrastructures a proposed policy is "**Community Construction Contracts**" which is based on the concept of active community participation in physical upgrading of their neighbourhoods. The expected advantage of this approach is the improvement of construction quality and the creation of responsibilities on the side of community for the design and construction as well as for the maintenance and repairs after its completion.

So, the "Community Construction Contracts" will be able to place integration between the technical and managerial aspect such as:

#### Technical Aspect

- Higher quality of works will be ensured because the community has a stake in the product; and
- Due to community ownership a provision of community required services can be attained more rapidly than a commercial contractor.

#### Managerial Aspect

- Job opportunity will be generate for skilled and unskilled persons in the settlement;
- The participants will be able to get the technical, administrative and management experiences practically on the job; and
- Such type of small scale 'Bio-Gas' plant will save the fuel wood and fertility of soil and overall for sure it will keep the soundness of environment through pathogen free discharge and pollution free air leading to a healthy atmosphere for the inhabitants. In the long run it will be great deals of sustainability through conserve the soil productiveness and the trees.

## 5.0 CONCLUSION

The great examples of 'Water Point' and 'Barrel Composting' show that the enhanced community participation in decision level become really successful for most of the pioneering technology. 'Community Participation' successes for many country as well as Bangladesh and hopefully it will be succeed to improve the slum dwellers' lifestyle in terms of sustainable safe water supply, sanitation and waste management. As the study illustrates cent percent respondents from unserved slum group showed willingness to pay for betterment so 'Community Construction Contract' will bring the targeted achievement incorporation with the integrated 'Bio-Gas' system. Although more intensive research and field works are required for Dhaka slums.

## REFERENCES

- ADB 1996. *Urban Poverty Reduction Project (ABD TA 2410- BAN. ADB Draft Final Report*. ADB, Government of the People's Republic of Bangladesh, Local Government Engineering Department, International Development Support Services, Bangladesh Consultants Limited and Proshika, November, Bangladesh.
- Akter A. 2003. *Water Supply, Sanitation and Solid Waste Management Situations of Selected Slums in Dhaka City*. M. Engg. Thesis, Department of Civil engineering, Bangladesh University of Engineering and Technology, Dhaka, Bangladesh.
- Akter A. and Mamtaz R. 2004. *Integration of Urban Facilities: A Great Sustainable Remedy to Urban Slum Dwellers in Dhaka (Bangladesh)*. Pro of the 1st KMITL International Conference on Integration of Science & Technology for Sustainable Development Bangkok, Thailand, 25-26 August 2004. Vol: 183-186.
- Coalition for the Urban Poor (CUP) 1998. *Baseline survey of environmental sanitation, hygiene and water supply in urban slums of Dhaka City*. Dhaka, Bangladesh.
- Center for Urban Studies (CUS), Dhaka 1996. *A comprehensive Summary Report*.
- Nawaz T., 2002. *Dhaka City and possible slum resettlement programme*. CUS Bulletin (No. 42) January - June (Special Issue: Thirteenth CUS Anniversary).
- Rahman, M.H., 1996. *Biogas: environmental aspects and potential for generation in Bangladesh*. International J. Env. Educ. & Inf., (Published by Environmental Resources Unit, University of Salford, U.K.
- UN-HABITAT, United Nations Human Settlement Program 2003. *The Challenge of Slums-Global Report on Human Settlements 2003*. Waste Concern, 2000. *Aborjona O Poribesh*, September, Dhaka , Bangladesh.
- World Summit on Sustainable Development, Rio+10, Johannesburg 2002. *Poverty eradication, sanitation, energy, financing, integrated water resources management*. Africa.

# **THE NEED FOR AN INTEGRATED DISASTER MANAGEMENT STRATEGY IN NORTH AFRICAN MEGACITIES: A CASE STUDY OF ALGIERS**

DJILLALI BENOUAR

USTHB, Civil Engineering Faculty, Alger, Algeria.

*dbenouar@yahoo.com*

## **ABSTRACT**

*As many other countries of the world, the northern African countries also suffer from environmental and geological problems, among others, the large cities and their suburbs. The capitals, particularly, represent gravitational poles constitute true economic metropolises of them, recording a considerable migratory flow in addition to one important demographic growth, a fast industrialization and an anarchistic urbanization, which make of it the receptacle of various sources of pollution, where ground, air and sea do not escape the consequences of these plagues. Furthermore, Algiers have had also suffered from storms, floods, landslides and earthquakes. Algiers in this research work, capital of Algeria, is taken as a case of study because it introduces most of the risks met in the other countries of North Africa. Algiers counts more than 3 million inhabitants for an area of 809.19 km<sup>2</sup>. From the independence of Algeria in 1962, Algiers was found constituted of a dense urban fabric where various functional scales were overlapped. The town of Algiers experienced a significant development as well on the urban level as industrial and of this fact it is seen confronted with a degraded environment and a multiform pollution. The industrial sector and the factories established in urban fabric and its periphery are at the origin of the existing or potential sources of pollution in addition to the consumption of space.*

## **1.0 INTRODUCTION**

For the North African countries, geological, environmental and technological hazards constitute a constant threat to human life and property, sometimes causing major economic losses and disruption. The rapid urbanization, development of critical engineering works such as dams, decaying building stock, implementation of various industries within and around the main cities, industrialization of cities with modern types of buildings and the large concentration of populations, with a heavy dependency on infrastructure and services, living in large cities and/or settling in hazardous areas are matters of growing concern, as they contribute to heavier loss of life and seriously increasing the economic losses in future disaster damage. The environment concerns and an increased official and public awareness of various hazards have, in the last decade, led to a rapid rise of interest in hazard and risk evaluations and thus in disaster risk management.



In fact, there are various reasons for investigating the Mediterranean Africa as a unit and for evaluating the various hazards of the entire zone under similar criteria: (1) In terms of geological process: the countries limiting the southern part of the Mediterranean Sea and its adjacent continuation in the Atlantic Ocean have had, since hundred million years ago, the same tectonic process marked by a relative motion alternating between left and right lateral along the border of the African and Eurasian plates, (2) Similar present level of development: the actual state of development in the whole zone is dominated by a rapid urbanization, high density of population in most important cities, degradation of the environment, (3) at the present pace and patterns of rural-to-urban migration and unplanned urbanization are causing increased population densities in urban centers, such areas are a prime reason for increasing vulnerability, (4) Similar historical development: the historical development of the countries in the region shows many common factors, such as cultural background. Similarities in population settlements, building stock characteristics and socio-economic and demographic conditions, various types of pollution, climate, etc., are very important parameters in the whole process of disaster risk studies in most cities in the zone under consideration. For all these reasons, this research work is concentrated on the city of Algiers, which presents a general case of most of the geological, environmental and technological threats found in all the main cities across the Mediterranean Africa.

Algiers, the Capital of Algeria, including its surroundings communities, has a population of approximately three millions, represents the most important concentration of investment, government institutions and population in the whole country. It is the intellectual, social, political and economic center of the country. In recent years the disaster risks have increased due to overcrowding, faulty land use planning and construction, inadequate infrastructure and services, and environmental degradation and technological plants within and surrounding the city. In the last two decades, the city of Algiers and its surroundings have known an important development in the urban domain as well as in the industrial one and thus it is actually confronted to rapid environmental degradation and to a multiform pollution. The industrial sector implemented within the city itself and its surroundings increases considerably the risk of disasters. Algiers is confronted seriously to all risks as earthquakes, floods, landslides, as well as the industrial pollution (4 Industrial zones), atmospheric pollution (road traffic, main industries, Public dump Oued Smar), Solid wastes pollution (Public dump Oued Smar, units for wastes treatment), Hydro pollution (superficial and underground water), marine pollution, soil pollution, forests and green spaces degradation, as well as to geological risks. The topography, the waterfront location and the ancient neighborhoods (Casbah) make it difficult to affect radical solutions to most of its problems. Decision-makers need adequate integrated information on the likely (probabilities) intensity of the disaster the city will face if they are to reduce disaster vulnerability. This research work shows the need of an integrated disaster risk management in megacities.

## **2.0 INDUSTRIAL POLLUTION**

The industrial activity constitutes a most significant source of pollution and harmful effect in the city of Algiers. It is the origin of several forms of pollution as hydrous pollution and atmospheric; it is also generating dangerous and toxic wastes posing serious problems for the health of the people as well as their elimination.

Great Algiers represents one of the most significant areas of the country, from the point of view of the industrial activity. The total number of industrial units is approximately 735 public and private in the Wilaya of Algiers, that is to say 7.2% of the national total estimated at 10 200 units, of which 5 242 would be located on the coast.

The polluting industrial activity is localized with the periphery of Algiers, mainly in the East at the industrial zones of Gué de Constantine (8 km of the center town), of El Harrach (11 km of the center), Oued Smar (15 km) and Rouiba - Réghaia (27 Km).

The most polluting units on the level of Algiers are:

- Paper mills,
- Manufacture of batteries,
- Oils and soaps,
- Yeasts, detergents, metals heavy,
- Pharmaceutical products
- Fertilizers,
- Petroleum products: gas, gasoline, asphalt...

### **2.1 Air pollution**

The principal sources of pollution in Algiers are:

- Very intense road traffic,
- Rejections of pollutants by the industrial units established in urban fabric and by the various industrial zones,
- The combustion of the wastes at the public damp of Oued Smar.

#### **2.1.1 Road traffic**

The automobile park of Algiers counts approximately 560 000 vehicles all categories mixed (with a daily traffic of 1500 to 2000 vehicles/hour), which represents the quarter of the national automobile park. This pollution consists approximately to CO<sub>2</sub> 15%, 60 à 70% of CO, 40 to 50% of NO, 30% of the hydrocarbon none burnt residues, SO<sub>2</sub> 5%, black fume, dust, lead, etc.,.

A quantity of 180 tons lead/year is emitted in the streets of the capital at a rate of 0.5g of lead/liter of gasoline for the vehicles, that is to say an annual average of 3.8mg/m<sup>3</sup> (average higher than that of the capitals of the other countries). The annual average recommended by WHO, as a standard of quality of the air not to be exceeded, ranges between 0.5 and 1 mg/m<sup>3</sup>. Whereas lead concentration in the agglomeration of Algiers east of 2.01 mg/m<sup>3</sup> (Aoudia, 1996).

### **2.1.2 The main industries**

The most polluting industries are:

- The cement factory of Rais Hamidou which emits cement dust charged with combustion gas NO, CO<sub>2</sub> and of CO, is 30 tons of dust/day (the standard ranges between 15 to 250 tons/Km<sup>2</sup>/year) (Service environment and forests, 1990). This cement factory, localized within the heart of an urban zone (to 10 km west of the center of Algiers), unquestionably constitutes a significant harmful effect for the populations resident and the whole environment in the vicinity. Producing 750 tons of cement per day, this cement factory emits fine particles, made up mainly by products limestone, which generate respiratory diseases. The most visible impact is certainly the deposit of cement dust on the roofs, the vegetation and on the entire zone close to the cement factory. The threshold of 1000g of dust/100m<sup>2</sup>/month, determined by a model of dispersion as a norm, is largely exceeded on a radius of 3 km (INGECO, 1997).
- The tobacco production units of Bab El Oued and El Hamma (both located within the center of Algiers) emit harmful fume due to the use of fuel.
- The unit of cable-making of Oued Smar emits dust charged with lead,
- The industrial unit of the greasy substances in the harbor of Algiers emits fume with nauseous odors,
- The manufacturing plant of batteries of Oued Smar emits lead oxide dust,
- The manufacturing plant of painting within Oued Smar emits gas dust charged with asbestos and lead,
- The refinery of Baraki (localized to 12 km of the center of Algiers) releases various hydrocarbon gases,

### **2.1.3 Public dump of Oued Smar**

It releases nauseous fume, odors and gas emissions (CH<sub>4</sub>, CO<sub>2</sub>, NH<sub>3</sub>) from the combustion of the household refuse of the city of Algiers, its surroundings and the industrial zones. This pollution is visible at Oued Smar, El Harrach, Bab Ezzouar, Hamiz, Dar El Beida and Eucalyptus.

### **3.0 POLLUTION BY SOLID WASTE**

Solid urban wastes can be defined like the whole of the solid waste generated by the urban activity. In Algeria, in particular in Algiers, household refuses pose serious difficulties to the public services to collect them correctly, as they encumber the streets of Algiers and its surroundings. Wild waste dumps on which the inhabitants come to deposit their waste without paying any attention to the impact on the environment. In fact, the lack of information and awareness, and the non respect of the law, made that the citizen pours his solid waste anywhere, more particularly in the isolated places and thus the creation of wild discharges. The estimate of the quantity of the waste generated by the agglomeration of Algiers is about 1 408 tons per day (ANAT, 1996). The quantity of 2 500 tons per day is produced on the whole of Wilaya of Algiers, that is to say 910 000 tons/year. This quantity will pass to 3 200 tons/day in 2005.

As for the industrial facilities, they pour daily more than 2 000 tons of not controlled wastes, particularly asbestos, acid, cyanide, phosphorus, etc. It should be also noted that waste of the slaughterhouses is rejected directly into the public dump of Oued Smar.

The nature of solid waste is:

- Domestic Waste: 657 000 tons/year;
  - Industrial Waste: 930 000 tons/year;
  - Waste of the administrations (paper, paperboards, etc.) : 90 000 tons/year;
  - Waste of the markets: 50 000 tons/year;
  - Waste of hospital (syringes, bandages, etc.) : 3 900 tons/year;
  - Waste of trade: 80 000 tons/year;
  - Special Waste (toxic): 30 000 tons/year;
- (Service CPVA in Inspection of environment of Algiers).

#### **3.1 Public dump of Oued Smar**

Solid waste of the Wilaya of Algiers is forwarded to the single public dump of Oued Smar just as well as the waste of the industrial zones. The initial surface was 10 hectares and reached 37.5 hectares today. It is located at 13 km of the center of Algiers on a ground of a unit of clay. This public dump reached a very advanced degree of saturation where the mounds of stored waste exceed 6 meter high above the ground level. An investigation of a engineering and design department (Kaoula, 1996) estimated at 4 000 tons/day the quantity of waste which arrives on the discharge including 1 600 tons/day of domestic waste, that is to say approximately 1 000 000 tons/year coming from Wilayates of Algiers, Boumerdes and Tipaza.

#### **3.2 Hydrous pollution**

Hydrous pollution is related to the disposal of the liquid and solid wastes in the ground. Pollution reached today most of the hydrographic networks and poses serious problems, on the one hand by the insufficiency of the water resources, and on the other hand, because of the degradation of the living conditions in the aquatic environment.

### **3.3 Superficial waters**

The superficial water pollution is caused mainly by the sewage systems deteriorated and not maintained where also pour the effluents in the rivers. Sewage water of the of the city of Algiers and that of all the other communes of the Wilaya is rejected to the sea, either directly, or by the means of Oued El Harrach. Oued El Harrach in which flow all the waste water of the regions of El Harrach, Baraki, Eucalyptus, Bab Ezzouar, Dar El Beida, Oued Smar, Gué of Constantine and even part of Wilaya de Blida. The total volume of the wastewater poured in the Oued El Harrach is approximately 57 000m<sup>3</sup>/day (IEA, 1997).

### **3.4 Underground waters**

The water table of the plain of Mitidja constitutes the main water tank of the area. It is prone to many contaminations:

- Pesticides, nitrate fertilizers
- The liquid infiltrations of the water table
- Nitrates of the catchments basin of Oued El Harrach.

The pollution of the water tables by hydrocarbons is a serious problem since it can expand to surrounding collecting fields. Indeed, drillings of the water table of Algiers were subjected of pollution by hydrocarbons. Most of drillings analyzed present a very high degree of pollution, showing a largely higher index than the maximum permissible concentration (10mg/litre) for the water intended for human consumption (Bruchet, 1985).

The discharge of domestic and industrial waste water without treatment in the receiving medium constituted by a hydrographic network which is characterized by nonpermanent rivers and relatively low flow not allowing a process of self - purification, dangerously threatens the water table, the beaches, the dams as well as the public health.

### **3.5 Marine pollution**

The bay of Algiers covers a water area of 184 ha, characterized by a pollution of urban and industrial origin. Most of the cities in the Wilaya and industrial facilities established on the of Algiers littoral pour their waste water either directly to the sea, or by the means of the Oueds, without preliminary processing which causes the deterioration the sea water quality. At the Algiers harbor, 25 outlets of urban and industrial waste water were

listed, with presence of oils and greases coming from the harbor maintenance workshops, the sewage waters of Hamma, the hospital Mustapha Bacha, the factories of the fatty corps, the pasta production unit, oil company and electricity production unit in addition to the draining operated by the tankers and other ships either within the harbor or at large (Urbanis, 1998).

### **3.6 Soils pollution**

The pollution of the soil may have its origin from the industrial activities. The massive use of the artificial fertilizers, the use of certain organic soil conditioners and the systematic use to the pesticides result in a very significant increase in the agricultural outputs; unfortunately this rise of the productivity of the grounds is often accompanied by the increase in the contents of heavy metals in these grounds. Indeed, the contamination of the grounds by heavy metals constitutes a phenomenon which results mainly from the various human activities as the agricultural use of fertilizers (phosphates, fertilizers, organic soil conditioners,..), the industrial wastes, etc. The analysis carried out in various places of the Mitidja plain shows a content of nitrates between 50 and 250 mg/l, whereas the standard set by WHO is 45 mg/l (ANAT, 1996).

### **4.0 DETERIORATION OF THE FORESTS (DEFORESTATION)**

The forests of Wilaya of Algiers know actually a very advanced deterioration covering a surface of 633 ha for a total surface of 5 338 ha, including 37 forests whose majority were arranged as entertaining forests.

The principal causes of deterioration of the forests are:

- Attack of insects
- Fires
- Atmospheric pollution of origin generated by the industrial activity; case of the cement factory of Rais Hamidou which devastated the forest of Bainem
- Neglect of the sector of the forests in the land use decisions
- Anarchistic urbanization
- Proliferations of the cities

### **5.0 FLOODS**

Rapid urbanization is a major factor in the increase of floods. Flash floods is a growing concern due to concrete which absorbs little water, the decline of open spaces, engineering works that divert river flows and weak city drainage systems (neglect, lack of maintenance). inappropriate housing on river banks or near delta is a major concern.

The last Algiers flood and mudflow of 10 November 2001 which caused the loss of 712 human lives, injured 350, 116 are missing, and 1800

housing units suffered damage, 56 schools, scores of bridges, roads, public works were damaged. 1000000 m<sup>3</sup> (up to 10 m thick) of mud in the street of Bab el Oued, more than 350 vehicles (cars, trucks and buses) with passengers buried under mud. Preliminary cost U.S.\$ 250 000 000.

## **6.0 LANDSLIDES**

- Rocks and soil sliding rapidly downhill. Mudflows and rock falls triggered by earthquakes, storms, water logged soil and heavy constructions.
- Growing amounts of badly built housing on/below steep slopes, on cliffs, or at river mouths of mountain valley. Landslides have occurred with or without the help of earthquakes. During the last Algiers flood and mudflow of 10 November 2001, several landslide cases were recorded within Algiers and its surroundings.

## **7.0 EARTHQUAKES**

- Algiers, densely built, densely populated city located on seismic zone. The city suffered several damaging earthquakes in the past, occurring within the city or in adjacent zones. The earthquake catalogue for the Wilaya of Algiers goes back to 1365.
- The building stock of the capital Algiers presents a high vulnerability to earthquake loads and thus seismic risk management is really needed if the government wants to avoid surprises

## **8.0 CONCLUSIONS AND RECOMMENDATIONS**

Decision-makers need adequate integrated information on the likely (probabilities) intensity of the disaster the city will face if they are to reduce disaster vulnerability. This research shows the need of an integrated disaster risk management in megacities.

In a country which regrettably is a disaster-prone as Algeria or in other country, it is of crucial importance, at the macro-level, for the country to have a well established and well regulated disaster management plan. This will enable the government to avoid undue crisis management when future emergencies occur. It is also of crucial importance, again at the macro-level, to integrate disaster management in all its facets with government's mainstream policies and plans for national development.

Disaster management and economic development are not two separate disciplines that conflicts for resourcing. They are synonymous and their resourcing should be a combined administrative process.

To fulfil these goals, the proposal of the establishment of a national disaster research and management agency in Algeria has two objectives (1) to prepare the national disaster management plan and (2) to create a

sustainable cadre of disaster management staff at all levels, and to promote institutional and public awareness of disasters, their effects and likely relief activities. The permanently established national disaster management organisation is presented in what follows. The organisation chart describes the structure, the chain of control and reporting, and the main working relationships. It allows having a permanently established and functioning integrated data collection system to gather information relevant to disaster management in all its aspects. However, it has a wider application and provides an important step forwards an effective national data collection system, and this will require extensive research work. Several partial data bases are already available and these will be drawn upon in the creation of the agency which will attempt to provide a more general view within a single framework. The structure of the agency will then incorporate existing government, non-government and community information/data sources in order to provide an overall picture of potential danger zones, multi-sectoral early warning indicators and available resources. This enables particular attention to be paid to problem geographic sectors or problem functions, and the consequent mobilisation and allocation of resources in advance of disasters. A permanent structure for disaster management integrated in the Algerian government is presented in Figure 1.

## REFERENCES

- Abdelouaheb, N. and T. Sadoun 1996. *Evaluation de la pollution de l'eau par les métaux lourds à l'aide des moules de la région d'Alger*. in communications 1<sup>er</sup> Séminaire Maghrebin sur l'eau, Université de Tizi Ouzou (Algérie), Juin.
- ANAT (Agence Nationale d'Aménagement du Territoire) 1996. *Schéma d'organisation de l'armature urbaine de la région métropolitaine d'Alger*.
- Aoudia, T. 1991. *Pollution atmosphérique dans la région Est d'Alger*. in Etudes : Estimation des concentrations dans l'air à l'aide d'un modèle de boîte ; CERHYD, Alger.
- Bentir, M. 1995. *La problématique des déchets solides en Algérie*. Revue EEC-Edil.
- Bruchet, A. 1985. *Recherche d'hydrocarbures dans les forages de la nappe d'Alger*. Rapport Lyonnaise des Eaux, Laboratoire Central, France.
- DVAHA 1990. *Dossier Pollution et nuisances de la Wilaya d'Alger*. Division du développement des activités hydrauliques et agricoles, « Service Environnement des forêts de la Wilaya d'Alger », 241 pages.
- IEA 1997. *Rapport sur l'état environnementale*. Inspection de l'Environnement de la Wilaya d'Alger.
- INGECO 1997. *Audit environnemental de la cimenterie de Rais Hamidou* (Rapport préliminaire).
- Kaoula, A. 1996. *Alger, une capitale malade de ses ordures*. Revue « Symbiose », 34p).
- Melha, A. 2001. *Les enjeux environnementaux en Algérie*. Pifp, June, Alger. Programme du Gouvernement algérien pour l'an 2000.
- Revues : « Algérie – Environnement », No. 1 and 2, 1998 and 1999.



- Rouidi. L.1995. *Les déchets solides urbains du Grand Alger*. Revue Edil – Info. « Quantification, Caractérisation et propositions techniques pour leur élimination ».
- Sellali. B. 1995. *Influence des rejets urbain et industriels sur l'environnement du littoral : Quelques exemples en Algérie*. p.69. AGEP : Actes de la Conférence Nationale sur la Nouvelle Politique de l'Eau.
- Urbanis 1998. *Problèmes environnementaux dans le Gouvernorat du Grand Alger*.

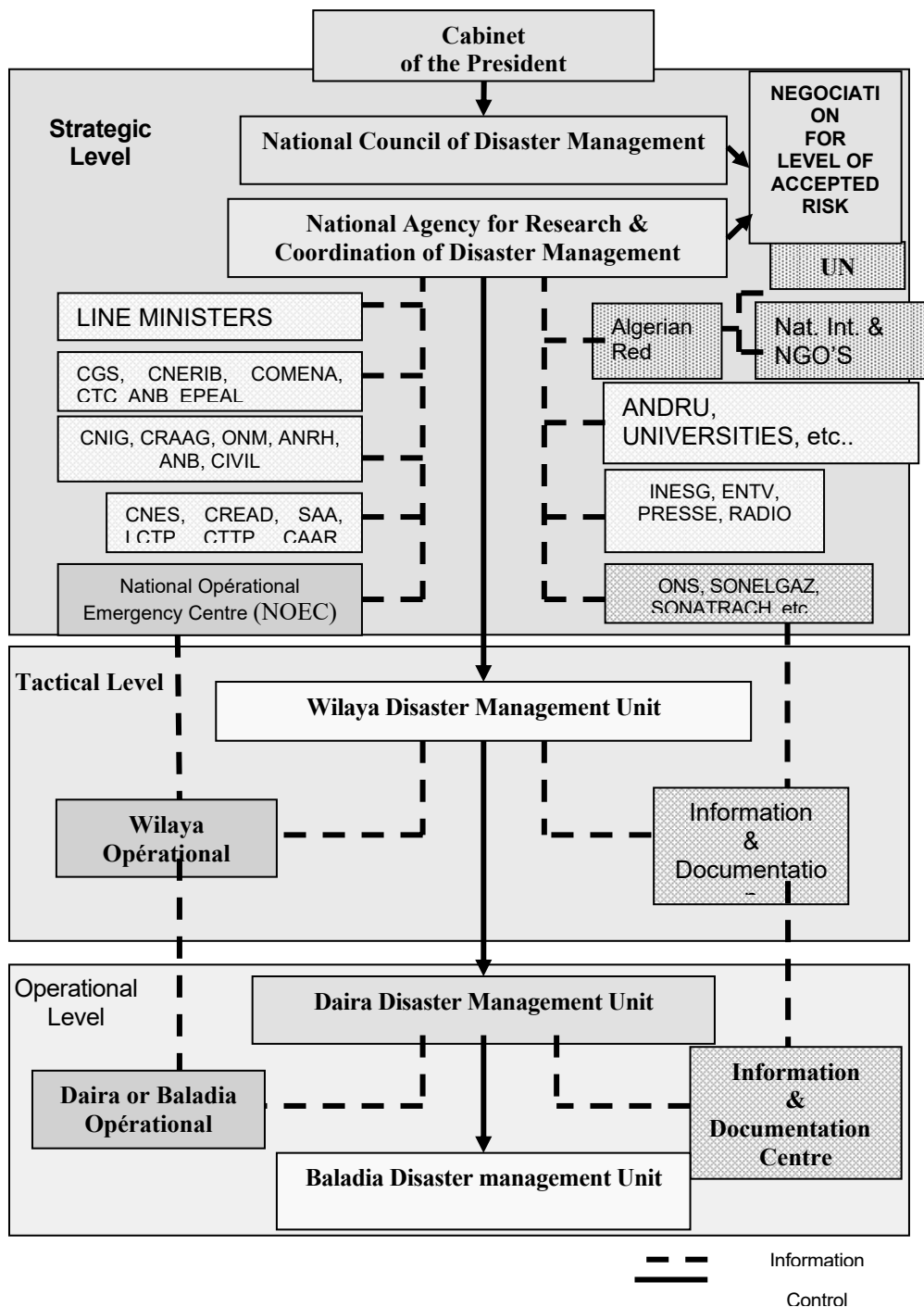


Figure 1: Structure of ANRCGCN in Algeria

# **APPLICATION OF POWER DEMAND CHANGES TO EVALUATE BUILDING AND DWELLING DAMAGES DUE TO EARTHQUAKE**

KIMIRO MEGURO<sup>1</sup> AND YASUNORI HADA<sup>2</sup>

<sup>1</sup> International Center for Urban Safety Engineering  
Institute of Industrial Science, The University of Tokyo

<sup>2</sup> Disaster Center and Human Renovation Institution  
*meguro@iis.u-tokyo.ac.jp*

## **ABSTRACT**

*Early earthquake damage evaluation is very important for the disaster-related organizations to take prompt action in order to minimize the hazard negative impact. This paper presents a methodology to evaluate the earthquake damage to buildings and dwellings using monitored power supply before and after the event. The electric power demand was used to evaluate regional characteristics and a high correlation was found between the demand changes and the earthquake damage. The proposed method allows a feasible real-time damage evaluation methodology that can be readily implemented with little investment and its applicability is not limited by the weather conditions or time.*

## **1.0 INTRODUCTION**

The accurate evaluation of earthquake damage is extremely important for disaster related organizations to efficiently plan their actions. After the 1995 Kobe Earthquake (Great Hanshin-Awaji Earthquake or Hyogo-ken Nambu Earthquake), several methodologies for quick disaster estimation were developed. Fragility curves combined with strong ground motion records as well as remote sensing techniques are among them (Noda and Meguro, 1995, Yamazaki et al, 1998, Takashima and Hayashi, 2000, Matsuoka et al, 2001). As an alternative to these methodologies, we propose the monitoring of power demand variations during and after the event as a means to evaluate earthquake damage. Power is permanently supplied to the users, with its demand strongly reflecting the people's response or actions. During a disaster, the damage level of an area is directly reflected by the activities of the people there. Therefore, the power demand after the occurrence strongly reflects the site damage situation.

The proposed methodology has several benefits. First, there is no need to develop new facilities to implement a power demand monitoring system. All the facilities are already available and provided by the power supply company. Second, a real time monitoring is possible. Third, there is no need to collect a database of the structure strength characteristics or to develop fragility curves before the event. Finally, the observation is not affected by weather conditions or time.

In this paper, the feasibility of the above mentioned methodology is explored. As a first approach, the power demand is monitored at a spatial unit defined by the substation supply area. This unit consists of one substation for the transformation of the power for ordinary consumers (Figure 1). At each substation, there are three transformers and approximately 20 distribution lines. Thus, from the system point of view, it is possible to reduce the spatial unit by monitoring the power demand at the distribution line level. However, at the present stage, the spatial unit is given by the substation supply area.

## 2.0 POWER DEMAND AND REGIONAL CHARACTERISTICS

The power demand and the substation supply area characteristics are strongly related. Meguro et al proposed a classification of a region according to its power demand. Four categories were defined: 1) residential type, 2) office type, 3) industrial (factory) type, and 4) entertainment (pubs and restaurant, etc.) type. By using a stochastic analysis, typical demand curves for each type according to the season were developed for the 23 wards of Tokyo. First, power demand characteristics in the Kobe area were assumed to be the same as those in Tokyo and demand curves obtained in Tokyo were used to calculate contribution rates of each type of demand curves in Kobe. However, the results were not appropriate as the power demand characteristics strongly depend on the regional characteristics. Therefore, in this report, we calculated the typical demand curves using power demand data in Kobe.

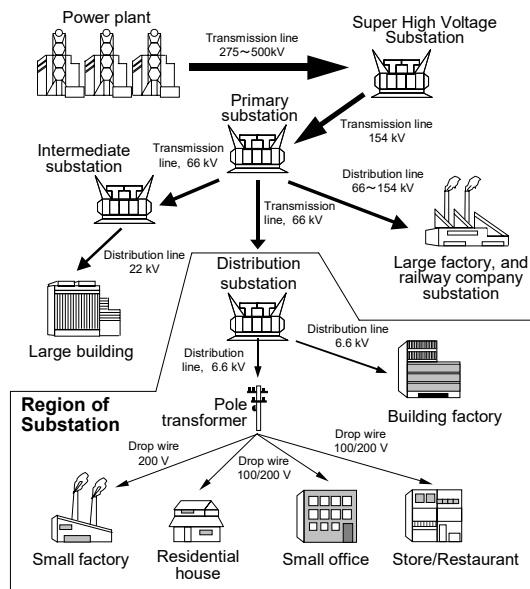


Figure 1: Electric power supply system

Figure 2 shows the distribution of the substation supply areas for the Hanshin region, which has 69 spatial units with an average area of 4.78 km<sup>2</sup>.

## 2.1 Power demand database

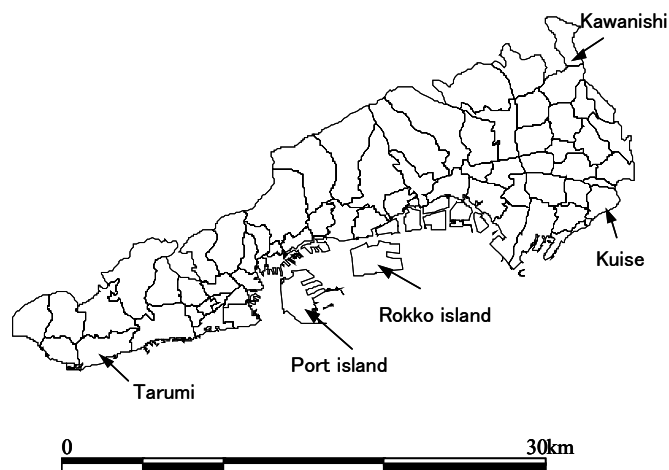
The Kansai Power Company, which supplied power to the affected areas during the Kobe earthquake, provided data of the power demand before and after the earthquake. The database includes hourly records from January 9 to 24, from January 28 to February 3, i.e. approximately two weeks after the event, and from February 18 to 24, i.e. one month after the event.

## 2.2 Calculation of the typical demand curves

The substation power supply area is composed of not only one of the categories defined before, but rather a combination of them. Thus, the power demand at each area can be evaluated as the summation of the contribution of each category. In order to calculate the typical demand curves, the selected spatial unit was the substation area. In this report, we selected 69 substation areas in the affected region. The calculation details may be found in Hada et al (2004). Figure 3 shows a comparison between the typical load curves of the four demand areas for Tokyo and Kobe.

## 2.3 Calculation of the contribution rate for each substation power supply area

Using the obtained elemental load curves, contribution rates for all substation areas were calculated. The contribution rate is the percentage of the power used in an area at peak-load time due to residences, offices, factories or restaurant consumption. Figure 4 shows a comparison between the recorded power demand and the demand calculated using the calculation of the contribution rate. A good agreement is clear. Therefore, it can be concluded that the nature of the substation power demand can be accurately estimated by the contribution rate concept.



*Figure 2: Distribution of substation areas in Kobe*

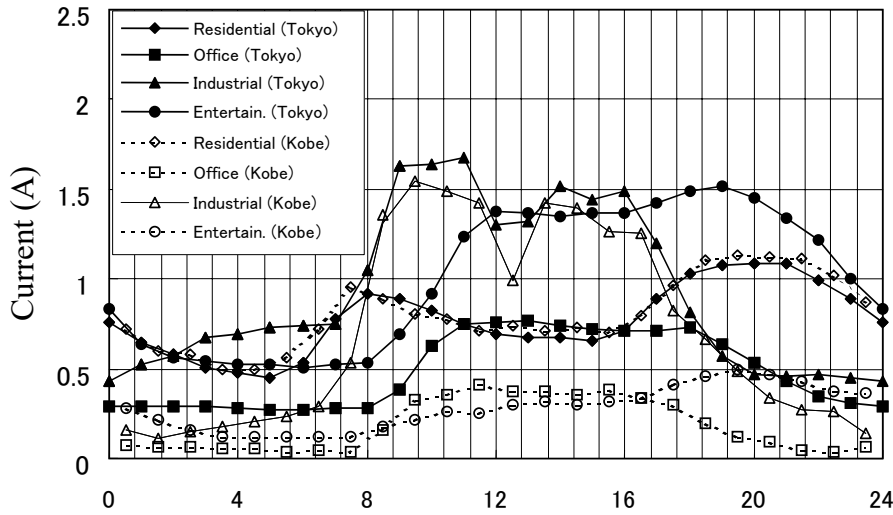


Figure 3: Typical power demand curves for Tokyo and Kobe

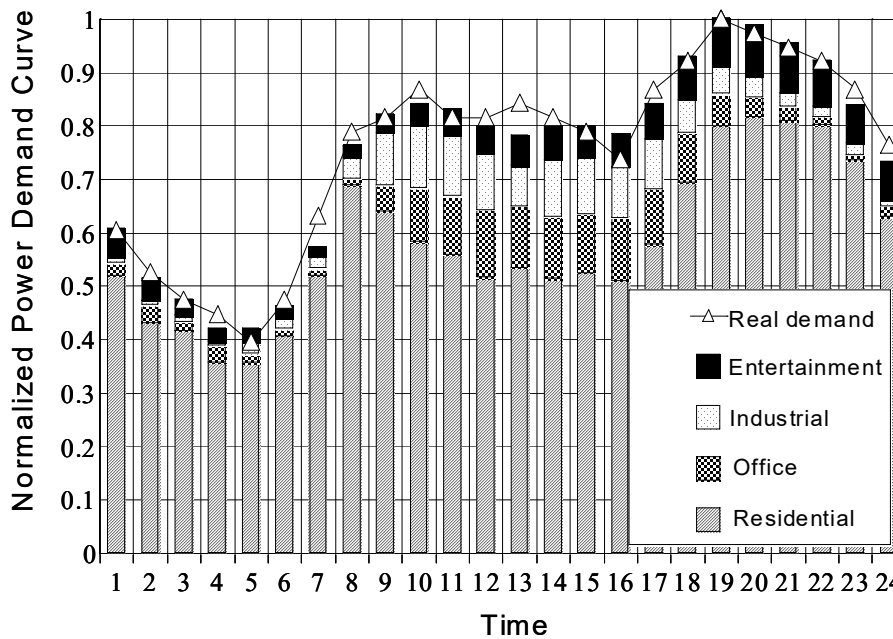


Figure 4: Comparison between real power demand and simulated demand by contribution ratios

### 3.0 CHANGES OF THE POWER DEMAND BEFORE AND AFTER THE KOBE EARTHQUAKE

#### 3.1 Overview of power outage due to the Kobe earthquake and its causes

As Figure 5 shows, due to the Kobe earthquake, 260 million customers lost power just after the event and 169 substations including 106 stations of Kobe branch office experienced malfunction. Although it took about one week for all the consumers to recover power supply in the affected area, with a quick recovery response such as switching of supply network, 80% of those substations recovered within 3 hours. Fukiai

substation, whose malfunction time was the longest, finally recovered at 7:23 am on January 18 (about 26 hours after the earthquake). From that point in time, a discussion of the power demand changes can be done. There were about 400 thousand consumers without power even after all the substations' function recovered because of damage to facilities at a level, lower than the substation. It can be argued that the demand might be affected by the falling of poles. This does not directly imply building damage. However, there is a strong correlation between poles and building damage. A collapsed pole is an indication of the severity of the earthquake. Thus, the probability of building damage in the area next to a fallen pole is very high.

### 3.2 Changes of power demand before and after the earthquake at the level of controlling office unit

Figure 6 shows that the power demand decreased immediately after the earthquake. Due to the large area of the spatial unit the demand drop was not so dramatic. The gap increases if a smaller area unit is taken into consideration.

### 3.3 Power demand changes at the substation unit level

Figure 7 shows the power demand variation on the day of the event, one and two weeks after, and one month after for the 69 substations observed in the study. Figure 7(b) shows the area where the seismic intensity was JMA7 in magenta color. The correlation between the power demand drop and the seismic intensity is very high.

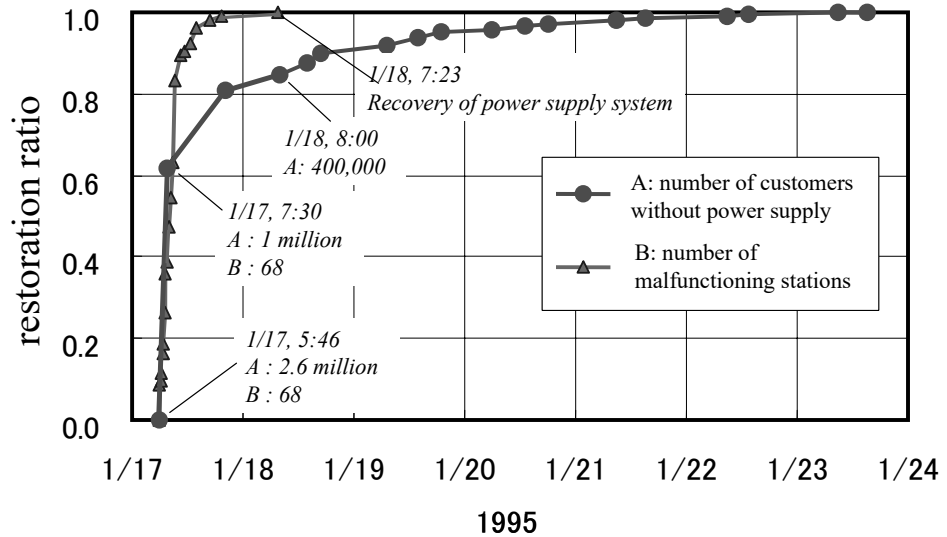


Figure 5: Electric power recovery time after the Kobe earthquake

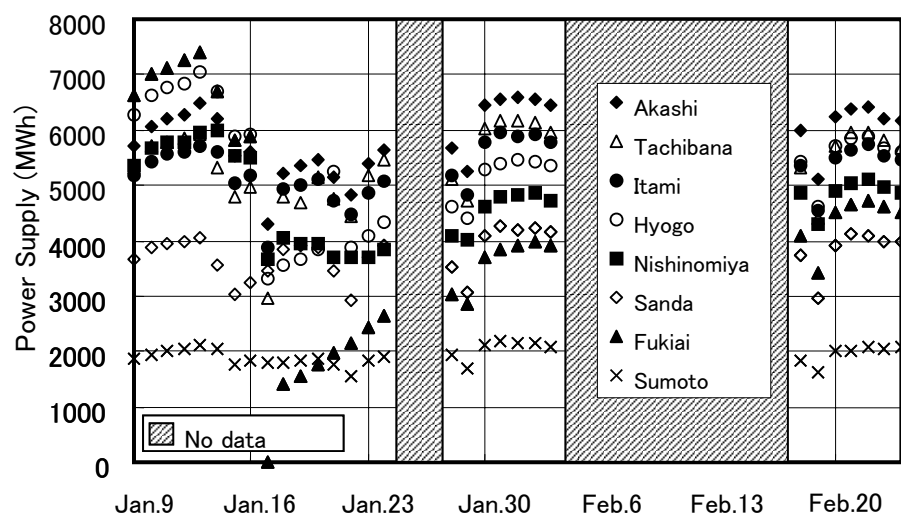


Figure 6: Changes of electric power supply before and after the 1995 Kobe Earthquake

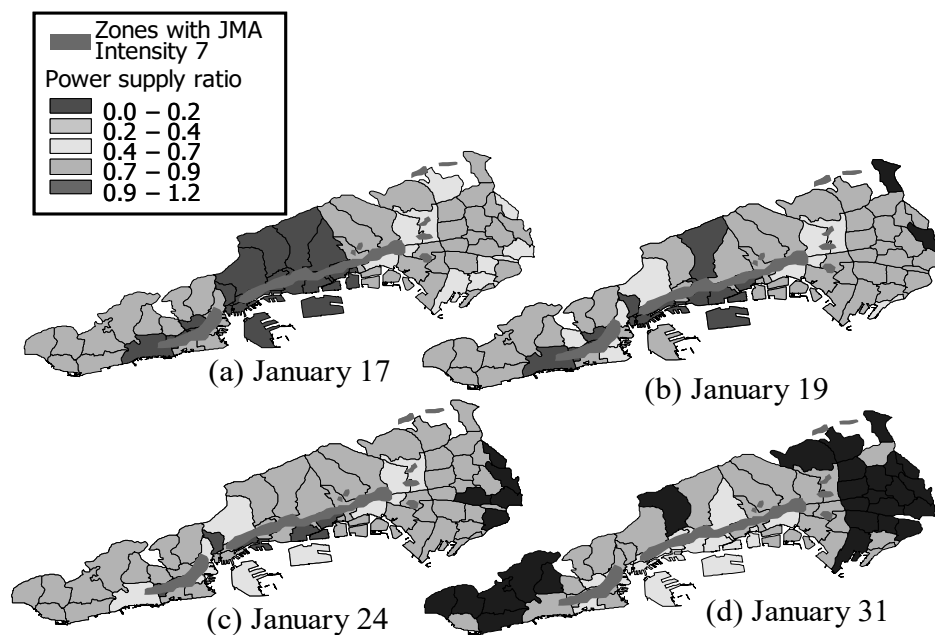


Figure 7: Distribution of power supply ratio in the affected areas (on the day, one- and two-week, and one-month later the earthquake)

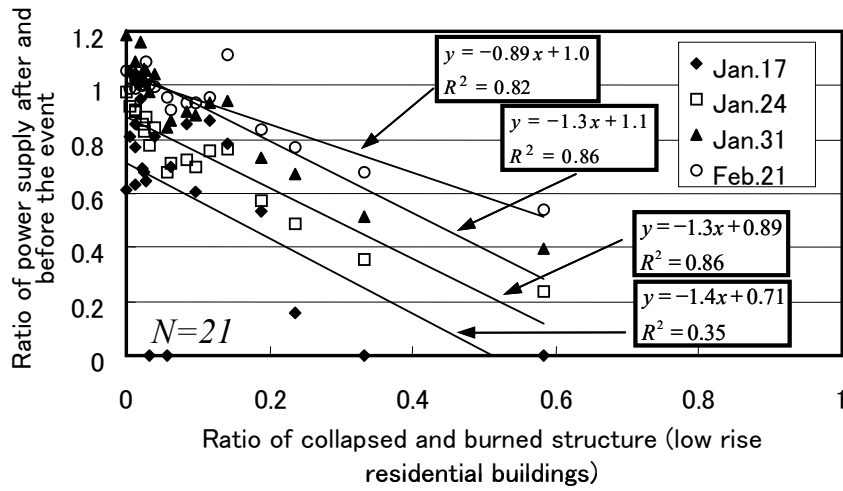
#### 4.0 DISCUSSION ON THE RELATION BETWEEN POWER DEMAND AND STRUCTURAL DAMAGE

Power demand can always be monitored. As time goes by, the peak value gradually increases until the original demand peak is reached. In order to analyze the relationship between structural damage and power demand, the ratio of power demand with respect to the original demand and the damage ratio (collapsed or burned buildings) are plotted against each other. Figure 8 shows the graphs corresponding to the substations where a) the residential area component contribution is over 70%, b) the office component contribution is over 30%, c) the industrial component contribution is over 35%, and d) the entertainment component contribution is over 20%. Each graph shows four curves corresponding to four different times: 1) the day of the earthquake, 2) one week after, 3) two weeks after, and 4) one month after. If damage is 0%, the power demand should be 100%. On the other hand, if damage is 100%, the demand should be null. However, it is clear that even in the cases where the damage is zero, a drop in the demand can be observed. The reason for this is that even if the damage is small or inexistent at the spatial unit under consideration, the peoples' activities change due to the damage in the surrounding areas. For instance, people cannot get to their offices or factories.

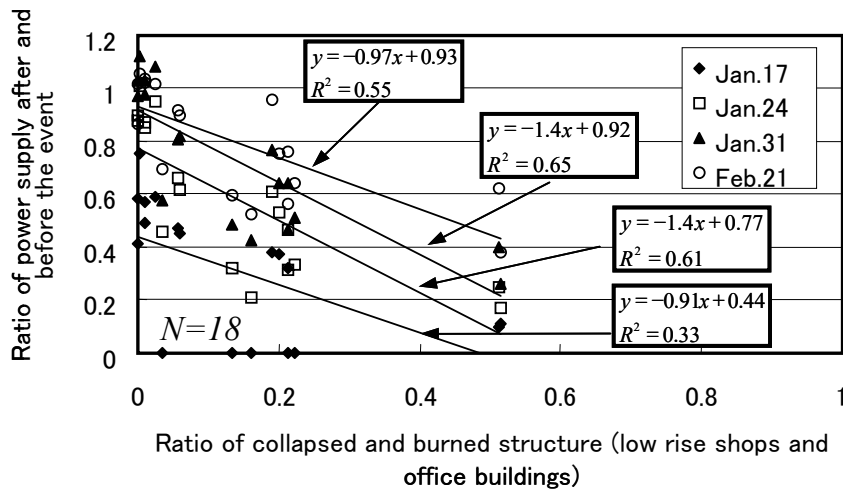
Figure 8 shows another interesting feature. In the four cases considered the correlation between power demand and structural damage increases as time elapses from the earthquake occurrence time. On the day of the earthquake, the correlation is low. For instance, in the case of residential area, it is 0.35. This is mainly due to the presence of substations that are not supplying energy, i.e. power supply system failure, which are nevertheless considered for the calculation of the correlation. As time passes, the correlation dramatically increases. This allows the proposed method to achieve accuracy levels superior to other damage estimation methods.

A general trend of power demand recovery is observed for the four cases as shown in Figure 9. Shortly after the earthquake, the areas where the damage is minor rapidly recover to the original levels of demand. The areas where damage is higher recover as well, but not until a significant period of recovery. Figure 9 depicts the mechanism of power demand recovery as a function of the damage ratio and time elapsed from the earthquake occurrence. At first, the regression line power demand versus the damage ratio shifts until the original demand at the locations where damage is null is reached. After this, the regression line slowly rotates until the entire region returns to the original demand level.

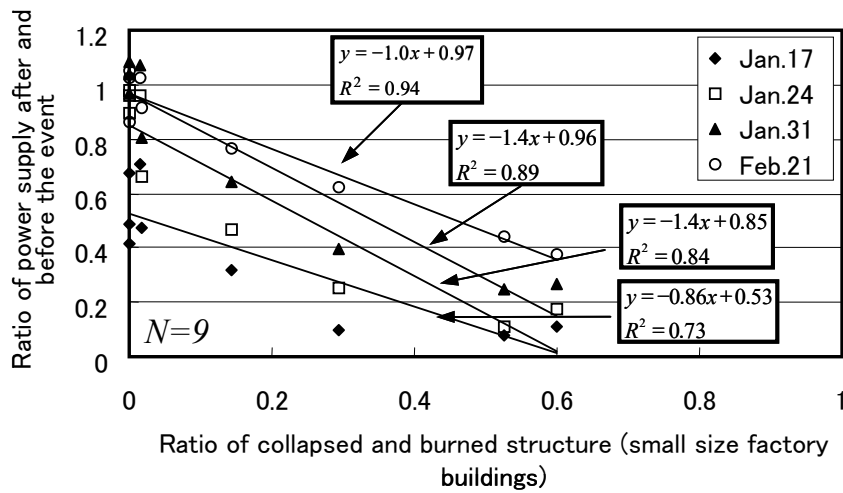




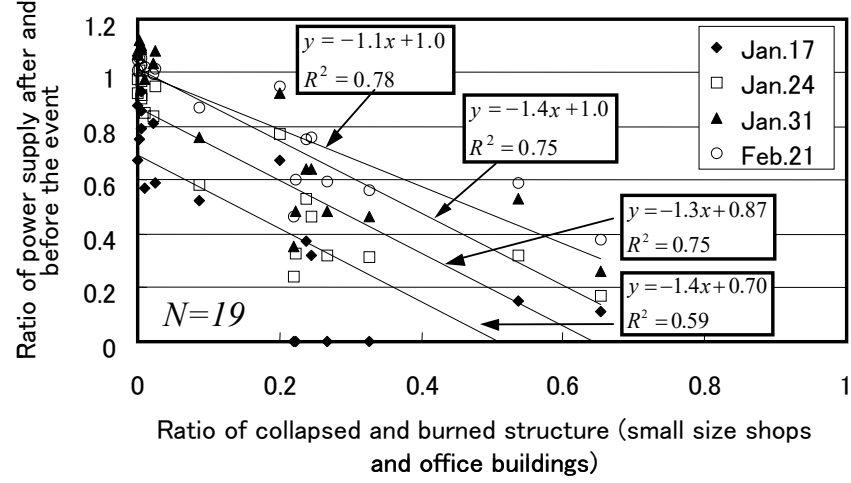
(a) Residential type substation areas (Contribution rate is more than 70%)



(b) Office type substation areas (Contribution rate is more than 30%)



(c) Industrial type substation areas (Contribution rate is more than 30%)



(d) Entertainment type substation areas (Contribution rate is more than 20%)

Figure 8: Changes of power supply after the earthquake at substations with different damage levels

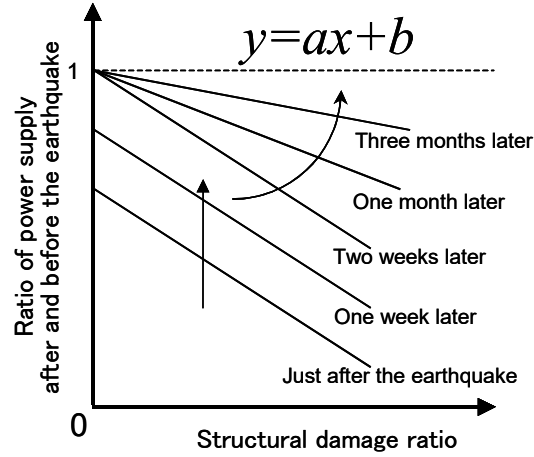


Figure 9: Model for discussion of structural damage and power supply changes (in case regional characteristics before and after the event are close to each other)

## 5.0 CONCLUSIONS

This paper presents a new technique for structural damage estimation based on the observation of the power demand variations. This methodology has several advantages. First, there are no limitations for the observation of the power demand such as weather conditions, time, etc. Second, there is no need to prepare new facilities such as aircraft or satellites for conducting the observation. All the required facilities are already provided by the power supply company. Third, the data can be monitored in real time. Forth, the model is continually updated since the power demand is continuously being observed, i.e. immediate feedback is possible. Fifth, the proposed

methodology is also useful to supervise the reconstruction progress by monitoring the power demand recovery. Even in case a certain area changes its type of use, i.e. from an industrial use to a residential use, the expected power demand can be easily estimated from the model and recovery supervision is possible.

## REFERENCES

- Yamazaki F., Noda S. and Meguro K. 1998. *Developments of Early Earthquake Damage Assessment Systems in Japan, Structural Safety and Reliability*. Proceedings of ICOSSAR 7, 1573-1580, Balkema.
- Meguro K., Soejima M., Yamazaki F. and Katayama T. 1995. *Classification of Urban Areas by Characteristics of Power Load Curves*. Proc. of 5th International Conference on Seismic Zonation, 60-67, Nice, France.
- Matsuoka M., Yamazaki F. and Midorikawa S., 2001. *Characteristics of Satellite Optical Images in Areas Damaged by the 1995 Hyogo-ken Nanbu Earthquake*. Journal of Japan Society of Civil Engineers, 668/I-54, 177-185, 2001.
- Takashima M. and Hayashi H., 2000. *Validation of Damaged Area Estimation using DMSP/OLS night-time imagery, - application for Marmara earthquake in Turkey (1999) and Hanshin-Awaji earthquake in Japan (1995)*. Journal of Social Safety Science, Institute of Social Safety Science, 2, 69-78.
- Noda S. and Meguro K., 1995. *A New Horizon for Sophisticated Real-Time Earthquake Engineering*. Journal of Natural Disaster Science, 17(2), 13-46.
- Hada, Y. And Meguro K., 2004. *Introduction of An Earthquake Damage Evaluation Method For Buildings And Dwellings By Monitoring Changes Of Power Supply*. US-Japan Cooperative Research For Urban Earthquake Disaster Mitigation Assessment Of Post Earthquake Management Processes Using Multimedia Disaster Simulation.

# **INTEGRATED EARTHQUAKE SIMULATION USING SIMULATION AND GIS**

MUNEO HORI AND KENJI OGUNI

Earthquake Research Institute, The University of Tokyo, Japan

hori@eri.u-tokyo.ac.jp

## **ABSTRACT**

*The advancement of computer technology and sciences enables us a large-scale numerical computation. As one of such, the authors have been simulating the whole processes of earthquake, i.e., the generation and propagation of earthquake, the response and damage of structures, and human and social action against disaster. With the aid of the latest geographical information system (GIS), a compute model can be constructed for a city of some hundred-meter scale; a structure model is automatically made for each building, and a suitable numerical analysis method is applied to calculate the dynamic response of each model for a given strong motion.*

*This paper presents the current state of this integrated earthquake simulation. The simulation is controlled by a computer system which combines numerical analysis methods and GIS. An example of a computer model of a city is presented. Discussion is made on the usefulness of the large-scale simulation of the integrated earthquake simulation, in order to form a common recognition of possible earthquake hazards among citizens, government officers and earthquake engineers.*

## **1.0 INTRODUCTION**

Local government officers play a major role in promoting earthquake disaster mitigation since they make and enforce regional mitigation plans against a possible earthquake. For the technical point of view, the local government officers are not in an ideal state. They are essentially administrators and do not have to understand seismology and earthquake engineering at high level. Even engineering-oriented officers do not have sufficient experiences on designing and constructing structures.

Improving the technical ability of the local government officers is an important issue. The technical ability means correct understanding of prediction of possible earthquake damages which is made by experts. The uncertainty of the prediction must be grasped, and the targets are all buildings and structures located in the city.

The technical ability must rely on a solid foundation such as earthquake resistant design codes. The codes, however, are written for a professional design engineers, and local government officers have some difficulty to read the codes; they must read the codes of various structures. Visualization of dynamic responses of all structures located in a city helps

understanding the earthquake resistant codes when the responses are computed by using the codes. Realizing such unified visualization of structure responses is the primary objective of the present paper.

Unified visualization is made with the aid of an integrated earthquake simulator (IES), a system which is aimed at simulating all processes of earthquakes, with the aid of data stored in geographical information system (GIS); see Yang *et al.* (2002). Numerical analysis methods based on actual earthquake resistant design codes are implemented in IES. An example of unified visualization which combines all the simulation results is presented.

## 2.0 SYSTEM FOR UNIFIED VISUALIZATION

Realizing unified visualization is not trivial, even if it is taken for granted that there is limitation in constructing computer models for all structures due to lack in available data. The major difficulty is the implementation of numerical analysis methods of various structures into one system. To solve this difficulty, we develop a mediator, a computer agent which automatically implements a numerical analysis method to IES.

### 2.1 Mediator in IES

First, we briefly explain IES (Yang *et al.*, 2002). As mentioned, IES is a system for numerically simulating all processes of earthquake; the processes are basically divided into three phases, namely, the generation and propagation of earthquake, the responses and damages of structures, and the human and social action against earthquake disaster. IES thus consists of three simulations, earthquake simulation (Ichimura and Hori, 2000), structure response simulation and action simulation; see Fig. 1.

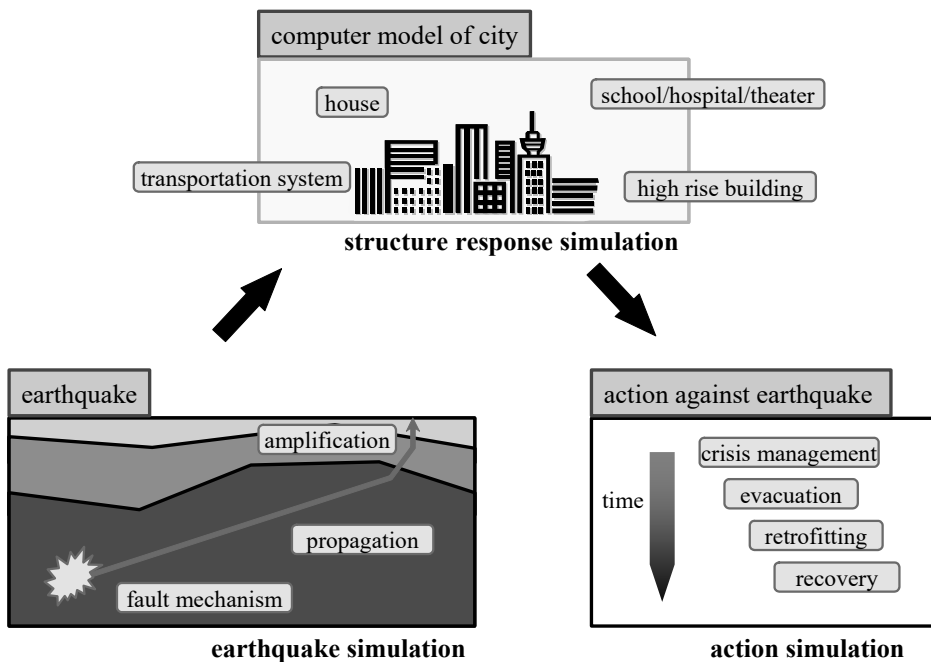


Figure 1: Overview of IES.

Major components of IES are kernel, GIS, simulation programs (SP) of structures and visualization tools. Kernel is a key component, as it controls other components; see Fig. 2. From GIS, kernel extracts data needed for model construction. Providing data for model and strong ground motion, kernel runs each SP. Kernel finally collects all simulation results and send them to visualization tools.

Plug-in is not suitable for implementation of SP's into IES, since it requires a laborious task of modifying a source code of SP. As an alternative, we adapt an agent, called a mediator, which translates all communications between kernel and SP; see Hammer *et al.* (1995). The communications are for data input, execution and result output. Thus, each mediator plays a role of an interpreter for its supporting SP (Uhlman, 1997, Gruber 1993).

It should be emphasized that each SP needs a particular mediator. Making a mediator requires a laborious task similar to modifying a source code since SP has its own description of input/output. However, the basic structure of all SP's is common; they are based on finite element method (FEM) which is a standard analysis method of earthquake resistant design. In principle, therefore, it is possible to automatically make a mediator for a given SP. In this paper, we seek to develop an artificial intelligence, called a mediator maker, for this purpose.

## 2.2 Mediator maker

When viewed from the point of input and output, an FEM-based SP basically consists of an input part and a loop part which further consists of a calculation subpart and an output subpart. The input part is literally for

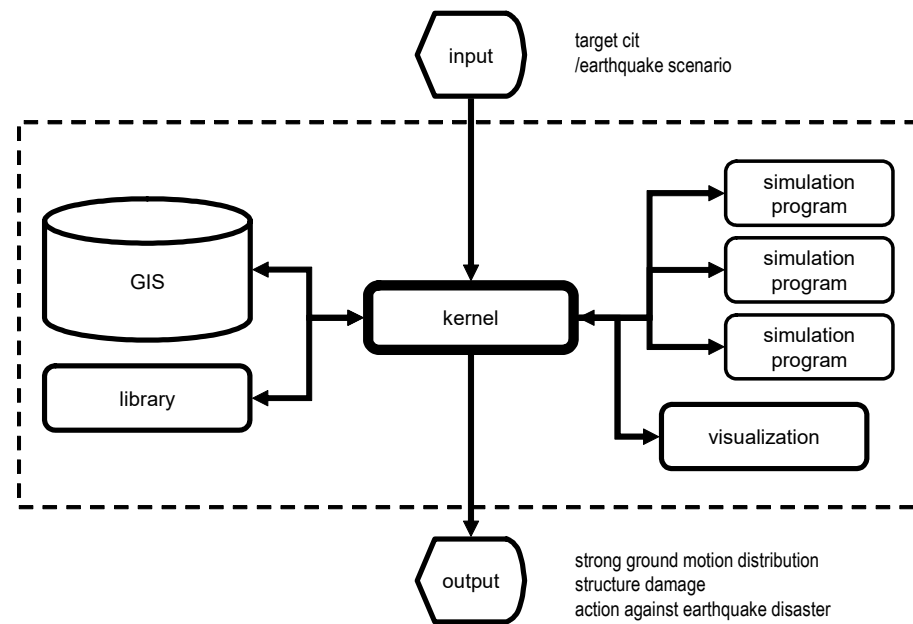


Figure 2: Kernel of IES.

inputting data such as configuration, material properties and boundary conditions. The loop part repeats calculation in the calculation subpart and output of temporal results in the output subpart. In view of this program structure, we specify basic functions of a mediator in Table 1. The first four functions correspond to the input part, and the sixth function is for the output subpart. The fifth function interprets kernel's command of execution and the seventh function is to construct files for the unified visualization.

When C++ is used, a mediator is programmed as a class and the basic functions shown in Table 1 are written as methods of the class. Making use of succession, we can efficiently construct the class; a source class for a mediator is pre-constructed, and a new class is construed by modifying the contents of data and methods of the source class.

A mediator maker is an artificial intelligence program which outputs a class of a mediator when a source code of SP is given. Making a class means describing the seven methods which are inherent to SP. The mediator maker does this task through the two phases, namely, the analysis of the source code and the construction of mediator; see Fig. 3.

In the first phase, the mediator maker generates a digested code, a simplified code which contains only input/output and loop sentences, from the source code of SP. When the source code is written in FORTRAN, the key points of analyzing SP are subroutines and common memories. In analyzing subroutines, the mediator maker finds all subroutines in the source code, picks up input/output statements, and examines the order of the input/output sentences and the type and format of input/output variables by considering mutual relations of subroutines.

*Table 1: Basic functions of mediator.*

basic function	content
identification of structure	identify structure and building in a target city from data extracted from GIS
selection of SGM site	select sites where SGM is computed and inform them to earthquake simulator
acquisition of structure data	construct data files for input of SP, by extracting data from GIS and library
acquisition of SGM data	construct data files for SGM at sites, using results of earthquake simulator
execution of SP analysis	run SP using data files which are constructed by mediator
acquisition of results	take results of simulation from SP, and make result files
visualization	make visualization files (VRML/POV/AVS) from result files made by mediator

SGM: strong ground motion

In the second phase, the mediator maker analyzes the digested code and describes the seven methods of the mediator class. Since the digested code mainly consists of input/output and loop sentences, the major tasks are 1) analysis of input/output, 2) analysis of loop and condition and 3)

presumption of variables which are used in input/output or loop and condition. The presumption of variables is important in describing the methods since the mediator makers match these variables with variables which are used in the original class in succeeding it to a new class.

It should be emphasized that constructing a robust artificial intelligence program is extremely difficult. The current mediator maker is not complete, as it requires some man power in describing a class for a mediator. However, it saves man power to some extent since the program structure of a source code is analyzed and some input/output variables are identified.

### 3.0 EXAMPLE OF UNIFIED VISUALIZATION

With the aid of the mediators which are produced by the mediator maker, IES constructs a virtual city (VC) as a computer model for an artificial city of 300x300[m] area; see Hirose *et al.* (1999) for a computer model of city. A small GIS is constructed for this city, such that data to construct computer models for the underground and structures are stored. The underground, up to depth of 40[m], consists of three distinct layers, and there are four gas pipe lines, five concrete piers, seven steel piers of two kinds and four ground molds. A schematic view of VC is presented in Fig 4. This figure is a result of visualization; IES automatically generates the static image of VC and each structure within VC as well as dynamic images (animation) of VC as for unified visualization.

The second phase of construction of mediator is not trivial, due to the difficulty in presuming variable. We seek to presume the meaning of some variables which are commonly used in FEM-based SP, namely, the node number, the element number and the time increment number. These variables are input in the beginning of the input part and used in the loop part, and the mediator maker seeks to find them as follows:

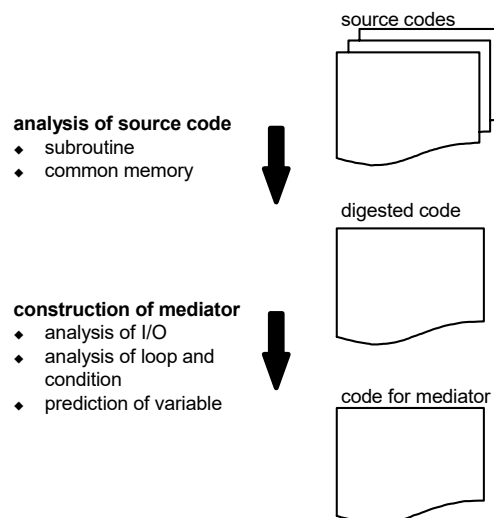


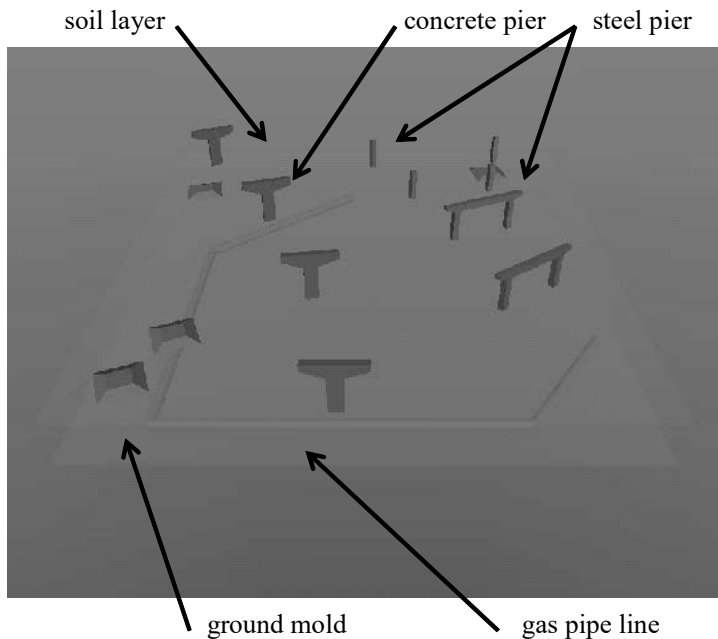
Figure 3: Two phases of mediator maker.



- the node number as a variable which controls the iteration of the input part and of the output subpart;
- the element number as a variable which controls the iteration of the output subpart;
- the time increment number as a variables which control the iteration of the loop part.

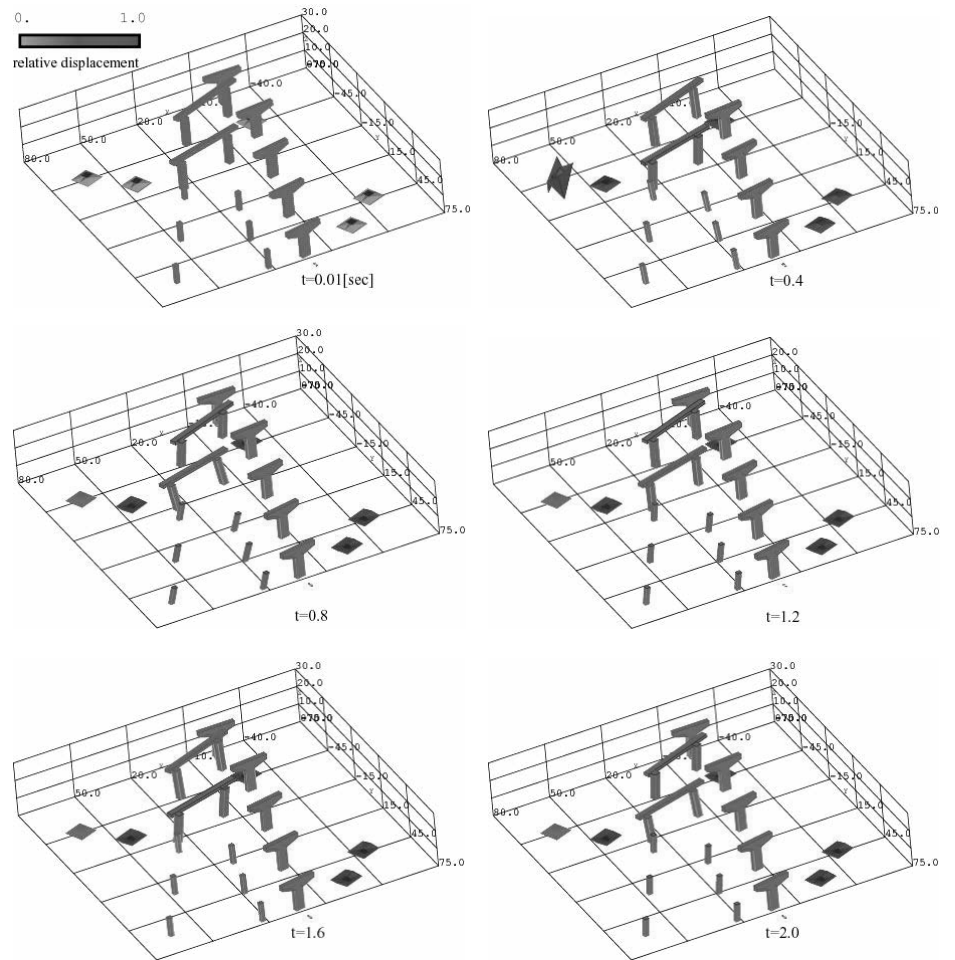
As an example, the frequency of all variables appearing in the digested code are shown in Fig. 6 for a digested code of concrete pier; read/write means input/output, and LL means the loop level (LL=0 or =1 is out of loop sentences or in the first nest of loop sentences). As is seen, variables INODE, IMEM, IJK are presumed as the node number, the element number and the time increment number, which is correct presumption.

Examples of the unified visualization is shown in Fig. 5; a half sinusoidal wave of amplitude 10[cm] and period 1.0[sec] is input at the bedrock mass, and figures are snapshots of bird-views of VC every 0.2[sec]. The displacement of structures is magnified by 10 times, and the norm is indicated by color. As expected, structures of the identical configuration and material properties have different responses since strong ground motion input to them is not the same due to the difference in local ground structures which results in different amplification of earthquake; see ground molds. Structures of different kinds have responses which is mainly governed by the natural frequency; for instance, concrete and steel piers located at the center of VC cause has large contrast in amplitude of displacement, and the maximum displacement of the concrete pier is just 20% of that of the steel pier.



*Figure 4: Static view of VC.*

It should be emphasized that SP's implemented into IES have been used to analyze dynamic non-linear responses of a structure for the research purpose. Hence, high reliability can be expected. The unified visualization of earthquake disaster which may happen in a city surely contributes to the improvement of the engineering ability of local government officers since it provides a vivid image of the disaster. While more realistic visualization will be needed, the unified visualization of quantitative information of the structure damages which are simulated by reliable numerical analysis methods results in making more efficient mitigation plans.



*Figure 5: Example of unified visualization.*

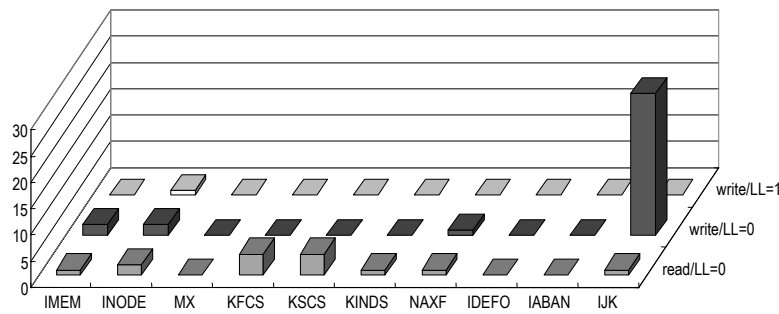


Figure 6: Frequency of variables at different loop level;  
frequency is counted by mediator maker.

#### 4.0 CONCLUDING REMAKRS

With the aid of the mediator and mediator maker, some SP's of analyzing dynamic structure response, which have been developed according to the earthquake resistant design codes, are implemented into IES. An example of the unified visualization is presented for an artificial city; it provides reliable images of possible damages of structures within the city. This example suggests the usefulness of IES that combines GIS and simulations for the unified visualization. The system of IES will be being improved as well as the mediator maker such that other SP's can be implemented into IES more freely.

#### REFERENCES

- Gruber, T. R., 1993. *A translation approach to portable ontology specification*, *Knowledge. Acquisition*, 5, 2, 199-220.
- Hammer, J., Gracia-Monlina, H., Ireland, K., Papakonstantinou, Y., Uhlman, J. D. and Widom, J., 1995. *Information translation, mediation, and mosaic-based browsing in the TSIMMIS system*. Exhibits Program of the Proceedings of the ACM SIGMOD International conference on Management of Data, 483.
- Hirose, M., Tanikawa, T. and Endo, T., 1999. *Building a virtual world from the real world*. *Mixed Reality - Merging Real and Virtual Worlds* (ed. by Ohta, Y and Tamura, H.), Springer-Verlag, 183-197.
- Ichimura, T. and Hori, M., 2000. *Macro-micro analysis for prediction of strong motion distribution in metropolis*. *J. Struct. Mech. Earthquake Eng.*, JSCE, 654/I-52, 51-61.
- Uhlman, J. D., 1997. *Information Integration Using Logical Views*. Proc. ICD'97, Springer LNCS 1186, 19-40.
- Yang, F., Ichimura, T. and Hori, M., 2002. *Earthquake simulation in virtual metropolis using strong Motion simulator and Geographic Information System*. *Journal of Applied Mechanics*, JSCE, 5, 527-534.

# UNDERSTANDING THE SEISMIC SOURCES IN INDIA: STRATEGIES FOR SEISMIC HAZARD REDUCTION

KUSALA RAJENDRAN AND C.P. RAJENDRAN  
Centre for Earth Science Studies, Trivandrum, India.  
*kusala@seires.net*

## ABSTRACT

*Seismic sources in the Indian subcontinent display varying characteristics, in their styles of deformation to earthquake recurrence. These sources, capable of generating moderate, large and great earthquakes occur in the interplate collision zone (Himalaya), ancient rift systems (Narmada, Kachchh) and unrifted crust (Killari) and the uplifted plateau (Shillong). Following are some of the key questions concerning the seismic hazard associated with these sources: Which faults are likely to generate damaging earthquakes in the near future? What is the maximum magnitude expected? How frequently do they generate earthquakes? What is the nature of ground acceleration and site amplification in these regions? In this paper, we address some of these questions in the context of some selected seismic sources in India (Killari, Jabalpur, Kachchh), that have generated moderate to large earthquakes in the recent times. The Killari earthquake of 1993 (M 6.3) occurred in a region of negligible background seismicity, considered as the zone of least seismic risk. The shallow source and site-specific amplification, together with the style of construction contributed to the severity of damage at this location. Paleoseismological investigations in the rupture zone suggested that the past earthquake in the same source may have occurred ~20000 years before present. The Kachchh seismic source presents a different picture where large earthquakes recur during shorter intervals of time (100s of years, as against 1000s at Killari). For example, the 1819 source appears to have generated a similar earthquake about 1000 years ago. Site amplification of energy and soil liquefaction, affecting locations as far as 150 km from the source, are considered major causes for the severity of damage, apart from the inadequate design of structures. Our studies have revealed existence of multiple sources in the Kachchh region, but their past histories remain largely unknown. We also present observations from the source zone of the great 1897 Shillong (Assam) earthquake, where we have dated the past earthquake in the same source as about 1200 years before present. Our study suggests that the seismogenic processes in the Shillong Plateau vary from that of the Himalaya and consequently, the hazard assessment in this region must consider these issues.*

## 1.0 INTRODUCTION

Hazard evaluation and mitigation measures such as developing appropriate design practices call for a reasonably good understanding of the

nature of earthquake sources. This understanding must include not only the knowledge about the location, size and potential (size and frequency, for example) of the structures concerned, but also the site-specific characteristics of damage (liquefaction potential, site amplification etc.). Attempts to assess the seismogenic potential of a fault based on its recent and historic activities reveal their histories during a small segment of time only, perhaps too short, compared to the interseismic interval. For example, instrumental data are available only for a few decades and the historic documents in most regions extent only to a few hundreds of years. Techniques such as archeo and plaeoseismology are often used to reconstruct the histories of such faults (see McCalpin, 1995). Knowing the timing of the past earthquakes often helps to obtain some handle on the future activity on the same fault. Obviously such information provide basic inputs for hazard assessment as well as information required in the planning of critical facilities such as nuclear power plants, in the proximity of seismogenic structures. These faults may not be active at the present time, but admittedly, the short period for which historic information is available does not really represent the seismogenic status of such structures. Ability to map a fault and develop its past histories may vary from one location to the other, based on the nature of activity on the fault (size and frequency of earthquakes, for example) as well as the site-specific nature of deformation. For example, in regions where large earthquakes have occurred in the recent/historic past and where the geological conditions are favorable for the generation and preservation of primary and secondary features, such studies are much easier, compared to regions of infrequent, low/moderate seismicity that does not lead to significant fault-related features such as fault scarps and offsets, liquefaction features etc.

Five damaging earthquakes occurred in India during the last ten years, causing substantial loss of life and damage to property. These were at Uttarkashi (1991,  $m_b$  6.5); Killari (1993,  $M_w$  6.2); Jabalpur (1997,  $M_w$  5.8); Chamoli (1999,  $m_b$  6.3) and Bhuj (2001,  $M_w$  7.7). Of these, the Chamoli and Uttarkashi earthquakes occurred in the Himalaya and these are not discussed in this paper. The other three events occurred in the peninsular India (Fig. 1), a part of the Stable Continental Region (SCR), characterized by slow deformation and low seismic productivity. In this paper we discuss the characteristics of these three seismic sources. We also present some observations about the source of the great 1897 Shillong earthquake in the NE India.

The Killari earthquake occurred in a region that had not experienced any notable seismicity in the past and was regarded to be of low seismic risk. This earthquake came as a total surprise and as a grim reminder that a damaging SCR earthquake can occur even at the least expected location. On the contrary, the 2001 Bhuj event occurred in a region that has experienced previous large earthquakes, the most notable being the one in 1819, a classic example of SCR-seismicity associated with passive rifts. It had caused more than 2000 deaths and brought about permanent changes to the landscape of the region. In comparison, to Killari and Bhuj earthquakes, the Jabalpur presents a different case; it was spatially coincident with the ENE-WSW

trending Narmada-Son lineament, which occasionally generates low-moderate earthquakes. These earthquakes are associated with an ancient rift system that closed subsequent to the Himalayan collision (see Rajendran and Rajendran 1999a and references therein). All of these earthquakes have been studied in detail and a large volume of information is available. The purpose of this paper is to use these examples to illustrate how moderate or large earthquakes in diverse tectonic settings can differ in their characteristics. Observations presented in this paper illustrate the need to adopt different strategies for hazard reduction, considering the diverse nature of these sources.

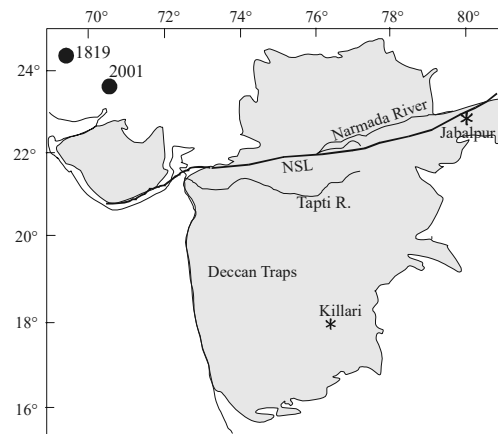


Figure 1: Map of western India showing earthquakes discussed in the text

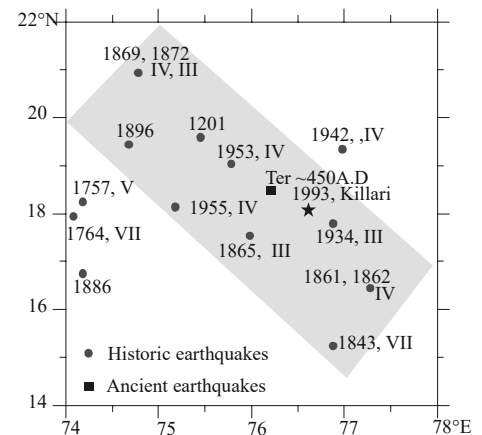


Figure 2: Historic seismicity in the Killari region. The shaded region indicates the NW corridor discussed in the text.

## 2.0 THE 1993 EARTHQUAKE AT KILLARI

The Killari earthquake occurred in the eastern margin of the Deccan Plateau, formed by Late Cretaceous-Eocene basalt flows (Fig. 1). The earthquake, which nucleated at shallow depth (5 km), was associated with hundreds of aftershocks (Kayal et al., 1996). Killari falls in zone I of India's seismic zonation map; this region has not experienced any significant earthquakes in the historic past and it was not considered as a potential site for a future damaging earthquake. Consequently, the level of awareness and preparedness, particularly in terms of construction practices was also very poor, a situation that increased the damages manifold. The generally low background seismicity, together with the perceived stability of the region made this earthquake appear as a total surprise. Its occurrence triggered many questions on the mechanism of SCR earthquakes. Some of these pertinent questions are: Do the SCR source zones share common characteristics? Are these earthquakes random or periodic? Do they repeat at the same source? Many of these questions remain to be answered fully, but the studies that followed the Killari earthquake provided a variety of data, helpful to address some of these questions.

Relatively inactive areas such as the source zones of the Killari earthquake seldom attract the attention of earthquake scientists. Thus, it is only after an earthquake actually strikes at such a location that one tries to examine whatever scanty data that may be available. We examined the earthquake catalogues for peninsular India (Rao and Rao, 1984), which indicate no earthquake of  $M > 6$  from this region during the recent or historic times ( $\sim 800$  years). The background seismicity associated with the Killari source seems to compare with those in other cratons, such as Australia. Interestingly, the locations of historic earthquakes during AD 1201-1960 (Geological Survey of India) appear to be mostly confined to a 400 km-long, NW corridor, passing through Killari (Fig. 2).

Spatial correlation of this corridor of activity with a structure inferred from a variety of field evidence as well as the fault plane solution of the main event suggested reactivation of a NW oriented fault (Rajendran et al., 1996). The 3-D distribution of aftershocks suggests that the earthquake originated at the intersection of the NW and EW oriented faults (Kayal et al., 1996). These observations suggest localization of strain build up, which may develop as future locations of earthquakes. Thus, the Killari-type earthquakes seem to occur in certain locations within the stable region, where the conditions for the localization and build up of stress are favorable. The next important question is if the Killari earthquake was a temporally isolated event or if any previous earthquakes have occurred on the same structure. We address this question through paleoseismological investigations in the rupture zone of the 1993 earthquake.

The Killari earthquake generated a small scarp (a few centimeters to about 80 cm) along a 1-km-long discontinuous rupture. Since very few SCR earthquakes are associated with surface ruptures, this earthquake presented a unique case for detailed field investigations. The deformation zone at Killari has since then been the site of many studies including trenching, deep drilling and other studies (Seeber et al., 1996; Rajendran et al., 1996 and Gupta et al., 1999). Initial studies in the rupture zone were concerned primarily with obtaining evidence for past earthquakes that may have occurred in the same source. Early shallow trenching suggested that the 1993 earthquake originated on a new fault (Seeber et al., 1996). However, deep trenches cut across the rupture zone exposed a wide impact zone comprising of minute fragments of rocks and grounded mass with yellowish clay, which was interpreted as evidence of previous movement (Rajendran et al., 1996). Indications of thrusting observed in the lateritized profile overlying the basalt flows were also considered as additional evidence for deformation in the layers basalt. Preliminary analysis based dating of gouge (based on thermo luminescence technique, TL) from the impact zone suggests an age of 18-20 ka for the penultimate earthquake at this source (Rajendran and Rajendran, 1999b). This appears to be in the range of repeat intervals observed for other cratonic regions, such as Australia. Evidence for previous movement has been obtained also from deep drilling in the rupture zone. A maximum displacement of about 6 m, observed in the deeper basalt layers is suggested as evidence for repeated reactivation. On a first approximation, this should suggest occurrence of at least six events

(assuming constant slip) subsequent to the last episode of basalt flow, suggesting interseismic intervals of the order of several 1000s of years, as suggested also by the TL data.

Search for paleoearthquakes in the vicinity of Killari led to the identification a deformation event dating to AD 350-450, at a location known as Ter, about 40 km northwest of Killari. Evidence for the occurrence of another earthquake in the NW corridor (Fig. 2) defined by historic earthquakes as well as structural trend is a possible indication that other discrete parts of this pre-existing weak zone may have been reactivated in different segments of time. We have no data on the older earthquakes on the Ter fault, but going by the example of Killari, it is reasonable to assume that the next event on this part of the fault may be thousands of years away.

The important question concerning the Killari source is whether there are other discrete segments of this fault that might be the next candidate for rupture? Because such structures seem hidden beneath the basalt and they are not expressed by any recent activity, will some of them spring another surprise? The biggest lesson to be learned from this earthquake is that seismic hazard assessment in the intracratonic regions must take into account, even the less prominent and perhaps unexposed faults. These may not be active in the current time window, but without an understanding of their past histories, hazard evaluation will not be complete. How did an M 6.3 earthquake lead to such total devastation in a few villages in the immediate vicinity of the epicentre? Apart from the poor style of rural construction, one aspect that compounded the damage is probably the amplification of seismic energy at the rock-soil interface. The thin soil profile (a few metres) overlying the basement rock appears to have provided an excellent medium for amplification of seismic energy as the waves passed from the high velocity basement to low velocity soil. The layered structure of the soil also provided ideal conditions for the generation of multiples. We believe that this peculiar site-specific behavior, together with the non-engineered nature of the rural houses were prime factors in the severity of damage at Killari.

### **3.0 THE 1997 EARTHQUAKE AT JABALPUR**

The Mw 5.8 earthquake near Jabalpur is spatially coincident with the ENE-WSW trending Narmada-Son rift (Fig 3). This earthquake killed 48 people and left many injured. Several thousands of houses were partially or completely damaged. The occurrence of this earthquake has perhaps guided to the conception and implementation of major project on microzonation of Jabalpur, which will put together a variety of information to prepare hazard zonation maps. Geological and geophysical surveys have unequivocally established this structure as deep fault zone, cutting across the entire breadth of central India. This structure is also associated with low-moderate seismicity and at least 4 earthquakes of magnitude > 5 have occurred in this region.



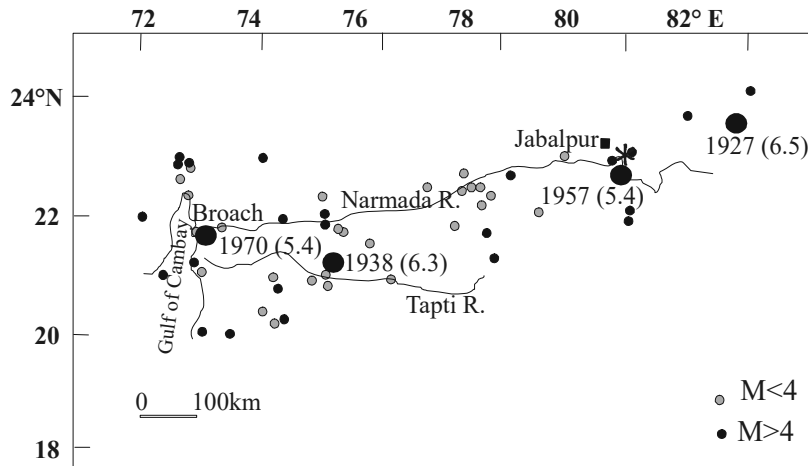


Figure 3: Historic and recent earthquakes in the Narmada rift region. The 1997 Jabalpur earthquake is indicated by a star.

In comparison to other shield-related earthquakes, those associated with ancient rift systems seem to be originating at mid-crustal or lower crustal depths. The Jabalpur earthquake also falls in this category, with its focus at a depth of 36 km. Another interesting aspect is the limited aftershock activity (see Rajendran and Rajendran, 1999a for details). While the Killari earthquake was followed by hundreds of aftershocks, the Jabalpur earthquake had only a few aftershocks. In terms of seismic hazard assessment, the nature of aftershock productivity is an important consideration, because a large number of aftershocks following a mainshock can lead to failure of structures already weakened by the main shock.

#### 4.0 SEISMIC SOURCES IN THE KACHCHH RIFT

##### 4.1 Allah bund: 1819

The 1819 earthquake (Mw 7.5) occurred on the northwestern flank of the Kachchh basin in NW India, a known seismic source in the Indian SCR (Fig. 4). The damage caused by this earthquake at Bhuj, located about 150 km southwest of its epicentral region is quite revealing of the severity of this earthquake. Nearly 7000 houses were destroyed in this town, killing more than 1150 people. The shock was felt in far away cities such as Ahmedabad (about 300 km from the epicentre) where a 400-year-old mosque was damaged (Oldham, 1926). This earthquake generated one of the most dramatic of the surface deformation features formed by an SCR earthquake—a nearly 60 km-long, warped zone with an average elevation of about 2.5 m high, popularly known as the *Allah Bund*. It caused widespread liquefaction in a large area, the farthest documented effect being at Porbandar, about 250 km south of its source zone (Oldham, 1926). Liquefaction of sediments appears to be the major cause for the submergence of the Sindri Fort, located about 8 km south of the *Allah Bund* (Rajendran and Rajendran, 2001). Damage from the 1819 earthquake suggested that a similar earthquake can affect distant cities such as Ahmedabad.

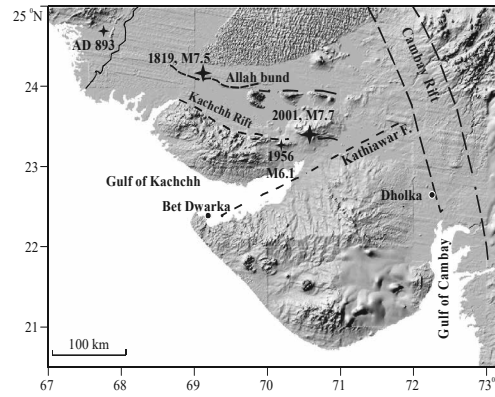


Figure 4: Map of Kachchh region showing the rifts, earthquakes and locations discussed in the text.

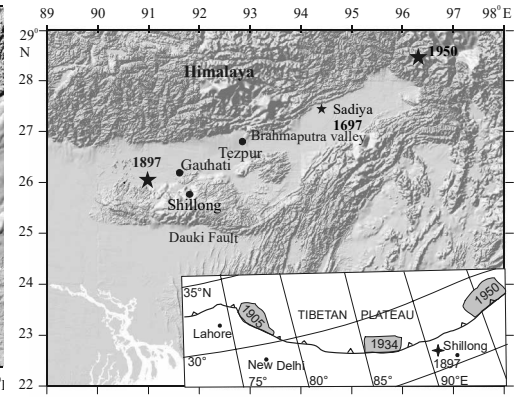


Figure 5: Map of NE India showing location of the 1897 Shillong earthquake. Inset shows the rupture areas of the 1905, 1934 and 1950 earthquakes. See text for discussion

With the experience of a large historic earthquake, we explored this region to understand its past activity. Paleoseismic investigations in the 1819 epicentral area suggested occurrence of another earthquake about 1000 years ago. By sifting through some historic documents, we could gather supplementary evidence suggesting that this event occurred in A.D. 893, providing additional constraints to the paleoseismic evidence. This is the first example from India, for constraining the date of past earthquake, in the source zone of a large earthquake, using paleoseismological as well as historical data (Rajendran and Rajendran, 2001, 2002).

Although our investigations helped to estimate the timing of the penultimate earthquake in the 1819 source, this information is still inadequate to suggest a recurrence interval for large earthquakes. One reasonable conclusion that we could derive is that the 1819 source has the potential to generate large earthquakes over a period of 1000 years. The occurrence of the 2001 Bhuj earthquake on an independent fault within the rift illustrated that earthquakes in the Kachchh rift are not just restricted to the *Allah Bund* source. The natural question that followed is whether there are other unknown sources, waiting to generate future large earthquakes. Paleoseismic data, although scanty, suggest the possibility for other potential sources, but their seismic histories remain to be explored.

#### 4.2 Bhuj: 2001

The 2001 source was not known to be associated with any previous large historical earthquakes, the only significant event in this region being the 1956 Anjar earthquake (Fig. 4). Compared to the 1819 earthquake, the surface effects of the 2001 earthquake were less dramatic in that it was not associated with any primary surface folding or rupture. However, this earthquake generated sandblows, ground fissures, minor strike-slip faults, linear mounds and small thrust scarps. Ground failure features include widespread liquefaction, lateral spreads and gas ejection, which were more intense within a radius of 50 km around the epicenter (Wesnousky et al.,

2001). The depth distribution of aftershocks suggested that the earthquake occurred on a fault that dips  $50^{\circ}$  toward the south, but the projection of this plane does not match with any mapped faults in the area. The depth range of aftershocks is from 10-35 km and the fact that there are no shallower events is consistent with the observation that there was no obvious main fault rupture for this earthquake. Based on the overall style of deformation, lack of a primary surface rupture and absence of aftershock activity at depths shallower than 10 km, the causative fault is considered as a blind thrust.

Compared to faults that are exposed and with well-expressed geomorphic features, possibly also associated with some discernible pattern of recent seismicity, blind thrusts pose more threat because of the lack of information on their existence. This situation can lead to severe earthquake-related damage at the least expected locations. The occurrence of a large earthquake on a hitherto unknown fault in the Kachchh rift pointed to the underestimation of seismic hazard associated with this structure. Whether this source has a similar history as the 1819 source and if there were more such unknown faults waiting to fail, became issues of immediate concern.

The Bhuj earthquake caused widespread liquefaction and related features in a large area. However, trenching in a few large craters in the epicentral area did not expose any significant evidence of older liquefaction. One example where a 2001 sand dike has cut an older sandblow was observed in a river valley at Dholka, near Ahmedabad, about 250 km south of the 2001 epicenter (see Fig. 4 for location). This trench provided a single TL age constraint of  $2948 \pm 295$  yr B.P., for the older dike (Rajendran et al., 2002). Causative source of this earthquake remains unknown, but the nearly 3000-year-long interval between the liquefaction events suggests two possibilities: one, that no earthquake may have affected this region during the intervening period and two, that the sandblows that formed during this period may have been eroded or disturbed by anthropogenic activities. Further work in this region has exposed more features belonging to the same vintage and we are inclined to believe that there are no missing events between the 3000-year-old and the 2001 earthquakes that have affected this region.

The history of damage to the ancient Harappan settlement at Mohenjo-daro (B.C. 2600 to B.C. 1600), located about 60 km north of the 2001 epicentre, offer additional constraints on the timing of the past earthquakes. Although this structure suffered only minor damages from the 2001 earthquake (some bricks at the entrance had fallen off), subtle evidence of a previous deformation event, in the form of a flexure is preserved on the brick wall in the central part of the fort. The 1819 earthquake did not cause any damage to this structure; paleoseismic investigations in this area did not expose any major features that could be related to that earthquake. However, this 4000-year fort underwent some significant repairs during the closing decades of Stage III of the settlement (B.C. 2500- B.C. 2200), possibly due to an earthquake (Joshi and Bisht, 1994). No major repair work is reported to have taken place since Stage III of this settlement. The question to be resolved is whether an older earthquake at the Bhuj source could have

caused this damage, requiring major reconstruction. Could the same earthquake have caused the damage at Dholavira and the liquefaction at Dholka? The underlying assumption here is that we know only about the Bhuj and Allah Bund sources, but this may not be the true situation. Paleoseismic studies suggest the possibility for a third source in the vicinity of Bet Dwarka where the last earthquake seems to have occurred around 2000 years ago.

### **4.3 A third source near Bet Dwarka?**

Bet Dwarka, a coastal island on the coast of Gulf of Kachchh, is known to have hosted human settlements dating back to more than 3000 years, this site offers opportunity to use archeological data in combination with paleoseismic evidence (see Fig. 4 for location). In one of the trenches excavated here, we observed a paleoliquefaction feature, which shares most attributes of seismically induced structures. Charcoal from the liquefied layer was dated to be  $1859 \pm 60$  yr B.P. (cal. A.D. 25-A.D. 328); the sediment immediately overlying this sandblow was dated as  $1980 \pm 40$  yr B.P. (cal. B.C. 50 - A.D. 100). We have proposed that an earthquake may have affected this area  $\sim 2000$  years ago, but its exact source remains to be constrained (Rajendran et al. 2003). The age data from Bet Dwarka does not compare with the data obtained from other sites and the obvious question is if we are dealing with a totally independent source. If these observations are correct, the Kachchh region features multiple sources which may show varying pattern of recurrence. We do not have a precise chronology on their past activities; nor do we know about their locations. However, going by the experience of the 1819 and 2001 earthquakes, one thing is very evident. Large earthquakes in this region tend to cause damage even at distant locations, due to liquefaction, lateral spreading and site amplification. The large range of distances in which liquefaction features are generated is itself a problem in pinpointing the exact source zones. But the knowledge that many seismic sources exist and that future earthquakes in each of these regions may affect far away locations should be an important criterion in the seismic hazard assessment of this region.

### **5.0 1897 SHILLONG EARTHQUAKE**

One of the largest earthquakes in the modern history, the mechanism of the 1897 Shillong (Assam) earthquake is still debated (see Fig. 5). While some workers relate it to the Himalayan fault system (Seeber and Armbruster, 1981 for example), there are other workers that view it as related to an independent source related to the Shillong Plateau (Bilham and England, 2001; Rajendran et al., 2004). Two issues regarding this earthquake remain poorly understood. One concerns the geometry of the fault and its relation to the Shillong Plateau and two, the age of the past earthquake in detail. Rajendran et al. (2004) have addressed these issues in detail and here we reproduced some of their important observations.

The 1897 earthquake generated massive liquefaction in the meizoseismal area, particularly within the Brahmaputra Valley (Oldham,

1899). We believe that identifying older generation liquefaction features and dating them would provide constraints on the previous earthquakes in this region. Previous workers conducted paleoliquefaction studies along the Krishnai and Chedrang Rivers, a region known for the 1897 coseismic secondary rupture (Sukhija et al., 1999a and b). These studies indicated evidence for at least two older earthquakes during A.D. 1450-1650 and A.D. 700-1050. Our re-evaluation of the published data suggests that the liquefaction features identified in this area can also be placed in two groups, based on their relative sizes. While the younger features (A.D. 1450-1650) are characterized by ~10 cm wide vents, the width of the older vents (A.D. 700-1050) is  $\geq 50$  cm. We conducted more excavations and came across multiple liquefactions- from 1897 and its predecessor. We highlight here the salient features of some interesting sedimentary features, exposed at two sites in the epicentral area (see Rajendran et al., 2004 for details).

Our observations data suggest that the penultimate earthquake in this region may have occurred between  $1250 \pm 80$  yr B.P. and  $2501 \pm 75$  yr B.P. In a region where history stretches to periods far beyond the probable timing of the penultimate earthquake, chronological constraints can be obtained also from monuments and other heritage structures. A catalogue of ancient monuments indicates that ruins of almost all of the stone temples discovered from various parts of the Brahmaputra valley belong to c. 9-10<sup>th</sup> century A.D. Historical data also reveal that during A.D. 9<sup>th</sup> –11<sup>th</sup> century, there was a wave of reconstruction activity in Assam (see Barua, 1966). Later generation construction in the contemporary style and inscriptions on some of these temples testify to their rebuilding. These reconstructions seem to have followed a massive destruction and the timing is in agreement with that of the large earthquake (~1200 yr B.P) inferred from the paleoliquefaction studies, discussed earlier.

Rajendran et al., (2004) made to important observations from the point of view of hazard evaluation in this region. Seeber and Armbruster (1981) proposed that the 1897 earthquake ruptured a 550-km-long segment of the Himalaya, filling the gap between the rupture zones of the great 1934 and 1950 earthquakes (see Fig 5, inset). Following this argument, it has been suggested that the 1897 earthquake has actually lowered the potential for a large earthquake in the Himalaya. If indeed the mechanism of the 1897 earthquake is unrelated to the thin-skinned tectonics of the Himalaya, the seismogenic processes and therefore the recurrence of earthquakes in the Shillong region will be independent of the Himalaya. In this scenario, the hazard assessment of the Shillong Plateau needs a different approach. The second issue concerns the potential of the Dauki fault (the southern boundary fault) which has not broken at least for the last 1000 years. The threats from the faults bordering the plateau remain underestimated; so also the hazard associated with the unbroken segment of the Himalaya, between the 1934 and 1950 ruptures.

## 6.0 DISCUSSION

The earthquakes at Kachchh and Killari may be considered as representative examples of two distinct types of SCR earthquakes. The former occurred in a pericontinental rift, where large earthquakes seem to recur during short intervals of time where as the latter originated in the shallow and un-rifted part of the SCR crust. The Jabalpur earthquake is somewhat different because of its association with a well-defined continental structure, known to have generated earthquakes in the past. Going by the nature of this structure, it appears that earthquakes of magnitude around 6 can be expected on any part of this structure and hazard assessment strategies must consider this possibility. The Kachchh seismic zone shares characteristics of other well-known sources associated with failed rifts elsewhere. For example, the recurrence period of the Kachchh-type earthquakes may be of the order of only 100s of years.

The current picture of the seismic history of the Kachchh region is very sketchy. Limited paleoseismic investigations in the region suggest existence of multiple sources associated with different fault systems. Seismic histories of these sources are barely known- two events separated by an interval of about 1000 years are known from the *Allah Bund* fault, but this data is insufficient to suggest a recurrence model. The Bhuj source, however is associated with a different recurrence rate, it does not seem to be generating large earthquakes in the same way as the 1819 source. The timing of the penultimate earthquake in the 2001 source is yet to be constrained and only after we gather more data, a comparison can be made with the 1819 source. Occurrence of another sandblow, belonging to an independent age bracket (2000 yrs), in the trench at Bet Dwarka brings up the possibility of a third source, whose location is not known. We need to constrain the sources of these earthquakes and develop better age constraints and this will be the focus of our future studies.

Hazard evaluation (which must start with estimation of timing, location and size of future earthquakes) is not a simple task, particularly in regions where multiple sources with complex seem to exist. In addition to the inherent uncertainties originating from the complexities of the source zone, what makes it more difficult at Kachchh is the lack of sufficient data. That some of the potential structures in this region remain hidden beneath the thick sediment deposits adds a more difficult dimension to this problem. A more or less complete picture of the active faults and their earthquake histories, quantification of strain using GPS-based observations are some of the important tasks to be completed. The investigations at Kachchh are only beginning and only through a concerted effort to combine geological observations with seismic reflection and GPS data, can we present a clearer picture of the seismic hazard associated with this important seismogenic source.

The Killari-type earthquakes in the unrifted crust may be considered as an outcome of slow tectonic processes, and by the very nature of that definition, earthquakes are expected to repeat only during much longer

intervals of time, compared to rift-type earthquakes. With its shallow focal depth, abundance in aftershock activity and subdued neotectonic expressions of the source zone, the Killari earthquake is comparable to typical SCR events in the Australian shield. Seismic hazard assessment of SCR regions is complicated also because of the incompleteness in data. In the absence of high quality data from each of the SCRs, assessment of the seismogenic processes may have to rely also on data from analogous settings elsewhere. As more data are generated from various source regions, it may be possible to identify analogies in their characteristic sizes, patterns of recurrence and deformation mechanisms.

Hazard evaluation must essentially combine a variety of information starting from details of active faults, site characteristics as well as population centres, life-lines etc., using latest tools such as the GIS. Geological and paleoseismological data can provide information on the location and past activities associated with some of the seismic sources. These include dimensions of the fault and expected style of deformation; they would also provide some estimates on the locations and sizes of past earthquakes and also identify regions of highest liquefaction potential. The most important input to this data base must come from ground acceleration and geotechnical studies. This is one area that requires more efforts. As more of such data become available, hazard maps indicating the probabilities of ground shaking can be prepared. Clearly, strategies to be followed in Kachchh region are different from that at Killari or Jabalpur, as has been demonstrated in this paper. Similarly, the hazard caused by the 1897-type earthquakes, associated with structures that are not part of the Himalaya may need re-evaluation. The important task right now is to expand the data base on the nature and history of active faults so that appropriate hazard assessment scenarios can be developed, for each region. Paleoseismological studies being carried out in the known sources of earthquakes is a step in that direction.

## REFERENCES

- Barua, R.K.L., 1966. *Early history of Kamarupa*, Lawyers's Book Stall, Gauhati, Assam, 234p.
- Bilham, R., and England, P., 2001. Plateau 'pop-up' in the great 1897 Assam earthquake, *Nature*, 410, 806-809.
- Gupta, H.K., Rao, R.U.M., Srinivasan, R., Rao, G.V., Dwivedy, K.K., Banerjee, D.C., Mohanty, R and Satyasradhi, Y.R., 1999. Anatomy of surface rupture zones of two stable continental region earthquakes, 1967 Koyna and 1993 Latur India. *Geophys.Res.Lett.*, 26, 1985-1988.
- Joshi, V.P. and Bisht, R.S. 1994. "*India and the Indus Civilization*" National Museum Institute, New Delhi, 1994, 22-31.
- Kayal, J.R., Reena De, Das, B and Chowdhury, S.N., 1996. Aftershock monitoring and focal mechanism studies; Killari earthquake. *GSI SPL PUB 37*, 165-185.
- McCalpin, J. 1996. *Paleoseismology*, Academic Press, 588pp.

- Oldham, R.D., 1899. Report of the great earthquake of 12th June, 1897, Mem. Geol. Surv. India, reprinted: 1981, *Geol. Surv. India, Calcutta*, 379p.
- Oldham, R.D., 1926. The Cutch (Kachh) earthquake of 16th June 1819 with a revision of the great earthquake of 12th June 1897. *Geological Survey of India Memoir*, 71-147.
- Rajendran, C.P., Rajendran, K., and John, B., 1996. The 1993 Killari (Latur), Central India, and Earthquake: An Example of Fault Reactivation in the Precambrian Crust. *Geology*, 24, 651-654.
- Rajendran, K., and Rajendran, C.P., 1999a. Seismogenesis in the Stable Continental Interiors: An appraisal based on two examples from India. *Tectonophysics*, 305, 355-370.
- Rajendran, C.P., and Rajendran, K., 1999b. Geological investigations at Killari and Ter, Central India and their Implications for Paleoseismicity in the Shield Region. *Tectonophysics*, 308, 67-81.
- Rajendran, C.P. and Rajendran, K., 2001. Characteristics of deformation and past seismicity associated with the 1819 Kutch earthquake, Northwest India. *Bull. Seism. Soc. Am.*, 91, 3, 407-426.
- Rajendran, K., Rajendran, C.P., Thakkar, M., Gartia, R.K., 2002. Sand blows from the 2001 Bhuj earthquake reveal clues on past seismicity, *Current Science*, 83, 5, 603-610.
- Rajendran, C.P. and Rajendran, K., 2002. Historical constraints on previous seismic activity and morphologic changes near the source zone of the 1819 Rann of Kutch earthquake: Further light on the penultimate event. *Seism. Res. Lett.*, 73, 470-479.
- Rajendran, C.P., Rajendran, K., Vora, K.H. and Gaur, A.S., 2003. The odds of a seismic source near Dwarka, NW Gujarat: An evaluation based on proxies. *Current Science*, 84, 5, 695-699.
- Rajendran, C.P., Rajendran, K., Duarah, B.P., Baruah, S. and Earnest, A., 2004. Interpreting the style of faulting and paleoseismicity associated with the 1897 Shillong, northeast India, earthquake: Implications for regional tectonism, *Tectonics*, 23, doi 10.1029/2003TC00165.
- Rao, B.R and Rao, S., 1984. Historical seismicity of peninsular India. *Bull. Seism. Soc. Am.*, 74, 2519-2533.
- Seeber, L., and Armbruster, J. 1981. Great detachment earthquakes along the Himalayan arc and long-term forecasting, in: *Earthquake Prediction: An International Review, Maurice Ewing Ser. Vol. 4, edited by D.W. Simpson and P.G. Richards, AGU, Washington, D.C.*, pp. 259-277, 1981.
- Seeber, L., Ekstron, G., Jain, S.K., Murty, C.V.R., Chandak, N and Armbruster, J.G., 1996. The 1993 Killari earthquake in central India: A new fault in Mesozoic basalt flows? *Journal of Geophysical Research*, 101, 8543-8560.
- Sukhija, B.S., Rao, M.N. Reddy, D.V. Nagabhushanam, P., Hussain, S., Chadha, R.K and Gupta, H.K., 1999a. Paleoliquefaction evidence and periodicity of large prehistoric earthquakes in Shillong Plateau, India. *Earth and Planetary Sci. Lett.*, 167, 269-282.
- Sukhija, B.S., Rao, M.N. Reddy, D.V. Nagabhushanam, P., Hussain, S., Chadha, R.K and Gupta, H.K., 1999b. Timing and return period of major paleoseismic events in the Shillong Plateau, India, *Tectonophysics*, 308, 1999b.



Wesnousky, S.G., Seeber, L., Rockwell, T.K., Takkur, V.C., Briggs, R., Kumar, S and Ragona, D., 2001. Eight days in Bhuj: Field Bearing on surface rupture and genesis of the 26 January earthquake in India, Seism. Res. Lett., 72, 514-524.

# **CAPACITY BUILDING IN INDIA TOWARDS EARTHQUAKE RISK REDUCTION - ROLE OF IIT KANPUR IN PAST TWO DECADES**

SUDHIR K. JAIN AND C.V.R.MURTHY  
Indian Institute of Technology Kanpur, India  
*skjain@iitk.ac.in and cvrm@iitk.ac.in*

India faces moderate to severe seismic hazard over 60% of its land area. The lessons learnt from earthquakes that occurred in the country in the last two decades indicate that the country is far from being prepared to face earthquakes with no fatalities and minimal economic setback. IIT Kanpur recognized this national need about decades ago, and undertook small initiatives that set out small goals that address different facets of this national challenge of marching towards earthquake preparedness. The major work undertaken at this institute is focused on developing seismic design and construction in the country. The various initiatives include:

- (a) Teaching the subject of earthquake engineering as part of the undergraduate and post-graduate programs, and to practicing professionals and teachers of other colleges in India as part of the continuing education programs;
- (b) Conducting research on specific aspects of earthquake resistant design and construction through research conducted by students and research sponsored by various governmental agencies in the country;
- (c) Undertaking a comprehensive review of the seismic codes in India, developing provisions for seismic design and construction afresh that eventually lead to new Indian standards, and proposing modifications to existing provisions;
- (d) Setting in place a national clearing-house at IIT Kanpur for collection and dissemination of information at the national level on earthquake resistant design and construction;
- (e) Working with the Ministry of Human Resource Development of the Government of India in planning and executing the first phase of a major initiative of developing a teaching resource in the subject of earthquake resistant design and construction in engineering and architecture colleges in India; and
- (f) Initiating a set of small projects and human resource nuclei that are expected to eventually create a professional environment of strong and vibrant community of professionals with a background in earthquake resistant design and construction.

Details of these macro and micro initiatives undertaken at this Institute are given in the documents listed below:

- \_\_\_\_\_, Earthquake Engineering at IIT Kanpur, [www.nicee.org/EQ\\_Engg/eq\\_engg.htm](http://www.nicee.org/EQ_Engg/eq_engg.htm).
- Jain, S.K., and Murty, C.V.R., “Some Capacity Building Initiatives in India on Earthquake Risk Reduction,” Proceedings of the World Congress on Natural Disaster Mitigation, New Delhi, 19-22 February 2004, Vol.1, pp 217-222.
- Jain, S.K., and Agrawal, P., “Earthquake Engineering Capacity Building in Educational Sector in India,” CD ROM Paper No. 3245, 13th World Conference on Earthquake Engineering, Vancouver, Canada, 1-6 August 2004.
- \_\_\_\_\_, Programme Implementation Plan, National Programme on Earthquake Engineering Education, Ministry of Human Resource Development, Government of India, New Delhi, [www.nicee.org/npeee](http://www.nicee.org/npeee).
- \_\_\_\_\_, National Programme on Earthquake Engineering Education (NPEEE), Ministry of Human Resource Development, Government of India, New Delhi, [www.nicee.org/npeee](http://www.nicee.org/npeee)
- \_\_\_\_\_, National Information Center of Earthquake Engineering (NICEE), Indian Institute of Technology Kanpur, [www.nicee.org](http://www.nicee.org).
- Murty, C.V.R., “IITK-BMTPC Earthquake Tips - Learning Seismic Design and Construction,” [www.nicee.org/EQTips/IITK\\_BMTPC.htm](http://www.nicee.org/EQTips/IITK_BMTPC.htm).

# **CASUALTY OCCURRENCE MECHANISM INDUCED BY TRAIN ACCIDENT DURING AN EARTHQUAKE**

JUNJI KIYONO AND KATSUMI NAGAI

Graduate School of Engineering, Kyoto University, Japan

kiyono@quake.kuciv.kyoto-u.ac.jp

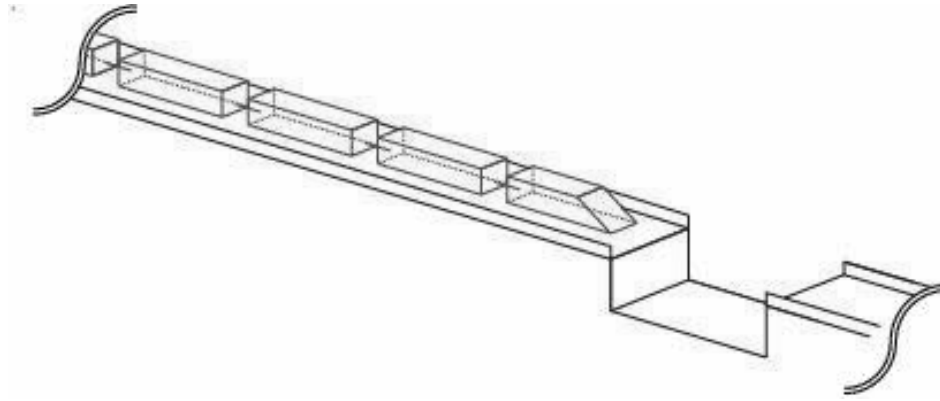
## **ABSTRACT**

*Damage to railway facilities is reported in the past earthquakes. Especially in the 1995 Hyogo-ken Nanbu Earthquake, totally thirty-two railway bridges were collapsed, and eight of which occurred at the San'yo super express line. Fortunately the train accidents caused by the damage to bridges have not been reported so far. Although the large earthquake that strongly affects the train behavior hardly occurs, the effect of the accident to the society is unpredictable once such large earthquake will occur. In this study, we modeled a train and passengers in the train as distinct elements and simulated their behavior by DEM. The impact force acted on the human body is computed and compared with the results from the experiments done by the automobile engineering field. It is found that the velocity of 80 km/h is a transition speed for both behaviors of trains and damage to passengers.*

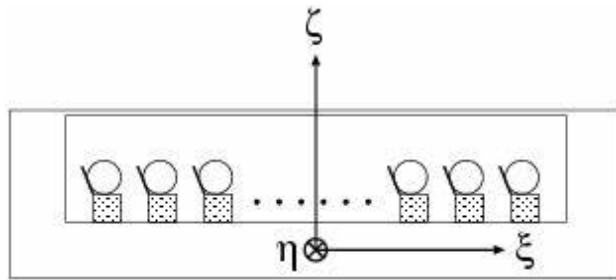
## **1.0 INTRODUCTION**

Many damages to railway facilities are reported in the recent historical earthquakes. Train accidents occur in nine past earthquakes in Japan. In the 1995 Hyogo-ken Nanbu Earthquake, seventeen trains were derailed, but fortunately nobody died by the accident. The trains of the Southern Pacific Railway in U.S. were also derailed during the 1994 Northridge earthquake. Damage to railway bridges was occurred in the 1964 Niigata Earthquake, the 1978 Miyagi-ken Oki Earthquake and the 1989 Loma Preate Earthquake. Thirty-two railway bridges including eight bridges of the San'yo super expressway were collapsed in the 1995 Hyogo-ken Nanbu Earthquake. Many train accidents induced by earthquakes have been reported, however, the terrible accident such that the trains crashed into a collapsed part of the bridges has never happened so far.

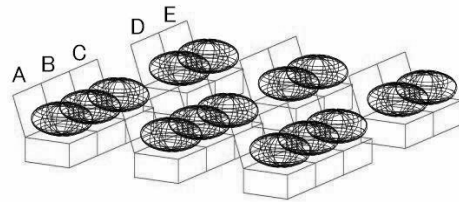
Although a large earthquake just beneath the urban area has seldom occurred, we have to anticipate and prepare for such a severe train accident. In this study, the case that the trains crash into a collapsed part of a destroyed overhead bridge is considered. Behaviors of the trains and passengers in them are simulated by use of the Distinct Element Method (DEM). We calculate the force that acts on the human body, and discuss the human casualty of the earthquake-induced train accident according to the damage criteria to the body for the car accident.



*Figure1: Train-collapsed bridge model*



*(a) 2D section of the train (interior space, seats and passengers)*



*(b) 3D model of seats and passengers*

*Figure 2: Analytical model of the inside of the train*

## 2.0 METHOD

A train and a human body are modeled as a three dimensional rigid element. The trains and the overhead bridge with a collapsed part are shown in Figure 1. The human bodies are expressed by spherical elements and arranged as shown in Figure 2 (a) and (b). The trains are numbered from a right side as No.1-No.16, and the human elements also from No.1 to No.20 for each row (A-E).

### 2.1 Equation of motion

The DEM, a numerical analysis method that computes the position of each element by solving the equations of motion step by step, was used.

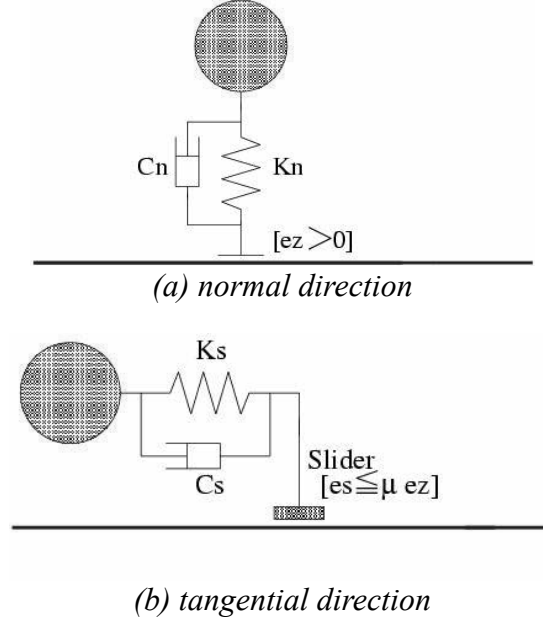


Figure 3: Contact model (virtual spring and dashpot)

All the elements are assumed to be rigid. Virtual springs and dashpots in the normal and tangential directions are generated when an element comes in contact with other elements (Figure 3). The contact force acts through these generated virtual springs and dashpots. By solving the equation of motion for each element step by step, the behavior of all the elements can be traced. The forces acting on an element are the external force  $(f_x, f_y, f_z)$  and the total sum of the contact forces between elements  $(F_x, F_y, F_z)$ . Accelerations of an element in a 3D case are calculated by:

$$\ddot{x} = (f_x + \sum F_x) / m \quad (1)$$

$$\ddot{y} = (f_y + \sum F_y) / m \quad (2)$$

$$\ddot{z} = (f_z + \sum F_z) / m \quad (3)$$

in which  $m$  is the element's mass and  $\Delta t$  the time increment in the analysis. Assuming that acceleration is constant for the short period,  $\Delta t$ , the velocity and displacement of each element can be calculated by the following difference scheme. Total structural behavior therefore can be traced.

$$\begin{Bmatrix} \dot{x}_t \\ \dot{y}_t \\ \dot{z}_t \end{Bmatrix} = \begin{Bmatrix} \dot{x}_{t-\Delta t} \\ \dot{y}_{t-\Delta t} \\ \dot{z}_{t-\Delta t} \end{Bmatrix} + \begin{Bmatrix} \ddot{x}_{t-\Delta t} \\ \ddot{y}_{t-\Delta t} \\ \ddot{z}_{t-\Delta t} \end{Bmatrix} \Delta t \quad (4)$$

$$\begin{Bmatrix} x_t \\ y_t \\ z_t \end{Bmatrix} = \begin{Bmatrix} x_{t-\Delta t} \\ y_{t-\Delta t} \\ z_{t-\Delta t} \end{Bmatrix} + \begin{Bmatrix} \dot{x}_{t-\Delta t} \\ \dot{y}_{t-\Delta t} \\ \dot{z}_{t-\Delta t} \end{Bmatrix} \Delta t \quad (5)$$

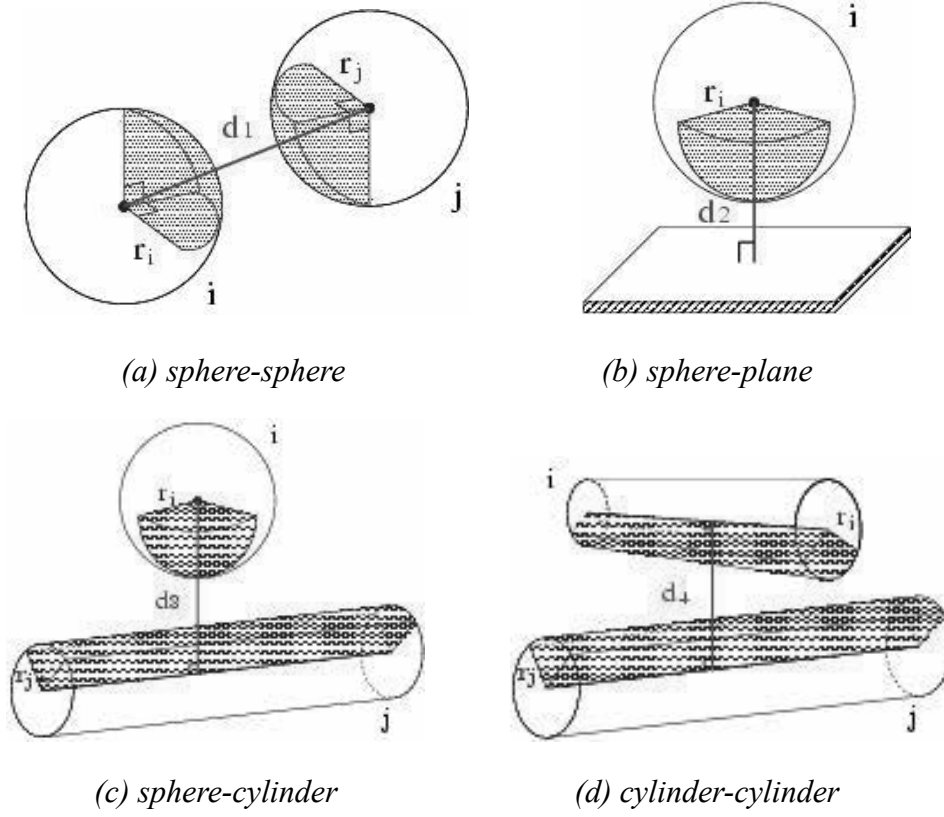


Figure 4: Contact patterns of the element

Rotation is obtained from Euler's equations of motion. Equations for the  $\xi$ -,  $\eta$ -, and  $\zeta$ -directions are

$$I_{\xi} \frac{d\omega_{\xi}}{dt} - (I_{\eta} - I_{\zeta})\omega_{\eta}\omega_{\zeta} = \left(\sum_i r_i \times F_i\right)_{\xi} \quad (6)$$

$$I_{\eta} \frac{d\omega_{\eta}}{dt} - (I_{\zeta} - I_{\xi})\omega_{\zeta}\omega_{\xi} = \left(\sum_i r_i \times F_i\right)_{\eta} \quad (7)$$

$$I_{\zeta} \frac{d\omega_{\zeta}}{dt} - (I_{\xi} - I_{\eta})\omega_{\xi}\omega_{\eta} = \left(\sum_i r_i \times F_i\right)_{\zeta} \quad (8)$$

in which  $\xi$ ,  $\eta$ , and  $\zeta$  are the inertia axes of the coordinates, and  $I_i$  and  $\omega_i$  ( $i = \xi, \eta, \zeta$ ) respectively are the moments of inertia and rotational velocities around the center of gravity in the inertial frame of reference.

## 2.2 Contact judgment

When elements come into contact, the spring and dashpot are generated in the calculation. Judgment of contact for the 3D analysis is based on the use of spherical and cylindrical elements, but the process is the same 2D circular elements. The contact models for the 3D analysis, shown in Figure 4; upper left is a case in which the spherical elements are in contact, upper right the spherical element and plane, bottom left the

spherical element and cylindrical element, and bottom right cylindrical elements. Judgment of contact is made by considering the collocation between the two elements concerned.

In order to make the judgment simple, the train was modeled by the use of 1/8-sphere and 1/4-cylinder for its corner and edge. The rail was modeled 1/2-cylinder.

### 2.3 Contact force

Increments of the restoring and damping forces in the normal and tangential directions,  $(\Delta e_n, \Delta e_s, \Delta d_n, \Delta d_s)$ , for the interval  $\Delta t$  are expressed by the increments of relative displacement in the normal and tangential directions,  $\Delta n$  and  $\Delta s$ ;

$$\Delta e_n = K_n \Delta n \quad (9)$$

$$\Delta e_s = K_s \Delta s \quad (10)$$

$$\Delta d_n = C_n \Delta n / \Delta t \quad (11)$$

$$\Delta d_s = C_s \Delta s / \Delta t \quad (12)$$

in which  $K_n$  and  $K_s$ , and  $C_n$  and  $C_s$ , respectively are the spring constants and damping coefficients in the normal and tangential directions. The restoring and damping forces in each direction,  $([e_n]_t, [e_s]_t, [d_n]_t, [d_s]_t)$  at the arbitrary time  $t$  are obtained from the preceding equations;

$$[e_n]_t = [e_n]_{t-\Delta t} + \Delta e_n \quad (13)$$

$$[e_s]_t = [e_s]_{t-\Delta t} + \Delta e_s \quad (14)$$

$$[d_n]_t = \Delta d_n \quad (15)$$

$$[d_s]_t = \Delta d_s \quad (16)$$

When the restoring force exceeds the friction limit, the tangential force is governed by dynamic friction. The total contact forces in both directions are

$$[F_n]_t = [e_n]_t + [d_n]_t \quad (18)$$

$$[F_s]_t = [e_s]_t + [d_s]_t \quad (19)$$

The forces,  $F_x$ ,  $F_y$  and  $F_z$ , in Eqs. (1), (2) and (3) are obtained by combining the above forces in the target direction.

## 3.0 PARAMETERS USED IN THE ANALYSIS

### 3.1 Element parameters of train and human body

The various parameters of the train are determined according to the 700-type bullet train [Table 1, and Figure 5 (a), (b)]. The parameters of the human body are given by using the experimental results (Kiyono *et al.*,



1998) as shown in Table 2. The speed of the train is defined when the train has reached to 5m behind the collapsed place. The contact parameters of the train and the human elements are used according to the previous study (Kiyono *et al.*, 2003).

Table 1: Element parameters for train

$m$ (ton)	44.25
$I_{\xi}$ (ton·m <sup>2</sup> )	42.28
$I_{\eta}$ (ton·m <sup>2</sup> )	2304.78
$I_{\zeta}$ (ton·m <sup>2</sup> )	2346.81
$l(m)$ [Car No.1 & No.16]	11.53
$l(m)$ [Car No.2 to No.15]	12.50
$b(m)$	3.38
$h(m)$	3.65
$l_G(m)$ [Car No.1]	11.53
$l_G(m)$ [Car No.2 to No.15]	12.50
$l_G(m)$ [Car No.16]	15.82
$b_G(m)$	1.69
$h_G(m)$ [Car No.1 & No.16]	0.636
$h_G(m)$ [Car No.2 to No.15]	0.650
$l_t(m)$	9.20
$h_b(m)$	1.30

Table 2: Element parameters for human body

$r(m)$	$m$ (kg)	$I_{\theta}$ (kg/m <sup>2</sup> )
0.219	64.00	1.228

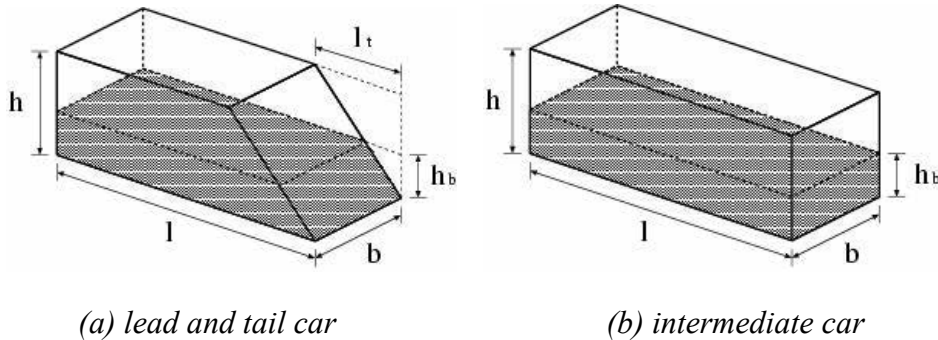


Figure 5: Parameter of the train

### 3.2 Chest-G and HIC

Damage to human body is assessed by the combination of the maximum impact acceleration (Chest-G) and Head Injury Criteria (HIC) frequently used in the field of car engineering. The value of HIC is calculated as follows;

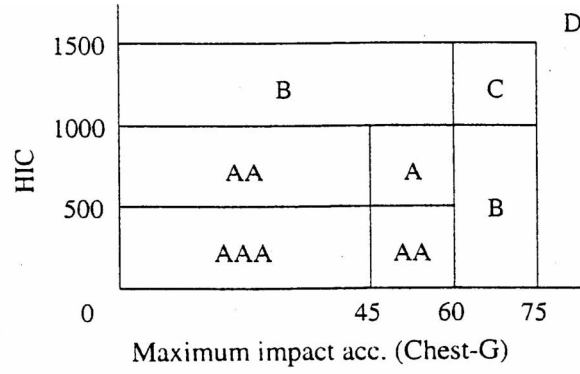


Figure 6: Classification of damage levels

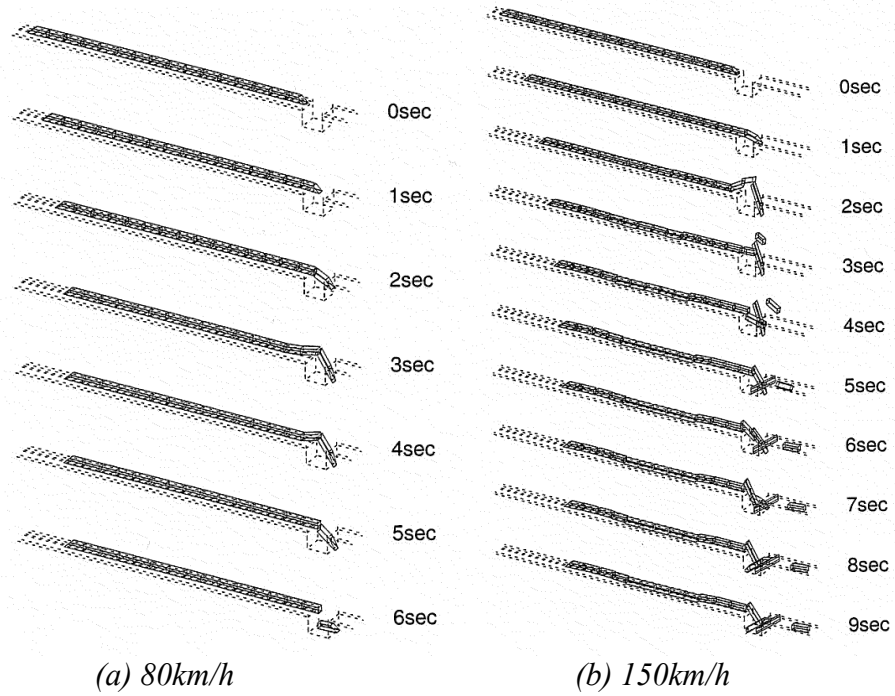


Figure 7: Behavior of the train with (a) 80km/h and (b) 150km/h in speed

$$HIC(t) = [T \{ \frac{1}{T} \int a(\tau) d\tau \}^{2.5}]_{\max} \quad (20)$$

In which  $t$  is an arbitrary time and  $T$  the duration time of the impact that satisfies  $T < 36$  (msec). The assessment of the damage based on the Chest-G and HIC is shown in Figure 6. We compared the simulation results of the car crash to the wall with those of the experiment in order to check the validity of the analysis. Both were in good agreement (Kiyono *et al.*, 2003).

#### 4.0 SIMULATION OF TRAIN ACCIDENT

The number of the trains is 16, the passengers in No.1 and No.16 car are 65 and intermediate car 100 persons. The span length and height of the

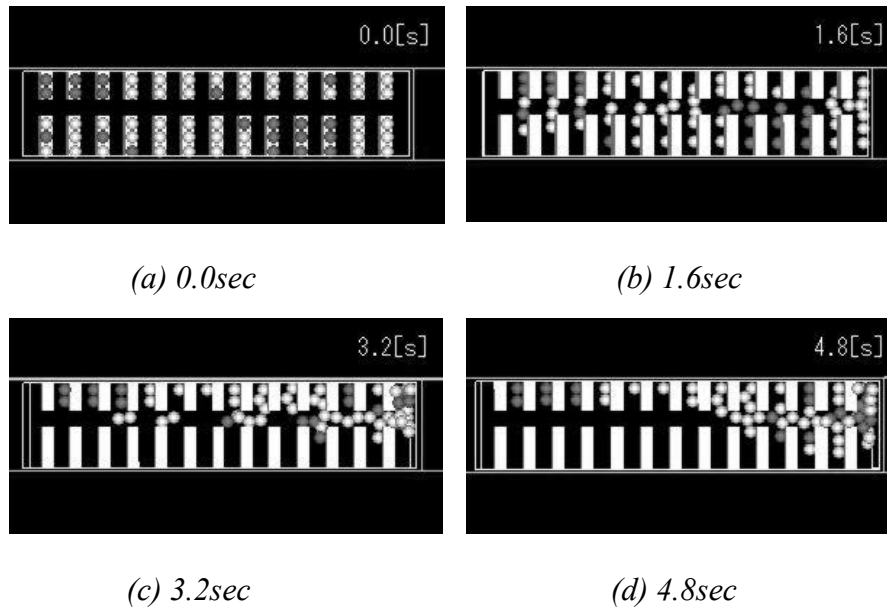


Figure 8: Behaviors of passengers in the car No.1 (80km/h)

collapsed overhead bridge are 30m and 10m, respectively. The reclining angle of the seat is 10 degree. The input ground motions used are the three components recorded at the Kobe Marin Observatory in the 1995 Hyogoken Nanbu earthquake. The input ground motion is assumed to propagate with an apparent velocity of 3km/sec in order to express three dimensional behavior of the train. The constraint of y-direction movement is released when the transversal acceleration exceeds 570gal or the uplift height from the rail exceeds 30mm, then the train derails.

Figure 7 (a) and (b) show the behaviors of the trains of which speeds are 80 and 150km/h, respectively. In case of 80km/h, the first train hits to the side wall directly, and the second car is lifted up. The deformation to the y-direction becomes large with increase in speed, however, each car almost collides head-on. In case that the speed exceeds 150km/h, the first two trains jump upward in order to release the energy. The behaviors of passengers in the car No.1 with 80km/h speed are shown in Figure 8 (a), (b), (c) and (d). As the train tilt and fall into the collapsed part of the bridge, the passengers in the train show the complex behaviors.

## 5.0 DAMAGE ASSESSMENT TO HUMAN BODY

The damage to human bodies is estimated by using the indexes of Chest-G and HIC. Analytical conditions of the train are same as the previous section. The speeds are varied such 6 cases as 50, 60, 70, 80, 90, and 100km/h. Damage levels for all passengers in the trains are calculated. The damage rate for each speed is shown in Figure 9. When the speed is less than 60-70km/h, more than 90% of passengers are ranked as triple-A. When the speed becomes 100km/h, more than 60% of passengers are ranked as D. The damage level of human body changes drastically around 70-80km/h.

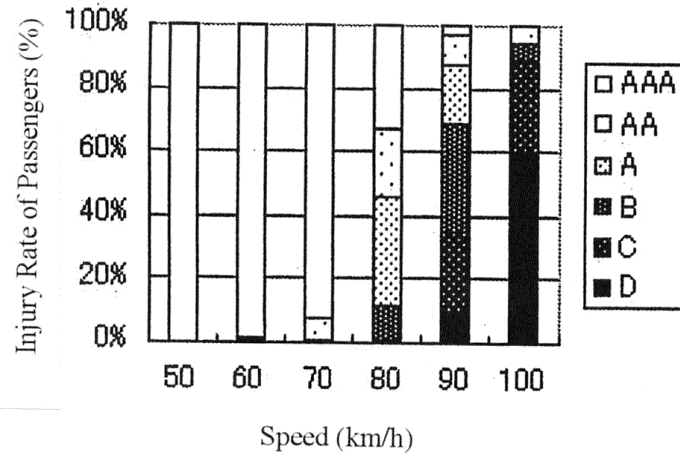


Figure 9: Damage rate for various speeds

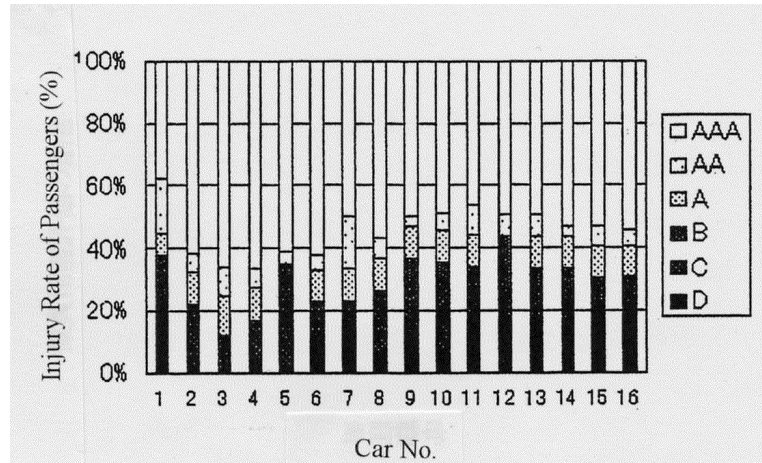


Figure 10: Average damage level for each car

Figure 10 shows the average damage level for each car. The rate of rank-AAA becomes large in the first car because its behavior is very complicated such like falling, crashing, and jumping. The rate of rank-D becomes smaller as the train is locating in the front position except Car No.1. The main reason that the force to the x-direction is decreased as the displacement to the y-direction becomes large for the front cars.

## 6.0 CONCLUSION

In this study, we simulated the earthquake-induced train accident when the overhead bridge collapsed by the strong ground motion. When the train speed exceeds 150km/h, the trains show very complicated behaviors such like falling, crashing, and jumping. The damage to passengers in the train was calculated according to the index of Chest-G and HIC. The damage level to human body also changes around the transition speed of 70-80km/h.

## ACKNOWLEDGEMENT

This research is supported by the Takahashi Industrial Economics and Research Foundation. The authors deeply acknowledge for this support.

## REFERENCES

- Kiyono, J., F. Miura and H. Yagi, 1998. *Simulation o Evacuation Behavior in a Disaster by Distinct Element Method*. Proc. of the Japan Society of Civil Engineers, No.591/I-43, 379-390 (in Japanese with English abstract).
- Kiyono, J. and K. Nagai, 2003. *Earthquake-induced Train Accident and Its Casualty Occurrence Mechanism*. Journal of Social Safety Science, **5**, 1-10 (in Japanese with English abstract).
- Nagase, K., K. Kondo and T. Nomura, 1997). *Train Damaged by the Quake in Kobe*. Proc. of the Japan Society of Mechanical Engineering, **63**(606), 300–307 (in Japanese).
- National Organization for Automative Safety and Victim's Aid, 2000. New Car Assessment, Japan (in Japanese).

# **DAMAGES TO MASONRY BUILDINGS IN DIEN BIEN PHU EARTHQUAKE**

PHAN QUANG MINH  
Hanoi University of Civil Engineering, Vietnam  
*pqminh1001@yahoo.com*

## **ABSTRACT**

*On February 19<sup>th</sup>, 2001, a 5.3 on Richter scale an earthquake struck Dien Bien Phu Town (North West Vietnam), where most of buildings are masonry. This paper presents an overview of damage to masonry buildings in the affected area and problems related to their strengthening.*

## **1.0 INTRODUCTION**

Vietnam is a country situated in seismically active region. Within the last 10 years a number of earthquakes have occurred in North West Vietnam, with the earthquakes in 1981 and 2001 measuring 6.6 and 5.3 respectively on Richter scale. The last event occurred at 22:53 local time on February 19<sup>th</sup> 2001. The epicenter was located 15 km from Dien Bien Phu Town, the focal depth was 12 km. Numerous aftershocks were recorded with magnitude of 4,2 to 4,9 on Richter scale. The earthquake resulted in economic consequences to the one of poorest regions of Vietnam.

For a long time, in Vietnam design norm, the earthquake load was not required for the design of buildings, except these of high importance. Up to now, Vietnam still has no official code for the seismic resistant design of buildings. The study of Dien Bien Phu earthquake damage plays a very important role in the compiling of Vietnamese norm for seismic design. In this article, the damages to masonry buildings and their strengthening are discussed.

## **2.0 DAMAGES OF MASONRY BUILDINGS**

Dien Bien Phu Town is located in the North West Vietnam with 227,000 citizens, a number of whom are from ethnic minorities. The majority of 1-storey and 2-storey buildings constructed before 1994 were unreinforced masonry with low strength of materials (burnt brick, lime mortar). Most of the bearing walls were 220 mm thick. Due to the local design preferences and climate conditions, the houses had high first storeys (about 4.2m) with large openings. The R/C slab of these constructions is made 70-80 mm thick. After 1994, reinforced concrete frames with infill masonry are used for buildings with 2 to 4 storeys in the town. In the suburbs, however houses with brick bearing walls and R/C slabs are widely used. None of the constructed buildings are following any seismic provision. The earthquake in 2001 caused:

- Up to 7700 damaged houses, 70% were 2-3 storey buildings, out of which 1257 buildings were heavy damaged. Most of the damaged buildings were unreinforced masonry. The bearing walls were subjected to the out-of-plane deformation, the width of cracks was to 4cm. The cracks of bearing walls were almost diagonal and often located between two openings or near the corners of buildings (Fig 1).



*Figure 1: Damage of bearing wall*

- The reinforced concrete frames were not affected, only observed cracks of infill masonry related to bond slip or openings.
- 2-storey building of Dien Bien Phu secondary school was heavy damaged. The structure of this building was brick bearing walls with R/C slabs. Interesting to note that another school building with the same structure, located down the hill and 30m far from first building, was experienced very little damage.
- 1 irrigation construction was damaged due to ground failure.
- There is one high structure in the area, the TV steel tower with 40m high, located on the hilltop. The tower was not affected, although some bracing elements were bent.

According to the investigation of the masonry buildings in affected areas, some main reasons for damage and failure were identified as given in Table 1.

*Table 1: Causes of failures in masonry structures*

(a) Defect of construction	(e) Openings close to corners.
(b) Lack of confining ties in unreinforced masonry	(f) High first storey
(c) Long walls (compared to their thickness)	(g) Soft first story
(d) Previously occurring cracks in walls (due to settlement, etc.)	(h) Low strength of materials
	(i) Bending of slabs
	(j) Poor connection between R/C frames and infill masonry

### 3.0 RESTORATION & STRENGTHENING OF MASONRY BUILDINGS

After the main earthquake, most damaged buildings were temporality supported. A decision to repair, restore or strengthen these needed to be taken urgently and depended on the level of damage. For example, it was decided to destroy and rebuilt buildings with very heavy damage, strengthen (with addition RC elements) those with substantial to heavy damage, and restore buildings with upto moderate damage. Also, the technique of restoration and strengthening took into consideration the short time and low cost of construction, locally available material, and the capability of the semi-skilled labors, etc.

#### 3.1 Restoration of buildings

For bearing walls with large cracks, the procedure adopted was – (a) Removal of portions of cracked masonry walls and rebuilding them in rich mortar, followed by (b) providing steel clamps, perpendicularly to cracks or reinforcement key to be inserted into the wall (Fig. 2) and replastering. In order to reduce the time involved in construction, the keys were precast.

#### 3.2 Strengthening of buildings

##### 3.2.1 Grouting

Grouting injection has gained popularity in recent years as an effective method for repairing or strengthening of masonry walls and requires equipment for mixing and pumping. In Dien Bien Phu, non-shrinking Portland cement grout mixture was used for strengthening of bearing walls of the school and some residential buildings with crack's width to 10mm. The technique of grouting injection requires equipment and skill labors, so its application is limited.

##### 3.2.2 Inserting new RCC elements

For unreinforced masonry, R/C framing columns and collar beams were provided. Columns were located in corners and junctions of walls. In some cases, in order to improve the bond of the new R/C structure with the wall, additional steel bars were inserted for connected existing slabs with columns (Fig. 3).

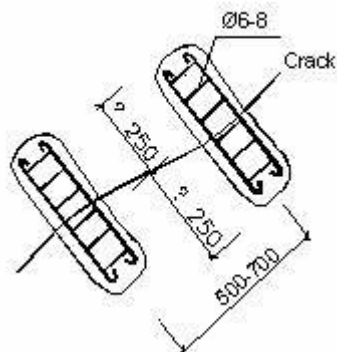


Figure 2: Inserting precast RC key into damaged wall

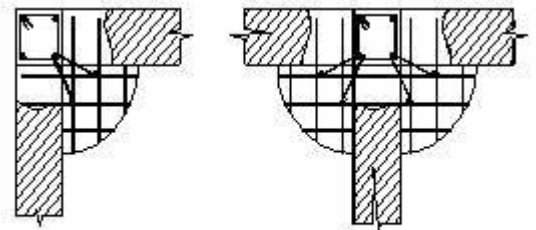


Figure 3: Inserting new R/C column





Figure 4: Strengthening of constructing building with new R/C columns

#### 4.0 CONCLUSION

After Dien Bien Phu earthquake in 2001, many newly constructed tall buildings in Vietnam were designed against the horizontal earthquake loading. Vietnam has not enough experience of earthquake damage and so study of foreign codes is very important in order to compile the Vietnamese code of practice for seismic resistant design of buildings.

#### 5.0 REFERENCES

- Arya, A.S, Teddy Boen, Yuji Ishiyama, Martemianov, A.I., Meli, R., Charles Scawthorn, Vargas Julio, N., Ye Yaoxian, 1986. *Guide-lines for earthquake resistant non-engineering construction*
- Hisaka Okada, 2001. *Report on Japanese activities on performance-based building structural design*. The 6<sup>th</sup> APEC workshop on International Alignment of Codes and standards in building construction. Hanoi, March 2001.
- Ninh N.L., Minh P.Q., 2002. *Seismic design of buildings*. Research Project, Hanoi (in Vietnamese).
- Paulay, T., Priestley, M.J.N., 1992. *Seismic design of reinforced concrete and masonry buidings*. John Wiley & Sonc, Inc.
- Phong N.T., Minh P.Q., Thanh, V.L., 2001. *Report on Lai chau Earthquake*. National workshop on "Buildings and constructions in seismically active regions". Hanoi, April, 2001 (in Vietnamese).
- RMS Event Report. 2003 *San Simeon, California Earthquake*.

# **SEISMIC VULNERABILITY ANALYSIS OF BUILDINGS IN JABALPUR URBAN AREA**

SHAILESH KR AGRAWAL AND AJAY CHOURASIA

Central Building Research Institute, Roorkee, India

*bdlcbri@datainfosys.net*

## **ABSTRACT**

*Experiences of earthquakes in last few decades have caused deep concern as regards to seismic vulnerability and resulting nature of disaster. The rapid industrial growth, population explosion and consequent escalation of urbanization with accelerated pressure on housing industry, render the entire domain of built environment vulnerable to earthquakes. The interest of social and economic stability requires recognition of earthquake risk, commitment & preparedness to encounter the hazard and their mitigation, through seismic vulnerability studies of urban centers. The paper presents an approach for assessment of seismic vulnerability of buildings whereat seismic vulnerability of existing building stock has been estimated quantitatively and qualitatively. The quantitative approach covers demand-capacity computation, while qualitative procedure estimates structural scores based on national & international state-of-the-art procedures viz. Rapid Screening Procedure (RSP). The study presented here is aimed to carry out seismic vulnerability of existing building stock to prognosticate the damage pattern of existing building stocks of Jabalpur urban area in the event of future earthquake. The results are mapped for different types of buildings viz. Adobe/Mud houses (Type-A), Masonry buildings (Type-B) and reinforced concrete (Type-C) buildings and collated using Arch Info and GIS, compatible for planning of pre-disaster mitigation measures.*

*The study concludes that most of the buildings in Jabalpur are constructed based on socio-economic consideration rather than engineering approach. The construction practices, materials used and quality of construction for Type-A buildings are varied in nature from one region to other region in the area lacking seismic resistant measures and are likely to fail in the event of an earthquake. The majority of building stock (70%) composed of Type-B buildings out of which 16% buildings are safe, while 84% buildings are likely to suffer damages in form of excessive cracking, falling of walls, falling hazard of non-structural components and then combinations. Similarly, RC constructions (15%), are mainly designed for vertical loads and no special provisions are being accounted as far as earthquake resistance is concerned. In case of an earthquake, around 45% buildings are safe whereas rest of Type-C buildings are likely to suffer damages in the form of excessive cracking, diagonal cracking, falling hazard and its combination.*

## **1.0 INTRODUCTION**

The semi-urban and urban parts of India are being visited by earthquakes recurrently. The resulting disaster caused by Uttarkashi (1991); Latur (1993); Jabalpur (1997); Chamoli (1999); & Bhuj (2001) are testimony to the vulnerability of our existing built environment. In this context, not only the well known seismic belts of Himalayan-Nagaland region, Indo-Gangetic Plain, Western India, Kachchh and Kathiawar regions in geologically unstable parts of the country, where most devastating earthquakes of the world have been witnessed, but also other seismic zones where events such as Latur (M6.3, 1993) and Jabalpur (M6.0, 1997) earthquakes have wreaked devastation in recent past are of equal concern. The damages in huge proportions to the engineered and non-engineered structures during Bhuj earthquake have shown that not only the source ground characteristics but also the vulnerability of the built environment render the domain susceptible to earthquake hazards.

A deterministic approach to hazard and risk analysis (DHRA) has been resorted and based on the experiences of preliminary studies on microzonation, a conceptual model for SHRM has been evolved (Mishra, P.S. et al, 2001; Agrawal et al, 2003). It envisages four level microzonation viz. (a) base or 1<sup>st</sup> level geoscientific microzonation, (b) microzonation with geotechnical inputs on ground characterization, (c) microzonation improvised with parameters on site effect and ground response, and (d) seismic risk microzonation with engineering, seismological inputs on vulnerability of engineered and non-engineered structures and anthropic parameters of population living in dwelling susceptible to damage and other exposure factors. The seismic vulnerability is a measure of the seismic strength or capacity of a structure, hence it is found to be the main component of seismic risk assessment and microzonation thereof is being presented here.

## **2.0 SEISMIC VULNERABILITY OF BUILDINGS FOR JABALPUR**

The seismic vulnerability study comprise mainly review of the existing buildings of Jabalpur in the light of guidelines for earthquake resistant construction in India, behavior of buildings during 1997 earthquake, construction practices being adopted in Jabalpur urban area (pre & post earthquake), building typologies, designing of questionnaire for survey of buildings, zoning of the Jabalpur urban area, selection of representative building samples, detailed survey of selected buildings, and creation of database. Subsequently, seismic vulnerability of existing building stock estimated quantitatively and qualitatively. The quantitative approach covers demand-capacity computation, while qualitative procedure estimates structural scores using Rapid Screening Procedures (RSP). The results are mapped using ArcInfo and GIS which are later synergized with seismic hazard microzonation to deliver seismic risk.

## 2.1 Existing building scenario in Jabalpur urban area

India has a very complex socio-cultural environment and its built environment encompasses the widest possible range from non-engineered dwellings built with traditional skills to the most modern buildings, and Jabalpur is no exception. The Jabalpur urban area under study is spread over 290 sq. km., comprising of around 6.2 lakhs dwellings of different typology (Table-1).

*Table 1: Distribution of Houses by Predominant Materials of Roof/Wall\**

Wall & Roof Combination		Census Houses	
		No. of Houses	%
Type-A	Urban	74,825	20.75
	Rural	2,85,650	79.25
	Total	3,60,475	58.42
Type-B	Urban	1,82,655	79.50
	Rural	47,115	20.50
	Total	2,29,770	37.24
Type-C	Urban	9,405	84.10
	Rural	1,775	15.90
	Total	11,180	1.81
Type-X	Urban	9,480	60.75
	Rural	6,125	39.25
	Total	15,605	2.53
Grand Total		6,17,030	

### Building Category

Type-A: Buildings in field-stone, rural structures, unburnt brick house, clay houses

Type-B: Ordinary brick building, buildings of the large block and prefabricated type, half-timbered structures, building in natural hewn stone

Type-C: Reinforced building, well built wooden structures

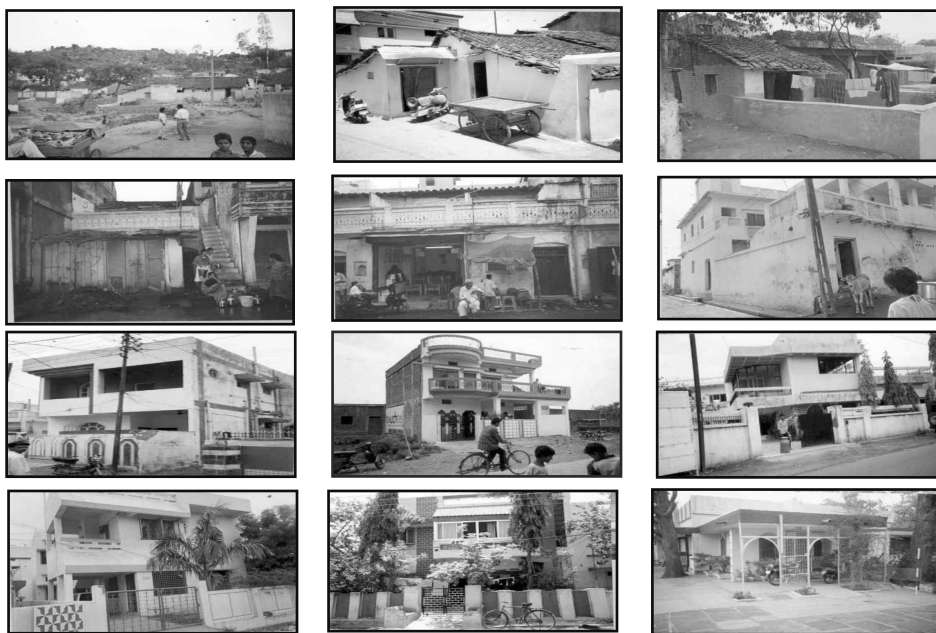
Type-X: Other types not covered in A, B, C.

\*Source: *Vulnerability Atlas of India (1999)*

The majority of houses in villages under Jabalpur urban area are of (a) mud (reinforced with straw), having 60 – 75 cm thick walls, (b) thick stone strips in mud/lime mortar, having wall thickness of 35 to 60 cm, (c) unburnt clay bricks in mud/lime mortar having wall thickness of 35 - 50 cm (Type-A Structures). The roofs are made of thatch of bamboo or other plants, covered with earthen tiles supported on wooden purlins. The roof and cantilever projections all around the houses are supported on wooden ballies/wooden columns/mud pedestals. There is no interlocking / connection between the wall and roof, making the same more vulnerable during earthquake. The supporting columns are connected with wooden

rafters by wedge kind of triangular wooden element. The various elements of trusses made-up of wooden ballies are interconnected using nails and all gable ends found without any connection/gable band.

The existing building stock (around 70%) in Jabalpur city is comprised of brick masonry in cement mortar (1:8)/ lime / surkhi / mud mortar, with 230 mm to 750 mm thick load bearing walls (Type-B Structures). These dwellings are mainly 2 to 3 storey with 3.00 to 3.3 m storey height. The construction practices and material used for these houses seem to vary with time. It has been found that no earthquake resistant measures have been adopted in buildings constructed before 1997 earthquake. Implementation of BIS codal provisions regarding earthquake resistant design & construction (IS: 4326-1993), were found to be absent almost in all the sample buildings surveyed, rendering the large percentage of structure seismically vulnerable. However, the post 1997 construction make use of four RCC columns of size 230 x 230 mm in corners, and RCC beams at lintel and floor level. In some of the newer construction lintel and plinth bands were found to be present.



*Photo 1: Existing building typologies in Jabalpur urban area*

The RC framed buildings are not much prevalent (around 15%) in Jabalpur urban area. General construction of RC framed buildings are of nominal concrete of M15 grade (1:2:4) ranging from 3 to 4 story with story height of 3.00 to 3.30 m (Type-C Structures). Among majority of RC frame building, around 90% buildings are soft story, with uniform cross section of columns although, having RCC slab of 120-140 mm thickness and 200-250 mm thick brick masonry in CM (1:6) as infill. These RC buildings are mainly designed for gravity loads without giving much attention to ductility provisions as enumerated in BIS: 13920-1993.

## **2.2 Experiences of Jabalpur earthquake of 1997 (M6)**

Jabalpur lies close to a mature zone of seismic source with recurrent seismic activity. On 22<sup>nd</sup> May 1997, the area was rocked by an earthquake of 6.0 magnitude (focal depth ~ 35 km) with epicenter at latitude 23.08°N and longitude 80.06°E. The Jabalpur urban domain lied in the near field of the seismic event and was in meizoseismal zone having undergone wide spread damage of MSK intensity VIII. The post-earthquake reconnaissance survey during 1997 in the area carried out by difference agencies viz. GSI (Mishra, P.S. et al, 2000), CBRI (Agrawal, S.K. et al, 2002), IIT Kanpur (Jain, S.K. et al, 2001), IIT Roorkee (Rai, D.C. et al, 1997), revealed that the performance of existing building stock was poor. The obvious reason has been that earthquake resistant measures prescribed in Indian codes were not made mandatory.

## **2.3 Past attempts for assessment of vulnerability**

The first attempt to create Vulnerability Atlas of India (MP) – 1997 (Arya, 1997) details out housing vulnerability tables wherein damage risk levels for earthquakes are defined based on the intensity scale such as Very High, High, Moderate, Low, and Very Low, and categorization of houses has been carried out based on distribution of houses by predominant materials of roof and wall, according to 1991 Census. The statewide Vulnerability Atlas, describing districtwise damage risk due to earthquake, wind and flood has been prepared. Accordingly, the earthquake damage risk associated for Jabalpur urban area varies from very low, low, & medium to Type-C, Type-B, & Type-A houses respectively. However, May 1997 Jabalpur earthquake caused severe damages leading to collapse of Type-A and Type-B houses, in particular, based on various damage survey reports. There has not been any other reported literature on seismic vulnerability of existing building stocks of Jabalpur urban area, which is one of the important modules for any SHRM study.

## **3.0 SEISMIC EVALUATION: METHODOLOGY**

Indian buildings built over past two decades are seismically deficient because of lack of awareness regarding seismic behavior of structure, constant upgradation of knowledge as regards earthquake resistant design & construction. Also seismic design is not practiced in most of the buildings being built. It calls for seismic evaluation of existing building stocks in an area.

Evaluation is a complex process, which has to consider not only the design of building but also the deterioration of the material and damage caused to the building, if any. The difficulties faced in the seismic evaluation of a building are manifold. There is no reliable information/database available for existing building stock, construction practices, in-situ strength of material and components of the building. The seismic evaluation mainly relies on set of general evaluation statements.

The unavailability of a reliable estimate of earthquake parameters, to which the building is expected to be subjected during, its residual life poses another challenge. Probabilistic approach to evolve needful parameters, would call for elaborate studies. Hence, for preliminary appraisal, the ground motion parameters available in the present code (IS:1893-2002) have been estimated at the macro level. As regards the effect of local soil conditions, which are known to greatly modify the earthquake ground motion, experiences of ground accentuation and data generated through collateral studies on site response have been considered. Also, in view of above constraints, the present study is limited to seismic evaluation of representative buildings of different typology viz. Type-A (Mud/RR Masonry, Adobe), Type-B (Brick Masonry Buildings), and Type-C (RCC Buildings), and projects a generalized pattern of building response to future seismic ground motion in different wards/zones of Jabalpur urban area.

The seismic evaluation leading to seismic vulnerability of existing building stock at Jabalpur has been estimated quantitatively and qualitatively. The quantitative approach, covers demand-capacity computation (ATC-40, 1996), while qualitative procedure estimates structural scores based on national & international state-of-the-art procedures viz. Rapid Screening Procedure (ATC-21, 1988, ATC-21-1,1988). The general procedures for seismic evaluation of existing buildings adopted in the present study are: site visit & data collection; selection & review of evaluation statements; follow-up fieldwork; and analysis of buildings by quantitative and qualitative approach.

### **3.1 Designing of questionnaire**

Designing of questionnaire comprising of set of evaluation statements is the first and foremost step for any seismic vulnerability analysis. The questionnaire would help the surveyor to determine any weak links in the structure that could precipitate structural or component failure. Although for macroseismic/post-earthquake damage investigations several questionnaires (Gunthal, 1993) are devised, however, for pre-earthquake seismic evaluation of existing building stocks there is no standard questionnaire at international & national levels. Hence, a need was felt to design exhaustive questionnaire to uncover the flaws and weaknesses of buildings/built environment. In the backdrop of available practices being adopted all over the globe, a comprehensive questionnaire has been designed. The questionnaire involves the use of sets of evaluation statements which cover structural configuration & specification, condition of structure & ambience, scenario of distress in non-structural components, seismic vulnerability parameters, damage during previous earthquake and repairs carried out thereof, and assessment of scientist/surveyor. The questions are in form of fill-in-the-blanks and evaluation statements highlighting building characteristics which are essential to avoid failures during earthquake.

## **3.2 Site visit and building survey**

### ***3.2.1 Administrative units of Jabalpur urban area***

In order to evaluate seismic vulnerability of huge number of building stocks in Jabalpur urban area, it is practically impossible to survey each and every house; hence it is imperative to divide Jabalpur urban area into number of small zones based upon structural/population density. The Jabalpur urban area is divided into 60 numbers of municipal wards as delineated by Jabalpur Nagar Nigam (Municipal Corporation of Jabalpur). These 60 wards are taken as zone in the present analysis. In addition, Jabalpur Cantonment Area and surrounding villages have been considered as a separate zone. Detailed reconnaissance survey of existing buildings stocks of each ward has been conducted. Based upon the observations, 3-4 representative building samples of different building typologies are selected for detailed investigation from each ward.

### ***3.2.2 Selection of building samples***

During the detailed survey, buildings of each type (i.e. Type-A, Type-B, and Type-C) have been identified, with the assumption that selected building represents construction practices being prevalent in that particular ward/zone. This was done with the mutual consensus amongst the team members and Corporator of the ward. Wherever the construction practices varied drastically in a ward, more number of samples were identified so as to cover the each type of construction in a ward. The sample survey was done with the aim that the seismic vulnerability analysis to be carried out on those sample buildings which would represent seismic vulnerability of each type of building in that zone.

### ***3.2.3 Detailed survey of selected buildings***

Apart from filling-up of questionnaire for the selected buildings, surveyor has to inspect the health of structure critically to assess its seismic resistance. In the process, surveyor has to face several difficulties. The foremost problem is of uncovering the structure. In many buildings the structure is concealed by architectural finishes, and the surveyor will have to get into attics, crawl spaces. Non-availability of plans, and design calculations is yet another problem, and is particularly frustrating with respect to reinforced concrete work. Assessing material quality and associated allowable stresses is also difficult preposition, and one has to rely on local available reports/information or otherwise one has to go for destructive testing, which is seldom possible. Destructive and non-destructive testing of reinforced concrete and masonry elements are necessary to determine strength and quality of construction. The rebound hammer is used to assess the compressive strength of concrete structural members, wherever access is provided in reinforced concrete structure. If reinforcement details are available, a limited amount of exposure of critical reinforcement is needed to verify conformity to the plans/structural details.



If the plans are not available, the quality of reinforcement is assessed by exposing reinforcement to a limited extent.

The sample survey was carried out for about 474 buildings spread over 62 zones of Jabalpur urban area including 22 surrounding villages, out of which 33% are of Type A, 52% are of Type B and 15% are of Type C.

### **3.3 Seismic vulnerability analysis**

The seismic vulnerability analysis of all types of buildings have been carried out by two different approaches. For qualitative assessment of buildings, Rapid Screening Procedure is used to assess vulnerability of all types of structures, while for quantitative approach, DCR computation has been used for Type B & C buildings and later it is related with the possible failure modes.

### **3.4 Quantitative seismic vulnerability for masonry buildings**

Since earthquake is a random process, all the load bearing walls in a structure are to be evaluated for their shear resistance. The demand placed by an earthquake i.e. lateral forces at various levels, as per IS:1893-2002, along with gravity load calculations were carried out for sample buildings, and later check in terms of Demand –Capacity ratio (DCR) for shear resistance, combined stress, overturning, and stability of non-structural failures for long and short walls. The capacity of wall is defined as its allowable stress depending upon mortar type in accordance with the relevant codal provisions. The DCR greater than unity, indicates that the building is seismically vulnerable in respective criterion, whereas DCR less than one implies the building to be safe under earthquake loads. As indicated earlier, earthquake demands for better shear resistance and hence the DCR in shear should be less than one, otherwise the building will have diagonal (X) cracking. The DCR greater than one for combined stresses means that the building is not even designed for gravity loads and would lead to collapse on seismic shaking. The failures in overturning corroborates falling of walls. The check for non-structural element implies the falling hazard of parapet wall. The above analogy has been used to estimate seismic vulnerability in terms of various failure modes i.e. collapse, excessive cracking, falling of walls including parapet walls.

### **3.5 Quantitative seismic vulnerability for RC buildings**

In order to critically evaluate the RC framed buildings, selected building sample were modeled using sophisticated structural analysis software under combination of earthquakes & other loads for computing the member end forces in each structural member. Apart from the dead & live loads, is analyzed for design basis earthquake (DBE) loads, the earthquake loads which can reasonably be expected to occur at least once during the lifetime of the structure. Accordingly, dead load, live load and their combination as suggested in IS-1893-2002 have been considered for

analysis. The analysis directly computes member end forces and then each member is designed for worst load combination. The design module of analysis engine gives the longitudinal and transverse reinforcement for each member. This reinforcement corresponds to the demand of a member due to earthquake forces, whereas the actual reinforcement provided in a particular member would correspond to capacity. In order to calculate the DCRs, the calculated reinforcement of structural members has been compared with provided reinforcement. The DCRs for longitudinal and transverse reinforcement reflects DCRs for flexure and shear of member. The DCRs calculated for flexure and shear gives the idea about inherent ductility and strength of member to ensure safety & serviceability during severe shocks.

The DCR greater than one for flexure indicates that the longitudinal reinforcement in columns & beams are inadequate leading to failure. The possibility of failure of such buildings is excessive cracking leading to collapse. Whereas DCR greater than one in shear indicates that the lateral ties provided are not sufficient leading to brittle failures i.e. catastrophic failure. In this case, there is possibility of diagonal cracking in structural elements. The check for non-structural element implies the falling hazard of parapet wall. Based upon above analogy, DCRs for flexure, shear and non-structural members leading to estimate seismic vulnerability in terms of failure modes i.e. excessive cracking, diagonal cracking and falling hazard respectively, for all the representative RC buildings under consideration have been computed.

### **3.6 Qualitative seismic evaluation for buildings**

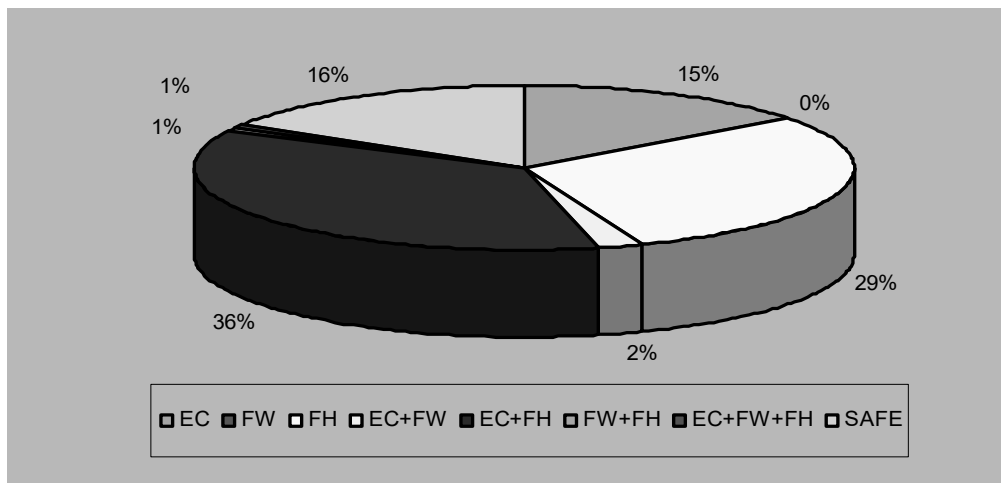
The Rapid Screening Procedure (RSP) is aimed to identify potentially hazardous buildings in the study area, without going into detailed analysis. RSP utilizes a methodology based on visual inspection of a building and noting the structural configuration. The methodology begins with identifying the primary structural lateral load resisting system and materials of the building. The method generates a Structural Score 'S', which consists of a series of 'scores' and modifiers based on building attributes that can be seen during detailed survey. The Structural Score 'S' is related to probability of the building sustaining life-threatening damage in the event of occurrence of a severe earthquake in the region. A low S score suggests that the building is vulnerable and needs detailed analysis, whereas a high 'S' score indicates that the building is probably adequate. RSP helps in developing a list of potentially hazardous buildings without a high cost of detailed analysis of each building. In the present study, this method has been used for qualitative assessment of seismic vulnerability of existing buildings in Jabalpur urban area.

### **3.7 Prognostic damage scenario of Jabalpur urban area**

The prognostic damage scenario of a ward reflects the structural and non-structural damages induced in the existing building stocks. The damage scenario of a ward given here is based on representative building surveyed for different building typologies.

Based on the survey & analysis of data, the seismic vulnerability of Jabalpur urban area obtained through qualitative approach. It is found that Type-A, Type-B & Type-C buildings are 100%, 87% and 33% vulnerable respectively.

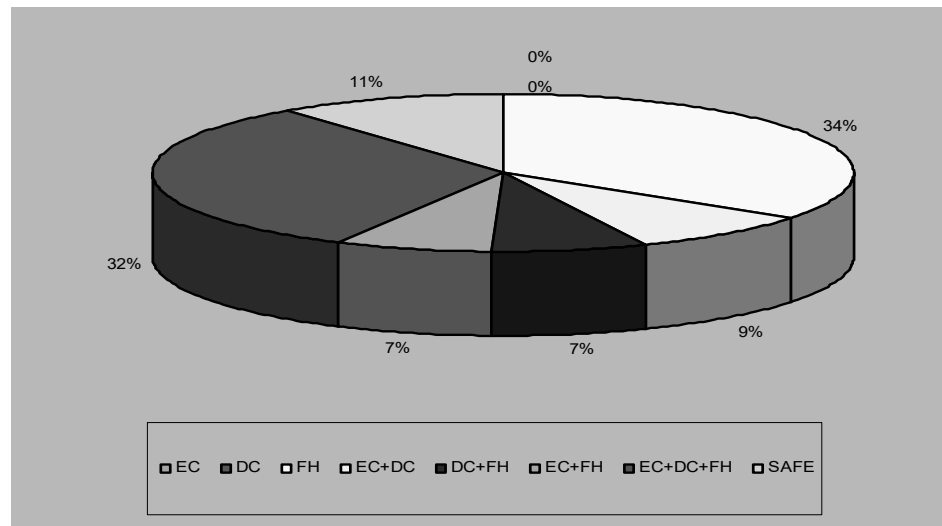
In order to present the prognostic damage scenario for Jabalpur urban area using quantitative approach, the failures modes of different type of buildings are collated, and indicates that all the Type-A houses are 100% vulnerable since they are built from socio-economic consideration rather than engineering. For Type-B buildings, the postulated failure modes have been categorized as excessive cracking (EC); falling of walls (FW); falling hazard of non-structural members (FH); and combination thereof - Excessive cracking + falling of wall (EC+FW); excessive cracking + falling hazard (EC+FH); falling of wall + falling hazard (FW + FH); excessive cracking + falling of wall + falling hazard (EC + FW + FH); and safe buildings (which do not have any failure). At the first instance, wardwise seismic vulnerability has been derived, and later the ensemble is projected to present prognostic damage scenario for Jabalpur urban area. The prognostic damage scenario for Jabalpur urban area for Type-B structures obtained as “Excessive Cracking (EC) works out to 15%; Falling of Walls (FW) – 0%; Falling Hazard of non-structural members (FH) – 29%; and combination thereof - Excessive Cracking + Falling of Wall (EC+FW) – 2%; Excessive Cracking + Falling Hazard (EC+FH) – 36%; Falling of Wall + Falling Hazard (FW + FH) – 1%; Excessive Cracking + Falling of Wall + Falling Hazard (EC + FW + FH) – 1%; and Safe buildings – 16% (Fig. 1).



*Figure 1: Prognostic damage scenario of Type-B buildings in Jabalpur*

Similarly, the various failures modes for assessing seismic vulnerability of Type-C buildings are identified as excessive cracking (EC), diagonal cracking (DC); falling hazard of non-structural members (FH); and combination thereof and safe buildings. The prognostic damage scenario for Type-C buildings in Jabalpur urban area obtained as “Excessive Cracking (EC) – 0%; Diagonal Cracking (DC) – 0%; Falling Hazard (FH) –

34%; Excessive & Diagonal Cracking (EC+DC) – 9%; Diagonal Cracking + Falling Hazard (DC+FH) – 7%; Excessive Cracking + Falling Hazard (EC+FH) – 7%; Excessive Cracking + Diagonal Cracking + Falling Hazard (EC + DC + FH) – 32%; and safe buildings – 11%. The overall prognostic damage scenario of Jabalpur urban area for this kind of buildings is presented in Fig. 2. The falling hazards are essentially non-structural failures and therefore these buildings may also be deemed to be safe after minor modification to non-structural elements making around 45% safe RC structure.



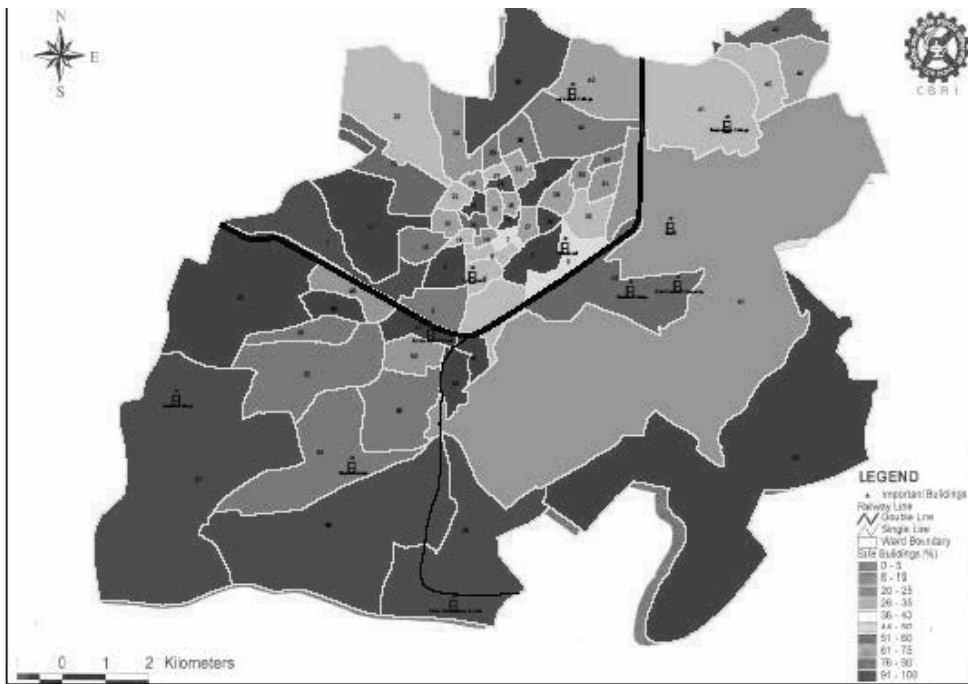
*Figure 2: Prognostic damage scenario of Type-C buildings in Jabalpur*

Figure 3 presents Prognostic Seismic Vulnerability Map of Masonry Buildings in Jabalpur. The vulnerability map can be effectively used to project the risk associated with existing building stock in Jabalpur Urban area. Further, these maps may act as guidance for future planning, risk reduction and disaster mitigation and management.

#### 4.0 CONCLUSIONS

Based on qualitative and quantitative analysis of the data collected during the survey and its analysis & interpretation, the following conclusions for predicting seismic damage scenario for Jabalpur are drawn:

- The buildings in field-stone, rural structures, unburnt brick house, clay houses (**classified as Type-A**), comprises of **15% of total building stock** in Jabalpur urban area. The construction practices, materials used and quality of construction for Type-A buildings are varied in nature from one region to another region in the area. All the buildings lack seismic resistant measures and are **likely to fail** in the event of an earthquake.



*Figure 3: Prognostic seismic vulnerability of masonry buildings in Jabalpur urban area*

- The majority of building stock (**70%**) in Jabalpur area composed of **Type-B buildings** which include ordinary brick buildings, buildings of the large block, half-timbered structures, buildings in natural hewn stone. As regards to seismic damage scenario, around **16% buildings are safe**, while 84% buildings are likely to suffer damages in form of excessive cracking, falling of walls, falling hazard of non-structural component and combination thereof.
- The engineered RC construction in the region typically consists of RC Moment Resisting Frames (**Type-C**) with infilled brick masonry walls, which constitutes about **15% of total building stock**. The buildings are found to be designed for vertical loads only with no special provisions for earthquake resistance. In case of an earthquake around **45% buildings are safe** whereas rest of Type-C buildings are likely to suffer damages in the form of excessive cracking, diagonal cracking, falling hazard and its combination.
- The study presents the seismic damage scenario of Jabalpur urban area taking into account all prevalent construction practices, material of construction, quality/workmanship of construction, types of buildings, ambience, geological / geotechnical parameters based on ground realities. However, the limitation of study has been that it is based on a limited sample size of 474 representative building from different microzones of Jabalpur urban area.

- The present study on vulnerability when integrated for damage scenario analysis on incidence of earthquake with collateral geoscientific studies corroborates the finding of revalidated intensity map of Jabalpur Earthquake 1997.

These risk microzonation studies demands special attention with reference to heritage/monumental buildings, lifelines like rail/road, water supply, electric supply, sewage, communication, dams, hospitals & schools, vulnerable industries, which is missing in the present study. Also there is a need to identify safe zones/domains/structures and secure routes to work as a relief centers and relief dispersion on incidence of future disaster.

## ACKNOWLEDGEMENTS

The authors gratefully acknowledge the financial support from the Department of Science & Technology, Government of India for financial support for the above study. Authors are thankful to Dr P.S. Mishra, Director, Geological Survey of India, Nagpur for valuable suggestion & guidance offered during the study. The authors also thank Shri V.K. Mathur, Director, Central Building Research Institute, Roorkee, for granting permission to publish the paper.

## REFERENCES

- Arya, A. S. 1997. *Madhya Pradesh: Vulnerability Atlas of India*. BMTPC, Ministry of Urban Development, New Delhi, India.
- Agrawal, Shailesh Kr., and Chourasia, Ajay 2004. *Estimation of Seismic Vulnerability of Buildings in Delhi*. World Congress on Natural Disaster Mitigation organized by Institution of Engineers (I), Kolkata, Feb. 2004.
- Agrawal, Shailesh Kr., Chourasia, Ajay, and Parashar, J. 2003. *Seismic Vulnerability of Buildings in Jabalpur Urban Area*. Vol V, DST Report, Central Building Research Institute, Roorkee.
- Agrawal, S.K., Chourasia, Ajay, and Parashar, J. 2002. *Seismic Evaluation & Retrofitting of Existing Buildings*. 12<sup>th</sup> Symposium on Earthquake Engineering, Indian Institute of Technology, Roorkee.
- Agrawal, S.K., Chourasia, Ajay, Parashar, J and Dutta, J. 2002. *Experimental Investigation on Earthquake Resistance and Retrofitting Measures of Masonry House*. Advances in Concrete & Construction Technology, Publication –3, Interline Publishing, Bangalore.
- ATC-21, 1988. *Rapid Visual Screening of Buildings for Potential Seismic Hazards: A Handbook*. Applied Technology Council, Redwood city, CA, USA.
- ATC-21-1(1988), “*Rapid Visual Screening of Buildings for Potential Seismic Hazards: Supporting Documentation*”, Applied Technology Council, Redwood city, CA, USA.
- ATC-40, 1996. *Seismic Evaluation and Retrofit of Concrete Buildings*. Vol. I, Applied Technology Council, Redwood city, CA, USA.

- Grunthal G., 1993. *European Macroseismic Scale 1992 (up-dated MSK-scale)*. European Seismological Commission, Luxembourg, 1993.
- IS:1893-2002, 2002. *Criteria for Earthquake Resistant Design of Structure*. Bureau of Indian Standards, New Delhi.
- IS:4326-1993, 1993. *Code of Practice for Earthquake Resistant and Construction of Buildings*. Bureau of Indian Standards, New Delhi.
- IS:13920-1993, 1993. *Ductility Detailing of Reinforced Concrete Structures Subjected to Seismic Forces-Code of Practice*. Bureau of Indian Standards, New Delhi.
- Jain, S. K., Murty, C. V. R., Dayal, U., Arlekar, J. N., and Chaubey, S. K., 2001. *A Field Report on Structural and Geotechnical Damages Sustained During the 26<sup>th</sup> January, 2001 M7.9 Bhuj Earthquake in Western India*. NICEE Report.
- Mathur, V.K., Agrawal, Shailesh Kr., and Chourasia, Ajay 2004. *Microzonation Studies as Impacted by Recent Earthquakes in India*. World Congress on Natural Disaster Mitigation organized by Institution of Engineers (I), Kolkata, Feb. 2004.
- Mathur, V.K., Agrawal, S.K., and Chourasia, Ajay 2003. *Demand-Capacity Approach for Seismic Rehabilitation of RC Residential Buildings*. 9<sup>th</sup> International Conference on Civil & Structural Engineering Computing (CIVIL-COMP 2003), Heriot Watt University,, Edinburgh, UK.
- Mishra, P.S. et al 2000. *Jabalpur Earthquake – 22 May 1997- A Geoscientific Study*. GSI Special Publication No. 51, Geological Survey of India, Calcutta.
- Mishra, P.S. et al 2001. *Base Level Seismic Hazard Microzonation of Jabalpur Urban Area, MP*. National Symposium on Role of Integrated Development & Related Issues, GSI Special Publication No. 65(iii), Calcutta, pp 249-258.
- Rai, D.C., Narayan, J.P., Pankaj, Kumar, A. 1997. *Jabalpur Earthquake of May 22, 1997 – Reconnaissance Report*. Department of Earthquake Engineering, University of Roorkee, Roorkee.
- Vulnerability Atlas of India* 1999. Building Materials & Technology Promotion Council, New Delhi.

# **AN INNOVATIVE SEISMIC STRENGTHENING METHOD FOR UNREINFORCED MASONRY STRUCTURES USING PP-BAND MESHES**

PAOLA MAYORCA AND KIMIRO MEGURO

IIS, The University of Tokyo, Japan

*paola@iis.u-tokyo.ac.jp*

## **ABSTRACT**

*Rapid urbanization and city grow are common features worldwide. This phenomenon is transforming city skylines due to the remarkable increase of high-rise buildings and infrastructure. In spite of this, numerous existing structures are and will be used in the future. Many of these buildings are made of seismic vulnerable materials, such as unreinforced masonry, posing a great danger to urban development in seismic prone regions. The potential risk that these structures represent to human lives in large metropolis is aggravated by the high concentration of people. Therefore, increasing their seismic resistance is imperative.*

*In order to effectively promote seismic retrofitting, one of the key issues is to enable inexpensive technical solutions which could be executed without highly skilled labor. In this context, this paper discusses an innovative strengthening technique for unreinforced masonry structures using polypropylene band (PP-band) meshes embedded in a mortar overlay. These bands, which are commonly used for packing, are resistant, inexpensive, durable and worldwide available. The PP-band meshes are easily attached on both sides of the wall and connected with wires passed through holes drilled in the wall. In this way, the structure disintegration under seismic loads is prevented.*

*In order to verify the suitability of the proposed method, a series of masonry walls, with and without retrofit, were tested under in-plane loads. Although the retrofitted wall peak strength was almost the same as that of the bare wall, its post-peak strength became much larger and sustained for lateral drifts over 2%.*

## **1.0 INTRODUCTION**

Masonry is a construction material widely used around the world due to its low cost and construction easiness. More than 30% of the world's population lives in a house of unbaked earth, which is one type of unreinforced masonry (Houben and Guillaud, 1989). During the last century, human casualties during earthquakes were mainly caused by structural damage, being the failure of unreinforced masonry structures responsible of more than 60% of them (Coburn and Spence, 1992). The vulnerability of masonry structures under seismic loads has being recognized long ago and



efforts to provide guidelines for the construction of sound earthquake resistant houses have been remarkable. In spite of this, every year casualties due to collapsing masonry houses during earthquakes are reported.

Several types of retrofitting have been developed for unreinforced masonry structures. A comprehensive review of them can be found in Lizundia et al (1997). The existing retrofitting techniques can be categorized in: 1) grout and epoxy injections, 2) surface coatings, 3) reinforced or post-tensioned cores, and 4) addition of structural elements. There is no doubt that these methods are useful for strengthening masonry structures. Depending on the purpose of the retrofitting works, one method is more appealing than the other.

For strengthening unreinforced masonry houses in developing countries, a suitable retrofitting technique should guarantee not only its efficiency in terms of improvement of the seismic resistant characteristics of the structure (strength, ductility and energy dissipation). It should also be considered that: 1) the used material is economical and locally available and 2) the required labor skill is minimum. In this context, a new retrofitting method for unreinforced masonry structures is proposed.

## **2.0 RETROFITTING METHOD PROPOSAL**

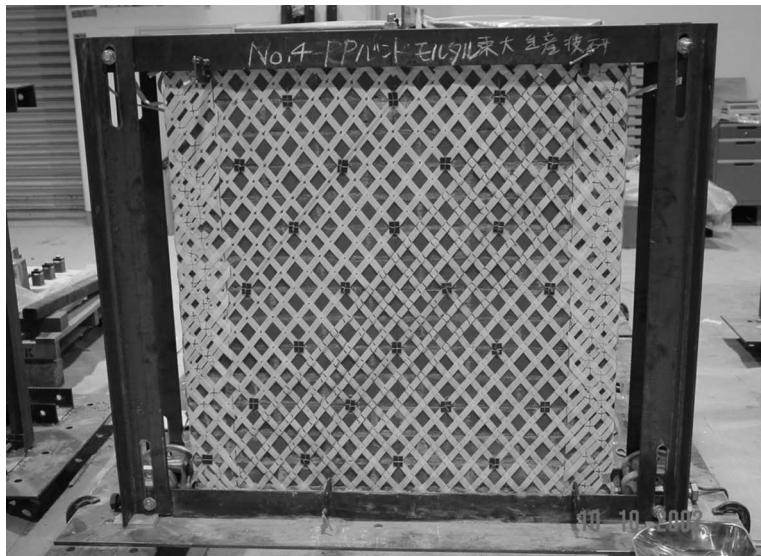
Considering the above-mentioned conditions, a novel retrofitting method consisting of polypropylene bands (PP-bands) arranged in a mesh fashion and embedded in a cement mortar overlay is proposed. These bands are worldwide used for packing. They are cheap, resistant, and easy to handle. The details of the retrofitting technique are discussed elsewhere (Mayorca and Meguro, 2003). Only a brief explanation of the installation procedure is presented below.

At first, the meshes are prepared with the PP-bands. The pitch and inclination may vary according to the required earthquake resistance. Then, the masonry wall surfaces are cleaned and holes are drilled through the wall at a spacing of approximately 4 times the mesh pitch. After this, the PP-band meshes are set on both wall sides and fixed at the borders. Galvanized steel wires are passed through the wall holes and used to fix the meshes. Photo 1 shows the wall at this stage of the process. Finally, a mortar overlay is placed on the wall surface.

## **3.0 EXPERIMENTAL PROGRAM**

In order to assess the retrofitting by PP-band mesh, eight masonry walls were constructed: four with and four without reinforcement. The wall dimensions were  $985 \times 1072 \times 100 \text{ mm}^3$  and consisted of 15 brick rows of 4.5 bricks each. Clay bricks were used. The mortar mix proportion in volume was cement: sand=1:4.5 and the joint thickness was 10mm. The bottom and top brick layers were embedded in steel channels. The walls were cured with water spray for 14 days. At the end of the curing process,

the upper channel was installed. Figure 1 shows the test setup and specimen dimensions.



*Photo 1: Retrofitted wall before mortar overlay setting*

Two meshes were prepared per retrofitted wall. The mesh pitch, equal to 45mm, was chosen so that each brick would be crossed by at least three bands. Because the bricks were very strong, the connectors, 27 in total, were placed only at the mortar interface. This constrain defined the band inclination, which was 50°. A cement mortar mix (cement: sand=1:3) was used for the protection overlay of 8mm thickness.

At first, a vertical pre-compression load was applied by closing the bolts at the bottom end of six vertical rods. The force increment at the bars was closely monitored. Then, the actuator was positioned and the forces at the vertical rods were readjusted in case of unbalance. Finally, the horizontal loading, which consisted of 5 steps, was applied with a hydraulic pump operated manually. In the first step, the wall was loaded until diagonal cracking. The second step consisted on additionally pushing the wall 10mm in the same direction. In the third step, the actuator displacement direction was reversed and the specimen was loaded until the diagonal crack in the opposite direction occurred. In the fourth step, the wall was loaded 10mm more in the same direction. Finally, the wall was unloaded. Table 1 shows the experiment program summary.

Due to the brick high strength, the resulting masonry was stronger than the material typically available in developing countries. In order to intentionally reduce the wall strength and highlight the retrofitting effect, holes were drilled through some of the walls. Two hole distributions were considered, uniform and diagonal. Further details of the experimental program may be found in Mayorca (2003).

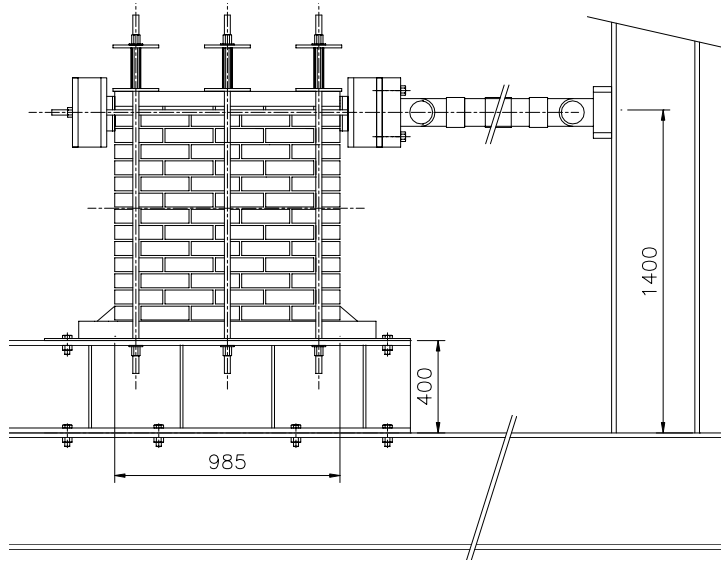


Figure 1: Test setup and dimensions in mm

Table 1: Summary of experiment conditions

Case name	VL (kN)	PP- band	Mortar	Holes
Bare wall	9			None
Bare wall w/ holes	9			Uniform
Bare wall w/mortar	9		O	None
Reinforced wall	9	O	O	None
Reinforced wall w/holes	9	O	O	Uniform
Bare wall w/mortar	30		O	None
Reinforced wall	30	O	O	None
Reinforced wall w/diagonal holes	30	O	O	Diagonal

VL=Vertical pre-compression load

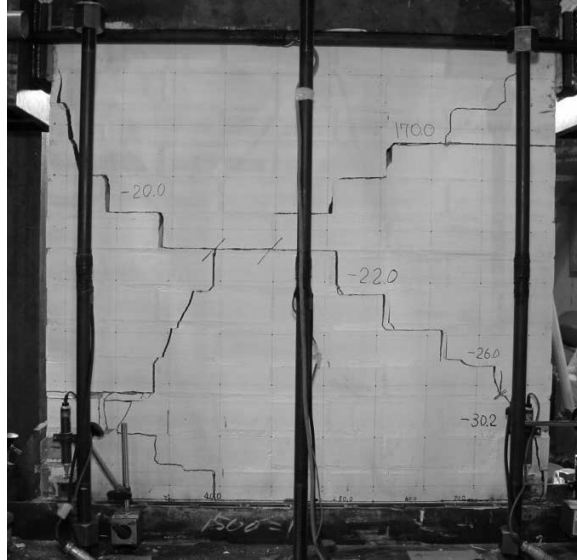
## 4.0 RESULTS DISCUSSION

Photos 2 and 3 show typical crack patterns. Figures 2 and 3 show the force-deformation curves obtained in the experiments grouped according to the pre-compression load. The experimental observations are briefly discussed below.

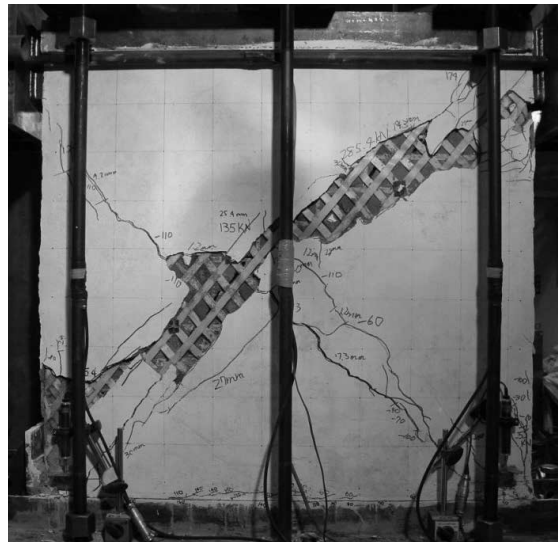
### 4.1 Crack pattern

As observed in Photos 2 and 3, the crack pattern did not change considerably due to the reinforcement presence. In both cases, the flexural stresses caused a crack at the lower most mortar layer at an early load stage. This crack became gradually longer and wider as the horizontal load increased. In the case of the reinforced walls, the crack propagated slowly and as a result, a wall strength drop was not observed in the force-deformation curve. This effect was identified in the walls with VL=9kN.

The flexural crack caused the horizontal force, which was originally transferred to the support by a shear-flexural mechanism, to be resisted through a compression strut along the wall diagonal. As the bottom crack stopped propagating, the specimen stresses continued to build up and were eventually released through a diagonal crack.



*Photo 2. Unreinforced wall crack pattern*



*Photo 3. Reinforced wall crack pattern*

After the first diagonal crack, the wall strength was notoriously reduced and the subsequent imposed deformation was related to the movement of the upper half of the failed wall. Because of this, when the load was reversed it did not produce any additional flexural cracking. It was mainly the upper wall displacement. After the initial shear crack closed, the stresses started to build up again and the second diagonal crack, along the

other diagonal, appeared. The main difference between the unreinforced and reinforced walls was the crack propagation speed rather than the location.

## 4.2 Stiffness

The force-deformation curves presented in Figure 2 may suggest that the reinforced walls have a slightly higher stiffness than the unreinforced ones. However, it must be noted that the deformations showed in the figures correspond to two effects, the wall deformation itself and the wall rotation. The later is larger. Figure 4 shows the deformation along the wall diagonals, which is a direct measurement of the wall shear deformation. Note that the deformation of both reinforced and unreinforced walls is small and almost the same. This shows the high stiffness of the masonry wall and suggests that the stiffness difference observed in the force deformation curves is mainly due to the reinforcement restrain to the wall rotation.

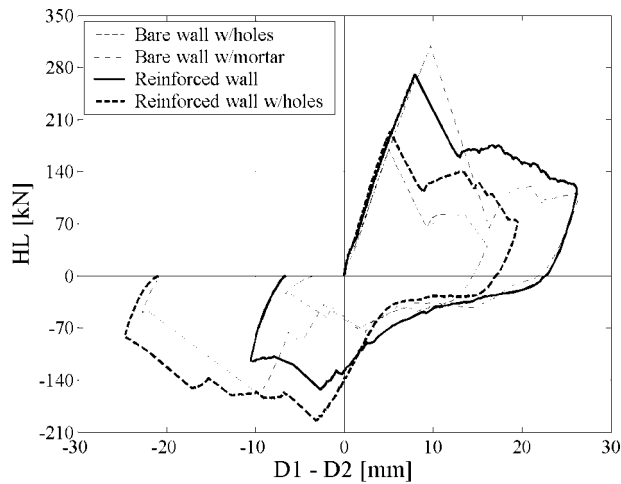


Figure 2: Force-deformation curve ( $VL=9kN$ )

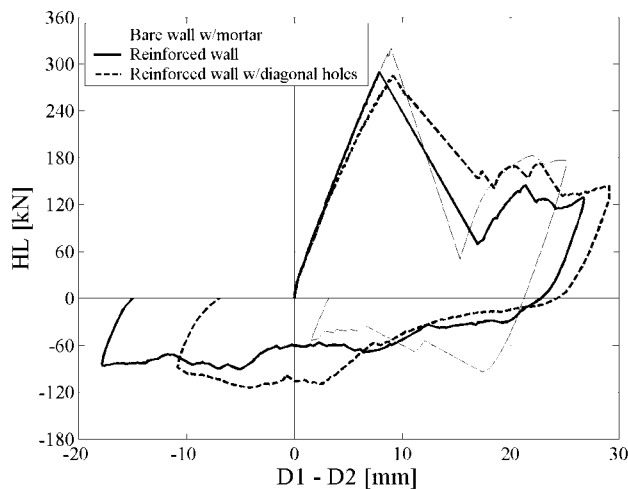


Figure 3: Force-deformation curve ( $VL=30kN$ )

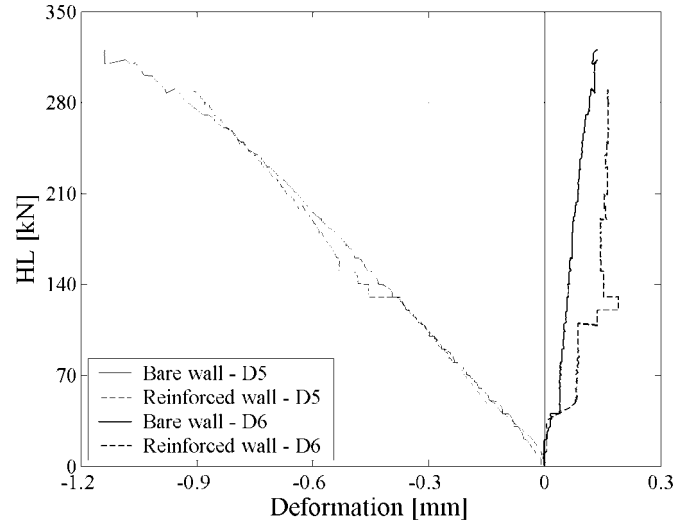


Figure 4: Diagonal deformation ( $VL=30kN$ )

### 4.3 Peak strength

The PP-bands have a relatively low stiffness compared to the masonry walls (Mayorca, 2003). Because of this, they did not contribute to increase the wall peak strength. Although some differences are observed, these are due to: 1) mortar overlay presence, 2) bonding between mortar overlay and masonry wall, and 3) variability of masonry properties due to the workmanship effect. The PP-band mesh contribution was only observed after the wall cracked.

### 4.4 Post-peak strength

Figure 5 shows the force-deformation relation normalized to the peak strength and corresponding deformation for the group of walls with  $VL=9kN$ . It is observed that immediately after the peak, the normalized strength dropped to 10 to 40% for the unreinforced walls. On the other hand, the reinforced walls exhibited a 60% residual strength after the peak, which was sustained for drifts over 2%. In the reverse direction, the reinforced walls also exhibited a larger normalized strength.

### 4.5 Effect of connectors and mortar overlay

The reinforced wall with  $VL=30kN$  deserves special attention because the wall strength after the diagonal crack dropped to almost 25% of the peak strength. This was the only reinforced wall that exhibited such a sharp drop. After the test, the specimen was examined and broken wire connectors were found. Furthermore, a severe cracking of the mortar overlay due to drying shrinkage was observed before the experiment. This may have caused a reduction of the mortar support to the bands resulting in a larger demand to the wire connections, which ultimately caused their failure. It is worth noting that this was the first retrofitted wall constructed and eventually the steel wires may have been damaged during the installation process.

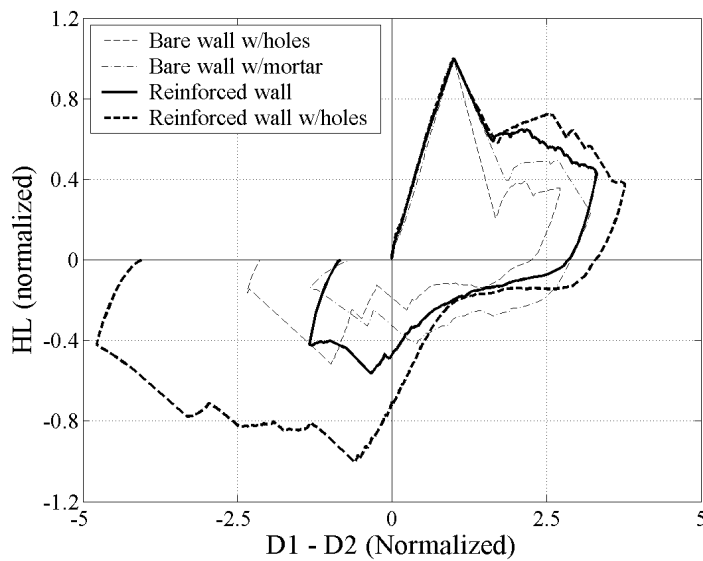


Figure 5: Normalized force-deformation relation ( $V_L=9kN$ )

## 5.0 CONCLUSIONS

A new technique for strengthening masonry structures using PP-bands is proposed. The results of shear wall tests showed the reinforcement effect on the masonry wall behavior. Although the reinforcement did not increase the structure peak strength, it contributed to improve its performance after the crack occurrence. The reinforced walls exhibited a larger post-peak strength and were capable of better sustaining their strength even for drifts over 2%. The importance of the connectors and the mortar overlay for the retrofitted wall performance was recognized.

## REFERENCES

- Houben H. and Guillaud, H, 1989. *Earth construction – A comprehensive guide*. ITDG Publishing, London.
- Coburn A. and Spence R., 1992. *Earthquake Protection*. John Wiley & Sons Ltd, West Sussex.
- Lizundia, B., Holmes, W. T., Longstreth, M., Kren, A., Abrams, D. P., 1997. *Development of Procedures to Enhance the Performance of Rehabilitated URM Buildings*. NIST GCR 97-724-1.
- Mayorca, P. and Meguro, K., 2003. *Efficiency of polypropylene bands for the strengthening of masonry structures in developing countries*. Proc. of the 5<sup>th</sup> International Summer Symposium, JSCE, 125-128.
- Mayorca, P., 2003. *Strengthening of unreinforced masonry structures in earthquake-prone regions*. PhD Dissertation, The University of Tokyo.

# **RESPONSE OF A BASE ISOLATED MASONRY STRUCTURE**

KRISHNAMOORTHY<sup>1</sup>, KIRAN KUMAR SHETTY<sup>2</sup>  
AND RAVI KUMAR<sup>1</sup>

<sup>1</sup>Manipal Institute of Technology, Manipal, India

<sup>2</sup>N.M.A.M. Institute of Technology, Nitte, India  
*hodcivil2002@yahoo.com*

## **ABSTRACT**

*A masonry building resting on laminated rubber bearing and subjected to ground acceleration due to Koyana earthquake is analyzed using three dimensional finite element method. The building and bearing is modeled using eight noded isoparametric brick element with three degrees of freedom at each node. The response of building isolated at base is compared with the response of the building fixed at base. The response of isolated building is found to be less in comparison to the corresponding response without isolation system, implying that the isolation is effective in reducing the response of the masonry structure. It is also found that the displacement at top and base of the isolated building are almost same at all time intervals. This indicates that the building moves rigidly during earthquake.*

## **1.0 INTRODUCTION**

Masonry buildings are increasingly used in all countries except perhaps in the relatively more developed ones. Masonry walls are known to suffer maximum damage during earthquakes. A number of base isolation systems have been developed to isolate these buildings subjected to earthquake. Base isolation is an aseismic design approach in which the building is protected from the severe earthquake forces by a mechanism, which reduces the transmission of horizontal acceleration into the building. One of the concepts to protect a building from the damaging effects of an earthquake is by introducing some type of support that isolates it from the shaking ground using specially designed bearing. These bearings are placed between the structure and its foundation. These bearings can carry the gravity load of the superstructure in normal way and simultaneously provide the horizontal flexibility necessary to shift its first mode natural frequency away from predominant frequency of the design earthquake motion. This results in the reduction of inertial forces and accelerations several times in the structure. Base isolation is therefore recommended for life saving and life threatening structures. Kelly (1986) carried out an extensive review on the historical developments of the many mechanisms that have been developed. Among the numerous designs of base isolators, the laminated rubber bearings offer perhaps the simplest method of isolation and are relatively easy to manufacture. In the present study a one-story masonry building resting on laminated bearing and subjected to Koyana ground motion is analyzed. The response obtained from the analysis of the building



fixed at base is compared with the response obtained from the analysis of the building isolated at base so as to study the effectiveness of base isolation.

## 2.0 ANALYSIS

The various assumptions made for analysis of the building mounted on bearing are as follows:

- The superstructure remains in the elastic range during the earthquake excitation.
- The force – deformation behavior of the laminated rubber bearing is considered to be linear

A three dimensional building frame resting on bearing and subjected to earthquake ground acceleration is analyzed by finite element method of analysis. The three dimensional building and bearing is divided into number of eight noded isoparametric brick element. The element is having three translational degrees of freedom at each node.. For each element, the stiffness matrix  $[k]$  and consistent mass matrix  $[m]$  are obtained. The mass matrix and stiffness matrix of each element are added by direct stiffness method to get the overall mass matrix  $[M]$  and overall stiffness matrix  $[K]$  for the entire structure. The overall damping matrix is obtained by using Raleigh's equation.  $[C] = \alpha [M] + \beta [K]$  where  $\alpha$  and  $\beta$  are the constants. The overall dynamic equation of equilibrium for the entire structure can be expressed in matrix notations as

$$[M] \{\ddot{u}\} + [C] \{\dot{u}\} + [K] \{u\} = \{f(t)\} \quad (1)$$

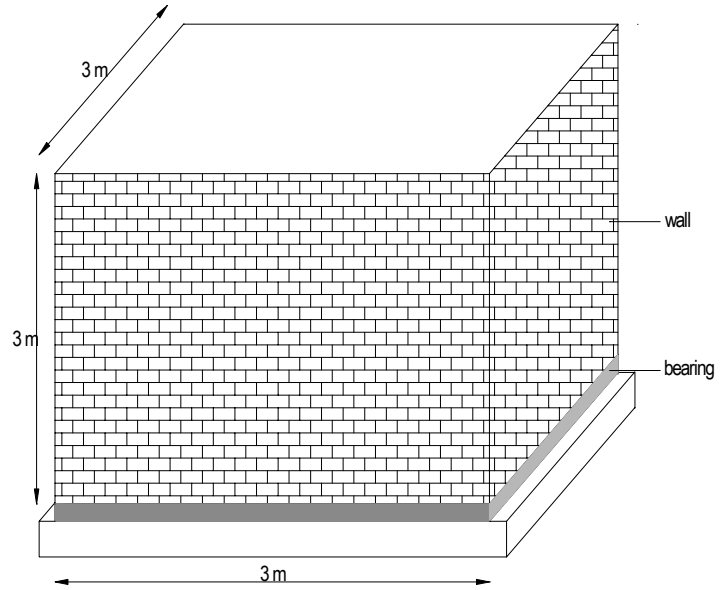
where  $[M]$ ,  $[C]$  and  $[K]$  are the overall mass, damping, and stiffness matrices.  $\{\ddot{u}\}$ ,  $\{\dot{u}\}$ ,  $\{u\}$  are the acceleration, velocity and displacement vectors and  $f(t)$  is the nodal load vector. The nodal displacement vector is equal to  $\{u\} = \{u_1, v_1, w_1, u_2, v_2, w_2, \dots, u_n, v_n, w_n\}$  where  $n$  is the number of nodes.

The nodal load vector due to earthquake is obtained using the equation

$$f(t) = -M I \ddot{u}_g(t) \quad (2)$$

where  $M$  is the overall mass matrix,  $I$  is the influence vector,  $\ddot{u}_g(t)$  is the ground acceleration. To determine the displacements and acceleration, the resulted equation of dynamic equilibrium is solved using Newmark's method. The displacement obtained at each node is assigned for each element. The stresses in each element are then obtained using these displacements.

### 3.0 RESULTS AND DISCUSSIONS



*Figure 1: One-storey masonry structure resting on laminated rubber bearing*

A response of a masonry building subjected to Koyna earthquake excitation is studied. A one-storey masonry building mounted on laminated rubber bearing considered for the analysis is shown in Figure 1. The modulus of elasticity and Poisson's ratio of wall is taken as  $2 \times 10^5 \text{ kN/m}^2$  and 0.2 respectively. The stiffness of the bearing is adjusted in order to get the isolation period equal to 2.0 seconds. Damping is assumed to be 5% and 10% for superstructure and bearing respectively. The top floor displacement, base displacement, top floor acceleration, Von Mises stresses at bottom due to this loading is computed at a time interval of 0.04 seconds for a total period of 30.0 seconds. The variation of response with time is shown in Figure 2 for fixed ( $T_s = 0.2 \text{ sec}$ ) as well as base isolated ( $T_b = 2.0 \text{ sec}$ ) structure. It can be seen from the figure that the maximum acceleration and maximum Von Mises stresses at bottom decreases due to isolation. However, the maximum horizontal displacement increases due to isolation. Also the displacement at top and base of the isolated structure are almost same at all time intervals. This indicates that the structure moves rigidly during earthquake.

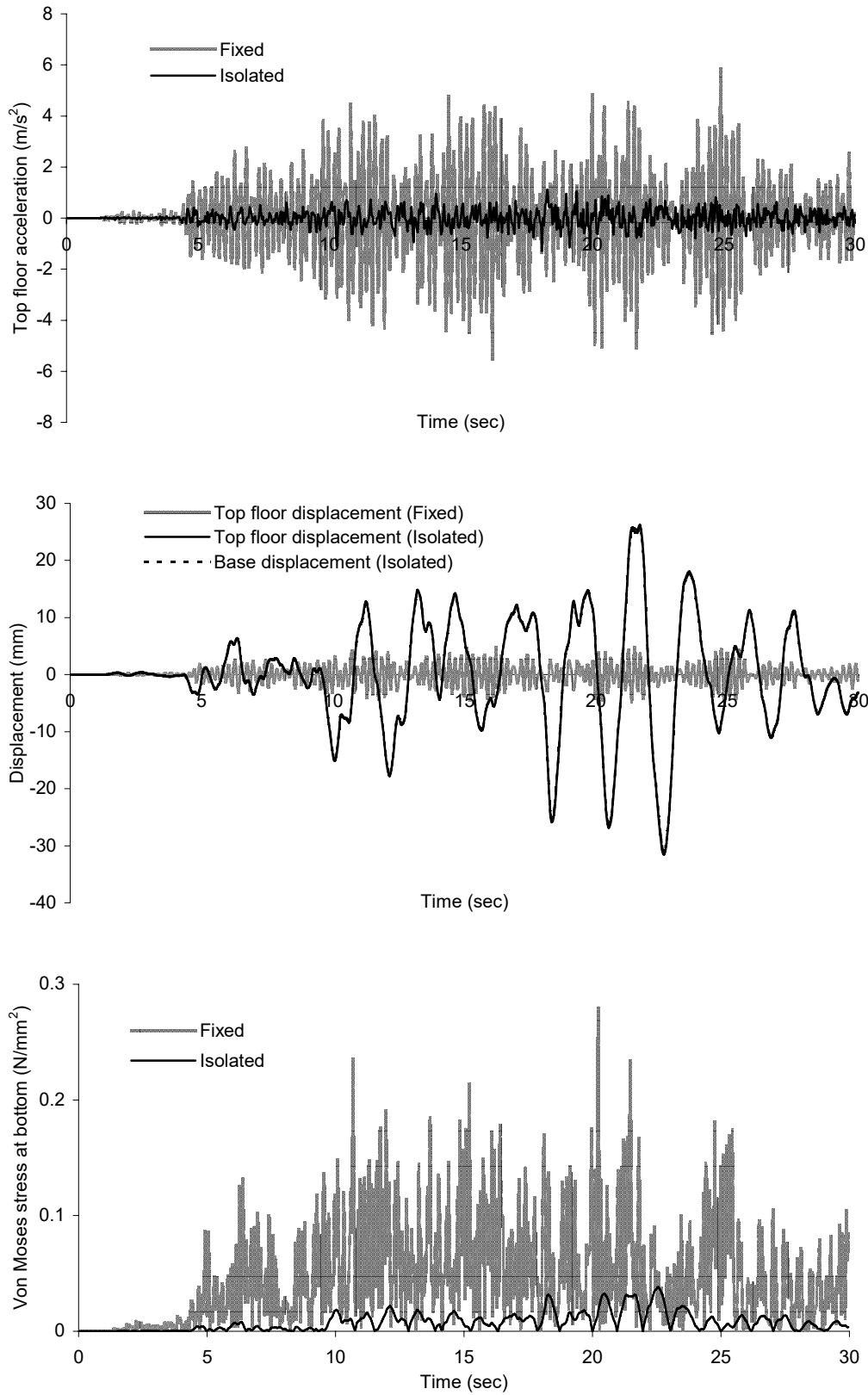


Figure 2: Response of masonry building for Koyuna earthquake

#### 4.0 CONCLUSIONS

The response of a masonry building resting on laminated rubber bearing subjected to Koyna earthquake ground motion is studied. A one-storey masonry building resting on bearing is considered for study. The effectiveness of base isolation is studied by comparing the response of base isolated structure with the response of the fixed base structure. Based on the analysis it can be concluded that the maximum acceleration and stresses in the building decreases considerably. The maximum base displacement is also within the limit. Hence the isolation using bearing can be used effectively used to reduce the effect of earthquake on masonry buildings.

#### ACKNOWLEDGEMENTS

This research was supported by grants from the University Grants Commission, New Delhi. This support is gratefully acknowledged.

#### REFERENCES

- Bhasker P, Jangid RS. 2001. *Experimental study of Base isolated Structures*. Journal of Earthquake Technology ISET; 38, 1, 1-15.
- Jangid RS, Dutta TK. 1992. *Seismic behaviour of torsionally coupled base isolated structure*. European Earthquake Engineering. 3, 1-13.
- Kelly JM.,1986. *Seismic base isolation: review and bibliography*. Soil dynamics and Earthquake Engineering. 5, 202-216.
- Paz M, 2001. *Structural dynamics – Theory and Computation*, 3<sup>rd</sup> Ed, Van Nostrad Reinhold, New York.

# **URBAN BUILDING INVENTORY FROM VHR REMOTE SENSING IMAGERY FOR EARTHQUAKE RISK ANALYSIS IN BANGKOK**

N.H.M. KAMRUJJAMAN SERKER<sup>1</sup>, PENNUNG WARNITCHAI<sup>2</sup> AND  
DUSHMANTA DUTTA<sup>3</sup>

<sup>1</sup>Rajshahi University of Engineering and Technology, Bangladesh

<sup>2</sup>SCE, Asian Institute of Technology, Thailand

<sup>3</sup>ICUS, IIS, University of Tokyo, Japan

ddutta@ait.ac.th

## **ABSTRACT**

*Bangkok, the capital city of Thailand, is one of the mega cities in Asia and a regional hub. The city has a very high economic growth and is going through changes as new buildings and other structures are built. Bangkok is considered free of seismic risk. Recent studies shows that the risk due to distant earthquakes needs to be evaluated because of high population density and construction of concrete structures considering a little or no seismic loading. It is imperative to update the building and infrastructure inventory to evaluate seismic risk and to establish proper management plans for disaster reduction. Therefore, very high resolution (VHR) satellite images are used to develop an inventory for building and infrastructures located in the region considering their spectral, spatial and contextual properties. Seismic risk due to scenario earthquake is evaluated using the HAZUS methodology and inventory data obtained from image analysis in combination with the existing database. Scenario results are presented for an earthquake in the region.*

## **1.0 INTRODUCTION**

Bangkok (Figure 1), the capital city of Thailand, is one of the major cities in Asia and is a regional hub. The city has a high economic growth and a rapid urbanization and a massive scale of building construction have taken place in Bangkok. Since Bangkok has long been considered by most people as being free from seismic risk, most buildings and structures were designed and constructed without any consideration on seismic loading. However, recent studies indicate that there are several active faults located at about 120 to 300 km from Bangkok (Warnitchai, 2003). Warnitchai (2003) also found that these active faults exhibit very low levels of seismicity, however, their expected rupture dimensions indicate that a large earthquake of magnitude 7.5 could be generated. Instrumental records of earthquakes in the Thailand-Burma-Indochina region over the past 90 years also show that the active seismic sources, capable of generating large magnitude earthquakes, are located at about 400 km to 100 km from Bangkok. Moreover, Bangkok has the qualitatively similar surficial geologic setting of Mexico City, and hence by analogy, Bangkok appears

similar to be susceptible to the same soil amplification of ground motions (Warnitchai, et. al, 2000).

Disaster risk analysis is important not only to estimate the losses from future event (or events) but also to make recommendations for prevention, preparedness and response. Building inventories are essential for all types of disaster risk analysis models. With a slight difference in characterization of building types, all models require an estimate of number of buildings or total square footage (Eguchi *et al.*, 2000). Land use information is very important for disaster risk analysis in urban areas. Traditional land surveying methods, such as field surveys, aerial photography, etc. are costly and time consuming. Padermkul (1999) developed an inventory methodology for Bangkok using the multiple data sources. However these sources contain old data and these files are not updated regularly. Also the available building inventories for Bangkok are old, paper-based and do not contain the spatial information. In order to rapidly derive detailed land use information in broad areas, it is necessary to use remote sensing techniques.

The launches of the IKONOS and Quickbird satellites in 1999 and 2001, respectively, have improved the resolution power of the previously most powerful commercially available satellite images by factors greater than 10. The Quickbird images provide 2.8 meter detail in multispectral mode (blue, green, red and near-infrared bands) and 0.6 meter in panchromatic mode. This detail is comparable to aerial photography, but satellite imagery has the advantage of being continuously updated without having to cover great areas using an aeroplane with expensive equipment. The availability of such images has given new possibilities to use satellite images in high detail Geographic Information Systems, including city-planning, real-estate inventory, natural risk management and any other kind of cartography.

A few studies, in the past years, were done to use satellite imagery to develop building and other infrastructures inventories for the selected areas. Yamazaki *et al.* (2000) investigated the capability of developing building inventory used for seismic risk analysis using satellite images from LANDSAT, IRS, JERS-1, ADEOS and IKONOS. They used principal component analysis and found this method as a possible solution to classify urban structures. However, Sande *et al.* (2003) proposed a segmentation and classification approach for IKONOS-2 imagery for land cover mapping to assist flood risk and flood damage assessment using object oriented image analysis technique

This research was aimed to develop an up-to-date building inventory using information obtained from remote sensing data analysis and existing databases. The main objectives were as follows:

- Analysis of very high-resolution satellite remote sensing data for developing an inventory for buildings for an urban area,
- Use of the building inventory for earthquake risk analysis.

## 2.0 STUDY AREA

The study site selected is a part of the Bangkok Metropolitan Area (Figure 1). The area, measured about 52 km<sup>2</sup>, comprises of mainly residential areas along with a few industrial sites. Most of the buildings are single housing type. Only a few numbers of high-rise buildings was found in the selected site. The common practice of building houses in the selected area is with concrete moment resisting frame with in filled non-reinforced masonry walls. Reinforced concrete roofs, concrete tiled roofs, and metal roofing's are very common in the selected study area. However, details about the individual buildings were not found from any existing database. The roads are found as cement concrete roads with foot over bridges at regular intervals. The roads are separated with wide road dividers and at road intersections flyovers exist. There are trees along the roadsides and part of roads and building roofs are found shaded with tree.

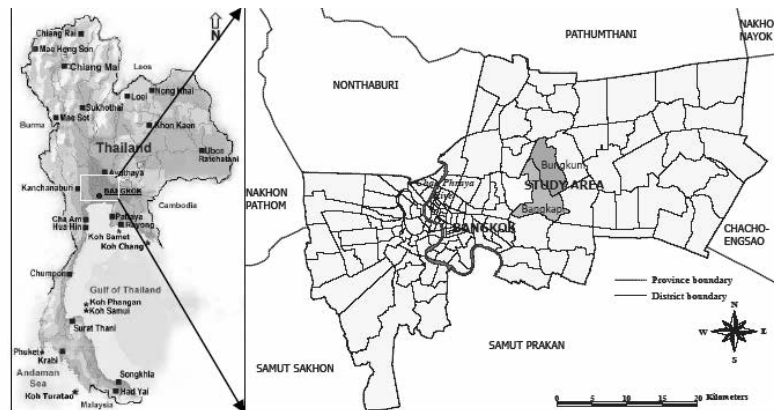


Figure 1: The study area

## 3.0 METHODOLOGY

The overall approach adopted for development of an up-to-date building inventory is shown in Figure 2. The existing building database was supplemented with the outcomes of the image analysis of very high resolution remote sensing data for the study area. AGIS platform was utilized to integrate the extracted information from image analysis and existing information of the region.

QuickBird (panchromatic and multi-spectral) images were used in this study, for development of urban building inventory. QuickBird image specification is shown in Table 1. The primary objective of this study was to obtain information on buildings and other important structures, from very high-resolution remote sensing data, located in the selected site.

There are two different approaches, visual interpretation and thematic classification, of gathering information from satellite imagery. Pixel based classification and object oriented classification are two common methods of thematic classification. In this study object oriented image analysis

technique was applied to extract the desired information. The basic elements of an object-oriented approach are image objects. Image objects are contiguous regions in an image. Segmentation is the subdivision of an image into separated regions. Image segmentation was done using multi-resolution image segmentation (eCognition, 2002).

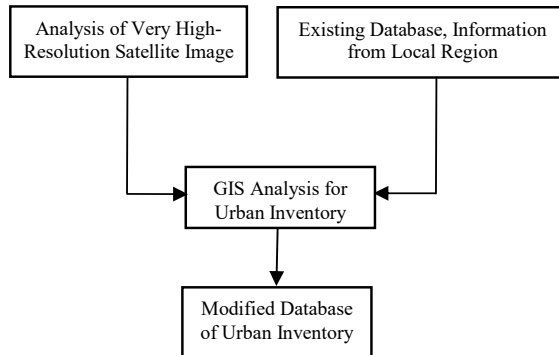


Figure 2: Overall inventory methodology

Table 1: QuickBird image properties.

Acquisition date	11/07/2002
Spatial resolution	2.80 m multi-spectral bands 0.60 m panchromatic
Spectral wavebands	0.45-0.52 $\mu\text{m}$ (Blue) 0.52-0.60 $\mu\text{m}$ (Green) 0.63-0.69 $\mu\text{m}$ (Red) 0.76-0.90 $\mu\text{m}$ (Near IR)
Map projection	Universal Transverse Mercator
View angle	Nadir
Swath width	16.5 km

Fuzzy classification is beside neural networks and probabilistic approaches (Curlander and Kober, 1992), a very powerful soft classifier (Benz et.al., 2004). As an expert system (Tsatsoulis, 1993) for classification it takes into account the followings (Benz *et.al.*, 2004):

- Uncertainty in sensor measurements
- Parameter variations due to limited sensor calibration
- Vague class descriptions
- Class mixtures due to limited resolution

Four different levels were chosen to extract features of interest from different levels. Table 2 shows the segmentation parameters used as relative values and as a function of thematic land cover. As shown in the Table 2 and Figure 3, the spectral bands can either be included or excluded from the



segmentation process. The scale parameter was the most important factor to control the size of the objects. The classification was done on the image objects using multi level classification approach based on fuzzy methods. Fuzzy classification technique was applied with the help membership function. Membership functions were developed based on the spectral reflectance characteristics and shape properties of the image objects. Different features were separated using different membership functions. One-dimensional membership functions were used in this study. To separate different urban features, (e.g., concrete surfaces, nonconcrete surfaces, green areas, Bareland, water bodies, etc) spectral information based on image objects was used. Buildings were separated from roads based on their shape properties. The classified image view is shown in Figure 4. Field survey was carried out to obtain information about the features and to obtain 'ground truth' data. Field survey data was used as the primary knowledge base and was combined with the spectral information obtained from the image objects to develop membership functions for different classes.

*Table 2: Segmentation parameters used for analysis of QuickBird image.*

Segmentation & classification level	Land use types	QuickBird bands used				Scale	Homogeneity criterion			
		Blue	Green	Red	NIR		Color	Shape	Shape settings	
									Smoothness	Compactness
Level I	All	Yes	Yes	Yes	Yes	5	0.7	0.3	0.9	0.1
Level II	Buildings & Roads	No	Yes	Yes	Yes	10	0.5	0.5	0.9	0.1
Level III	Major Roads	No	Yes	Yes	Yes	25	0.5	0.5	0.9	0.1
Level IV	Large Water bodies	No	No	Yes	Yes	40	0.9	0.1	0.9	0.1

*Table 3: Features extracted from QuickBird image analysis and digitization (% of total area)*

Class		QuickBird	Digitized
Build up	Road	3.29	4.24
	RC Building	10.65	10.20
	NRC Building	23.33	20.10
Green		42.79	57.61
Bareland		13.81	
Water		3.20	3.85
Shadow		0.60	3.30
Others		3.33	

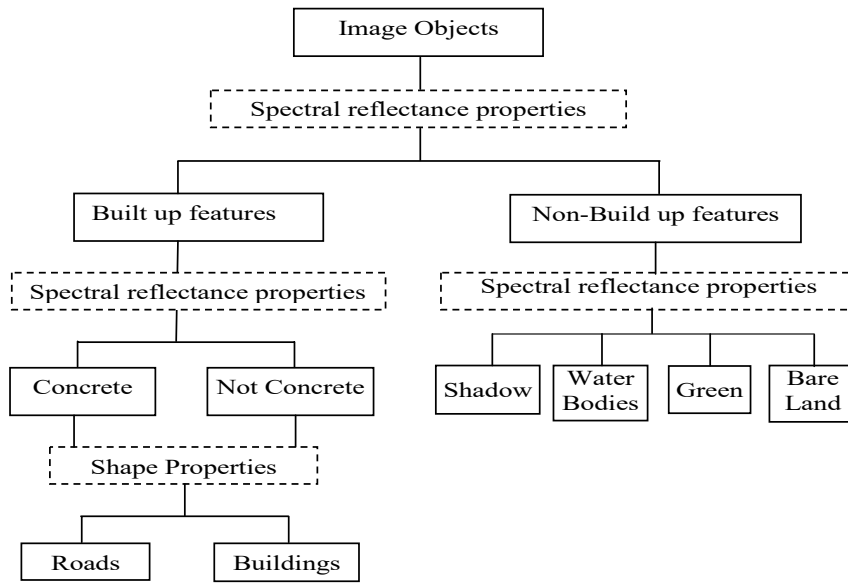


Figure 3: Class hierarchy for analysis of QuickBird image

## 4.0 RESULT ANALYSES

In this study buildings and roads were given primary importance to be extracted. Buildings were extracted from segmentations at levels 1 and 2. Buildings were classified as reinforced and non-reinforced concrete buildings depending on their roofing materials and types. Small roads were extracted from extracted from segmentation at level 2 where as large roads were extracted from segmentation at level 3. Segmentation at level 4 was used to classify the large objects, e.g. large water bodies, in the study area. The classification results are summarized in Table 3. About 38% of the total area was classified as built up area of which approximately. 35% of the total area was classified as building area. From visual interpretation of the panchromatic image of 60cm, approximately 36% of the total area was classified as built up area, which is about 95% of the area obtained from image analysis. It was possible to separate shadows from other features, however, 33% shadow objects were classified as water.

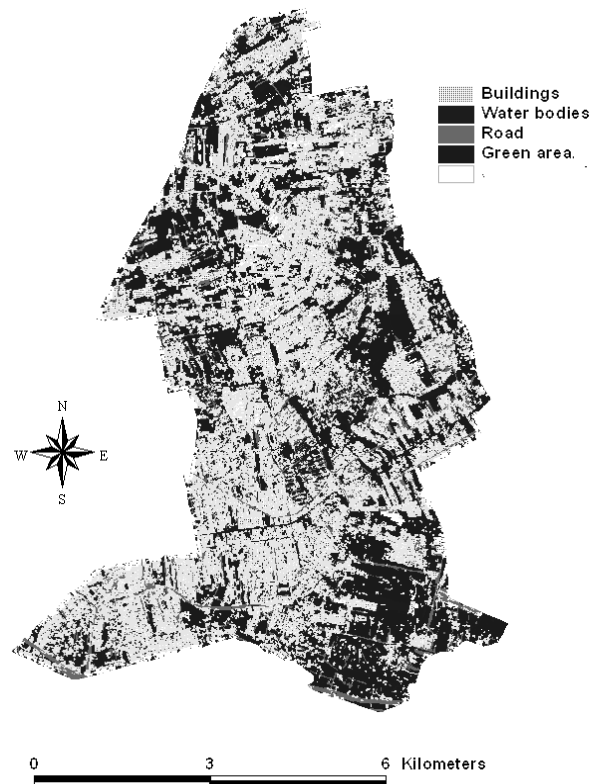
### 4.1 Accuracy assessment

Verification of the classification results with the help of ground truth data is a common technique in remote sensing data analysis. However, in this study two different approaches, verification of results with ground truth data and comparison of the results with the results obtained from digitization, were applied to verify the classification results. Table 4 shows the verification of the classification results with ground truth data. In general pixels are considered to verify the classification results. In this study, image objects were considered to verify the classification system. An overall accuracy of 85% was achieved with the classification scheme. However some of the classes, e.g. RC buildings, green areas and bareland, were classified with high level of accuracy up to 100%. Non RC buildings

and roads were classified with accuracy of 70% and 80% respectively. Digitized data of the study area was developed using manual classification with the help of visual interpretation and photographs obtained from field survey. The areas of different features extracted from image analysis were compared with the areas obtained by digitizing. The comparison of the results obtained from two analyses is shown in Table 3. RC buildings area extracted from image analysis was 95% of the area obtained by digitization. Non RC buildings area was extracted as 116% of the digitized area. Shapes of buildings, roads and water bodies, extracted from image analysis, were overlaid on the shapes obtained from digitization. There was large deviation, in terms of regularity of shape, between two shapes.

*Table 4: Error matrix for QuickBird image.*

	Building	Road	Not Concrete	Water	Shadow	Green	Bareland	Total
Building	10							10
Road	2	7						10
Not Concrete			7			1	2	10
Water				8				8
Shadow				3	6			9
Green						10		10
Bareland							5	5
Total								62



*Figure 4: Classified map with QuickBird image*

## **5.0 SEISMIC RISK ANALYSIS**

The recent studies show that Bangkok can be experienced to a large earthquake of magnitude 7.5. Also the site response analyses show that the surficial deposits of Bangkok have the ability to amplify earthquake ground motions about 3 to 4 times, and the amplified ground motions can be describes as narrowband random motions with long predominant period of about 1 second. Considering these factors an earthquake of magnitude 7.5 was selected to observe the building damage.

HAZUS99-SR2 was used for earthquake loss estimation in this study. HAZUS has been developed by the Federal Emergency Management Agency (FEMA) under the agreement with National Institute of Building Sciences (NIBS). HAZUS is designed to produce loss estimate in different levels (e.g. state, regional, and local government levels). HAZUS can be used in ARC View or ARC Info environment. An earthquake loss estimate can be performed using HAZUS for any location using only the methodology and user supplied databases. The HAZUS methodology is outlined in Figure 5.

### **5.1 Inventory development for risk analysis**

The study was focused only on the damage of buildings and distribution of damaged buildings. The classification of buildings was made on the building structure types. Other classifications e.g. social function classes, essentially needed for monetary and non-monetary loss estimation, were not considered. The inventory was compiled using the extracted results from remotely sensed data and combining it with field survey data and existing databases. From the field survey it was found that there exist mostly single housing residential buildings. Most of the buildings are low-rise building. The number of high-rise buildings is not large. For the classification of building the methodology provided by HAZUS was followed. The total number of building was estimated from the QuickBird panchromatic image as 7000. Approximately 79% of the buildings are associated with residential housing. The land use statistics as obtained from JICA report on “The Study on Urban Environmental Improvement Program in Bangkok Metropolitan Area” are shown in Tables 5 and 6.

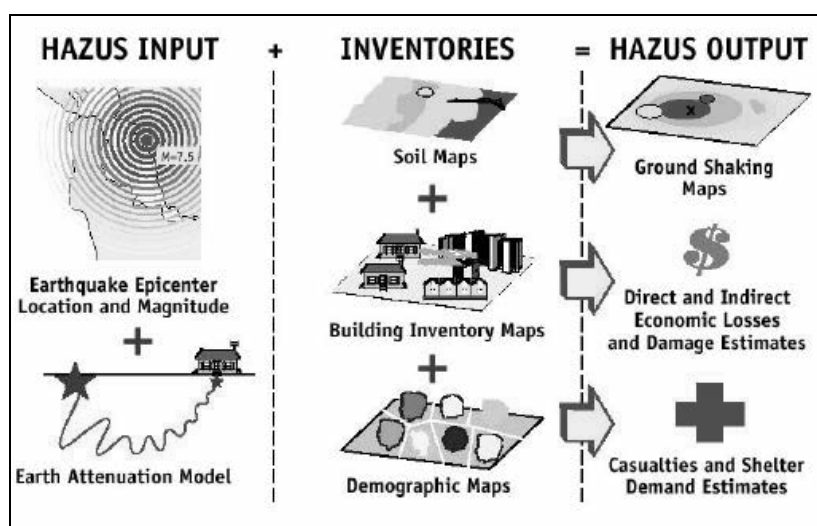
### **5.2 Building damage estimation**

Structural fragility curves were evaluated for spectral displacement and spectral acceleration defined by the intersection of the capacity and demand curve. The fragility curves for different types of structural classification that are used in this study were taken from HAZUS. Figure 6 shows the building damage distribution in the study region due to an earthquake of magnitude 7.5. The damage states are used from the HAZUS. The analysis shows that about 1.5% of the low-rise building got slight damaged and 0.5% of the mid-rise building damaged slightly. None of the high-rise building received any damage due to the ground shaking caused by

the selected earthquake. The results of the building damage estimation are given in Table 7.

*Table5: Types of building according to function  
(% of total building constructed)*

District	Residential	Commercial	Office	Industrial	Others
Bangkapi	37.41%	30.56%	26.46%	0.18%	5.39%
Bungkum	48.52%	30.42%	14.56%	1.37%	5.13%



*Figure 5: Earthquake loss estimation using HAZUS (HAZUS99-SR2)*

*Table 6: Types of buildings according to height*

Type of Building	No. of stories	Bangkapi	
		% of total Building	Total no of Buildings
Low Rise	1~3	66.45	4,573
Mid Rise	4~7	21.94	1,607
High Rise	8+	11.61	1,036

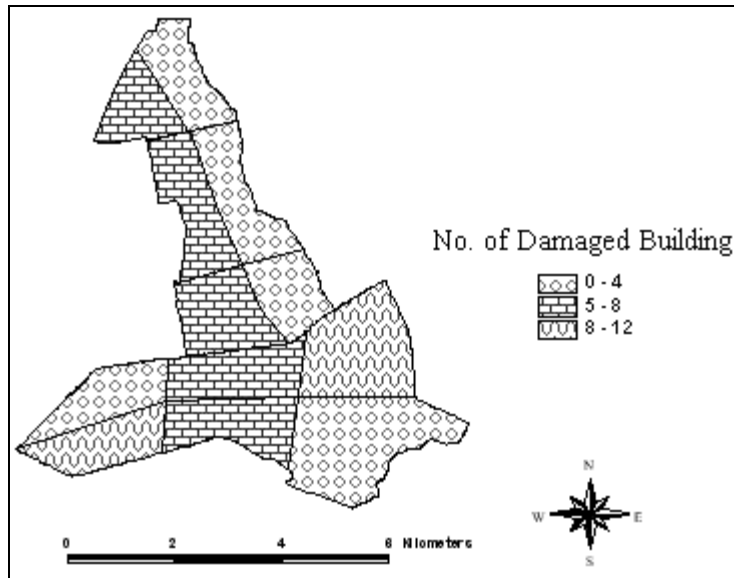
*Table 7: Building damage data*

Building Type	No of Buildings	No. of Building Damaged				
		No Damage	Slight	Moderate	Extensive	Complete
C3L*	4,573	4,505	68	Nil	Nil	Nil
C3M*	1,607	1,599	8	Nil	Nil	Nil
C3H*	1,036	1,036	Nil	Nil	Nil	Nil

\* C3L, C3M, and C3H represent low rise, midrise and high rise concrete frame with unreinforced masonry infill wall building respectively as described in HAZUS manual.

## 6.0 CONCLUSIONS

This study was aimed to develop a GIS ready inventory for buildings in selected districts of Bangkok city using remotely sensed data. Building areas were classified with approximately 90% accuracy. The shapes of the roads and water bodies were found as regular shapes. However, the regular shapes of the buildings were not found from the image analysis. Finally seismic risk due to an earthquake of magnitude 7.5 was evaluated using HAZUS methodology.



*Figure 6: Building damage distribution (low-rise buildings)*

From this study, the following conclusions can be drawn:

- QuickBird image can be a very good choice to develop an inventory for urban features. City area consists of small and large buildings and roads along with other structures. Small houses, roads, water bodies and other features are clearly visible and identifiable from QuickBird image.
- In the selected study site, the roofing material consists of concrete, metal sheets, wood etc. However, buildings were classified, based on their roofing materials, as concrete and non-concrete buildings.
- With the object-oriented classification scheme used in this study, an overall accuracy of 85% was achieved in detailed classification of urban landcover in the study area. The building area was extracted with a high level of accuracy.
- From this study, it was found that many urban features completely or partly covered with trees and shadows. From analysis of QuickBird image it was found that 0.6% of the total land area covered by shadow. Using Remote sensing data, it is difficult to extract accurately the features covered with trees or vegetal cover.

- Dynamic properties of buildings are needed to be evaluated to perform the risk analysis accurately. In this study all properties of buildings were directly used from HAZUS. So the results may vary due to change in building properties.

## REFERENCES

- Benz, U.C., Hofmann, P., Willhauck, G., Lingenfelder, I., Heynen, M., 2004. *Multi-resolution, object-oriented fuzzy analysis of remote sensing data for GIS-ready information*. ISPRS Journal of Photogrammetry & Remote Sensing, vol. 58, pp. 239–258
- Curlander, J., and Kober, W., 1992. *Rule Based System for Thematic Classification in SAR Imagery*. Proceedings of IGARSS, IEEE Press, New York
- eCognition, 2002. *User Guide*. Definiens Imaging, GmbH, Munich, Germany.
- Eguchi, R.T., Huyck, C.K., Houshmand, B., Tralli, D.M., and Shinozuka, M., 2000. *A new Application for Remotely Sensed Data: Construction of Building Inventories using Synthetic Aperture Radar Technology*. Proceedings of the 2<sup>nd</sup> Multi-lateral Workshop on Development of Earthquake and Tsunami Disaster Mitigation Technologies and Their Integration for the Asia-Pacific Region, Kobe, Japan.
- HAZUS 99 Service Release 2 (SR2), *User Manual-Arc View*, Maryland, U.S.A.
- Padermkul, S., 1999. *An Integrated Inventory Methodology for Seismic Damage Assessment of Bangkok*. Asian Institute of Technology, Thailand, Thesis no. ST-99-29.
- Sande, C.J. van der, Jong, S.M. de, and Roo, A.P.J. de, 2003. *A segmentation and classification approach of IKONOS-2 imagery for land cover mapping to assist flood risk and flood damage assessment*. International Journal of Applied Earth Observation and Geoinformation, vol. 4, pp 217-229.
- Tsatsoulis, C., 1993. *Expert systems in remote sensing applications*. IEEE Geoscience and Remote Sensing Newsletter June, 7–15.
- Warnitchai, P., 2003. *Assessing Impact of Distant Earthquakes on Buildings and Structures in Bangkok*. Proceedings of the 6<sup>th</sup> Multi-lateral Workshop on Development of Earthquake and Tsunami Disaster Mitigation Technologies and their Integration for the Asia-Pacific Region, Kashikojima, Japan.
- Warnitchai, P., Sangrayangkul, C., and Ashford, S.A., 2000. *Seismic hazards in Bangkok due to long distance earthquakes*. Proceedings of the 12<sup>th</sup> world conference on Earthquake Engineering, Auckland, paper no. 2145.
- Yamazaki, F., Mitomi, H., Matsuoka, M., and Honda, K., 2000. *Inventory Development for Natural and Built Environments- Remote Sensing Technologies for Inventory Development and Risk Assessment- Characteristics of Satellite Images in Bangkok, Thailand*. Report on 'The Development of Earthquake and Tsunami Disaster Mitigation

Technologies and Their Integration For the Asia-Pacific Region,  
Earthquake Disaster Mitigation Research Center, Japan.  
[http://www.edm.bosai.go.jp/eqtap/3rdws\\_yamazaki\\_e.pdf](http://www.edm.bosai.go.jp/eqtap/3rdws_yamazaki_e.pdf) (April  
2004).



# **QUANTITATIVE APPROACH FOR SEISMIC RETROFITTING OF STRUCTURES USING PUSHOVER ANALYSIS**

PRABIR C. BASU, A. D. ROSHAN, AJAI S. PISHARADY  
Atomic Energy Regulatory Board, Mumbai, India.  
*adroshan@aerb.gov.in*

## **ABSTRACT**

*Seismic fragility of structure is the conditional frequency of its failure for a given value of seismic response parameter, which is generally taken as peak ground acceleration. A method for determining the seismic fragility using deflection based structural analysis (pushover analysis) has been developed. Application of deflection based fragility analysis method is illustrated with an example problem of reinforced concrete frame structures taken from a safety related concrete building of PHWR based nuclear power plant.*

## **1.0 INTRODUCTION**

Fragility of a system, be it building structures or equipment or a safety system, is defined as the conditional probability of its failure for a given value of the input parameter such as stress, moment, spectral acceleration, peak ground acceleration.

Seismic fragility is generally defined in terms of peak ground acceleration (PGA). The objective of fragility evaluation is to estimate the PGA value for which the seismic response of a given component (i.e. structural elements or equipment) located at a specified point in the structure exceeds the component capacity resulting in its failure. Because there are many sources of variability in the estimation of this ground acceleration capacity, the component fragility is described by means of a family of fragility curves. A probability value is assigned to each curve to reflect the uncertainty in the fragility estimation (Kennedy et. al., 1980). System fragility is derived by combining suitably the component fragility.

In case of structures, failure can be viewed in more than one way, strength failure (collapse) and functional failure. Fragility analysis of concrete structure of a nuclear power plant (NPP) is worked out in most cases in terms of element stresses, i.e. basically with reference to strength failure. The structures have generally considerable margin against strength failure. However, safety against such failure may not guarantee the safety against functional failure.

Seismic fragility of reinforced concrete structures for functional failure could be worked out using deflection based method. Deflection

based method is also believed to be suitable for re-evaluation of concrete structures subjected to near field earthquakes. The scope of the present paper covers determination of seismic fragility of reinforced concrete structures using deflection based method.

## 2.0 FRAGILITY ANALYSIS OF STRUCTURAL SYSTEM

The ground acceleration capacity,  $A$ , of a component can be expressed in terms of best estimate of the median ground acceleration capacity,  $\tilde{A}$ , and two random variables,  $\varepsilon_R$  and  $\varepsilon_U$ , and is given by (Kennedy et. al., 1984),

$$A = \tilde{A} \cdot \varepsilon_R \cdot \varepsilon_U \quad (1)$$

$$\tilde{A} = A_m \cdot F \quad (2)$$

$$F = F_S \cdot F_\mu \cdot F_{RS} \quad (3)$$

$$F_{RS} = F_{SA} \cdot F_{SS} \cdot F_\delta \cdot F_M \cdot F_{MC} \cdot F_{EC} \quad (4)$$

Where,

$\tilde{A}$  : Median ground acceleration capacity

$\varepsilon_R$ : Random variable representing the inherent randomness about the median value

$\varepsilon_U$ : Random variable representing the uncertainty in the median value.

$A_m$ : Median value of ground acceleration PGA

$F_S$ : Strength factor.

$F_\mu$ : Inelastic-absorption factor.

$F_{RS}$ : Structure-response conservatism factor.

$F_{SA}$ : Factor for ground motion and associated response spectra for a given PGA.

$F_{SS}$ : Soil structure interaction factor.

$F_\delta$ : Factor energy dissipation i.e. damping.

$F_M$ : Structural modeling factor.

$F_{MC}$ : Factor for combination of modes and earthquake analysis results.

$F_{EC}$ : Factor for combination of earthquake components

If  $\{F_{()}\}$ 's follows log-normal distribution, the median ( $\bar{F}$ ) and standard deviation ( $\beta_F$ ) of "F" can be calculated from the median values  $\{\bar{F}_{()}\}$  and logarithmic standard deviation  $\{\beta_{()}\}$  of the factors given in equations (3) and (4). Therefore,

$$\bar{F} = \bar{F}_S \cdot \bar{F}_\mu \cdot \bar{F}_{SA} \cdot \bar{F}_{SS} \cdot \bar{F}_\delta \cdot \bar{F}_M \cdot \bar{F}_{MC} \cdot \bar{F}_{EC} \quad (5)$$

and

$$\beta_F = \sqrt{\beta_S^2 + \beta_\mu^2 + \beta_{SA}^2 + \beta_{SS}^2 + \beta_\delta^2 + \beta_M^2 + \beta_{MC}^2 + \beta_{EC}^2} \quad (6)$$

$\beta_F$  is further divided into random variability  $\beta_R$  and uncertainty  $\beta_U$

The fragility i.e., the frequency of failure  $f$  at any non-exceedence probability level  $Q$  can be expressed as:

$$f = \Phi \left( \frac{\ln \left( \frac{a}{A} \right) + \beta_U \Phi^{-1}(Q)}{\beta_R} \right) \quad (7)$$

Where,  $Q = P[f' < f | a]$  = the probability that the conditional frequency of failure, “ $f'$ ”, is less than  $f$  for a peak ground acceleration, ‘ $a$ ’; and  $\Phi(.)$  is the standard Guassian cumulative distribution function. From the equation above  $f'$  is determined for discrete values of non-exceedence probability level such as 5%, 50% and 95% etc for each structural elements.

Fragility of the overall structural system can be determined by combining suitably the component (structural element) fragility. One example of such combination approach is fail-safe condition. The seismic fragility of overall structural system can be determined as follows using fail-safe combination approach. Let  $f_i$  is the conditional frequency of failure of the element for a PGA value of “ $a$ ”. The conditional frequency failure of the overall structure for PGA value of “ $a$ ” is given by the following expressions (Moses F and Kinser D.E., 1967) for a given value of “ $i$ ”, say  $i = 4$ ;

$$P_F = f_1 + (1 - f_1)[f_2 + (1 - f_2)\{f_3 + (1 - f_3)f_4\}] \quad (8)$$

Where,  $f_i$ 's are arranged in descending order, i.e.,  $f_1 > f_2 > f_3 > f_4$

### 3.0 SEISMIC FRAGILITY OF REINFORCED CONCRETE FRAME STRUCTURES USING DEFLECTION BASED METHOD

A structure can be considered to fail functionally when the deformations under seismic loads are estimated to be sufficient to potentially interfere with the operability of the safety related equipment attached to the structure, or fractured sufficiently to cause the failure of equipment attached to it. Two important failure modes of structures are indicated above; deformation of the structure beyond a desired value, and fracture of components to which equipment is attached. First one may be viewed from the consideration of functional failure, while the second one is associated with the strength failure of component.

The functional failure of a structural system can be defined by the exceedence of deflection at a given location beyond a specified value, or storey drift exceeding a given value. Such type of deflection-based criteria can be incorporated in the fragility evaluation of reinforced concrete frame structures by means of deflection-based method.

In deflection-based method, a pushover curve, i.e. load (base shear) deformation (roof deflection) curve of the structure is first determined and then the maximum displacement,  $\Delta_{ag}$ , under the effect of given seismic excitation is calculated. Methodology described in either FEMA 273 (1997)

or ATC-40 (1996) is suitable for this purpose. It is to be noted that the pushover curve (load deformation curve) is the property of the structure and not related to ground motion parameters. The limiting value of deflection parameters can be specified considering the constraints imposed upon the structure from the operability condition of systems or equipment housed in it. These limiting values of deflection parameters represent the capacity of the structure for given criteria. Typical deflection parameters on which the limitations could be imposed are roof deflection, storey drift, etc. Once the deflection parameters are identified and the limits,  $\Delta_a$ , are specified, the ground acceleration capacity of the structure can be determined from equation (1) through (7). The governing relation of ground acceleration capacity of equations (2) and (3) reduces to

$$\bar{A} = \bar{A}_m * F_{C\Delta} * F_{RS} \quad (9)$$

$$F_{C\Delta} = \frac{\Delta_a - \Delta_{an}}{\Delta_{ag} - \Delta_{an}} \quad (10)$$

Where,

$F_{C\Delta}$  = Capacity factor

$\Delta_a$  = Limiting value of structural deflection.

$\Delta_{an}$  = Deflection induced by non-seismic load

$\Delta_{ag}$  = Maximum deflection corresponds to the given ground motion parameter determined from the deflection based method.

When  $\Delta_{an}$  is very small compared to  $\Delta_a$  and  $\Delta_{ag}$ , for example in case of dead load, equation (10) reduces to

$$F_{C\Delta} = \frac{\Delta_a}{\Delta_{ag}} \quad (11)$$

It may be noted from equation (9) that the capacity factor  $F_{C\Delta}$  replaces  $F_s$  and  $F_\mu$  of equation (3). The factor  $F_\mu$  of equations (3), (4), and (6) is not considered explicitly in equation (9), because the contribution of structural ductility is already considered in establishing pushover curve. But the variability associated with  $F_{C\Delta}$  and other factors related to  $F_{RS}$  are to be considered similar way as expressed in equations (5) and (6). The exceptions are that the terms ' $\bar{F}_s * \bar{F}_\mu$ ' and ' $\beta_s^2 + \beta_\mu^2$ ' would be replaced by ' $F_{C\Delta}$ ' and ' $\beta_{C\Delta}^2$ ' respectively.

The methodology described in FEMA 273 has been adopted for the present work, though ATC-40 methodology is also equally good for calculating  $\Delta_{ag}$ . FEMA 273 outlines a procedure for calculation of the expected maximum displacement (usually, roof displacement), which is also termed as target displacement, during an earthquake using a number of factors for modification of structural deflection. To derive the target displacement, the spectral acceleration corresponding to the effective period of the structure is multiplied by these modification factors, which accounts for non-linear and dynamic behavior of the structure. The target displacement expected during an earthquake is given by

$$\delta_t = C_0 C_1 C_2 C_3 S_a \left( \frac{T_e}{2\pi} \right)^2 g \quad (12)$$

The detailed procedure for calculation of target displacement as per FEMA 273 is given in the Appendix.

#### 4.0 EXAMPLE PROBLEM

The formulation derived in the preceding section is illustrated with an example of reinforced concrete frame structure taken from a safety related building of PHWR based NPP. Figure 1 depicts configuration of the frame structure and the sectional parameters of beams and columns are given in Table-1A and Table-1B respectively. The ground acceleration spectrum that was used in design of the frame is given in Figure 2.

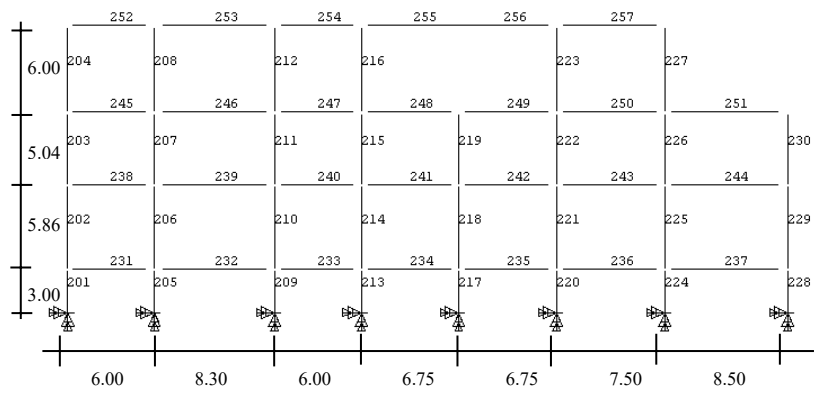


Figure 1: Configuration of the frame structure of the example problem  
(All dimensions are in meters)

Table 1A: Section parameters of beams

Group	Element Numbers.	Size (mm) b x d	Percentage of reinforcement			
			End 1		End 2	
			Top	Bottom	Top	Bottom
B1	231	450x1000	.84	.84	.88	.88
B2	237	450x1000	.78	.78	.87	.87
B3	232,234,236	450x1000	.66	.66	.67	.67
B4	233,235	450x1000	.74	.74	.76	.76
B5	245,238	800x500	1.82	.61	1.3	.65
B6	244	500x1200	.91	.54	1.26	.55
B7	239	500x1200	1.22	.61	.92	.56
B8	240,241,242,243	500x1200	.99	.61	.95	.62
B9	252	800x500	1.16	.61	.95	.62
B10	246	700x1200	.95	.6	.7	.54
B11	247,248,249,250,251	700x1200	.65	.55	.67	.59
B12	253,254,255,256,257	700x950	.85	.55	.88	.61

Table 1B: Section parameters of columns

Group	Element Numbers	Size (mm)	Percentage of reinforcement
C1	201	800x800	3.5
C2	202, 204	800x800	2.42
C3	203	800x800	1.27
C4	205, 206, 207	1200x1200	1.26
C5	208	1200x1200	1.45
C6	209, 210, 211, 213, 214, 215, 216, 217, 218, 220, 221, 222, 224, 225, 226	1000x1000	1.62
C7	212, 219	1000x1000	1.97
C8	223, 227	1000x1000	1.89
C9	228, 229, 230	1200x1200	1.26

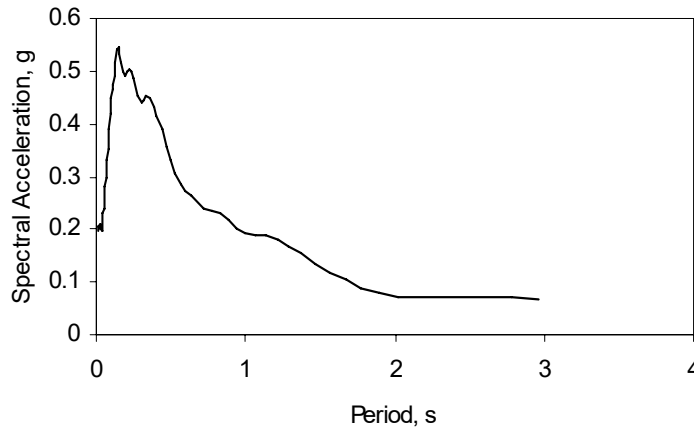


Figure 2: Ground acceleration response spectra (7% damping)

Push over analysis of the frame was carried out for failure in flexure mode. The moment curvature relationship of elements are determined from the cross sectional data of Table-1 using the method given in (SS/CSE-1). A typical moment curvature relation of a concrete beam (end 1 of element group B2) is shown in Figure 3. The fragility parameters, i.e. median values of factors associated with  $F_{RS}$  and the variability of  $F_{C\Delta}$  and different factors related to  $F_{RS}$  is tabulated in Table – 2 (Kennedy et. al., 1984).

Table 2: Fragility Parameters

Factors	$\bar{F}_{(.)}$	$\beta_{(.)U}$	$\beta_{(.)R}$
$F_{C\Delta}$	-	0.25	0.14
$F_{SA}$	1.25	0.10	0.20
$F_{\delta}$	1.25	0.075	0.075
$F_M$	1.0	0.15	0.00
$F_{MC}$	1.0	0.00	0.075
$F_{EC}$	1.0	0.00	0.075
$F_{SS}$	1.3	0.20	0.20

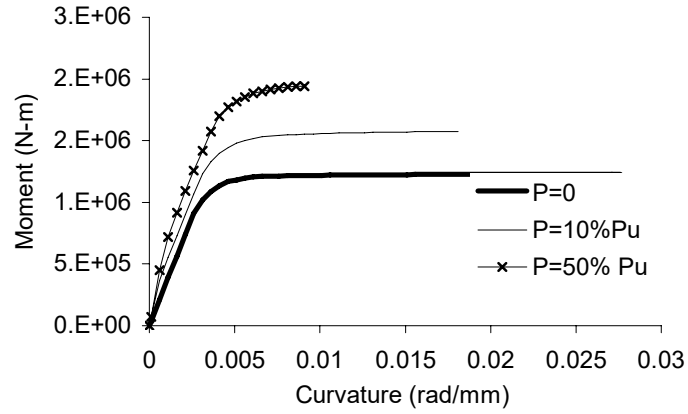


Figure 3: Typical moment curvature curves for a concrete beam for different values of axial load ( $P$ ) in terms of ultimate load ( $P_u$ )

The frame was pushed by the load distribution given in Figure 4, determined from storey shear corresponding to first mode of vibration. The push over analysis was carried out using ANSYS software. Figure 5 contains the deflected shape of the frame when mechanism is formed. The corresponding pushover curve, i.e. variation of roof displacement with base shear is given in Figure 6. The load displacement data obtained from the pushover analysis is given in Table-3.

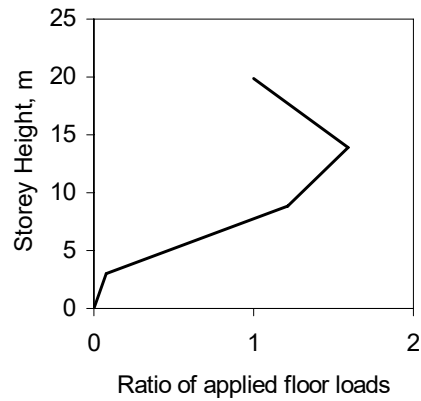


Figure 4: Load distribution used for pushover analysis

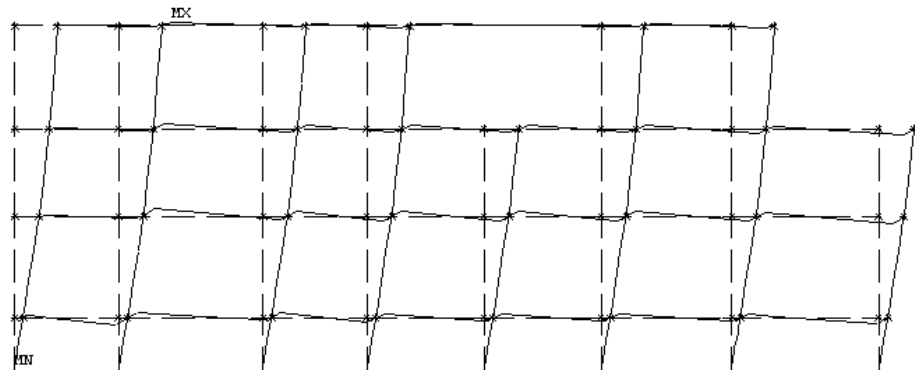


Figure 5: Deflected shape of the frame after the formation of mechanism.

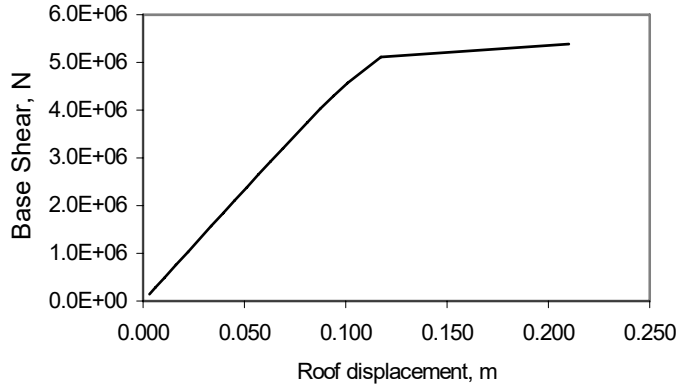


Figure 6: Pushover curve (Base shear Vs roof deflection) of the frame

Table 3: Load – Load – deflection data of the frame

Step No.	Base shear, (N)	Roof		Fourth floor	
		Floor Drift, (m)	Drift Ratio %	Floor Drift, (m)	Drift ratio, %
1	1.46E+05	0.0032	0.0162	0.0010	0.0160
2	2.82E+05	0.0061	0.0307	0.0018	0.0296
3	4.86E+05	0.0104	0.0525	0.0030	0.0499
4	7.58E+05	0.0162	0.0816	0.0046	0.0771
5	1.03E+06	0.0220	0.1108	0.0063	0.1044
6	1.30E+06	0.0279	0.1400	0.0079	0.1317
7	1.57E+06	0.0337	0.1693	0.0095	0.1591
8	1.85E+06	0.0395	0.1986	0.0112	0.1867
9	2.12E+06	0.0454	0.2279	0.0128	0.2142
10	2.39E+06	0.0512	0.2572	0.0145	0.2417
11	2.66E+06	0.0570	0.2866	0.0162	0.2692
12	2.93E+06	0.0629	0.3161	0.0178	0.2968
13	3.21E+06	0.0688	0.3459	0.0195	0.3245
14	3.48E+06	0.0749	0.3763	0.0211	0.3524
15	3.75E+06	0.0810	0.4071	0.0228	0.3804
16	4.02E+06	0.0873	0.4387	0.0245	0.4089
17	4.29E+06	0.0940	0.4722	0.0263	0.4379
18	4.57E+06	0.1011	0.5080	0.0281	0.4677
19	4.84E+06	0.1091	0.5482	0.0299	0.4989
20	5.11E+06	0.1175	0.5903	0.0318	0.5307
21	5.38E+06	0.2100	1.0553	0.0407	0.6779

The median value of  $F_{C\Delta}$ , i.e.  $\bar{F}_{C\Delta}$ , is calculated from the median value of  $\Delta_a$  and  $\Delta_{ag}$  using equation (11). The corresponding value of variability  $\beta_{C\Delta R}$  and uncertainty  $\beta_{C\Delta U}$  are taken as 0.14 and 0.25 respectively. The displacement,  $\Delta_{ag}$ , corresponding to PGA value 0.2g is calculated from equation (12) and the pushover curve of Figure 6, which is 9.44 mm. The fragility curve considering the value of maximum roof deflection,  $\Delta_a=210\text{mm}$  (from Figure 6) as its capacity is given in Figure 7. It may be noted that Figure 7 gives the fragility curve of the frame when its capacity is



defined by the maximum roof deflection. The acceleration capacity of the frame corresponding to high confidence (95%) low probability of failure (5%) is 2.8g.

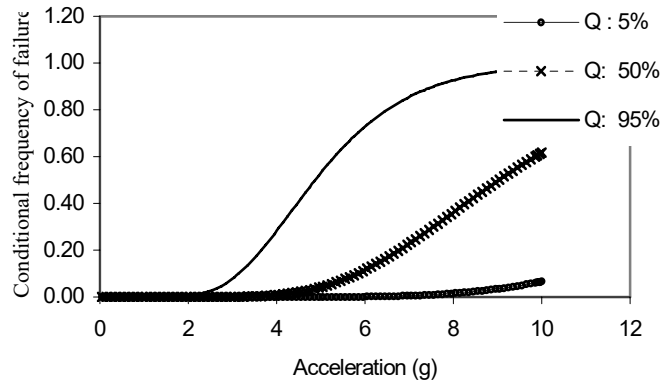


Figure 7: Fragility curve of the frame corresponding to the collapse state.  
HCLPF = 2.8g

The pushover calculation of the frame indicates a very high roof deflection 210mm prior to collapse, no concrete structure of NPP is allowed to deflect so high. Generally limit on deflection, from functionality consideration, is imposed. The fragility curves of structure can be easily determined for this condition. If roof deflection of the example frame is limited to height/300, the  $\Delta_a$  becomes 66mm. This is less than the maximum deflection determined by pushover analysis. The fragility curves thus determined by putting this value of  $\Delta_a$  in equation (9) and (11) are given in Figure 8.

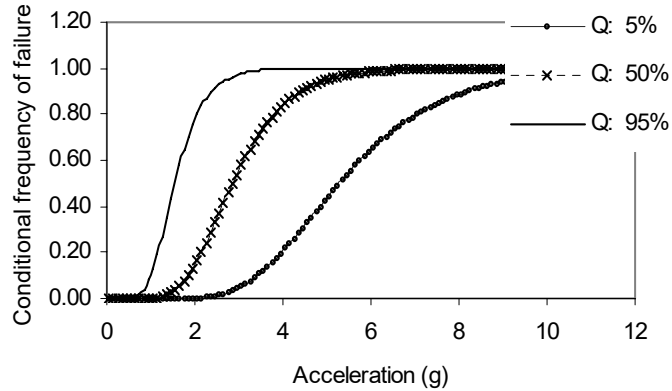
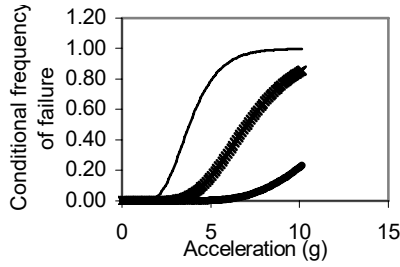


Figure 8: Fragility curve of the frame corresponding to the roof deflection of height/300, HCLPF= 0.875 g.

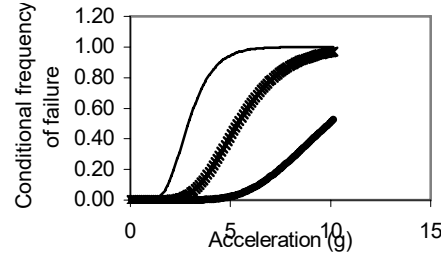
Functional failure criteria are also defined in some cases by limiting particular storey drift. Fragility curves can also be determined for such cases using the method described in the present paper. If functional failure is defined as a given floor drift, the roof deflection corresponding to this specified floor drift will represent the capacity  $\Delta_a$ . Once  $\Delta_a$  is known, the fragility curves are determined using the same procedure. Fragility curves of the example problem are determined for four cases of story drifts as given in Table-4. These fragility curves are given in Figure 9.

Table 4: Calculation of  $F_{c\Delta}$  for different performance parameters

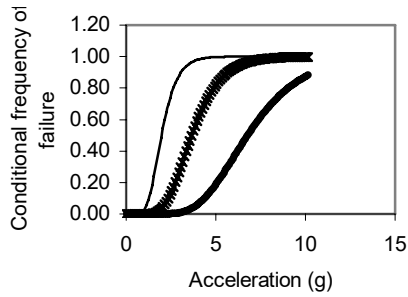
Case	(% drift of second floor)	Roof deflection, $\Delta_a^*$ (m)	$F_{c\Delta}$	$\overline{A}_m \overline{F}_{c\Delta}$ (g)
1	1	0.164	17.32	3.64
2	0.75	0.125	13.06	2.61
3	0.5	0.085	9.00	1.80
4	0.25	0.037	3.87	0.77



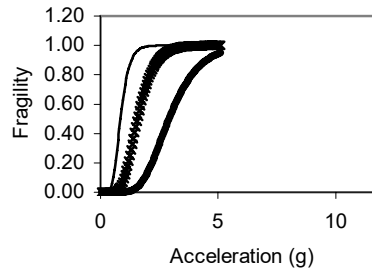
(a) Case – 1 (drift = 1%)  
HCLPF = 2.175g



(b) Case – 2 (drift = 0.75%)  
HCLPF = 1.65g



(c) Case – 3 (drift = 0.5%)  
HCLPF = 1.125 g



(d) Case – 4 (drift = 0.25%)  
HCLPF = 0.485 g

Figure 9: Fragility curve of the frame corresponding to limits on floor drift

## 5.0 CONCLUDING REMARKS

Deflection based method has been in use for the safety assessment of reinforced concrete structures of buildings in non-nuclear field for some time. This method is believed to be an efficient tool for examining safety significance of structures subjected to near field earthquakes in addition to that for far-field earthquake.

A formulation, using deflection based method, is outlined in the present paper to calculate the fragility curves of reinforced concrete structures when failure criteria is described in terms of deflection parameters of structure. The newly formulated deflection based method for fragility analysis is applied to determine the fragility curves of the example problem conveniently with the failure criteria is expressed as follows,

- Roof deflection at collapse of structure
- Limit on roof deflection expressed as a fraction of height of the building
- Storey drift

Further work is necessary to assign suitable value of different fragility parameters, i.e.  $\bar{F}_{(.)}$ ,  $\beta_{(.)U}$  and  $\beta_{(.)R}$ .

## REFERENCES

- Applied Technology Council. *Seismic Evaluation and Retrofit of concrete buildings*. ATC-40 (1996), Vol. 1, California Seismic Safety Commission, California.
- Atomic Energy Regulatory Board. *Design of Concrete Structures Important to Safety of Nuclear Facilities*. SS/CSE-1 (2001), AERB, Mumbai.
- Federal Emergency Management Agency. *NEHRP Guidelines for the Seismic Rehabilitation of Buildings*. FEMA-273 (1997), Washington, DC.
- Kennedy R.P., Cornell C.A., Campbell R.D., Kaplan S., Perla H.F., 1980. *Probabilistic seismic safety study of an existing nuclear power plant*. Nuclear Engineering and Design, 59, 315-338.
- Kennedy R. P., Ravindra M.K.. *Seismic fragilities for nuclear power plant risk studies*. Nuclear Engineering and Design, 79, 47-68.
- Moses, F., Kinser, D.E.. *Optimum structural design with failure constraints*. AIAA Journal, 6 (1967), 1152-1158
- U.S. Nuclear Regulatory Commission. *Assessment of the Relevance of Displacement Based Design Methods/Criteria to Nuclear Plant Structures*. NUREG-6719 (2001), USNRC, Washington DC.

## APPENDIX

### CALCULATION OF TARGET DISPLACEMENT AS PER FEMA 273

FEMA 273 outlines a procedure for calculation of the expected maximum displacement (usually, roof displacement) during an earthquake. For this purpose, the spectral displacement corresponding to the effective period of the structure is multiplied by a series of coefficients, which accounts for non-linear behavior of the structure. The procedure could be briefly described as follows:

1. Calculate the fundamental period ( $T_i$ ) of the structure
2. From the non-linear force displacement curve (Base shear vs. roof displacement), derive a bilinear form of force displacement curve. The intersection of the two linear segments is termed as the yield strength of the structure ( $V_y$ ) of the structure. The bilinear segments should also satisfy the criterion that the first segment of the bilinear approximation should intersect the non-linear curve at a base shear of  $0.6V_y$ . The initial slope of the bilinear curve is termed as effective lateral stiffness,  $K_e$  (Figure A1). The effective period of the structure is

$$T_e = T_i \sqrt{\frac{K_i}{K_e}}$$

$K_i$  : Elastic lateral stiffness of the building.

3. The target displacement ( $\delta_t$ ) is given by

$$\delta_t = C_0 C_1 C_2 C_3 S_a \left( \frac{T_e}{2\pi} \right)^2 g$$

Where

$S_a$  is the spectral acceleration at period,  $T_e$ , and the damping ratio of the building under consideration

$C_0$  is the modification factor to relate the spectral displacement and likely building roof displacement.

$C_1$  is the modification factor to relate expected maximum inelastic displacements to displacements calculated for linear response.

$C_2$  is the modification factor to represent the effect of hysteresis shape on the maximum displacement response.

$C_3$  is the modification factor to represent the increased displacements due to dynamic P- $\Delta$  effects.

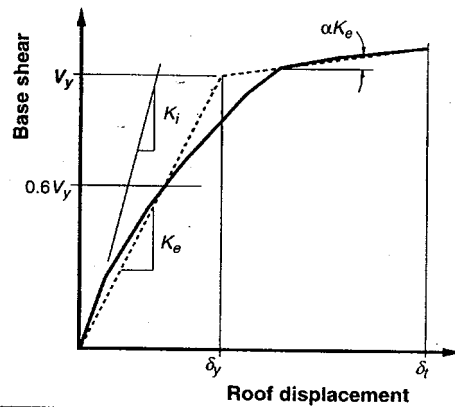


Figure A1: Calculation of effective stiffness (From FEMA 273)

# **EVALUATION OF EARTHQUAKE CAUSED DAMAGES USING NON-LINEAR DYNAMIC ANALYSIS**

T.G. SUNTHARAVADIVEL<sup>1</sup>, YOZO FUJINO<sup>1</sup> AND PING ZHU<sup>2</sup>

<sup>1</sup>The University of Tokyo, Tokyo, Japan.

<sup>2</sup>Research Institute of Science and Technology for Society, Tokyo, Japan

[zhu@ristex.jst.go.jp](mailto:zhu@ristex.jst.go.jp)

## **ABSTRACT**

*The inter-dependent socio-economic development of the world has led to dramatic increase of losses due to natural and anthropogenic catastrophes such as earthquakes, floods, and nuclear accidents. The ever increasing loss and casualty of earthquakes in the past several decades have warranted commitments and cooperative endeavors by the insurance sector, as well as the emergency management agencies at a national and international level, toward reducing the loss and casualty caused by earthquake disasters.*

*This paper focuses on the analysis of damage of wooden house using numerical simulation. In Japan, the wooden house represents one of the society's largest investments in the built environment and common wood frame house is usually an individual's largest assets. But the wooden houses have higher risk during an earthquake. During the Great Kanto earthquake (1923) and Kobe Great Hanshin Earthquake (1995) many human casualties are associated with the wooden residential houses. So that the wooden houses damage have a significant role in risk assessment in Japan cities and need to estimate the damage of wooden houses with more concern. However unlikely other type of structures, the wooden house seismic behavior is highly affected by many uncertainties such as joint type, material properties of timber. In this study an advanced technique has been used to simulate the wooden houses and study the effect of the joint properties and building type on the damage of a wooden house. The influence of joint strength on the damage of wooden houses has discussed.*

## **1.0 INTRODUCTION**

Earthquake cause a large impacts on human properties and life as well. However its occurrence time and place or magnitude could not predict exactly with existing technology. This critical situation makes a higher demand in pre-earthquake damage and loss assessment to reduce the damages of human life and properties. It has been estimated that within the next 50 years, more than a third of the world's population will live in seismically and volcanically active zones (Serguei et al. 2002). Therefore a proper risk management policy is important to serve the building damage and human vulnerability. To achieve this aim, an effective methodology is needed to estimate the building damage caused by an earthquake. The

seismic hazard assessment (estimate the building and human vulnerability) methodology consists of several steps, some of which are interactive. In general these events are treated separately and combining together in a probability manner to get total damage and loss due to an earthquake scenario.

Unlike other type of structures, wooden houses behavior is highly complex and varies with their material properties and dynamic characteristics as well as the scenario earthquake. Therefore the statistical data or probabilistic based estimation will not satisfy the decision makers' demand. Thus, a numerical based damage estimation system is important for buildings, especially for wooden houses.

## **2.0 MODELING OF WOODEN HOUSES**

### **2.1 Background**

Wood structures consist of interacting components (or subassemblies) such as walls, floors, roof, and a foundation that are fastened together by nails, bolts, steel straps, and/or cleats forming a three – dimensional, highly indeterminate system. A common observation from the cyclic test data of typical lateral – load – resisting systems is that the hysteresis trace of wood subsystem or subassembly is governed by the hysteretic characteristics of its primary connections. Thus, we only need to characterize the hysteretic behavior of wood joints to characterize the behavior of wood structural systems (Greg C. Foliente, 1995).

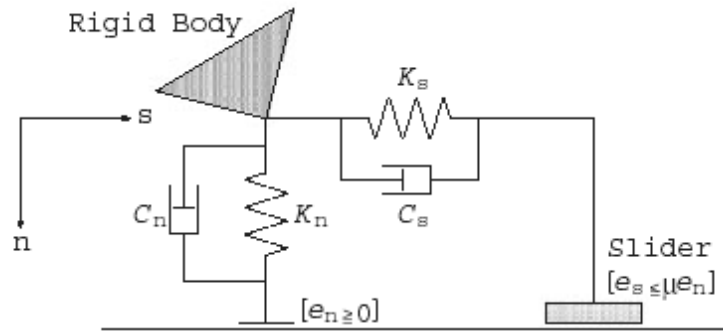
In Japan several models have been used in dynamic analysis of Japanese wood houses. Sakamoto and Ohashi (1998) proposed two hysteresis models for conventional Japanese wooden houses. Kamiya (1988) proposed another model that was developed from pseudo–dynamic tests of wood – sheathed shear walls. A third model was proposed by Miyazawa (1990) for Japanese wood – framed construction.

### **2.2 Numerical tool – DEM**

Although these models satisfied some of the specific features of the joints or systems that they meant to model, they may be inappropriate for joints and systems with different configurations and material components. Furthermore, all the available models for wooden systems use either a complex set of force – history rules or very limited empirical relations. Because there are hundred of combinations of materials and joint configurations in wood systems a general constitutive model, that both simulates the general hysteretic features of wooden systems and is mathematically tractable in dynamic analysis is preferred.

Junji Kiyono and Aiko Furukawa (2004) developed three – dimensional analytical model using distinct element model (DEM). The main advantage of this DEM is that, it can analyze until the collapse of the

house (DEM is a numerical analysis method that compute the position of each individual elements by solving equations of motion step by step) and able to simulate collapse of each element individually as well. In usual DEM, connectivity between elements is not considered, the elements acting independently as a discontinuum. Joints, however, connect the columns and beams of a real structure, and the structure acts as a continuum. The contact model (*Figure 1*) allows a structure to behave as a continuum until its joints being broken.



*Figure 1: Contact Models of Elements (2D)*

The joint model consists of spring and dashpot to represent the respective hysteretic loop of the wooden houses. However, in this analysis it is assumed that damping coefficient of the joint model as zero in all directions and springs behave as bilinear elastic - plastic elements.

### 3.0 NUMERICAL ANALYSIS OF WOODEN HOUSES

In this study, wooden houses were modeled using DEM. Because of the number of combination in the materials as well as joint configurations, the damage may differ significantly even with same structural configurations. The major sources for the variation in the damage of wooden houses were identified as:

- Earthquake Input – for same spectral displacement depends on the input earthquake motion may change the response of the buildings.
- Type of building – different type (frequency) of structure has different response for same earthquake.
- The joint property of the wooden houses – Type and configuration of joints [for analytical purpose Dowrick (1986) classified joint types into yielding plates, yielding nails and yielding bolts]

#### 3.1 Input parameters

A number of two story wooden buildings were analyzed for 1995 Kobe earthquake ground motion with different joint strengths. In reality wooden house joint strengths have a large range from 4000 – 12000 N/m<sup>2</sup> (Sarwar, 2003) depends on the material properties, age and joint configuration. According to the IISSE report about wooden houses, the

natural frequencies have changes from 2.2 – 4.0 Hz. Based on these studies following range of joint strengths and frequencies has used for this study.

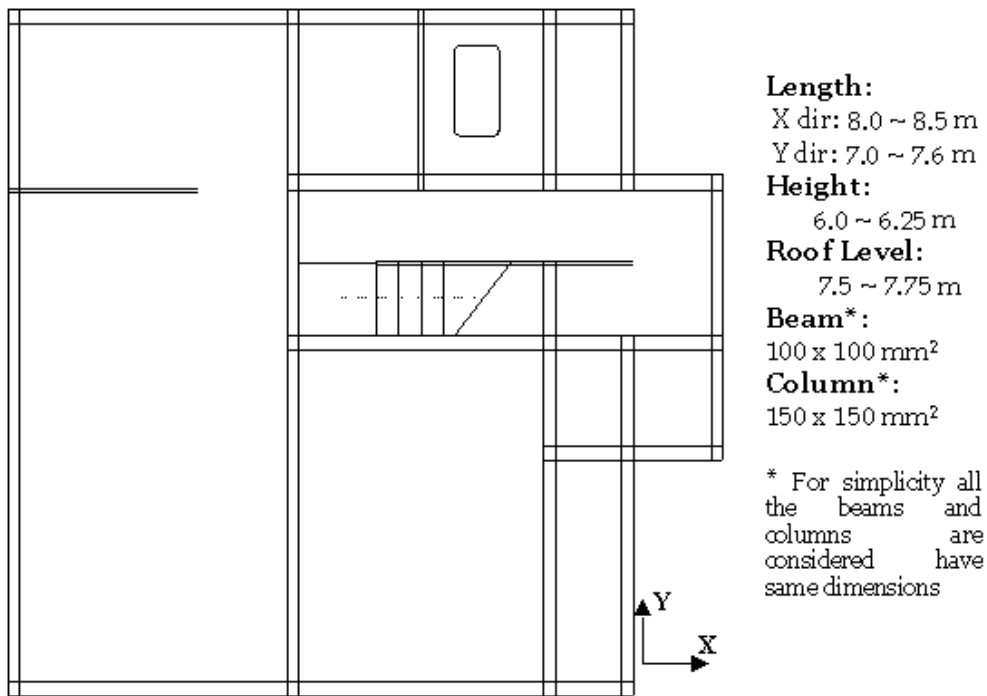


Figure 2: Typical plan of wooden house used in this study

Table 1: Model properties for the analysis

Model Property	Range
Joint Strength (N/m <sup>2</sup> )	4500 – 25000
Natural Frequency (Hz)	2.5 – 4.0

### 3.2 Simulation results

The story drift angle (story drift divided by the height of the story) was obtained from the numerical simulation as a measure of damage. The mean and variation is plotted in Figure 3.



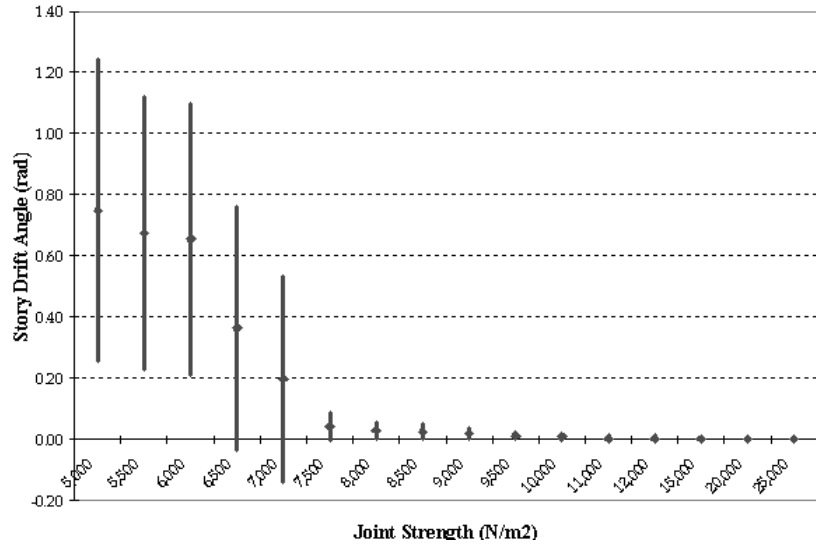


Figure 3: Story drift angles for different joint strengths

#### 4.0 DAMAGE ANALYSIS OF WOODEN HOUSES

The simulation results show a large variation of story drift angle measurement in low joint strength range. Most of the residential houses in Kobe were on this range and served a severe damage.

##### 4.1 Damage classification

Because of the higher variation of the story drift angle (damage) in wooden houses, the mean value of damage may leads a large difference in decision-making towards improve the building performance. However to use the numerical simulation result for damage estimation we need a relationship between story drift angle and damage of wooden houses. Based on the post earthquake assessment guidance used in Japan, we proposed a simple relation as in Figure 4. The story drift 1/5 is considered as limit of safety of the building.

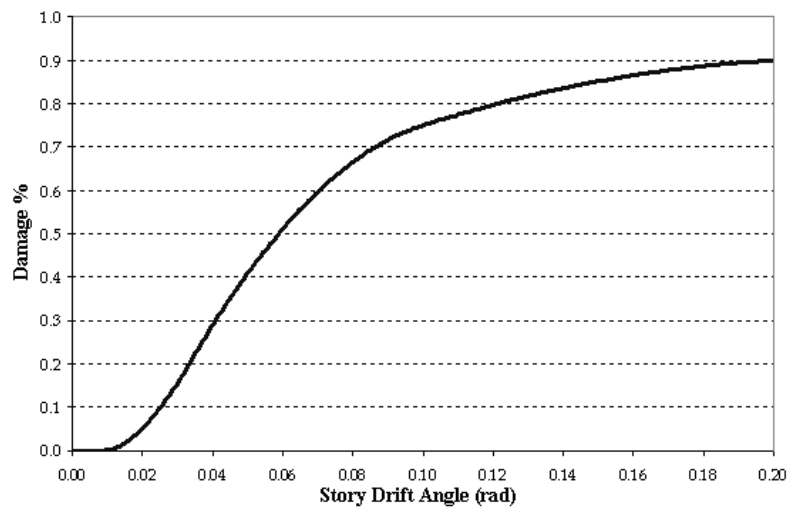


Figure 4: Defined relationship between story drift angle and damage of wooden house

## 4.2 Damage distributions

The wooden house damages were estimated for different wooden house groups. According to Sarwar (2003), Joint strengths of Kobe wooden houses having a mean of 6000 N/m<sup>2</sup> and standard deviation (STDIV) 1050 N/m<sup>2</sup>. Based on this other joint strength distributions were assumed to study the effect of joint strength on the damage of wooden houses.

*Table 1: Distribution of wooden house damage with different joint strength distributions*

Joint Strength (N/m <sup>2</sup> )		Damage (%)	
Mean	STDIV	Mean	STDIV
6000	1050	58.0	43.3
7000	1300	45.9	32.5
8000	1450	28.7	28.5
9000	1600	22.1	21.0

According to the analytical results, when the joint strength increased by 50%, the damage of wooden houses could be reducing by nearly 60%. This is an important advantage in numerical damage estimation; it is easy to predict the future retrofitting scheme for a wooden house or a group of wooden houses.

## 5.0 CONCLUSIONS

In this paper, the earthquake caused damage and loss of wooden houses was analyzed using non-linear dynamic response analysis. The variation in the conventional damage estimation methodology has discussed for different joint properties and different wooden house types. A numerical based damage estimation methodology has been developed. This study can conclude that:

- There is a large variation observed in the damage of wooden houses for different joint strengths and different natural frequency of the structures. In reality the joint strength of wooden house has a large range depending not only on the age of the structure but also in the joint type and timber properties.
- The story drift angle could be a better measure than the fragility curve for more reliable damage estimation. With the advanced computation technology the story drift angle can be estimated in a short time with good accuracy.
- The numerical computation also gives a better estimation of the human vulnerability (not discussed in this paper).

At present the existing wooden houses were not strictly follow code of practice; therefore, the material and joint properties are highly unknown. Therefore it is quite difficult to categorize into groups. Therefore numerical

analysis methodology is a better replacement for the conventional damage estimation (fragility curve) of wooden houses. It can be estimate the stability of the wooden frame construction as well as effect of retrofitting.

## ACKNOWLEDGEMENTS

The authors wish to thank Professor Muneo Hori and Dr. Masato Abe for thier guidance and patient advice during this study.

## REFERENCES

- American Institute of Timber Construction, 1966. *Timber Construction Manual*. AITC, Washington, D.C.
- Applied Technology Council, 1985. *Earthquake Damage Evaluation Data for California*. ATC, California.
- Disaster Presentation Urban Development Section, 2002. *The Fifth Report on Disaster – based Assessment of Vulnerability to Earthquake Disaster*. Bureau of City Planning, Tokyo Metropolitan Government, Japan
- Dowrick, D.J., 1986. *Hysteresis loops for Timber Structures: Bulletin of New Zealand National Society of Earthquake Engineering*. Waikanoe, New Zealand, Vol. 19(20), 143-152.
- Federal Emergency Management Agency 1999. *HAZUS®99 Technical and User Manual*. FEMA, Washington D.C.
- Greg C. Foliente, 1995. *Hysteresis Modeling of Wood Joints and Structural Systems*”, *Journal of Structural Engineering*. Vol. 121(6), 1013–1022.
- International Institute of Seismology and Earthquake Engineering. *Assesment of Building Damage due to Ground Motion*. Web publication of IISEE, [http://iisee.kenken.go.jp/net/yokoi/methodology/04bld\\_damage\\_motion.htm](http://iisee.kenken.go.jp/net/yokoi/methodology/04bld_damage_motion.htm)
- Junji Kiyono, and Aiko Furukawa, 2004. *Casualty Occurrence Mechanism in the Collapse of Timber – frame Houses during an Earthquake* Earthquake Engineering and Structural Dynamics. Vol. 33, 1233–1248.
- Naoya Yamaguchi, and Fumio Yamazaki, 2001. *Estimation of strong motion distribution in the 1995 Kobe earthquake based on building damage data*. Earthquake Engineering and Structural Dynamics. Vol. 30, 787– 801.
- Osamu Murao, Hiroyuki Tanaka, and Fumio Yamazaki, 2000. *Risk Evaluation Method of Building Collapse from the Experience of the Kobe Earthquake*. Proceedings of the 12<sup>th</sup> World Conference on Earthquake Engineering, Auckland New Zealand, January 2000.
- Sarwar Muhammad Waheed, 2003. *Parametric Identification of Joints in Wooden Houses based on Past Earthquake Damage using DEM Collapse Simulation*. Master Thesis, University of Tokyo, Japan.
- Serguei Baranov, Boris Digas, Tatiana Ermolieva, Valerii Rozenberg, 2002. *Earthquake Risk Management: A Scenario Generator*. Interim Report of the Project No IR-02-025, International Institute for Applied Systems Analysis, Austria. <http://www.iiasa.ac.at>

# SEISMIC BEHAVIOR OF URBAN HIGHWAY TUNNEL IN VICINITY OF EMBANKMENT

YUSUKE ONO, JUNJI KIYONO AND TATSUKI TAMAI  
Department of Urban Management, Kyoto University, Japan  
ono@quake2.kuciv.kyoto-u.ac.jp

## ABSTRACT

*A new construction of the highway tunnel is planned in Osaka, Japan. The features of this structure are that it is a semi-underground structure and in the vicinity of the existing embankment. The steel sheet piles will be installed on the both sides of the tunnel during the construction. The seismic responses of both the highway tunnel and the embankment may decrease due to the large stiffness of steel sheet piles. The sheet piles, however, are usually removed after the construction and their effects on the seismic responses are not cleared yet. Thus, effects of the steel sheet pile on the seismic behavior of the semi-underground highway tunnel and the embankment are discussed in this paper.*

*The three-dimensional dynamic finite element technique is used to calculate earthquake responses. Our analysis is composed of two steps. First, the earthquake ground motions are inputted below the bottom of the finite model spontaneously. Second, the input ground motions are applied along the longitudinal direction with time delay and the propagation effects of seismic waves are considered.*

*It is concluded that the steel sheet pile installed the both side of the tunnel have effects that make the residual displacement and the rocking of structure decrease. Furthermore, it is cleared that the effects of the sheet pile are strongly affected by the propagating velocity of the seismic wave.*

## 1.0 INTRODUCTION

A new highway construction is planned due to the dissolution of the heavy traffic jam in Osaka region. The part of this new highway will be a half-buried structure and combined with the existing embankment. Few construction examples of tunnel structures combined with the embankment are known and the seismic behavior of this kind of system has not been cleared yet.

Moreover, the steel sheet piles are planned to be installed along the both sides of the half-buried tunnel. The steel sheet piles are generally used as the temporally retaining wall during the construction and they are removed when the construction is finished. However, it is expected that the sheet piles improve the stability of the embankment during earthquakes.

The purpose of this study is to investigate the seismic behavior of the half-buried tunnel-embankment system with steel sheet piles, and to make

clear the propagation effect of the input ground motions. Three dimensional finite element analysis is used in this study.

## 2.0 ANALYTICAL MODEL

In this study, the viscous boundary developed by Miura et al (1989) was used. The viscous boundary we used can take into account the free field ground motion on the outside of the analytical region. Soils including the embankment were modeled as an elastic-plastic solid element except for base diluvial clay while the tunnel structure was modeled as elastic solid element. The steel sheet pile was modeled as a Mindlin shell element. The yield criterion of soil element obeys the Drucker-Prager model. The geological survey at the construction site has already been done. The soil properties we used are listed in Table 1.

*Table 1: Soil profiles*

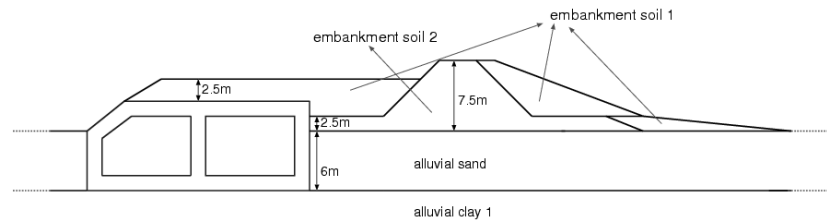
Soil	Unit Weight (tf/m <sup>3</sup> )	Poisson's ratio	Shear Wave Velocity (m/s)	Cohesion (tf/m <sup>2</sup> )	Internal Friction Angle (deg)
B-1	1.90	0.490	200.0	0.00	35.0
B-2	1.78	0.384	200.0	0.86	37.4
As	1.89	0.494	153.0	0.88	35.7
Ac-1	1.79	0.493	157.0	7.15	0.0
Ac-2	1.75	0.492	194.0	7.64	0.0
Tc	1.83	0.492	218.0	12.8	0.0

The sectional view of the tunnel-embankment system is illustrated in Figure 1. As shown in Figure 2, the steel sheet piles are installed in the both side of 1m away from the structure. The embankment consists of two soil materials. Properties of the embankment materials were also shown in Table 1. The half-buried tunnel is a reinforced concrete structure. The properties are shown in Table 2. The unit weight, Poisson ratio and Young's modulus of steel sheet pile are also shown in Table 2.

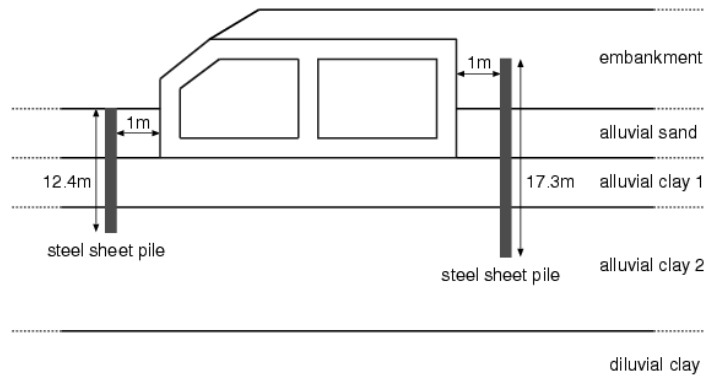
*Table 2: Structural parameters*

Structure	Unit Weight (tf/m <sup>3</sup> )	Poisson's ratio	Young's Modulus (tf/m)
RC tunnel	2.35	0.167	2.8x10 <sup>6</sup>
Steel Sheet Pile	7.85	0.300	2.1x10 <sup>7</sup>

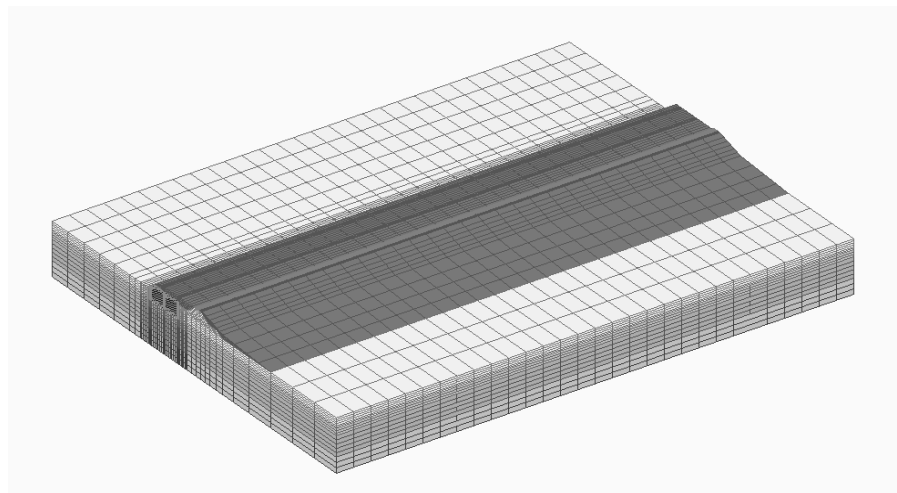
The FEM mesh used in this analysis is shown in Figure 3. The width and depth of the analytical model in the cross section are 233m and 38.5m, respectively. The length of longitudinal section is 300m.



*Figure 1: Sectional view of the half-buried tunnel and the embankment*



*Figure 2: Soil profiles and installation position of steel sheet piles*



*Figure 3: Bird view of finite element mesh*

### 3.0 INPUT GROUND MOTION

Figure 4 shows the time histories of the observed records at the Port-Island during the 1995 Kobe Earthquake. The vertical seismographs array had been built at the site. The records at G.L.-83m are used in our analysis. Three components of the ground motion are inputted simultaneously.

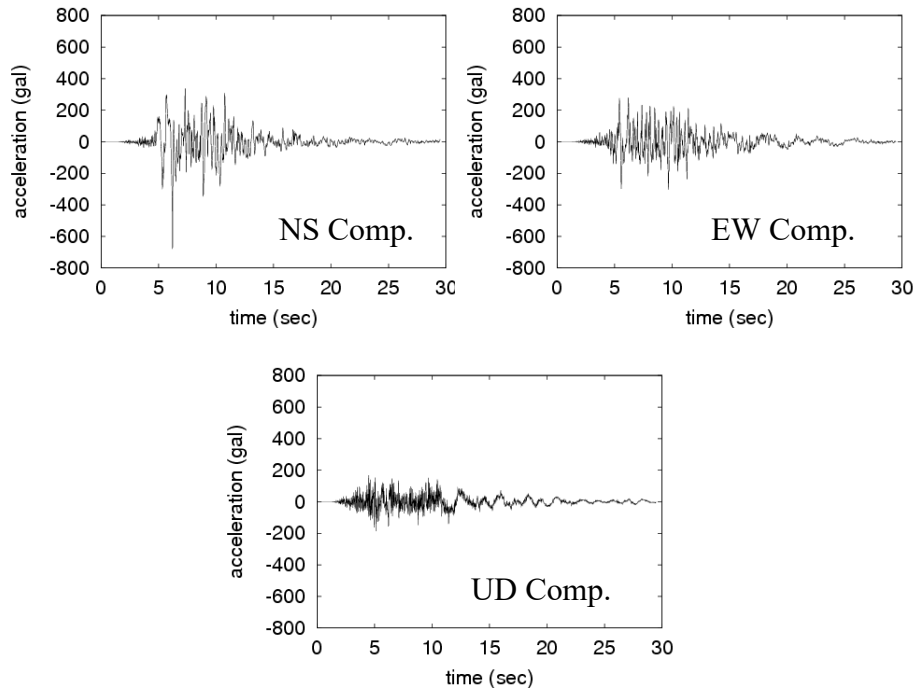


Figure 4: Observed record at G.L.-83m, Port Islands during 1995 Kobe earthquake.

## 4.0 RESULTS

### 4.1 Effects of steel sheet pile

The horizontal responses at the top of the embankment in the cross section which locates at center of the longitudinal direction are shown in Figure 4. The responses are obviously reduced by leaving steel sheet piles. The reduction rate of the maximum acceleration is 12.3%. With respect to the peak values of the velocity and the residual displacement, the reduction rates are 14.6% and 56.3% respectively.

On the other hand, the vertical direction responses of the same node are shown in Figure 5. Although the remarkable reduction is not seen about acceleration and velocity responses, the residual displacement is decreased by steel sheet piles. The reduction rate due to the steel sheet piles is 47.8%.

Table 3 shows the summary of the comparison of the peak values of the acceleration, velocity and residual displacement with and without the steel sheet piles. It is known that the horizontal responses in the cross direction and the residual vertical displacement are decreased. This phenomenon is also seen at the top of the half-buried RC tunnel.

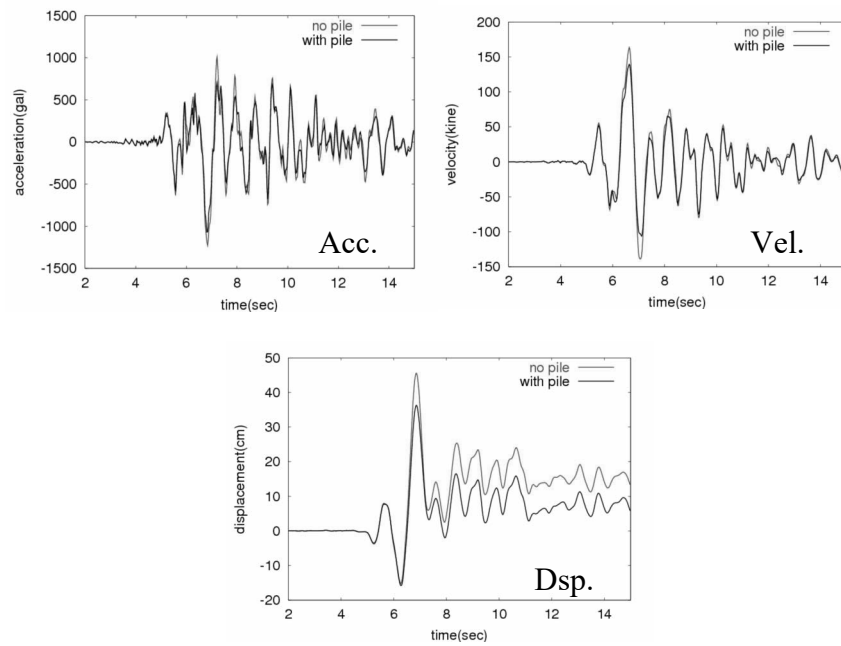


Figure 4: Horizontal responses at the top of the embankment in the cross section

Table 3: Peak values of responses at the top of the embankment

	Acc. (gal)	Vel. (kine)	Residual Dsp. (cm)
<b>Horizontal response in the cross section</b>			
<b>without steel sheet pile</b>	1228.1	163.6	13.38
<b>with steel sheet pile</b>	1069.3	139.6	5.84
<b>Horizontal response in the longitudinal section</b>			
<b>without steel sheet pile</b>	690.7	84.4	1.09
<b>with steel sheet pile</b>	680	86.4	2.82
<b>Vertical Response</b>			
<b>without steel sheet pile</b>	382.8	22	1.68
<b>with steel sheet pile</b>	400.6	31.7	0.88

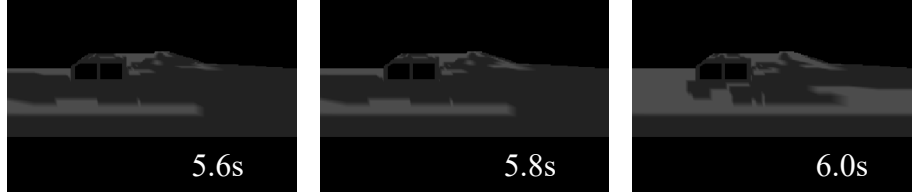
Figures 5(a) and (b) show the growth of the yielded soil area in the case without and with steel sheet pile in the cross section at the center of longitudinal direction, respectively. These results show that the steel sheet piles have effects of increasing the shear strength of soil closed between steel sheet piles. Figures 6(a) and (b) show the spatial distribution of the maximum strain in the case without and with steel sheet piles, respectively. It is found that the axial strains near the surface are decreased by the steel sheet piles. On the other hands, the axial strains in the depth deeper than sheet piles are increasing as compared with the case without steel sheet piles.

Additionally it is seen that strains in the region between the tunnel and the embankment is quite small. This phenomenon implies that the structure



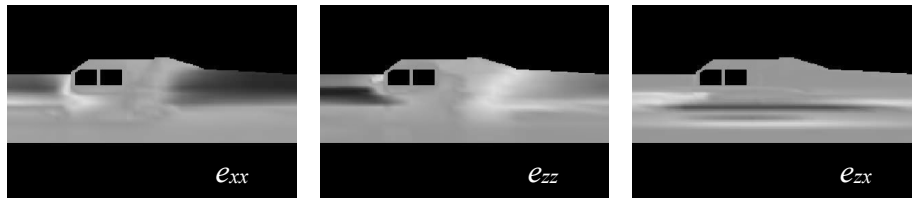


(a) Without steel sheet piles

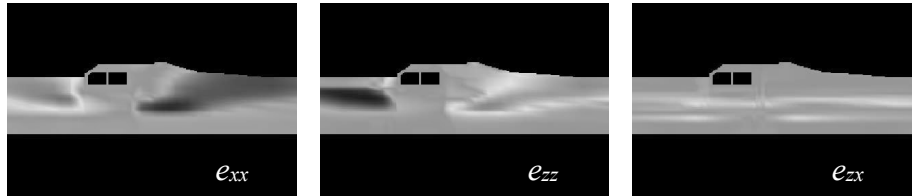


(b) With steel sheet piles

Figure 5: The growth of the yielded soil area



(a) Without steel sheet piles



(b) With steel sheet piles

Figure 6: Distribution of the maximum strain

and embankment behave as one structure. The maximum value of strain  $e_{zx}$  is reduced by 50% by the steel sheet piles and the steel sheet piles restrain the share deformation of the soil in the cross section.

Figure 7 shows the behavior of the structure from 5.9 to 6.05 sec. The nodal displacements are multiplied by 300 and the results without steel sheet piles are shown. On the other hands, Figure 10 corresponds to the case with steel sheet piles. Compared with these figures, it is found that the rocking of structure is decreased by the steel sheet piles. In vertical component, the

residual relative displacement between the both ends of the bottom is 0.47cm with steel sheet piles while it amount to 2.8cm in the case without them. This is because steel sheet piles restrain the deformation of the soil under the structure. We can conclude the steel sheet piles have desirable effects that make the rocking of the structure decrease.

#### **4.2 Propagation effects of input ground motion**

Each part of a long structure, like as a highway tunnel, is excited by a different input motion each other and it becomes a problem on a seismic performance of a structure. Thus the responses of our highway tunnel-embankment system excited by the propagating seismic wave are analyzed in this study.

Figure 8 shows the nodal responses at the top of the embankment in the case without the steel sheet piles while the propagation velocity of the input wave change from 500 to 1000 and 2000m/s. In this figure, the maximum response is getting smaller when the propagation velocity becomes small.

Figure 9 and 10 show comparison of the nodal responses at the top of the embankment between the case with and without the steel sheet piles. The propagation velocity in Figures 9 and 10 are corresponding to 500 and 2000m/s respectively. From these figures, it can be seen that the steel sheet piles have small effect on the response of the embankment as long as the propagation velocity is small.

#### **5.0 CONCLUSIONS**

The dynamic behavior of the embankment neighboring on semi-underground structure excited by the seismic motion is discussed. The conclusions obtained through this study are summarized as follows:

- By installing the steel sheet piles along the tunnel structure, the maximum values of horizontal acceleration and velocity on the cross section are decreased 10% at least.
- The steel sheet piles have effects that make the residual displacement and the rocking of the structure decrease.
- Taking into account the propagation of seismic waves, the maximum response both of the structure and the embankment become small.
- The effects of the steel sheet piles become small when the propagation velocity is getting small.



(a) Without steel sheet piles



(b) With steel sheet piles

Figure 7: Rocking motion of the RC tunnel

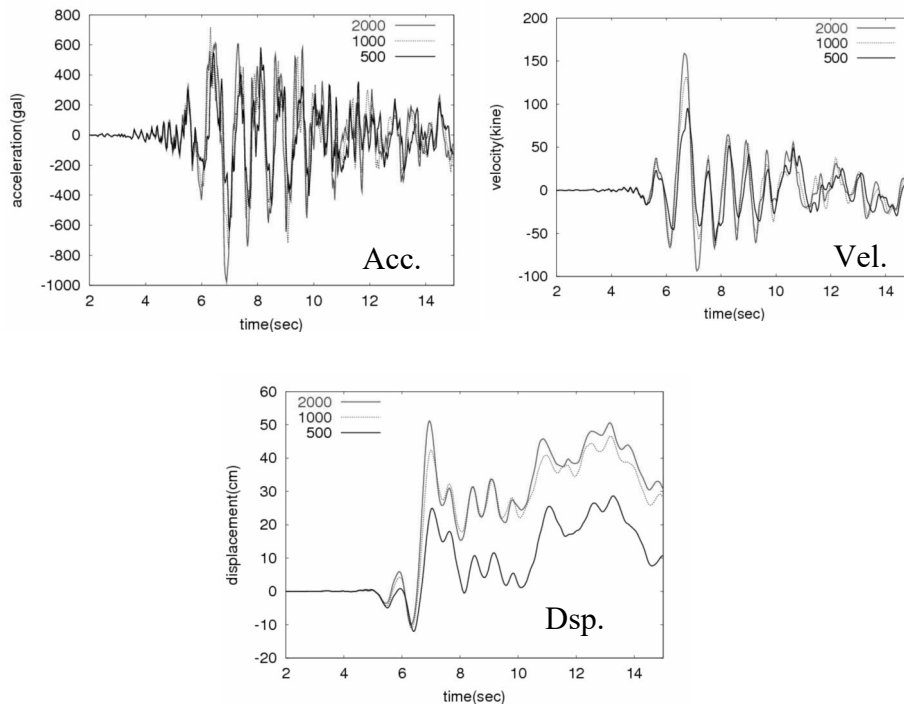


Figure 8: Variation of the response at the top of the embankment due to the propagation velocity of the input motion

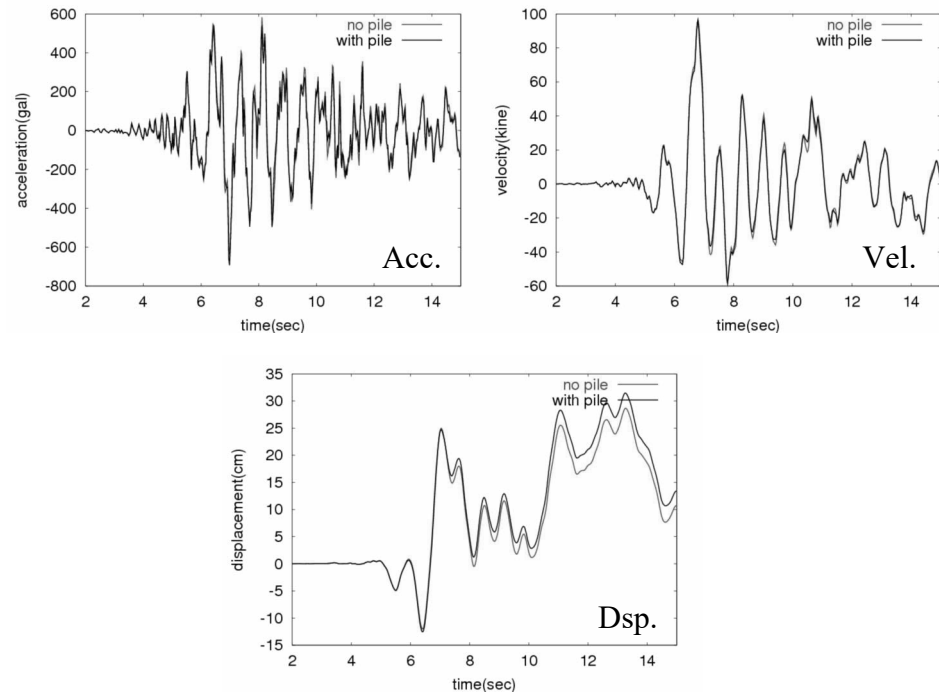


Figure 9: Effect of the steel sheet piles ( $V=500\text{m/s}$ )

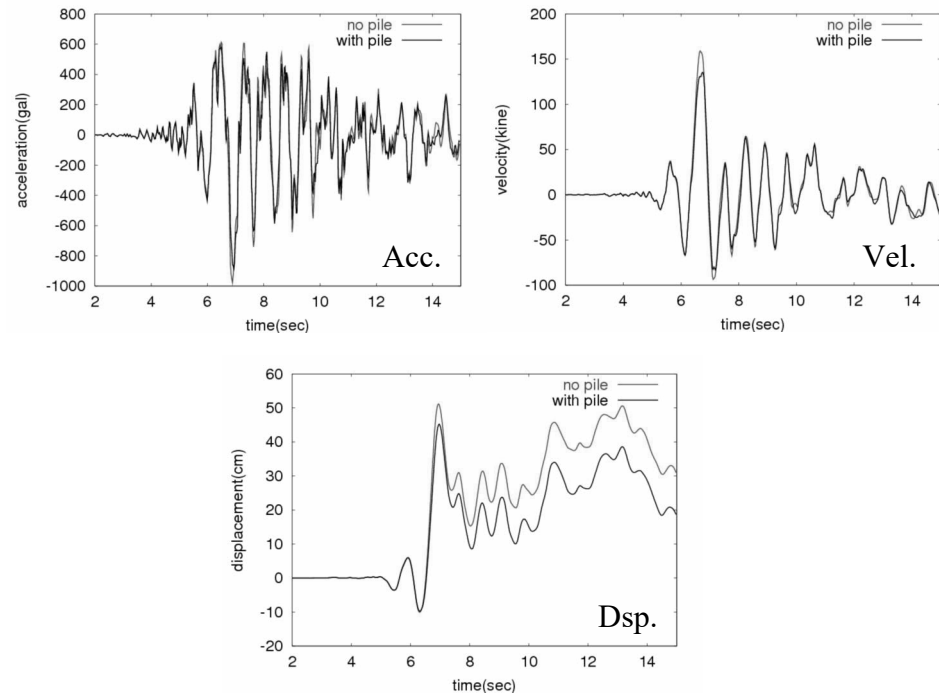


Figure 10: Effect of the steel sheet piles ( $V=2000\text{m/s}$ )

## REFERENCES

Miura, F and Okinaka, H, 1989. *Dynamic Analysis Method for 3-D Soil-Structure Interaction System with the Viscous Boundary based on the Principle of Virtual Work*. Journal of Structural Engineering, JSCE, No404, pp.395-404.

# **SEISMIC BEHAVIOR OF REINFORCED CONCRETE PIERS DETERIORATED BY CORROSION OF REINFORCEMENT**

KOJI TAKEWAKA<sup>1</sup> AND GOVINDA RAJ PANDEY<sup>2</sup>

<sup>1</sup>Kagoshima University, Japan

<sup>2</sup>Saitama University, Japan

*takewaka@oce.kagoshima-u.ac.jp*

## **ABSTRACT**

*The corrosion of reinforcement is the main cause of serious and rapid degradation of the performance of reinforced concrete structures. Apart from the problems on serviceability such as cracking and rust staining, corrosion on reinforcement causes significant deterioration in the static and dynamic behavior of the reinforced concrete structures leading to the reduction of their mechanical capacities.*

*The main objective of this research is to evaluate the seismic behaviors such as, stiffness, ductility and energy absorption of the piers deteriorated by corrosion of reinforcement. It is aimed to obtain the nature of degradation of these properties with increase in the weight loss of reinforcing steel due to corrosion. Moreover, the combined effect of the axial load and the corrosion is also to be evaluated.*

*In the examination, an experimental study is carried out on sixteen reinforced concrete piers with exactly same size and identical loading cycles while axial load, design method and corrosion condition were being varied. And, the following results can be obtained:*

- The seismic behaviors of reinforced concrete structures are seriously affected by corrosion of reinforcement, and the reduction rate of strength, ductility and total energy absorption with corrosion loss of reinforcement can be quantitatively evaluated by experimental equations.*
- Rate of degradation of ductility and energy absorption with corrosion loss is found to be much larger than that of strength. Therefore, even when only a slight reduction of strength of structure due to corrosion of reinforcement has been observed from static loading test, it should be considered that the corrosion is responsible for much larger reduction of ductility and energy absorption.*

## **1.0 INTRODUCTION**

The corrosion of reinforcement is the main cause of serious and rapid degradation of the performance of reinforced concrete structures. Apart from the problems on serviceability such as cracking and rust staining,

corrosion in reinforcement causes significant deterioration in the static and dynamic behavior of the reinforced concrete structures leading to the reduction of their mechanical capacities.

Experiences from recent earthquakes, like the Great Hansin Awaji Earthquake, clearly show that piers in bridges are relatively vulnerable to earthquake because it is suffered with very large inertial force. On the other hand, some of the piers in chloride-attacked environment, such as marine environment, have already deteriorated due to corrosion of the reinforcement. Particularly in the regions of high seismic risk, the behavior of these deteriorated piers against earthquake becomes the matter of prime concern. In addition, now the trend of repairing, renovating and rehabilitation is increasing rather than just demolishing and reconstruction. Under such condition, it becomes necessary to evaluate the dynamic behavior of the deteriorated bridge piers.

The main objective of this research is to evaluate the dynamic properties such as, stiffness, ductility and energy absorption of the piers deteriorated by corrosion of reinforcement. It is aimed to obtain the nature of degradation of these properties with increase in the loss of steel weight due to corrosion of reinforcement. Moreover, the combined effect of the axial load and the corrosion is also to be evaluated.

The purpose is also to study the behavior of the corroded piers against the seismic loading, which were designed with two different ways. The first one was designed by using the design method for ordinary structures in JSCE code. The second one was designed with the seismic design part of JSCE along with the verification of ductility.

## 2.0 OUTLINE OF EXPERIMENT

### 2.1 Test specimen

The overall size of the specimen is shown in Figure 1. The height of pier part was 1.2 meter, whereas the point of application of load was 1 meter above the base. The specimen was designed for the axial load and the moment corresponding to the lateral load at the point of application of load. In the design, lateral seismic load was assumed as 20 % of the axial load. Using the strength interaction diagram, specimens less than 200 kN of axial load were designed with two design philosophies, which were design methods specified by Japan Society of Civil Engineer (JSCE) code for ordinary reinforced concrete structures and by the seismic design part of JSCE code in conjunction with the Japan

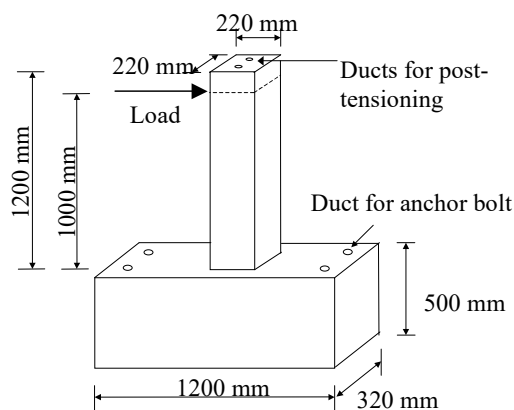


Figure 1: Size of specimen

Road Association (JRA)'s specification for the verification of ductility against the seismic load. Figure 2 shows the detail of the specimen designed by both philosophies.

Mix proportion and the average strength of the concrete used were shown in Table 1.

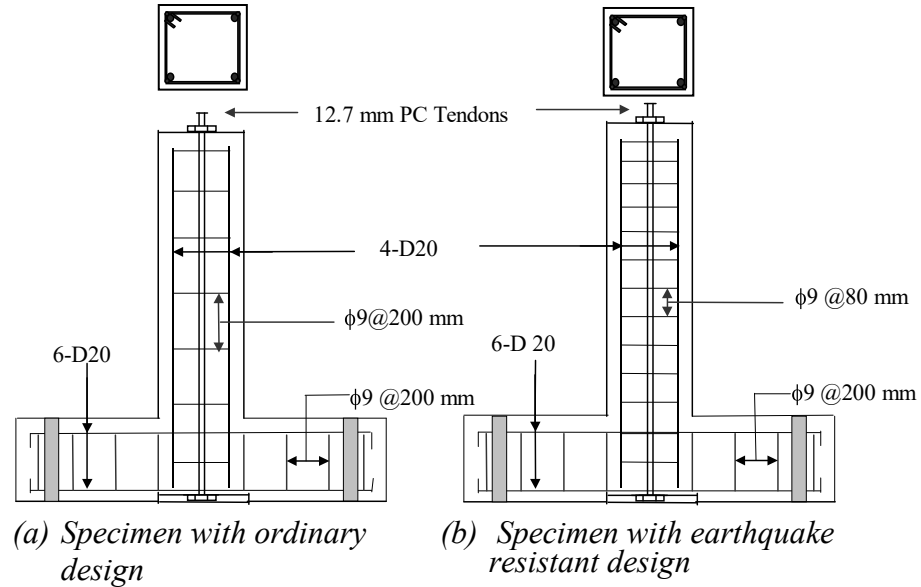


Figure 2: Detailing of the specimens  
Size of specimen

Table 1: Mix proportion of concrete

W/C (%)	Unit weights (kg/m <sup>3</sup> )				Compressive Strength (Mpa)
	W	C	S	G	
.55	192	349	828	935	35

## 2.2 Experimental parameters and number of specimens

The main parameter that was considered in the experiment was degree of corrosion of the reinforcement. The experiments were carried out for four different degrees of corrosion including non-corrosion condition.

Another important parameter that was varied in the experiment was the condition of axial load. Two sets of experiments were performed with and without axial force. The third important parameter was the design principle mentioned in 2.1. With all these combinations, the total specimen number was sixteen. The designation and its corresponding conditions are as shown in Table 2.

## 2.3 Accelerated corrosion test of reinforcing bars

To simulate the deterioration of concrete structure due to rebar corrosion in the laboratory in a short time, accelerated galvanic corrosion



technique has to be used. Specimens were cured for fourteen days before accelerated corrosion test was performed. To have galvanic accelerated corrosion, specimen was immersed into a tank with 3.5% sodium chloride solution that

Table 2: Test specimens

No.	Designation	Axial load	Expected corrosion(*)	No.	Designation	Axial load	Expected corrosion(*)
Ordinary design				Seismic design			
1	POA-1	200 kN	0.00	9	PEA-1	200 kN	0.00
2	POA-2		0.19	10	PEA-2		0.19
3	POA-3		0.38	11	PEA-3		0.38
4	POA-5		0.56	12	PEA-5		0.56
5	PON-1	0	0.00	13	PEN-1	0	0.00
6	PON-2		0.19	14	PEN-2		0.19
7	POA-3		0.38	15	PEN-3		0.38
8	PON-5		0.56	16	PEN-5		0.56

acts as an electrolyte. In this method, rebars of the specimen that had to be corroded was made anode and titanium mesh was used as cathode. The schematic circuit diagram for the experiment is shown in Figure 2.

The weight loss in the rebars by this technique can be obtained by using Faraday's law. The relation is as follows;

$$\Delta w = \frac{AIt}{ZF\alpha} \quad (1)$$

where,  $\Delta w$  : metal weight loss due to corrosion,  $A$  : atomic weight of iron (56 g),  $I$  : corrosion current in ampere,  $t$  : time elapsed in sec.,  $a$  : reinforcing bar surface area before corrosion,  $Z$  : valence of the reacting electrode (iron) which is 2,  $F$  : Faraday's constant (96,500 amp sec),  $\alpha$  : constant depending on the concrete quality and cover thickness

The value of  $\alpha$  depends on the quality of concrete and the cover thickness. This factor had to be determined by the preliminary tests. Poudel (2001) had carried out experiments in the similar conditions for the case of beam and found the value of  $\alpha$  to be 1. Therefore, the result obtained from that experiment was used as preliminary test results.

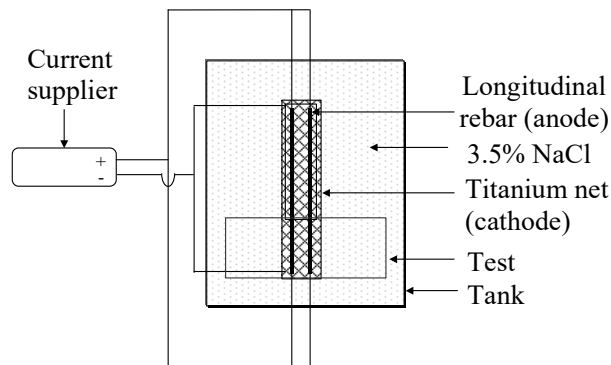


Figure 2: Circuit diagram for accelerated corrosion test

## 2.4 Experimental setup

The experiment was carried out with the experimental setup as shown in Figure 3. Figure 4 shows the lateral loading cycle on the specimens in terms of displacement. Design yield lateral loads were 33.1kN and 36.3kN for the specimens with and without the axial load, respectively. Therefore, in the first three cycles until 30kN of the lateral load, the loading was controlled by load and then it was changed to be in displacement control condition; that was, the fourth cycle was started with the maximum displacement was 16 mm and then followed by the cycles in which the maximum displacement was increased by 8 mm each. Consequently, the order of the cycles was  $\pm 15$  kN,  $\pm 21$  kN,  $\pm 30$  kN,  $\pm 16$  mm,  $\pm 24$  mm,  $\pm 32$  mm,  $\pm 40$  mm and so on, until the specimen was collapsed.

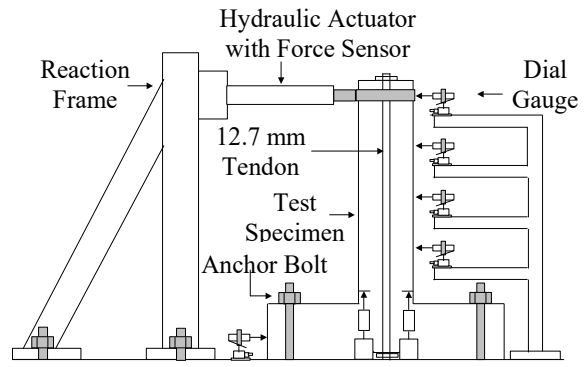


Figure3: Experimental setup

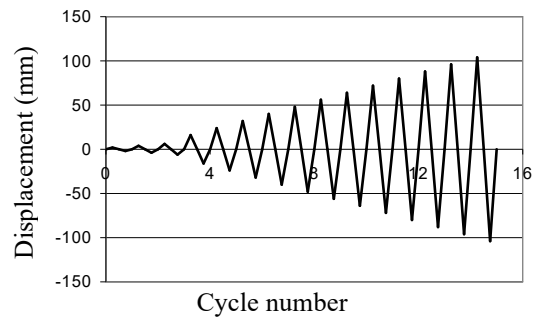


Figure 4: Lateral load history

## 3.0 RESULTS

### 3.1 Deterioration condition of specimens

Typical deterioration conditions on the specimens after accelerated corrosion test are shown in Figure 5 and Table 3. Corrosion loss in rebars that were taken out from the specimens was measured after the lateral loading test. Though the average corrosion loss was smaller than the expected ones calculated by using equation (1), all of the specimens suffering corrosion of rebars had the corrosion cracks on the concrete surface along with the main rebar's direction.

Figure 6 shows the relationship between corrosion loss in rebar and average corrosion crack width. In the lower degree of corrosion, the entire specimen showed very close value in crack width with the same corrosion loss, while in higher corrosion condition some difference arose. However, nearly the linear behavior was also observed in the relation between average crack width and corrosion loss.

### 3.2 Load-displacement curve

The typical load displacement curves of the specimens under the loading test are shown in Figure 7. The shape of the curve for specimens, in which the average corrosion loss in rebars was less than 0.20 and the

average corrosion cracks width was smaller than 0.5mm, was almost the same and had relatively the large area enclosed by the hysteretic loop in the all series

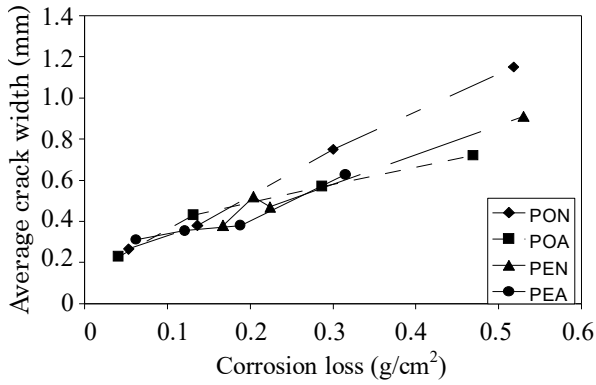


Figure 6: Relationship between corrosion loss in rebar and average crack width on concrete surface

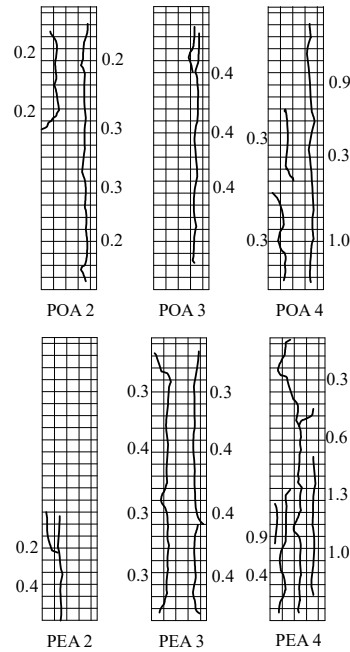
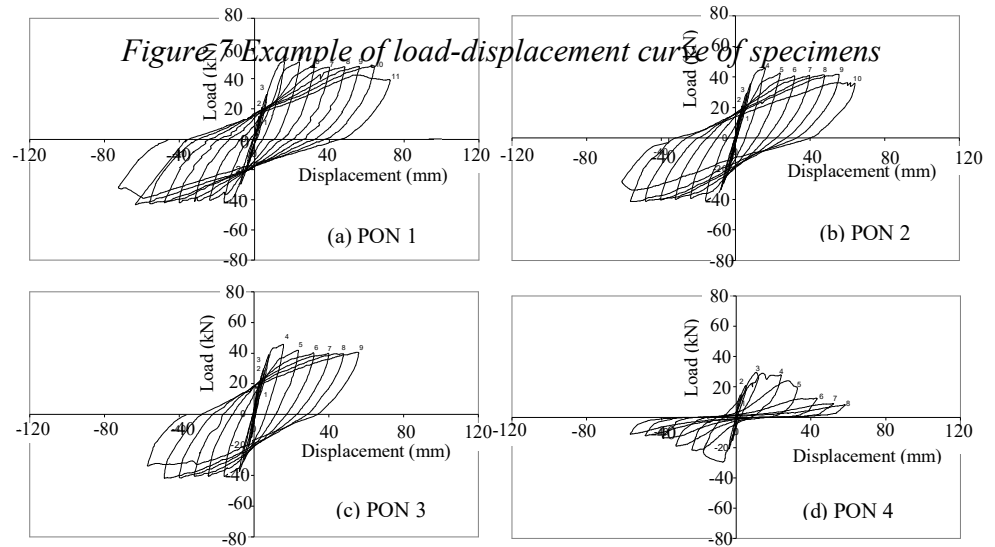


Figure 5: Typical corrosion crack pattern with its width

Table 3: Degree of deterioration and loading capacity of specimen

No.	Designation	Corrosion loss (gm/cm <sup>2</sup> )		Duration of test (days)	Crack width (mm)		Failure load (kN)	
		Expected	Actual		Max.	Avg.	Calculated	Actual
1	POA-1	--	--	--	--	--	55.21	58.66
2	POA-2	0.19	0.04	6.6	0.3	0.23		54.25
3	POA-3	0.38	0.13	13.2	0.5	0.43		54.59
4	POA-4	0.56	0.47	19.7	1.3	0.72		46.71
5	PON-1	--	--	--	--	--	42.07	47.70
6	PON-2	0.19	0.05	6.6	0.4	0.26		44.30
7	PON-3	0.38	0.14	13.2	0.5	0.38		44.20
8	PON-4	0.56	0.52	19.7	2.0	1.15		30.00
9	PEA-1	--	--	--	--	--	55.21	61.31
10	PEA-2	0.19	0.17	6.6	0.6	0.38		60.18
11	PEA-3	0.38	0.22	13.2	0.9	0.47		54.05
12	PEA-4	0.56	0.53	19.7	1.3	0.91		51.84
13	PEA-1	--	--	--	--	--	42.07	48.95
14	PEN-2	0.19	0.06	6.6	0.50	0.31		48.87
15	PEN-3	0.38	0.12	13.2	0.50	0.35		48.87
16	PEN-4	0.56	0.31	19.7	1.60	0.63		33.01

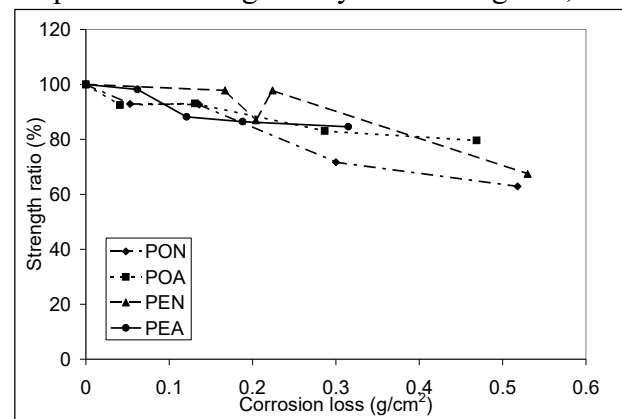


of PON, POA, PEN and PEA. In consideration of both the curve shapes and crack development condition during loading, the specimens with axial load (POA and PEA types) were seemed to be in the typical bending failure nature, while the specimens without the axial load (PON and PEN types) might be in a combination of bending and shear failure nature.

On the other hand, in the specimens having most severe corrosion loss of rebars and the corrosion cracks with about 0.5mm or more of their average width, the curve shows a typical bond failure condition with very narrow loop area.

### 3.3 Strength

Strength of each specimen, which is explained as the maximum load bearing capacity acting on the specimen during the cyclic loading test, is also shown in Table 3. Figure 8 shows the strength ratio of the corroded specimen to the non-corroded one with corrosion loss of rebars. With the small increase in degree of corrosion within  $0.05 \text{ g/cm}^2$  the strength had shown only 10 % or less in reduction. Then it remained stable with only 5% more of strength reduction with some more corrosion loss around  $0.15 \text{ g/cm}^2$ . With further increase in corrosion loss, the strength started to reduce rapidly.



*Figure 8: Trend of reduction in load bearing capacity of specimen with corrosion loss*

From the figure, it seems that the strength mainly depends on the deterioration condition such as the corrosion loss and occurrence of the longitudinal corrosion crack, regardless of design method and axial load condition. Therefore all the data can be fitted by an approximate curve as shown in Equation (2). With the known flexural strength of non-corroded pier, the strength of the corroded pier may be predicted for the various corrosion condition by this equation.

$$P_c = (1 - 0.1703 \Delta w^2 - 0.5244 \Delta w) P_u \quad (2)$$

where,  $P_c$  : strength of corroded specimen,  $P_u$ : strength of non-corroded specimen,  $\Delta w$ : corrosion loss ( $\text{g}/\text{cm}^2$ )

### 3.4 Ductility

Ductility of a structure is defined as the ratio of ultimate displacement to the yield displacement. In this study, the ultimate displacement was determined from the load displacement curve at the point of collapse where the load bearing capacity has been reduced by 20 percent from the strength of the specimen.

Figure 9 shows the degradation of the ductility with increase in corrosion loss. It can be clearly observed that the ductility in the specimens without corrosion was larger in the case of specimens designed for seismic resistance, though there was not any

significant change in ductility due to axial load condition. The ductility is also found to be very susceptible to the corrosion of reinforcement. Especially, when the corrosion loss was more than  $0.15 \text{ gm}/\text{cm}^2$ , ductility was reduced significantly and became less than 2 with corrosion loss more than  $0.4 \text{ gm}/\text{cm}^2$ , which was around one third to one fourth of the ductility on the specimen without corrosion.

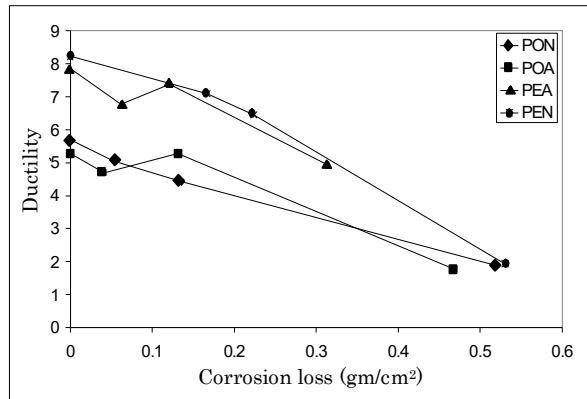


Figure 9: Relationship between ductility of specimen and corrosion loss on rebars

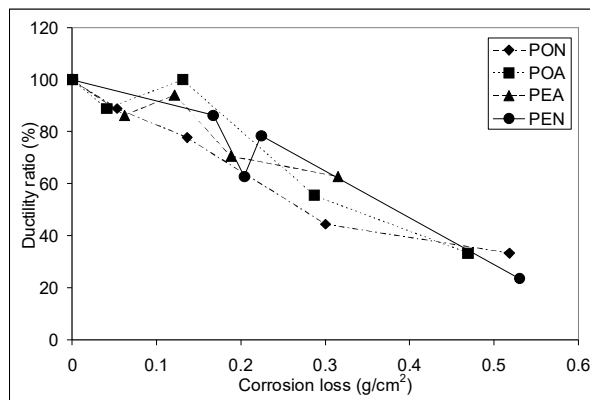


Figure 10: Trend of reduction in ductility of specimen with corrosion loss

Figure10 illustrates the trend of ductility reduction with increase in corrosion loss. The theoretical calculation considering the effects of corrosion on both main rebars and lateral ties showed that the rate of reduction of ductility in the specimens with seismic design was higher than the specimens with ordinary design under the same condition of corrosion loss. However, for corrosion loss up to  $0.5\text{gm/cm}^2$ , the difference in the reduction rate of ductility with corrosion loss was found to be small in the all series. Therefore, for the simplicity in ductility estimation, the best fit parabolic curve was evaluated from all the results, and ductility of corroded specimen may be predicted by using Equation (3).

$$\mu_c = (1 - 1.149\Delta w^2 - 0.7927\Delta w)\mu_u \quad (3)$$

where,  $\mu_c$ : ductility of corroded specimen,  $\mu_u$ : ductility of non-corroded specimen,  $\Delta w$ : corrosion loss ( $\text{gm/cm}^2$ ).

### 3.5 Energy absorption

Energy absorption was obtained by calculating the area under the hysteretic curve. Figure 11 shows the degradation of total energy absorption of specimen with the increase in corrosion loss. The total energy absorption of the specimens with seismic design was much larger than the specimen with ordinary design in the case of non-corroded condition. However, it was sharply decreased with increase in corrosion on the specimens designed not only by the ordinary design method but also by the seismic one.

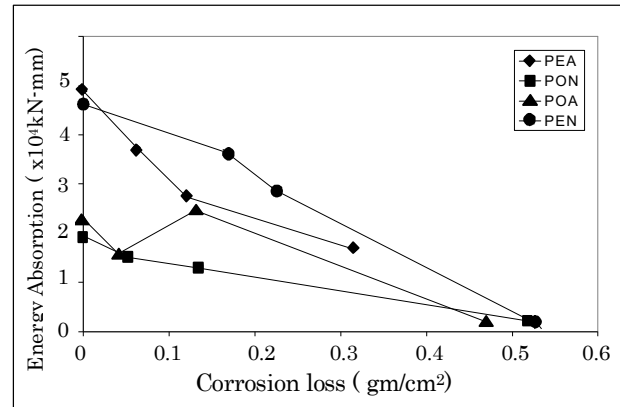


Figure 11: Relationship between energy absorption of specimen and corrosion loss on rebars

Figure 12 shows the ratio of energy absorption of corroded specimen to that of non-corroded one. Total energy absorption is very sensitive to the corrosion of reinforcement. Consequently, in higher corrosion condition with corrosion loss of  $0.5\text{ gm/cm}^2$  or more, the

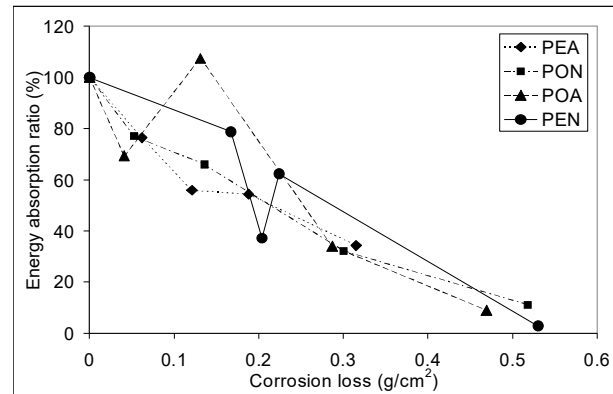


Figure 12: Trend of reduction in energy absorption of specimen with corrosion loss

energy absorption dropped drastically down by 10% for non-corroded specimen, regardless of the difference of design method. The trend of reduction of energy absorption had a little effect of design condition. The rate of the reduction was found to be larger in the specimens with seismic design especially in the lower corrosion condition than about 0.3 g/cm<sup>2</sup> of corrosion loss. However, the relationship between the rate of energy absorption and the corrosion loss for the specimens designed by both methods were not much difference from each other. Consequently, the energy absorption of the corroded specimen was explained as an equation (4).

$$E_c = (1 - 1.8517\Delta w)E_u \quad (4)$$

where,  $E_c$ : energy absorption of corroded specimen,  $E_u$ : energy absorption of non-corroded specimen,  $\Delta w$ : corrosion loss (gm/cm<sup>2</sup>).

#### 4.0 CONCLUSION

From the experimental results on the dynamic properties of the piers deteriorated due corrosion of reinforcement, the following conclusions were obtained:

- Seismic performances of reinforced concrete structures such as strength, ductility, stiffness and energy absorption are seriously affected by corrosion of reinforcement.
- With the increase in the corrosion loss of reinforcing bars, reduction rate of ductility and energy absorption of the pier is much higher than that of strength. Therefore, even when only a slight reduction of strength of structure due to corrosion of reinforcement has been observed from static loading test, it should be considered that the corrosion is responsible for much larger reduction of ductility and energy absorption. Corrosion of reinforcement becomes much more critical parameter for the deteriorated structures in earthquake action.
- Reduction rate of strength, ductility and total energy absorption with corrosion loss of reinforcement can be quantitatively evaluated by experimental equations.

#### REFERENCES

- Takewaka, K and Poudel, U. P., 2001. *Bending Property of Reinforced High Strength Concrete Structure Deteriorated by Corrosion of Steel Reinforcement*. Proceedings of the Third International Conference on Concrete under Severe Conditions, Vol.2, CONSEC'01.
- Takewaka, K. and Matsumoto, S., 1984. *Influence of Corrosion of Reinforcement on Mechanical Property of Reinforced Concrete Beams*. Proceedings of JCI, Vol. 6, Japan Concrete Institute.

# SEISMIC PERFORMANCE OF POST-TENSIONED INTERIOR FLAT SLAB-COLUMN CONNECTIONS

PENNING WARNITCHAI<sup>1</sup>, SOMMAI PONGPORNUP<sup>1</sup>,  
UNNOP PRAWATWONG<sup>1</sup> AND AMORN PIMANMAS<sup>2</sup>

<sup>1</sup>Asian Institute of Technology, Thailand

<sup>2</sup>Sirindhorn International Institute of Technology, Thailand  
*pennung@ait.ac.th*

## ABSTRACT

*This paper presents the results of reversed cyclic loading test of a 3/5 scale slab-column connection model, which was carefully designed and constructed to represent a typical connection between interior column and post-tensioned flat slab with bonded tendons in Thailand. A conventional displacement-controlled cyclic loading test with monotonically increasing drift levels until failure was adopted to investigate the seismic performance of the connection. The lateral force-deformation relation indicated that for each loading cycle the connection model essentially behaved like a linear elastic system with low energy dissipation. As the drift level increased, cracks on the slab surface grew in size and number and concentrated around the column, and the lateral stiffness of the model degraded significantly. Shortly after attaining its maximum lateral strength at 2% drift, the specimen abruptly failed by punching shear. The drift at which the non-ductile failure occurred is considered to be rather low, and hence design improvement for slab-column connections is deemed desirable. The test results on cyclic properties of the response, including stiffness degradation, hysteretic shape, and failure mode, will be useful for the evaluation of seismic performance of the entire slab-column frame buildings in the future.*

## 1.0 BACKGROUND

Over the past three decades, rapid urbanization and massive scale of building construction have taken place in Bangkok and several major cities in Thailand. As the country has long been considered as being free from seismic risk, most existing buildings have been designed and constructed without any consideration on seismic loading. Recently, however, there has been a significant improvement in the understanding of seismic risk. New probabilistic seismic hazard studies indicate that northern and western Thailand can be regarded as regions of moderate seismic hazard, and that Bangkok, though located at a remote distance from seismic sources, is still at risk from long-period, damaging ground motions induced by distant large earthquakes (Warnitchai 2004). The risk in Bangkok is primarily caused by the ability of thick soft surficial deposits in the city area to amplify earthquake ground motions about 3 to 4 times.



To mitigate the risk, seismic design requirements in the form of mandatory ministerial regulations were introduced in 1997. The regulations stipulate that public buildings, essential facilities, hazardous facilities, and all other buildings with height above 15 meters in 10 provinces in northern and western Thailand must be designed for a moderate level of earthquake ground shaking. A revision of the regulations is currently being made to include the design requirements against the effects of distant large earthquakes for buildings in Bangkok and 4 neighboring provinces.

Despite the introduction of statutory seismic design requirements, their actual implementation in design practices seems to have many difficulties and limitations. Most design engineers are not familiar with seismic design concepts and procedures, and they normally do not understand the need for seismic detailing. Many engineers believe that buildings typically designed for gravity loads and wind load (but no seismic detailing) do have sufficient inherent capacity to withstand the expected moderate earthquake ground shaking.

Under these circumstances, a research program on the seismic performance of several typical buildings in Thailand is currently being conducted by the authors. The main objectives are to: (1) determine the inherent seismic capacity of typical buildings of various forms; (2) identify their typical weak spots, detailing deficiencies, and poorly performed structural configurations; and (3) find out economic and practical ways to improve the design of new buildings and to retrofit existing buildings. One key element in this research program is a study on the performance of some critical building components under reversed cyclic loading. These components include, for example, RC columns with short lap splices, beam-column joints with no joint reinforcement, and slab-column connections, etc.

In this paper, a study on the seismic performance of post-tensioned interior flat slab-column connections is presented. A quasi-static, reversed cyclic loading test of a 3/5 scale connection model was carried out, and its behavior and failure mode were examined in detail. The results from this study will be critical ingredients for the evaluation of seismic performance of slab-column frame buildings in Thailand.

## **2.0 SLAB-COLUMN FRAME BUILDINGS IN THAILAND**

Post-tensioned flat slab construction is popular in Thailand for medium to high rise buildings such as office buildings, hospitals, residential buildings and parking buildings. A slab-column frame is normally designed to carry only gravity loads, while the lateral wind load is assumed to be taken care of by concrete shear walls. The slab-column frame is neither designed for lateral seismic load nor checked for lateral deformation compatibility with shear walls to ensure that it can undergo the maximum lateral drift (due to seismic load) without losing gravity load carrying capacity.

It is widely known that the slab-column connection is a critical component in the slab-column frame system. This is the region of slab immediately adjacent to the column that has to transmit large torsion, shear and bending moments between slab and column and is therefore susceptible to punching shear failure. In Thailand, slab-column connections are typically not designed and detailed for seismic effects. No shear reinforcement (such as stirrups or stud-rails) is provided at slab-column connections. Although slab bottom reinforcement bars are provided in an orthogonal mesh to satisfy a minimum requirement for temperature and shrinkage effects, there may be no continuous bottom bar passing through the column to protect against progressive collapse after punching shear failure. Furthermore, due to the congestion of reinforcement bars in the column section, prestressing tendons are normally arranged such that none of them passes through the column.

Despite the fact that a reasonably large number of research studies on the behavior of slab-column connections under seismic loading have been carried out in the past, most of them were made for reinforced concrete slab-column connections. Only a few focused on post-tensioned flat slab-column connections (e.g. Hawkins 1981, Burns et al. 1985, Martinez-Cruzado et al. 1994, Kang et al. 2004), and none of them were made for ‘bonded’ post-tensioning tendons system with non-seismic reinforcement detailing, which is the prevailing type of flat slab construction in Thailand.

### 3.0 KEY STRUCTURAL INDICES

As the objective is to study the seismic performance of post-tensioned slab-column connections that are typical in Thailand, an effort was made to acquire architectural and structural drawings of five representative buildings with post-tensioned floors in Bangkok. The number of stories of these buildings varies from 15 to 30. Some important structural parameters associated with seismic behavior are computed from the drawings; they are herein called ‘structural indices’. These indices are: gravity shear ratio ( $V_g/V_0$ ), critical section perimeter-to-depth ratio ( $b_0/d$ ), side ratio ( $b_1/b_2$ ), gravity shear-to-moment ratio ( $e_r V_g/M_g$ ), prestressing ratio ( $f_{pc}/\sqrt{f'_c}$ ), negative moment reinforcement ratio ( $\rho_s$ ), and gravity moment ratio ( $M_g/M_h$ ).

In the above,  $V_g$  is the gravity shear acting on the slab critical section,  $V_0$  is the direct punching shear strength as defined by ACI 318-95,  $b_0$  is perimeter of the critical section,  $d$  is the effective depth,  $b_1$  is the width of the critical section measured along the direction of loading,  $b_2$  is the other dimension of the section orthogonal to  $b_1$ ,  $M_g$  is the negative moment at the slab-column connection caused by gravity load,  $e_r$  is the ratio of the shear stress caused by a unit direct shear to the maximum shear stress caused by a unit unbalanced moment on the critical section,  $f_{pc}$  is the compressive stress in concrete slab at the centroid of cross section due to prestressing force,  $\rho_s$  is the ratio of total area of top reinforcement bars to  $(c_2 + 3d)d$ ,  $c_2$  is the

column width measured orthogonal to the direction of loading,  $M_n$  is the nominal slab moment capacity. Note that the gravity load here is the dead load (without load factor) plus ‘likely live load’ of which the value is given by ATC-40 (ATC 1996) based on the building occupancy type.

The indices’ values of interior slab-column connections in five representative buildings are given in Table 1. The values do not vary much from case to case, indicating the structural similarity between all these cases. Among these indices, the gravity shear ratio ( $V_g/V_0$ ) appears to be the most important one, as many test results in the past indicate that the lateral drift level at which a connection punching shear occurs is strongly influenced by this index (Hueste et al., 1999). For gravity shear ratios higher than 0.4—which is the maximum limit recommended by ACI 318-02, the drift capacity could be unacceptably low, say below 1.5 % in some cases. Table 1 shows that the gravity shear ratio of every representative building falls within the limit, with a moderately high average value of 0.289.

*Table 1: Structural indices of interior slab-column connections in five representative buildings and those of test specimen*

Building	Span (cm)	Column Size (cm x cm)	$\frac{V_g}{V_0}$	$\frac{b_0}{d}$	$\frac{b_1}{b_2}$	$\frac{e_r V_g}{M_g}$	$\frac{f_{pc}^*}{\sqrt{f'_c}}$	$\rho_s$	$\frac{M_g}{M_n}$
Office 1	800	40x100	0.267	21.5	2.07	1.72	0.84	0.014	0.13
Office 2	700	40x80	0.296	19.0	1.71	1.67	1.01	0.011	0.11
Office 3	800	40x80	0.287	19.0	1.71	1.21	0.84	0.010	0.16
University	800	50x80	0.231	18.8	1.44	1.40	1.04	0.008	0.11
Hospital	840	50x70	0.366	18.3	1.30	1.52	0.87	0.009	0.15
Average	800	40x80	0.289	19.3	1.65	1.50	0.92	0.010	0.13
Specimen	480	25x50	0.280	18.3	1.70	3.25	0.93	0.011	0.07

\* unit =  $kg/cm^2$

#### 4.0 TEST SPECIMEN AND EXPERIMENTAL SETUP

The test specimen is a 3/5 scale slab-column interior connection model as shown in Figure 1. As the inflection points in the slab-column frame system under seismic loading are assumed to occur at slab mid-span and column mid-height, the model slab extends to mid-span on two sides of the connection and the column extends above and below the slab to story mid-height. The slab was supported along each transverse edge by 5 pin-ended bars to simulate a moment-free boundary condition. Similarly, to produce moment-free condition at the column ends, the column bottom end was set on a hinged support, and the top end was connected to a hydraulic actuator through a pivoted connection. The test specimen was designed to have the values of structural indices close to the average values of representative buildings as shown in Table 1.

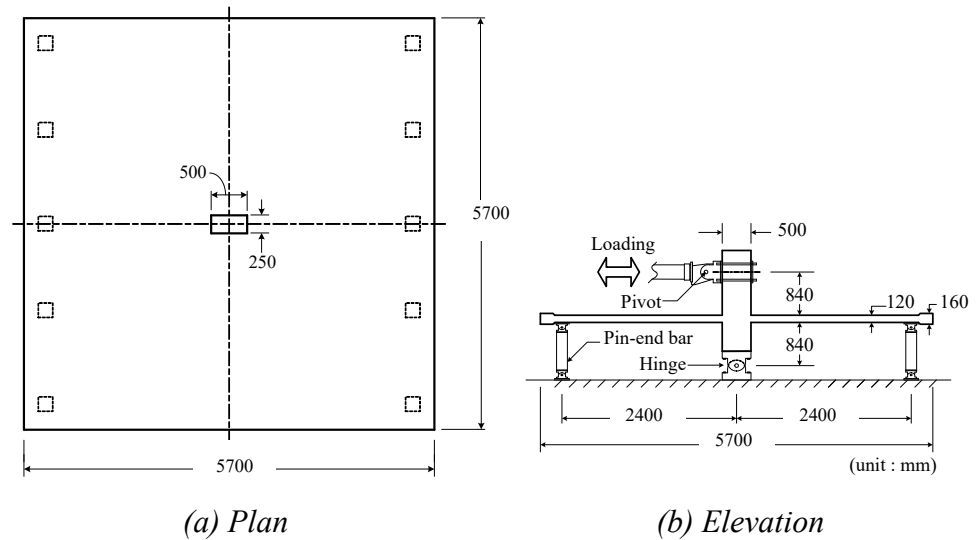


Figure 1: Interior slab-column connection specimen and its dimensions

The prestressing strands are grade 270, seven-wire, stress relieved type with a nominal diameter of 12.7 mm. Eight strands were banded in the direction of loading with a spacing of 350 mm. Other eight strands were placed uniformly in the direction perpendicular to the loading with a spacing of 700 mm as shown in Figure 2. Each strand was inserted into a galvanized duct to prevent bonding with concrete before prestressing. Three days after casting slab, all these strands were tensioned one by one to about 80 % of their ultimate strength ( $0.80 f_{pu}$ ). Shortly afterward, all galvanized ducts were filled in by non-shrink cement grout.

Top slab reinforcement bars were placed symmetric about both centerline axes as shown in Figure 3. The top bars were concentrated only at the slab-column connection region and have a spacing of 80 mm. These bars were cut off at a distance of 1.0 m from the center of the column. Figure 3 also shows the layout of bottom slab reinforcement which is symmetric about both center line axes. The bottom bars were spaced at 550 mm intervals throughout the slab. Although the specified steel grade of all slab reinforcement bars was SD-30, their tested yield and tensile strengths were about 440 and 580 MPa, respectively. The average compressive strength of concrete cylinders for slab at 4, 14, and 28 days were 20, 39, and 40 MPa, respectively.

Before applying a lateral reversed cyclic load, a large number of sand bags were piled up on and hanged underneath the slab as shown in Figure 4 in order to correctly simulate the gravity load effects. The amount and distribution of sand bags were determined by a finite element analysis such that the computed gravity shear ratio was close to the average value of representative buildings. The lateral load was applied to the top column by an MTS servo controlled hydraulic actuator mounted horizontally to a rigid reaction wall (Figure 4).

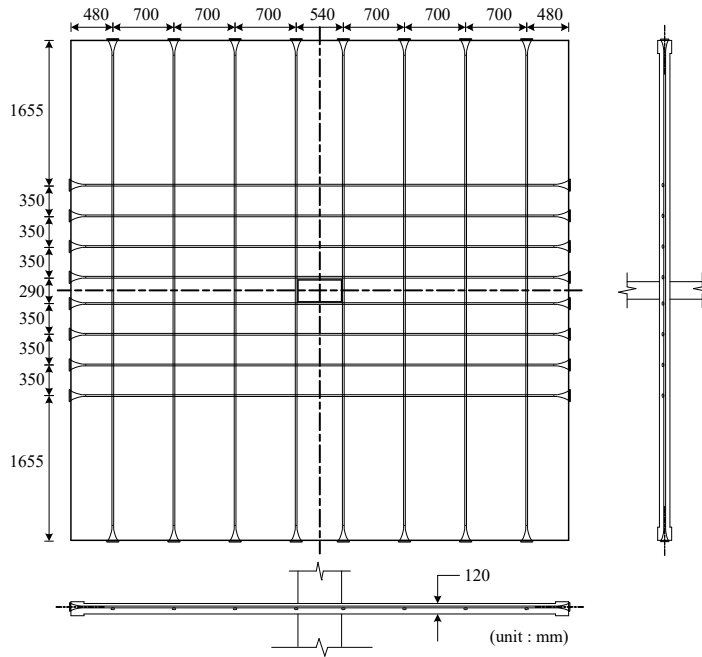


Figure 2: Layout of prestressing strands

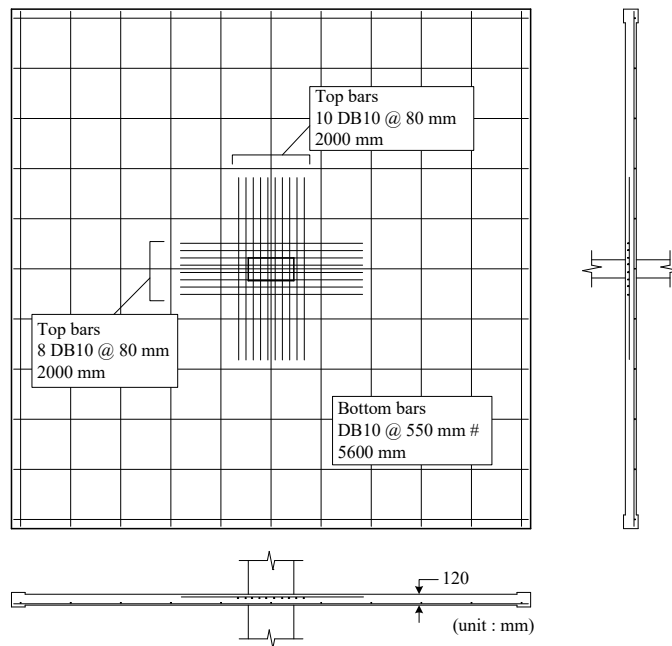


Figure 3: Layout of top and bottom steel deformed bars

Note that this test setup was found to be rather weak in torsion, so a torsional restraining system was attached to the test specimen. A typical displacement-controlled cyclic loading test was then carried out with monotonically increasing drift levels of  $\pm 0.25\%$ ,  $\pm 0.5\%$ ,  $\pm 0.75\%$ ,  $\pm 1.00\%$ ,  $\pm 1.25\%$ ,  $\pm 1.50\%$ ,  $\pm 2.00\%$ , .... For each drift level, two complete cyclic displacement loops were made.



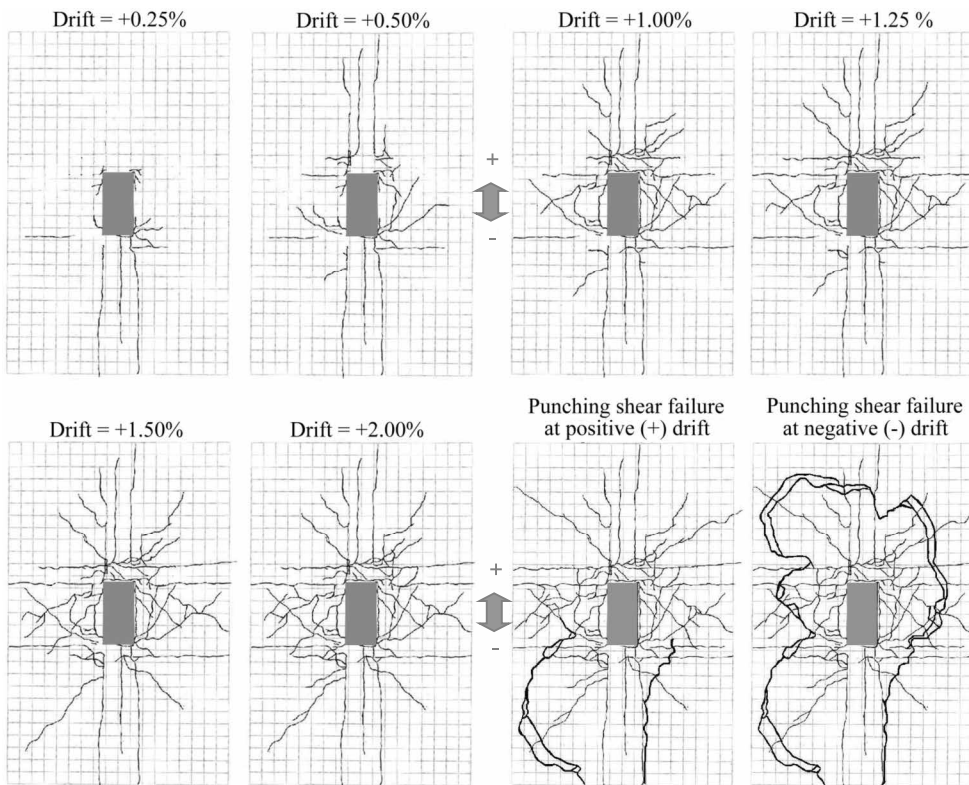
*Figure 4: Setup for reversed cyclic loading test*

The data measured and recorded in the experiment include: (1) lateral force and displacement at the top column end, (2) lateral displacement and rigid-body twisting angle of slab, (3) bending curvature of slab in front of and behind the column, (4) strain in top and bottom bars of slab at various locations, (5) strain distribution along some prestressing strands, and (6) strain of longitudinal bars of column. Photos were also taken at peak positive and negative drifts in every cycle of loading to record the development of visible cracks on top slab surface in the connection region. Full details of the test specimen instrumentation can be found in (Pongpornsup 2003).

## **5.0 EXPERIMENTAL RESULTS**

Due to space limitation, only some results are presented here in this section. First, the development of cracks on the top surface of the slab around the column is shown in Figure 5. The first observable cracks were longitudinal cracks running in the direction of loading and passing through the column sides. They initiated at the lateral drift of 0.25%. The development of diagonal cracks radiated from column corners followed afterward and became more obvious at 0.5% drift. These diagonal cracks might be caused torsion in the slab, which was resulted from the difference in flexural deformation of slab strips near and far from the column faces. The flexural deformation of the slab strip adjacent to the column face was found to be the highest. Transverse cracks were clearly developed at about 1.0% drift. As the drift level increased, these longitudinal, diagonal, and transverse cracks widened and lengthened and grew in number around the connection.

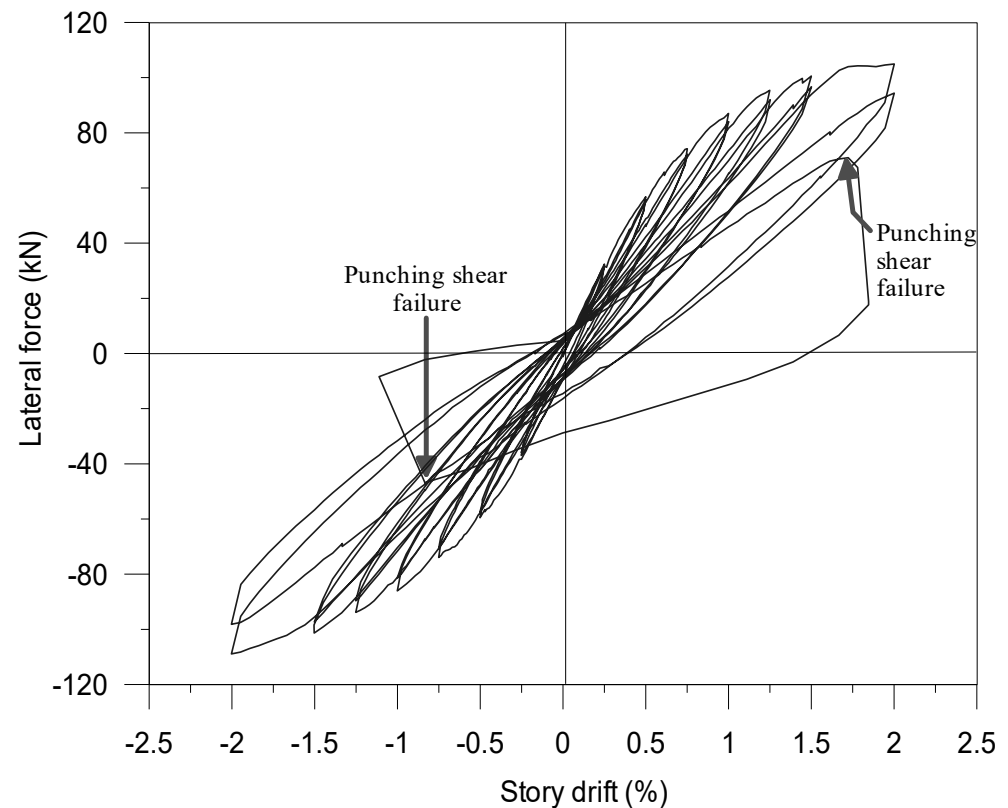
While the slab was pushing toward the positive direction after completing two cycles at 2.0% drift, a punching shear failure suddenly occurred on one side of the connection at about 1.70% drift. After that, the slab was then pulling back toward the negative direction, and another punching shear failure suddenly developed on the other side of the connection at about -0.8% drift, thus forming a complete loop of punching shear failure as shown in Figure 5. Note that the punching shear failure did not occur at the critical section.



*Figure 5: Development of cracks on the top surface of slab*

The relation between lateral load and lateral drift is shown in Figure 6. The hysteretic loop in every loading cycle before punching shear failure was long and narrow, indicating a limited ability to dissipate energy. Neither pinching behavior nor plastic residual deformations were observed. As the drift level increased, the peak lateral load also increased, but the average stiffness (secant stiffness) reduced. The test specimen essentially behaved like a linear elastic system with significant stiffness degradation. The stiffness degradation is believed to be caused by the extensive and progressive cracking of slab in the connection region. Strains in slab bottom bars, prestressing strands, and column longitudinal bars fluctuated within the limit of linear elastic, while strains in slab top bars exceeded the yield limit at about 1.5% drift. The maximum lateral load of 105 kN was attained at 2.0% drift. After the punching shear failure occurred at around 2.0% drift, the test specimen completely lost its lateral strength and stiffness.

Compared with other test results on slab-column connections done elsewhere (e.g. Hueste 1999), the drift of about 2.0% at which the punching shear failure occurred appears to be rather low. Improvement in the design of post-tensioned slab-column connections is deemed desirable.



*Figure 6: Relation between lateral load and lateral drift*

## 6.0 CONCLUSIONS

A 3/5 scale model was designed and constructed to represent a typical connection between interior column and post-tensioned flat slab in medium to high rise buildings in Thailand. The model was tested under a conventional reversed cyclic loading with monotonically increasing drift levels until failure to investigate its seismic performance. During the test, the specimen essentially behaved like a linear elastic system with low energy dissipation, as indicated by its long and narrow hysteretic loops. As the drift level increased, cracks on the slab surface around the column grew in size and number, and the lateral stiffness of the specimen degraded significantly. Shortly after attaining its maximum lateral strength at 2% drift, the specimen abruptly failed by punching shear. The drift at which the non-ductile failure occurred is considered to be rather low, and hence design improvement for slab-column connections is deemed desirable. The test results on cyclic properties of the response, including stiffness degradation, hysteretic shape, and failure mode, will undoubtedly be useful for the evaluation of seismic performance of the entire slab-column frame buildings in the future.



## ACKNOWLEDGEMENTS

This research work was funded by the EDM-EqTAP Project of the National Research Institute for Earth Science and Disaster Prevention (NIED) of Japan and also by the Thailand Research Fund (TRF). We wish to express our sincere appreciation to both organizations for providing the opportunity to undertake this research work.

## REFERENCES

- ATC, 1996. *Seismic evaluation and retrofit of concrete buildings*. Volume 1, ATC- 40 Report, Applied Technology Council, Redwood City, California.
- Burns, N.H. and Roongroj, Hemakom, 1985. *Test of post-tensioned flat plate with banded tendons*. Journal of the Structural Division, ASCE, Vol. 111, No. 9, 1899-1915.
- Hawkins, N. M., 1981. *Lateral load resistance of unbonded post-tensioned flat plate construction*. PCI Journal, Vol. 26, No.1, 94-116.
- Hueste, M. B. D., Wight, J. K., 1999. *Nonlinear punching shear failure model for interior slab-column connections*. Journal of Structural Engineering, Vol. 125, No. 9, 997-1008.
- Kang, T. H. K., Wallace, J. W., 2004. *Shake table tests of reinforced concrete flat plate frames and post-tensioned flat plate frames*. Proc. 13<sup>th</sup> World Conference on Earthquake Engineering, International Association for Earthquake Engineering, Vancouver, Canada, Paper No. 1119.
- Martinez-Cruzado, J. A., Qaisrani, A.N., and Moehle, J. P., 1994. *Post-tensioned flat-plate slab-column connections subjected to earthquake loading*. Proc. 5<sup>th</sup> U.S. National Conference on Earthquake Engineering, Vol. 2, Earthquake Engineering Research Inst., Oakland, California, 139-148.
- Pongpornsup, S., 2003. *Seismic performance of post-tensioned interior flat slab-column connections*. M. Eng Thesis, Thesis No. ST.-03-18, Asian Institute of Technology.
- Warnitchai, P., 2004. *Development of seismic design requirements for buildings in Bangkok against the effects of distant large earthquakes*. Proc. 13<sup>th</sup> World Conference on Earthquake Engineering, International Association for Earthquake Engineering, Vancouver, Canada, Paper No. 744.

# **EQUIVALENT STATIC ANALYSIS AS PER IS 1893:2002 – A SIMPLE SOFTWARE TOOL**

N. CHANDRA SEKHAR<sup>1</sup>, K. B. S. SUNIL BABU<sup>1</sup>  
AND PRADEEP KUMAR RAMANCHARLA<sup>2</sup>

<sup>1</sup>M.Tech (CASE) and <sup>2</sup>Assistant Professor & Coordinator,  
Earthquake Engineering Research Centre, IIT Hyderabad, India.  
*ramancharla@iiit.net*

## **ABSTRACT**

*This paper presents a software tool for performing the static and dynamic analysis of regular and simple multi-storied structures. This analysis procedure is based on IS 1893:2002 (Part I), Criteria for Earthquake Resistant Design of Structures. This tool is a windows based software program developed in Visual Basic. The tool provides a user-friendly GUI for the calculation of base shear and its distribution over the height of the structure, depending on the input parameters. Usual input parameters are structural dimensions, type of structure, soil type, purpose of structure and location. Though this tool is simple, can be used for verification of design within short time. This tool is aimed to help students, architects and engineers during design of earthquake resistant structures.*

## **1.0 INTRODUCTION**

Earthquake engineering education in India though started early, it has not picked up to the extent what is required at present. This is clearly evident from the damages during previous earthquakes. Recent earthquake in Bhuj, Gujarat on 26th Jan 2001 has also stressed the need for increasing the awareness about earthquakes among the professional involved in construction activity. To address this issue, Ministry of Human Resources Development, Govt. of India, (MHRD) initiated a programme called National Programme on Earthquake Engineering Education (NPEEE) <sup>1</sup>. Under this programme, a large number of teachers from engineering colleges, architecture colleges and polytechnics are trained in the subject of earthquake engineering. It is also felt that there is a need to develop teaching aids and printed resource material relevant to India in this field. In this connection, we plan to develop simple software tools that will help students, professionals, and faculty members in understanding, teaching the basics of earthquake resistant design of structures. As a preliminary attempt, this tool is developed. Provisions of IS 1893 2002 are used in this tool for performing equivalent static analysis and dynamic analysis of a simple structure. The program has been adequately validated and found to provide satisfactory results under all possible cases. This tool provides fast analysis of simple structures.

## 2.0 BRIEF OVERVIEW ON PROVISIONS OF IS 1893: 2002

Earthquake motion causes vibration of the structure leading to inertia forces. Thus a structure must be able to safely transmit the horizontal and the vertical inertia forces generated in the super structure through the foundation to the ground. Hence, for most of the ordinary structures, earthquake-resistant design requires ensuring that the structure has adequate lateral load carrying capacity. Seismic codes will guide a designer to safely design the structure for its intended purpose.

Seismic codes are unique to a particular region or country. In India, IS 1893 is the main code that provides outline for calculating seismic design force. This force depends on the mass and seismic coefficient of the structure and the latter in turn depends on properties like seismic zone in which structure lies, importance of the structure, its stiffness, the soil on which it rests, and its ductility. Part I of IS 1893:2002 (here after we refer it as the code) deals with assessment of seismic loads on various structures and buildings. Whole the code centres on the calculation of base shear and its distribution over height. Depending on the height of the structure and zone to which it belongs, type of analysis i.e., static analysis or dynamic analysis is performed.

### 2.1 Static analysis

#### 2.1.1 Calculation of design horizontal seismic coefficient

The total design seismic base shear ( $V_B$  along any principal direction shall be determined by following expression.

$$V_B = A_h * W \quad (1)$$

where,  $W$  is the total weight of the building calculated using the structural details and  $A_h$  is calculated as shown below:

$$A_h = \left(\frac{Z}{2}\right) * \left(\frac{I}{R}\right) * \left(\frac{S_a}{g}\right) \quad (2)$$

where,  $Z$  is zone factor,  $I$  is Importance factor,  $R$  is response reduction factor and  $S_a/g$  is spectral acceleration coefficient.

#### 2.1.2 Design lateral force at each floor $i$

The design lateral force,  $V_b$  shall be distributed along the height of the building using equation 3.

$$Q_i = \frac{V_B * W_i * h_i^2}{\sum_{j=1}^n W_j * h_j^2} \quad (3)$$

where,  $Q_i$  = Design lateral force at floor  $i$

$W_i$  = Seismic weight of floor i  
 $h_i$  = Height of floor I measured from base and  
 $n$  = Number of storeys in the building

## 2.2 Dynamic analysis

Dynamic analysis shall be performed to obtain the design seismic forces, and its distribution to different levels along the height of the building and to the various lateral load resisting elements under any of the following conditions:

- For regular buildings, if the height is greater than 40 m in Zones IV and V or greater than 90 m in Zone II and III
- For irregular buildings, if height is more than 12 m in Zones IV and V and more than 40 m in Zones II and III.

Dynamic analysis can be performed either by time history method or response spectrum method. In this paper, response spectrum method is discussed.

The peak response of the structure is calculated from the modal combination, where the following two methods can be used

Square root of sum of squares (SRSS) method

$$\lambda = \sqrt{\sum_{k=1}^r \lambda_k^2} \quad (4)$$

Where  $\lambda_k$  = absolute value of quantity in mode k, and  
 $r$  = number of modes being considered

Complete Quadratic Combination (CQC) method

$$\lambda = \sqrt{\sum_{i=1}^r \sum_{j=1}^r \lambda_i \rho_{ij} \lambda_j} \quad (5)$$

where  $r$  = number of modes being considered

$\lambda_i$  = response quantity in mode i (including sign)

$\lambda_j$  = response quantity in mode j (including sign)

$\rho_{ij}$  = cross-modal coefficient

$$\frac{8\zeta^2(1+\beta)\beta^{1.5}}{(1+\beta^2)^2 + 4\zeta^2\beta(1+\beta)^2}$$

Where  $\zeta$  = modal damping ratio

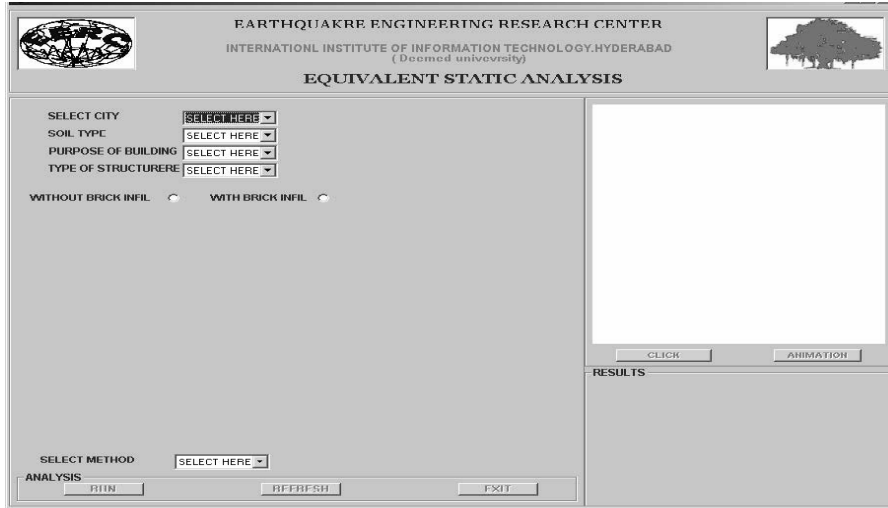
$\beta$  = frequency ratio =  $\omega_j / \omega_i$

$\omega_i$  = circular frequency in  $i^{th}$  mode

$\omega_j$  = circular frequency in  $j^{th}$  mode

### 3.0 GUI OF THE TOOL

The user interface of the tool is shown in figure 3.1. It requires user to provide certain input parameters such as location, type of soil, purpose of building, type of structure and dimensions of the structure.



*Figure 3.1: The interface of the tool*

The screenshot displays a software interface with four main sections for selection:

- Location:** A vertical list box with 'HYDERABAD' selected. Other visible options include DURGAPUR, GANGTOK, GAYA, GOA, GORAKHPUR, GULBARGA, GUWAHATI, and HYDERABAD.
- SOIL TYPE:** A dropdown menu with 'SELECT HERE' selected. The expanded list shows HARD SOIL, SOFT SOIL, and MEDIUM SOIL.
- PURPOSE OF BUILDING:** A dropdown menu with 'SELECT HERE' selected. The expanded list shows SELECT HERE, IMPORTANT SERV, and ALL OTHER BUILD.
- TYPE OF STRUCTURE:** A dropdown menu with 'SELECT HERE' selected. The expanded list shows SELECT HERE, OMRF, SMRF, LBMW UNREIN, LBMW REINFO, LBMW RC BAN, ORDINARY REI, and DUCTILE SHEA.

Figure 3.2: Selection of different options from drop down menu

The screenshot displays a software interface for selecting brick infill options and dimensions:

- WITHOUT BRICK INFIL** ☐ **WITH BRICK INFIL** ☒
- ALL UNITS IN m**
- NUMBER OF STOREYS:** Input field.
- EACH STOREY HEIGHT:** Input field with **ADD** and **REMOVE** buttons.
- BASE DIMENSION:** Input field.
- WALL THICKNESS:** Input field.
- COLUMN DIMENSIONS:**
  - BREADTH:** Input field
  - DEPTH:** Input field
- BEAM DIMENSIONS:**
  - BREADTH:** Input field
  - DEPTH:** Input field
- SLAB DIMENSIONS:**
  - BREADTH:** Input field
  - DEPTH:** Input field
- SELECT METHOD:** Dropdown menu with 'SELECT HERE' selected.
- OK** button.

Figure 3.3: Selection of brick infill option

Based on the past seismic activity, India is divided into four zones. Each zone is assigned one zone factor and for ready reference zone factors for some important towns are mentioned in Annex E of the code. All these city names and assigned zone factors are stored in a database and can be retrieved after selecting the city name from the drop down menu in the user interface. Similarly, the other parameters like soil type, type of structure and purpose of building are stored in the database. Selection of soil type decides which curve to be used in figure 2 of the code, type of structure decides what should be the value of response reduction factor and purpose of building retrieve the importance factor to be used in the analysis. Another parameter that helps us in selecting the formula for calculating fundamental natural period is option that selects the structure with or without brick infill.

Basic theory includes the idealization of whole structure into a lumped mass at each floor level. The tool will take all the input values mentioned above and calculate the weights, lateral forces, time periods, frequencies of each floor and mode shapes. Finally the maximum response of the structure is calculated using SRSS or CQC method depending on the natural frequencies.

#### 4.0 EXAMPLE PROBLEM

For testing the correctness of the developed software tool, we are comparing the results of analysis of a simple 3-storied structured shown in figure 4.1. First, analysis by hand calculation is performed and later results are compared with software analysis results.

Given structure: 3-storeyed building  
 Location : Hyderabad (Zone II)  
 Soil type : Medium soil  
 Purpose : Residential  
 Structure type: Ordinary moment resisting frame with brick infill  
 Storey height : 3m  
 Column dimensions: 230 mm x 230 mm  
 Beam dimensions : 230 mm x 230 mm  
 Slab dimensions : 6 m x 6 m  
 Number of columns: 9  
 Number of beams: 6  
 Unit weight of concrete: 25 kN/m<sup>3</sup>  
 Unit weight of brick : 18 kN/m<sup>3</sup>  
 Live load is 2 kN/m<sup>2</sup>

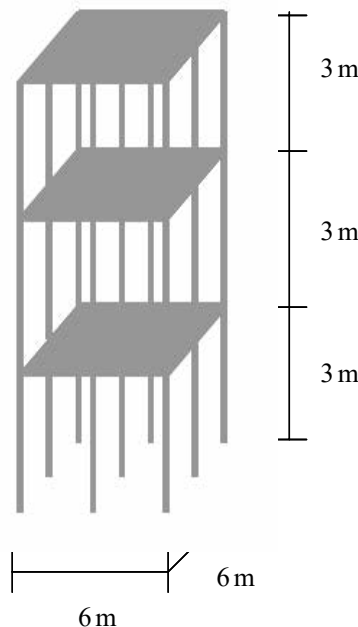


Figure 4.1: Example problem

#### 4.1 Analysis by hand calculation

Slab weight =  $(25 * 6 * 6 * 0.12) = 108$  kN

Beam weight =  $(25 * 0.23 * 6 * 6) = 47.61$  kN

**Column weight:**

$$\text{First floor} = (25 * 0.23 * 0.23 * 3 * 9) = 35.7 \text{ kN}$$

$$\text{Second floor} = (25 * 0.23 * 0.23 * 3 * 9) = 35.7 \text{ kN}$$

$$\text{Third floor} = (25 * 0.23 * 0.23 * 1.5 * 9) = 17.8 \text{ kN}$$

**Wall weight:**

$$\text{First floor} = (18 * 0.23 * 6 * 3 * 6) = 447.12 \text{ kN}$$

$$\text{Second floor} = (18 * 0.23 * 6 * 3 * 6) = 447.12 \text{ kN}$$

$$\text{Third floor} = (18 * 0.23 * 6 * 1.5 * 6) = 223.56 \text{ kN}$$

$$\text{Live load} = (2 * 6 * 6) = 72 \text{ kN}$$

$$\text{First floor weight} = 108 + 47.61 + 35.7 + 447.12 + (0.2 * 72) = 652.83 \text{ kN}$$

$$\text{Second floor weight} = 108 + 47.61 + 35.7 + 447.12 + (0.2 * 72) = 652.83 \text{ kN}$$

$$\text{Third floor weight} = 108 + 47.61 + 17.85 + 223.56 + (0.2 * 72) = 411.42 \text{ kN}$$

$$\text{Total weight (W)} = 652.83 + 652.87 + 411.42 = 1717.094 \text{ kN}$$

Fundamental natural time period for brick infill panel:

$$T_a = \frac{0.09 * h}{\sqrt{d}} = 0.33 \text{ sec}$$

$$Z=0.1, I=1, R=3, S_a/g = 2.5 \text{ (depends on } T_a \text{ and type of soil)}$$

$$A_h = 0.0416 \text{ from equation (2)}$$

$$V_B = 71.43 \text{ kN from equation (1)}$$

Distribution of seismic force to each floor: From equation (3)

$$Q_1 = 6.69 \text{ kN (for first floor)}$$

$$Q_2 = 26.77 \text{ kN (for second floor)}$$

$$Q_3 = 37.96 \text{ kN (for third floor)}$$

In addition to static analysis, we performed dynamic analysis also;

Stiffness of each floor:

$$1^{\text{st}} \text{ floor stiffness} = 20858.116 \text{ kN/m}$$

$$2^{\text{nd}} \text{ floor stiffness} = 20858.116 \text{ kN/m}$$

$$3^{\text{rd}} \text{ floor stiffness} = 20858.116 \text{ kN/m}$$

Mass matrix

$$\begin{bmatrix} 652.837 & 0 & 0 \\ 0 & 652.837 & 0 \\ 0 & 0 & 411.420 \end{bmatrix}$$



Stiffness matrix

$$\begin{bmatrix} 41716 & -20858 & 0 \\ -20858 & 41716 & 20858 \\ 0 & -20858 & 20858 \end{bmatrix}$$

Solving  $|K-\lambda M| = 0$ , frequencies (rad/second) are

$\omega_1 = 2.80$ ,  $\omega_2 = 7.67$  and  $\omega_3 = 10.57$  and mode shapes for  $\lambda_1, \lambda_2, \lambda_3$  are

$\lambda_1$	$\lambda_2$	$\lambda_3$
0.481	-1.025	0.804
0.845	-0.161	-1.204
1.000	1.000	1.000

Since natural frequencies are distinct, SRSS method of modal combination can be used. In such case, maximum displacement response of the structure is 0.357 m.

#### 4.2 Analysis using software tool

After having performed the analysis by hand calculation, we will now do the same using software tool. In this tool, it is required to input the parameters by selecting options using the drop down menu as shown in figure 3.1.

##### Step 1:

In GUI, select city for deciding zone factor, select the purpose of building for deciding importance factor, select structural framework for deciding response reduction factor and select soil type for choosing the curve from table 2 of the code to read spectral acceleration.

##### Step 2:

Since the example problem is with brick infill, we have to input all physical dimensions of the structure including wall and base dimensions.

##### Step 3:

After entering all the dimensions, click on the 'RUN' button. Then, base shear and its distribution as shown below will be displayed on the screen.

Base shear is 71.43 kN

$Q_1 = 6.69$  kN (for first floor)

$Q_2 = 26.77$  kN (for second floor)

$Q_3 = 37.96$  kN (for third floor)

In addition to these, natural frequencies, mode shapes and maximum displacement responses will be displayed. All these values are matching well with the results of hand calculations

## 5.0 CONCLUSION

This paper discusses the simple software tool for performing equivalent static analysis of structures as per IS 1893: 2002 (Part I). For this purpose a simple VB GUI has been developed in order to make the calculations simple. This can be a handy tool for the civil engineers who wish to do structural calculations in least time.

## REFERENCES

- Project Implementation Plan: National Programme on Earthquake Engineering Education.* A Ministry of HRD Initiative, Government of India, March 2003.
- Indian standard Criteria for earthquake resistant design of structures, Part1: General Provisions and Buildings, IS 1893(part1): 2002.* Bureau of Indian standards, New Delhi.
- Evangelos Petroutrisos, 2002. *Mastering Visual Basic 6.0.* B.P.B. Publishers, New Delhi.

# **INTRODUCTION TO JSCE STANDARD SPECIFICATION FOR CONCRETE STRUCTURES**

TAKETO UOMOTO

ICUS, IISc, University of Tokyo, Japan  
[uomoto@iis.u-tokyo.ac.jp](mailto:uomoto@iis.u-tokyo.ac.jp)

## **ABSTRACT**

*Japan has been constructing a large quantity of concrete structures since 1950. In case of concrete structures, JSCE standard specification has played an important role in the field of civil engineering, and most of the civil structures in Japan are designed and constructed in accordance with these specifications. Now, not only the materials of construction but also the design and construction methods, procedures inspection and maintenance have also changed drastically since the specification was published in 1914. JSCE has endeavoured to incorporate the latest development in the area of research by suitably modifying the specifications. A change in the design philosophy from the allowable stress to limit state design and now to a performance based design concept, is only one example of these changes. This paper provides a brief historical background to JSCE specifications and an insight into the latest edition, where the performance and durability based design and maintenance has been introduced for the first time.*

## **1.0 INTRODUCTION**

Since the end of 19<sup>th</sup> century, Japan has been constructing a large quantity of structures introducing European and American methods, modifying the method a little by little acceptable to Japanese culture. At the beginning of 20<sup>th</sup> century, many new materials and design and construction methods were introduced - such as to construction of structures using steel, bricks, plain and reinforced concrete. The first cement plant was setup by the government in 1875 and handed over to a private company in the 1884, which marked the beginning of cement production in Japan.

In 1923, the great Kanto earthquake shook the metropolitan area, destroying numerous structures made of bricks and, and the ensuing fire burnt down wooden structures after the earthquake. This experience showed the weakness of brick structures without enough reinforcement, and engineers decided to construct important civil structures using either steel or concrete.

For large scale construction of these structures it was necessary for the engineers to standardize the material to be used and the design and construction methods. Considering these, Concrete Committee of Japan Society of Civil Engineers (JSCE) began publishing Standard Specifications for concrete structures with the help of academicians, public officers,

researchers and engineers from consulting and construction companies. These standard specifications which have been published since 1931 have played a leading role in the field of civil engineering, and most of the civil structures in Japan are designed and constructed in accordance with them.

Modifications have been introduced in these specification from time to time to incorporate findings from on going research and development, and development in materials and construction technology. As an example, the design philosophy for concrete structures was ‘allowable stress’, which was changed to limit state design in 1986 to meet the requirements of safety and economy. The concept has undergone a further revision, and performance based design was introduced in 2002 to allow the use of many newly developed materials and methods of design considering performances other than strength: safety, aesthetics, durability, hazards to the public, environmental issues, etc.

This paper provides a brief historical background to JSCE specifications and an insight into the latest edition, where the performance and durability based design and maintenance has been introduced for the first time. The titles of chapters in some of the latest specifications are listed in the Appendix for ready reference.

## 2.0 BRIEF HISTORY OF JSCE STANDARD SPECIFICATION

As shown in Figure 1, the first Standard Specification of Concrete Structure was published in 1931, and dealt with the design and construction of reinforced concrete structures including bridges and other facilities. The specification for non-reinforced concrete was published in 1943 to meet the requirements of construction of tunnels, concrete dams and other facilities.

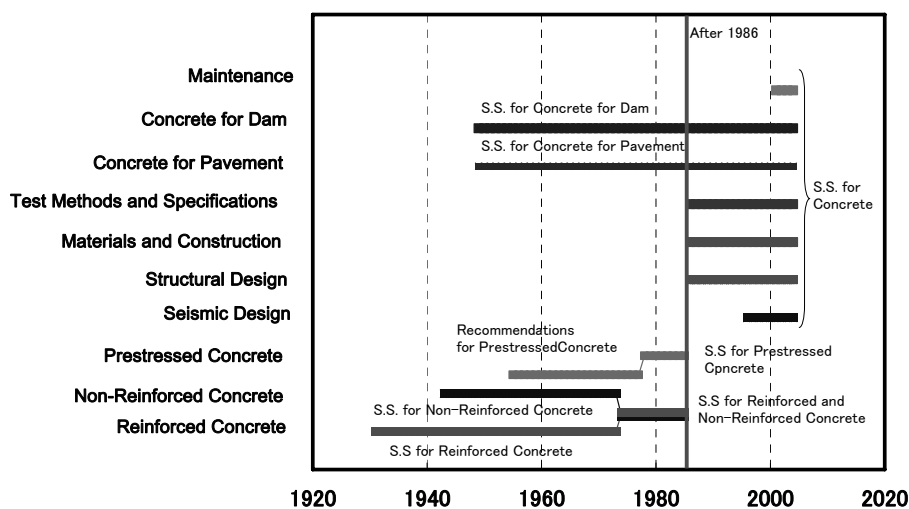


Figure 1: Publication of the Standard Specifications of JSCE

Considering the importance and the differences of concrete to be used in dams and pavements, new specifications were published for dams and pavements in 1949. After the Second World War, power generation and transportation were the most urgent needs of the nation, and civil engineers were involved in construction of concrete dams and roads across the country.

To prepare for the 1964 Tokyo Olympic Games the nation had to prepare not only stadiums but also highways and ultra-rapid trains connecting Tokyo and Osaka. Although Japan has large number of earthquakes all year around, prestressed concrete was introduced in the construction of longer span bridges. In 1955, recommendation for prestressed concrete was published and after years of discussions, standard specifications for prestressed concrete were published in 1978.

In 1986, all the specifications were combined into a single set called “Standard Specifications for Concrete” and individual specifications (volumes) became a part of these - design, construction, etc.. In this year, limit state design was introduced for the first time, though an option to use the allowable stress method was still retained, depending upon the requirements and wishes of a client.

In the 21<sup>st</sup> century, there was a pressure from both – clients and the society to use waste materials, reduce energy consumption, keep the environment clean, etc. To deal with the problem, performance based specification was introduced in the 2002 edition of the Specifications, containing durability design. A new volume titled “Maintenance” was added to the specifications to specially take care of the issues related to already existing structures. Learning from the disasters of the Great Hanshin Awaji Earthquake (1995), more emphasis was placed on seismic design, which was published as an independent volume separated from the volume of design. Salient features of the durability design and maintenance volumes are briefly discussed in the following sections.

### **3.0 EXAMPLES OF THE CHANGES**

Figure 2 shows the changes of the maximum design strength of concrete in the specifications. As can be seen, this value has been increasing since 1931, and has now reached 1000kg/cm<sup>2</sup> (since 1986), which is practically six times that in 1931. The increase is more pronounced with the introduction of prestressed concrete. This increase in strength of concrete has become possible by improved methods of cement production, better understanding of hydration processes and proportioning of concrete mixes, better methods of production of concrete, and quality control.

However, this dramatic increase in design strength does not imply that all structures are built with such ‘high strength concrete’, but simply that the option is available for the use of such concrete, and the issues related to design and construction using such material have been resolved at least to the extent that allows their actual use.

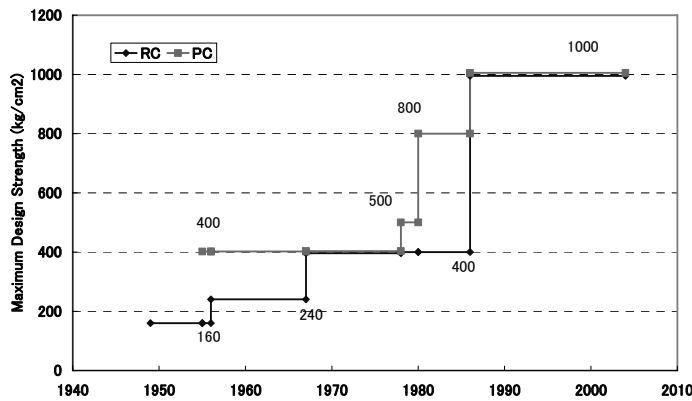


Figure 2: Changes in maximum design strength of concrete

Figure 3 shows the change of maximum water cement ratio when freeze thaw durability needs to be considered, and this change has been possible due to changes of material quality. In fact, presently, the maximum water cement ratio of concrete is restricted by other factors, such as strength, durability against corrosion etc.

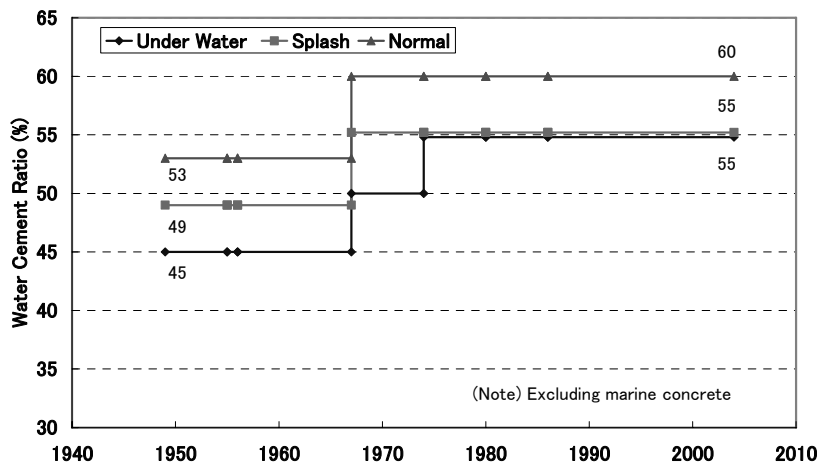


Figure 3: Changes in maximum water-cement ratio of air entrained concretes considering freeze-thaw durability

#### 4.0 NEW STANDARD SPECIFICATIONS OF JSCE

The Concrete Committee of JSCE, the leading committee in the field of concrete, published revised editions of the Standard Specifications for Concrete Structures in 2000, 2001 and 2002 to address problems related to durability and maintenance, which were becoming difficult to handle in the earlier specifications. The following two proposals can be considered the most important of the changes proposed in these documents:

- Proposal for a new method for design and construction of new concrete structures, wherein the structures can be used for a specified lifetime at low cost of maintenance

- Proposal for an effective, economic and rational system for maintenance of existing concrete structures, with minimum investment in manpower. This aspect is important not only from the technical point of view but also considering the overall manpower available for carrying out such jobs.

Addressing the above, the following two volumes have been published – The Standard Specification for Construction Works of Concrete Structures, (Jan. 2000), and, The Standard Specification for Maintenance of Concrete Structures (Jan. 2001).

#### 4.1 Durability design of new concrete structures [4]

Performance-based durability design was introduced in the “Standard Specification of Concrete Structures” by the Concrete Committee of JSCE in 2000. Although durability of concrete structures was considered important in the previous specifications, performance-based design method was not used. The previous specifications described the importance of durability by proposing that the concrete structures are durable for a long time when specified materials, mixes, covers, etc. are used. But these specifications did not account for the time, in an explicit manner.

The proposed performance-based new durability design can be summarized requires that the concrete structure should be quantitatively checked whether the structure possesses required performance over the entire designed period. Thus, the degree of deterioration of the structure in service on account of a specific cause (mechanism) needs to be specified. Also, to ensure that performance of a structure remains above the specified degree of deterioration, the required performance also, needs to be specified.

To examine the performance on durability, a scheme similar to the limit state design scheme was introduced, and the required equation can be written as follows:

$$\gamma_i \cdot A_d / A_{\text{lim}} \leq 1.0$$

where,  $A_d$  and  $A_{\text{lim}}$  are the designed performance of the structure at specified time considering the specified deterioration cause, and the limit of the performance of the structure, respectively, and  $\gamma_i$  is a coefficient to take into account the importance, etc. of the structure.

Generally, the following deterioration items need to be examined, though sometimes, others such as fatigue loading, may also be examined.

- Corrosion of steel bars due to carbonation of concrete
- Corrosion of steel bars due to chloride penetration into concrete
- Deterioration of concrete due to freezing and thawing
- Deterioration of concrete due to chemical attack
- Deterioration of concrete due to alkali-aggregate reaction
- Water-tightness of concrete
- Deterioration of concrete due to fire

Figure 4 shows an example of the calculated result for minimum cover thickness to prevent carbonation induced corrosion at different design service lives for concretes with ordinary Portland and blast furnace slag cements. As shown in the figures, the required cover thickness and water-cement ratio changes substantially, depending upon the type of cement used, the environment (dry or wet) around the structure.

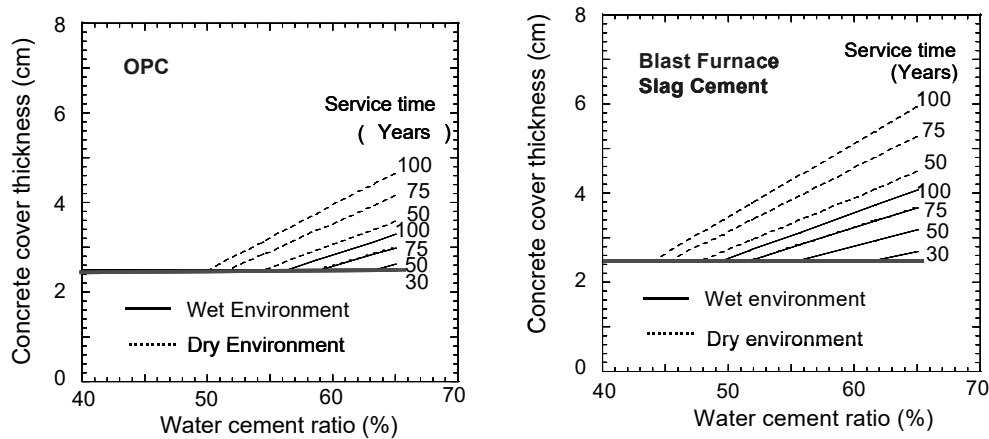


Figure 4: Concrete cover and water-cement ratio for concrete made using Ordinary Portland and Blast Furnace Slag cement

#### 4.2 Methods of maintenance of existing structures [6])

The methods used in the new Standard Specification are basically the same as the conventional method. The difference is that the new method requires maintaining the structure within their required performances throughout their service lives, using the following basic principles:

- To maintain a structure, performances required for the structure must be clearly defined,
- The performance(s) required for general structures are “safety”, “serviceability”, “hazards to the public”, “aesthetics and landscape” and “durability” (See Figure 5).
- Structures must be maintained according to the designated maintenance category by formulating an appropriate maintenance program to retain the performances within the specified tolerances throughout their service life. The system for maintenance includes adequate “initial inspection”, “deterioration prediction”, “inspection”, “assessment/judgment”, “remedial measures”, and “record” (See Figure 6).

As mentioned in items (1) and (2), Figure 5 shows the classification of required performances of a general structure. Compared to other performances, “durability” performance is to keep the structure within their tolerances throughout their lives.



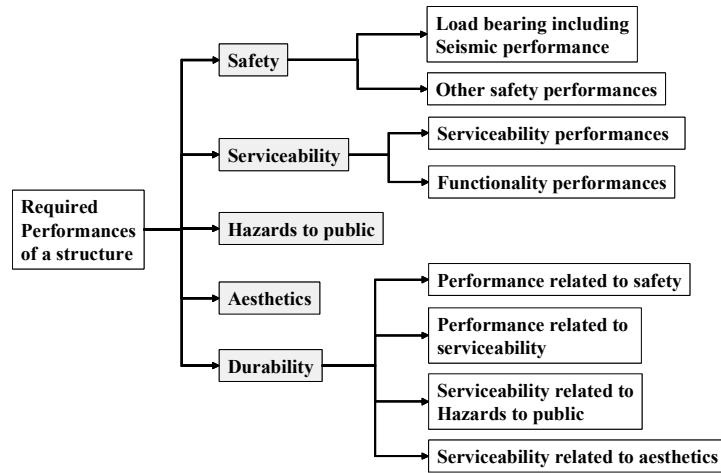


Figure 5: Classification of required performance(s) of a structure [6]

Also, considering item (3), Figure 6 shows how the maintenance operation should be carried out. The details are highlighted below.

- Structures must be maintained according to a designated maintenance category by formulating a maintenance program to retain the performance within the specified tolerances throughout their service life. And maintenance system includes adequate “initial inspection”, “deterioration prediction”, “inspection”, “assessment/judgment”, “remedial action”, and “record”.
- To maintain a structure, in addition to assessment and evaluation at the time of inspection, assessment and evaluation should be carried out throughout the service life based on prediction of deterioration.
- To predict the deterioration, required performances of the structure, and the design service life must be clearly defined and stated
- Records for design, construction, initial inspection, deterioration prediction, periodical inspection, assessment and/or evaluation, and remedial actions must be kept throughout the service life.

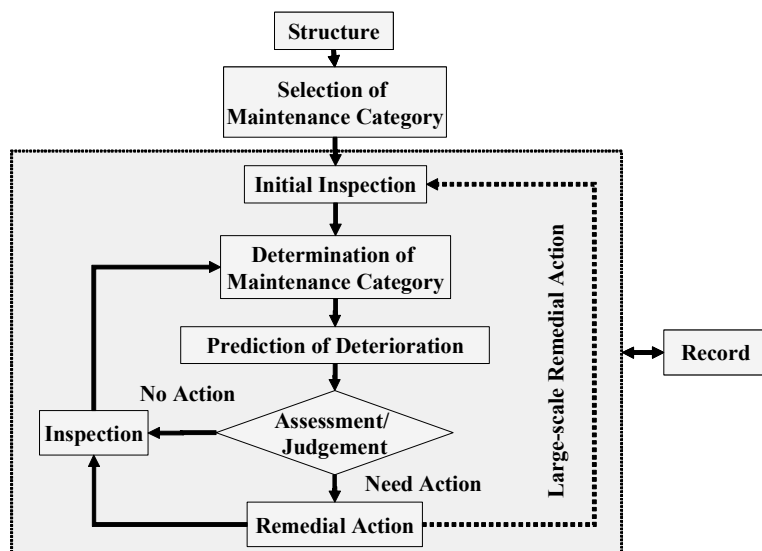


Figure 6: Flowchart for maintenance of concrete structures [6]

One of the difficulties in the maintenance operation is prediction of degree of deterioration at the end of their service lives. Several efforts have been made to quantify deterioration [5,6]. In the published Standards, several quantitative prediction methods have been cited as references for structures suffering cyclic fatigue loads, carbonation induced corrosion and chloride induced corrosion. Whereas in case of cyclic fatigue, S-N curves are used to predict the service life, in the case of carbonation and chloride induced corrosion of steel bars, diffusion equations for carbon dioxide and chloride are used to predict the degree of corrosion. Using these methods, an estimate of the degree of deterioration can be made. But for other deterioration problems, for whom a quantitative model is presently not available, a qualitative method “Grading method” has been suggested, and it is hoped that research effort in the future in these areas will enable development of appropriate tools.

The commonly used grading of apparent defects related to the progress of deterioration is to classify the deterioration stages to “initiation”, “propagation”, “acceleration”, and “deterioration” stages. From the results of detailed inspection, the degree of deterioration can be estimated as shown in Figure 7. This is an example of corrosion induced deterioration. As can be seen from the figure, initiation of corrosion takes place some years after the structure is in service. Even when corrosion starts, it is difficult to inspect whether corrosion has already started or not by visible inspections. When corrosion proceeds to certain amount, cracks on concrete may appear due to expansion of corroded steel bars. This shows that when cracks are observed on concrete, it is already in the stage of propagation.

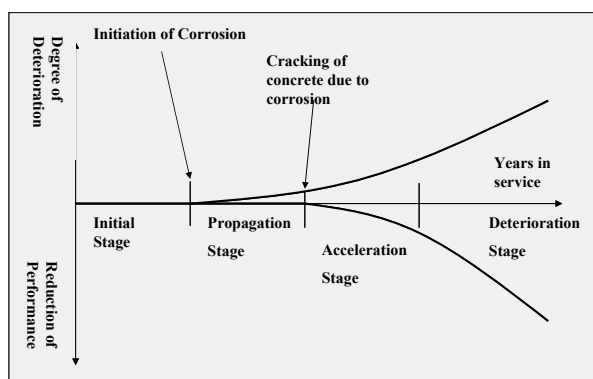


Figure 7: Estimation of deterioration degree by grading method [6]

## 5.0 CONCLUDING REMARKS

Engineering is not always complete, and further research works are needed. To sustain existing structures, durability of the structure is important. One good method is to construct durable structures, but for the existing structures maintenance is the only way to deal with the problem. Although concrete committee of JSCE has set up a good system for maintenance of existing concrete structures, there are still many things to be done: not only researches but also education to the students and engineers

about durability and maintenance. I hope this paper may become a help to the concrete engineers of the world who are trying to design, construct and maintain concrete structures.

## ACKNOWLEDGMENT

The author would like to send sincere thanks to Dr. Sudhir Misra (IIT, Kanpur, India) and the members of Concrete Committee of JSCE (Chairman: Prof. Kyuichi Maruyama) allowing me to explain some of the outputs of the committee works related to the Standard Specification of Concrete Structures. English version of the specification is now being translated by the Translation Committee (Chairman: Dr. T. Ueda) and will be published by March 2005.

## REFERENCES

- [1] Uomoto T. and Misra S. *Role of Engineers to Improve Quality of Concrete Structures*. Proceedings of EASEC-8, 2001.10
- [2] Izumi S. et al. *Non-destructive Inspection of Concrete using High Energy X-ray CT/DR*. Proceeding of 54th General meeting of JSCE, Vol. 5, JSCE, 1999.9 (in Japanese).
- [3] Hirata T. et al. *Application of High Density Ultra-sonic Measurement to Inspect Internal Defects of Concrete*. SEIKEN Leaflet 308, IIS, University of Tokyo, 2001.6 (in Japanese).
- [4] Concrete Committee. *The Standard Specification for Construction Works of Concrete Structures*. JSCE, Jan. 2000 (in Japanese).
- [5] Concrete Committee. *References for "The Standard Specification for Construction Works of Concrete Structures"*. JSCE, Jan. 2000 (in Japanese).
- [6] Concrete Committee. *The Standard Specification for Maintenance of Concrete Structures*. JSCE, Jan. 2001 (in Japanese).

## APPENDIX

The contents of the Standard Specifications for Concrete Structures (2002) "Structural Performance Verification" are reproduced below:

Chapter 1	General
Chapter 2	Basic of design
Chapter 3	Design values for materials
Chapter 4	Loads
Chapter 5	Structural analysis
Chapter 6	Verification of structural safety
Chapter 7	Verification of serviceability
Chapter 8	Verification of fatigue resistance
Chapter 9	General structural details
Chapter 10	Prestressed concrete
Chapter 11	Composite steel and concrete structure
Chapter 12	Design of members
Chapter 13	Strut-and-tie model

The contents of Standard Specifications for Concrete Structures (2001) “Maintenance” are reproduced below:

#### PART 1: MAINTENANCE

Chapter 1	General
Chapter 2	Required performance for concrete structures
Chapter 3	Basic principles for maintenance
Chapter 4	Identification of deteriorating mechanism
Chapter 5	Initial inspection
Chapter 6	Routine inspection
Chapter 7	periodic inspection
Chapter 8	Detailed inspection
Chapter 9	Extraordinary inspection
Chapter 10	Techniques of testing and surveying
Chapter 11	Remedial measures
Chapter 12	Records

#### PART 2: STANDARDS FOR MAINTENANCE

Chapter 13	Standard maintenance method for carbonation induced deterioration
Chapter 14	Standard maintenance method for chloride induced deterioration
Chapter 15	Standard maintenance method for frost attack
Chapter 16	Standard maintenance method for chemical attack
Chapter 17	Standard maintenance method for alkali aggregate reaction
Chapter 18	Standard maintenance method for fatigue of RC slab of road bridge
Chapter 19	Standard maintenance method for fatigue of RC beam of railway bridge

# **RECENT ADVANCES IN ASSESSMENT TECHNOLOGY OF INFRASTRUCTURES IN KOREA**

KEUN JOO BYUN  
Yonsei University, Seoul, Korea  
byun@yonsei.ac.kr

## **ABSTRACT**

*Infrastructures are very important, capital equipments for a country. In spite of their importance, Korea is still suffering from the global competitiveness of the infrastructures nowadays. This would lead the role of government in investment and maintenance for our social overhead capital (SOC) to be increased.*

*While most of developed countries have continually invested on expansion of the SOC and development of the assessment technology for their infrastructures, we have just recognized the need of investment for maintenance and assessment of the infrastructures in the 1990's and recently started to propose high-tech health monitoring systems and assessment technologies for our infrastructures.*

*In this paper, we present the status of assessment techniques for our infrastructures and also introduce a road map for the development of an assessment technique in a long-term point of view including the service life prediction technique, durability serviceability load-carrying capacity assessment technique, health monitoring technique, and safety assessment technique.*

## **1.0 INTRODUCTION**

The SOC is an infrastructure that offers the basis of national economic activities. Hence, principal infrastructures (road, railroad, harbor, airport, etc.) would be appropriately supplied and continuously maintained for the global competitiveness, and an assessment technique for the infrastructures would be also systematically developed for the effective investment of infrastructures as well. That is because the collapse and reconstruction of the infrastructures are able to lead not only human life and property to be lost, but also national economy to be damaged, for examples.

As the construction business has been rapidly grown with the construction boom of Middle East in the 1970's, a lot of infrastructures in Korea have been constructed in a short time period due to the increased demand for the infrastructures along with the high growth of economy. However, it is true that the investment for developing an assessment technique has been rather neglected compared with the quantitative growth of the SOC projects (Oh and Park, 2000).

In this paper, an assessment technique for the Korean infrastructures and its road map are introduced for the effective investment of the infrastructures.

## 2.0 CURRENT STATUS OF INVESTMENT AND ASSESSMENT TECHNOLOGY FOR INFRASTRUCTURES

### 2.1 Current status of investment in infrastructures

The SOC investments have been increased to stimulate the economic activities and to strengthen the global competitiveness. In 2002, the SOC investment against gross domestic product (GDP) of Korea is 17.7% of the Korean GDP. Figure 1 shows the ratios of the SOC investments against the national budgets between 1995 and 2002. Figure 2 shows the statistics of the infrastructures in Korea. As shown in Figure 1, the demand for the infrastructures and national investments are increasing by about 2% every year. Although Figure 1 is not enough to completely show a comparison with the developed countries, it still shows that the SOC projects have great importance as a fundamental interest in Korea (Ministry of Construction and Transportation, 2001).

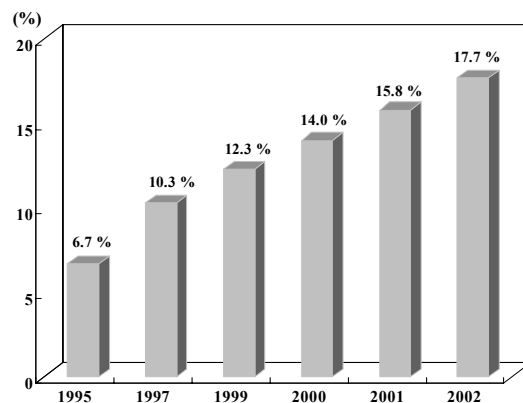


Figure 1: Ratio of investment in SOC to national budget

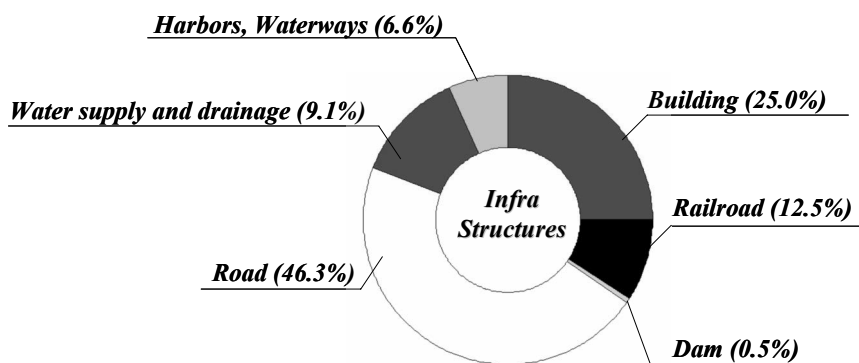


Figure 2: Statistics for infrastructures in Korea

## 2.2 Current status of assessment technology of infrastructures

For several decades, the need of the SOC expansion has consistently existed, and the demands for construction of the infrastructures, such as bridge, road, railroad, harbor and bay, dam, waterway, water supply and drainage system, and underground structure have also rapidly increased. As for their effective maintenance, some research institutes (e.g., specified organizations and structural consultant companies) have carried out the SOC assessment, but the results are not enough for the current Korean infrastructures. Figure 3 shows the levels of design, construction, and maintenance technologies of infrastructures in Korea. It is also shown that the maintenance techniques of infrastructures (road, bridge and tunnel) in Korea are only ranging from ~67% to ~72% in comparison of the technically developed countries (Oh and Park, 2000).

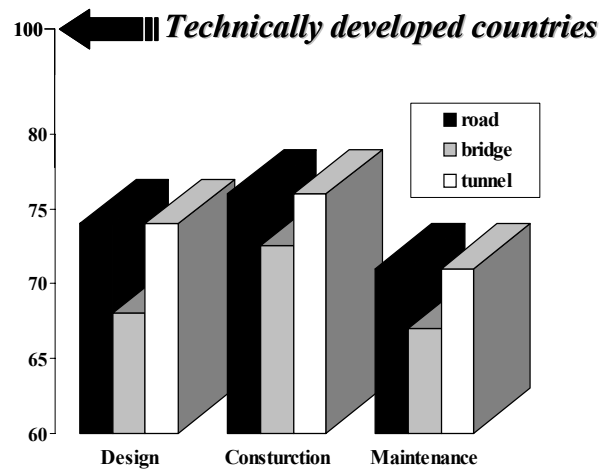


Figure 3: Level of design, construction, and maintenance of infrastructures in Korea

Until the 1960's, the developed countries have spent a lot of costs for the replacement of infrastructures because of the lack of the SOC assessment and maintenance systems. However, since the 1980's, the developed countries have consistently conducted researches to develop the efficient maintenance technologies for the infrastructures. As a result of the development of partially integrated SOC maintenance systems, the developed countries were able to get rid of the inefficiency due to double investments and reconstructions. In case of the United Kingdom, the SOC investment in the maintenance and assessment systems had already been up to 28% of the total construction volume in 1973 and reached out 38% in 1983. However, the SOC maintenance and assessment costs in Korea were only 8% of the total construction volume. This means that the international competitiveness of overall management of the infrastructures in Korea was very low in 1983. It was from the middle of the 1990's in which the importance and the necessity of investment for maintenance and assessment of infrastructures were understood and made researchers in the academies

conduct basic researches on the durability, serviceability and life cycle cost of infrastructures in Korea. Then, these efforts made possible for extensive researches on integrated analysis, design and construction, and maintenance system for infrastructures. Recently, completed National Technology Road Map (NTRM) considers an essential technology in advanced infrastructure construction technologies and Korean government continuously invests for the technical developments of maintenance and assessment in the infrastructures (Byun, 2003).

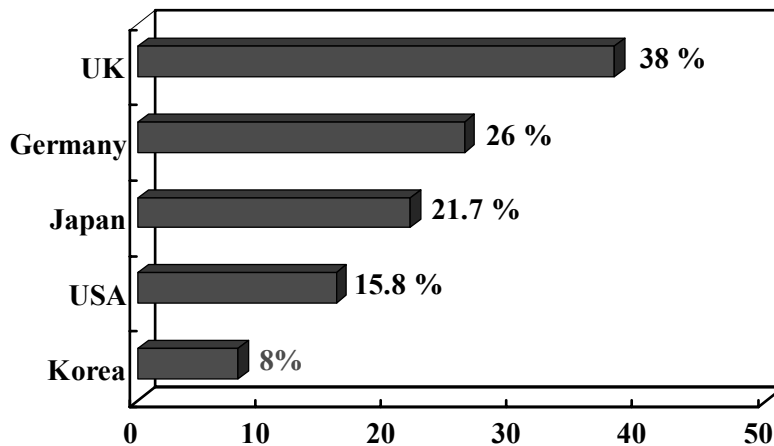


Figure 4: Comparison of investment in maintenance to total construction volume.

### 3.0 ROAD MAP IN ASSESSMENT TECHNOLOGY OF INFRASTRUCTURES IN KOREA

#### 3.1 Master plan

As for the systematic assessment of infrastructures, it is necessary to develop the assessment technologies of infrastructures based on the application of a new technique and the development of new inspection equipments. An investment from the government for efficient maintenance of infrastructures is also essential. Requirements of the master plan to develop assessment technologies are as follows:

- The assessment technique must be compatible with general maintenance system of infrastructures.
- The technique must be set as the objective of standardization because nonstandard techniques may induce additional expense.
- The technique must be innovative, intelligent developments including the integration with IT technology and database of information.
- In order that all users are easy to use, the automatic measuring technique is essential.
- The developed individual technique on the element level must be utilized with a good application and be able to commonly expand.



Hence, the assessment technique must be a generalized technique with the capacities of analysis, estimation, and management during the service period.

### 3.2 Road map

As for the effective management of infrastructures, the optimized assessment technique is essential. To achieve this purpose, four requirements must be focused as shown in Figure 5. (1) health monitoring technique, (2) safety assessment technique, (3) durability assessment technique, and (4) modeling for service period and life time. Through these techniques, the unified assessment system for infrastructures can be established, so that the advanced assessment technology for infrastructures under various conditions can be integrated and widely used. Figure 5 shows the road map of related researches on the assessment technology.

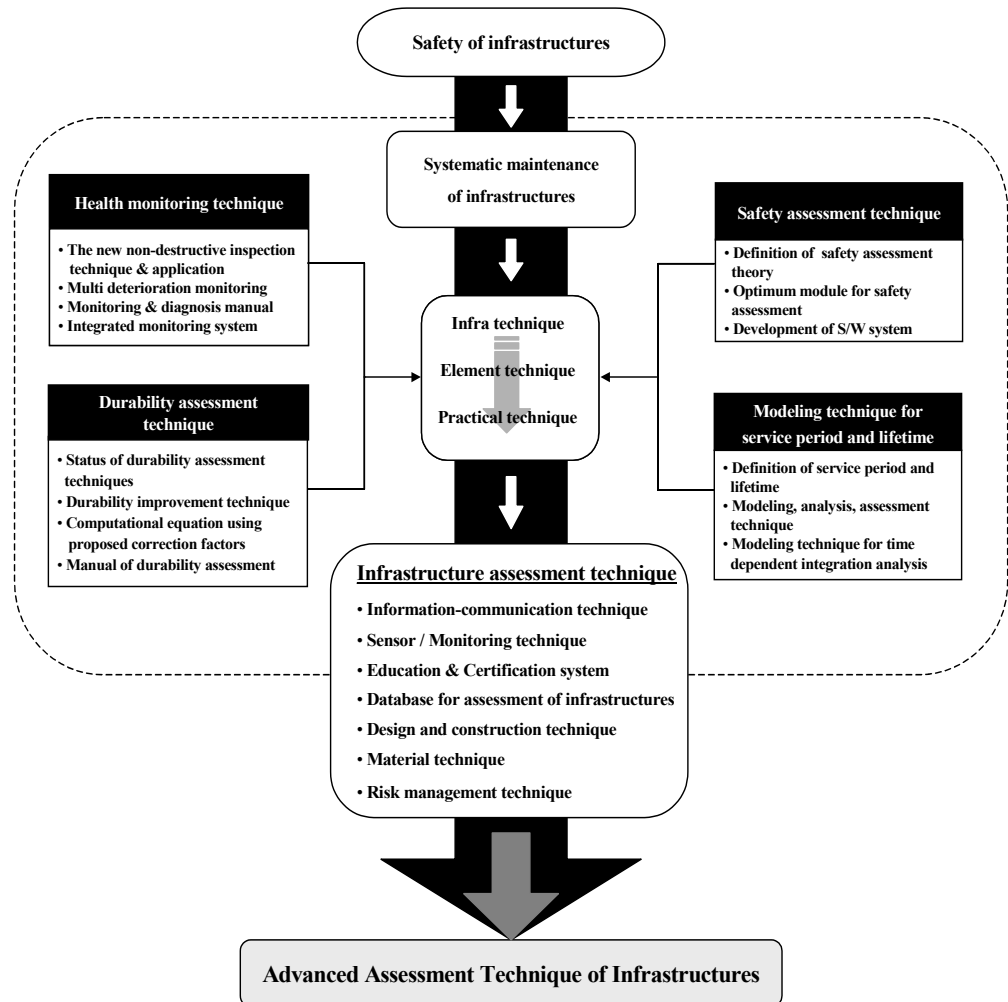


Figure 5: Road Map of related research on assessment technology

## 4.0 CONCLUSION

There exist many subjects to improve for the assessment technologies of infrastructures. Recently, the advanced assessment technologies including health monitoring technique, safety assessment technique, durability assessment technique, and modeling technique for service period life time are proposing in Korea as the first stage.

In this paper, a technical road map on the assessment technology of infrastructures was proposed. A main concept of the road map is the integration of individual developments and combination of all the related technologies even in initiation stage of the research. The ultimate goal of these techniques is to develop an advanced assessment technique of infrastructures in Korea.

## REFERENCES

- Byun, K. J., Kim, M. K., and Song, H. W., 2003. *Advanced Lifeline Systems in Korea*. Proceedings of the 2<sup>nd</sup> International Symposium on New Technologies for Urban Safety of Mega Cities in Asia, ICUS/INCEDE.
- Kim, M. K., and Byun, K. J., 1999. *The Status of Bridge Maintenance in Korea*. Korean Society of Civil Engineers.
- Lee, H. E., and Choi, H. J., 1999. *Sensitivity of Time Domain Modal Identification Technique to Measurement Noise and It's Application to Cable Stayed Bridges*. 5<sup>th</sup> Korea-Japan Joint Seminar on Steel Bridges.
- Ministry of Construction and Transportation, 2001. *Development of Design & Construction Guide for Strengthening Method and Standardization of Load-carrying Capacity Assessment Technique*.
- Oh, K. C., and Park, K. C., 2000. *Evaluation Procedure on Concrete Durability in Korea*. ACI, The Forth ACI/KCI International Conference, 37-46.
- Sim, J., Song, H. W., and Hong, S. G., 2001. *Concrete Technology in Korea*. Workshop on Concrete Issues in Asia, Asian Concrete Forum, Sapporo, Japan, 27-32.
- Song, H. W., Byun, K. J., and You, D. W., 2000. *Evaluation of Retrofitted Capacity of Deteriorated Reinforced Concrete Beams*. ACI Supplementary paper, 47-64.

# **A RISK-BASED DECISION SUPPORT SYSTEM FOR INSPECTION AND MAINTENANCE OF CROSS-COUNTRY PETROLEUM PIPELINES**

PRASANTA KUMAR DEY<sup>1</sup> AND STEPHEN O. OGUNLANA<sup>2</sup>

<sup>1</sup>University of the West Indies, Bridgetown, Barbados, West Indies

<sup>2</sup>Asian Institute of Technology, Pathumthani, Thailand  
ogunlana@ait.ac.th

## **ABSTRACT**

*Pipeline failure can have devastating effect on the health and livelihood of people living within the pipeline corridor. The existing method of pipeline health monitoring, which requires an entire pipeline to be inspected periodically, is unproductive. A risk-based decision support system (DSS) that reduces the amount of time spent on inspection has is presented.*

*The risk-based DSS uses Analytic Hierarchy Process (AHP), a multiple attribute decision-making technique, to identify the factors that influence failure on specific segments and analyzes their effects by determining probability of risk factors. The severity of failure is determined through consequence analysis. From this, the effect of a failure caused by each risk factor can be established in terms of cost, and the cumulative effect of failure determined through probability analysis. The technique does not totally eliminate subjectivity, but it is an improvement over the existing inspection method selection.*

## **1.0 INTRODUCTION**

Cross-country pipelines are the most energy-efficient, safe, environmentally friendly, and economic way to ship hydrocarbons (gas, crude oil, and finished products) over long distances, either within the geographical boundary of a country or beyond it. A significant portion of many nations' energy requirements is now transported through pipelines. The economies of many countries depend on the smooth and uninterrupted operation of these lines, so it is increasingly important to ensure the safe and failure-free operation of pipelines.

While pipelines are one of the safest modes of transporting bulk energy, and have failure rates much lower than the railroads or highway transportation, failures do occur, and sometimes with catastrophic consequences. A number of pipelines have failed in the recent past, with tragic consequences. In 1993 in Venezuela, 51

people were burnt to death when a gas pipeline failed and the escaping gas ignited. Again in 1994, a 36-inch (914 mm) pipeline in New Jersey failed, resulting in the death of one person and more than 50 injuries. Similar failures also have occurred in the UK, Russia, Canada, Pakistan, and India (Hopkins 1994). While pipeline failure rarely causes fatalities, disruptions in operation lead to large business losses. Failures can be very expensive and cause considerable damage to the environment.

Traditionally, most pipeline operators make safety provisions for a theoretical minimum failure rate for the life of the pipeline at the design stage. Safety is considered when selecting pipes and other fittings. To prevent corrosion, providing a high resistance external coating materials electrically isolates a pipeline. As a secondary protective measure, a low-voltage direct current is impressed in the pipe at pre-calculated distance to transfer any corrosion that occurs due to breaks in the coating caused by a heap of buried iron junk, rails, etc. This is called impressed current cathodic protection. The quality of the commodity that is being transported through the line is also ensured, and sometimes corrosion-preventing chemicals (corrosion inhibitors) are mixed with the commodity. To avoid deliberate damage of the pipeline in isolated locations, regular patrolling of the right-of-way from the air as well as on foot is carried out, and all third party activities near the route are monitored.

Various techniques are routinely used to monitor the status of a pipeline. Any deterioration in the line may cause a leak or rupture. Modern methodologies can ensure the structural integrity of an operating pipeline without taking it out of service (Jamieson, 1986).

The existing inspection and maintenance practices commonly followed by most pipeline operators are formulated mainly on the basis of experience. However, operators are developing an organized maintenance policy based on data analysis and other in-house studies to replace rule-of-thumb based policies. The primary reasons for this are stringent environmental protection laws (DOT, 1995), scarce resources, and excessive inspection costs. Existing policies are not sharply focused from the point of view of the greatest damage/defect risk to a pipeline. The basis for selecting health monitoring and inspection techniques is not very clear to many operators. In many cases, a survey is conducted over an entire pipeline or on a particular segment, when another segment needs it more. Avoidable expenditures are thus incurred.

A strong reason exists, therefore, to derive a technique that will help pipeline operators select the right type of inspection/monitoring technique for segments that need it. A more clearly focused inspection and maintenance policy that has a low investment-to-benefit ratio should be formulated.

This article introduces a DSS for predicting the risk factor for pipeline failures. This model allows management to formulate a cost-effective, customized, flexible, and logical inspection model. It is established through risk analysis, with the application of the analytic hierarchy process (AHP) (Saaty 1980).

## **2.0 THE ANALYTIC HIERARCHY PROCESS**

Risks are by nature subjective, so to analyze their potential contribution to a failure, the AHP developed by Saaty (1980) is used here. This technique allows subjective and objective factors to be considered in risk analysis and also provide a flexible and easily understood way to analyze subjective risk factors. It is a multiple criteria decision-making technique that permits the active participation of those involved, and provides managers a rational basis on which to make decisions.

Formulating the decision problem in the form of a hierarchical structure is the first step. In a typical hierarchy, the top level reflects the overall objective (focus) of the decision problem. The elements affecting the decision are represented in intermediate levels. The lowest level comprises the decision options. Once the hierarchy has been constructed, the decision-maker begins the prioritization procedure to determine the relative importance of the elements in each level of the hierarchy. The elements in each level are compared pair-wise with respect to their importance in making the decision under consideration. The verbal scale used in AHP enables the decision-maker to incorporate subjectivity, experience and knowledge in an intuitive and natural way.

After the comparison matrices have been created, the process moves on to the phase in which relative weights are derived for the various elements. The relative weights of the elements of each level with respect to an element in the adjacent upper level are computed as the components of the normalized eigenvector associated with the largest eigenvalue of their comparison matrix. The composite weights of the decision alternatives are then determined by aggregating the weights through the hierarchy. This is done by following a path from the top of the hierarchy to each alternative at the lowest level, and multiplying the weights along each segment of the path. The outcome of this aggregation is a normalized vector of the overall weights of the options. The mathematical basis for determining the weights has been established by Saaty (1980).

The AHP has been applied to pipeline project control (Dey *et al.*, 1994), route selection (Dey and Gupta, 2000) and feasibility analysis (Dey, 2001).

### 3.0 METHODOLOGY

The methodology adopted in this study involves the following steps.

**Step 1:** Cross-country petroleum pipeline passes through various terrains and requires originating and a few intermediate pumping stations for transporting petroleum products or crude oil. Therefore, the entire pipeline is classified into a few stretches (preferably in line with its natural stretch i.e. pipeline sections in between two stations).

**Step 2:** All information related to the pipeline including the terrain detail under study is prepared and documented section wise.

**Step 3:** Risk factors that can cause failures are identified. Generally, pipelines fail because of one of these reasons: (i) corrosion; (ii) external interference; (iii) construction and materials defects; (iv) acts of God; and (v) human and operational error.

**Step 4:** A risk structure model is formulated in the AHP framework. Based on the identified risk factors, a hierarchical risk structure is formed (see Figure 1). The goal here is to determine the relative likelihood of pipeline failures. Level II is criteria (risk factors), level III is sub-factors, and level IV is alternatives (the pipeline stretches). Figure 1 shows the AHP model for analyzing risk from a failure perspective.

**Step 5:** Comparison between pairs of risk factors and sub-factors are done to determine the likelihood of pipeline failure due to each factor and sub-factor.

**Step 6:** Pair wise comparison of alternative pipeline stretches, with respect to each risk factor, to determine the likelihood of failure for each pipeline stretch due to each factor is done.

**Step 7:** The results are synthesized across the hierarchy to determine the likelihood of failure of a pipeline stretch and relative comparison with other stretches from failure perspectives.

**Step 8:** Determine specific inspection/maintenance requirements for specific segments, to mitigate risk.

**Step 9:** Determine the expected failure cost of each line by a Monte Carlo simulation.

**Step 10:** Establish a cost-benefit analysis to justify the proposed investment, to suggest design, construction and operation

improvement of future pipelines and to formulate a cost-effective insurance plan for pipeline.

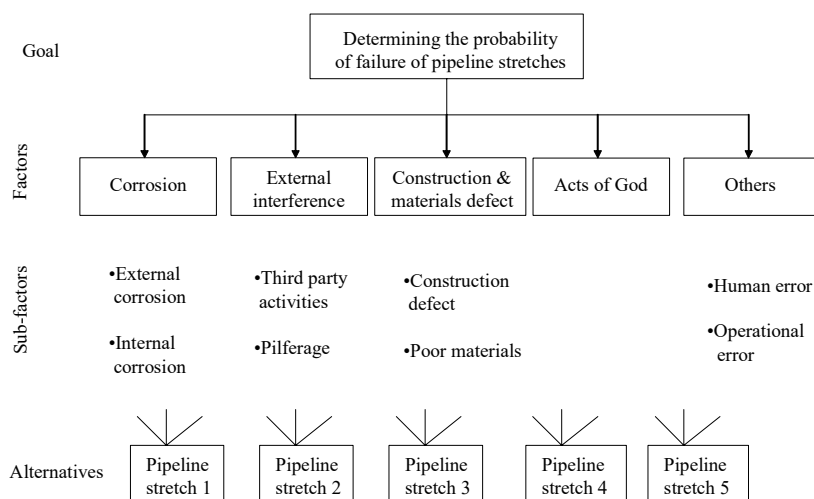
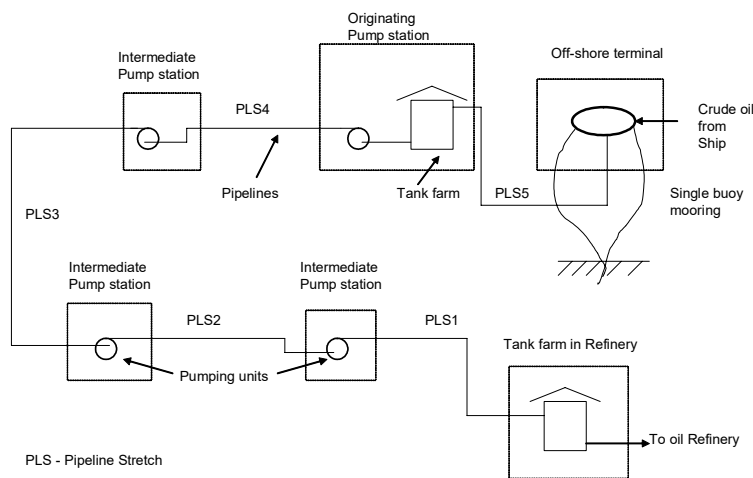


Figure 1: Hierarchical risk structure

#### 4.0 APPLICATION

The entire methodology has been illustrated by a case study application. For reasons of space, only the first seven steps in the methodology are demonstrated in this paper. A crude oil pipeline (length 1500 km) in the western part of India was studied. The throughput of the pipeline is 9 million metric ton per annum (MMTPA) with augmentation capability of 12 MMTPA, having three intermediate booster stations and a offshore terminal. The schematic of the pipelines is shown in Figure 2. The pipeline is 19 years old and has a history of corrosion failure. The poor condition of the coating, as revealed during various surveys and an unreliable power supply to cathodic protection stations are the reasons for this. The line passes through long stretches of socio-economically backward areas and is vulnerable to pilferage and sabotage. In some regions, the right-of-way is shared with other agencies, as such, the chance of external interference is high. Failure data revealed numerous pre-commissioning failures, raising doubts about the quality of construction.

The risk analysis model for the pipeline is formulated by applying the methodology described above. The entire pipeline was classified into five stretches. The risk structure and pair wise comparisons were established through a workshop of the executives who operate various pipelines. Thirty executives participated, each having more than 15 years of experience in pipeline operations.



*Figure 2: Schematic of oil pipelines*

Before formulating the model, they were given full knowledge of pipeline conditions through the database of various pipeline stretches (Table 1) and pipeline record sheet.

A decision-maker can express a preference between each pair as equal, moderate, strong, very strong, and extremely preferable (important). These judgments can be translated into numerical values on a scale of 1 to 9 (Table 2). Elements at each level of hierarchy are compared with each other in pairs, with their respective “parents” at the next higher level. With the hierarchy used here, matrices of judgments are formed. A brainstorming session was held to compare the risk factors. The pipeline executives established a common consensus for the AHP hierarchy, pair wise comparison in factors, sub-factors and alternative levels through group decision making. Disagreements were resolved through reasoning and collecting more information. Their hierarchy contained the details necessary for risk analysis. Table 3 shows the matrix of judgments that resulted.

The final outcomes of each of the pipeline stretch against the risk factors are summarized in Table 4. Both local probability and global probability for each of the five stretches are summed up to derive the probability of a pipeline stretch failure and its position with respect to other stretches. The results of the analysis (Table 4) reveal that the chances of pipeline failure due to corrosion and external interference are greater than other factors.



Table 1: Database of pipeline stretches (figures in km)

Description	Pipe LS 1	Pipe LS2	Pipe LS3	Pipe LS4	Pipe LS5
Length	260	210	180	230	25
Terrain detail:					
Normal	170	95	35	169	7
Slushy	36				
Rocky (hilly)			115	20	
River & canal crossings	4	2		6	
Populated	50	88		35	
Offshore					18
Coal belt		25			
Forest			30		
Soil condition	corrosive	corrosive	Less corrosive	Less corros.	Less corrosive
3 <sup>rd</sup> party activities		More due to coal belt			
Chances of pilferage	Higher due to populated area	Higher due to populated area		Higher due to populated area	
Construction complexity			More due to rock and forest	More due to river crossing	More due to offshore piping
Operational complexity					More due to offshore terminal

Table 2: Scale of relative importance for pair-wise comparison

Intensity	Definition	Explanation
1	Equal importance	Two activities contribute equally to the object
3	Moderate importance	Slightly favors one over another
5	Essential or strong importance	Strongly favors one over another
7	Demonstrated importance	Dominance of the demonstrated in practice
9	Extreme importance	Evidence favoring one over another of highest possible order of affirmation
2, 4, 6, 8	Intermediate values	When compromise is needed

Table 3: Pair wise comparison in factor level

Factors	Corrosion	External Interference	Construction & materials defect	Acts of God	Others	Likelihood
Corrosion	1	2	3	7	3	0.40
External Interference	1/2	1	3	5	3	0.29
Construction & materials defect	1/3	1/3	1	3	2	0.14
Acts of God	1/7	1/5	1/3	1	1/4	0.05
Others	1/3	1/3	1/2	4	1	0.12

The following additional observations were made from the risk analysis study:

- The pipeline stretches 1 and 2 are vulnerable from external corrosion due to slushy terrain, whereas pipeline stretches 4 and 5 are vulnerable to internal corrosion due to long submerged pipe sections.
- External interference due to the third party activities is a major problem in pipeline stretches 2 because of coal mining activities, whereas in stretches 4, it is due to major river crossings and canal crossing.

- External interference due to malicious reasons prevail in stretches 1 and 2 because they pass through a long and highly populated industrial areas.
- The pipeline stretch 3 passes through mostly rocky terrain, exposing the pipe to various types of failure due to construction and poor materials. As this stretch is vulnerable to subsidence problem, the likelihood of pipeline failure from acts of God is quite high along with high chance of failure due to construction defect and poor materials.
- The stretch 5, i.e. the offshore pipeline is very sensitive to operational and human errors as well as failure due to various natural calamities.
- All pipeline stretches are ranked with respect to their failure chances, the failure prone pipeline stretches 5, 1, 2, 4, and 3 in decreasing order of vulnerability.

*Table 4: Likelihood of failure of various pipeline stretches*

Factors	Like- lihood	Sub-factors	Like- lihood	PLS <sub>1</sub>	PLS <sub>2</sub>	PLS <sub>3</sub>	PLS <sub>4</sub>	PLS <sub>5</sub>
Corrosion	0.40	External	0.221	0.108	0.064	0.007	0.011	0.031
		Internal	0.181	0.038	0.022	0.020	0.042	0.060
External Interferen ce	0.29	3 <sup>rd</sup> party activities	0.186	0.030	0.078	0.011	0.061	0.006
		Malicious	0.100	0.033	0.039	0.005	0.018	0.005
Constructi on & mat. defect	0.14	Constructio n defects	0.072	0.012	0.007	0.028	0.007	0.018
		Poor mats.	0.072	0.006	0.007	0.027	0.016	0.017
Acts of God	0.05		0.05	0.006	0.001	0.014	0.006	0.020
Others	0.12	Human error	0.048	0.001	0.005	0.003	0.008	0.030
		Operational error	0.072	0.001	0.003	0.009	0.003	0.056
Likelihood of failure of various pipeline stretches				0.236	0.227	0.123	0.172	0.242
Ranking				2	3	5	4	1

PLS – Pipeline stretch

## 5.0 SUMMARY AND CONCLUSIONS

As pipelines pass through varied terrain, the condition of pipelines varies widely across the entire length and throughout the service life. Inspecting entire pipelines through specific a inspection methodology/ tool cannot detect problems in the entire length as inspection tools are designed to detect specific problems only. On the

other hand, inspecting the entire pipeline by various tools to detect the entire associated problems is not cost effective.

A decision support system (DSS) model in AHP framework, which determines the likely problems associated with each stretch with the involvement of the experienced pipeline operators has been presented. This leads to the development of a cost-effective inspection and maintenance strategy for the pipelines. The same methodology can be used for any operating unit to develop strategic DSS for inspection and maintenance.

The method of analysis described here can be used to: (i) reduce subjectivity in the decision making process when selecting an inspection technique; (ii) identify the right pipeline or segment for inspection and maintenance; and (iii) demonstrate the risk level to governments and other regulatory agencies.

The technique does have limitations, because subjectivity is not totally eliminated. For instance, the weightage against each of the failure factors is based upon experience, available data and perception of the pipeline executives and decision-makers. Despite these limitations, a cross-country petroleum pipeline inspection and maintenance policy formed on the basis of the methodology can be an effective tool to mitigate risk

## REFERENCES

- Dey, P K, Tabucanon, M T, and Ogunlana S O., 1994. *Planning for project control through risk analysis: a case of petroleum pipeline laying project*. International Journal of Project Management, 12:1, 23-33.
- Dey, P. K. and Gupta, S. S., 2000. *Decision support system yields better pipeline route*. Oil and Gas Journal, 98.22:10, 68-73, May 29.
- Dey, P K., 2001. *Integrated approach to project feasibility analysis: a case study*. Impact Assessment and Project Appraisal, Forthcoming 2001.
- Hopkins, P., 1994. *Ensuring the Safe Operation of Older Pipelines*. International Pipelines and offshore Contractors Association, 28<sup>th</sup> Convention. September.
- Jamieson, R. M., 1986. *Pipeline Integrity Monitoring*. Pipeline Integrity Conference Aberdeen, Scotland. October 29-30.
- Saaty, T. L. The Analytic Hierarchy Process. New York: McGraw-Hill, 1980.
- Pipeline Safety Regulations*. Department of Transportation(US), 1<sup>st</sup> October 1995.

# **IMPACT RESISTANCE OF FRP-CONCRETE SANDWICH PANELS**

KIANG HWEE TAN

Department of Civil Engineering,  
National University of Singapore, Singapore  
cvetankh@nus.edu.sg

## **ABSTRACT**

*Structures may be subjected to impact loads caused by events like earthquakes or strong winds or terrorist acts or accidents, during their service life. This study examined the use of fiber-reinforced polymer (FRP) panels and FRP-concrete sandwich panels to resist impact loads. Repeated impact tests using a hemispherical impactor of 43 kg falling from a height of 4 m in a drop-weight test rig, were carried out on square panels of different thicknesses, with or with concrete, and with carbon and glass FRPs as the reinforcing material. Both the FRP and FRP-concrete sandwich panels exhibited good impact characteristics in terms of resisted impact force, impulse and energy absorption capacity. For FRP panels, the impact resistance improved with the number of plies of FRP sheets. On the other hand, the impact resistance improved with the thickness of the FRP system in the case of glass FRP-concrete panels but not for the carbon FRP-concrete panels, due to the brittleness of carbon fibers under transverse shear. A 5-mm thick concrete panel sandwiched between two 4-ply glass FRP sheets suffered a punch through failure only after twelve impacts.*

## **1.0 INTRODUCTION**

Concrete structures may be subjected to impact or impulsive loads during their service life due to falling or flying objects, due to events such as earthquakes, strong winds, explosions or vehicular accidents. These include protective structures to shield motorways from falling rocks, or bridge decks and piers against impact by vessels (Struck and Voggenreiter, 1975). They also include defence shelters, ammunition bunkers, and firing ranges, which are designed to resist small weapon effects or sometimes, fragmentation from small bombs.

The objective of this study is to examine the impact resistance of fibre-reinforced polymer (FRP) and FRP-concrete panels, thereby determining the suitability of the material in protective works. The advantages of using FRP systems are its low unit weight, and its installation speed. To achieve the objective, a series of impact tests using a drop-weight test rig was conducted on FRP panels as well as FRP-concrete sandwich panels. The test parameters included two types of FRP composites, and the thicknesses of the FRP and concrete layers. The impact resistance was evaluated in terms of resisted impact load, impulse, energy absorption capacity and number of impacts to failure.

## 2.0 TEST PROGRAMME

Two series of specimens, as shown in Table 1, were prepared. Series P consisted of FRP panels, each measuring 1000 mm by 1000 mm on plan, and made with four, six or ten plies of carbon or glass fibre sheets. Series S comprised FRP-concrete sandwich panels, in which a concrete lay, 5 or 10 mm thick, was bonded with two or four plies of glass or carbon FRP sheets on each face. The FRP sheets were of uni-directional fibres, and were laid ply by ply in alternating orthogonal directions.

*Table 1: Test Specimens*

Series	Specimen Designation	Concrete thickness (mm)	Type of FRP Reinforcement	Measured FRP thickness (mm)	No. of FRP plies
P	PC4	-	Carbon sheet	3.45	4
	PC6	-	Carbon sheet	5.75	6
	PC10	-	Carbon sheet	10.14	10
	PG4	-	Glass sheet	5.75	4
	PG6	-	Glass sheet	6.95	6
	PG10	-	Glass sheet	10.61	10
S	SC25	5	Carbon sheet	9.52	2x2
	SC45	5	Carbon sheet	12.31	2x4
	SC210	10	Carbon sheet	14.14	2x2
	SG25	5	Glass sheet	13.40	2x2
	SG45	5	Glass sheet	16.50	2x4
	SG210	10	Glass sheet	17.29	2x2

## 2.1 Materials

Ordinary Portland cement, potable water and natural river sand passing through 4.75 mm sieve, were mixed in the proportion of 1:2:0.5 to form the mortar concrete layer in Series S specimens. As specified by the manufacturers, the carbon fibre sheet weighs 300 g/m<sup>2</sup>, and has a design thickness of 0.165 mm, and a tensile strength of 3500 MPa, with a modulus of elasticity of 230 GPa and a rupture strain of 1.5 %. The glass fibre fabric has a weight of 900 g/m<sup>2</sup> and design thickness of 0.355 mm, tensile strength of 1700 MPa, and rupture strain of 2.0 %. The primer and saturant for the bonding of the fibre sheets were each supplied in two parts, consisting of a main and a hardening agent, to be mixed in the ratio of 3:1 by weight.

## 2.2 Fabrication of Specimens

A template for making the FRP panels was constructed. It consisted of two aluminum strips set 1000 mm apart and adhesively attached to a plastic sheet placed on a wooden plank. A piece of Perspex was used to form the third side. The plastic sheet was waxed to facilitate demoulding. The first FRP sheet was then placed onto the plastic sheet and taped down on one edge. The FRP sheet was flipped over and saturant was applied to

the bottom plastic sheet. The FRP sheet was then flipped back onto the plastic sheet, and a coat of saturant was applied. Care was taken to flatten the FRP sheet so as to prevent any air voids from appearing. The second FRP layer was laid in the orthogonal direction, and the same procedure was repeated, until the required number of plies of FRP sheet was placed. After that, a piece of perspex was placed with some weights on the FRP panel, to achieve uniform thickness. The panel was left to cure overnight and demoulded the next day. Mild steel plates measuring 50 mm wide and 2 mm thick were bonded along the four edges of each panel to facilitate clamping down during testing.

In the case of sandwich panels, the concrete layers were cast in wooden formwork, demoulded after a day, and placed under wet gunny sacks for 7 days. Six 100 mm cubes were also cast and cured in the same manner for each panel for the purpose of strength determination. After the concrete panels had gained sufficient strength, they were ground on both faces using a sandpaper grinder. Primer was applied to one of the faces evenly and allowed to dry before the FRP sheets were installed, taking care to remove air bubbles and excess saturant using a roller. The installed FRP sheets were left to cure. The specimen was turned over the next day and the process of FRP installation was repeated on the other face of the concrete layer to form the sandwich panel.

### 2.3 Test set-up and instrumentation

The impact tests were carried out using a drop weight test frame, consisting of a square horizontal frame welded to columns which were bolted on to the floor. Each panel was placed on the horizontal frame on four edges with its centre aligned with the impactor. The panel was restrained at the supports using steel bolts and/or clamps. Electrical strain gauges and potentiometers were used to measure strains and displacements during impact, near the center of the specimen, as shown in Fig 1.

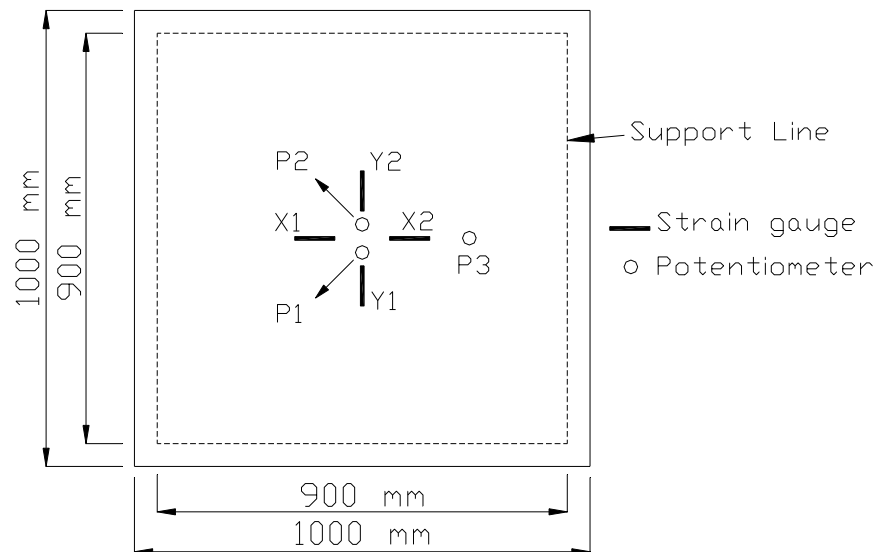


Figure 1: Location of strain gauges and potentiometers (plan view)

For each test, a 43-kg striker with a hemispherical head was raised to a height of 4 m and allowed to drop under its free weight on the centre of the specimen. Its line of fall was kept in the vertical direction by smooth rollers running along the aluminum guides. An accelerometer was fixed at the tip of the impactor to measure its deceleration and hence the impact force. The impact velocity was measured by two laser diodes. The strain gauges, potentiometers, laser diodes and accelerometer were connected to a data acquisition system, and data collection was triggered by the laser diode first crossed by the impactor upon release.

The recorded data was filtered to remove electrical noise due to the electronic systems and the mechanical system. A cut-off frequency of 3 kHz was selected using a trial and error method based on Fast Fourier Transform (FFT) computation.

### **3.0 TEST RESULTS AND DISCUSSION**

#### **3.1 Behavior of FRP panels**

Panels PC4 and PC6 were punched through at the first blow. PG4 took six blows before the potentiometers were damaged. The remaining panels (PC10, PG6 and PG10) were subjected to a maximum of ten blows.

##### **3.1.1 Failure characteristics**

Failure was catastrophic for PC4 and PC6 as the impactor perforated the carbon FRP panels. The measured FRP strains around the perforation were as high as 0.8%. Besides rupture of fibres as shown in Fig. 2, inter-ply delamination between the carbon fibre sheets was observed.



*Figure 2: Appearance of FRP panels after failure*

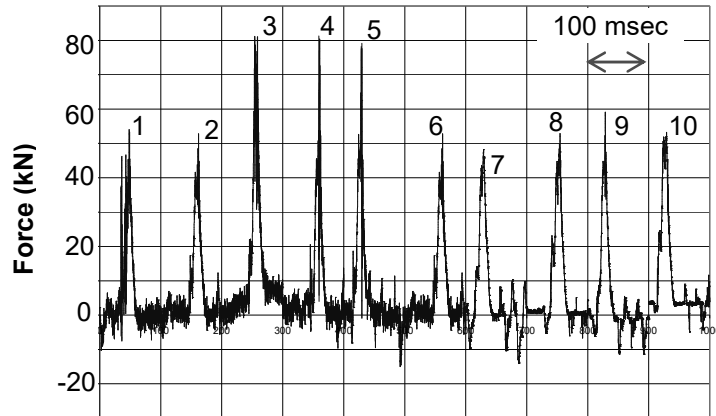
##### **3.1.2 Impact force**

The impact force on the panel, determined from the mass and deceleration of the impactor, was found to increase with the panel thickness

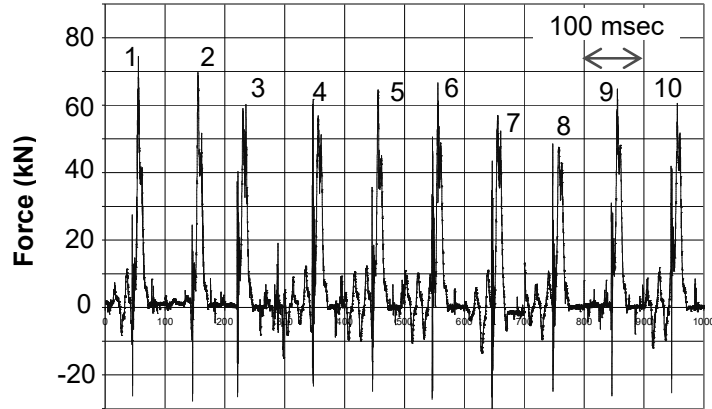


and hence stiffness. For the carbon FRP panels, it measured 80 kN for PC4 and 110 kN for PC6 for the first impact. The value was low at 55 kN for PC10, but it rose to about 80 kN for the third impact. For the glass FRP panels, the values were about 32 kN, 68 kN and 75 kN, respectively, for PG4, PG6 and PG10.

Also, the impact force generally decreased with the number of impacts, due to the loss of stiffness of the panels. Fig. 3 shows that the loss in stiffness appears to be more drastic in carbon FRP panels.



(a) PC10



(b) PG10

Figure 3: Impact force-time characteristics of FRP panels

### 3.1.3 Impulse

The area under the impact force-time graph gives the impulse, which is a measure of the intensity of the impact load. Test results indicated that the impulse increased with the panel thickness in the initial few impacts. Thereafter, the impulse was about the same and equal to about 550 Ns regardless of the type and thickness of the panels, as shown in Fig. 4, in

which the value for PC10 at the third impact is probably due to measurement error.

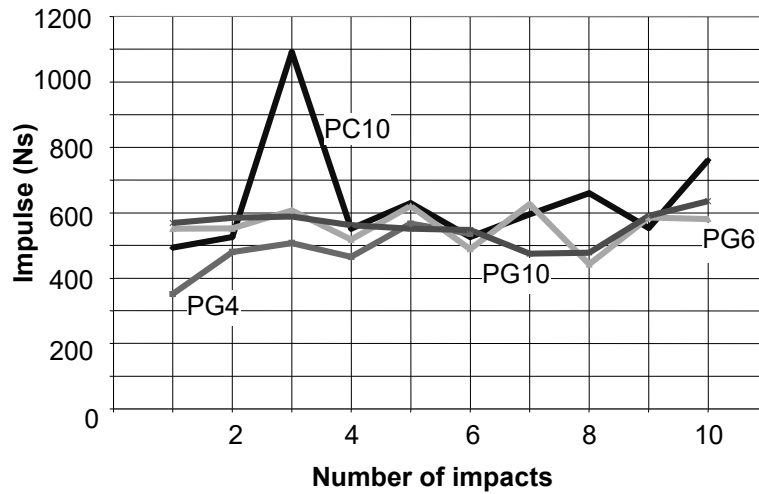


Figure 4: Impulse on FRP panels

### 3.1.4 Energy absorption

The maximum instantaneous displacement was lower for thicker panels as expected. However, the variation in maximum displacement was observed to be small for the glass FRP panels tested. Also, despite being thicker, PG10 registered a slightly higher maximum displacement than PC10, probably due to the lower modulus of elasticity of glass FRP compared to carbon FRP. The number of impacts did not affect the maximum displacement, probably as the panels continued to behave elastically and there was no permanent deformation.

The energy absorbed and dissipated by the panel was determined from the force-time and displacement-time relations. The cumulative energy absorbed with the number of impact is shown in Fig. 5. Specimen PC10 absorbed the most energy due to a higher impact force. Among the glass FRP panels, the energy absorbed generally increased with the panel thickness, although the results of PG4 and PG6 did not differ much.

## 3.2 Behavior of FRP-concrete sandwich panels

At the time of testing, the concrete compressive strength averaged 54 MPa for carbon and 60 MPa for glass FRP-concrete sandwich panels. All panels were punched through at the first or second impact, except SG45 which took twelve impacts without failing. The strains measured at the bottom of the carbon FRP-concrete panel near the centre were between 0.3 and 0.7%, with the higher value in the fibre direction of the outermost FRP ply. The strains were higher in glass FRP-concrete panels at between 1 and 2%, except for SG45 where the strains were lower at between 0.4 and 1%. The lower strains in carbon FRP-concrete panels indicated that the punching

failure was more localized as the load could easily shear through the carbon FRP sheets.

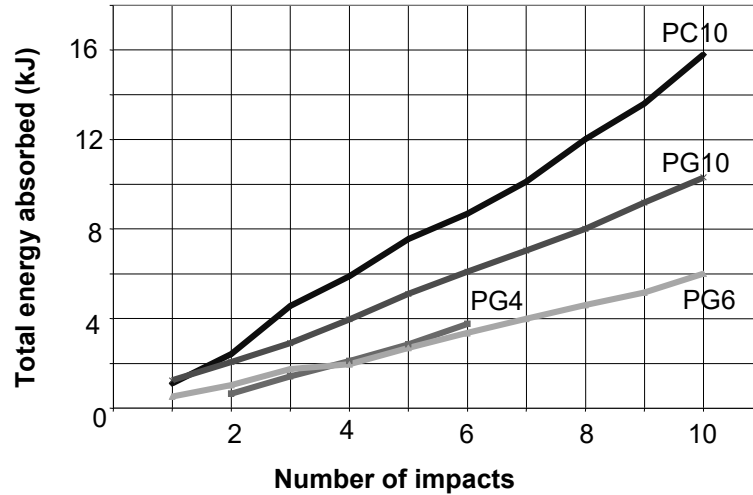


Figure 5: Energy absorption capacity of FRP panels

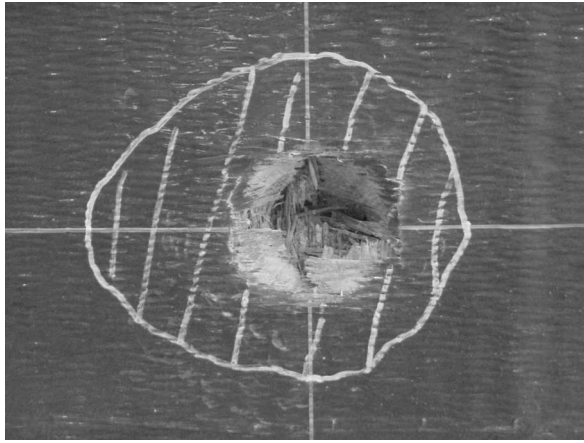
### 3.2.1 Damage and failure characteristics

The damage to the specimens due to the impacts was observed on the top face. At the first impact, the top FRP layer was punched through, and the impactor penetrated easily into the concrete layer. Since SC25 and SC210 each effectively had only two plies of carbon FRP sheets at the bottom and the concrete layer was thin, the impactor immediately punched through the slab. SC45, SG25 and SG210 suffered the same fate at the second impact.

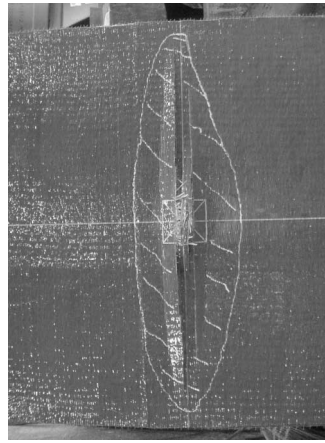
For Panel SG45, with a 5 mm thick concrete layer sandwiched between two 4-ply FRP sheets, a depression was observed at the top face of the specimen after several impacts, and the appearance after punching failure at the twelfth impact is shown in Fig. 6(a). Part of the top FRP sheets had debonded around the depression, as shown shaded. Upon turning the panel over, it was observed that the bottom FRP plies had also delaminated near the centre of the slab, and this had spread along the fibre direction towards the edges as shown in Fig. 6(b). Similar delamination was observed in the other slabs that were punched through.

### 3.2.2 Impact force

In general, the impact force increased with the concrete thickness or the number of plies of FRP sheet. Also, it decreased with the number of impact, as observed from the panels that failed under the second impact, indicating a deterioration of stiffness due to cracking of the concrete layer. The impact force-time characteristics for Panel SG45 shown in Fig. 7, however indicates an unexpected increase in impact force initially, followed by a drop for subsequent impact beyond the sixth impact. The unexpected increase could only be attributed to noise interference.



(a) Top view



(b) Bottom view

Figure 6: Appearance of FRP-concrete sandwich panel SG45

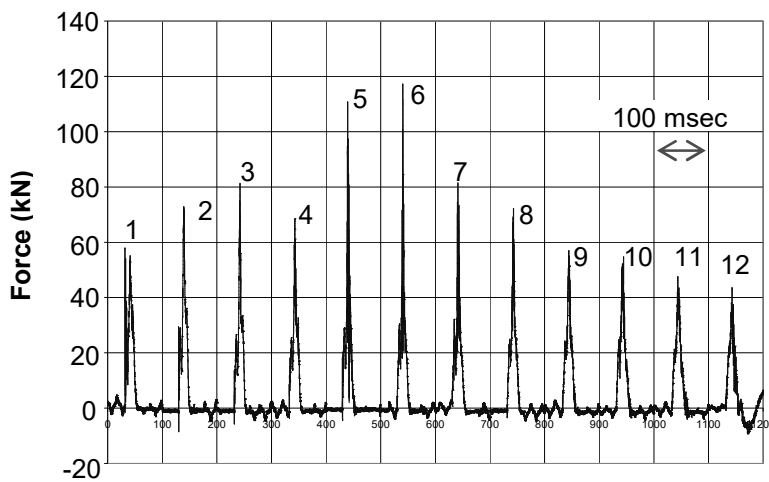


Figure 7: Impact force-time characteristics of panel SG45

### 3.2.3 Impulse

The impulse, like the impact force, increased with an increase in thickness in concrete layer or number of FRP ply. In general, the impulse on the glass FRP-concrete panels was higher than that on the carbon FRP-concrete panels, as glass FRP was more resistant to transverse shear and thicker than carbon FRP, sheet by sheet. Fig. 8 shows that the impulse for SG45 decreased after the sixth impact, due to damage and loss in stiffness.

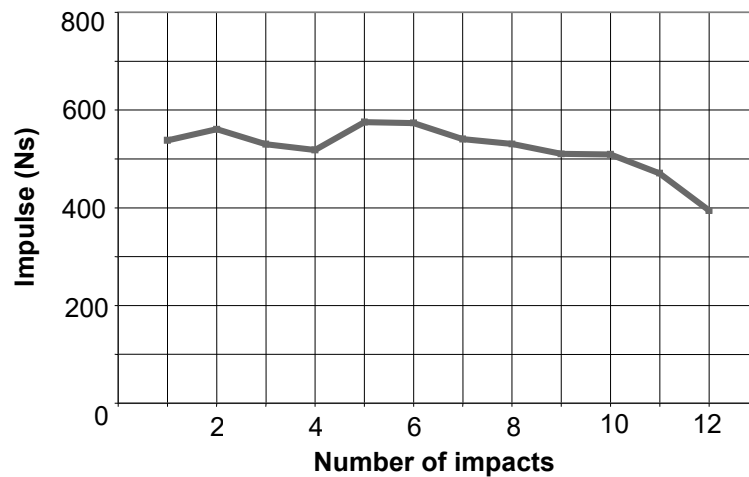


Figure 8: Impulse on panel SG45

### 3.2.4 Energy absorption characteristics

The maximum deflection of the panel under each impact decreased with the thickness of the concrete and FRP layers in the case of carbon FRP-concrete panels, being about 70 mm, 50 mm and 55 mm under the first impact, for SC25, SC45 and SC210, respectively. The glass FRP-concrete panels sustained higher deflections of between 65 to 75 mm, probably due to the lower modulus of glass FRP, but did not show any clear trend in the influence of thickness of the concrete and FRP layers.

The energy absorption capacity increased with the thickness of either the concrete layer or FRP layer. The values were 480 J, 1200 J and 720 J for SC25, SC45 and SC210, and 1350 J, 1500 J and 1500 J for SG25, SG45 and SG210, respectively. The cumulative energy absorbed in Panel SG45 is shown in Fig. 9. The energy absorbed per impact decreased after the eighth impact, indicating that significant damage had been imparted on the panel.

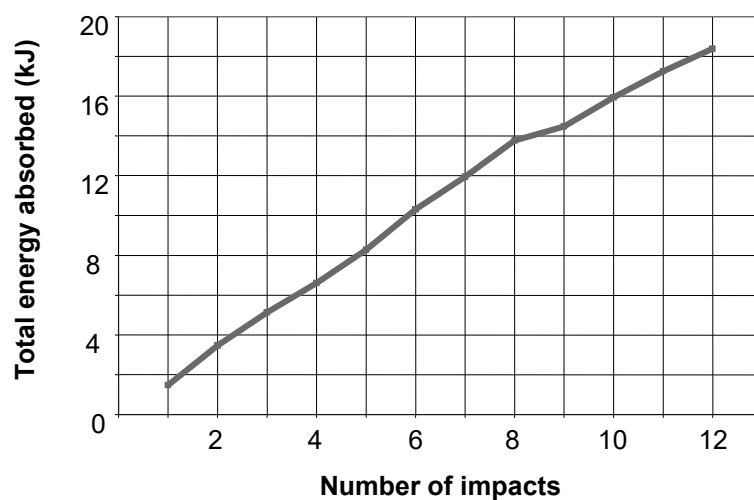


Figure 9: Energy absorption capacity of panel SG45

#### **4.0 CONCLUDING REMARKS**

Carbon FRP panels are more susceptible to punching failure than glass FRP panels as the fibers are less resistant to transverse shear. However, they provide higher stiffness, thereby enabling the panels to resist higher impact force and absorb greater energy, when compared to glass FRP panels with the same number of plies of FRP sheets. Also, the impact resistance improves with the panel thickness in general, but was not affected by the number of impact covered in the study.

Similarly, for the sandwich panels, punching failure was more localized and likely to occur in carbon FRP-concrete panels. The impact resistance was also found to improve with thicker concrete or FRP layers. Repeated impacts cause damage to the concrete layer, thereby reducing the resistance of the panel.

#### **ACKNOWLEDGMENT**

The study was carried out with the assistance of Mr W. X. Lim, and staff of the Structural Engineering Laboratory at the National University of Singapore.

#### **REFERENCES**

Struck, W. and Voggenreiter, W. 1975. *Examples of Impact and Impulsive Loading in the Field of Civil Engineering*. Materials and Structures, Vol. 8, No. 44, pp. 81-87.

# **DURABILITY DESIGN FOR CONCRETE STRUCTURES FOR URBAN SAFETY IN THAILAND**

SOMNUK TANGTERMSIRIKUL

Sirindhorn International Institute of Technology,

Thammasat University, Thailand

somnuk@siit.tu.ac.th

## **ABSTRACT**

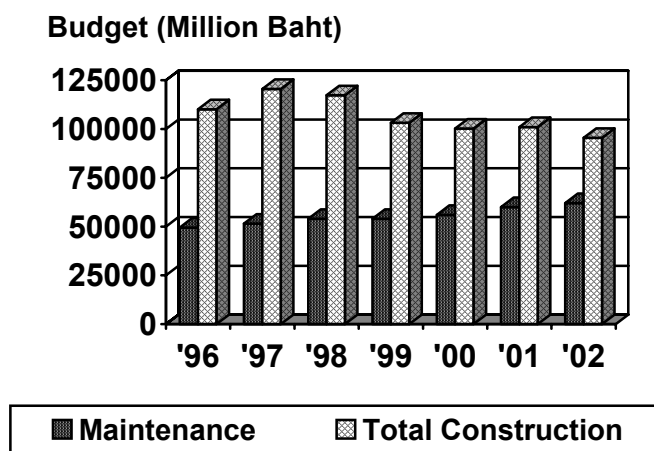
*This paper introduces some problems on deterioration of concrete structures in Thailand and some concepts on their future solutions. A survey of damages due to durability problems of some structures in the central and eastern parts of Thailand was carried out to explore the level of severity of the problem. It could be summarized that problems occurred in various states of the works i.e. from design, material selection, construction and maintenance. Some examples of problems in each state are illustrated. Solutions were offered in two categories i.e. that for new construction and that for the existing structures. For new construction, the performance based analysis and design taking into account the service life of the structures is proposed. For the existing structures, good protection, repair, strengthening shall be carried out.*

## **1.0 INTRODUCTION**

The current practices for design and construction of concrete structures in Thailand are based mainly on short-term properties of concrete. Civil engineers concern much only on a few properties of the concrete such as workability and mechanical properties like strength and Young's modulus, etc. at the design age which is usually 28 days. Unfortunately, those considered properties are just a few of the overall properties of concrete when considering the whole service life of the concrete. There are still many properties that should be considered especially those in long-term state such as durability properties. The current development plan of the current Thai government has set ground for enormous investment on infrastructures especially in the transportation and communication sectors. It is an urgent task for Thailand to change the way of practice from the mentioned strength concept to be a more rational design taking into account overall properties throughout service life of the structures. In addition, with many infrastructures constructed within the past decades, already there is now a huge stock of infrastructures that requires proper maintenance programs. Figure 1 shows the distribution and trend of annual total construction budget of a major public organization in Thailand in the past decade from 1996 to 2002 as an example to demonstrate the critical situation in the near future. The figure shows that the ratio of maintenance/total construction budget has surged from 45% in 1996 to 65% in 2002 while the total budget tends to be constant or even decreased. It is

then expected that this organization will have financial difficulty to expand new infrastructures and may even have difficulty to properly maintain the existing infrastructures. This situation is similar for all public organizations but only with different seriousness. The situations in many countries are not much different.

This paper introduces the results of surveys on current situation of concrete structures in some parts of Thailand, indicating various problems. Many evidences deterioration with various degrees from light to serious were observed. The deterioration was caused by insufficient knowledge and attention in various steps of the practices starting from analysis and design, material selection, construction and maintenance. It is necessary to plan for a solution to this problem for the sake of economic and safety.



*Figure 1: Budget situation of a major public organization in Thailand*

## 2.0 SURVEYS ON DETERIORATION OF CONCRETE STRUCTURES SHOWING DETERIORATION PROBLEMS

Surveys on situation of deterioration of some concrete structures in Thailand have been conducted since 1997 with the aim of gathering data on the types and degree of deterioration of the surveyed structures [1, 2, 3]. Two regions were selected for the survey namely central region (including Bangkok) and eastern region of Thailand. The two regions have different types of environment. The main difference of the two regions is on the existing of chloride attack. Eastern part of Thailand is the region closed to sea and is subjecting to attack by salts. Figure 2 shows the map of Thailand and the survey area denoted by the name of the provinces in the map. According to this survey, the following summary can be drawn:

- There were various causes of deterioration including those due to load and due to environmental attack such as drying shrinkage, thermal crack, sulfate attack, acid attack, alkali aggregate reaction, carbonation, chloride attack, etc., and those occurs during construction like plastic shrinkage, bleeding and settlement, etc.

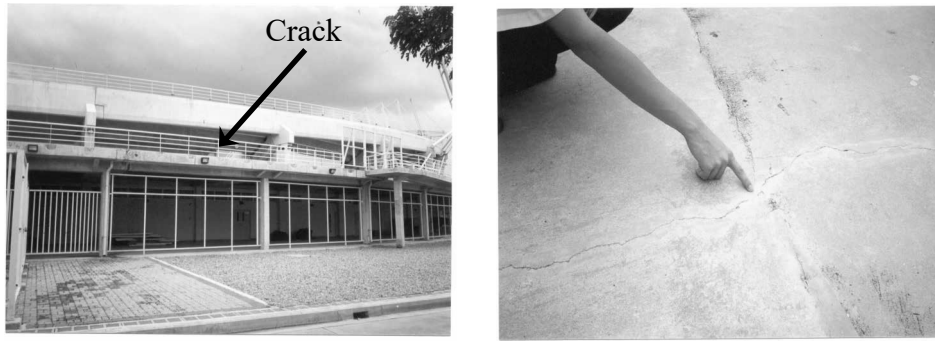


- Most damages were visible in form of steel corrosion. Damages due to steel corrosion are much more serious in the eastern part than in the center of Thailand. The steel corrosion problems in the eastern part are due to chloride attack but those found in Bangkok area are mostly due to carbonation.
- Many of the steel corrosion problems were due to poor construction such as insufficient concrete cover or honeycombing, etc.
- Very few maintenance programs are in action for those structures.
- The selection of raw materials and mix proportion of concrete was only based on a few performances such as strength and workability. The concept of selecting proper materials and proper mix proportion for different environment was not practiced in the past but has been just started in these few years.



*Figure 2: Map of Thailand showing the surveyed regions*

The problems in all stages of practice can be observed, starting from stage of analysis and design, raw materials selection and mix proportioning, construction and maintenance. Figures 3 to 8 show some examples of the problem in each stage.



*Figure 3: Crack on a roof slab of a stadium (Analysis and design problem)*



a) Cracks due to AAR

b) Sulfate and acid attack in sewer water

*Figure 4: Material selection problem*



*Figure 5: Severe honeycombing due to segregation (Problem of concrete mix proportion)*



*Figure 6: Plastic shrinkage (left) and plastic settlement cracking (center and right) showing construction problems*



*Figure 7: Steel corrosion due to insufficient concrete cover under a bridge (left) and in a building (right) (Construction problem)*



*Figure 8: Concrete spalling due to carbonation induced steel corrosion in Bangkok area (left) and chloride induced corrosion in eastern part of Thailand (right) (Maintenance problem)*

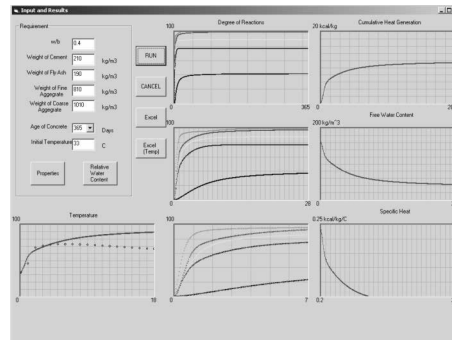
### **3.0 SOLUTIONS**

The solution to this problem can be implemented by considering 2 measures, first for new structures to be constructed from now on and second for the existing structures that had been built. For new structures, the following measures are to be implemented:

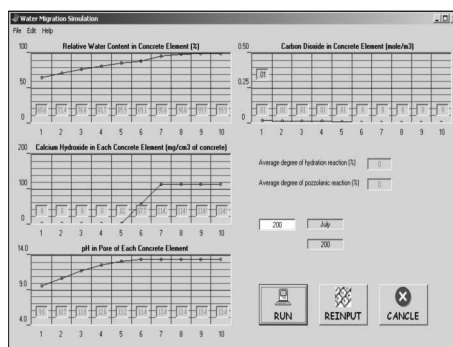
- A better analysis and design considering not only short term but long term performances of the structures (Performance based analysis and design). Design code shall be modified in the mentioned way. At present, the design regulation is modified by the Department of Public Work and Urban Planning to incorporate the durability into the design.
- Selecting proper raw materials and mix proportion of concrete for each type of structure and different types of environment. The concept of proper concrete for each structure type and each environment must be seriously considered. Shown in Figure 9 are some computer program for analysis and design of concrete mix proportion by considering requirements of concrete performances such as workability, strength, temperature rise, carbonation and chloride content of the concrete.



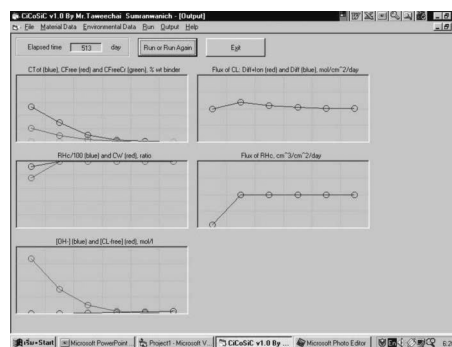
a) Slump and strength design



b) Analysis of temperature



c) Analysis of carbonation depth



d) Analysis of chloride profile

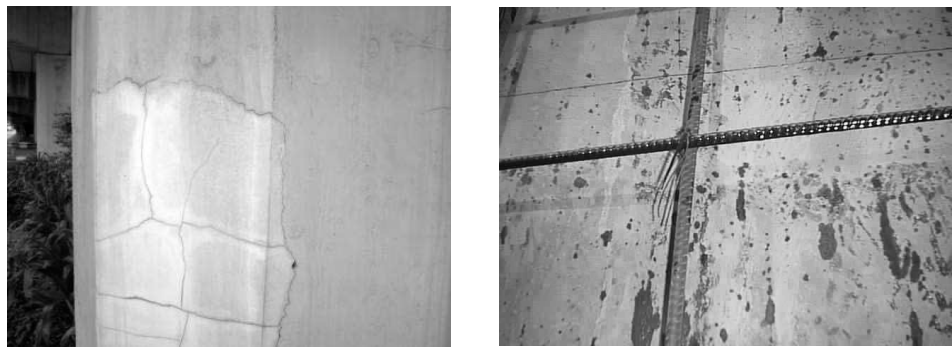
Figure 9: Examples of performance based computer software for analysis and design of concrete mix proportion (An effort to cope with problems on material)

- A much more seriousness in quality control and quality assurance of construction must be practiced. The Engineering of Thailand and Thai Concrete Association are now modifying their codes of

practice for construction and to conduct seminar courses for the practice engineers.

- The existing of good plan of protection and maintenance which will prevent intensive repair or strengthening in the future has to be considered from the beginning of the project.

For the already built structures, there is an urgent need to create a database indicating the cause and degree of deterioration of the existing structures in order to conduct a proper protection, maintenance, repair, strengthening or reconstruction program for each case. There is a strong need to publish higher level of appropriately advanced codes and standards of practice and to provide more education in order to get the problems solved. The Thai Concrete Association is now drafting various codes and guideline for maintenance of concrete structures and preparing for seminar and training using the drafted codes and guidelines in the near future. These will include the code and guideline for selecting repair materials and repair methods that will prevent the wrong practice as those shown in Figure 10.



*Figure 10: Cracking in the patching material due to incompatible shrinkage property (left) showing improper selection of repair material. Improper sequence of construction causing epoxy to adhere on the steel reinforcement (right) showing low quality handling.*

#### **4.0 CONCLUDING REMARKS**

Based on a survey on the deterioration situation of some concrete structures in the central and eastern parts of Thailand, it was found that even though most of those structures were constructed just in the past decade, there were many problems regarding deterioration which would lead to future burden or even accident unless a proper plan for maintenance, repair and rehabilitation is realized. Not only the existing damaged structures, but also the newly constructed ones and those to be constructed must be considered. A proper protective maintenance plan for newly and still undamaged structures and proper practices in analysis, design, materials selection, construction and maintenance plan for those to be constructed must be available.

## ACKNOWLEDGEMENTS

A part of the survey was partially funded by the International Center for Urban Safety of the University of Tokyo where the author would like to acknowledge for the support. The author would like to also express appreciation to Dr. Toshiharu Kishi of the University of Tokyo, former seconded faculty member to Asian Institute of Technology and many graduate and undergraduate students from Sirindhorn International Institute of Technology and Asian Institute of Technology for their contributions to the survey.

## REFERENCES

- Tangtermsirikul, S., 2003. *Information Acquisition and Structural Health Monitoring of Bridges in Bangkok*. A report submitted to the International Center for Urban Safety, the University of Tokyo.
- Tangtermsirikul, S., et.al., 2000. *Durability of Concrete*. Engineering Institute of Thailand, ISBN 978-974-87684-5-7, Thailand.
- Wongtanakitcharoen, T., 1999. *A Study of Deterioration of RC Structures in Central and Seaside Areas of Thailand*. A Master thesis No. ST-99-32, Asian Institute of Technology, Thailand.

# **AN EXPERIMENTAL STUDY ON COMPLEX DETERIORATION OF CONCRETE USING GROUND GRANULATED BLAST-FURNACE SLAG**

TOSHINOBU YAMAGUCHI<sup>1</sup>, KOJI TAKEWAKA<sup>1</sup>,  
JUNICHI MATSUMOTO<sup>1</sup> AND YOSHIKAZU AKIRA<sup>2</sup>

<sup>1</sup> Department of Ocean Civil Engineering, Kagoshima University, Japan

<sup>2</sup> Port and Airport Research Institute, Japan  
yamaguch@oce.kagoshima-u.ac.jp

## **ABSTRACT**

*Recently, a complex deterioration due to plural deterioration factors has posed one of serious problems in RC structures. The effect on complex deterioration is not clear, especially as for concrete using ground granulated blast-furnace slag which, in Japan, commonly applied in coastal environment.*

*In this study, the experimental examinations on the deterioration due to each/both salt attack and neutralization were carried out using mortar with substitution ratios of the ground granulated blast-furnace slag by accelerated tests. As the results, by using GGBS, though neutralization depth increases, penetration of chloride ion and corrosion properties of re-bar can be improve. However, to use GGBS as admixture of concrete, content of GGBS and initial curing time must be considered.*

## **1.0 INTRODUCTION**

Recently, a complex deterioration due to plural deterioration factors has posed one of serious problems in RC structures (Saeki, T., 2002). The effect on complex deterioration is not clear, especially as for concrete using ground granulated blast-furnace slag which, in Japan, commonly applied in coastal environment. The reasons to use GGBS are to inhibit alkali-aggregate reaction, to reduce hydration heat, to improve diffusivity of chloride ion, and so on (Matsushita, H.,2003, Kokubu, k.,1988).

In this study, the experimental examinations on the deterioration due to each/both salt attack and neutralization were carried out using mortar with substitution ratios of the slag by accelerated tests. Corrosion areas of re-bar were also measured to examine its effectiveness as an index for the corrosion under complex deteriorative environment.

## 2.0 EXPERIMENTAL PROGRAM

### 2.1 Specimens

Properties of used materials, ordinary portland cement, river sand and GGBFS, are shown in Table 1. Mix proportions for mortal specimens are shown in Table 2. The shape of specimen is shown in Figure 1. Cylindrical mortar specimens with a size of 10 cm in diameter and 10 cm in height, having a re-bar embedded with a cover depth of 3 cm were prepared. The side and bottom of each specimen was coated by epoxy resin. To examine the effect of initial curing time before exposure, three periods, 7, 28, and 91 days, were carried out for each mix proportion.

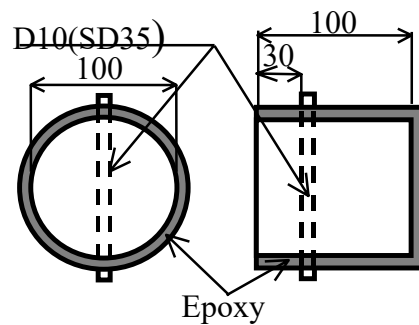
*Table 1: Properties of materials*

Materials	Density	Specific surface area / F.M.	CI (%)
Ordinary portland cement	3.16 g/cm <sup>3</sup>	3290 cm <sup>2</sup> /g	0.009
Ground granulated blast furnace slag	2.90 g/cm <sup>3</sup>	4010 cm <sup>2</sup> /g	0.002
River sand	2.63 g/cm <sup>3</sup>	F.M. : 2.68	

*Table 2: Mix proportions*

Series	W/B (%)	past volume (%)	GGBS/B (%)	Unit weight (kg/m <sup>3</sup> )			
				W	B	GGBS	S
50-S00	50	45	0	275	550	0	1447
50-S50	50	45	50	271	271	271	1447
50-S70	50	45	70	269	161	377	1447
70-S00	70	41	0	282	403	0	1552
70-S50	70	41	50	278	199	199	1552
70-S70	70	41	70	277	119	277	1552

\* Mortar flow: 200 mm for every mix proportion



*Figure 1: Size of specimen (mm)*



## 2.2 Accelerated condition

In the experiment, 3 types of accelerated test were performed, assuming deteriorations, such as salt attack, neutralization, and complex of both. Table 3 shows each accelerated conditions. Setting 7 days in each accelerated conditions as 1 cycle, chloride ion content, neutralization depth, corroded area of re-bar were measured every 10 cycles. Picture 1 shows the acceleration system originally developed by authors (Akira, Y.,2001).

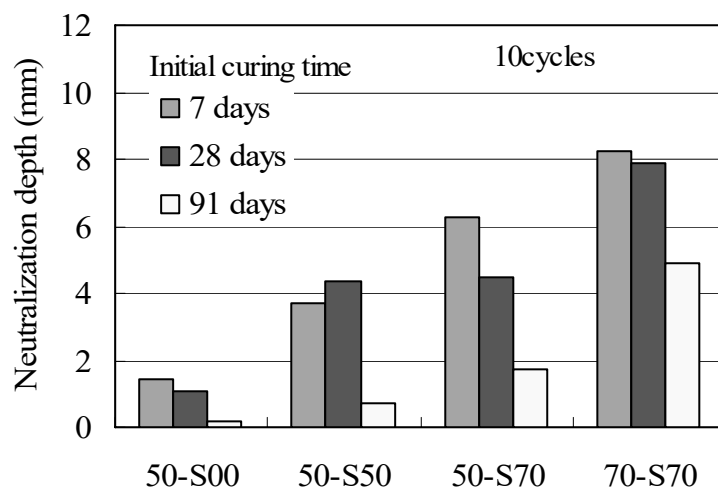
*Table 3: Cycle condition for each accelerated test*

Deterioration	Immersion (3.5days)	Drying (3.5days)
Salt attack	5% NaCl solution	Normal Air
Nutralization	Distilled water	CO <sub>2</sub> 5%
Complex	5% NaCl solution	CO <sub>2</sub> 5%

## 3.0 RESULTS AND DISCUSSION

### 3.1 Neutralization depth

Figure 2 shows neutralization depth of each type of specimen, after 10 cycles of complex deterioration test. As previously reported, neutralization depth increases with increasing GGBS content and water binder ratio, and decreasing initial curing time. However, this unbeneficial characteristic of concrete and mortar using BBGS can be partly reduced in complex deterioration as shown in Figure 3.



*Figure 2: Neutralization depth (complex)*

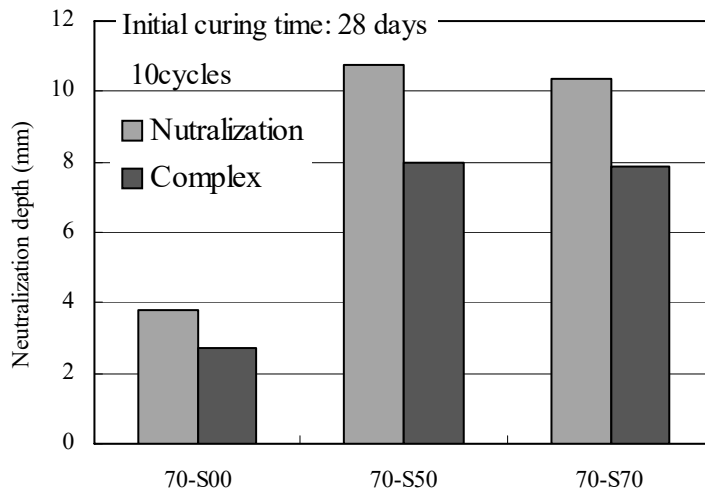


Figure 3: Neutralization depth in different deterioration tests

### 3.2 Penetration of chloride ion

Figure 4 and 5 show the diffusion properties of each type of specimen in complex deterioration test, and Figure 6 shows the comparison of chloride diffusion coefficients obtained from the results of both single and complex deterioration tests. However, the beneficial characteristic of BBGS reduces due to the effect of neutralization, the great improvement in resistance against the penetration of chloride ion due to the GGBS can be still observed in both water binder ratio.

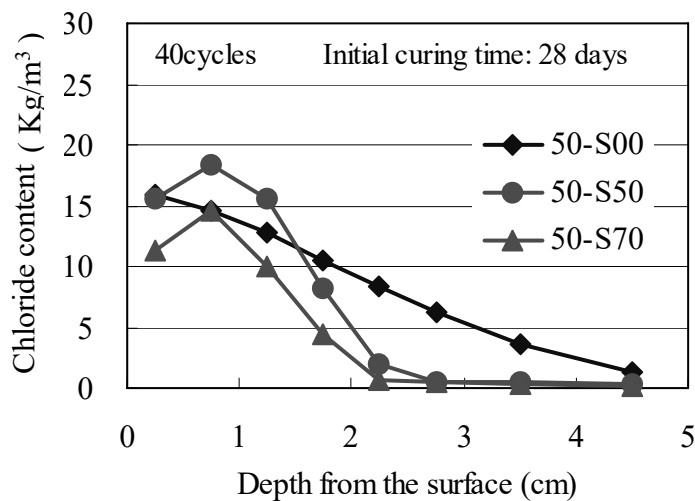


Figure 4: Chloride content in specimen (complex, W/B 50%)

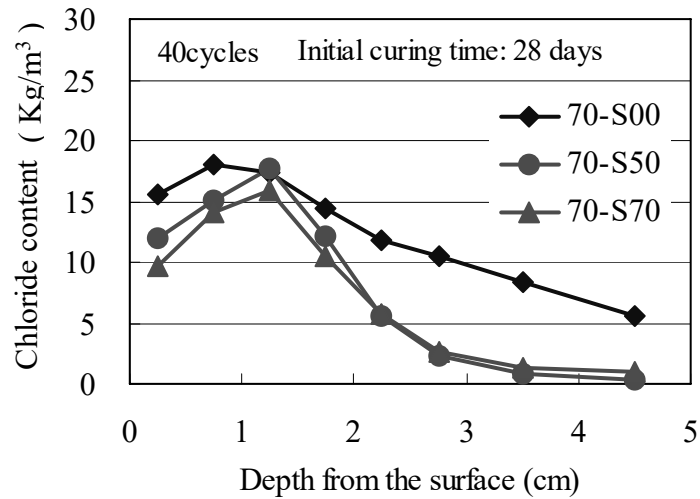


Figure 5: Chloride content in specimen (complex, W/B 70%)

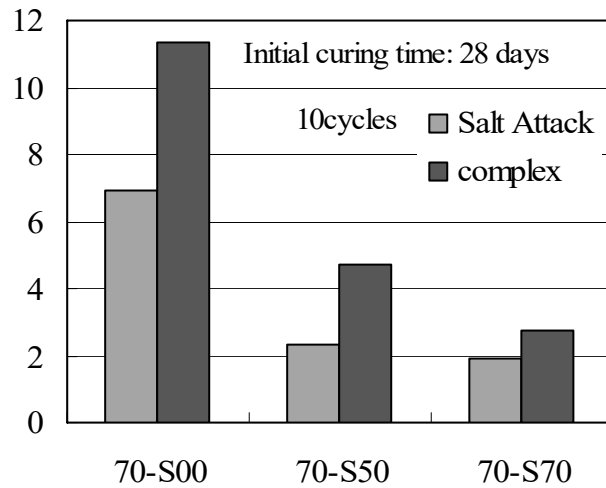


Figure 6: Chloride diffusion coefficient in different deterioration tests

### 3.3 Corrosion properties

Figure 7, 8, 9, and 10 show the corrosion area of re-bar in each type of specimen, during complex deterioration test. Figure 11 shows the comparison of corrosion area of re-bar between salt attack deterioration and complex deterioration. From these figures, it is found that corrosion area of the re-bar increases with increasing water binder ratio and GGBS content. Up to 50% GGBS content, corrosion area can be reduced by using GGBS.

However, the most important point is the conflicting phenomenon between chloride content and corrosion area in high GGBS content specimen. That is to say, in spite of high resistance against chloride penetration which GGBS mortar has as shown Figure 4 and 5, re-bar inside of high GGBS mortar, such as 70% GGBS content can be corroded even the very little chloride content. For the phenomenon, initial curing time is also

very essential parameter to maintain the durability of GGBS concrete. Therefore to use GGBS concrete for the complex deterioration environments concerning to neutralization and salt attack, the GGBS content and initial curing are should be considered carefully.

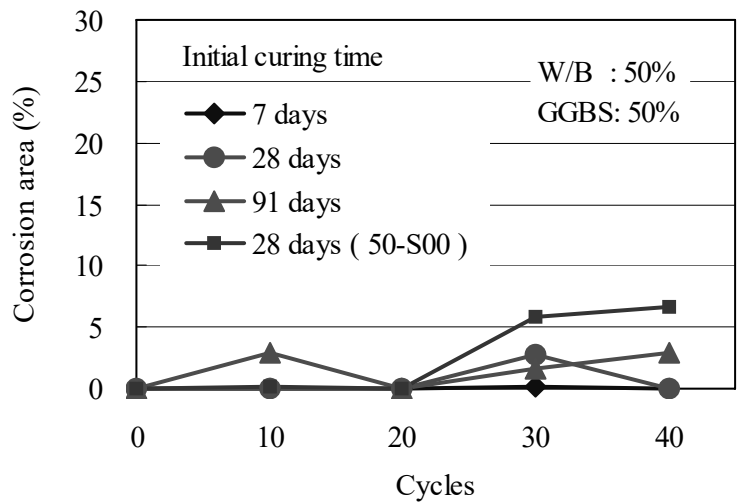


Figure 7: Corrosion area of re-bar (complex, W/B 50%, GGBS 50%)

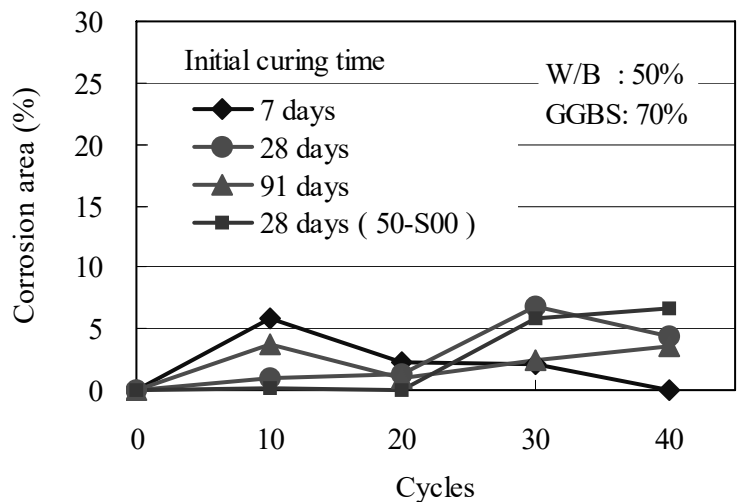


Figure 8: Corrosion area of re-bar (complex, W/B 50%, GGBS 70%)

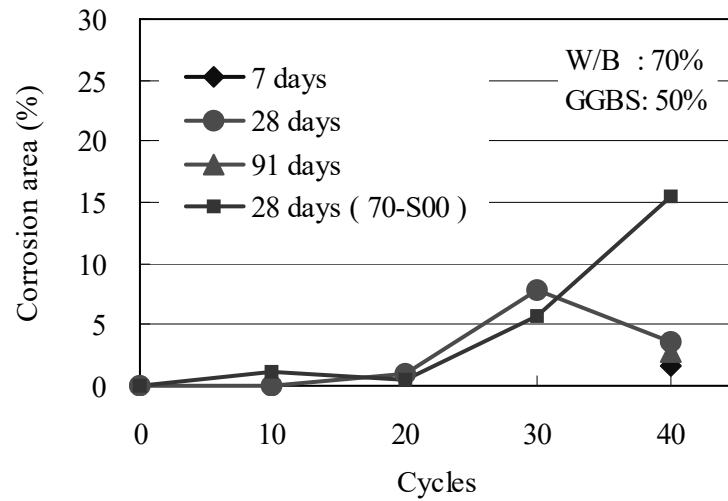


Figure 9: Corrosion area of re-bar (complex, W/B 70%, GGBS 50%)

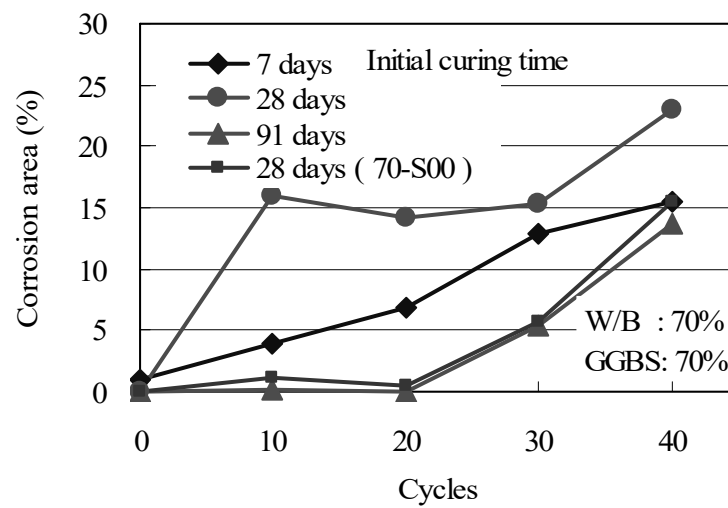


Figure 10: Corrosion area of re-bar (complex, W/B 70%, GGBS 50%)

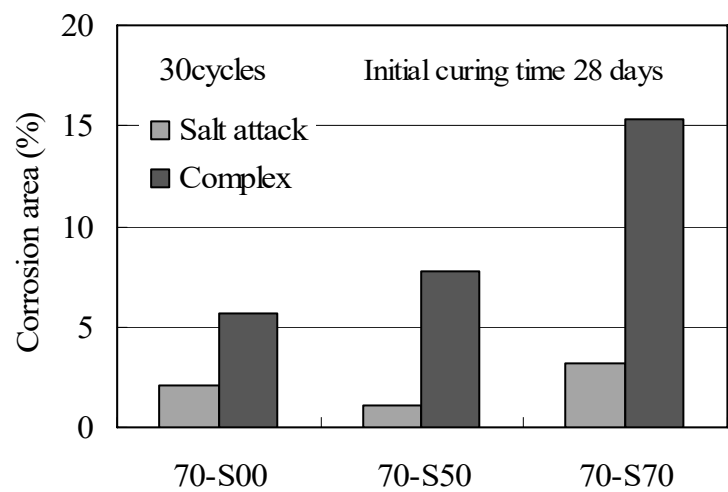


Figure 11: Corrosion area of re-bar between different deteriorations

## 4.0 CONCLUSIONS

In this study, experimental examinations were performed in order to grasp the complex deterioration properties of concrete using GGBS (ground granulated blast-furnace slag), especially for the complex between salt attack and neutralization. As the results, it is found that an interactive deterioration of concrete can be occurred in the complex deterioration environment.

By using GGBS, though neutralization depth increases, penetration of chloride ion and corrosion properties of re-bar can be improve. However, to use GGBS as admixture of concrete, content of GGBS and initial curing time must be considered.

## REFERENCES

- Saeki, T., Ueki, S., and Shima, T., 2002. *A model for predicting the deterioration process of concrete due to the compound interaction of salt damage and carbonation*, *Journal of material*. Concrete structures and pavements, Vol.697, No.54, 131-142.
- Matsushita, H., Harada, T., Soeda, M., Ryu, R., and Yoshitake, T., 2003. *Durability design and thermal cracking control of concrete piers of shin-kita-kyushu airport bridge*. *Journal of construction management and engineering*, Vol.728, VI-58, 79-92.
- Kokubu, K., Murata, Y., Takahashi, S., and Anzai, H., 1988. *Studies on adiabatic temperature rise and hydration of portland cement concrete incorporating ground granulated blast furnace slag*. *Journal of materials, concrete structures and pavements*, Vol.396, V-9, 39-48.
- Akira, Y., Takewaka, K., Sato, T., and Yamaguchi, T., 2001. *Experimental study on deterioration of concrete structure due to acid rain*. First international structural engineering and construction conference.

# **CASE STUDY OF THE REPAIR OF A MAJOR BRIDGE AND SOME THOUGHTS ON REPAIR MATERIALS**

MANJREKAR S. K.  
SSCPL, Mumbai, India  
[sscpl1@bom5.vsnl.net.in](mailto:sscpl1@bom5.vsnl.net.in)

## **ABSTRACT**

*The paper discusses repair and rehabilitation of a major road over bridge connecting eastern and western suburbs of Andheri, Mumbai. While the case study is described, the author dwells upon some of the important aspects involved in selection of appropriate materials and methodologies of repair / rehabilitation.*

## **1.0 INTRODUCTION**

Rehabilitation of reinforced concrete (RC) bridges prematurely or otherwise damaged, continue to be a major problem throughout India. The problem is more serious in the coastal areas and is aggravated further in the highly polluted city like Mumbai. Many a bridge needs major repairs. In view of the need to maintain continuous traffic flow on the bridge the repair methodology assumes great importance. A case in point is the repair to the Gopalkrishna Gokhale (GKG) Bridge, connecting S. V. Road and the Western Express Highway in a suburb of Mumbai.

Major rehabilitation work of the western approach of this bridge has been just concluded. It was carried out in very trying conditions of continuous traffic flow matched with the serious damage taken place over the years. This paper is an effort to understand the nature of damage and then the logical solution to repairs based on the latest understanding of the materials, particularly polymers and polymer-modified mortars/ concretes. An attempt is also made to explain the mechanisms involved. This is with the expectation that this case study which is possibly first example of its type in terms of the expanse of the job and large quantities of materials required can be a guidance for posterity to assess and carry out such bridge repairs in the future.

## **2.0 DETAILS OF THE CASE STUDY**

### **2.1 Salient features of the bridge**

The salient features of the GKG Bridge are as below:

- |                         |   |         |
|-------------------------|---|---------|
| 1. Year of construction | : | 1969    |
| 2. Width of bridge      | : | 27.45 m |

3. Superstructure
  - On railway track : Structural steel
  - On approaches : RCC T-beam and slab
  - (Total length 160m: 100 m on the western side and 60m on the eastern side.)
4. Substructure : 12 RC columns  
(the area below RC approach is enclosed and used as offices)
5. No. of girders per span : 12
6. Thickness of deck Slab : 250 mm
7. Bearings : Roller and rocker-roller type steel bearings
8. Foundation : open
9. Total length of approaches : Eastern side- 240 m  
Western side- 220 m

## 2.2 Nature of damage

Detailed visual inspection revealed the following types of damage:

- Heavy and continuous leakages
- Development of cracks in deck, girders and columns
- Chunk of concrete mass fell off from western approach deck exposing the deck reinforcement steel
- Parapet walls cracked extensively.

Non-destructive testing was carried out involving ultrasonic pulse velocity tests, carbonation test, half-cell potential mapping, determination of pH of concrete and chloride content estimation, etc. Based on the visual observations and results of non-destructive testing, consultants worked out a detailed procedure for the repairs which constituted following specifications.

- Support the RC members by steel props and spans appropriately, depending upon loading conditions and extent of damage of the members to be repaired.
- Expose the member by means of chisel and hammer. Remove the loose concrete beyond the reinforcement.
- Remove loose rust from reinforcement by means of *tacha* and wire brush (mechanical/manually). Apply phosphate-based rust converter- **RUSTICIDE** capable of removing corrosion products to the reinforcement by brush or cotton waste. After 24 hours wash the reinforcement by clean water jet.
- Providing and applying slurry of 1 part of specially formulated alkaline acrylic-based polymeric solution - **POLYALK FIXOPRIME** with 1.5 part of fresh cement and mix the solution by means of stirrer and apply it on the reinforcement by paint brush. This will act as protective coating on the reinforcement. After 24 hours apply similar second coat of such slurry. Make sure no area is left uncovered.
- Providing and applying bond coat of single-coat acrylic co-polymeric admixture - **POLYALK EP** and cement in 1:1



proportion to RC members and applying polymer-modified mortar to build up the thickness upto 10 mm.

- Repairing of damaged RC member by single coat co-polymeric mortar in 1:5:15 (acrylic co-polymer (**POLYALK EP**): cement: Quartz sand) proportion and required proportion of water.
- Curing the same by spray pump after 24 hours.

This paper lays emphasis on the material science dealing with the properties, behavior and mechanisms of various repair materials / polymers used in the above work. For various steps involved in the work corresponding cross-references are also provided for better understanding.

### 3.0 REPAIR: SOME THOUGHTS

For effectiveness of any repair the following points need thorough consideration from material properties and compatibility point of views, besides the important considerations of structural parameters:

- Ascertaining the extent of corrosion and carbonation
- Near total removal of corrosion products from the steel.
- Application of a corrosion resistant barrier film on the reinforcement (such film should inhibit further corrosion)
- Application of a useful bond coat which assures good bonding.
- Rendering a strong, passive carbonation resistant polymer modified / polymer concrete cover of proper generics, wherever necessary.
- Applying protective seal coat on the entire surface to guard against any aggressive chemical attack.

Carbonation is one of the principle causes of corrosion and it brings about various physical changes in the quality of concrete. However, it affects the alkalinity of the concrete by bringing it down considerably. Generally, the pH of good concrete which is in the vicinity of 12.5 to 13 comes down to around 9. This loss in pH causes the reinforcing steel to be susceptible to corrosion. The carbonation plane moves into the concrete from the outer surface as a result of external attack and it is dependent upon the moisture content of the concrete. This plane moves rapidly when relative humidity is between 50 to 70 percent<sup>1</sup>. One can find out the depth of carbonation from a formula  $d = k_c \sqrt{t}$  where,  $d$  = the depth of the carbonation reaction plane in mm, after time  $t$ , years. Coefficient of carbonation  $k_c$  is related to the permeability of the concrete, the amount of available free time, relative humidity<sup>1</sup> and the carbon dioxide (other related gases in case of polluted environments) content of the given environment.

As reported<sup>2</sup> in the present case study, the carbonation attack was seen to be upto 70 mm depth which was associated with highly undesirable low pH in the range of 5 to 8.0. Half cell readings also were fairly negative in the range of - 450 to - 600 mv. These data corroborated well with the

physical state of the bridge. Thus, ascertaining the extent of corrosion and carbonation proved to be very useful first step in the sequence of repairs.

The next step consisted of the process of removal of diseased/ loose concrete and removal of corrosion products from the steel and preparing the surface for further applications. It needs to be mentioned here that howsoever effective the materials are, the basic surface treatment plays very important role in the efficacy of the repair operation. In addition, it is very important to see that the surrounding good concrete is not damaged. In this case chipping was done by hammers, which is most widespread method of concrete removal if the deterioration is deeper than 15 mm or more. ACI committee 546<sup>3</sup> also stresses on proper selection of chipping tools, which will avoid the damage of surrounding concrete. However in recent years the introduction of the water jet technique (hydro demolition or hydro jetting or hydro blasting) has changed the prevalent method of concrete removal<sup>4</sup>. Besides high efficiency several other advantages listed below add to the success of this method:

- A rough and clean surface made available.
- No micro cracks are introduced into the remaining concrete.
- The reinforcement is undamaged and cleaned from rust, and
- Only bad concrete is removed leaving the good concrete intact.

In fact, some comparative studies also have been made on the interface strength of a repaired matrix between sand blasted surface, mechanically chipped surface and the water-jetted surface. In water jetted surface, maximum bond strength was shown followed by mechanically chipped and the sand blasted surface showed the least bond. In the present work it was however decided to adopt the chipping method, using chipping tools which fits in the recommendations of ACI Committee 546.

The next important step was to ensure that the corrosion products on the steel are removed effectively. For this, it is reported that the mechanical means prove quite inadequate. Hence, it was correct to use the chemical rust remover-cum-converter material. The application of this material does not reduce the section of steel (like in sand blasting) after having removed the loose oxidation scales. It, in fact, consolidates the left over section. This treatment also helps in resisting the corrosion to an extent, though, subsequent process of pacifying the steel is very essential.

Neither chemical cleaning nor rust converting processes are permanent relief from corrosion. Hence, a protective barrier film is generally applied on the treated steel. One of the options is to apply liquid epoxy on the bars which on setting becomes almost plastic-like, resulting in substantial loss of bond with subsequently laid concrete. It is reported that as much as 40 percent bond is lost<sup>5</sup>. In order to overcome this bond loss fine quartz sand is sprinkled on the wet epoxy on many occasions. In addition, this treatment being only a barrier film does not do anything so as to create non corrodible conditions around the steel. However, despite these drawbacks epoxy

treatment for bars has been found to be more effective than any other coating treatment like zinc chromate priming<sup>6</sup>, etc.

*Table 1: Indicative properties of the polymers*

Sr. No.	Properties		Polymer / Cement ratio (on Wt/Wt basis)		
			0	0.2	0.4
1	Adhesion to concrete, N/mm <sup>2</sup>	Dry	0.07	2.0	3.4
		Wet	0.03	1.0	1.4
		Wet	0.00	1.4	2.1
2	Adhesion to steel, N/mm <sup>2</sup>	Dry	0.0	2.0	1.6
		Wet	0.0		1.3
3	Tensile strength, N/mm <sup>2</sup>	Dry	3.0	6.0	4.3
		Wet	1.8		3.9
4	Compressive strength, N/mm <sup>2</sup>	Dry	56.0	50.0	
5	Flexural strength, N/mm <sup>2</sup>	Dry	7.1		10.6
		Wet	5.8		9.6
6	Effects of chemicals on dry flexural strength after six months immersion, N/mm <sup>2</sup>				
		• Untreated	7.2	13.2	
		• 10% potassium hydroxide	6.1	12.3	
		• 10% magnesium sulphate	4.3	13.2	
		• 5% lactic acid	5.9	8.0	
		• 5% hydrochloric acid	0.0	2.2	
7	Effects of extremes of temperature N/mm <sup>2</sup>				
		• untreated	7.1	10.6	
		• after 6 freeze/ thaw cycles at 18°C ( in 10% brine)	0.0	10.4	
		• after 1 year at 70°C	5.2	14.3	
8	Adhesion to concrete (dry) , N/mm <sup>2</sup>	• untreated	0.1	3.4	
		• after 6 months at 70°C	0.0	2.6	
9	Shrinkage to concrete (dry) , N/mm <sup>2</sup>	• water-cement ratio	0.40	0.34	0.30
		• percent shrinkage	0.07	0.02	0.01
10	Water penetration, g/ m <sup>2</sup> /24 hours		46.9	38.1	1.9
11	Water penetration with Revinex 29Y 40 in mortar, Kg/ m <sup>2</sup> /24 hours		100.0	35.0	0.0

### 3.1 Need of a bond coat

In order to overcome the above mentioned shortcomings, a slurry of water based polymer emulsions and cement is applied on steel. This mixture

being highly alkaline in nature keeps the environment around steel in an alkaline state. This situation helps greatly in maintaining a passive,  $\gamma\text{-Fe}_2\text{O}_3$  film on the steel, thereby preventing corrosion<sup>7</sup>. Besides, this film being cement based, it is a compatible material with concrete and does not result in any loss of bond strength making the structural engineer's work easy. Moreover, the film is quite tough as well as flexible. In addition, being a one-pack polymer system, hardening of unused material or setting of the material due to delayed use, etc is more or less eliminated. For reasons mentioned earlier, pure acrylates, modified acrylates, modified styrene-butadiene rubber (SBR), etc are used as concrete modifiers, preference being in that order too. These tailor-made formulations are easily available. For the current job the material used was acrylate-based polymeric solution which is tailor-made to protect  $\gamma\text{-Fe}_2\text{O}_3$  film that is to prevent further corrosion for long time to come. As a matter of fact, this material is specially formulated to withstand even the stress corrosion when used with suitably-formulated cementitious and supplementary cementitious materials<sup>8</sup>. This step is one of "the important" steps to avoid further deterioration as well as to enhance the life of the repaired system.

Earlier we have discussed the mechanism of improving the bond strength at the stage of pretreatment of the method of removal of diseased concrete. In addition to this, in terms of additional and assured bonding methods one must consider the 'Swedish Regulations for Concrete Structures' which do not permit shear transfer at interfaces of composite concrete structures. European and American concrete codes prescribe comparatively low values for the permissible shear stress at the interfaces like 0.22 to 0.62 N/mm<sup>2</sup> (dependent on characteristic compressive concrete strength<sup>9</sup>) and 0.55 N/mm<sup>2</sup>, respectively. Consequently, reinforcement crossing the interface is needed as soon as the applied design shear stress exceeds these small values. This means the shear capacity in composite repairs can be provided by shear connectors or dowels at very close intervals which on a large area could prove very impractical and expensive. That is why to ensure further adhesion between two phases, namely, between the original concrete and the new repair material, a polymer cementitious adhesive bonding coat is considered essential.

In several cases, where traditional repairs are executed by replastering or mere concrete jacketing, or even guniting, it is often seen that the new concrete / mortar mass separates from the old concrete. This obviously happens due to dissimilar behavior patterns of the old, already set concrete and the subsequent new concrete or mortar, which is undergoing stresses and strains while stiffening, mainly due to shrinkage. To an extent this drawback is nullified by using steel wire mesh. Although the wire mesh helps to distribute shrinkage stresses evenly it may introduce additional corrosion problems. To overcome this, galvanized wire mesh is used, but this may prove to be costly. Hence, years of experience has taught the repair specialists to use a bond coat which ensures mechanical bond between old and new concrete. However, sometimes inappropriate quantity / quality of bonding coat together with the shortcomings in workmanship results in an undesirable performance.

Liquid epoxy in tacky conditions is found to be an excellent bonding coat. However, sometimes if a large area is to be concreted, for example, jacketing of all four sides of the column, or when due to the negligence on the part of workmen, the time lag between application of the epoxy bond coat and subsequent placement of new concrete increases, it results in the epoxy being partially or fully set and consequently it acts as debonding agent rather than a bonding agent. In such cases, separation cracks at the interface can be seen. This is not because of the failure of the material but due to the two-pack epoxy not being utilized properly. Hence, use of user-friendly material is necessary and this should preferably be a one-pack system. Bonding polymers, which are based on polymer latexes, when used along with cement, give equally excellent adhesion both to old concrete as well as the new one. There is substantial reduction in cost too and the one pack nature of the polymer keeps the tackiness of the surface for a long time. It also helps to keep the conditions around the exposed steel and exposed concrete generally alkaline, thereby preventing corrosion of steel and carbonation of the adjacent concrete. Those latexes which are mentioned earlier for steel protection are good for bonding purposes too.

In the present case study we have used a bonding coat of acrylate based co-polymeric solution and cement in 1:1 proportion (part by weight) as a slurry. Such polymeric materials are reported to show added bonding to concrete and steel which is approximately thirty times more in concrete to concrete and almost 100 times more in case of steel and concrete<sup>10</sup>. Such a bonding coat can effectively replace the use of dowels at very close intervals.

### **3.2 Polymer modified mortar/ concrete**

Providing a new cover to a repairable structure should be done only wherever necessary and the temptation to expose the entire surface – even if a part of it is unaffected strong concrete, should be avoided. Judicious removal of diseased concrete is therefore essential. If the replacement is done by unmodified concrete, it can deteriorate due to carbonation and chemical attacks.

The most important factor encountered in selecting methods and materials for repair is the compatibility of existing concrete and new materials. Many materials change volume as they initially set, and practically all of them change volume with temperature and moisture changes. Tensile stresses are induced in one material and compressive stresses in the other, causing a substantial shear at the interface. Identical patterns of stress will result from the differential shrinkage and different moduli of elasticity<sup>11</sup>.

In the initial stages of advent of polymers for repairs, the only reliable material used for making up the lost concrete as epoxy. It is a very strong material and can easily give compressive strength of 80 to 100 N/mm<sup>2</sup> and high tensile strength of 20 to 30 N/mm<sup>2</sup>. In addition, epoxy mortars which fall under the category of polymer mortars are not affected by chemical

attack or carbonation. However, the following few points have made engineers and materials scientists ponder over alternatives to this system:

- Most of the reinforced concrete members to be repaired are having concrete strengths between 20 and 25 N/mm<sup>2</sup>. Hence, how correct is it to introduce in it intermittent pockets of very high-strength mortar?
- The cost of epoxy repair can be high, particularly if large areas are to be rehabilitated.
- If faulty application is done, basically due to two-pack nature of epoxy and negligence on the part of the labourers (due to its user unfriendly character), bonding and integrity of mortar suffers resulting into undesirable behavior of the concrete.
- Epoxy mortars are found to be susceptible to fires or fire-prone areas, wherein the mortar itself catches fire readily. This not only leads to loss of earlier repairs but the fire also increases.
- If user-friendly, one-pack polymer cementitious mortar is used, such mortar will be more compatible with the existing reinforced concrete members and it will have good properties like chemical resistance, carbonation resistance etc.
- Preparation of cementitious polymer mortar is easy for construction workers, since it is a plain cement mortar in which the polymer is to be simply mixed. This does not require any specialized training and hence the problems of poor workmanship can be minimised.

Due to above points, the trend is shifting in favour of polymer modified cementitious mortars which have improved chemical and physical properties as compared to ordinary cement /concrete mortar. In addition to above reported properties, studies of comparative photomicrographs have shown that the addition of polymer emulsions to concrete results in bonding of the latex to the aggregates and helps in bridging the cracks as they form. As a result, the polymer relieves the internal macro stresses, retards the formation and enlargements of cracks and increases the concrete's overall strength. Moreover, as the voids and cracks are bridged by the polymer, it results in substantially reducing the penetration of moisture and corrosion chemicals. The indicative properties of the polymers used in these mortars are given in Table 1<sup>10</sup>. The cost of these mortars is approximately 33 percent of the cost of epoxy mortar. In addition, the polymer mortar cover is of the order of 10 to 15 mm in thickness above steel. Such thickness itself can adequately take care of further chemical attack or subsequent carbonation. Remaining part of the cover can be simply finished with well-controlled plain cement / concrete mortar to get proper level. Such judicious use of polymers can further bring down the cost of rehabilitation without sacrificing on performance. In many countries such mortars find large application in repair of bridge decks where the cost of repairs due to corrosion would otherwise be colossal.

### 3.3 Surface protection treatment

The final step in the rehabilitation project is the application of the penetrating sealer to entire surface including the repaired concrete parts. This helps to minimize the moisture and chloride penetration and related continuous environmental attack. Repairs are carried out on patch-work basis and these patches are repaired with polymer concrete/mortars or polymer modified mortars/concretes. Obviously at these repaired patches environmental attack or carbonation attacks are not effective, though the adjacent area may get affected. Hence, to protect the entire area from attacks and to avoid subsequently repair expenses, application of the surface coating becomes imperative. Generally, these protective seal coats are suitably pigmented so that besides protection, aesthetics of the structure can also be taken care of simultaneously. Various coatings like polyurethane, epoxy, alkyds, chlorinated rubbers, acrylic emulsions can be used for this purpose. However, selection is done keeping following points in mind:

- Adhesion to the surface
- Compatibility with alkalinity of concrete
- Breathing capacity at the same time the coating should be impermeable enough
- Resistance to aggressive attacks
- Expected longevity of the treatment
- Capacity to absorb irregularities of the surface like slight dampness or imperfect cleaning of the surface.
- Ease in application and availability of color shades.

In the case study reported here, specially formulated material suiting above requirements, an acrylate based copolymer formulation - **POLYALK WP** was mixed into colored cement to form a water resistant coating to avoid any ingress of moisture / water in the concrete.

### 4.0 PARTICIPANTS IN THE PROJECT

Client	:	Municipal Corporation of Greater Mumbai
Consultants	:	S. J. Group, Mumbai, and Structural Designers & Consultants Pvt. Ltd., Mumbai
Contractors	:	Manjalankal Construction
Supplier of Construction	:	Sunanda Speciality Coatings Pvt. Ltd, Mumbai Chemicals

## REFERENCES

- Smolcyk, H.G., 1976. *Physical and chemical phenomena of carbonation*. Proceedings RILEM International symposium on carbonation of concrete, Cement and Concrete Association, Wexham Springs, UK, pp.10.
- Bahadurpurkar, M.G., Godbole, U.B., 1999. *Major structural repair to GKG bridge at Andheri*. National Conference on Corrosion Controlled Structure, India Society of Structural Engineers, pp.345.
- Guide For Repair Of Concrete Bridge Superstructures*. ACI 546.1 Ir-80, 1980. American Concrete Institute, Detroit, pp.20
- Ingvarsson, H., And Ericksson, B., 1998. *Hydrodemolition for bridge repairs*. Nordisk Betong (Stockolm), No 2-3. pp 49-54.
- Caims John And Abdullahramli. July-August 1994. ACI Materials Journal, Vol.91, no.4.
- Sieely Carrol N. And Kelly Thomas Enp., 1991. *Concrete surface preparation coating and lining and inspection*. National Association of Corrosion Engineers, Houston.
- Brett, M.A. And Brett, A.O., 1993. *Electro-chemistry methods and application*. Oxford University Press, pp.361.
- Manjrekar, S.K., Manjrekar R.S. And Nair P.R.C., July 1996. *Role of polymer – Cement-inhibitor comatrix in corrosion control of reinforcing steel*. The Indian Concrete Journal, Vol 70, No.7, pp 389-392.
- CEB/FIP Model Code for Concrete Structures*, 3<sup>rd</sup> Edition, 1978. Comite Euro-international du Beton / Federation Internationale de la Precontrainte, Paris, pp.348
- Ohama Y., 1973. *Study of properties and mix proportioning of polymer modified mortars for buildings (in Japanese)*. Report on the Building Research Institute, No.65, Tokyo, Japan.
- Bullock, R.E., 1980. *Factors influencing concrete repairs materials*. Concrete International: Design and construction, Vol 2 No.9, September, pp.67-68.



# **DEVELOPMENT OF NEW METHOD TO INSPECT DETERIORATED CONCRETE USING NIR SPECTROSCOPIC TECHNIQUE**

H. KANADA<sup>1</sup>, Y. ISHIKAWA<sup>2</sup> AND T. UOMOTO<sup>3</sup>

<sup>1</sup>Graduate School of Engineering, The University of Tokyo, Japan

<sup>2</sup>Graduate School of Engineering, Shibaura Institute of Technology, Japan

<sup>3</sup>Institute of Industrial Science, The University of Tokyo, Japan

kanada@iis.u-tokyo.ac.jp

## **ABSTRACT**

*Many non-destructive inspection methods have recently been developed for concrete structures. However, these methods can obtain only physical information of concrete, such as crack depth, delamination or position of reinforcement etc. near its surface. Core boring or sampling may be carried out for componential analysis in order to cover the lack of chemical information. A remote non-destructive method that can detect deterioration factors such as carbonation, chloride content or sulfate attack would be an outstanding innovation in inspection methodologies. In this research, remote non-destructive material detection of concrete is attempted using near-infrared [NIR] spectroscopy. The first step requires the measurement of optical properties of components generated due to deterioration. A specific wavelength that can detect the target component was determined from measured spectrums. Further, the capability of quantitative analysis was confirmed using chemometrics. This enables us to obtain chemical information of concrete by just sensing reflected near-infrared rays from the measuring plane. Since the existing methods are restricted to measurements on small areas, a new near-infrared imaging system was assembled using equipment already available. This system consists of near-infrared irradiation equipment, imaging spectroscopy and near-infrared CCD camera. Dispersed near-infrared rays through the spectroscopy can be received in each wavelength by light-sensitive element on CCD camera. Finally, distribution or concentration of the target component can be observed as an image. This paper describes the detection method of carbonation, chloride and sulfate attack as examples. Applicability of this method for inspection has been corroborated by experimental results.*

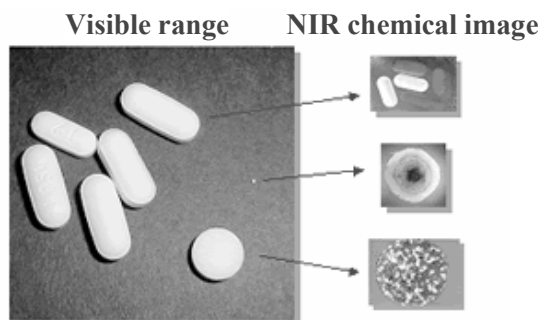
## **1.0 INTRODUCTION**

Visual inspection is carried out as the first step of diagnosis of deteriorated concrete structures. Then, detailed inspections such as non-destructive testing methods or constitutive analysis may be done if necessary. For example, delamination or loose portion of concrete can be detected by using the infrared thermography method, and the ultrasonic method is used for measurement of crack depth. But deleterious substances of concrete can not be detected by non-destructive inspection method. Core

boring or sampling may be carried out for constitutive analysis in order to obtain chemical information. In the case of social infrastructures, the inspection area is large, and environmental condition or location may be tough, therefore, it often requires high labor and cost in order to inspect concrete structures. The applicability of diagnosis of deteriorated concrete using near-infrared spectral imaging system is examined in this paper. This method would prove to be a very effective technique for inspectors since it can be remotely used to obtain chemical information on concrete surface.

## 2.0 APPLICATION EXAMPLE OF SPECTROSCOPIC TECHNIQUE

Near-infrared [NIR] spectroscopy had been developed in the area of agriculture or food. Electromagnetic waves are absorbed or reflected from any substance depending on the characteristics of their components. Therefore, unknown components can be estimated if its optical properties have been understood. Figure 1 shows the near-infrared image of tablets. Left figure was captured in the visible range, right figure was captured by near-infrared spectral imaging system.



*Figure 1 Near-infrared image of tablets (S. T. Japan Inc.)*

Distribution of components can be observed from NIR image. Each component of tablet has its own characteristic optical properties, so concentration of the component can be visualized as shading by capturing spectral image at a specific wavelength. Figure 2 shows the optical properties of tablet components.

In this figure, the x axis shows the 2nd derivative spectrum, and y axis the wavelength. 2nd derivative spectrum has local minimal value at absorption peak of raw spectrum, and it has local maximum value at reflecting peak of raw spectrum (Figure 3).

As shown in Figure 2, Aspirin has a unique reflecting property at 1637nm, Acetaminophen and Caffeine also have unique absorption properties at 2042, 2420nm respectively. Figure 4 shows component distributions of tablets. Mixing ratio of components can be measured remotely by image analysis, and these systems have already been installed at production lines of medicine manufacturing plants in order to check its quality.

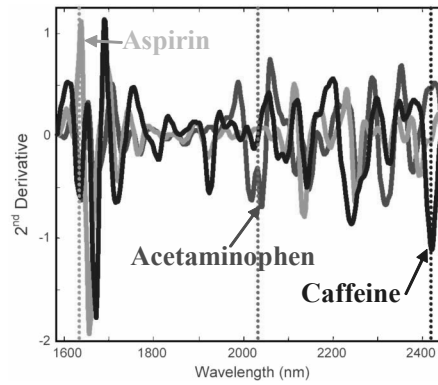


Figure 2: Optical properties of tablet components

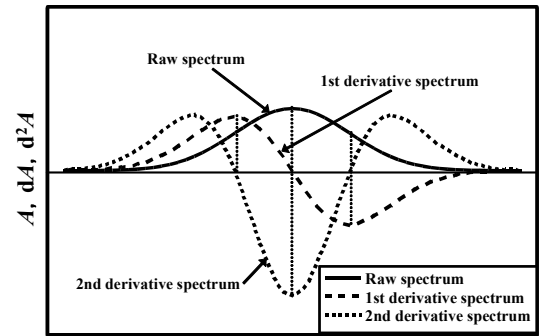


Figure 3: Relationship between raw spectrum and 1st, 2nd derivative spectrum

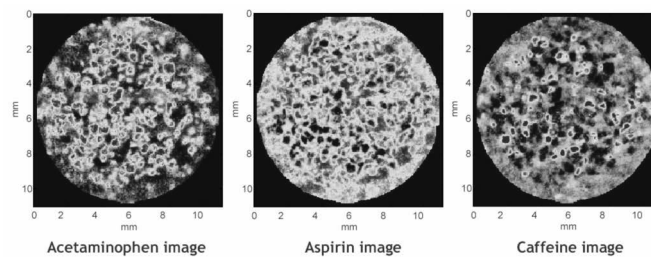


Figure 4: Component distributions of tablets (Spectral Dimensions Inc.)

### 3.0 APPLICATION OF NEAR-INFRARED SPECTROSCOPY TO DETECT DELETERIOUS SUBSTANCES IN CONCRETE

Causes or grades of deterioration can be estimated from presence of substances such as chloride, calcium carbonate, calcium sulfate, alkali silica gel, rust etc. on concrete surface. In this research, steel corrosion due to carbonation, chloride penetration and sulfuric acid attack were primarily focused upon, and spectrum change due to deterioration was investigated.

#### 3.1 Preparation of samples

Considering deterioration mechanisms, degeneration of cement hydrates or penetration of detrimental constituent are main causes except in cases of fracture due to external force or use of harmful aggregates. Moreover, sand or coarse aggregate do not have unique optical properties in near-infrared range, so spectrum change of cement hydrates due to deterioration was focused. Cement paste samples were prepared in so as to obtain basic optical properties of concrete components. Samples, 40×40×160 mm in size, of chloride containing cement paste specimens (Table 1) were prepared. These proportions were determined according to the chloride content on concrete surface described in “Standard Specification for Design and Construction of Concrete Structures”(Japan society of civil engineers). Chloride (sodium chloride) was directly added

into the mixing water. Remixing was carried out to prevent segregation and to keep uniformity before casting.

Table 1: Mix proportions of samples

Cement	Ordinary Portland cement	W/C	50%
Sample No.	Chloride content (kg/m <sup>3</sup> )	Sample No.	Chloride content (kg/m <sup>3</sup> )
N-50	Not contained	N7-50	9.0
N1-50	1.2	N8-50	11.0
N2-50	1.5	N9-50	16.0
N3-50	2.0	N10-50	20.0
N4-50	3.0	N11-50	25.0
N5-50	4.5	N12-50	30.0
N6-50	6.0		

To verify spectrum change due to carbonation, specimen of N-50 was placed in carbonation chamber until fracture plane pink coloration was not noticed upon spraying phenolphthalein alcohol solution. To verify spectrum change due to sulfuric acid attack, it was soaked in sulfuric acid.

### 3.2 Measurement of near-infrared spectrum

The near-infrared spectrums of samples were measured using a near-infrared spectrometer (FOSS NIRSystems 6500 Series). The Spectral reflectance can be obtained from reflex ratio between sample and barium sulfate used as standard white surface. The absorbance was adopted as the parameter of optical properties by converting reflectance (equation 1) in this case

$$\text{Absorbance} = \log(1 / \text{Reflectance}) \quad (1)$$

Figures 5 to 9 show the relationship between absorbance and wavelength of sample. The values shown have been averaged across fifty measurements for the same sample. Measurement can be completed in several tens of seconds for one sample.

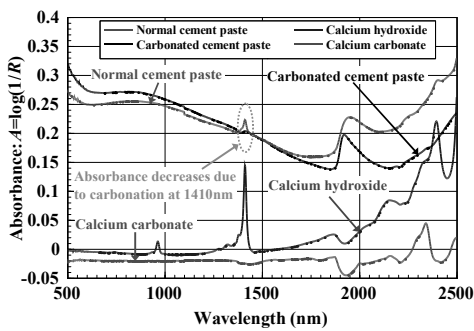


Figure 5: Spectrum change due to carbonation

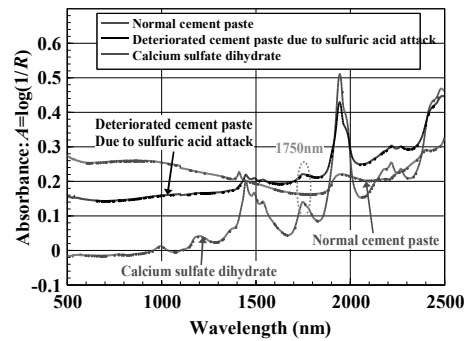


Figure 6: Spectrum change due to sulfuric acid attack

Figure 5 shows spectrum change due to carbonation, spectrums of  $\text{Ca}(\text{OH})_2$  and  $\text{CaCO}_3$  are also shown for reference. Decrease of absorbance at 1410nm can be observed due to carbonation.  $\text{Ca}(\text{OH})_2$  in hydrated cement changes to  $\text{CaCO}_3$ , therefore, absorption properties of hydroxyl (-OH) were found absent. Absorption peak at the wavelength is caused by 1st overtone spectroscopy of the hydroxyl stretch vibration in calcium hydroxide. Wavelength of 1410nm can be selected as characteristic waveband to verify carbonation.

Deterioration due to sulfuric acid attack is often concerned for sewage treatment equipments or structures in hot-spring area. Figure 6 shows spectrum change due to sulfuric acid, and the spectrum for  $\text{CaSO}_4 \cdot 2\text{H}_2\text{O}$  has been shown for reference. Calcium sulfate dihydrate is produced due to chemical reactions between calcium hydroxide and sulfuric acid (eq. 2).

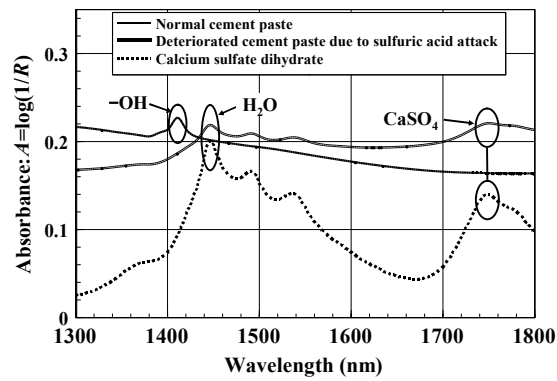
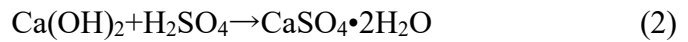


Figure 7: Assignment of absorption peak of deteriorated samples due to sulfuric acid attack

Some optical absorption peaks can be observed after deterioration (Figure 7), and absorption peak at 1410nm was found absent due to neutralization. Wavelength 1750 nm was selected as characteristic waveband to verify deterioration caused by sulfuric acid since, compared to other peaks, it was independent and clear (F. M. Howari, et.al., 2002).

Figure 8 shows spectrum change from different chloride contents. Increase of absorbance at 2266nm can be observed as chloride content increases. The optical absorption peak can be seen clearer in Figure 9, showing the enlarged figure at 2266nm after baseline offset. This behavior is attributed to the fact that the vibration mode of cement hydrates is changed by the action of chloride. Further details regarding this phenomenon are currently being investigated. 2266 nm can be selected as characteristic waveband to quantify chloride content of cement paste.

Second derivative can remove the baseline offset and slope of the turbid interference, and emphasizes the peak of the spectrum (Figure 3). This method is widely used for spectral analysis. Figure 10 shows the 2nd derivative spectrums of samples. The effectiveness of second derivative method can be seen by the accentuation of the absorption property at 2266nm when compared to Figure 9.

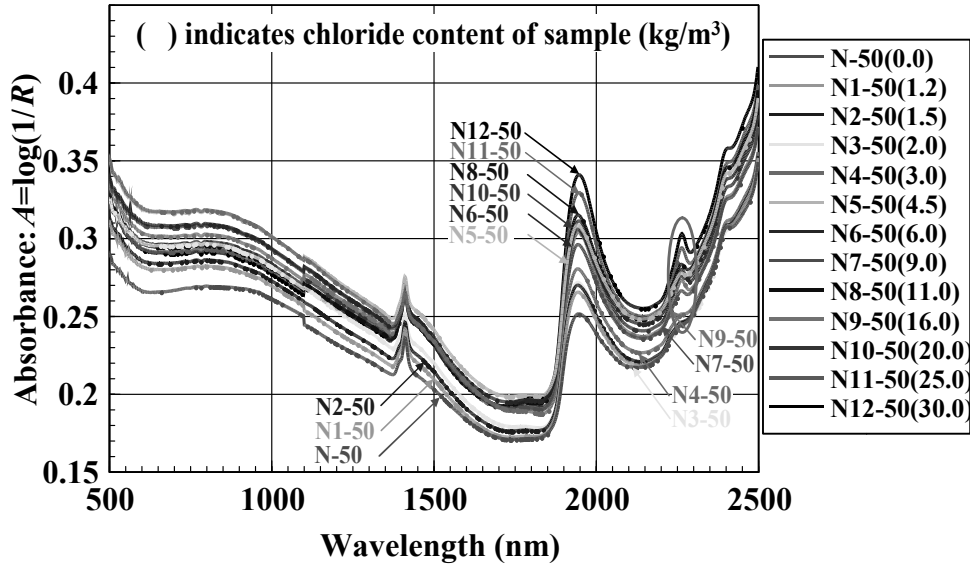


Figure 8: Spectrum change from different chloride contents

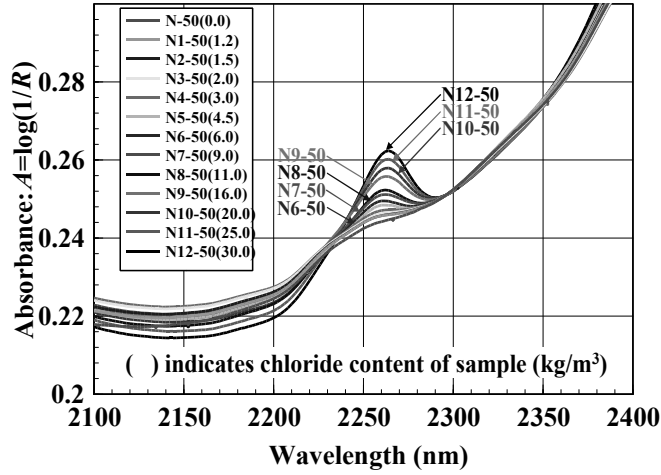


Figure 9: Enlarged figure at 226.6 nm after baseline offset

### 3.3 Introduction of regression analysis

Regression analysis should be carried out when the relationship between component and optical properties is required. The simplest method of calibration is based on a single independent variable (wavelength), and used for estimation of chloride content. The assumption is that constituent value  $c$  (concentrations) are linear function of the 2nd derivative spectrum  $A''$  at some wavelength  $i$ :

$$c = K(0) + K(1) \cdot A_i'' \quad (3)$$

The least squares approach fits the line so as to minimize the sum of squares of deviations between data points and the calibration line and yields two calibration constants: intercept  $K(0)$  and slope  $K(1)$ . Those deviations are taken along the concentration axis, and are hence called concentration residuals. Chloride content of concrete can be easily estimated from the

calibration curve. In this case, this curve was determined from second derivative spectrums and concentrations:

$$c = 0.79 - 2461 \cdot A''_{(2266)} \quad (\text{kg/m}^3) \quad (4)$$

The chloride content of sample can be estimated by substituting the value of second derivative spectrum at 2266 in equation 4. Figure 11 shows the relationship between calculated value from calibration curve and actual value, a very high correlation ( $R^2=0.99$ ) was obtained. Therefore, accurate calibration curve can be obtained in above steps, and chloride content can be estimated from optical spectrum.

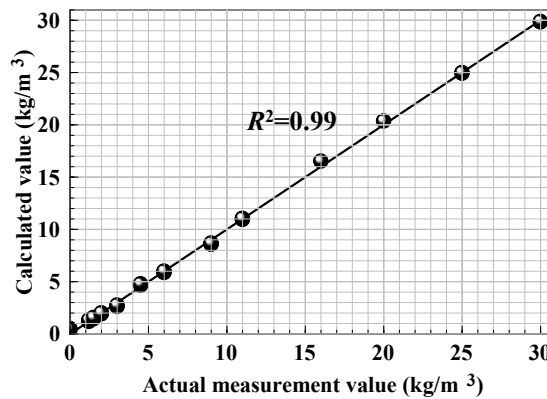


Figure 11: Relationship between calculated value and actual

#### 4.0 DETECTION OF DELETERIOUS SUBSTANCES OF CONCRETE USING NEAR-INFRARED SPECTRAL IMAGING SYSTEM

Since the near-infrared spectrometer can be used to measure the spectrum only at a fixed point, the spectral imaging system is required for two-dimensional scans.

##### 4.1 Introduction of near-infrared spectral imaging system

Near-infrared spectral imaging system was introduced in order to detect distribution or concentration of deterioration factors remotely. This system consists of near-infrared irradiation equipment, imaging spectroscopy and near-infrared CCD camera. This system consists of near-infrared irradiation equipment, imaging spectroscopy and near-infrared CCD camera. Dispersed near-infrared rays through the spectroscopy can be received in each wavelength by light-sensitive element on CCD camera (Figure 12).

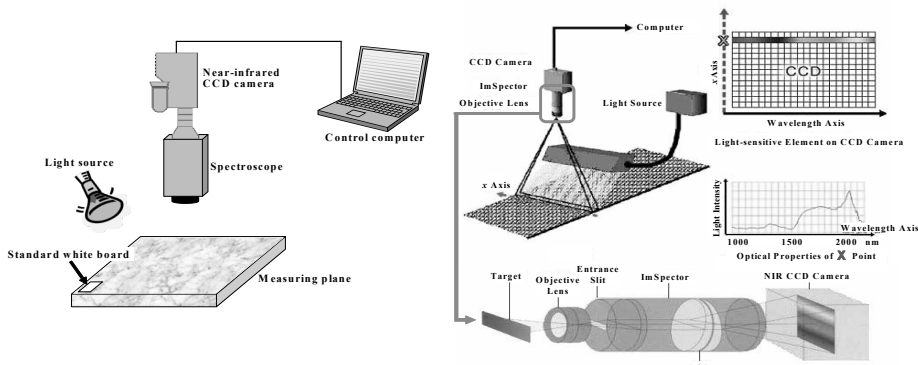


Figure 12: Near-infrared spectral imaging system

#### 4.2 Detection of carbonated area by NIR spectral imaging system

Detection of carbonation area was attempted by the system referring the result from obtained optical properties by spectrometer. Reflected near-infrared light from measuring plane through the spectroscopy is received, and then spectral image at arbitrary wavelength can be shown (Picture 1).

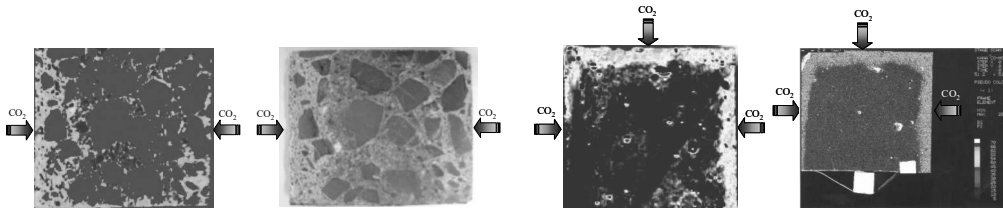
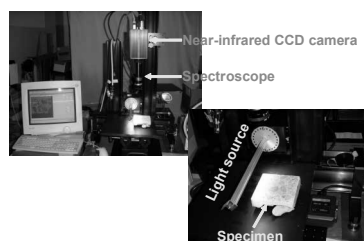


Figure 13: Spectral image and visible image of concrete specimen

Figure 14: Spectral image and result of EPMA analysis (Carbonation)

Figure 13 shows spectral image at 1410nm and optical image of a concrete specimen. The image in the left was obtained using the near-infrared spectral imaging system. Red pixels indicate non-carbonated area because calcium hydroxide absorbs near-infrared light of 1410nm, so the area is captured as dark. The image in the right was captured using a normal digital camera. Measuring plane was colored by spraying phenolphthalein alcohol solution. Figure 14 also shows spectral image at 1410nm and result of EPMA analysis (Target:C) of cement paste specimen. Good agreements between carbonated area detected by spectral image and traditional methods were observed.



Picture 1: Actual scanning in laboratory



### 4.3 Detection of chloride penetration by NIR spectral imaging system

Detection of chloride penetration was also attempted using the system. Figure 15 shows spectral image of 2266nm and result of EPMA analysis (Target:Cl). Cement paste specimen was soaked in salt water, so chloride was penetrated from its surface. Chloride containing cement paste absorbs near-infrared light of 2266nm, so high chloride concentration area appears dark.

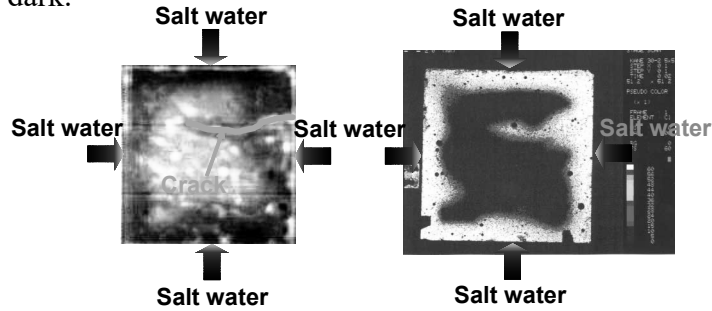


Figure 15: Spectral image and result of EPMA analysis (Chloride)

Distribution of chloride concentration can be obtained by image analysis (Figure 16). It was confirmed that chloride penetration can be also detected by the system from the experimental results.

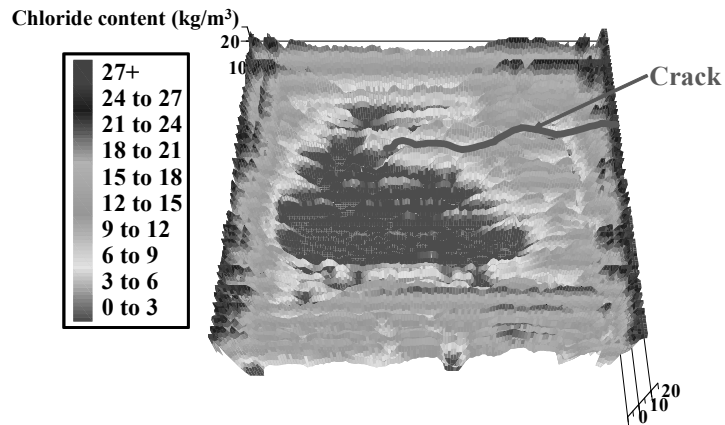


Figure 16: Distribution of chloride concentration

## 5.0 APPLICATIONS FOR FIELD INSPECTION

At the present stage, laboratory experiments have been carried out because performance of NIR spectral imaging system is not high. Some applications for field inspection will be expected. In case of concrete structures near seashore, chloride content on concrete surface or cover may be measured in order to estimate or investigate corrosion level of steel bars. If distribution of chloride concentration on concrete surface can be detected remotely, chloride penetration will be estimated approximately using Fick's diffusion equation. Moreover, number of core sampling would be proved to reduce since high chloride concentration area can be scanned two-dimensionally. As shown in Figure 17, unnecessary sampling can be

reduced and inspectors can designate the positions of boring from NIR spectral image. Fiber sensors can be also used for inspection of interior of concrete when information of internal deterioration is required. Carbonation depth, deterioration depth due to acid attack or chloride content at arbitrary depth can be measured using NIR fiber optic sensor (Figure 18).

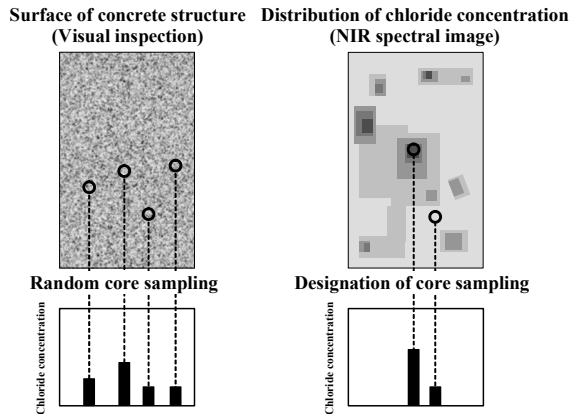


Figure 17: Core sampling using NIR spectral

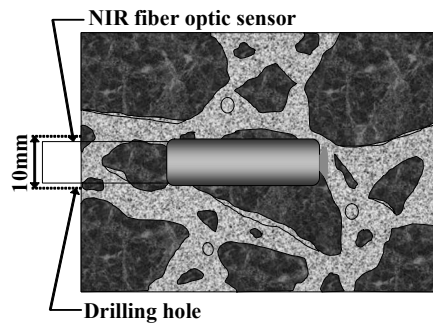


Figure 18: Inspection of interior of concrete using NIR fiber optic sensor

## 6.0 CONCLUSIONS

It has been shown that deterioration factors of concrete such as carbonation, sulfuric acid attack or chloride penetration can be detected from their optical properties, and methods for obtaining quantitative values of chloride content, etc. have been illustrated in this work. This method would be applicable to other deleterious substances too, if they have characteristic optical properties in near-infrared range. The Near-infrared spectral imaging system was also introduced to obtain the two-dimensional spectrum of the measuring plane. The applicability of the method has been corroborated by comparison of the results with those obtained using traditional methods.

## REFERENCES

- S. T. Japan Inc. *Product catalogue of near-infrared spectral imaging system*. (In Japanese).
- Spectral Dimensions Inc.: *Product catalogue of MatrixNIR*.
- Japan society of civil engineers. *Standard Specification for Design and Construction of Concrete Structures*, 2002. (In Japanese).
- F. M. Howari, P. C. Goodell, S. Miyamoto. 2002. *Spectral Properties of Salt Crusts Formed on Saline Soils*. *Journal of Environmental Quality*, 31:1453-1461.

# **VULNERABILITY ASSESSMENT OF EXISTING ENGINEERED AND NON ENGINEERED STRUCTURES OF DHAKA CITY USING RVS AND NDT TECHNIQUES**

MEHEDI A. ANSARY AND MUNAZ A. NOOR  
Department of Civil Engineering, BUET, Dhaka, Bangladesh  
[ansary@ce.buet.ac.bd](mailto:ansary@ce.buet.ac.bd)

## **ABSTRACT**

*Bangladesh is an earthquake-prone country. Although, a large part of the urban building stock is engineered but the quality of the construction is unsatisfactory. Luckily, the recent major earthquakes have occurred away from the city. The history of the region indicates that there is a strong possibility of major earthquakes occurrence that could cause extreme devastation. In fact recent studies demonstrated that even moderate earthquakes could be fatal in populated, unplanned cities. General public and the engineering community are becoming more and more aware of the situation. However, neither the possible extents of seismic damage of existing buildings are known nor there is any guideline for their strengthening measures. Even the performance of the engineered buildings under a seismic event is questionable, as enough work has not yet been done in this field.*

*The methodology for conducting a successful insitu investigation includes: strategic planning, preliminary visual inspection, loading assessment, material property evaluation and load testing techniques. The single most sought after material property used for the evaluation of residual load capacity and structural adequacy of deteriorated concrete structures is the insitu concrete strength. This study has presented the results of seismic vulnerability assessment of some existing engineered and nonengineered buildings of Dhaka City using Rapid Visual Screening Technique and has also estimated insitu concrete strength of some existing buildings by carrying out non-destructive tests. Finally using the collected insitu information seismic performance of one-engineered building has been assessed by structural modeling.*

## **1.0 INTRODUCTION**

The 1997 Chittagong Earthquake (Sabri, 2002), the 1999 Moheskhali Earthquake (Ansary et al., 2001) and the 2003 Rangamati Earthquake (Ansary et al., 2003) revealed the vulnerability of “non-earthquake-proof” cities and villages in southeastern part of Bangladesh. In 1897, an earthquake of magnitude 8.0 caused serious damages to buildings in the northeastern part of India (including Bangladesh) and 1542 people were killed. Recently, Bilham et al. (2001) pointed out that there is high possibility that a huge earthquake will occur around the Himalayan region

based on the difference between energy accumulation in this region and historical earthquake occurrence. The population increase around this region is at least 50 times than the population of 1897 and cities like Dhaka, Chittagong, Kathmandu, Guwahati have population exceeding several millions. It is a cause for great concern that the next great earthquake may occur in this region at any time. According to a report published by United Nations IDNDR-RADIUS Initiative, Dhaka and Tehran are the cities with the highest relative earthquake disaster risk (Cardona et al., 1999). Once a great earthquake occurs, Dhaka will suffer immense losses of life and property and will not be able to function as the capital of Bangladesh.

After the recent 2003 Rangamati Earthquake people of Dhaka City which is one of the densest areas in the world has become frightened regarding the quality of their houses. Especially the students of residential halls of Dhaka University (DU) have requested their authority to assess their halls and strengthen them. Under this circumstance, the authors have been requested by the DU authority to provide expert advice on this issue. Figure 1 shows the location of Dhaka and DU with respect to Bangladesh.

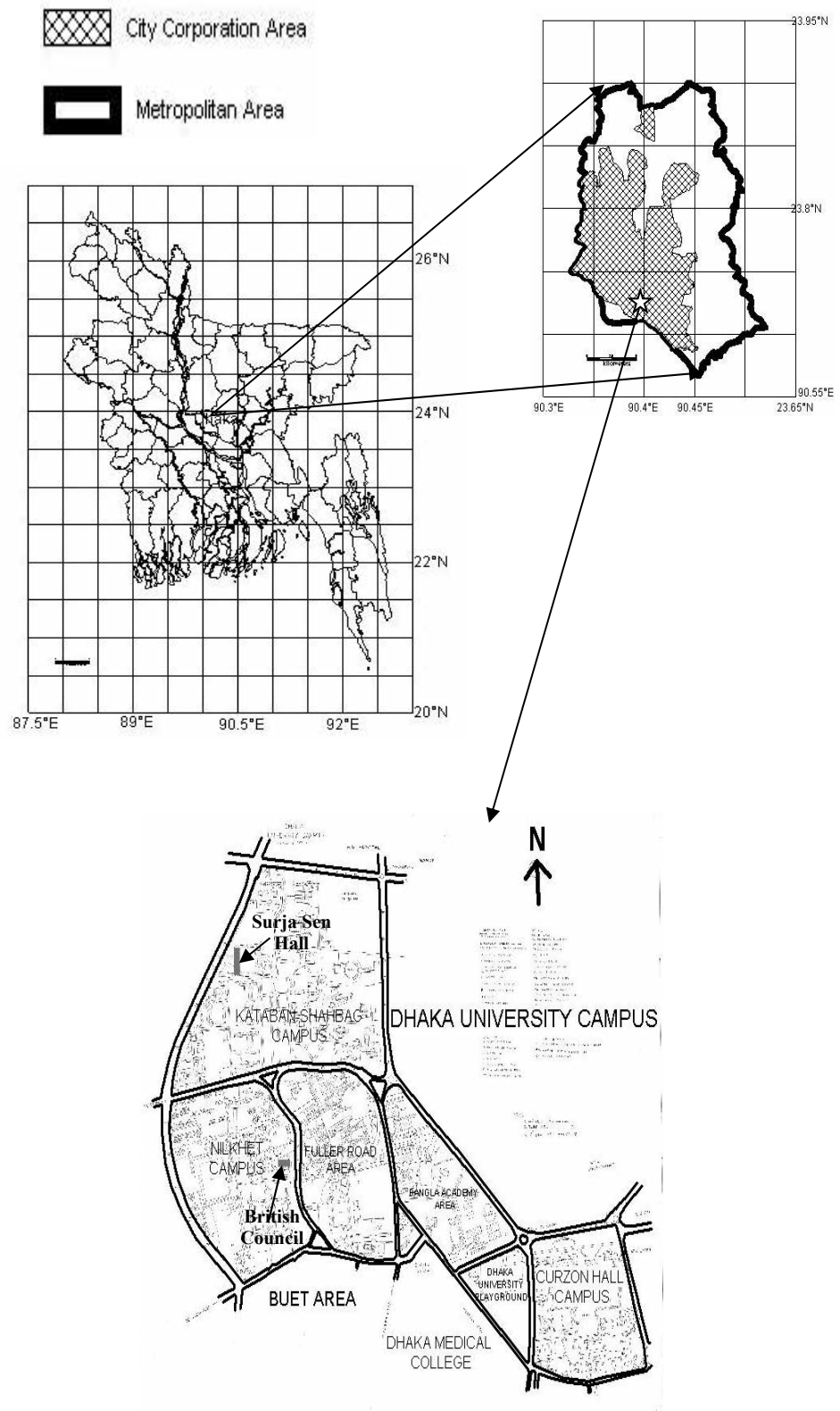
Accordingly, a Rapid Visual Screening (RVS) (FEMA-154, 2002) survey has been carried out for all the buildings of DU. A detailed evaluation for some of the buildings with low RVS score have also been undertaken. Initially two buildings one nonengineered and the other engineered have been selected for detailed evaluation. For this purpose non-destructive testing have been planned and carried out for the selected buildings. The obtained material data and other information have been used in the analysis of the structural model of the engineered structure.

This paper presents the findings of the non-destructive tests undertaken for the two buildings and the findings of the structural analysis of the engineered building. It also includes discussion of the results and provides recommendations for future study.

## **2.0 EXISTING STRUCTURES OF DHAKA UNIVERSITY**

Dhaka University (DU) is the premier university in Bangladesh, it was established in 1921. According to a recent survey (DU Chief Engineer, 2004) of the DU buildings, it has been found that there exist 165 official buildings within the campus. The buildings can be mainly classified into three categories: British Period (1757-1947), Pakistan Period (1947-1972) and Bangladesh Period (1972 to date).

Table 1 shows that among 165 buildings of DU, 61% are of Brick Masonry and the rest 39% are of reinforced concrete (RCC). This pattern of building construction has also been observed from the existing building typologies of Dhaka City (Ansary, 2004). Before undertaking a detailed survey, Rapid Visual Screening method (FEMA-154, 2002) has been undertaken for each of those 165 buildings. RVS for moderate seismic zone has been used as Dhaka falls in Zone-2 of Seismic Zoning Map of Bangladesh (BNBC, 1993) as shown in Figure 2.

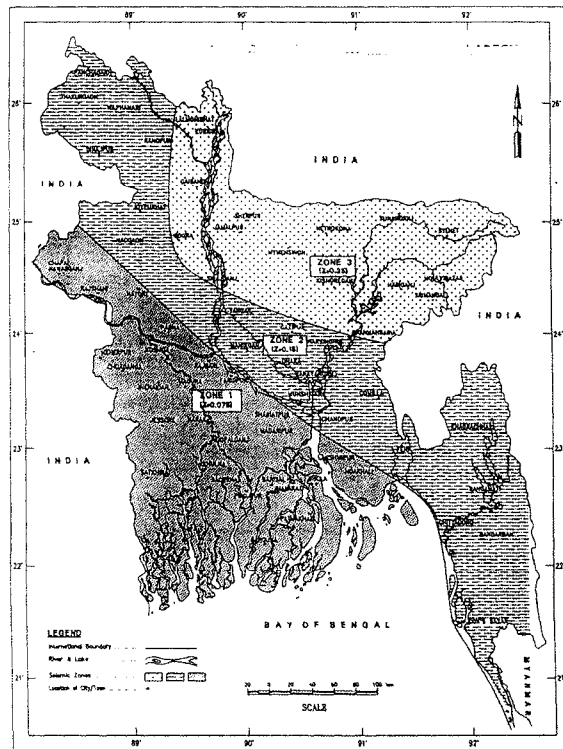


*Figure 1: Location map of Dhaka City and Dhaka University*

Almost all of the buildings have got a final score less than two. The primary reasons for this is that the buildings have either horizontal or vertical irregularities or both. The soil in DU area is stiff soil, which also reduces the score. Figure 3 shows two typical buildings of British and Bangladesh periods.

*Table 1: Types of existing buildings within DU*

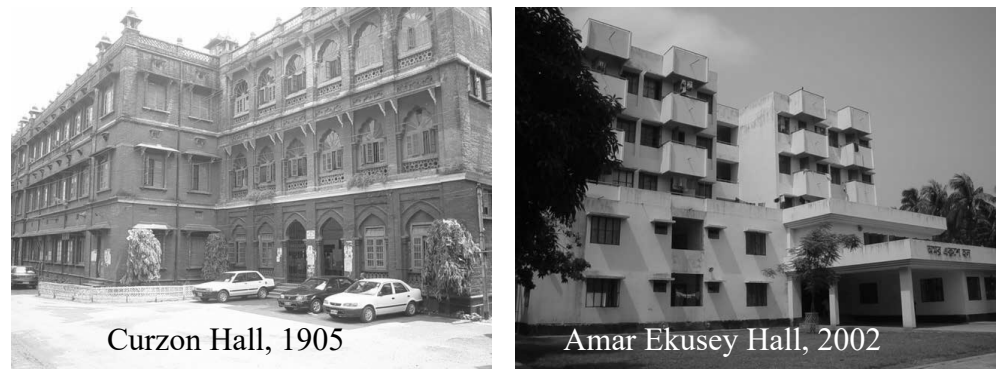
Period	Brick Masonry Structure			RCC Structure		
	Number	Maximum Storey	Construction Period	Number	Maximum Storey	Construction Period
British	7	3	1905-1942	-	-	-
Pakistan	61	5	1952-1970	23	6	1958-1970
Bangladesh	32	5	1972-2003	42	10	1972-2003



*Figure 2: Seismic zoning map of Bangladesh (BNBC, 1993)*

### 3.0 NON-DESTRUCTIVE TESTING

Among the DU buildings, two buildings have been selected for carrying out necessary non-destructive tests to obtain required in-situ concrete strength and other parameters for developing structural model and analysis. One is brick masonry and the other is reinforced concrete building. Figure 1 also shows the locations of these buildings.



*Figure 3: Typical buildings of British and Bangladesh periods*

### **3.1 British council complex**

This complex is located at Fuller road, Dhaka University. The complex has four brick masonry buildings all constructed in late 1950s. Schimdh Hammer and Micro Covermeter tests at selected locations of three of the buildings have been carried out. Also concrete core tests on collected samples and tensile strength tests on collected mild steel bar have been performed. Figure 4 shows the above mentioned tests been carried out on British Council buildings.

After conducting Schimdh Hammer test, following concrete strength have been obtained for roof slab:  $26 \pm 7$  MPa (9 locations); for beam:  $31 \pm 6$  MPa (3 locations). Using the Micro Covermeter equipment, main bar diameter and spacing and concrete clear cover have been determined for roof slabs and beams. Also three 48 mm diameter concrete cores have been collected from roof slab. Average concrete strength from the cores is  $28 \pm 2$  MPa. Three 6 mm diameter plain bars have been collected and tested in the laboratory with average yield strength of  $280 \pm 33$  MPa.

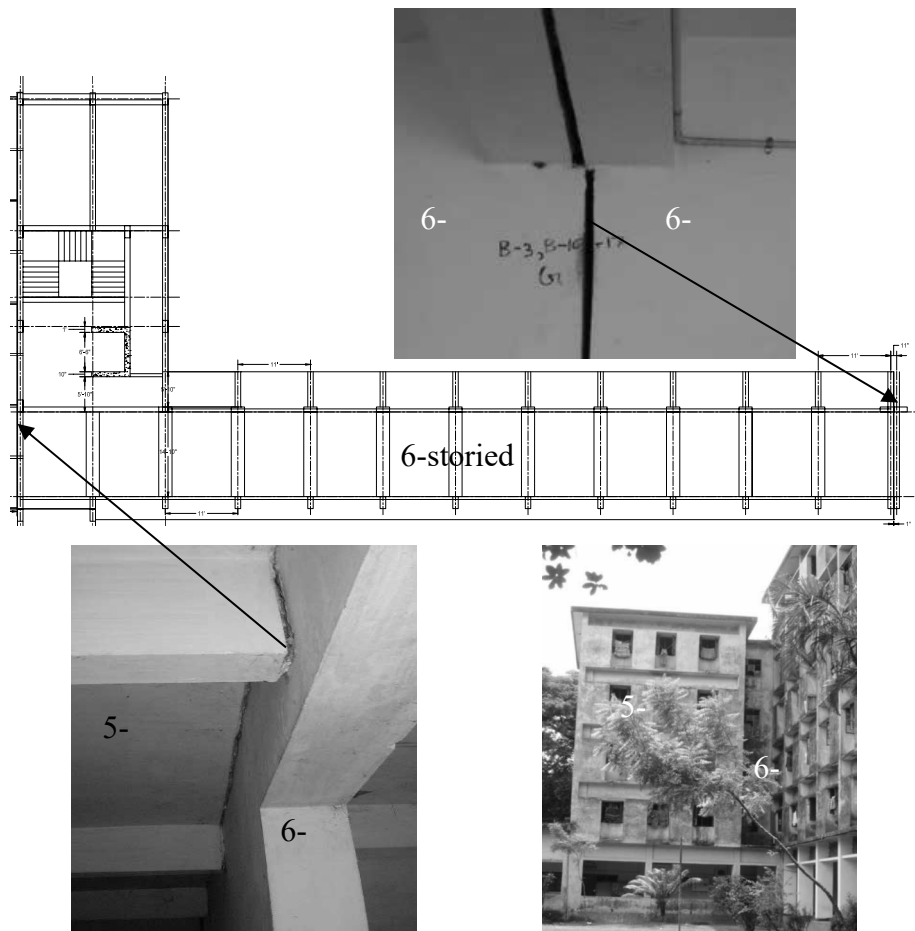
### **3.2 Surjo sen hall complex**

This student hall complex is located close to the Administrative office of DU. About 1200 students reside here. There are altogether twelve different buildings in the complex: five 5-story, two 6-story, one 3-story, three single-story and one auditorium. Except one 5-story house tutors bungalow, other 5 and 6-story buildings are connected with 1-inch expansion joint in between. All these buildings are ordinary moment resisting frame structures of reinforced concrete and were constructed in 1965. Figure 5 shows the plan of a 6-story building with two expansion joints at two ends. This building has a lift core and stair at one end.

Schimdh Hammer test have been carried out on the lift core, beams, columns and slabs of ground floor, third floor and the top floor of a 6-story building. Following concrete strength have been obtained for roof slab:  $19 \pm 5$  MPa (6 locations); for beam:  $16 \pm 5$  MPa (6 locations); for column:  $16 \pm 5$  MPa (6 locations); for lift core  $12 \pm 4$  MPa (6 locations).



*Figure 4: Non-destructive tests being carried out*



*Figure 5: Plan, elevation and expansion joints of a 6-storey building, Surjo Sen Hall*



#### 4.0 STRUCTURAL MODEL AND ANALYSIS

Figure 5 shows plan and elevation of a 6-story building of Surjo Sen Hall, which has been used for this investigation. The building has utilized a structural system with moment resisting frames having a lift core. All columns are 255x610 mm size and beams are of variable sizes: 150x610 mm, 150x1020 mm, 255x455 mm and 255x610 mm.

The analyses of the buildings have been carried out separately in the longitudinal and transverse directions using a finite element software ANSYS (1999). The first five modes and mode shapes of the elastic building without and with slabs are presented in Table 2. Figure 6 shows the first mode of the building without slab and Figure 7 shows the first mode of the building with slab.

*Table 2: Periods for different modal vibrations.*

Modes	Without Slab Period (s)	Mode Shape	With Slab Period (s)	Mode Shape
1	6.52	Cantilever along long direction	5.99	Torsional
2	5.72	Torsional	4.71	Cantilever along long direction
3	4.78	Torsional	3.77	Cantilever along short direction
4	3.83	Torsional	1.93	Double crossing
5	2.77	Double crossing	1.46	Breathing

The building has been analyzed for equivalent static load method (EQSM) and response spectrum method (RSM) following BNBC (1993) guideline. According to BNBC (1993), the design earthquake response spectrum for different types of soils is as shown in Figure 8. For the present study design response spectrum for soil type S<sub>2</sub> i.e., stiff clay has been used. The building has been analyzed without considering any vertical loads. The analysis results are presented in the next article.

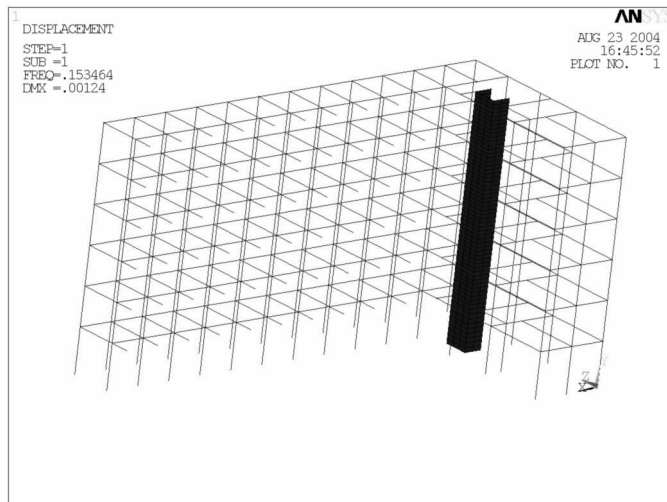
#### 5.0 RESULTS AND DISCUSSIONS

From the finite element analysis of the engineered structures of Surja Sen hall maximum top floor displacement have been estimated using the equivalent static load method (EQSM) and response spectrum method (RSM). The results are provided in Table 3. Figure 9 presents the structural analysis solution of the building without slab using RSM.

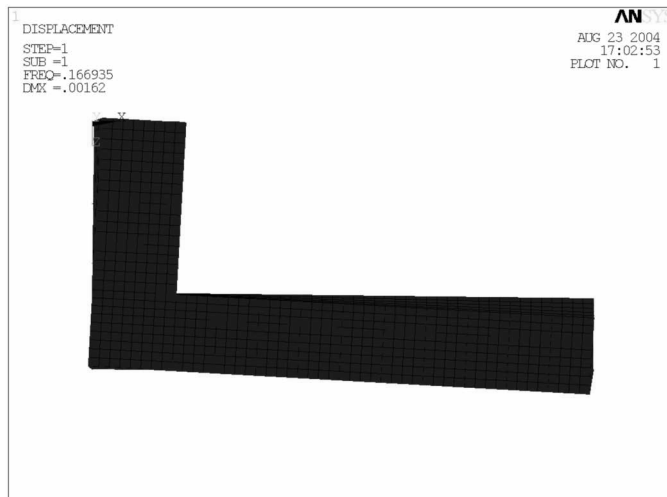
*Table 3: Maximum top floor deflection (mm).*

Method of Analysis	Without Slab Period (s)		With Slab Period (s)	
	Long Direction	Short Direction	Long Direction	Short Direction
EQSM	47	16	9	10
RSM	111	73	56	106

Non-destructive test (NDT) has provided very low insitu concrete strength and modulus as discussed earlier. Due to this the building has very long time period, which makes the building very flexible. From earthquake point of views, the building may absorb high energy but the deflection limit may be exceeded (as observed from Table 3), which demands high member ductility. But from the structural drawing, it has been found that the ductility detailing is absent in this building. During an earthquake this building may not be able to generate the desired deflection and eventually may collapse. To obtain the actual behavior of the building pushover analysis will be required. Also this building will need some strengthening to satisfy the earthquake demand.



*Figure 6: First mode of the building without slab*



*Figure 7: First mode of the building with slab*

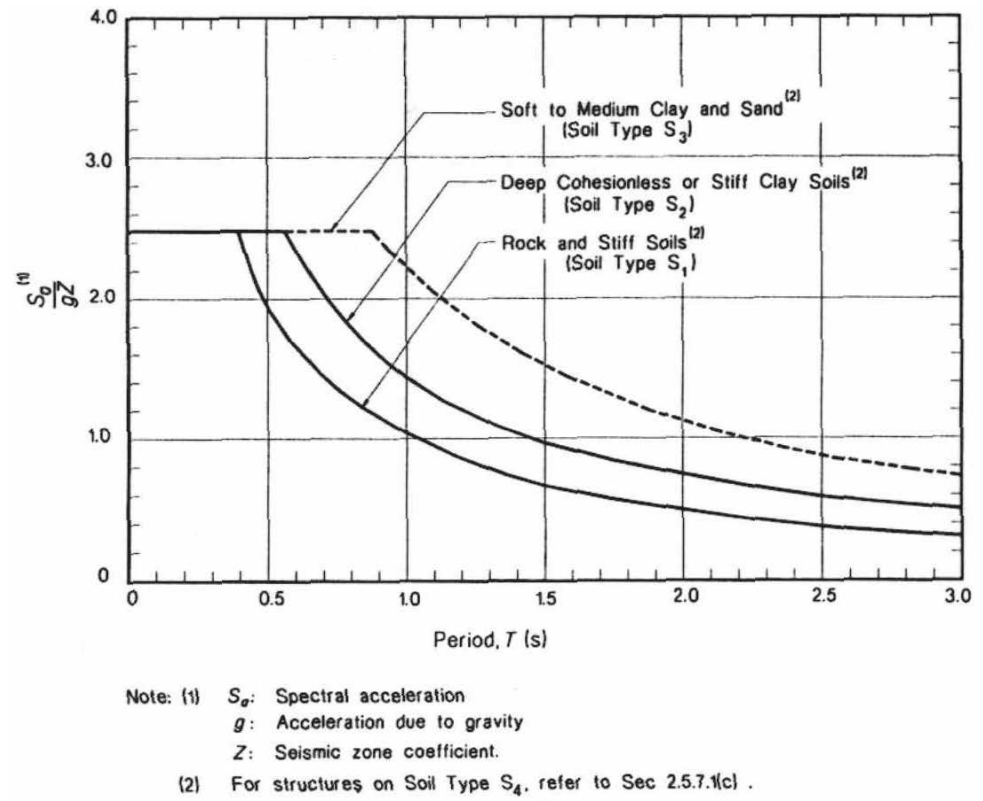


Figure 8: Normalized response spectra for 5% damping (BNBC, 1993)

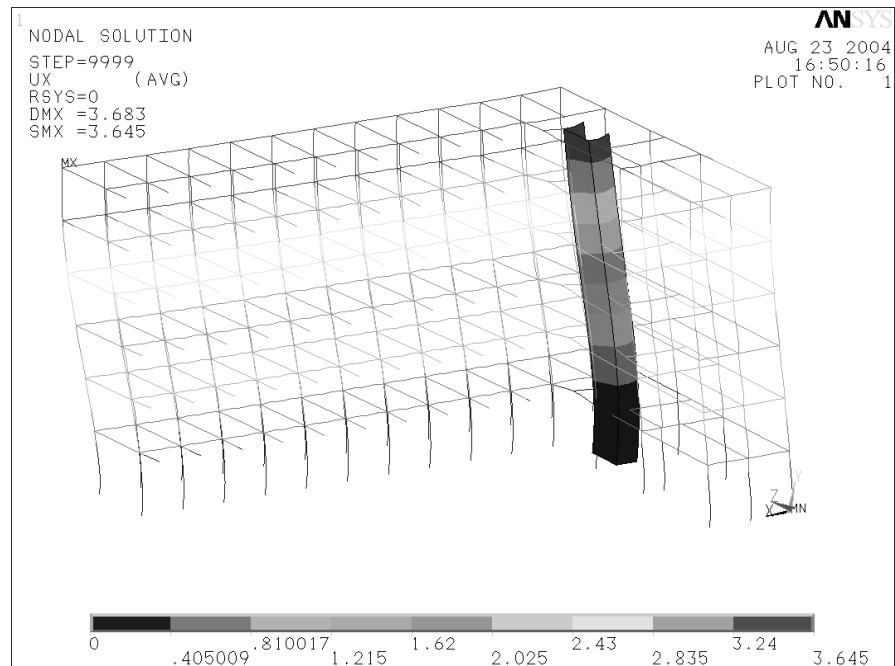


Figure 9: Deflected shape of the building without slab using RSM

## ACKNOWLEDGEMENTS

The authors would like to acknowledge the financial support provided by CASR, BUET. Also they would like to thank DU authority to allow them to carry out RVS survey and NDT test.

## REFERENCES

- Ansary, M.A., T.M. Al-Hussaini, M. Sharfuddin and J.R. Choudhury, 2001. 1999. *Moheshkhali earthquake: a damage study*. Journal of Asiatic Society of Bangladesh, 27 (2), 139-149.
- Ansary, M.A., A. Sadek and T.M. Al-Hussaini, 2003. 2003. *Rangamati earthquake – an engineering assessment*. Proc. of the Seminar on 2003 Rangamati Earthquake, Organized by Disaster Management Bureau, Ministry of Disaster Management and Relief, Government of Bangladesh and Bangladesh Earthquake Society, Dhaka, September 4, 2003.
- Ansary M.A., 2004. *Seismic loss estimation of Dhaka for an earthquake of intensity VII*. Oriental Geographer, 48(1), 1-16.
- ANSYS 5.6, 1999. ANSYS Inc., USA.
- Bilham, R., V.K. Gaur and P. Molnar, 2001. Himalayan seismic hazard. SCIENCE, 293.
- BNBC, 1993. Bangladesh National Building Code. HBRI-BSTI.
- Cardona, C., R. Davidson and C. Villacis, 1999. *Understanding urban seismic risk around the world*. Summary Report on the Comparative Study of the United nations International Decade for Natural Disaster Reduction, RADIUS Initiative.
- DU Chief Engineer, 2004. Building data collection of Dhaka University campus. Personal Communication.
- FEMA-154 (ATC-21), 2002. Rapid Visual Screening of Buildings for Potential Seismic Hazards: A Handbook.
- Sabri, S.A., 2002. *Earthquake intensity-attenuation relationship for Bangladesh and its surrounding region*. M. Engg. Thesis, BUET, Dhaka.

# **MAINTENANCE MANAGEMENT OF CONCRETE STRUCTURES BY USING REPAIR-RISK**

YOSHITAKA KATO

Institute of Industrial Science, University of Tokyo, Japan  
katoyosh@iis.u-tokyo.ac.jp

## **ABSTRACT**

*Prediction of deterioration of concrete structures was often executed using uncertain information, because the quality of concrete structures differed from the design due to construction errors. Therefore, it was very difficult to judge what repair/reinforcement should be selected, or when the repair/reinforcement should be done. To deal with that problem, it was considered to be very useful to acquire the information to predict the deterioration of concrete structures by inspection. Though physical inspection of actual structures can lead to more accurate results and predictions, such inspections are time consuming and are not as beneficial for application to large structures requiring maintenance. In this research, evaluation of the value of inspection technique in maintenance management was quantitatively done using repair risk, a factor proposed in this research.*

## **1.0 INTRODUCTION**

The Ministry of Land, Infrastructure and Transport (2003) forecasted that infrastructure maintenance cost in Japan would be about 9 trillion yen in 2025 which would be about 70 to 80 % of the entire construction investment. Especially, huge stocks which were constructed at the high economic growth period will be about 50 years old in 2020. As a result, the maintenance cost will drastically increase from that time. To deal with that problem, some researchers tried to apply “Asset Management” to maintain the stocks efficiently. But, it doesn't go well easily.

In order to do “Asset Management” appropriately, it is a minimum requirement to predict the future performance of structures. But, the prediction of deterioration of a concrete structure should be often executed under uncertain information, because the quality of concrete structures may differ from the design due to construction errors. Therefore the accuracy of prediction results may be low. This leads to difficulty in the selection of the repair/reinforcement methods and its timing. To deal with this problem, it is very useful to acquire the information by using several kinds of inspection techniques, such as ultra-sonic test, infrared thermograph, etc. Though physical inspection of actual structures can lead to more accurate results and predictions, such inspections are time consuming and are not as beneficial for application to large structures requiring maintenance.

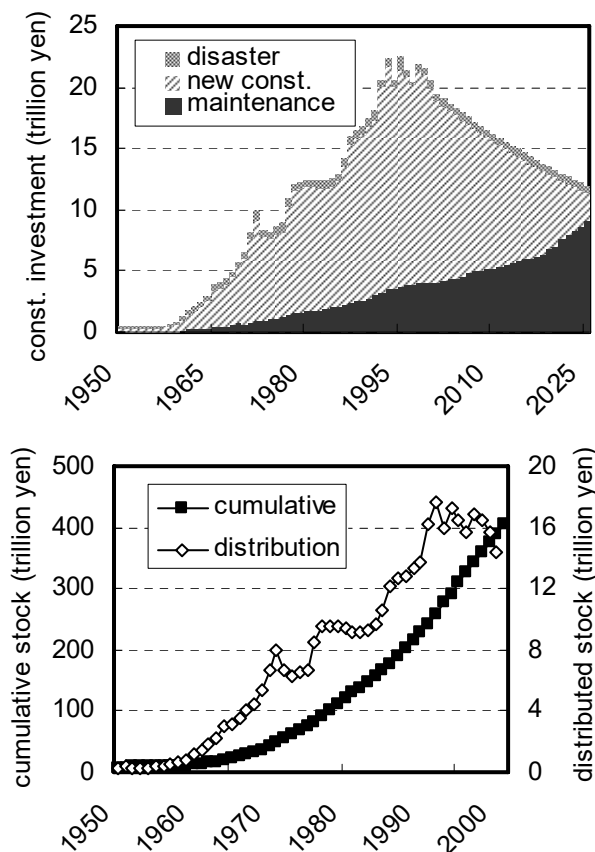


Figure 1: Construction investment and transition of amount of stock

In this research, evaluation of the value of inspection technique in maintenance management was quantitatively done using “Repair-Risk”, a factor proposed in this research.

## 2.0 WHAT IS UNCERTAIN INFORMATION?

In this research, corrosion-induced damage due to salt attack was selected as the case study of evaluating the value of inspection technique under uncertain information, because this phenomenon causes the serious deterioration of concrete structures and also can be predicted by moderate accuracy. When the prediction of this phenomenon is performed, the required information that depends on the applied model is as follows. 1) apparent diffusion coefficient of  $\text{Cl}^-$  in cover concrete, 2) thickness of cover concrete, 3)  $\text{Cl}^-$  content at surface concrete (environmental condition). Then,  $\text{Cl}^-$  content at surface concrete is governed by environmental condition such as distance from seashore, wind, temperature, humidity, and so on.  $\text{Cl}^-$  content at surface concrete is also uncertain information, but there is little research available for its calculation. Therefore, the influence of  $\text{Cl}^-$  content at surface concrete was neglected in this research. In addition, the accuracy of prediction result is also governed by the applied model. The model is also considered to be a kind of uncertain information. But in this research, the same model was applied to predict that phenomenon, the influence of

applied model was considered to be negligible. As a result, the apparent diffusion coefficient of  $\text{Cl}^-$  of cover concrete and the thickness of cover concrete were considered as the uncertain information in this research.

### 3.0 MODEL OF CORROSION-INDUCED DAMAGE DUE TO SALT ATTACK

The deterioration process of corrosion-induced damage due to salt attack is shown in Fig. 2. The corrosion of steel reinforcement begins at the end of stage1. According to JSCE (2002), this time is defined such that the density of  $\text{Cl}^-$  at surface of steel reinforcement reaches  $1.2 \text{ (kg/m}^3\text{)}$ . Next, the corrosion crack is generated at the end of stage2. This time is also defined such that the amount of corrosion reaches  $10 \text{ (mg/cm}^2\text{)}$ . In order to simulate stage1 situation, the diffusion analysis based on Fick's second law was conducted and for stage2, the proposed model by Matsumura et al (1999) was used.

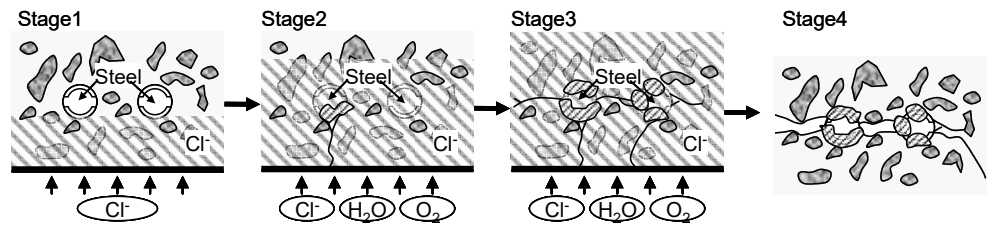


Figure 2: Deterioration process of corrosion-induced damage due to salt attack

The period of stage1 was calculated by equation (1). This equation is theoretical solution of Fick's second law of diffusion under the constant boundary condition.

$$C(x, t) = C_0 \left( 1 - \operatorname{erf} \frac{x}{2\sqrt{D_0 t}} \right) \quad (1)$$

where,  $C$ :  $\text{Cl}^-$  content ( $\text{kg/m}^3$ ),  $C_0$ :  $\text{Cl}^-$  content at surface of concrete ( $\text{kg/m}^3$ ),  $x$ : distance from concrete surface (cm),  $D_0$ : apparent diffusion coefficient of  $\text{Cl}^-$  ( $\text{cm}^2/\text{year}$ ),  $t$ : time (year), erf: error function

The period of stage2 was calculated by equation (2). This model was based on the relation between corrosion speed of steel reinforcement and concrete resistance.

$$\begin{aligned}
\log V_{\text{corr}} &= 33.1(R_{\text{RC}}) + Y \quad (R_{\text{RC}} \leq 0.04) \\
\log V_{\text{corr}} &= 33.1 \times 0.04 + Y \quad (R_{\text{RC}} \geq 0.04) \\
Y &= 0.457 \cdot C - 9.79 \quad (C \leq 6.89 \text{ kg/cm}^3) \\
Y &= -6.64 \quad (C \leq 6.89 \text{ kg/cm}^3) \\
\log((R_c)_{\text{L,H}}) &= A + B_{\text{L,H}} \sqrt{t} \\
B_{\text{L,H}} &= -0.007744 + 0.0018 \times L + 0.00037 \times H
\end{aligned} \tag{2}$$

where,  $V_{\text{corr}}$ : corrosion speed ( $\text{mg/cm}^2/\text{year}$ ),  $R_{\text{RC}}$ : reciprocal of concrete resistance ( $1/\Omega$ ),  $A$ : constant ( $-1.216$ ),  $L$ : thickness of cover concrete (cm),  $H$ : relative humidity (%).

#### 4.0 SETUP OF UNCERTAIN INFORMATION

The apparent diffusion coefficient of  $\text{Cl}^-$  and the thickness of cover concrete were considered as uncertain information. Setups for of each set of information are described in the following sections.

##### 4.1 Setup of apparent diffusion coefficient of $\text{Cl}^-$

There were a lot of measurement results of apparent diffusion coefficient of  $\text{Cl}^-$ . However, these results could not be simply compared because the method of calculating the apparent diffusion coefficient of  $\text{Cl}^-$  was different among researchers. To deal with that problem, Maeda et al (2002) re-analyzed 1500 data sets that were reported by the investigations in 27 years. Figure 3 is one example of analysis results. The relation between water cement ratio ( $W/C$ ) and apparent diffusion coefficient of  $\text{Cl}^-$  ( $D_{\text{Cl}}$ ) is shown in this figure. And the dispersion of  $D_{\text{Cl}}$  is also shown in this figure. This result was used in this research.

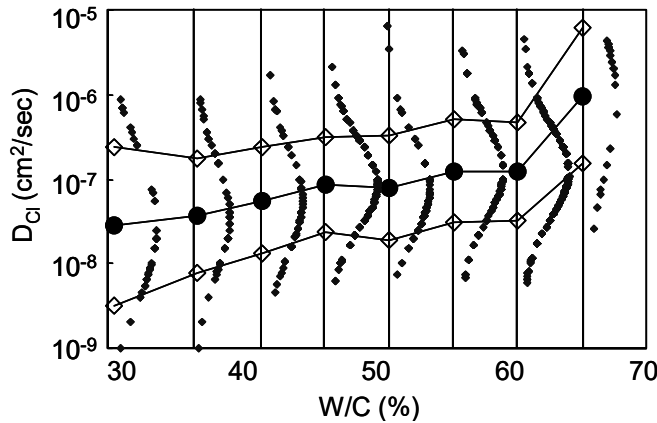


Figure 4: Relation between  $W/C$  and  $D_{\text{Cl}}$  [4]



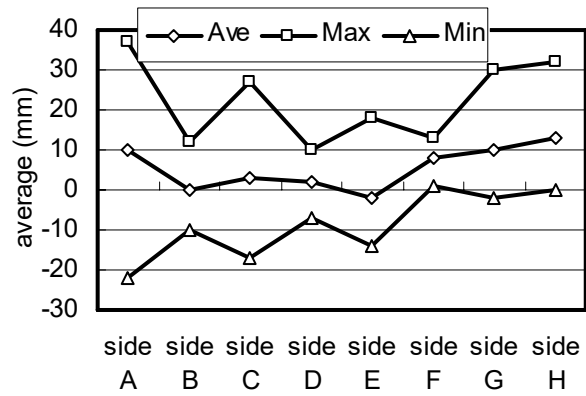


Figure 5: Average of construction error

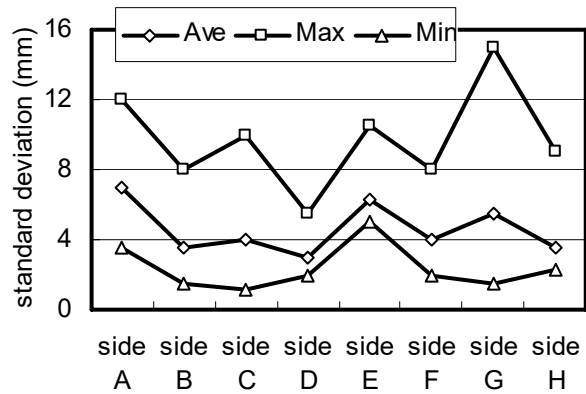


Figure 6: Standard deviation of construction error

## 4.2 Setup of thickness of cover concrete

It is very difficult to quantitatively evaluate the dispersion of thickness of cover concrete due to construction error. Setup of that dispersion was conducted based on the investigation results (Tanimura et al. 2003). Figure 5 shows the average of construction error. The plus value of vertical axis means that the thickness of cover concrete is thicker than that of design, and the minus value means the opposite situation. Figure 6 shows the standard deviation of construction error. These results were utilized in this research.

## 5.0 EVALUATION OF VALUE OF INSPECTION TECHNIQUE

### 5.1 Prediction of corrosion-induced damage due to salt attack

Figure 7 shows the examples of prediction results ( $T_{cc}$  means thickness of cover concrete). Analytical conditions are  $W/C = 0.5$ ,  $T_{cc} = 10$  (cm) and  $C_0 = 13$  (kg/m<sup>3</sup>) and the dispersion of  $D_{Cl}$  and  $T_{cc}$  were set based on Section 4. From this figure, it could be found that the corrosion crack occurs from 8 to 114 years. The probability density distribution of corrosion crack generation time are shown in Figure 8. Then,  $T_{cc}$  being kept at 10 (cm),  $W/C$  and  $C_0$  were changed in this simulation.

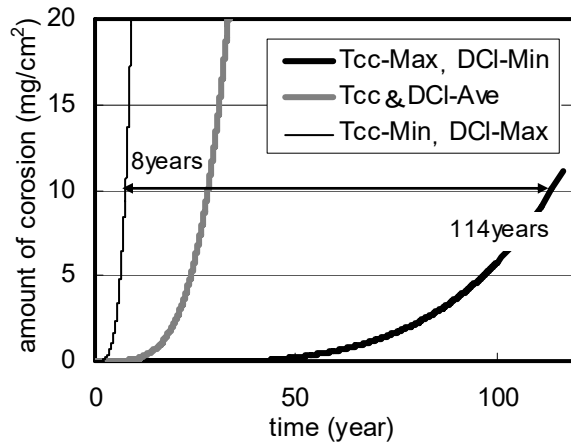


Figure 7: Calculation result of amount of corrosion

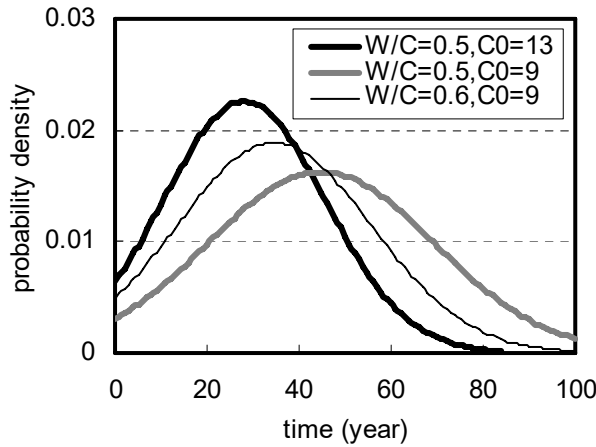


Figure 8: Probability density distribution of corrosion crack generation time

## 5.2 Calculation of “Repair-Risk”

In this research, the dispersion of prediction result was measured with “Repair-Risk (RR)” and it was calculated with probability density distribution of corrosion crack generation time ( $P_c$ ), repair cost ( $R_c$ ) and repair frequency ( $R_f$ ). The calculation conditions are as follows:

- Repair method: Desalination (cost = 1, validity time = 20 (years))
- Service period: 100 years
- Periodic inspections are conducted in every 5 years
- $(RR)_i = (P_c) \times (R_c \times R_f)_i \times (R_c \times R_f)_d$  at time =  $i$
- $(RR)_i$  was calculated at each periodic inspection (see Figure 9). Then,  $(R_c \times R_f)_d$  means total repair cost at design (design means there are no dispersions of  $DCI$  and  $T_{cc}$ ).
- $RR = \sum_{i=p}^{100} (RR)_i$  :  $p$  means the time when the value is evaluated (see

Figure 10)

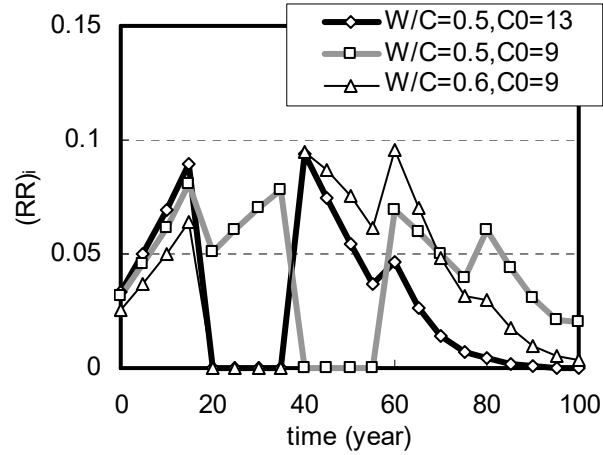


Figure 9: Calculation result of  $(RR)_i$

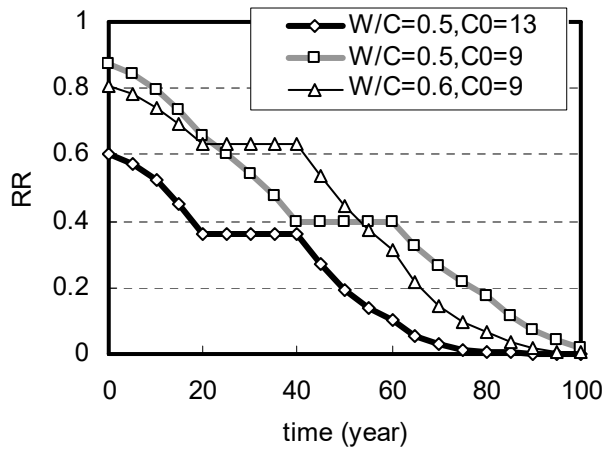


Figure 10: Calculation result of  $RR$

### 5.3 Evaluation of value of inspection technique

Figure 11 shows  $RR$  in case of measuring  $D_{Cl}$  or  $T_{cc}$  ( $W/C = 0.5$ ,  $C_0 = 13$  ( $\text{kg/m}^3$ )). In case of measuring  $D_{Cl}$ ,  $D_{Cl}$  was constant, but dispersion of  $T_{cc}$  remained. In case of  $T_{cc}$ , the opposite situation can be seen. From this figure, it could be found that measuring  $D_{Cl}$  can decrease  $RR$  more than measuring  $T_{cc}$  in this case study. Figure 12 shows the result of subtracting Figure 11 (measuring  $D_{Cl}$ ) from Figure 10. Vertical axis shows the amount of decreasing  $RR$ , meaning the value of inspection. Naturally, larger values denote higher values of inspection. From this figure, the order of the height of value of inspection depends on the time. Therefore, it was concluded that the structure that should be inspected by priority that can be judged by using this evaluation method.

### 6.0 CONCLUSION

In this research, the evaluation method of value of inspection technique under uncertain information was proposed. The proposed model can judge structures requiring inspection by proprietors. However, cost-effectiveness of inspection was not examined, and also the number of case

study was limited. The proposed model should be modified to deal with such a problem.

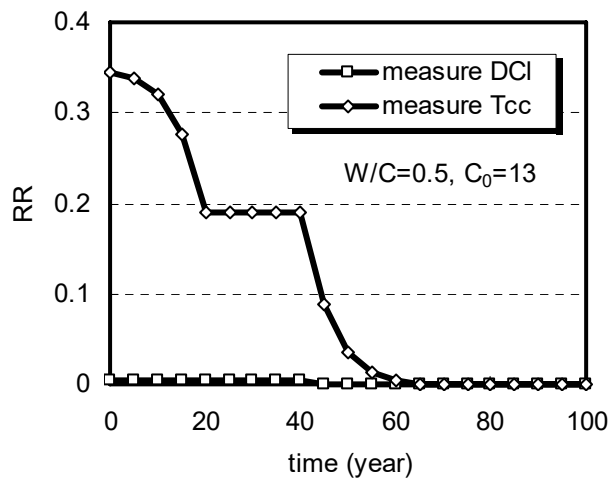


Figure 11: RR in case of measuring  $D_{CI}/T_{cc}$

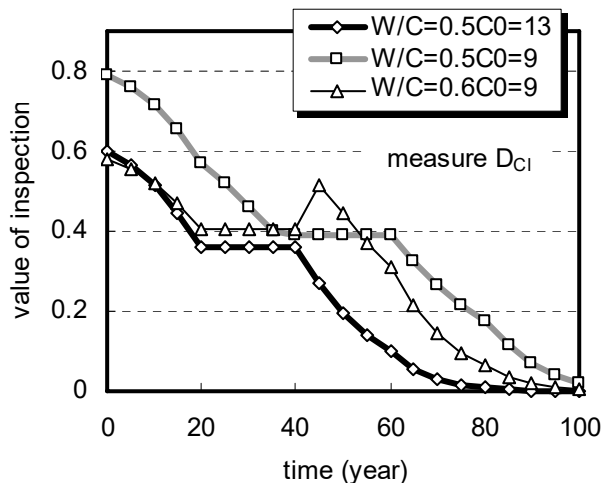


Figure 12: Calculation result of value of inspection

## REFERENCES

- JSCE, 2002. Concrete standard specifications (construction) (in Japanese)
- Maeda, S., Takewaka, K., Yamaguchi, T. and Yoshimoto, K., 2002. Analysis of Data on Chloride Diffusion Process into Concrete, proceedings of the JCI, Vol.24 (in Japanese)
- Matsumura, T., Kanazu, T. and Nishiuchi, T., 1999. An Evaluation Method for Corroding of Reinforcement in Concrete Structure Located in Seashore Atmosphere, Journal of Materials, Concrete Structures and Pavements, JSCE, Vol.634, pp.303-314(in Japanese)
- Tanimura, Y., Hasegawa, M., Sogabe, M. and Sato, T., 2003. Construction Error of Concrete Cover in Railway Viaduct, proceedings of the JCI, Vol.25, No.2, pp.1843-1848(in Japanese)
- The Ministry of Land, Infrastructure and Transport, 2003. White paper on Land, Infrastructure and transportation in Japan (in Japanese).

# **INFLUENCE OF FIBRE WRAP RETROFITTING ON GRAVITY DESIGNED RC BEAM-COLUMN JOINTS UNDER CYCLIC LOADING**

K K BAJPAI, C V R MURTY AND DURGESH C RAI

Department of Civil Engineering, Indian Institute of Technology Kanpur  
kunwar@iitk.ac.in

## **ABSTRACT**

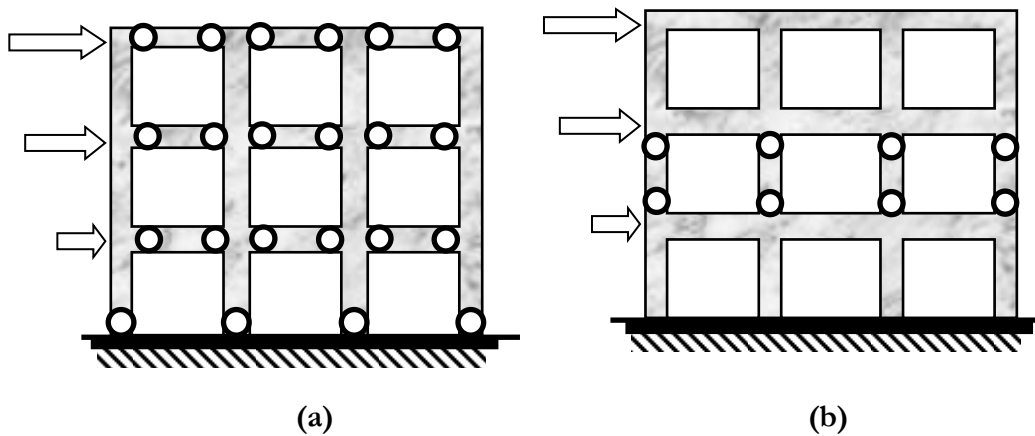
*Some RC frame buildings in India suffered severe damage in recent earthquakes due to poor detailing of joint reinforcement. Indian standards do not have detailed design guidelines for determining the amount of transverse shear reinforcement in joints and anchorage of longitudinal beam bars in columns. It is therefore important to evaluate the performance of beam-column joints of existing buildings and to devise suitable retrofitting techniques for improved seismic behavior of these lateral load resisting moment frames.*

*This paper presents details of one of a series of twelve beam-column specimens with different joint details tested up to failure under reverse cyclic loading and retrofitted in the joint failure region using glass fabric reinforced plastic (GFRP) composite. The effectiveness of retrofitting using GFRP composite for RC beam-column specimens was studied for improving the seismic performance of RC joints. The specimen retrofitted with GFRP composite showed improved strength and marginally improved energy dissipation characteristics under reverse cyclic testing when compared with original specimen. However, there is no improvement in the ductility of the joint.*

## **1.0 INTRODUCTION**

Much of the civil infrastructure is in need of repair or replacement as a result of damage caused by heavy use and exposure to the environment. There is additional demand on repair and retrofitting caused by natural disasters like earthquakes. The fiber reinforced polymers (FRP) are relatively new materials but they have already become important engineering materials. The properties of FRP's like high strength-to-weight and stiffness-to-weight ratios, corrosion resistance, light weight and potentially high durability make them very attractive for use in civil infrastructure. Recently, the new retrofit method for reinforced concrete (RC) structures using FRP's is getting attention due to its advantages over conventional retrofitting techniques like steel jacketing and shotcreting etc. Their use has significantly increased in the retrofitting of RC structures due to their tailor able performance characteristics.

Good seismic performance of RC frames is achieved in frames that have the ability to (a) avoid a sudden development of collapse mechanism during strong earthquake shaking, and (b) absorb seismic energy through inelastic deformations. These objectives are met at global and local levels while designing a RC frame system. At the global level, a suitable collapse mechanism is chosen which distributes the inelasticity uniformly throughout the structure but at specific regions, which enhances overall energy dissipation potential and limits the inelastic demand at each of these specific regions to a low level. And, at the local level, these regions designated for inelastic activity are so detailed that they can undergo large deformations without losing much strength and stiffness. For typical RC frames, a *strong column-weak beam* (SCWB) collapse mechanism (Figure 1a) satisfies the above global objective much better than by a *strong beam-weak column* (SBWC) mechanism (Figure 1b). In SCWB systems, flexural capacities of beams at a joint are developed before (i) the shear capacities of the beams themselves, (ii) the shear capacity of the joint, and (iii) the flexural capacities of the columns.



*Figure 1: Collapse mechanisms of frames (a) overall sway mechanism owing to strong-column weak-beam design, and (b) storey sway mechanism owing to strong-beam weak-column design*

Moreover, some RC frame buildings suffered damage in recent earthquakes due to poor detailing of joint reinforcement (amount of transverse shear reinforcement in joints and anchorage of longitudinal beam bars in columns) (Rai and Murty, 2003). In the Indian context, most buildings were designed by the Indian Concrete Code IS:456:1978 (IS:456:1978) and IS:456:2000 (IS:456:2000), in which there is no mention of beam column joints. It is therefore important to evaluate the performance of beam-column joints and to devise superior detailing techniques for improved seismic behavior of lateral load resisting moment frames. Further, the suitable retrofitting technique to rehabilitate the failed beam-column joint in existing structures is very important to bring back the damaged structure in its normal life.

Extensive research work has been reported in literature on retrofitting of columns (Priestle et. al., 1996, and Seible et. al. 1997). Circular, square, and rectangular bridge columns have been strengthened externally using continuously wrapped carbon FRP (CFRP) composites and steel jacketing. Confinement, ductility, and shear effects were studied and design guidelines were developed. An experimental investigation was conducted by Sadatmanesh et. al. (1996) to study the effect of retrofitting using composite straps on seismic performance of RC columns. The retrofitted columns had a improved ductility (up to 6) compared to low level of ductility (1.5) observed for specimens without FRP retrofitting. Janoes Gergely et. al. (2000) studied the viability of carbon FRP composite for shear strengthening of RC T-joints. The use of CFRP has increased the joints's shear strength greatly and in addition there was better damage control and the joints had the minimal residual strength at the end of the test sufficient for supporting dead loads. Malek and Saadatmanesh (1998) studied the ultimate shear capacity of RC beams strengthened with web-bonded FRP plates. Older concrete structures do not meet the modified code criteria

This paper reports the findings of two specimens of an experimental study on retrofitting of damaged exterior RC beam-column joint sub-assemblages that are typical of gravity-only designed RC frames in low seismic regions and of pre-seismic code constructions in India and many other developing countries. Full details of all specimens tested in this series are given elsewhere (Murty et al. 2004).

## **2.0 OBJECTIVES**

Retrofitting of different beam-column joints damaged under reverse cyclic testing is done by using glass fabric reinforced polymer (GFRP) overlays. The performance of this FRP retrofitting technique is evaluated based on hysteretic behavior and energy absorbed under cyclic loading.

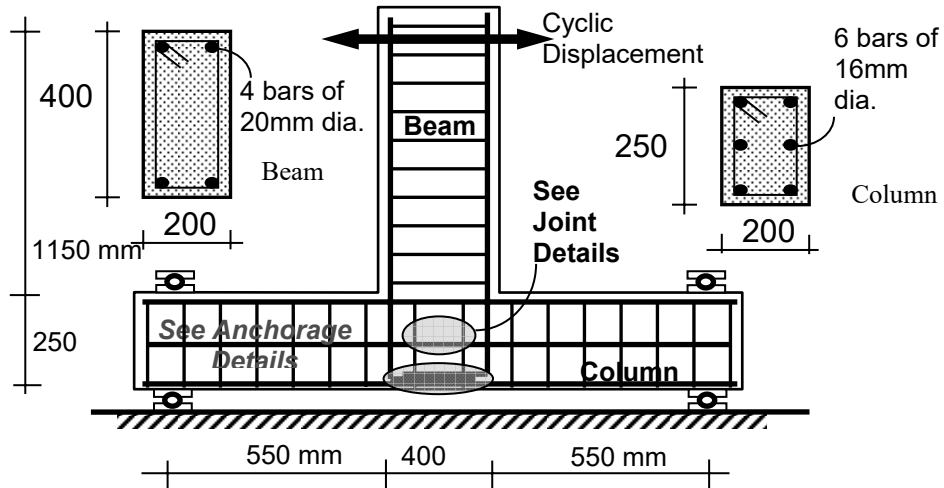
## **3.0 EXPERIMENTAL DETAILS**

### **3.1 Specimen design**

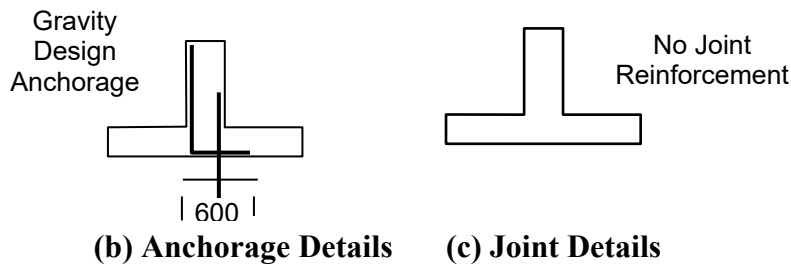
Two specimens of half scale RC beam-column joint sub-assemblages were tested, one original and another retrofitted. The original specimen represented reinforcement detailing for anchorage of beam bars and transverse reinforcement of joint core as practiced in most RC frame building constructions in India (Figure 2). The anchorage in the specimen is typical for non-seismic (gravity) frames where only tension rebars are anchored (Indian Standard Handbook on Concrete Reinforcement and Detailing, 1987). This type of anchorage is least effective against pullout in strong seismic shaking. The original specimen S1 was tested under cyclic loads up to failure as reported in a previous study (Murty, et. al., 2003). The photograph of a typical specimen failed in joint is shown in Figure 3.

### 3.2 Application of GFRP overlays

The failed joint was retrofitted by GFRP overlays (4 layers) in the joint region after replacing the cracked concrete with fresh concrete (Figure 4). The balanced weave glass fabric (area density: 350 g/m<sup>2</sup>) has been used



(a) Frame Geometry



(b) Anchorage Details (c) Joint Details

Figure 2: Geometry and reinforcement details of specimen

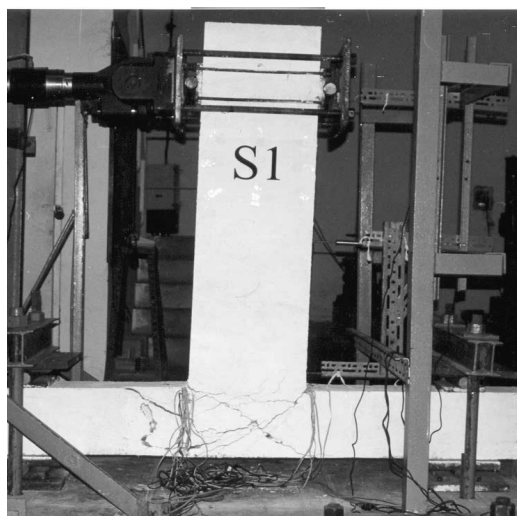


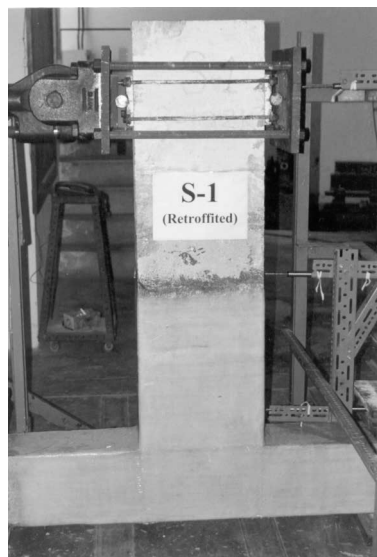
Figure 3: The original specimen tested up to failure



as reinforcement along with epoxy resin system for application of GFRP overlays to retrofit all the twelve specimens damaged under cyclic testing. The epoxy resin has two components: Resin PG-100 and Hardener PH-851 available from local manufacturer M/s Parikh Resins Limited, Kanpur. The hardener is mixed in the resin (50% by weight) with gel time of 180-200 minutes (sufficient for retrofitting one joint at a time) and curing time of 24 hours at room temperature. After cleaning the finished surface of the repaired joint a thick coat of epoxy resin was applied first. Subsequently, layers of cut glass fabric sheets in T-shape were applied in the joint region (total four layers). The glass fabric was impregnated with epoxy resin in each layer by using rollers and brushes so that extra resin from below comes on top ensuring proper impregnation. The cracked concrete in the beam and column surrounding the joint was also covered with GFRP overlays. The photograph of the specimen with GFRP overlays in the test set-up is shown in Figure 5.



*Figure 4: Putting fresh concrete after the removal of cracked concrete from failed joint*



*Figure 5: Photograph of the GFRP retrofitted specimen*

### 3.3 Test set-up

The isolation of sub-assemblages from the frame structure requires that proper boundary conditions be simulated in the test set-up for faithful emulation of stresses inside the test specimen akin to the prototype. A schematic of the test-setup used in the study is shown in Figure 6. The sub-assemblage was rotated  $90^\circ$  such that the column member is in the horizontal position and the beam member in the vertical position.

A 250 kN hydraulic actuator was used to apply cyclic displacements at the beam end. The column ends are held against the reaction floor through an arrangement, which not only restricts the horizontal movement but also provides moment-free rotation through an external hinge fixture (Figure 6). The loading program used was the same as for original specimens, consisted of a simple history of reversed symmetric cycles of increasing displacement amplitudes in predetermined steps (Figure 7). At each step of loading, three cycles were performed. This simplified history permits the evaluation of parameters such as energy dissipation potential, and failure mode, which are important for understanding the seismic performance of any system. The load cell in the actuator arm measured the applied horizontal force and the DC type LVDTs mounted on the specimen monitored the displacements and were recorded online on a data acquisition system.

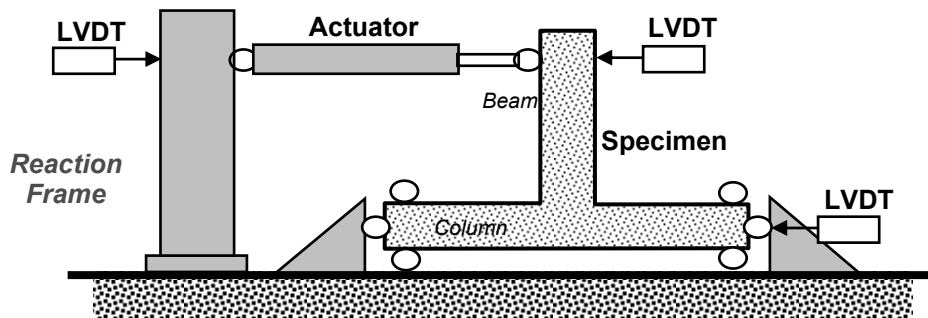


Figure 6: Test set-up for cyclic displacement loading of joint sub assemblage in a  $90^\circ$  rotated position

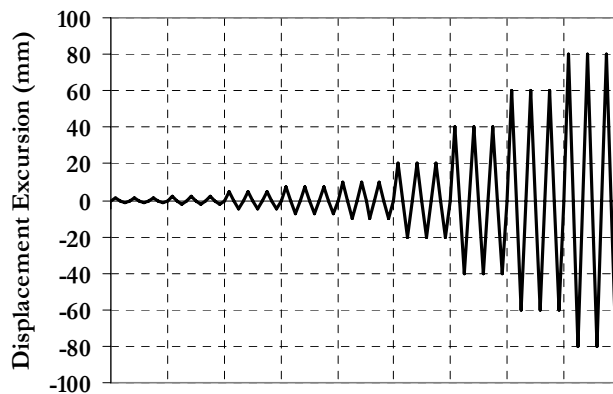


Figure 7: Cyclic displacement loading history applied on joint sub-assemblages

#### 4.0 RESULTS AND DISCUSSIONS

The effect of retrofitting using GFRP overlays for twelve different RC beam column specimens damaged under cyclic loads (Murty et. al., 2003) has been studied. The retrofitted specimen has been tested under same cyclic loading like original specimen. The overall hysteretic behavior of the two specimens is summarized in Table 1 and Figures 8 and 9. In general, the retrofitted specimen has been able to regain its original strength. The specimen failed at the same displacement excursion levels as the original undamaged specimen. The increase in peak load is between 33.7% as observed from envelope backbone curves (Figures 10) for the specimens. Observed pinched hysteretic curves (Figures 8-9) of the sub-assemblages (for both original and retrofitted specimens) are primarily due to premature shear failure of the joint region exhibiting performance of joint reinforcement.

Comparing hysteretic loops (Figures 8-9) and envelope backbone curves of the specimens (Figures 10), the ultimate displacement (the displacement at 15% drop of peak load) is 20.0 mm for original specimen and 18.1 mm for retrofitted specimen. The cumulative energy dissipated during the hysteretic loops has been plotted for different specimens in Figure 11 and the total cumulative energy values are given in Table 1 to compare the performance of different specimens. A comparison of the energy dissipation of the specimens (Figure 11) shows that the specimen with no joint reinforcement indicates the poor energy dissipation potential. It has been observed that use of GFRP overlays for retrofitting has been able to achieve the original strength and marginally increase the energy dissipation characteristics. However, there is no improvement in the ductility.

*Table 1: Comparison of observed Ultimate displacement and load, and computed cumulative energy dissipated during hysteretic cycles*

<b>Specimens</b>	<b>Ultimate Displacement <math>\delta_u</math>, mm</b>	<b>Ultimate Load, <math>P_u</math>, kN</b>	<b>Total Energy dissipated in hysteretic cycles, <math>E_{cummu}</math>, kN-m</b>
(1)	(2)	(3)	(4)
S1	21.0	70.6	5.90
S1 Ret	18.1	94.4	7.55

#### ACKNOWLEDGMENTS

The experimental study reported in this paper is conducted at the Structural Engineering Laboratory, Indian Institute of Technology Kanpur (India). The untiring efforts of N. Satyanarayana, (Technical Officer), Snehal Kaushik (Senior Project Associate), and staff members of the

laboratory in the timely completion of the experiments are sincerely acknowledged.

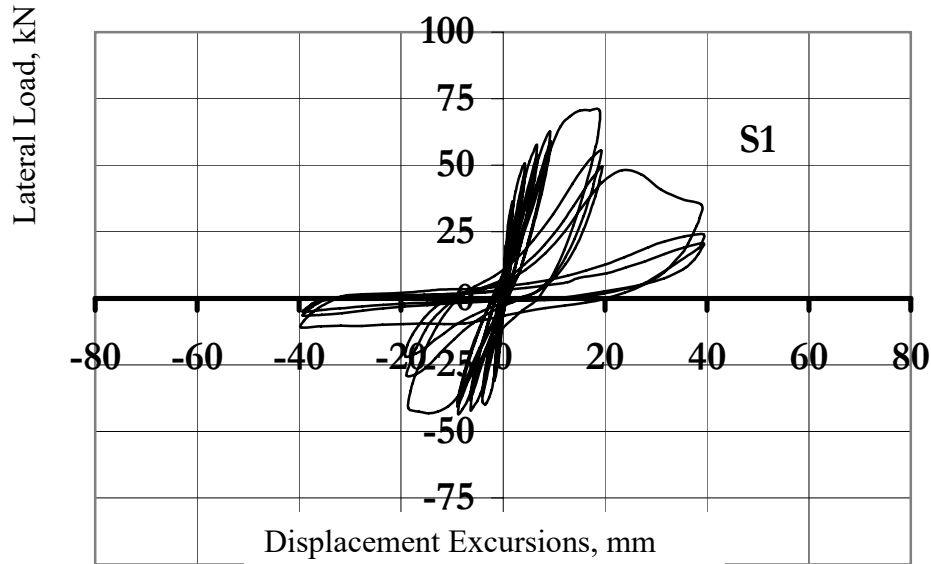


Figure 8: Lateral load-displacement hysteresis loops of original sub-assembly specimen

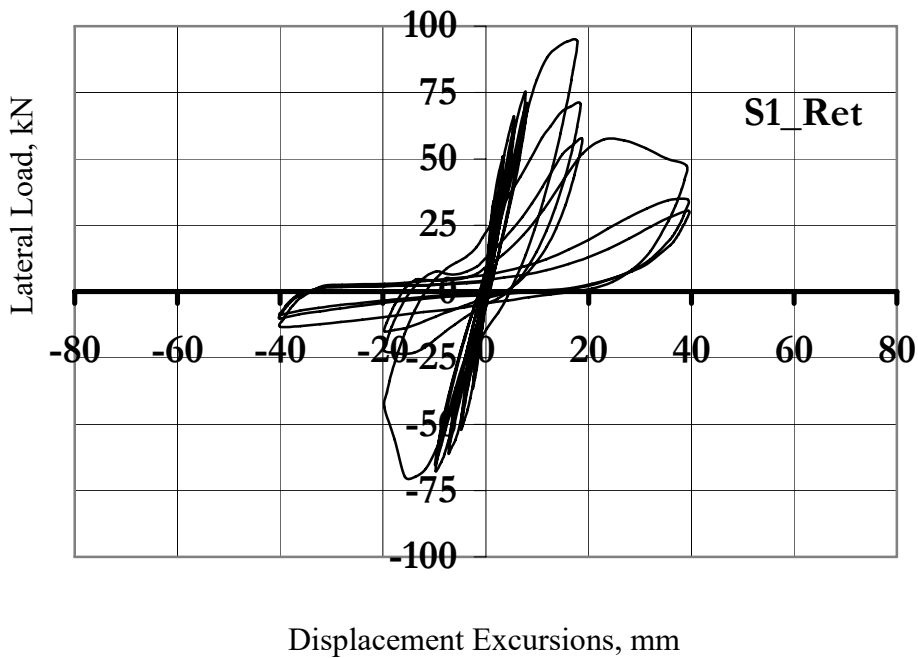


Figure 9: Lateral load-displacement hysteresis loops of retrofitted sub-assembly specimen

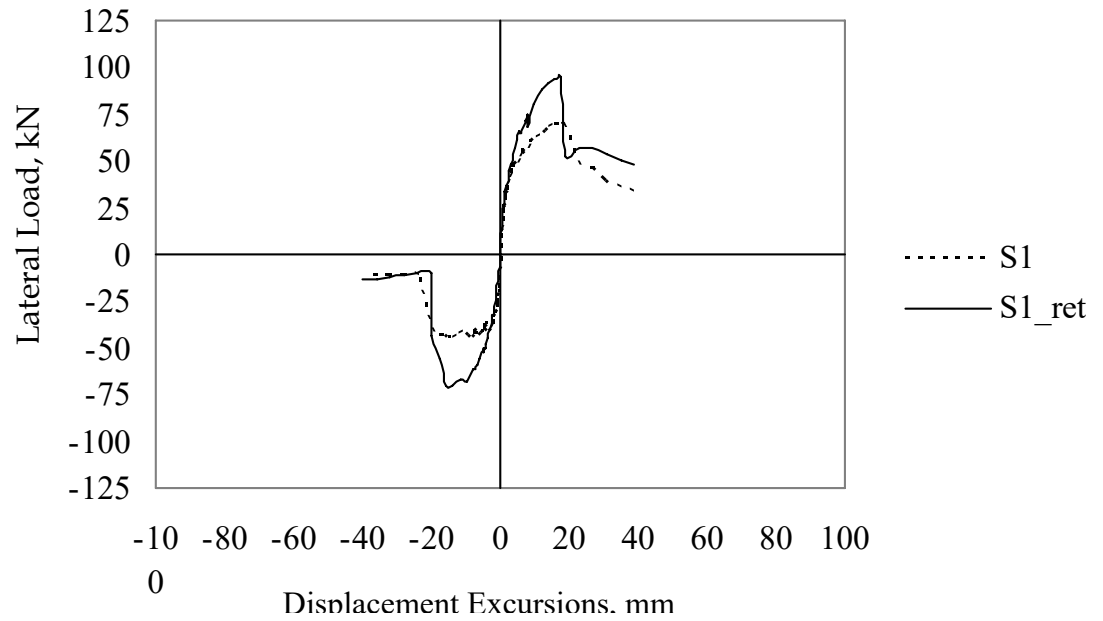


Figure 10: Comparison of envelope backbone curves (original and retrofitted specimens)

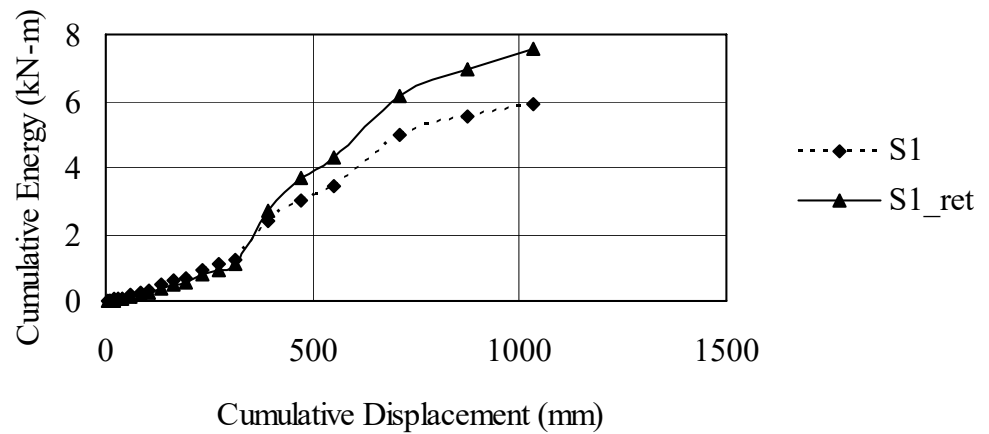


Figure 11: Comparison of energy dissipation

## REFERENCES

- Gergely Janos, Pantelides Chris P., and Reaveley Lawrence D. 2000. *Shear Strengthening of RCT-Joints using CFRP Composites*. Journal of Composites for Construction, ASCE, 4(2), 56-64.
- Indian Standard Handbook on Concrete Reinforcement and Detailing 1987. (SP 34(S&T):1987), Special Publication, Bureau of Indian Standards, New Delhi.

- Indian Standard Plain and Reinforced Concrete Code of Practice, (IS-456:2000), Bureau of Indian Standards, New Delhi, India, July 2000.
- Malek A.M., and Saadatmanesh, H. 1998. *Ultimate Shear Capacity of RC Beams Strengthened with Web Bonded FRP Plates*. ACI Structural Journal, 95(4), 391-399.
- Murty, C. V. R., Rai, D. C., Bajpai, K. K., and Jain, S. K., 2003. *Effectiveness of Reinforcement Details in Exterior Reinforced Concrete Beam-Column Joints for Earthquake Resistance*. ACI Structural Journal, 100(2), 149-156.
- Murty, C. V. R., Rai, D. C., Bajpai, K. K., and Jain, S. K., 2004. *Effectiveness of Fibre Wrap Retrofitting on Exterior RC Beam-Column Joints for Earthquake Resistance*. Submitted to ACI Structural Journal.
- Nilsson, I.H.E., and Losberg, A. 1976. *Reinforced Concrete Corners and Joints subjected to Bending Moment*. Journal of Structural Div. ASCE, 102 (ST6), 1229-1254.
- Priestley, M.J.N., Seible F., and Calvi, G.M. 1996. *Seismic Design and Retrofit of Bridges*. Wiley, New York.
- Priestley, M.J.N., Seible F., MacRac, G.A., and Chai Y.H. 1997. *Seismic Assessment of the Santa Monica Viaduct Bect details*. ACI Structural Journal, 94(5), 513-524.
- Rai, D.C., and Murty C.V.R., 2003. *North Andaman (Diglipur) Earthquake of 14 September 2002*. Reconnaissance Report, Department of Civil Engineering, IIT Kanpur, April 2003.
- Saadatmanesh, H., Ehsani, M.R., and Jin, L. 1996. *Behavior of Concrete Columns Retrofitted with Fiber Composite Straps under Cyclic Loading*. Proc., Ist International Conference on Composites in Infrastructure, 842-856.
- Seible, F., Priestley, M.J.N., Hegemier, G.A., and Innamorato, D. 1997. *Seismic Retrofit of RC Columns with Continuous Carbon Fiber Jackets*. Journal of Composites for Construction, ASCE, 1(2), 52-62.

# **NEW CONCEPT FOR RETROFITTING CONCRETE STRUCTURES WITH UNCONVENTIONAL MATERIALS**

UEDA TAMON  
Hokkaido University, Sapporo, Japan  
egpsee@eng.hokudai.ac.jp

## **ABSTRACT**

*This paper presents some new concepts for retrofitting concrete structures. These concepts can be recognized as new due to the facts that materials other than steel, which is a truly conventional reinforcement material, possess quite different mechanical properties and the bond of retrofitting materials to concrete is quite different from conventional steel reinforcement embedded in concrete.*

*The first concept is an application of material with small stiffness but high fracturing strain. In order to assure high deformability with concrete members, reinforcement material should have a high fracturing strain otherwise concrete deformability cannot be utilized fully. Low stiffness can be compensated by providing more material, however low fracturing strain cannot. Reinforcement materials with lower elastic modulus than steel can be more effective than steel reinforcement if developed strain in the reinforcement at member's ultimate deformation is significantly higher than the steel yield strain. This is because the steel stiffness at the ultimate deformation could be less than that of those materials.*

*The second concept is an application of soft adhesive for bonding reinforcement externally. For reinforcement embedded in concrete, it is not necessary to consider adhesive for bonding, however external bonding, which is a typical retrofitting method, must have adhesive for bonding. Mechanical properties of adhesives are not of primary interest in the past. In fact adhesive properties affect mechanical properties of members after retrofitting. Soft adhesive decreases member stiffness but increases ultimate member strength.*

*This paper presents experimental evidences of the above concepts as well as numerical models to express the advantages of the new concept.*

## **1.0 INTRODUCTION**

In the 20<sup>th</sup> century human beings had accumulated so many infrastructures, especially in mega cities. During the 21<sup>st</sup> century human beings must maintain those infrastructures not only for safety reason but also for conservation of resources and energy. As a major remedial action for maintenance, retrofitting is one of the primary interests to civil engineers.

Retrofitting methods vary greatly in terms of structural type and material type. External bonding and over/under-laying as retrofitting needs

special attention different from that for monolithic structure. Many retrofitting materials are not steel hence possess different mechanical properties from steel which shows yielding and a high fracturing strain.

The difference in structural type and material properties, however, bring us a new concept for material property to achieve retrofitting effects most efficiently. This paper introduces some of the new concepts. The first one is the importance of fracturing strain of material rather than strength/stiffness. The second is the soft adhesive (or bond) layer for external bonding.

## 2.0 HIGH FRACTURING STRAIN FOR ACHIEVING DUCTILITY

### 2.1 Stress – strain relationship of various fiber sheets

Generally a material with a high strength shows a high stiffness but low fracturing strain. Figure 1 illustrates stress – strain relationships of various fiber sheets. Carbon is known to be a high strength and stiffness material. The stiffness is as high as steel, and the strength is ten times of steel. However, the fracturing strain is around 1.5 %. Polyacetal fiber (PAF), polyethylene terephthalate (PET) and polyethylene naphthalate (PEN) show a much lower strength/stiffness than carbon but a much higher fracturing strain (see Table 1). PAF sheet jacketing as seismic retrofitting shows a good performance to enhance ultimate ductility and even shear strength (Ueda, 2001). In this paper experimental evidences on enhancement of ultimate ductility with PET and PEN are presented.

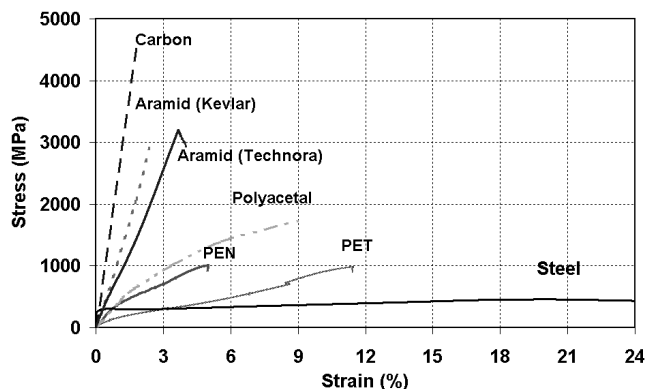


Figure 1: Stress – strain relationships of various fiber sheets

### 2.2 Outline of experiment

Ten specimens were prepared in order to see ductility enhancement by the duplex fiber sheet jacketing of reinforced columns. The DFS jacketing applies two types of fiber, one of which is applied in hinge zone for ductility enhancement and the other is in zone above the hinge zone for shear strength enhancement. The former is PET, PEN or aramid 1 (Technora)



whose fracturing strain is rather high, while the latter is aramid 2 (Kevlar) whose stiffness is rather high. The details of materials used and specimens are shown in Table 1 and 2 respectively. All the specimens were subjected to reverse cyclic loading with a loading system as shown in Figure 2.

Table 1: Material constants

Items	$E$ (GPa)	$f_y$ (MPa)	$f_t$ (MPa)	$\epsilon_{fu}$
Axial Reinforcement D19	176	394	-	-
Tie Reinforcement D6	188	340	-	-
Aramid 1 (Technora)	79.5	-	3246	0.041
PEN	22.6	-	1028	0.045
PET	6.7	-	923	0.138
Aramid 2 (Kevlar)	122	-	2670	0.022

Table 2: Details of specimens

Items	Unit	SP-1	SP-2	SP-3	SP-4	SP-5
Dimension	mm	400×400				
Shear span (a)	mm	1150				
Axial load	MPa	1.0				
$\rho_{\square t}$	%	0.98				
$\rho_s$	%	0.16				
$M_y$	kNm	257				
$M_u$	kNm	327				
$V_u$	kN	284				
$V_c$	kN	118				
$V_s$	kN	73				
$(V_c+V_s)/V_u$		0.67				
<u>Sheet reinforcement above plastic hinge zone</u>						
Material type		-	Kevlar	Kevlar	Kevlar	Kevlar
$\rho_f$	%	-	0.097	0.097	0.097	0.048
$V_f$	kN	-	231	231	231	134
$(V_c+V_s+V_f)/V_u$		0.67	1.48	1.48	1.48	1.14
<u>Sheet reinforcement on plastic hinge zone</u>						
Material types		-	Technora	PEN	PET	PET
$\rho_f$	%	-	0.126	0.382	0.377	0.187
$V_f$	kN	-	213	205	181.6	90.8
$(V_c+V_s+V_f)/V_u$		0.67	1.42	1.39	1.31	0.99
Ductility (Exp)		4.9	11.8	12	13.7	7.9

Table 2: Details of specimens (Continued)

Items	Unit	SP-6	SP-7	SP-8	SP-9	SP-10
Dimension	mm	400*400				
Shear span (a)	mm	1500				
Axial load	MPa	1.0				
$\rho_{\square t}$	%	0.98			1.18	0.78
$\rho_{\square s}$	%	0.16				
$M_y$	kNm	257			310	210
$M_u$	kNm	327			393	260
$V_u$	KN	218			262	173
$V_c$	KN	118			120	107
$V_s$	KN	73				
$(V_c+V_s)/V_u$		0.88			0.74	1.04
<u>Sheet Reinforcement above Plastic Hinge Zone</u>						
Material Type		Kevlar	Kevlar	-	Kevlar	-
$\rho_f$	%	0.024	0.024		0.024	
$V_f$	KN	67	67		67	
$(V_c+V_s+V_f)/V_u$		1.18	1.18	0.88	0.99	1.04
<u>Sheet Reinforcement on Plastic Hinge Zone</u>						
Material Types		PET	PET	-	PET	PET
$\rho_f$	%	0.125	0.063		0.125	0.063
$V_f$	kN	60.5	30.3		60.5	30.3
$(V_c+V_s+V_f)/V_u$		1.15	1.01	0.88	0.97	1.21
Ductility (Exp)		8.7	7.9	6.6	8.8	11.3

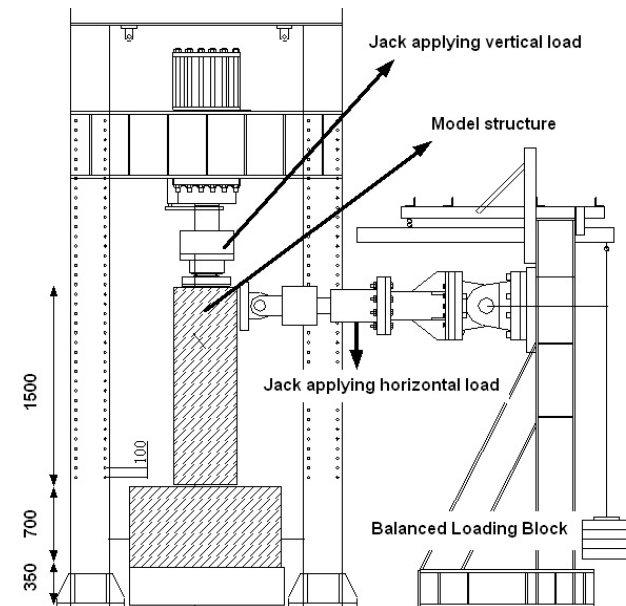
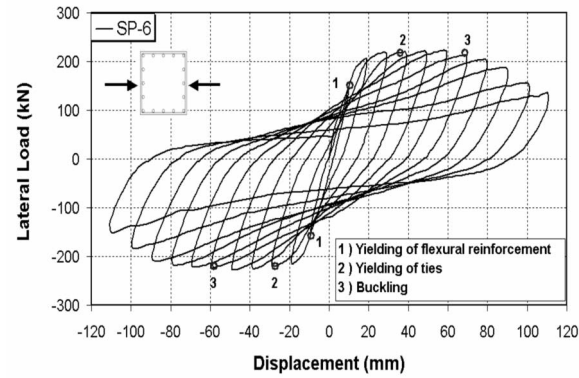


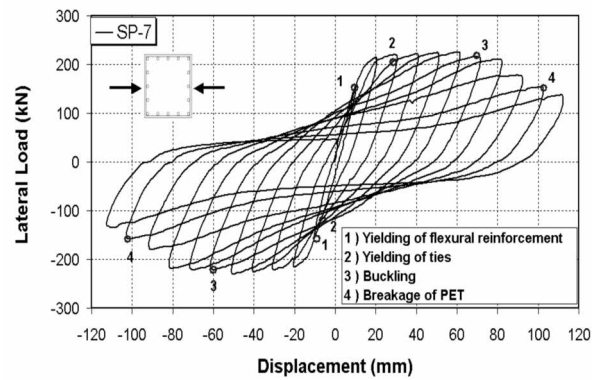
Figure 2: Loading system for columns specimen

### 2.3 PET sheet performance for enhancement of ductility

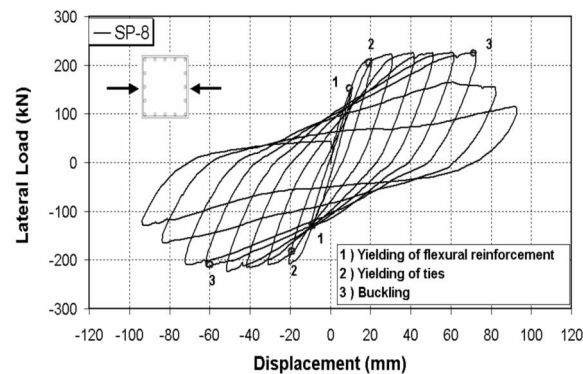
The load-displacement relationship of specimens SP-6 and SP7 with PET sheet jacketing in the hinge zone are compared with that of specimen SP-8 without jacketing (reference specimen) in Figure 3. It can be seen that the reduction in load carrying capacity after the peak load with increase in displacement is much smaller in the retrofitted specimens (SP-6 and SP-7) than in the un-retrofitted specimen. This difference is believed to be due to non-fracture of PET sheet even after buckling of the longitudinal reinforcement, which can confine concrete in the hinge zone (see Figure 4).



(a) Specimen SP-6 (retrofitted)



(b) Specimen SP-7 (retrofitted)



(c) Specimen SP-8 (un-retrofitted)

Figure 3: Load-displacement relationships

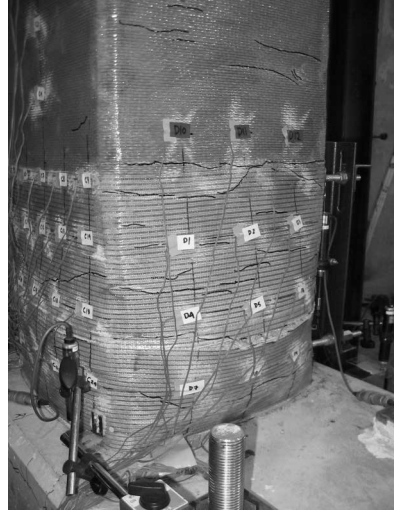
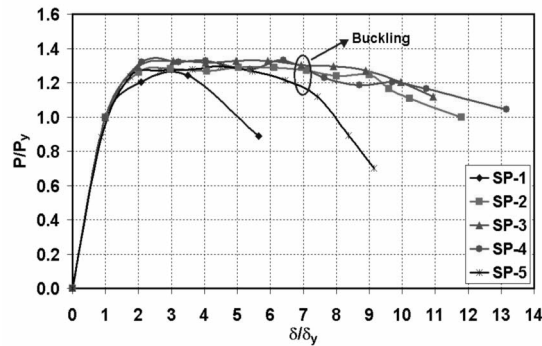
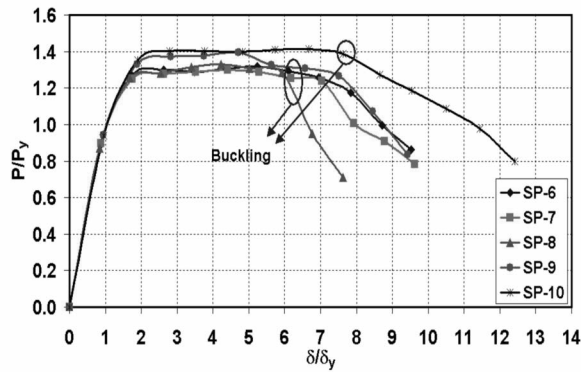


Figure 4: PET sheet in hinge zone

Enhancement of ultimate ductility can be seen in the normalized envelope curve ( $P/P_y$ - $\delta/\delta_y$  relationship) as shown in Figure 5. Among specimens SP-1 to SP-5 where the shear strength to flexural strength ratio of the specimens before retrofitting is rather low (0.67), the enhancement effect can be seen more clearly than among specimens SP-6 to SP-10 where the shear strength to flexural strength ratio of the specimens before retrofitting is higher (0.74 to 1.04).



(a) Specimens SP-1 to SP-5



(b) Specimens SP-6 to SP-10

Figure 5: Ultimate ductility

The prediction formula for ultimate ductility available in a report of the Research Committee on Upgrading of Concrete Structures with FRP Reinforcement, (2001), which was thought to be the best fitting of experimental data for carbon and aramid fiber sheet, most of which show sheet fracture at ultimate deformation. However this formula overestimates the observed ultimate ductility with PET sheet indicating that a new formula needs to be developed.

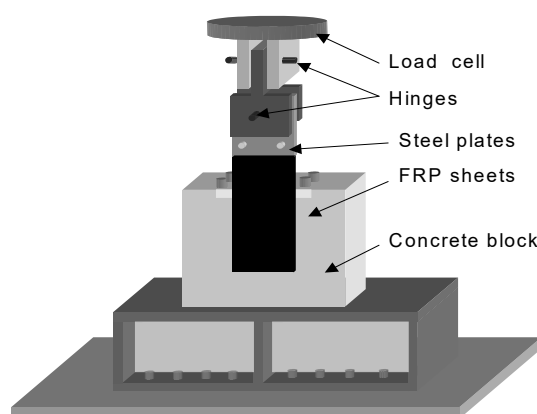
In comparison with steel reinforcement there is an advantage with fiber whose fracturing strain is high. Around ultimate deformation any tie (shear) reinforcement is subjected to a high strain, therefore stiffness of steel is likely to be reduced significantly due to its yielding. The fiber stiffness whose initial stiffness is smaller than steel can be greater than steel at this stage. This implies that the fiber reinforcement can provide a higher stiffness, so that confinement of core concrete is more efficient.

### **3.0 SOFT ADHESIVE RESIN FOR ENHANCEMENT OF DEBONDING STRENGTH**

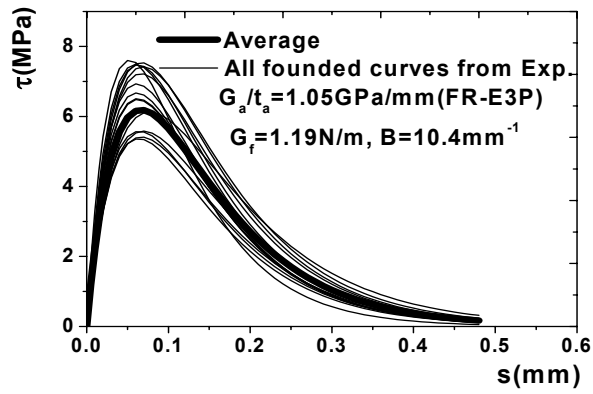
For external bonding, adhesive must be provided. However, in the past almost no attention had been paid to mechanical property of adhesive to achieve better interface bonding characteristics. This paper shows experimental evidences for significant effects of adhesive on the interface bonding characteristics and that soft adhesive is one of the means to improve debonding strength.

#### **3.1 Local bond stress – slip relationship and adhesive stiffness**

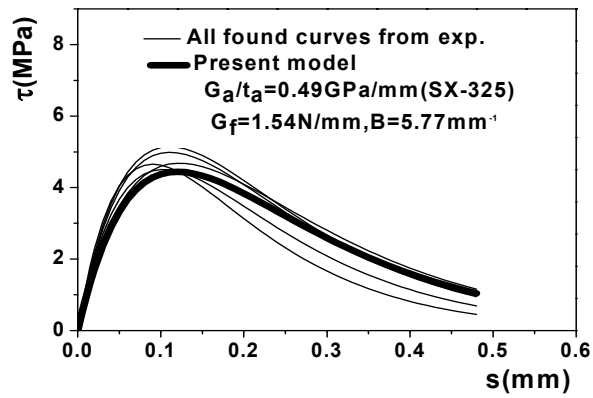
The pullout bond test of FRP sheet was conducted as shown in Figure 6. Local bonds stress – slip relationships observed in the test are compared among cases of different adhesive stiffness (see Figure 7) (Dai, et al, 2005). The initial stiffness and the peak bond stress are smaller for softer adhesive, however ductility is much better in the case of soft adhesive. As a result, the interfacial fracture energy increases with decrease in adhesive shear stiffness (see Figure 8).



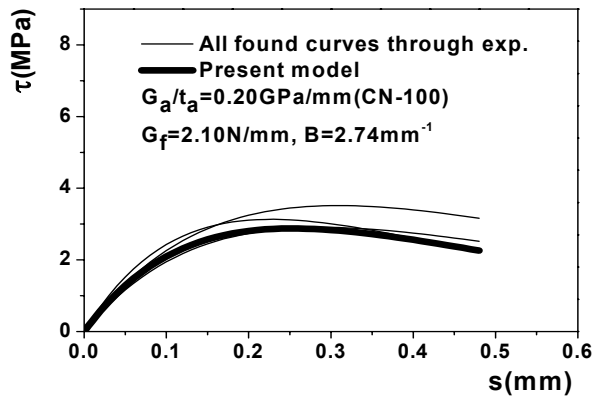
*Figure 6: Pull-out bond test*



(a) Adhesive with a high stiffness



(b) Adhesive with a medium stiffness



(c) Adhesive with a low stiffness

Figure 7: Effect of adhesive stiffness on local bond stress – slip curve

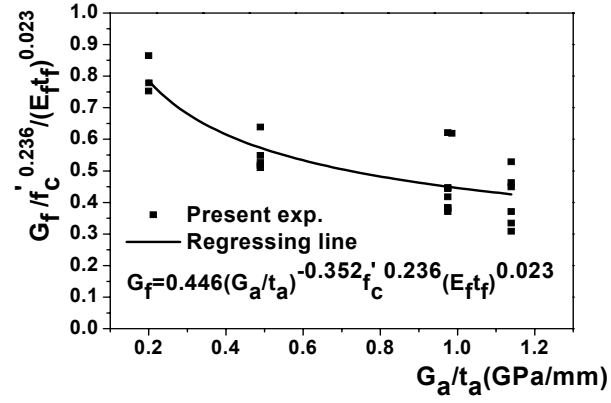


Figure 8: Effect of adhesive shear stiffness on interfacial fracture energy

The bond stress – slip model ( $\tau - s$ ) based on sheet strain – slip relationship at loaded end (Dai, et al, 2005), shown in equation (1), can predict the effects of adhesive stiffness very well (see Present model in Figure 8).

$$\tau = A^2 B E_f t_f \exp(-Bs)(1 - \exp(-Bs)) \quad (1)$$

where 
$$A = \sqrt{\frac{2G_f}{E_f t_f}} \quad (2)$$

$$B = 6.846(E_f t_f)^{0.108} (G_a / t_a)^{0.833} \quad (3)$$

and  $G_f$  is interfacial fracture energy,  $E_f$  and  $t_f$  are elastic modulus and thickness of FRP sheet, and  $G_a$  and  $t_a$  are shear modulus and thickness of adhesive.

### 3.2 Enhancement of Debonding Strength of Beam with Flexural Strengthening by Soft Adhesive Resin

Ultimate strength of beam with external bonding of carbon fiber sheet can be increased by applying soft adhesive resin because of improvement of interfacial fracture energy as described in 3.1. Figure 9 shows the comparison of load – deformation relationship of strengthened beams. All the strengthened beams show greater ultimate loads than the un-strengthened one (SP-C0). In all the cases of one, two and three layers of sheet the ultimate loads with soft adhesive layer are greater than those without soft adhesive layer (Ueda, 2002).

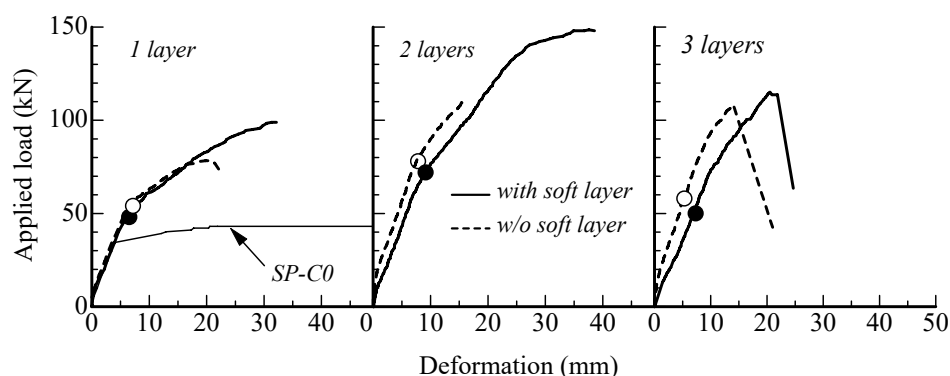


Figure 9: Load – deformation curves of beams strengthened by carbon fiber sheet with soft adhesive layer

## 4.0 CONCLUSIONS

Through retrofitting technology, which utilizes structure and material types different from the ordinary newly constructed structures, new mechanical concepts for reinforcing concrete can emerge. Two examples: high fracturing strain rather than high strength/stiffness and soft bonding layer, are introduced with experimental evidence. It is hoped that these new concepts could widen selections of structure and material types for practical use.

## ACKNOWLEDGEMENTS

The author is grateful to Mr Hadiyono Jaqin and Dr Dai Jianguo for their efforts in carrying the studies whose results are used in this paper.

## REFERENCES

- Dai J. G., Ueda T. and Sato Y., 2005. *Development of the Nonlinear Bond Stress-slip Model of Fiber Reinforced Plastics Sheet-concrete Interfaces with a Simple Method*. Journal of Composites in Construction, ASCE (to be printed).
- Research Committee on Upgrading of Concrete Structures with FRP Reinforcement, 2001. *Guideline on Upgrading of Concrete Structures with FRP Sheet*. Concrete Engineering Series 41, JSCE.
- Ueda T., 2001. *Bond behavior and seismic retrofitting effect of polyacetal fiber sheet*. FRP Composites in Civil Engineering. Proceedings of the International Conference on FRP Composites in Civil Engineering, Vol 2, 1041-1050.
- Ueda T. and Sato Y., 2002. *New Approach for Usage of Continuous Fiber as Non-Metallic Reinforcement of Concrete*. Structural Engineering International 12-2, IABSE, 111-116.



# ***SIMULATION OF PLATE BEHAVIOUR UNDER NON UNIFORM WIND LOADS***

TIJO THOMAS<sup>1</sup> AND PRADEEP KUMAR RAMANCHARLA<sup>2</sup>

<sup>1</sup>Former Graduate Student, <sup>2</sup>Assistant Professor & Coordinator  
IIIT Hyderabad, India  
[ramancharla@iiit.net](mailto:ramancharla@iiit.net)

## ***ABSTRACT***

*Procedure for finding out wind pressure at any given location in Indian subcontinent is outlined in IS-875 Part III 1987. This procedure is made convenient to the user by developing a tool named 'WindSim'. An efficient algorithm has been developed for finding out deflection, when the plate is subjected to uniform wind pressure. Finite difference method is used to solve the equation of plate in bending. It has been observed that the wind pressure varies with height. Hence, the algorithm is further modified to take care of the non-uniform wind loads and different support conditions. The deflection of the plate is graphically simulated by drawing contours on a VB GUI. The values of deflection obtained from the program can be compared with allowable deflection values, to check the safety of the structural component.*

## **1.0 INTRODUCTION**

The number of buildings increases year by year. So is the number of high-rise buildings. The effect of wind on these buildings and its components cannot be ignored. In many of these buildings, a major part of its vertical components can be modeled as plates. Example being glass walls in glazed building. When safety is a concern, behavior of these components under wind forces can be a subject of interest. The work presented here explains the program to simulate the linear behavior of building components that can be modeled as rectangular plates. The program has two major objectives:

- To find out the wind loads at a given location in India.
- To analyze the building component for deflection and simulate its behavior.

The safety of the structural component is assured if its deflections are within the allowable limits. The paper gives a quick glance over the provisions of IS 875, Part III (here after we mention this as the code) and its programming implementation. It deals in detail with equation of plate in bending, finite difference method, the algorithm for numerical simulation and the behavior of plate for different boundary conditions.

## 2.0 BRIEF OVERVIEW ON THE PROVISIONS OF IS 875-PART III

### 2.1 Basic wind velocity

Basic wind velocity ( $V_b$ ) is the speed of wind based on peak gust velocity averaged over a short time interval of about 3 seconds and corresponds to mean heights above ground level in an open terrain. The code provides basic wind speeds worked out for 50-year return period. This is applicable for 10 m heights above mean ground level for different zones of the country (Figure 1).

### 2.2 Risk coefficient

The risk coefficient ( $k_1$  factor) is dependent on the design life of the structure and the basic wind velocity. The  $k_1$  factors for different class of structure are given in the Table-1 of code.

### 2.3 Terrain, height and structure size factor

The code has classified the terrain into four categories with regard to the effect of obstructions that constitute the ground surface roughness. The terrain categories are as discussed below.

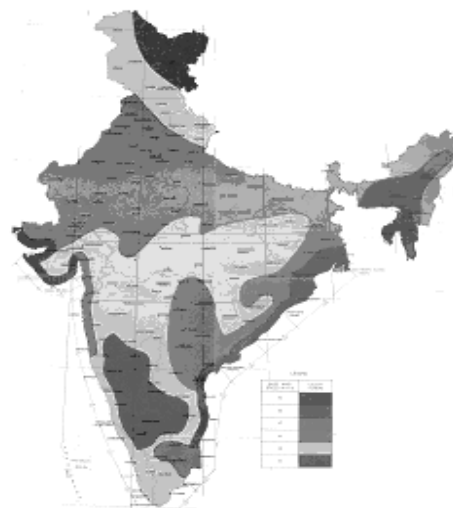


Figure 1: Basic wind velocity (IS 875, part 3)

Category – 1: Exposed open terrain with no obstruction and in which the average height of any object surrounding the structure is less than 1.5 m.

Category – 2: Open terrain with well-scattered obstructions having heights generally between 1.5 to 10 m.

Category –3: Terrain with numerous closely spaced obstructions having the size of building structure up to 10 m in height with or without a few isolated tall structures.

Category-4: Terrain with numerous large high closely spaced obstructions.

The structures are classified further according to following three classes depending up on their sizes:

Class A: Structures and/or their components whose maximum dimension is less than 20 m.

Class B: Structures and/or their components whose maximum dimension is between 20 and 50 m.

Class C: Structures and/or their components whose maximum dimension is greater than 50 m.

The table relating  $k_2$  factor to terrain category, class and height of the structure is given below Table-2 of the code.

## 2.4 Topography factor

The effect of topography is to accelerate wind near the summits of hills or crests of cliffs, escarpments or ridges and decelerate the wind in valleys or near the foot of cliffs, steep escarpments, or ridges. The effect of topography will become significant only when upwind slopes ( $\theta$ ) are greater than 3 degrees. When  $\theta$  is less than 3 degrees, topography factor  $k_3$  is taken as 1. If the slope is more than 3 degrees the value of  $k_3$  is obtained from the following expression:

$$k_3 = 1 + Cs \quad (1)$$

Where,  $C = 1.2 (z / L)$ , when  $3^\circ < \theta \leq 17^\circ$   
 $= 0.36$  when  $\theta > 17^\circ$

Here,

$L$  = horizontal distance of the slope

$Z$  = effective height of the feature

And for finding value of  $s$ , please refer the code.

## 2.5 Design wind pressure

The code provides us with the following formula for calculating the Design wind pressure:

$$P_z = 0.6 V_z^2 \quad (2)$$

Where  $P_z$  = Design wind pressure

$V_z$  = Design wind velocity

Design Wind Velocity:

$$(V_z) = V_b k_1 k_2 k_3 \quad (3)$$

The pressure coefficients are provided in the code, which when multiplied with  $P_z$  gives the normal wind pressure on a surface.

## 3.0 PROGRAMMING IMPLEMENTATION

The program displays the map of India as shown in figure 1. The user is prompted to click on the map corresponding to the location of his structure. The basic wind velocity, obtained by sensing mouse click is modified to get the design wind velocity as demonstrated later in this paper. By clicking an appropriate button, user is entering the design life of the structure. With the values of  $V_b$  and design life of the structure in hand, the value of  $k_2$  is obtained from the Table 2 of the code.

To find out the value of  $k_2$  factor a form has been created, which allows the user to select the type of terrain category where his structure belongs to. From the main form, text boxes are provided to enter the

dimensions of the structural component. The program accesses these values and finds out the class of the structure. Now Table 2 of the code is made use by the program to find out the value of terrain factor  $k_2$ .

Separate form has been introduced to enter the values of upwind slope, dimensions of the feature such as horizontal dimension, height. Digitizing the graphs given in the code, data files are created for finding out  $s$ . Program has been written to access the value of  $s$  from these files corresponding to the values of dimensions of the feature.

### 3.1 Application of the design wind pressure on plate

The design wind pressure serves as the uniform force per unit area on the plate. Using this force, the plate equation is solved to find out the deflections at any particular node of the plate. This process is explained in later. Wind pressure is calculated at the center of the plate and applied uniformly.

### 3.2 Equation of plate bending

The equation for plate in bending is given by:

$$\frac{\partial^4 w}{\partial x^4} + 2 \frac{\partial^4 w}{\partial x^2 \partial y^2} + \frac{\partial^4 w}{\partial y^4} = q / D$$

Where  $w$  = Deflection of the plate

$q$  = Force per unit area

$D$  = Elastic constant

$$D = \frac{E t^3}{12 (1 - \nu^2)}$$

$E$  = Modulus of elasticity

$t$  = Thickness

$\nu$  = Poisson ratio

In the analysis of plate in bending, deflection is obtained by solving the above equation satisfying the condition at the plate boundaries. The solution for deflection is obtained by the method of finite difference.

### 3.3 Method of finite difference

In finite difference method (FDM), numerical solution of the differential equation for displacement or stress resultant is obtained for

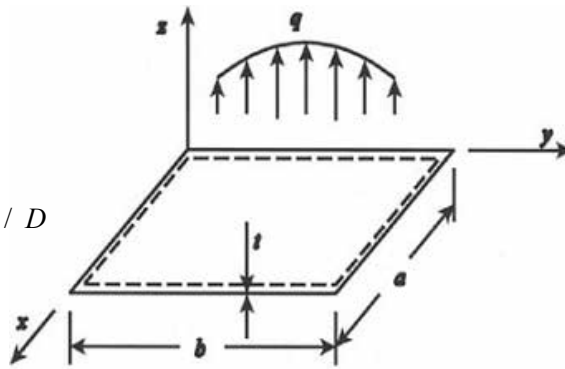


Figure 2: Bending of plate under uniform loads

chosen points of the structure, referred to as nodes. This solution is applicable to the actual continuous structure. To apply FDM at a node, the differential equation is replaced by finite difference expression, relating the given node and the nodes in the vicinity of that node. This equation is equated to the applied load. When FDM is applied to all the nodes in the same way, sufficient number of simultaneous equations for displacement or stress is obtained. The finite difference expression at nodes near the boundary has to be modified before solving for the unknown. The following paragraphs demonstrate how this is done for a plate.

### 3.4 Finite difference equations at an interior node of plate in bending

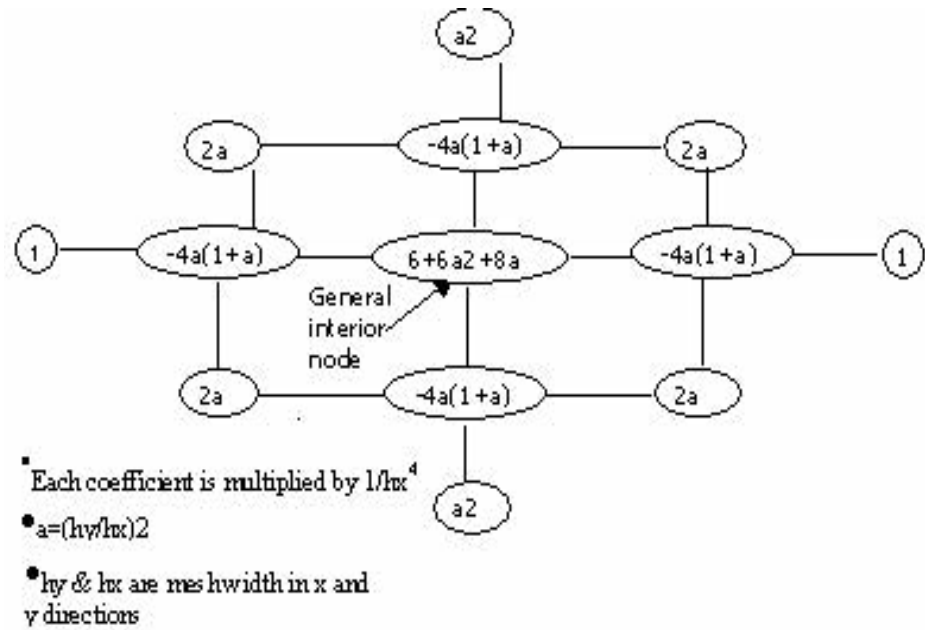


Figure 3: Biharmonic operator in central difference form

The partial differential equation presented in section 3.1 is replaced by appropriate finite difference expression. Figure 3 shows the central-difference approximation of the partial differential expression for an interior node of rectangular plate. These coefficients are used in the following form for a general interior node  $i$

$$[\text{Coefficients}] \{w_i\} = q_i/D \quad (5)$$

$w_i$  represents the deflection at a general interior node,  $q_i$  represent the pressure at a general interior node and  $D$  is the elastic constant of the plate.

Similar equations are written for all the nodes in a plate. The coefficients of nodes at or near the boundary are modified with appropriate boundary conditions. Next section explains the modeling of the boundary. These simultaneous equations are written in the form of a matrix, which is then solved to obtain deflection at each node. Algorithm for finding out deflection of plate subjected to uniform load is shown in figure 4.

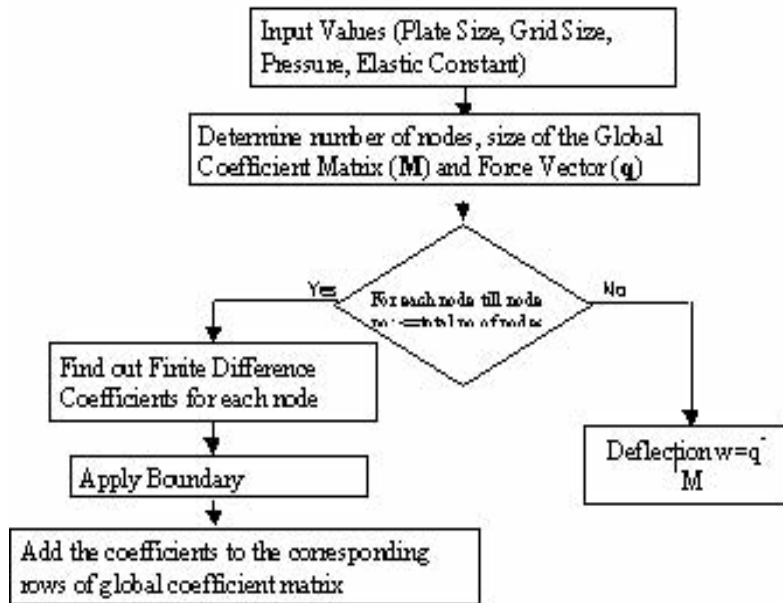


Figure 4: Flow chart of the program

### 3.5 Modeling of built-in edge

The deflection at all points on a built-in edge and slope of the deflected surface normal to the edge are zero. The equation shown in figure 5 is the algebraic representation of the boundary condition. Internal nodes such as 'A' here are modified to take care of the boundary condition. For example the coefficient at 'A' gets added with that of 'C' to take care of  $W_C = W_A$ .

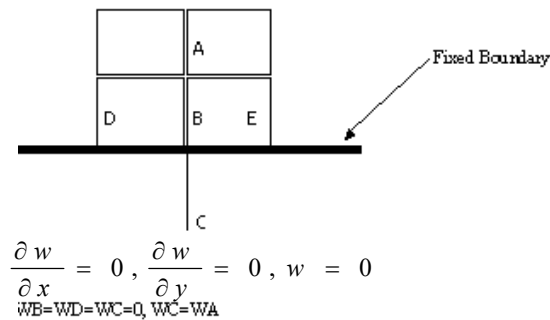


Figure 5: Built-in edge modeling

### 3.6 Modelling of simply supported edge

The deflection and the moment vanish at all boundary points. Here, coefficient at 'A' gets subtracted from that of 'C' to take care of  $W_C = W_A$  as explained in figure 6.

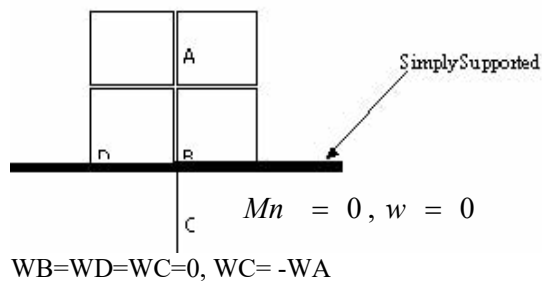
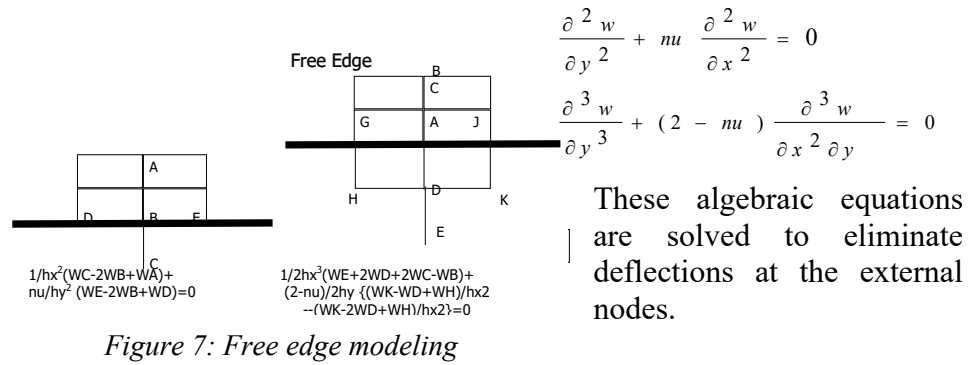


Figure 6: Simply supported edge modeling

### 3.7 Modeling of free edge

At a free edge bending moment at any free edge is zero and there should not be any transverse forces. For an edge parallel to the x-axis following are the conditions.

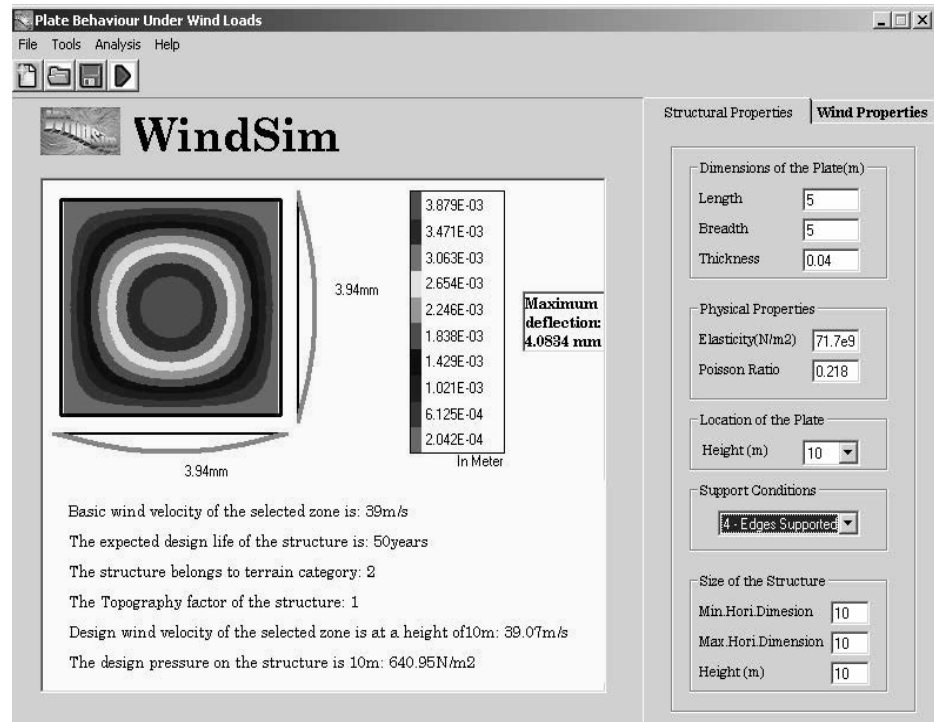


### 3.8 Modification for non-uniform wind pressure case

While constant pressure is applied in uniform case, pressure varying with height is applied for non-uniform case. To find out the force vector for this case, the height from the bottom of each row of nodes is calculated. Factor  $k_2$  factor for this particular height is obtained from the standard. Using  $k_2$ , design wind velocity and hence design wind pressure is modified. In short all the nodes in any particular row are subjected to the same pressure and this pressure varies from row to row.

### 4.0 GRAPHICAL USER INTERFACE

The GUI as shown in figure 4.1 has been developed using Visul Basic 6.0. The VB GUI provides user with convenient means to enter the properties of both the plate and wind. Text boxes are provided to enter dimensions such as length, breadth and thickness and material properties



such as elasticity and poisson ratio of the plate. To enter structural properties such as dimensions of structure and location of the plate separate text boxes are given. User can enter the support condition by selecting from the combo boxes. To enter the wind properties, forms have been provided where in user can enter the basic wind velocity and its modification factors by mouse click. Appropriate messages are displayed when improper values are fed in or to in confirmation of the entered value. The main program accesses these input values processed for the results such as deflection. These are then displayed as text in the main form. They are then graphically simulated as shown in next section. Utilities such as save, print, help are provided to assist the user further. Program provides the option of analysing for uniform pressure or non-uniform wind pressure.

#### 4.1 Graphical simulation of the deflection

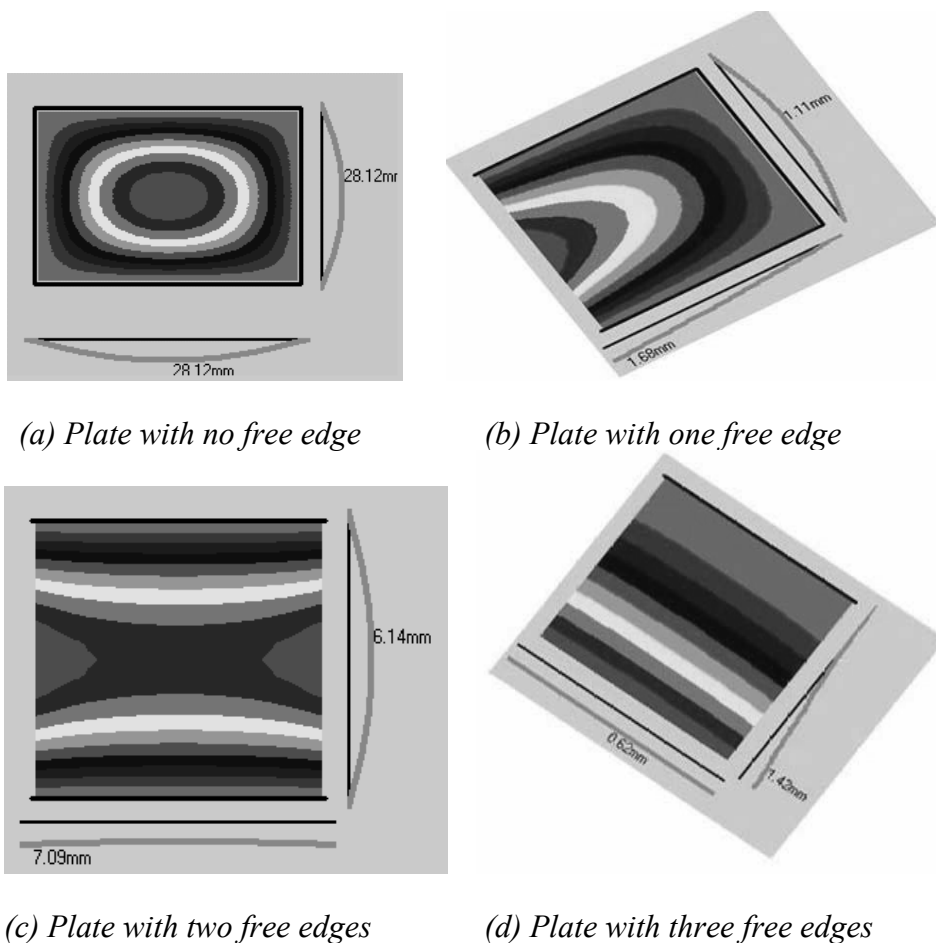


Figure 9: Deflection contours for different edge conditions

The deflection obtained by the procedures explained in the preceding sections is presented in the form of banded contour map on the VB GUI. In the contour map at different parts of the plate is represented by different colors. In general around 10 colors are used. The red color indicates the



maximum value while pink indicates '0' value of deflection. The other color indicates deflection between '0' and maximum. The contour maps for plates with different support conditions are given below.

#### ***4.1.1 Plate with no free edge***

All the edges of the plates are simply supported as shown in figure 9 (a). On applying uniformly load on to 4-edge supported plate, maximum deflection occurs at the center of the plate. This is indicated by the red color. The supported edges shows the minimum, i.e., '0' deflection. The deflection uniformly varies from the center to the edges. Deflections at the different part of the plates are between the maximum (Central deflection) and minimum (deflection at edges) limits.

#### ***4.1.2 Plate with one free edge***

On applying uniformly load on to 3-edge supported plate as shown in figure 9 (b), maximum deflection occurs at the center of the free edge of the plate. The supported edges show the minimum, i.e., '0' deflection. The deflection uniformly varies from the center of the free edge to the supported edges. Deflections at the different part of the plates are between the maximum (Central deflection-shown by red color) and minimum (deflection at edges) limits.

#### ***4.1.3 Plate with two free edges***

Two edges of the plates are simply supported and two are free as shown in figure 9 (c). When uniform load is applied on to 2-edge supported plate, maximum deflection occurs at the center of both the free edges of the plate. This is indicated by the red color. The supported edges show the minimum, i.e., '0' deflection. The deflection uniformly varies from the center of the free edge to the supported edges. Deflections at the different parts of the plate are between the maximum (Central deflection-shown by red color) and minimum (deflection at edges) limits.

#### ***4.1.4 Plate with three free edges***

One edge of the plate is fixed, while all other edges are free as shown in figure 9 (d). When uniform load is applied on a 1-edge supported plate, maximum deflection the center of the free edge, which has two unsupported corners. This is indicated by the red color. The supported edges show the minimum, i.e., '0' deflection. The deflection uniformly varies from the center of the free edge to the supported edges. Deflections at the different part of the plates are between the maximum (Central deflection-shown by red color) and minimum (deflection at edges) limits.

## 5.0 RESULTS AND DISCUSSIONS

The maximum deflection obtained from the analysis is compared for non-uniform application of wind loads and uniform application of wind loads. Values of the deflection for 5 X 5 m glass plate, located in a general building in wind

Table 1: Deflection of plate

Support Conditions	Deflection under non-uniform wind loads (in mm)	Deflection under uniform wind loads (in mm)
4-Edge Supported	4.083	4.0516
3-Edge Supported	12.1537	12.0569
2-Edge Supported	14.2409	14.3554
1-Edge Supported	66.3064	66.3515

zone-1, has been compared in the Table 1 given above. It is found that the deflection values are comparable. Maximum of the two deflection values can be taken for checking the safety of the structural component. For example, in the case of glass panels, the deflection value obtained from the program can be compared with the allowable deflection for standard glass types. If the value from the program is within the allowable deflection the glass panel is safe.

## 6.0 CONCLUSIONS

A software tool is created to find out design wind pressure at any given location in Indian subcontinent. The GUI of the program can take most of the input values from user through mouse click. The wind pressure so obtained confirms to IS 875 Part III, 1987. In second part of the program, deflection of plate under the action of this force is found out. An efficient algorithm has been developed to find out the deflection of any structural component that can be modelled as a rectangular plate. Algorithm is generalised to take care of different boundary condition. The algorithm is suitably modified to take care of the non-uniform wind loads. Of the two types loading condition, one which gives the maximum value of deflection, can be used for checking the safety of the plate. The deflection is then graphically presented on VB GUI, in the form of banded deflection contour map for better understanding about the plate behaviour. If the values of allowable values of load or deflection of any material is known, the tool can be used for checking the safety of the structural component.

## REFERENCES

- IS 875 Part 3 1987,1997. Bureau of Indian Standards, New Delhi.  
A Ghali and A. M. Neville, 1997. *Structural Analysis, A unified classical and matrix approach*. E & FN SPON, Taylor and Francis Group.  
C. V. Girija Vallabhan, 1982. *Iterative analysis of Nonlinear Glass Plates*. Journal of Structural Engineering, Vol 109, ASCE .  
Tirupathi R. Chandrupatla and Ashok D. Belegundu,2002. *Finite Elements in Engineering*. Prentice Hall – India.

# **URBAN SAFETY AND SECURITY ISSUES, CONSTRAINTS AND CHALLENGES AHEAD - AGRA**

TAHSINUR RAHMAN WARSI<sup>1</sup> AND ANURAG KHANDELWAL<sup>2</sup>

<sup>1</sup>Senior Lecturer, <sup>2</sup>Visiting Faculty, Aligarh Muslim University, India  
trwarsi@rediffmail.com

## **ABSTRACT**

*Agra in 1991 census has been added to the list of Mega Cities. Agra being synonymous with Taj, one of the most beautiful structures built by man and is among the most visited building in the world. With a total population of 11.5 lacks in 2001 census the city cater 8000-10000 tourists per day. Agra being the most important landmark of India still faces the brunt of government negligence. The issues of safety and security of Taj are focused more than the inhabitants and citizens of Agra.*

*The present paper discusses the various issues and challenges related to urban safety and security of environment, health, socio-economic and urban design parameters with reference to Agra- The City of Taj.*

## **1.0 INTRODUCTION**

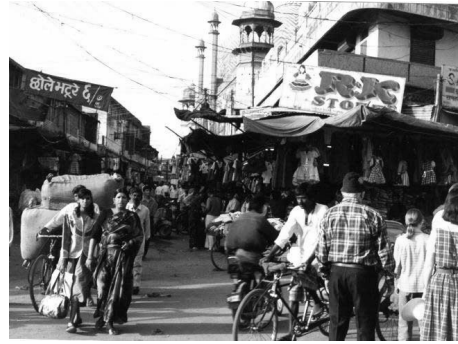
Agra in 1991 census has been added to the list of mega cities. The growth of the city with its ever-increasing population has been putting up pressure on the infrastructure available in the city, thereby challenging the core issues of Cities Urban Safety and security. Agra synonymous with Taj Mahal, one of the most beautiful structures built by man and today it is among the most visited monuments in the world. This adds up to the pressure on the Available infrastructure of the city.

## **2.0 TAJ MAHAL- BEYOND THE LOVE STORY**

Taj Mahal – one of the world’s greatest architectural wonders – is under threat. Taj situated in Agra, one of India’s most chaotic and polluted cities, this majestic monument is gradually being consumed by fumes and chemicals emanating from vehicles, diesel generators, factories, foundries, and refineries. The government is prepared to close these industrial units, to protect Taj, thus threatening jobs of millions. *Taj Mahal: beyond the love story* raises a question—in a poor country like India, can protecting a monument is more important than livelihood needs?



*Taj Mahal*



*Traditional Steet - Agra*

*Figure 1: Scenes of Agra*

### **3.0 AGRA–ITS DEVELOPMENT AND OVERCOMING CONSTRAINTS**

Strategically located and well connected by roads and railways to the major town especially the capital city Delhi, the city attracts a lot of people from the nearby by villages cities and districts for the opportunities for work, business, medical care, higher education, entertainment and shopping. With the total population of 1.15 million in 2001 Census, Agra attracts a minimum of 8000-10000 visitors per day and the figure during the peak can reach upto 80,000 to 100000 visitors per day.

Emperor Akbar founded Agra because of its strategic location, ever since Agra has been the hub of commercial activity. Akbar made Agra his capital and the development of the city experienced the golden era. During the reign of Emperor Shahjahan a feather in the cities cap was added –TAJ MAHAL. During the British Rule, the British Lords also realized the importance of the city and intended to make Agra the Capital, which finally was changed to Delhi.

A network of railways was set up and Agra was made one of the Military bases for British Army. Its Geographical Location provided a strategic advantage for the mobilization of the forces. Because of the infrastructure development city always provided the opportunities for employment and business to the people. After independence, Agra received a large number of refugees and migrants. The Business flourished and soon Agra became the commercial hub of northern India. Iron Foundries and Brick Kilns mushroomed after Independence. At present about 40% of the total economy of Agra depend on industry (Directly or indirectly). Over 7200 Small Scale Industrial Units are spared all over the district. Agra city is famous for the Leather Goods, Handicrafts, Marvel and Stone carving & inlay work. Agra is also well known for eats sweets (Petha) and Snacks (Dalmoth & Gajak). The Leather industry grew multifold as the city dwelled skilled labour, the specialty sweet ‘Petha’ Industry grew as the agriculture conditions favoured the cultivation of the pumpkins. Iron Foundries favored the growth of allied industries of casting. Agra became the hub of Generator

and diesel pump sets, automobile spares, and moulds. Agra supported the growth of Glass industry of nearby town Firozabad.

Education centers groomed as the universities, Technical and Medical institutions established to cater the vast population of the city, nearby areas and even abroad. The abundant availability of the technical and skilled manpower supported the industrial growth and Agra became the biggest medical center in northern region. Nursing Homes mushroomed as the demand for basic medical facilities to cater to the people of Agra and its nearby towns grew leaps and bounds.

The City Agra having all the advantages of factors of growth was not able to sustain the development and in the present state stands as an example of among the most chaotic and polluted cities in the world having lots of urban safety and security challenges..

## **4.0 INFRASTRUCTURE AND URBAN SAFETY AND SECURITY**

### **4.1 Socio economic scenario**

The City has a total population of 1.15 million and 43% population still lives in Slums. There are 182 identified slums in Agra. These Slums are in very bad Conditions. With the Supreme Court ordering for closure of the Polluting Units for the safety of the heritage monument viz., Iron Foundaries, Brick Kilns, Leather processing industries, without making provisions for alternate solutions has led to millions losing there jobs and work. The increasing unemployment and poverty results increase in crimes in the city.

### **4.2 Roads**

The Physical infrastructure of the city, the total length of roads ads is 142 kms. Out of which 75% are two lanes. Near about all the streets are narrow and hinders the smooth flow of traffic, creating health hazard due to vehicular pollution. The existing road network is inadequate for both intercity and intra city traffic movement. The vehicles are highly varied in character and at the same time one can observe the most basic form of transport (Bullock Cart) to the most advanced Automobile on the streets. The three National highways and few other highways passing through the city further aggravate the traffic chaos. It increases the traffic volume and traffic jams, results in increase in air pollution. The chaotic and unregulated traffic results in road accidents.

### **4.3 Power**

Per Day electricity deficiency is about 250 MVA and inadequate transmission infrastructure is leading to power breakdowns. Agra Faces regular severe power break approximately 4-6 hours per day. This has led to operating of large number of Diesel generator sets compounding considerable amount of air pollution.

#### **4.4 Water supply**

Situated on the bank of river Yamuna the major river of the Country, city faces the major drinking water scarcity. The river is dry for almost nine months and is being heavily polluted by city and industrial waste. The water supply from the Yamuna is for only 1-2 hours per day. About 24 drains are directly discharging effluent and sewage in Yamuna making the water totally non potable. The fishes in Yamuna in Agra died due to the fact that the BOD in Water has reached to zero levels. The water quality is low for most part it is having high coli form count due to breakages in pipe. Iron content in water is exceptionally high and residual chlorine and TDS are considerably high. The Most of the inhabitants sustain on underground water, which also has very high TDS and Salinity.

#### **4.5 Waste and sewage**

Only About 30% of the city is covered by sewerage network, the rest still survives on the most primitive techniques of sewage system. The total Sewerage generation of the city is 128.6 mld., there is no sewage treatment plant. The open drains which usually get choked by solid waste results in sewerage flowing on the roads and streets. The Waste disposal facilities are also lacking in the city. The city generates 450 tones of solid waste, which is uncollected. The situation in the area of 'petha' industry is even worst. Even the Biomedical waste of 400 odd nursing homes and clinics without being incinerated find its way into the general garbage bins.

#### **4.6 Air pollution**

Vehicular traffic is one important source of pollution in this mega city. The number of vehicles in Agra has increased manifold. The increase has been characterized by boom in private transport. The total air pollution in Agra from domestic sources, D.G Sets, Industrial sources, 'Petha' units and vehicular sources are 51t/day. In General the air quality is poor with SO<sub>2</sub>, NO<sub>2</sub> and SPM content in the air is above permissible limit.

With an Adverse Chaos and unmanaged situation the city lacks any facilities to counter adverse situations and any calamities. The lacking basic amenities and infrastructural facilities has made a city a dumps of Garbage and Chaos. The Urban Safety and Security has been put to ultimate Test. The Social and Environmental Safety and Security of its inhabitants and of its world heritage monuments are at stake.

#### **5.0 SUGGESTIONS**

Following are some suggestions to solve above mentioned challenges:-

- The new technology for power generation and solid waste disposal, which are eco-friendly, should be adopted.

- A citizens' committee should be constituted specifically for the improvement of heritage areas having representatives from local residents and user of those areas.
- NGOs should be provided with greater opportunities to participate in monitoring the state of the environment and Networking amongst NGOs in the region should be further strengthened.
- Governments should ensure wider participation and empowerment of women, youth, local communities and indigenous people in environmental management.
- Public awareness about environmental issues in Agra must be increased. Awareness has to be managed through various innovative means of communications in view of large illiterate population.
- Recognizes the importance of Agra as a world heritage and extends its support to the efforts being made by local communities and NGOs to protect its beautiful environment.
- Identify polluting industries in the Taj Trapezium and to suggest measures to control such pollution, which is harmful to the Taj as well as human being.
- Governments of India need to develop and adopt pro-people and pro-environment policies.
- Empirical evaluation of every problem has to be worked out to find out their economic viable and sustainable solutions.

## 6.0 CONCLUSION

Agra is on tourist map of world because of 'Taj Mahal' one of the wonders of world. Various efforts are being made to preserve and make this monument everlasting but unfortunately no serious attention have been given towards safety and security of more than one million inhabitants of this town. Who is more important 'human being' or 'Taj'? Who is really responsible for this? These are some questions, which need to be answered.

In present paper various issues regarding urban safety and security in context of Agra have been discussed. We think each and every issues may be elaborated further in order to investigate causes of various problems and to evolve sustainable solutions.

## REFERENCES

- Asher, C.B., 1995. *Architecture of Mughal India*. Cambridge University Press, U.K.
- Carmona M., 1996. *Controlling Urban Design-Part 1: A Possible renaissance?*. Oc Taner(editor). Journal of Urban Design. Volume 1, Carfax Publishing Company UK.
- Lang, J., 1994. *Urban Design the American Experience*. Van Nostrand Reinhold. ISBN 0442013604

- Moughtin, C., Cuesta. R., Sarris, C., and Signoretta, P., 1999. *Urban Design Methods and Techniques*. Architectural Press, Great Britain. ISBN 0750641029.
- Nath, R., 1997. *Agra & its Monumental Glory*. Taraporevala, Bombay, India.
- Nath, R., 1976. *Some Aspects of Mughal Architecture*. Abhinav Publications, New Delhi. India.



# **URBAN SAFETY IN ASIAN CITIES: FOR THE CITY DWELLERS, BY THE CITY DWELLERS**

MAHUA MUKHERJEE

Indian Institute Technology Roorkee, Roorkee, India

*mahua1965@rediffmail.com*

## **ABSTRACT**

*Today's mega-city in Asian context can be compared with dinosaur, one of the largest ever animal on earth. Strong apprehension is there, in near future, if corrective measures are not applied to these mega-cities they can be extinct species of human settlement like dinosaurs. Haphazard growth pattern coupled with uncontrolled population explosion are now a serious global concern. Natural or manmade disasters make them more vulnerable.*

*Policymakers, planners and programme developers are working on war-foot to maintain and recreate a safe environment. Situation of Asian mega cities are rapidly deteriorating due to extreme shortage of infrastructural facilities. The very purpose of city dwelling (i.e. safety and quality living) is being defeated at every steps. Not that effort is absent; new technological innovation/ developments are making the process smoother and more flawless. With easy communication (physical and informatics) sharing of experience from successful attempts are quite common today. But until and unless the common people would be involved in the process of problem solving starting from analysis to implementations of decisions, this is partly futile exercise. If the users feel changes proposed/made as worthy to follow, practice and pass on to next generation optimal success can be achieved. The scope of researchers has to be extended beyond planning and development of physical environment and use of new technologies like GIS etc. User's friendly technology or planning has to be initiated to take common people into the wing of development process. Many important information or research results never reach the target group. In this paper the author explores situations which are different as bridging between planners/policymakers/ researchers and the common city dwellers was appropriate. Dissemination of knowledge on behalf of researchers and awareness, local governments' effort to bridge the gap and active participation from common city dwellers have changed the situation.*

## **1.0 INTRODUCTION**

### **1.1 Urbanization**

The human settlement pattern in today's cities is far from ideal. Ordered planning in central cores with haphazard growths in transitional zones is a common feature. The global imbalance in the quality of life makes things more difficult. In developing countries the confusion of planning with general urban destitution is certainly severe than in the developed societies. In a book of Politics, Aristotle has described the urban settlement as habitable, when it can satisfy two main requirements—security and a good life [Gottmann, 1990]. According to him, the families form dense settlements for purposes of defense and once security are achieved, they remained there for the sake of a good life; i.e. happiness and safety are the aims of any human settlement. The terms like 'good life' or 'happiness'. 'Security' and 'safety' are subjective- but the notion they convey, can be easily appreciated. Cities are major contributors to the country's economy and resource development. To sustain this powerful engine of growth and development, the cities must be planned, managed and governed soundly.

### **1.2 The impending crisis**

Cities are places where social issues such as poverty, homelessness, crime and unemployment are becoming more far-reaching and complex than ever before. Urbanisation compounds issues like access to safe water, transport, education, security, health services, solid waste disposal and drainage etc. – often for the worse. One of the major challenges at the end of this century is the need to develop practical strategies for safe quality living in urban areas. Good governance, sustainable development and security are indivisible. Today's mega-city in Asian context can be compared with dinosaur, one of the largest ever animal on earth. Strong apprehension is there, in near future, if corrective measures are not applied to these mega-cities they can be extinct species of human settlement like dinosaurs. Haphazard growth pattern coupled with uncontrolled population explosion are now a serious global concern. Natural or manmade disasters make them more vulnerable.

### **1.3 Urban safety and security: a major issue in Asia**

Urban areas in Asia have become the place where social dysfunctionalities are exposed and unattended for longer time. Situation is rapidly deteriorating due to huge pressure of population coupled with shortage of resources and infrastructural facilities. The very purpose of city dwelling (i.e. safety and quality living) is being defeated at every steps. Not that effort is absent; new technological innovation/ developments help to make the process smoother and more flawless. But they are not enough to ensure safety in urban life. Absence of safety creates a feeling of insecurity among inhabitants, tearing the social fabric of cities and threatening the

foundations of democratic institutions. It is not pleasant to think that one cannot attend social events, classes in the evening, nor visit friends without feeling afraid for one's own safety.

World-wide, urban crime and violence is increasing. Because of the relative anonymity of city life, it becomes an attractive place for thieves, burglars, muggers, car hijackers and others, who can commit crime without fear of recognition. The role of city governments in local crime prevention is quite recent. Environmental degradation has also reached a new height. Cities are gasping to ensure that air is cleaner, water purer, and plant and animal species better conserved and protected. Better economy and improved physical environment can provide a safe life to some extent. When they are coupled with conducive social environment are bound to provide quality living. In developing countries cohesive social fabric is on the verge of collapse. Revitalisation of social link is another difficult task for the urban authorities at present situation.

## **2.0 URBAN SAFETY**

### **2.1 Purview of the issue**

Urban safety has different meanings to people of different backgrounds. For a social scientist, this is an issue which deals with crime, violence, social exclusion, law and order, attitude towards women and children, active participation, social festivals etc. Economist views this as availability and security of job, adequate compensation, healthy GDP, growth in industry & trade. For engineers, architects and planners this is equivocal to healthy built environment, satisfactory (both qualitative & quantitative) infrastructures like road networking, water supply and drainage, waste disposal systems etc. Environmentalist can base her judgment on physical or natural environment. Her consideration is pollution free water, soil, air, sound etc; conservation of vegetation cover, water body, and above all bio-diversity conservation. Medico thinks in terms of medical safety i.e. healthcare facilities in quantitative or qualitative terms or both. For the Political leaders this is a question of healthy electoral process, control or instigation of conflicts, ethical power play. Government assesses safety in terms of prevailing law and order situation, prevention and control in crime and violence, poverty eradication, abolition of social exclusion, control of socio-politico-religious turmoil, establishment of corruption-free administrative and judiciary process. Mitigating emergency situation due to natural hazards or man made disaster is another important task for government.

Public safety and security is increasingly recognised as a key planning and management objective to ensure economic and social development, as well as a central aspect of the quality of life. Public security must be considered as a public good for social well-being to be promoted by public institutions and civil society together. The measures to protect communities from deprivation, unemployment, homelessness and injustice will also protect them from crime and violence. High crime rates are

attributable to causes like [United Nations- Safety for All,1998]: disparity between income and expectations; the exclusion of youth; violence as a means of solving conflict within homes and communities; poorly designed and secured property; easy access to firearms, alcohol and drugs; and increasing impunity and unaccountability

Road Accidents are currently ranked as the eighth biggest cause of fatalities in the world and it is predicted that by 2020 they will be the third largest cause of death [The Institution of Highways and Transportation Guidelines, 2004]. As well as economic costs, there are social costs in terms of pain, grief and suffering caused to road accident victims and their friends and relatives. A large proportion of road accidents take place in urban areas; this is because urban areas are more complex than rural ones and there is more potential for conflicts to occur. Motor vehicle traffic levels in Asia have grown substantially over the last 30 or so years and these levels are set to keep rising. As the number of vehicles and distance traveled increases, there is a greater chance of conflicts occurring on the road and therefore potentially more road accidents.

Political conflicts in countries prevent the suitable development of cities and the provision of security to citizens. Government must also work towards preventing the conflicts which make crime prevention that much harder, while envisioning strategies for urban crime prevention. Only through these measures can the proper development of cities and the stability of countries be assured. Many African cities are examples of what happens when the governing framework collapses or does not exist. Citizens become victims of poverty or civil war. Crime becomes rampant in the wake of population displacements, illegal weapons and economic need.

Urban Safety and Disaster Mitigation Division in government level will develop management technologies to ensure the structural safety of urban infrastructure from natural disasters such as earthquake, flood, etc., and their safety for use at the time of disaster.

## **2.2 Methods of control**

Urban crimes are of different hues – alcohol, drug abuse, petty or violent crime (murder, rape, and molestation), theft, dacoity, trade in women and children, neglect & insecurity of elderly people and children, crime against school children etc. Prevention and reduction of crime is now being ensured with better training of police force, improved communication systems, use of sophisticated instruments etc. Crime information, role of national as well as local governments, the police and judiciary, communities and partnership, monitoring and implementation of programme everything plays important role to curb crimes.

In many Asian countries the road accident trend has been towards control in fatalities even though there have been continued increases in vehicular and pedestrian traffic levels. This has been a function of

transportation engineering and traffic management, education, enforcement and increases in safety standards. There are many well-documented methods which can be used to make urban areas safer, including traffic calming, zoning according to speed etc. Road engineers have the solution to many of road safety problems, but they are not always implemented as widely as they could be. The reason is often that the public opinion and/or political support are missing.

Recent rapid development of information technologies, i.e., Internet, Mobile Computing, Remote Sensing, Virtual Reality, etc., have changed our social life in various fields. Government, both at national and local level aims to develop and evaluate technologies for monitoring information of urban infrastructure, ensuring their safety for daily use and in case of emergency. This remarkable innovation also affects the field of urban safety planning or disaster mitigation. Cooperating with these latest information technologies, some human activities for disaster mitigation could be shifted into a new paradigm. Especially, GIS technology will be an effective means, because the spatial viewpoint is indispensable not only for the field of physical environment like urban planning but also for human activities. In fact, a lot of researches with GIS have been carried out e.g. MUSE (the Method of Urban Safety Analysis and Environmental Design) to analyze a city from the viewpoint of urban safety [Murao and Yamazaki, 1999]. City safety and disaster prevention strategy includes engineering technique for utilization of earthquake-predicting information.

## **2.3 Limitations**

Safety and security have been identified as priority areas of urban development policies. In reality, responsibilities for these subjects belong to different institutions, which are dependant of various Authorities operating at different levels. In many cases they do not share any compatible platform to exchange information, knowledge or experience. Though theoretically, with easy communication (physical and informatics) system of present day, sharing of experience from successful attempts are not difficult. This shows that the creation of partnerships which are sometimes complex, is always necessary. Enforcement of safety is faced with a multitude of challenges including high rates of delinquency, violence and insecurity; fears and concerns of the public; lack of faith in the efforts of the police to combat crime; frustrations with criminal justice systems; scarce government resources to cope with crime; and the inherent risk to democracy and economic development if sustainable solutions to crime are not found.

Participation of common people in the process of problem solving starting from analysis to implementations of decisions will make it a good exercise. If the users feel changes proposed/made as worthy to follow, practice and pass on to next generation optimal success can be achieved. The scope of researchers has to be extended beyond planning and development of physical environment and use of new technologies like GIS etc. Many important information or research results never reach the target

group. User's friendly technology or planning has to be initiated to take common people into the wing of development process. Limitation of resource may be a problem for Asian cities; but the experience from unsafe cities of developed countries counterbalance the issue of resource availability for ensuing safety; and reinforces the argument in the favour of public participation.

### **3.0 COMMUNITY'S PARTICIPATION**

#### **3.1 Community and safety**

To make a safer world there should be a common vision. Such a vision has two components: a vision of what is wanted; and a plan of action for viable strategies that are implementable. This vision should include educating people, motivating them based on their education and organising from a planned, central body. Such a vision must incorporate long and short-term goals, and should be partnership-focused. In addition to vision, more practical information must also be gathered. Given these diverse causes, solutions must go beyond law enforcement and criminal justice to incorporate prevention. A prevention focus should include: potential victims, persons and families at risk, as well as the general public, who should be encouraged to promote collective and individual responsibility to discourage a culture that fosters crime.

Crime prevention programmes are most likely to be effective if developed locally (and not at national level), drawing in local players and local government. For crime prevention to succeed, it must involve the community it is meant to help, because crime flourishes when good people do nothing. Community involvement needs to be interactive and must be inclusive – everyone who wants to participate should be allowed to.

The traditional criminal justice institutions can no longer stop or control the escalation of urban violence. Today, reducing crime is everyone's responsibility: local authorities, Habitat, and key local actors working together in partnership. If we learn to take responsibility and action, our cities can be places where life is led in dignity, safety, happiness and hope.

Psychological pressure can be fought in groups. All are aware that people cannot deal with urban violence and insecurity by repression alone. One need to focus on prevention and awareness-building within communities to address the root causes of urban violence. 'Partnership' is the current buzz-word, but for it to become a sustainable alliance it must be based on equality and on the differing economic, social and political realities of our world. Information sharing becomes important in this regard.

### **3.2 Scope of community participation**

Based on experience in the Safer Cities programmes [UNCHS, 1995], preventive policy should be implemented and coordinated at the city level, while political guidance, monitoring and evaluation are performed by national government. The experience from implementation of such programmes in several cities across the globe is quite exploring. Both at national level and at local level following steps can be followed to combat urban insecurity. At national level:

- Improve socio-economic policies affecting excluded groups, particularly youth and those in urban areas;
- Create national responsibility centers for crime prevention;
- Increase safer city programmes;
- Engage public support; and
- Pursuit of strategies that have been effective world-wide.

At local level:

- Evaluate the process identification of existing problems (crime, drugs, quality of life);
- Verification of problems through analysis;
- Identification of who is affected by these problems and who should be involved in their resolution;
- Establishment of a community policing philosophy engaging all key stakeholders;
- Initiation of community mobilisation strategies;
- Establishment of realistic, manageable and measurable goals.

There are common challenges facing cities both in developed and developing countries. Notably, justice systems often function inadequately – or worse, not at all. The justice system is in crisis as a result of the increase in crime. The large amounts of money spent on fixing justice systems in countries around the world have not always improved the functioning of these systems. What is needed is a system that can assist policing which involves the role-players who are close to the situation in the community.

### **3.3 Appreciable efforts**

Throughout the globe persisting strong efforts are there to make the community equipped to ensure safety and security in their urban settlement. In the following paragraphs few of these examples have been cited. Most of the efforts have been initiated in Europe and USA.

In Côte d'Ivoire in Africa, thousands of refugees from Liberia have entered the country. While government policy has been to incorporate these people into the country, there have been repercussions from the massive growth of urban areas. For example, transmissions of communicable diseases and crime have increased and weapons and drug trafficking is in

evidence. Thus, the need for a framework of public-private partnerships becomes all important and government is working on it [United Nations-Safety for All,1998]. In Europe, several cities have undertaken safer city approaches to reduce crime. These programmes have made use of partnerships and co-operation exchanges which allow for the shaping of experiences and the sharing of best practices. In San Francisco of USA, Urban Safety Programs [Urban Safety Programs] has been created to make a statement and to combat the feeling of resignation (towards accepting that violence or crime may occur to anyone). One should not have to feel resigned, nor do they have to harbor a deep seated anger. It is possible to face these issues squarely, and do something through Martial arts.

Alternative community court can take care of less serious crime, local byelaws violation, family or neighbourhood disputes etc. This can provide relief to people from waiting lifetime to get justice. Punishment can be awarded as different community services depending on the degree of seriousness of the crime. In Singapore this is a common practice and it's effective too.

In 1996, the Towards World Change conference was held in Vancouver, Canada. The conference was built around the notion that crime, human rights and equality are closely related and that crime flourishes in the absence of the other two. Three main tracks were identified: cities and communities, social development and justice. All require the involvement of key role-players in order to bring about crime reduction. The conference resulted in an action plan which encouraged the strengthening of the International Network of Practitioners, exchange of best practices, national support and the holding of a second international conference in Johannesburg in 1998. The resulting International Crime Prevention Action Network (ICPAN) operates as a forum for the development and exchange of ideas, strategies, resources and training at the community level.

Urban Safety Management [DUMAS] is a structured approach to accident prevention and casualty reduction on urban roads introduced by European Commission. Deaths, injuries and damage in accidents on urban roads, and people's apprehensions about traffic risk in towns and cities can be reduced by applying the principles as developed in the programme. Local Area Safety Schemes like a roundabout, road humps, cycle lane, a bend in a road, can reduce accidents. Strategy to make it successful has been identified as consultation with local people & groups of people with mobility handicaps; acceptance of measures; evaluation of proposed schemes; implementation and monitoring; monitor progress towards safety objectives for a whole urban area etc. As conditions in urban areas are constantly changing, the safety management strategy should be kept continually under review. Objective Urban Safety [Objective Urban Safety] has been introduced in USA to boost confidence to live & work in office safely. Suggestions are to **avoid becoming the victim** by varying routine/ lowering the profile/ playing the 'chameleon' / recognising the danger signs /staying aware; **getting about safely** by on buses / the underground and



trains /taxis, by car and on foot; **protecting possessions** like wallets, purses, handbags, credit cards, mobile telephones, cars; and **protection at home through** on the telephone - nuisance calls etc, answering the door, rules about keys, during a break-in, fire, security of the home etc.

In urban India, efforts are to induct school children in the safety awareness and implementation schemes at young ages. School children observes traffic weeks, taking training to learn self defense, improving interactions within neighbourhoods, taking care of elderly people etc. It is too early to assess the impact of these initiatives.

#### 4.0 COMMENTS

The city authorities in Asia have begun to recognise the scope of the problem and are working towards proactive safety policies. Following EU countries, safety is on the political agenda of municipal elections and moves are being made to make lives safer. However, every city has its own priorities and accordingly set their target and deduces the policy for implementation. To be able to provide a safe and secured environment local governments and communities can work together with following targets:

- Ensuring efficient performance of municipalities through satisfactory service delivery functions;
- The creation or rebuilding of local networks;
- Hauling up of local economic activities to revitalize the community
- Introducing alternative judiciary system to make judiciary process faster and issuing pro-neighbourhood punishments.
- The promotion of environmental design that stimulates community interactions, using simple indicators for assessment which community people understands;
- The need to prevent social exclusion.

The successful undertaking of these measures will prepare Asians for an urban 21st century. In developing a capacity-building strategic plan, focus should be on priorities such as communities' abilities to assess and manage crimes of concern, undertake pollution prevention, participate in biodiversity conservation, and improve economic and social efforts.

#### REFERENCES

- DUMAS, *Urban Safety Management Programme*. European Commissions on Safety. <http://www.trl.co.uk/dumas/index.htm>
- Gottmann Jean, January 1990. *Political problems of Urban Growth*. Guest Editor's introductory statement, *EKISTICS*, No. 340-341.
- The Institution of Highways and Transportation, *Urban safety management guidelines*.  
[http://www.dft.gov.uk/stellent/groups/dft\\_roads/documents/page/dft\\_roads\\_504781.hcsp](http://www.dft.gov.uk/stellent/groups/dft_roads/documents/page/dft_roads_504781.hcsp).
- Murao, O., and Yamazaki, F., 1999. *Use of GIS for the Method of Urban*

*Safety Analysis and Environmental Design*. Proceedings of the 20th Asian Conference on Remote Sensing, Vol. 2, 951-956, Hong Kong.

Objective Urban Safety. <http://www.objectiveurbansafety.com/>

Urban Safety- Safety for All. *Report of the International Conference for Crime Prevention Partnerships to Build Community Safety*. 26-30 October 1998, Johannesburg South Africa, Edited by Sarah Meek, assisted by Kirsten Bowen-Willer.

United Nations - UNCHS, *Safer City Programmes*, 1996. <http://www.unchs.org/safercities.html>.

Urban Safety Programs. <http://www.angelfire.com/ca/usp/>

# **PER-FIELD CLASSIFICATION OF INDIAN URBAN ENVIRONMENT USING IRS-1C SATELLITE DATA**

VIRENDRA PATHAK<sup>1</sup> AND ONKAR DIKSHIT<sup>2</sup>

1. Department of Civil Engg., I.E.T. , Sitapur Road, Lucknow, U.P., India

2. Department of Civil Engg., I.I.T. Kanpur, Kanpur, U.P., India

vireniet@hotmail.com

## **ABSTRACT**

*The paper presents investigations to determine the suitability of conventional per-pixel approach and results of per-field (segment) classification for classifying Indian urban environment using high spatial resolution satellite data. Three different types of classifications were performed: the per-pixel classification, per-field GML classification and the per-field neural classification. Result showed that per-field classification improves overall classification accuracy up to 25% in comparison to per-pixel approach.*

## **1.0 INTRODUCTION**

The past five decades have seen a phenomenal increase in the growth of urban population in India. All this rapid and haphazard growth of urban sprawl and increasing population pressure is resulting in deterioration of infrastructure facilities, loss of productive agricultural lands and green open spaces besides causing air pollution, health hazards and micro-climatic changes. To address these issues effectively, one requires up-to-date and accurate data at regular intervals of time on the changing urban sprawl, urban land use, urban resources and urban environment. It is here that satellite remote sensing with its ability to provide reliable and accurate data may offers excellent possibilities to map, monitor and measure the various facets of urban development.

Conventionally, land use maps derived using remote sensing data have been prepared using coarse resolution satellite data with per-pixel spectral (PPS) classifiers like minimum-distance-to-means and Gaussian maximum likelihood (GML) classification methods (Mather, 1985). However, the levels of details that could be delineated were very limited. Later on the same techniques and features were used for classification with high-resolution satellite images of urban areas from SPOT HRV and Landsat TM sensors (Toll and Kennard, 1984). Unfortunately, the results were not encouraging. The main reasons for this apparent lack of success were that the conventional classification techniques and features were not sufficient for urban land use classification. Therefore, with the availability of high-resolution data some new alternative approaches need to be explored for information extraction.

Some of the new approaches which could be used for this purpose are based on artificial neural network, fuzzy approach, inclusion of spatial information in the classification process etc. Spatial information could be included in the form of texture or per-field basis. Inclusion of spatial information in the form of texture using the window-based approach has inherent drawback of choosing a suitable window size. The per-field or region base is important because a region as a whole contains more information than its individual pixels, but also because regions are atomic entities for structural and semantic analysis in middle and high level vision. This study presents investigation pertaining to the region-based approach of classification for a typical urban environment.

## **2.0 OBJECTIVE, STUDY SITE AND DATA RESOURCES**

The experiments reported in this work were mainly implemented to achieve the following main objectives:

- To investigate suitability of per-pixel spectral classifier for high-resolution data of urban environment.
- To investigate per-field method of incorporating spatial information in the classification process.
- To assess utility of the proposed per-field approach for classification of high spatial resolution satellite data.

The study has been carried for Lucknow city, the state capital of northern Indian state of Uttar Pradesh. It is situated in the upper Gangetic plains of the country, the geographical extent of study area lies within North latitudes  $26^{\circ}45'$  to  $27^{\circ}$  and the East longitudes  $80^{\circ}50'$  to  $81^{\circ}5'$ . From the study of available maps, field visits and previous knowledge about these study sites, it was observed that for Lucknow study site 12 classes covered the majority of urban land use features (Table 1).

The satellite data products used for the study was procured from linear image self scanning (LISS)-III sensors on board IRS-1C satellite through National Remote Sensing Agency (NRSA), Hyderabad, India (Table 2). A central extract of 512 x 512 pixels covering major portion of urban areas was extracted from the satellite image for the study. In addition to these satellite data products corresponding topographic and land use maps were also used.

## **3.0 EXPERIMENTAL METHODOLOGY**

In the first part, per-pixel spectral classifications were carried out using GML approach with pure spectral features to assess its suitability for Indian urban environment. It was also intended for making comparison with the results obtained using other approaches. Initially, classification was carried out using 3 bands (B2, B3, B4) and then short wave Infra red band (SWIR) was added to see its effect on classification. The training and test

pixels for different classes were selected with the help of various maps available for the city, field visits, and by employing the experience of the authors about various classes in the city. Sample size for training and test were calculated at a confidence level of 99% and a desired precision of  $\pm 5\%$  using equation suggested by Toratora (1976).

*Table 1: Classes in the study area and their brief description*

S. no.	Name	Description
1	Agriculture-1	Agriculture area having crops at middle stage of growth
2	Agriculture-2	Agriculture area having crops at early stage of growth
3	Commercial	Central business area of the city
4	Educational institutes	Various educational Institutions
5	Government establishment	Different Government establishments
6	Grassy land	Big patches of lands having grass only
7	High residential	Residential areas with more than 600 persons/hectare
8	Medium residential	Residential areas with 400 to 600 persons/hectare
9	Park	Parks for recreational activities
10	Reserve forest	A big portion of land reserved for forest
11	River	River Gomati flowing from left to right
12	Water body	Various small water bodies in the study area

*Table 2 Satellite data characteristics for study areas*

Sensor	Bands	Resolution (m)	Size (pixels)	Wavelength ( $\mu m$ )	Spectral Region	Path/Row
LISS III	B2	23.5	512 x 512	0.52-0.59	Green	100/52
	B3	23.5	512 x 512	0.62-0.68	Red	
	B4	23.5	512 x 512	0.77-0.86	NIR	
	B5	70.5*	512 x 512	1.55-1.70	SWIR	
PAN	-	5.8	2048 x 2048	0.50-0.75	Panchromatic	

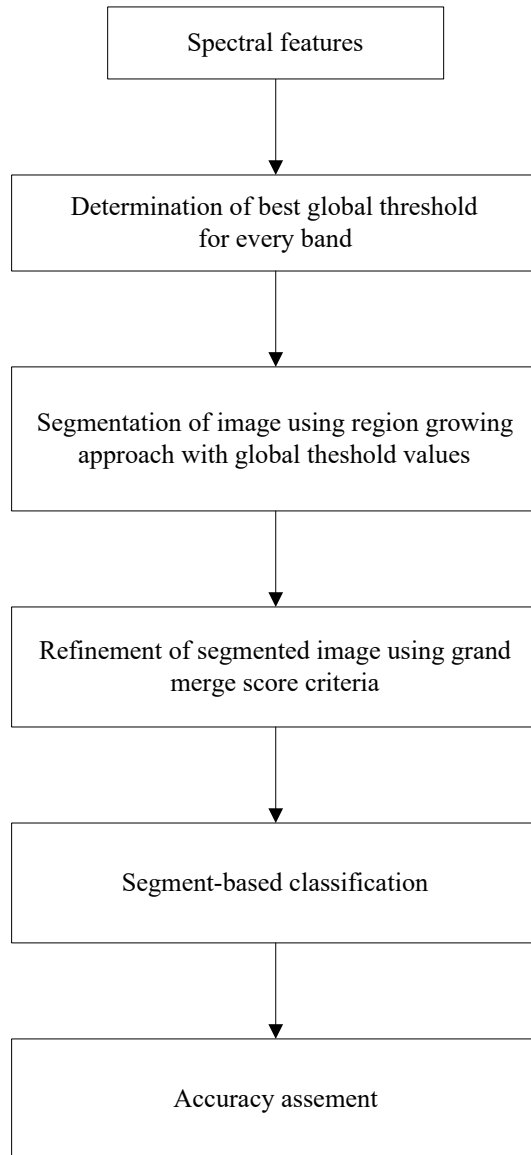
\* resampled to 23.5 m.

Experimental methodology for per-field based classification is divided into four stages i.e. Determination of threshold, segmentation of imagery, refinement of segmented imagery followed by classification based on per-field approach (Figure 1). For finding threshold for a given spectral band, an approach modified after Nagao and Matsuyama (1980) was implemented. The investigations used three different thresholding methods, namely Otsu (1979), Trussel (1979) and Kapur *et al.* (1980). These algorithms were applied using a sliding window approach with 5x5 window size.

Using thresholds obtained by using the aforementioned approach, the spectral bands were subjected to segmentation. There are two types of image segmentation that are based on detection of boundary or growth of region (Nevatia, 1982; Choo *et al.*, 1990).

A region-based approach was preferred because finding precise edges in such images is extremely difficult. The approach calculates a merge-score. A merge-score less than one indicates a preference for merging, while values greater than one dictates against merging. It is possible to incorporate many segment attributes to determine the merger of segments. The

segmentation algorithm operates in two phases. In the first phase, initial segments were grown from randomly selected seed pixels. After that the second phase started from the first pixel in the image by scanning from left to right and top to bottom. The second phase considered all those pixels that were not included in segments grown during the first phase.



*Figure 1: Overall methodology for per-field classifications*

The output of this process was a label image with a label number assigned to each segment. The label image obtained as a result of the initial segmentation was refined iteratively using region-merging approach proposed by Beveridge *et al.* (1989). After getting refined label image, various properties of segments like, minimum, maximum, mean, median, standard deviation, covariance, kurtosis and skewness values were calculated from spectral values of segments. Apart from these measures,

texture measures *Mean*, *Con* and *Entropy* (Haralick *et al.*, 1973) were also calculated.

In the final stage, these segments were classified using various spectral and textural properties of segments. Textural properties like standard deviation (SD), GLCM texture feature *Mean* were used. Three different types of classifications were performed, the per-pixel GMLC, per-field GMLC and per-field classification. For neural classification, Resilient Backpropagation method was used. The accuracy analysis was carried out using two approaches. The first measure of classification accuracy is based on the number of correctly classified segments. The other measure is based on  $\kappa$ -coefficient calculated using number of pixels corresponding to correctly classified segments. Pair-wise statistical tests were performed to assess the significance of any differences observed between two classifications using a Z statistic (Congalton and Green, 1999).

For testing the proposed per-field based classification approach on high resolution data, a simulated high spatial resolution data set of study site was generated by image fusion using wavelet based substitute principal component analysis (SPCA) approach (Li *et al.*, 1999). High spatial resolution PAN and low resolution LISS-III data were used for generating simulated high spatial resolution data set. Experiments were carried out using per-field based classification approach out in similar manner as it was done for normal data set.

## **4.0 RESULTS AND ANALYSIS**

This section presents results of various experiments carried out to achieve various objectives and to study importance of spatial properties in the classification of urban environment.

### **4.1 Classification using spectral features**

Classification results are presented in the Table 3. Classification accuracy for grassy land, reserve forest, river and water body was acceptable but for rest of the classes accuracy was poor. For classes commercial, educational institutes and government establishment  $\kappa$  - coefficient was lesser than 0.50. The overall accuracy was also very low. This low accuracy may be due to the fact that most of the classes were highly heterogeneous, there were many classes with low seperability values and few classes had similar biophysical environment.

Analysis of results suggests that classification results are less than acceptable due to high heterogeneity and non-normal behaviour of most of the classes. These poor classification results also suggest that spectral features alone are not sufficient for urban land use classification having high heterogeneity and non-normal behaviour and some additional information like spatial information in the form of texture, size, shape may be required.

Table 3 also presents result of GML classification after including SWIR band with three spectral bands B2, B3 and B4. It was observed that with the inclusion of SWIR band, there was improvement in classification accuracy for most of the classes. Though, this increase in classification accuracy was statistically significant only for one class (commercial) but due to increase in accuracy of all other classes, overall accuracy improved in a statistically significant manner. This shows that, although SWIR band has poor spatial resolution but its spectral properties help in improving classification accuracy when separation amongst classes is poor and the classes are highly heterogeneous.

*Table 3 Classification accuracy with spectral bands*

S. no.	Class name	Training			Test		
		<i>a</i>	<i>b</i>	$z_{ba}$	<i>a</i>	<i>b</i>	$z_{ba}$
1	Agriculture-1	0.65	0.75	1.33	0.74	0.78	0.71
2	Agriculture-2	0.61	0.82	3.16	0.73	0.77	0.58
3	Commercial	0.42	0.57	1.90	0.45	0.71	3.54
4	Educational institutes	0.44	0.51	0.91	0.49	0.53	0.49
5	Government establishment	0.15	0.19	0.69	0.05	0.11	1.49
6	Grassy land	0.87	0.92	1.02	0.87	0.89	0.49
7	High residential	0.80	0.85	0.83	0.75	0.81	0.81
8	Medium residential	0.81	0.91	1.90	0.74	0.85	1.77
9	Park	0.68	0.68	0.02	0.69	0.73	0.53
10	Reserve forest	0.94	0.93	-0.31	0.91	0.90	-0.26
11	River	0.95	0.95	0.00	0.92	0.92	0.00
12	Water body	0.84	0.87	0.44	0.92	0.93	0.29
	<b>Overall</b>	0.68	0.74	3.19	0.68	0.74	2.81

*a* 3 bands

*b* 3 bands + SWIR

$z_{ba}$  Z-statistic between *b* and *a*

## 4.2 Classification using per-field approach

Threshold values were determined for all bands considered for the study. It was observed that results of Otsu and Kapur *et al.* methods were similar while threshold values from Trussel were slightly higher than other two methods. Threshold values obtained using Otsu method were chosen to carry out further analysis. After selecting suitable threshold values for all four bands, multispectral segmentation of bands was carried out. It was observed from segmented image that inclusion of band B5 in the segmentation process produced poor segmentation. This could be due to very small thresholds values obtained for band B5. Segmentation carried out using three bands (B2, B3 and B4), produced good segmented image. Therefore, further analysis was carried out using only these three bands.

Table 4 shows the results of per-field based classifications. It was observed from the results that accuracy in terms of number of correctly classified segments was lower than the number of correctly classified pixels. The reason for this becomes obvious when we see test accuracy of classes



like commercial and educational institutes. In case of commercial class, only two out of eight segments have been correctly classified whereas in terms of number of pixels, more than 97% of the pixels have been correctly classified. Similarly for class educational institutes only one out of eight segments have been correctly classified whereas in terms of number of pixels, more than 90% of the pixels have been correctly classified for this class.

*Table 4: Results of per-field based classification*

S. no.	Class name	Test accuracy						
		In terms of segment			In terms of pixels			
		<i>a</i>	<i>b</i>	<i>c</i>	<i>d</i>	<i>e</i>	<i>f</i>	<i>g</i>
1	Agriculture-1	10	8	80.00	229	180	78.60	0.79
2	Agriculture-2	8	7	87.50	2623	1983	75.60	0.75
3	Commercial	8	2	25.00	2754	2691	97.71	0.98
4	Educational institutes	8	1	12.50	4943	4482	90.67	0.90
5	Government establishment	7	4	57.14	3477	3148	90.54	0.90
6	Grassy land	4	2	50.00	7768	7740	99.64	1.00
7	High residential	1	1	100.00	15558	15558	100.00	1.00
8	Medium residential	2	1	50.00	15412	15407	99.97	1.00
9	Park	5	2	40.00	1171	1125	96.07	0.96
10	Reserve forest	4	3	75.00	9954	7329	73.63	0.70
11	River	4	4	100.00	2297	2297	100.00	1.00
12	Water body	8	7	87.50	291	286	98.28	0.98
	<b>Overall</b>	69	42	60.87	66477	62226	93.61	0.92

- a* Number of segments for training / test  
*b* Number of correctly classified segments  
*c* % of correctly classified segments  
*d* Number of pixels corresponding to training / test segments  
*e* Number of correctly classified pixels  
*f* % of correctly classified pixels  
*g*  $\kappa$ -coefficient

Table 5 shows a comparison between classification results using per-field based GML and per-pixel GML classification approach. It was observed that except reserve forest, classification accuracy for most of the classes was statistically significantly higher using per-field based approach. The overall test accuracy in terms of  $\kappa$ -coefficient increased from 0.68 to 0.92 (increase of 24%). The classified image using per-field based approach looks more like a thematic map in comparison to per-pixel classified image.

For three fused bands obtained using wavelet based SPCA approach, threshold values were obtained from Otsu method. Segmentation of fused bands was carried out and subsequently merging was done for refinement of initially segmented image. Total of 550 iteration of segment merging algorithm were required before merging stopped. Corresponding to refined segmented image, per-pixel and per-field based GML classifications were carried out for simulated data set. The same approach of classification was adopted, which was used with the multispectral data set. Table 6 presents a comparison of per-field and per-pixel classification results. The overall test accuracy in terms of  $\kappa$ -coefficient increased from 0.70 to 0.95 (increase of 25%).

Table 5: Comparison of per-pixel and per-field based classification accuracy ( $\kappa$ )

S. no.	Class Name	Training			Test		
		$a$	$b$	$z_{ba}$	$a$	$b$	$z_{ba}$
1	Agriculture-1	0.65	0.61	-0.24	0.74	0.79	0.29
2	Agriculture-2	0.61	0.99	5.60	0.73	0.75	0.15
3	Commercial	0.42	0.99	8.29	0.45	0.98	6.87
4	Educational institutes	0.44	0.88	5.05	0.49	0.90	4.67
5	Government establishment	0.15	0.90	9.04	0.05	0.90	11.17
6	Grassy land	0.87	1.00	3.03	0.87	1.00	2.78
7	High residential	0.80	1.00	4.48	0.75	1.00	5.17
8	Medium residential	0.81	1.00	3.89	0.74	1.00	5.13
9	Park	0.68	1.00	6.20	0.69	0.96	2.87
10	Reserve forest	0.94	0.70	-3.26	0.91	0.70	-2.78
11	River	0.95	1.00	1.24	0.92	1.00	2.77
12	Water body	0.84	0.98	1.35	0.92	0.98	0.73
	<b>Overall</b>	0.68	0.93	7.26	0.68	0.92	6.60

$a$  per-pixel GML

$b$  per-field based GML

$z_{ba}$  Z-statistic between  $b$  and  $a$

Table 6: Comparison of accuracy ( $\kappa$ ) between per-pixel and per-field based classification with fused image

S. no.	Class name	Training			Test		
		$a$	$b$	$z_{ba}$	$a$	$b$	$z_{ba}$
1	Agriculture-1	0.79	0.78	-0.46	0.57	0.70	9.18
2	Agriculture-2	0.90	1.00	35.30	0.66	0.89	50.50
3	Commercial	0.48	0.95	196.19	0.49	0.95	195.73
4	Educational institutes	0.47	0.95	126.16	0.46	0.93	125.45
5	Government establishment	0.28	0.36	18.44	0.28	0.36	18.35
6	Grassy land	0.84	0.99	101.36	0.85	1.00	108.40
7	High residential	0.77	1.00	201.69	0.77	1.00	201.25
8	Medium residential	0.65	1.00	213.30	0.64	0.98	213.69
9	Park	0.63	0.87	45.45	0.62	0.82	36.38
10	Reserve forest	0.83	1.00	165.30	0.83	1.00	165.75
11	River	0.65	1.00	147.36	0.65	1.00	147.28
12	Water body	0.70	0.82	16.66	0.69	0.82	16.62
	<b>Overall</b>	0.71	0.96	388.40	0.70	0.95	390.24

$a$  Per-pixel classification

$b$  Per-field classification

$z_{ba}$  Z-statistic between  $b$  and  $a$

These results reveal that invariably for all the classes, accuracy increased in a statistically significant manner in case of per-field based classification approach. This clearly indicates that use of the proposed classification method would be appropriate even for high resolution data.

## 5.0 CONCLUSIONS

This paper has demonstrated the significance of spatial properties in the classification of urban environment using IRS-1C satellite data. This paper has also demonstrated that proposed approach of per-field (segment) based classification is suitable for classification of urban environment even with high resolution spatial data. The classification results with this approach showed significant improvement over per-pixel approach. The following conclusions can be drawn from the analysis carried out in this study:

- The poor classification results with pure spectral features suggest that spectral features alone are not sufficient for urban land use classification having high heterogeneity and non-normal behaviour. Therefore, some additional information like spatial information in the form of texture, size, shape may be required.
- Inclusion of SWIR band in the classification process with IRS-1C data helps in improving classification results for classes having high heterogeneity.
- Per-field based classification provides statistically significantly higher accuracy (up to 25%) than per-pixel approach.
- The per-field ANN classification provides slightly higher, though statistically insignificantly different, test accuracy than the per-field GML classification.
- Classified image obtained as a result of per-field based classifications looks more like a thematic map while making a comparison with results of per-pixel approach.
- Per-field based classification of fused data set obtained from high spatial resolution PAN and low spatial resolution LISS-III, provides significantly higher accuracy. This clearly indicates that per field approach would be appropriate for classification of urban environments from high spatial resolution satellite images.

## REFERENCES

- Beveridge, J. R., Griffith, J., Kohler, R. R., Hanson, A. R., and Riseman, E. M., 1989. *Segmenting Images using localised histograms and region merging*. International Journal of Computer Vision, 2, 311-347.
- Choo, A. P., A.J. Maeder and B. Pham, 1990. *Image Segmentation for complex natural Scenes*,. Image and Vision Computing, vol. 8, pp. 155-163.
- Congalton, R. G. and Green, K., 1999. *Assessing the Accuracy of Remotely Sensed Data: Principles and Practices*. CRC Press, Inc., U.S.A.
- Haralick, R. M., Shanmugam, K., and Dinstein, I., 1973. Textural features for image classification. *IEEE Trans. on Systems, Man, and Cybernetics*. SMC-3, 610-621.
- Kapur, J. N., Sahoo, P. K. and Wong, A. K. C., 1985. *A new method for grey-level picture thresholding using the entropy of the histogram*. Computer Vision and Image Processing, 29, 273-285.

- Li, J., Zoju, Y., and Li, D., 1999. *PCA and wavelet transform for fusing panchromatic and multispectral images*. SPIE's International symposium on Aero Scene: Image Exploitation and Target Reconstruction; Orlando, Florida, U.S.A, 3719, 5-9.
- Mather, P.M., 1985. *A computationally efficient maximum likelihood classifier employing prior probabilities for remotely sensed data*. International Journal of Remote Sensing. 6 (2), 369-376.
- Nagao, M. and Matsuyama, T., 1980. *A structural analysis of complex aerial photographs*. Plenum, New York.
- Nevatia, R., 1982. *Machine Perception*. Printice-Hall, Englewood Cliffs, NJ.
- Otsu, N., 1979. *A threshold selection method from grey-level histograms*. IEEE Trans. on systems, Man, and Cybernetics, SMC-9, 62-66.
- Toll, D. L. and Kennard, R. E., 1984. *Investigation of SPOT spectral and spatial characteristics for discriminating land use and land cover in Prince George's county, Maryland*. In SPOT simulation Applications Handbook, Falls Church: American Society for Photogrammetry, 165-170.
- Tortora, R., 1978. *A note on sample size estimation for multinomial populations*. The American Statistician, 32 (3) 100-102.
- Trussel, H. J., 1979. *Comments on 'Picture thresholding using an iterative selection method'*. IEEE Trans. on Systems, Man, and Cybernetics, SMC-9 (5), 311.

# **SURFACE CLIMATIC IMPACTS OF URBANIZATION IN THE HOCHIMINH CITY, VIETNAM: AN INTEGRATED STUDY WITH REMOTE SENSING AND MODELING**

TRAN HUNG<sup>1</sup> AND YOSHIFUMI YASUOKA<sup>2</sup>

<sup>1</sup>Institute of Meteorology and Hydrology, Hanoi, Vietnam

<sup>2</sup>Institute of Industrial Science, University of Tokyo, Tokyo, Japan  
*tranhung@iis.u-tokyo.ac.jp*

## **ABSTRACT**

*Hochiminh City, the biggest industrial, commercial center in Vietnam with population of more than 5 millions people, has experiencing rapid urban expansion during the last decade. A large amount of forest and agricultural land has been converted into housing, infrastructure and industrial estates. The resultant impervious urban surface alters the surface energy balance and surface runoff, which in turn could pose serious environmental problems for its inhabitants (e.g., urban waterlogged and thermal pollution). In this paper, we utilize satellite images (TM and ASTER) to derive surface biophysical parameters such as fractional vegetation cover ( $Fr$ ), surface radiant temperature ( $T_s$ ), surface moisture availability ( $M_0$ ) and evapotranspiration fraction ( $ET/R_n$ ) are derived for different years during 1989 – 2002 period. The changes over the years of surface biophysical parameters are, then, examined in association with land-use changes to illustrate how these parameters respond to rapid urban expansion in Hochiminh City and surrounding region. This study attempts to provide environmental awareness to urban planners in future urban development.*

## **1.0 BACKGROUND**

Hochiminh City, one of fast-expanding Asian Metropolis agglomerations with population of more than 5 millions, is the biggest industrial, commercial center in Vietnam. The population density in the urban area is reported as of 9,373 persons per square kilometers on April 01, 1999. High economic growth and increased employment opportunities caused substantial influx of labor immigration. The urban population has increased 1.5 times from 1977 to 1999 mainly due to immigration. Currently, the natural growth is 1.36% while the immigration growth is 0.77% annually. As the city expands, prime agricultural land and habitats such as forests and water basins are transformed into land for housing, roads, and industry. This has added more pressure on the land use demand and the drastic changes of land cover and land-use caused by urbanization could significantly affect social, economic and ecological conditions in a large urban footprint area. While effective urban land use planning can help guide urban development away from vulnerable ecosystems, it appears impossible without deep

understanding of processes governing the change dynamics and their inter-relations in urban and sub-urban areas.

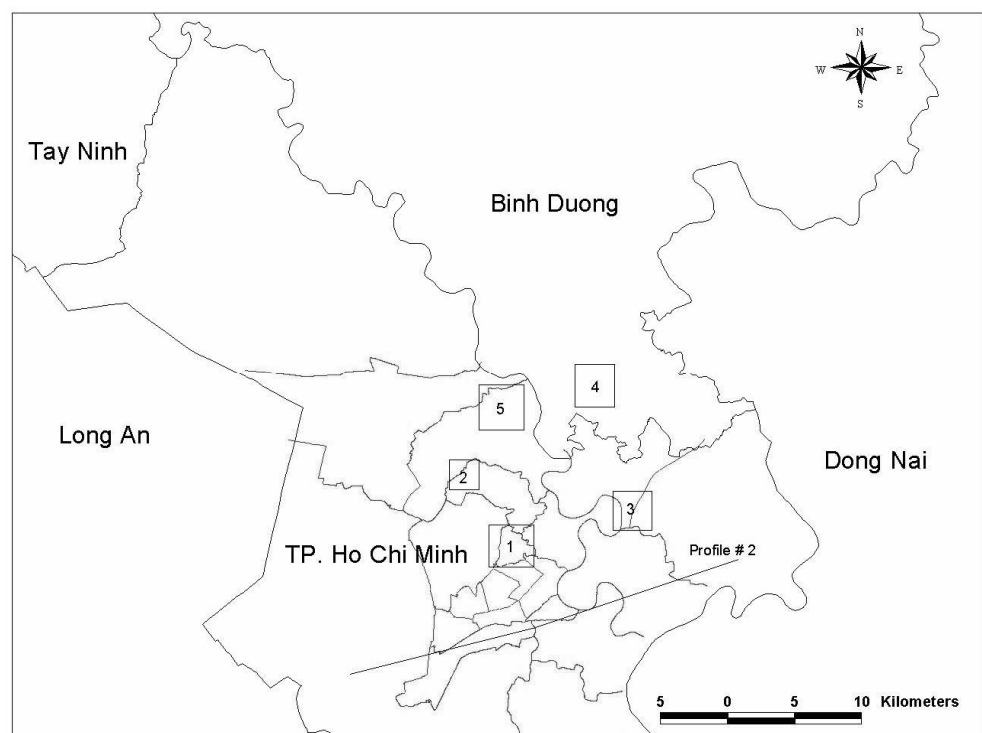
It is well recognized that the multi-spectral, multi-temporal satellite imageries provide the most reliable, up-to-date and consistent means of monitoring land cover changes associated with urbanization at the regional scale. The land cover information, properly classified, can provide a spatially and temporally explicit view of societal and environmental attributes and can be an important complement to in-situ measurements. In addition, Owen *et al.* (1998) noted that quantitative biophysical information could also be extracted from existing satellite data, thus adding a great potential for practical application to regional planning and urban ecology. Remotely sensed surface radiant temperatures were successfully used in the studies of the so-called urban heat islands, while various vegetation indexes have long been used in urban vegetation studies. Gillies *et al.* (1997) has described the characteristic triangular-shaped envelope of pixels as viewed on a scatterplot of vegetation cover and surface radiant temperature for satellite remotely sensed pixels. On the other hand, Soil-Vegetation-Atmosphere Transfer (SVAT) model can be used to predict changes in various meteorological variables, including substrate temperature, atmospheric temperature and surface moisture as a function of time. The remotely-sensed measured variables in terms of surface radiant temperature ( $T_s$ ) and NDVI (after normalizing to minimize the effects of surface and atmospheric variability) could be then fitted to the model's simulated ones in order to solve the inverse problem of estimating fractional vegetation cover, surface moisture availability and evapotranspiration fraction (Gillies *et al.*, 1997).

In this paper, we attempt to utilize satellite imageries in association with existing ancillary data to monitor and analyze land-use dynamics in Hochiminh City and surrounding region during 16 years (1986-2002). Based on revealed urban development patterns, major land-conversion zones are delineated. We then have applied the "triangle method" to derive surface biophysical parameters such as surface moisture availability ( $M_0$ ), evapotranspiration ( $ET/R_n$ ) fraction and vegetation fraction ( $Fr$ ) over the years from high-resolution TM, ETM+ and ASTER images. The main objective of this paper is to illustrate the expanded capability of remote sensing in studying the impacts of rapid urbanization on regional environment by analyzing the changes in the derived biophysical parameters associated with urban development in the Hochiminh City region between 1989 and 2002.

## 2.0 URBAN DEVELOPMENT PATTERNS BY REMOTE SENSING

The study area is located between  $106^{\circ}20'01''$  –  $106^{\circ}59'48''$  Longitude and  $10^{\circ}40'49''$  –  $11^{\circ}09'51''$  Latitude. Administratively, it composes of major part of Ho Chi Minh City and parts of surrounding Long An, Tay Ninh, Binh Duong and Dong Nai provinces, which is reported to have rapid built-up expansion since the last decade (Fig. 1). To provide temporal land cover and land use information, various satellite images such

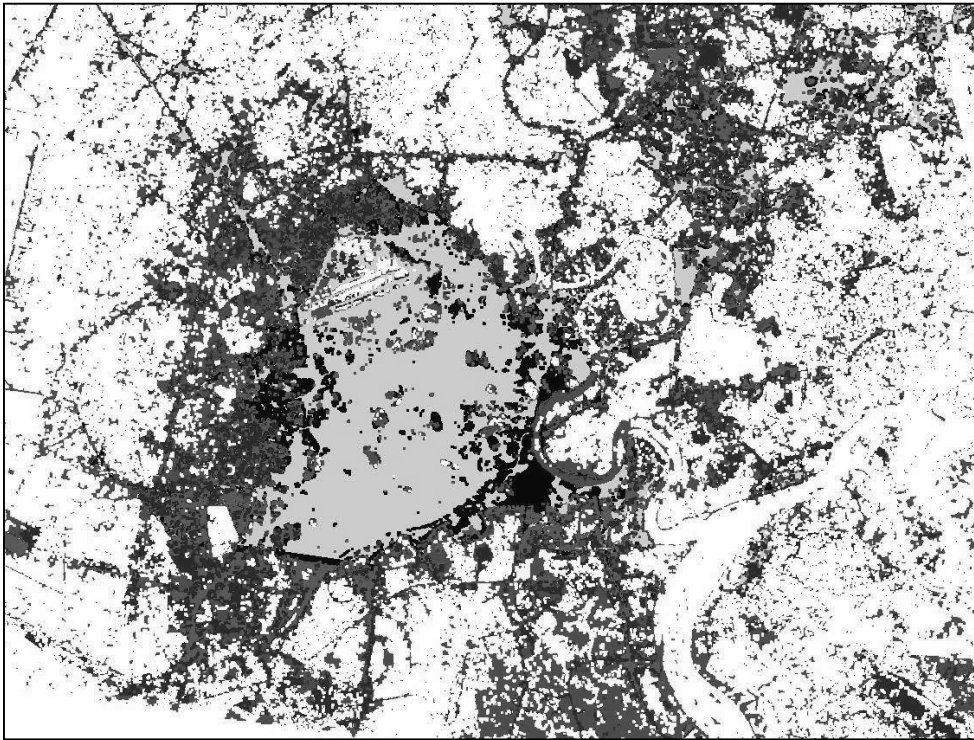
as MSS (1986), TM (1989, 1993), ETM+ (1999, 2001, 2002) and ASTER (2001) are obtained for the study area. Satellite images are corrected for atmospheric attenuation and geo-referenced to a common 1:50,000 UTM topographic map and re-sampled to 30m resolution. The image analysis is done on single-date images individually including ML classification and knowledge-based post-classification techniques incorporating texture, vegetation information and ancillary existing land-use maps of 1997. With biophysical characteristics of the land cover as the major focus of the study, the final analysis consolidates classified images into some major land-cover categories: built-up, paddy/irrigated agricultural land, plantation, forest, dry baresoil, wet baresoil, wasteland and water-body. Change detection is then applied based on overlaying classified images in order to understand the land-use conversion and to build time-series data for a particular land-use type for the 1986 – 2002 period.



*Figure 1: Map of the study area with some focus spots: for inner city – 1 (Q. Phu Nhuan); suburban - 2 & 3 (Q. Go Vap & Thu Duc); industrial zones – 4 (South of Binh Duong); agricultural area – 5 (H. Hoc Mon)*

As the result, the spatial patterns of urban development are found changing over the years (Fig. 2). Along with the continuing urban densification of highly urbanized areas in the inner city districts such as Quan 6, Phu Nhuan, the City significantly expands into northern and eastern suburban areas during 1989 – 2002 (e.g., Q. Go Vap, Quan 8, Q. Thu Duc, Q. 2 and southern part of Binh Duong province). The rate of urban expansion is observed of more than 7 percent per year in some neighborhoods of the Go Vap and Thu Duc districts. Figure 3 shows trend of urbanization of some representative districts in the inner city and suburban areas. The major to-

urban-land conversion is observed from: 1) irrigated land (paddy fields, wetland) to built-up; 2) agricultural land (cash crops, orchards) to built-up; 3) bush land / range land to pre-construction wasteland and industrial estates areas; and 4) urban densification. Here, we select 5 sub-areas representing different patterns, type and degree of urban development (1 – inner city, 2 – dry suburb, 3 – wet suburb, 4 - industrial zones & 5 – agriculture as control zone) for more detailed analysis of the changes in surface biophysical parameters (Fig. 1).



*Figure 2: RS-derived urban expansion around HCM area during 1989 – 2002 (white color shows non-urban; gray - urban area before 1989; blue, green, brown and red show new urban land by 1993, 1999, 2001 and 2002)*

### **3.0 REMOTELY-SENSED BIOPHYSICAL PARAMETERS**

#### **3.1 Surface temperatures and NDVI**

The Landsat TM raw data of 1989 and 1993, ETM+ of 1999, 2001 and 2002 and Terra ASTER data of 2001 are used to extract biophysical surface parameters (more details could be found in Tran & Yasuoka, 2001). Thermal radiances at the original spatial resolution are converted to at-sensor temperatures via the Planck equation and then to at-surface temperatures based on the equations and calibrating coefficients developed by the National Aeronautics and Space Agency (NASA) and ERSDAC respectively. Normalized Difference Vegetation Index (NDVI) is calculated from visible red (TM Band 3 or ASTER B2) and near infrared (TM B4 or ASTER B3) reflectance by equation:  $NDVI = (NIR - R) / (NIR + R)$ .



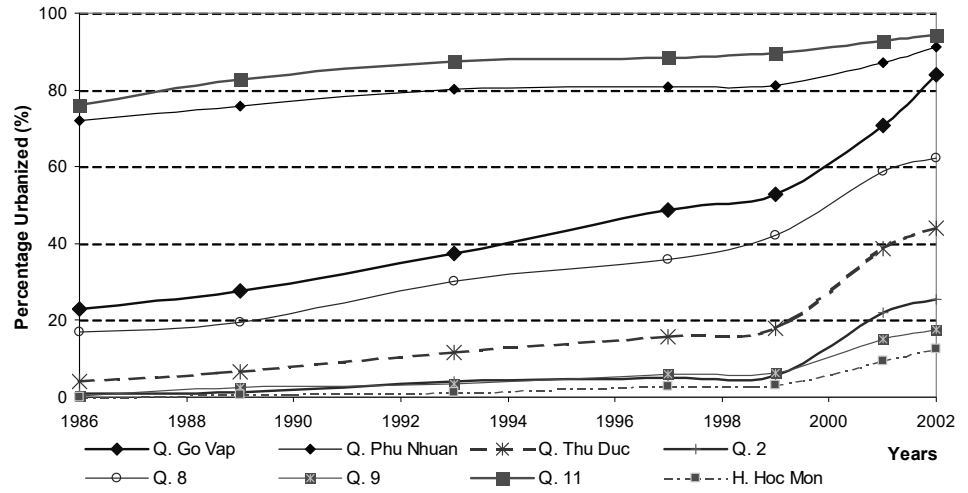


Figure 3: Increase in percentage of urbanized areas in selected inner and suburban districts of Ho Chi Minh City during 1986-2002

### 3.2 Universal triangle and biophysical parameters

We derive biophysical parameters from satellite images based on the triangle method (Gillies *et al.*, 1997). The water and cloud contaminated pixels, which tend to be localized at negative of NDVI and lower values of  $T_0$ , are excluded from the analysis. Firstly, we normalize the calculated NDVI and  $T_s$ , to reduce inter-scene variability in the state of the surface, the phenology of the vegetation and the condition of the atmosphere (e.g., haze, wind speed, humidity). Transformation of NDVI to a scaled NDVI ( $N^*$ ) is accomplished using equation:

$$N^* = \frac{NDVI - NDVI_0}{NDVI_s - NDVI_0}$$

where  $NDVI_0$  is limit for bare soil and  $NDVI_s$  is limit for 100% vegetation cover are selected empirically for each image. Then, the fractional vegetation cover ( $Fr$ ) is calculated as  $Fr = N^{*2}$  according to Carlson & Arthur (2000). Temperature values are also scaled between the warmest ( $T_{max}$ ) and coldest ( $T_0$ ) surface temperatures corresponding to dry bare soil and wet soil at 100% of vegetation cover. The temperature anchor values are determined by inspection of the NDVI/ $T_s$  scatterplots (Owen *et al.*, 1998) and observed ambient air temperature ( $T_a$ ) recorded at the Tay Ninh, Xuan Loc meteorological stations at the time of satellite overpass. Normalization to a scaled surface temperature is done based on equation:

$$T^* = \frac{T_s - T_0}{T_{max} - T_0}$$

The normalized  $Fr/T^*$  scatterplots are, then, constructed for the 1989, 1993, 2001 and 2002 images as the “universal triangle” as shown in Figure

4. With input parameters from observation data recorded from meteorological stations at Tay Ninh and Xuan Loc, the SVAT (soil-vegetation-atmosphere transfer) model of the Penn State University is used to derive fractional vegetation cover ( $Fr$ ), surface soil water content ( $M_0$ ) and evapotranspiration fraction ( $ET/R_n$ ). The SVAT model output in forms of  $M_0$  and  $ET/R_n$  isopleths are overlaid on the normalized  $Fr/T^*$  scatterplots using third-order polynomial relations to compute the  $M_0$  and  $ET/R_n$  from  $Fr$  and  $T^*$  for the 1989, 1993, 2001 and 2002 images in the study.

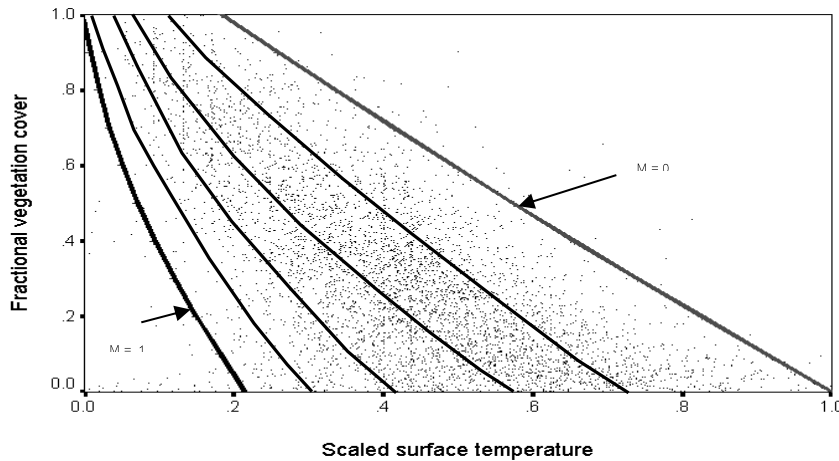


Figure 4: Universal triangle as scaled  $Fr/T^*$  scatterplot for the Feb. 04, 1993 TM scene and overlaid surface moisture availability isolines ( $M_0 = 0, 0.2, 0.4, 0.6, 0.8, 1$ ) based on the SVAT model output.

#### 4.0 URBANIZATION AND REGIONAL CLIMATIC PARAMETERS

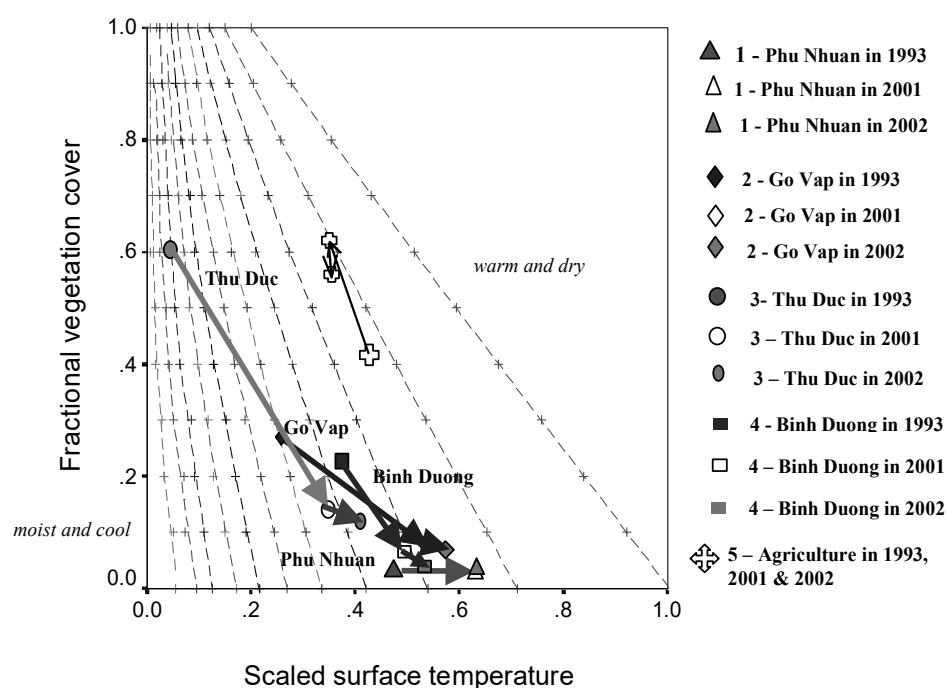
With the derived biophysical parameters over the years, it is interesting to examine the relationship between them and the urbanization process. As TM/ETM+ pixels are of small size,  $T^*$  and  $Fr$  have considerable large variations creating difficulties in tracing out representative changes over years, biophysical parameters are aggregated from 30x30m to 300x300m spatial resolution using average values. Examining the  $Fr/T^*$  scatterplots, there is a clear distinction between dense urbanized pixels from other land cover types in terms of  $T^*$  ( $> 0.6$ ) and  $Fr$  ( $< 0.1$ ), while suburban residential areas have large variability in  $T^*$  ( $0.3 \div 0.6$ ) due to variable vegetation covers. Statistically, it is found a significant negative relationship between % urbanized and  $Fr$  ( $r = 0.473$ ,  $p < 0.001$  for 2001 data) and significant positive correlation with  $T_s$  ( $r = 0.491$ ,  $p < 0.0001$ ).

The changes in  $T^*$ ,  $Fr$ ,  $M_0$  and  $ET/R_n$  between 1993 and 2001 for 5 selected subgroups are summarized in Table 1, showing the study area in general tends to become warmer and drier. Figure 5 shows the trajectories for aggregated TM pixels representing 4 urban development classes from 1993 to 2001 & 2002, which suggests urbanization is the primary cause of the migration of the pixels in the  $Fr/T^*$  scatterplot. However, the extent and direction of the path appeared to be governed by other factors such as the pixel's initial location in the triangle and pixel geographical neighborhood.

It seems that the conversion from agricultural lands, especially from lowland irrigated areas to dense residential areas (e.g., Thu Duc, Q.2) leads to most regional microclimate changes (e.g., significant decrease in Mo, ET/Rn and significant increase in urban run-off).

*Table 1: Comparison of mean migration of biophysical parameters from 1993 to 2001 for 5 distinct groupings based on urban development patterns*

	Sample size	Mean $\Delta T^*$	Mean $\Delta Fr$	Mean $\Delta Mo$	Mean $\Delta ET/Rn$
1- Inner City (Phu Nhuan)	164	+0.1438	-0.0001	-0.1983	-0.0619
2- Suburban (Go Vap)	218	+0.2519	-0.2134	-0.3121	-0.1032
3- Suburban (Thu Duc)	113	+0.3213	-0.4673	-0.5217	-0.1527
4- Industrial Zones (Binh Duong)	322	+0.0942	-0.1425	-0.2025	-0.1382
5- Agricultural area	525	-0.0214	+0.2031	+0.0118	-0.0025



*Figure 5: Migration of pixels (averaged for 5 focused sub-areas) on universal triangle between 1993, 2001 and 2002*

## 5.0 CONCLUDING REMARKS

Preliminary results from this case study in Hochiminh City demonstrate the capability of satellite remote sensing not only in monitoring the surface development but also in determining useful climate and land surface parameters such as  $T_s$ , Fr, ET/Rn and Mo. Significant changes in these surface climate variables ( $\Delta T^*$ ,  $\Delta ET/Rn$ ) are found to depend on the speed of urbanization as well as the initial percentages of urban coverage and vegetation amount. Continuing works are carrying out to include more ground observations and factors such as sub-region's urbanized structure and stage of urban developments into modeling of microclimate changes. This study is a part of an on-going research at the Institute of Industrial Science, University of Tokyo focusing on using remote sensing to study urban growth in Asian cities and its impacts on regional climate. We wish to thank Prof. Carlson T. N. at the PSU (US) and Dr. Tran Thuc at the IHM (Vietnam) for providing SVAT model & meteorological observations data to use in this study. We also wish to acknowledge the Japan Science and Technology Agency for the funding of this research at the IIS, University of Tokyo, Japan.

## REFERENCES

- Carlson T.N. & Arthur S.T., 2000. *The impact of land use – land cover changes due to urbanization on surface microclimate and hydrology: a satellite perspective*. Global and Planetary Change, Vol 25, 49-65
- Gillies R.R., Carlson T.N., Cui J., Kustas W.P. & Humes K.S., 1997. *A verification of the 'triangle' method for obtaining surface soil water content and energy fluxes from remote measurements of the Normalized Difference Vegetation Index (NDVI) and surface radiant temperature*. International Journal of Remote Sensing. Vol 18(15), 3145-3165
- Owen T.W., Carlson T.N. & Gillies R.R., 1998. *An assessment of satellite remotely sensed land cover parameters in quantitatively describing the climatic effect of urbanization*. International Journal of Remote Sensing. Vol 19(9), 1663-1681
- Tran H., Yasuoka Y., 2001. *Remote Sensing to Assess Regional Climatic Effects of Urban Expansion in Northern Bangkok, Thailand*. Proceedings of the Int'l Conference on Computer in Urban Planning and Urban Management. University of Hawaii at Manoa, USA.

# **SUBSURFACE GEOTECHNICAL CHARACTERIZATION MAP OF BANGALORE CITY USING 3-D ANALYST IN GIS**

T.G. SITHARAM<sup>1</sup>, C.S. VISWANATHA<sup>2</sup>, M.S. SUDARSHAN<sup>2</sup> AND  
P.S.R. NARASIMHA RAJU<sup>2</sup>

<sup>1</sup>Indian Institute Of Science, Bangalore, India

<sup>2</sup>Torsteel Research Foundation in India, Bangalore, India  
mssudarshan60@yahoo.co.in

## **ABSTRACT**

*The geotechnical characterization of the subsurface in a city leads to understanding the ground conditions, area wise, and to obtain details of soil stratification and soil characteristics. This helps in proper planning in positioning important structures and conceiving suitable foundation systems. Further, the regions of liquefaction and areas of magnification effects in the ground due to earthquakes can be mapped. The paper describes the development of a detailed map (on a scale of 1:20000), containing 852 borehole data upto a maximum depth of 40 m (rock depth), generated in 3-dimension for Bangalore region based on Geographic Information System (GIS) model using 3-D Analyst Package. GIS model helps in data management, visualization, spatial analysis and decision support. The project aims at creation of database on the existing information about subsurface geotechnical information upto refusal or hard strata for Bangalore region. GIS model consists of soil stratification with their geotechnical properties along the depth at all the borehole locations. The final objective of this work is to develop seismic microzonation maps and liquefaction zonation maps based on the geotechnical properties in the region.*

## **1.0 INTRODUCTION**

This project was aimed at mapping geotechnical data by developing a GIS based subsurface model. This project was taken with a visionary idea, to collate the enormous isolated geotechnical data that was available with various sources and frame in one single GIS model that could be used by whole range of geotechnical fraternity.

The GIS based model helps in data management, to develop geostatistical functions, 3D visualization of subsurface with geo-processing capability and future scope for web based subsurface mapping tool.

This is envisaged not only in economizing geotechnical investigations and avoid duplication of boreholes but would also provide geotechnical engineers with various 3-dimensional views of soil strata and their properties necessary for consultancy and general prediction of soil behavior.

The project is further intended for geotechnical site response and characterization studies for development of microzonation maps.

The work involved three major tasks as described below.

- Develop a digitized map of Bangalore city with several layers of information.
- Development of GIS database for collating and synthesizing geotechnical data available with different sources and,
- Develop 3 dimensional view of soil stratum presenting various geotechnical parameters with depth in appropriate format.

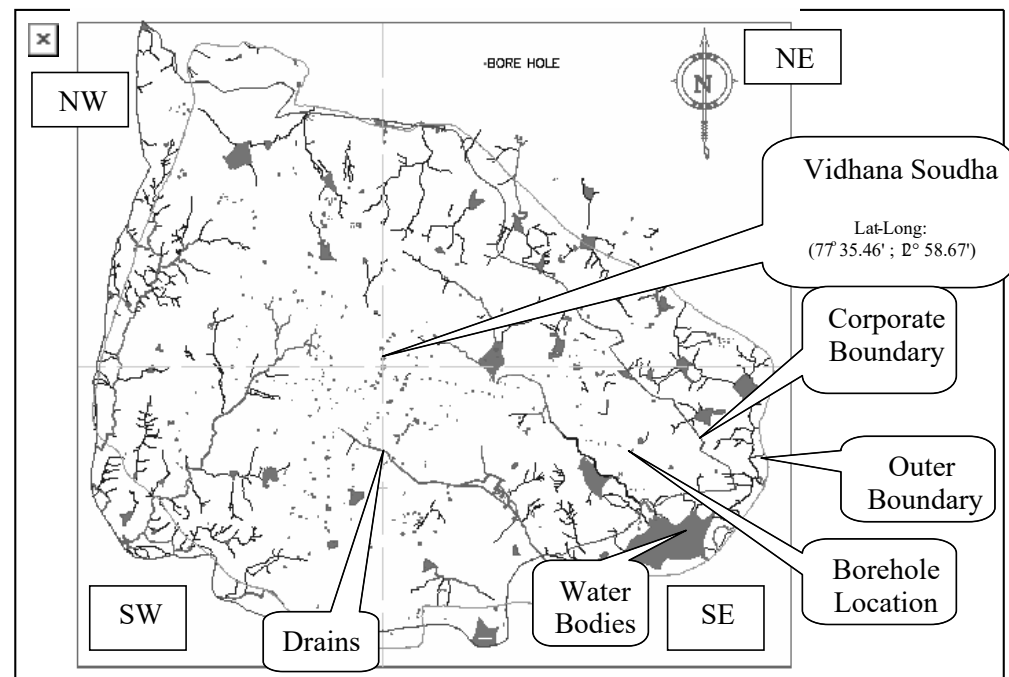
## **2.0 MAP AND 3-D SUBSURFACE MODELING**

GIS has been used in geosciences for data collection, organization and distribution of geological data and maps. The project in geosciences will have many types of data sources in which GIS is an invaluable tool for integration of many different types. Visualization is another GIS activity which is very useful in this project. This includes creating maps on screen, producing hard copy maps and delivering maps. Arc GIS 8.3 has been used here with 3D analyst extension.

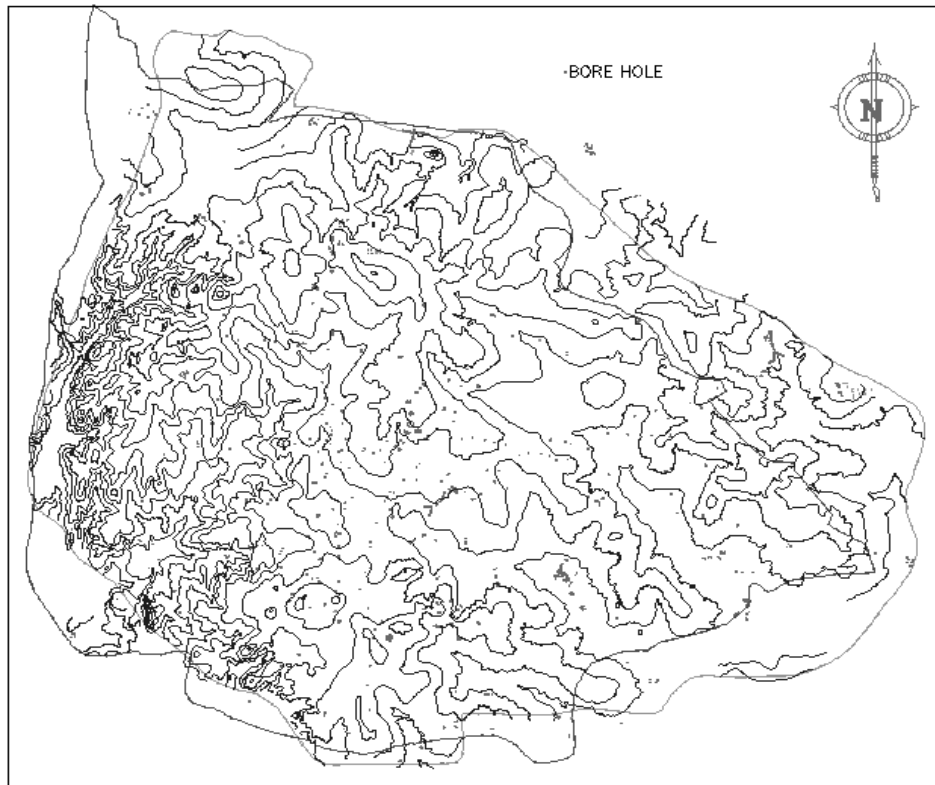
### **2.1 Digitization of map**

The Bangalore map forms the base layer for development of GIS model. The map entities were developed in view of two aspects, firstly for locating the bore logs to the utmost accuracy on a scale of 1:20000 and secondly for identification of bore logs by end user. With this scope of work the map was developed with several layers of information. Some of the important layers considered are the boundaries (Outer and Administrative), Contours, Highways, Major roads, Minor roads, Streets, Rail roads, Water bodies, Drains, Landmarks and Bore locations. Digitized map was developed mainly using hard copy of Bangalore guide map, published by Survey of India in 1983 and several other maps from standard publishers were used for reference. Digitization of the map layers was done in AutoCAD and then imported to Arc view GIS 8.1. Few combinations of layers that can be viewed in the map for various information are shown in Figures 1 & 2 below. Figure 1 depicts the location of boreholes with respect to water features like tanks, lakes and drains within the corporate boundary of Bangalore along with outer boundary circumscribing the ring road. It gives a clear view of the spatial distribution of boreholes in Bangalore region. Also this would be helpful in prediction of soil behavior and information can be derived for ground water management and planning. Figure 2 shows the location of boreholes with the elevation contours at 10m intervals. This would give information on availability of reliable geotechnical data on sloping terrains or valleys and could be used for land use planning or other planning purposes. Several other layers of information are available on the map like road (Highways, streets etc) and rail network, bridges, culverts, Landmarks and monumental structures etc, which would cater to the interest of many other engineering groups. Also the isometric

view of all boreholes can be viewed by overlapping of layers to get a 3-D projection. The 3-D modeling of boreholes is described in the section 2.3. This view gives a visual idea of the depth to which geotechnical data is available in each borehole.



*Figure1: GIS model of borehole locations with respect to water features*



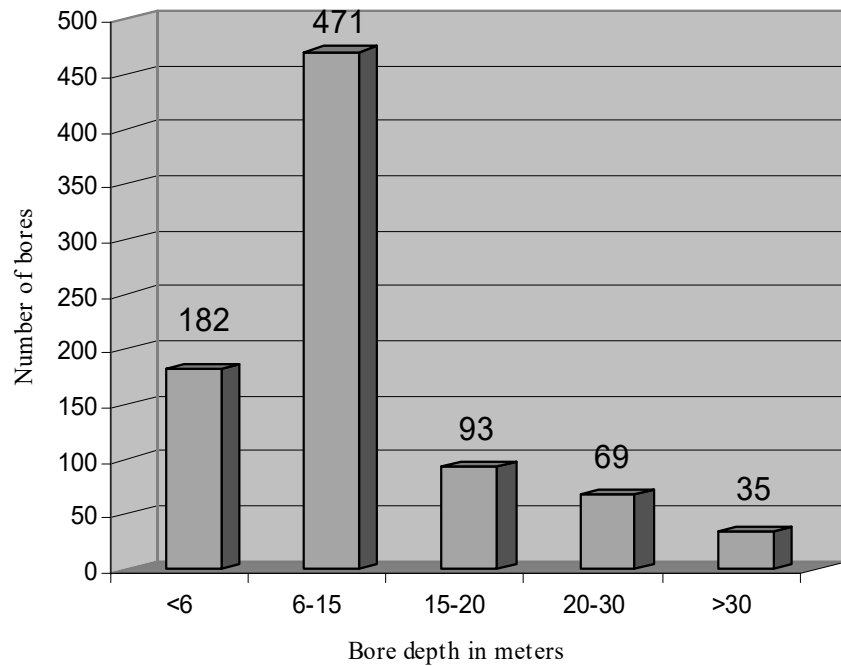
*Figure 2: GIS model of borehole locations with respect to contours*

## **2.2 Collation of geotechnical data**

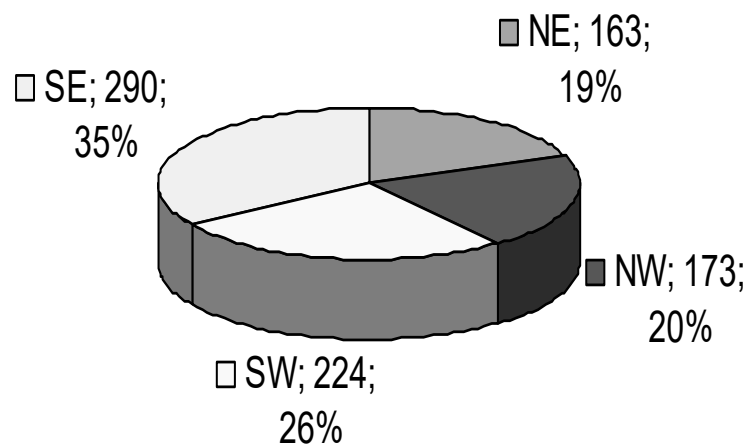
Geotechnical data was basically collated from archives of Torsteel Research Foundation in India (TRFI) and Indian Institute of Science (IISc) for geotechnical investigations carried out for several major projects in Bangalore. The data collected is of very high quality carried out by senior geotechnical engineers for important projects in Bangalore during the years 1990-2003. So far 850 bore-log information has been keyed into the database. Most of the data so far selected for the database is on average to a depth of 20m below the ground level with an interval of 0.5m. Another of about 600 borehole information is still available at different locations up to different depths (about 6-30m), which were carried out in connection with geotechnical investigations all over Bangalore. The bar chart shown in figure 3 clearly gives the distribution of the boreholes classified on the depth of bore below ground level. Majority of the bores with depths greater than 15m were carried out for several grade separator projects. Most investigations for residential and commercial complexes were below 15m. But wherever bed rock has been encountered investigation has been terminated at that depth. The properties keyed into the database at a particular depth are location details, physical properties, grain size distribution, Atterberg limits, and strength properties for soil and rock. These boreholes spatially cover most parts of the Bangalore city and more densely in the areas of high land use as shown in figures 1&2. Distribution of boreholes in four quadrants of Bangalore city considering Vidhana



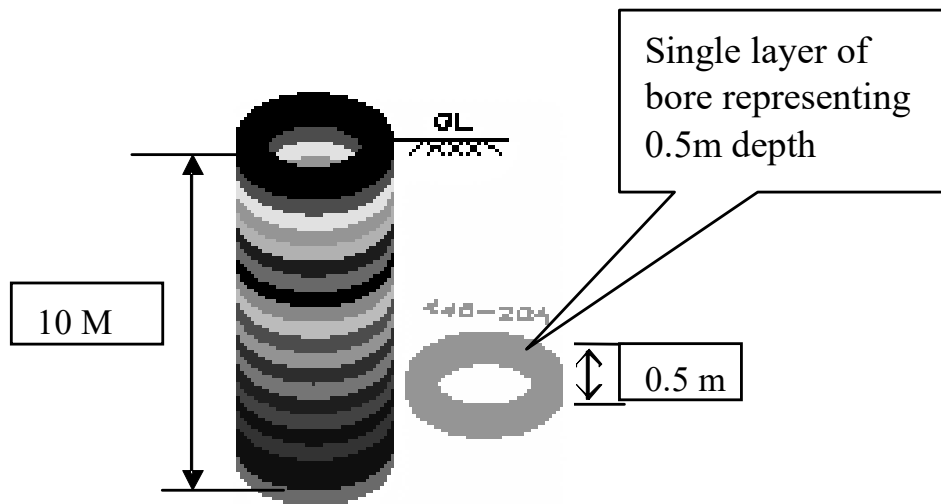
Soudha (shown in fig 1.) as the centre point is shown in figure 4. There is greater scope for geostatistical analysis of the collated data to study the subsurface features and their variation. One can use geostatistical analyst extension of Arc GIS to deal with the common situations of limited data availability in subsurface sampling and more effective decision making for site characterization.



*Figure 3: Distribution of bores based on depth*



*Figure 4: Distribution of bores in quadrants for bangalore city*



*Figure 5: A typical borehole in 3 D*

### 2.3 Subsurface 3-D model

The GIS model developed currently consists of 850 borehole locations marked on the digitized Bangalore map of 1:20000 scales. The boreholes are represented as 3 dimensional objects projecting below the map layer in 0.5m intervals. Also image files of bore logs and properties table has been attached to location in plan. These 3-D boreholes are generated with several layers with a bore location in each layer overlapping one below the other and each layer representing 0.5 m interval of the subsurface. Figure 5 shows a typical borehole viewed in isometric view. It consists of several donut elements in different layers placed coinciding one below the other. A single donut as shown on the right in figure 5 represents 0.5 m depth of ground in the model. Topmost donut represents the 0.5m depth of surface strata and thereon each donut cumulates to 0.5m below ground level.

Each borehole in this model is attached with geotechnical data along the depth. The data consists of visual soil classification, standard penetration test results, ground water level, time during which test has been carried out, other physical and engineering properties of soil. The model provides two options to view the data at each borehole in order to cater for various groups of geotechnical fraternity. In 2-D, by clicking on a borehole will display the standard bore log information as shown in figure 6 and the respective properties table consisting of index properties & shear strength parameters. Apart from this each donut of any borehole is attached with soil/rock properties at that particular depth. As such when this model is viewed in 3D geotechnical information on any borehole at any depth can be obtained by clicking at that level (donut).

### 3.0 SUMMARY AND CONCLUDING REMARKS

Digitized map of Bangalore on a scale of 1:20000 with about 12 layers of information has been prepared and presented. Geotechnical data for 850 boreholes up to a depth of about 40m has been collated and attached to the locations in the map using ARC View GIS 8.1 with 3D analyst package. Further work is under progress in locating additional borehole data, which is available for greater Bangalore region (Map development & extension work is also under progress). Once the database is fairly complete, attempts will be made to develop models of regions by contouring of various properties at various depths along with the data exploration, fitting a semivariogram model, performing diagnostics to find how well the model predicts the unknown values and comparing several models to find better predictions of the unknown.




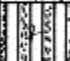
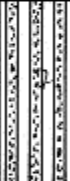
#### TORSTEEL RESEARCH FOUNDATION IN INDIA BORE LOG

Date of Commencement : 17.09.99

LOCATION : Banashankari, Bangalore.  
RL : -  
BH/FP-NO. : 1

Date of Completion : 18.09.99

GWL : -

Depth Below GL (M)	Soil Description	Thickness of Strata (M)	Legend	Details of * Sampling		Standard Penetration Test Data		
				Depth (M)	Type	Depth (M)	'N' Value	Rel. density or consistency
1	Filled up soil.	2.00		2.50	SPT UDS *			
2	Reddish/Yellowish Silty Sand with Clay.	1.00				2.0	6/10/14 N = 24	
3	Yellowish/Whitish/ Greyish Silty Sand (soft rock)	3.00				3.0	10/18/23 N = 41	
4								
5								
6	Bore Hole terminated at 6.0m				SPT	6.0	65R for 5 cm penetration.	
7								
8								
9								
10								

UDS - Undisturbed sample  
DS - Disturbed sample  
\* - Sample not Retrieved

SPT - Standard Penetration Test  
Remarks:

Figure 6: A typical display of bore log sheet

## **ACKNOWLEDGEMENTS**

Authors thank Seismology division, Department of Science and Technology, Government of India for funding the project titled “Geotechnical and site characterization of greater Bangalore region” (Ref no. DST/23(315)/SU/2002 dated October 2003). Thanks to Mr. G.U Mahesh and K.Shamanth, Project Associate who were very help full in preparation of the paper.

## **REFERENCES**

ARC View GIS 8.1, Manuals and Handouts.  
Torsteel Research Foundation in India, Geotechnical Investigation Reports  
(1988-2003).  
Indian Institute of Science, Geotechnical Investigation Reports.  
Survey of India, Bangalore guide map, 1983.  
Eicher Good Earth, Bangalore map, 2002.  
ESRI publishing, Subsurface Modeling with GIS.

# **REGISTRATION OF LASER SCANNER POINT CLOUDS FOR A LARGE AND COMPLEX BUILDING**

EKTA AMAR AND BHARAT LOHANI  
Indian Institute of Technology Kanpur, Kanpur, India  
*blohani@iitk.ac.in*

## **ABSTRACT**

*Terrestrial Laser scanners (TLS) can measure 3-D co-ordinates of large number of points in a short span of time. Scanning a large building requires scanning from more than one position. Thus, registration of point clouds acquired from different positions is important and essential for preparing a complete 3D model of a building. This paper deals with the registration of the different point cloud scans considering the common overlapping areas in between successive scans. The detail procedure is discussed and also the problem faced while registering is outlined.*

## **1.0 INTRODUCTION**

The new technique of laser scanning for obtaining 3D information of any object has revolutionized the surveying world. This technique is popularly known as terrestrial laser scanning (TLS). Notwithstanding its recent emergence, the TLS is becoming an industry standard technique for 3D data capture. The main advantage of this technique is the availability of geometric information of thousands of points on an object in a short span of time. TLS, as a new method of surveying, may replace the use of conventional surveying data collection techniques by faster and more complete data collection (Boehler et al., 2003). Colombo and Marana (2002) called these systems as natural successors to motorized total stations. It has become an additional technique for geodetic applications (Schulz and Ingensand, 2004). Some of its application areas are creation of 3D digital models, 3D imaging of buildings and structures, measurement tasks, particularly for engineering projects and cultural heritage recording. Laser scanner has also been used in topographic mapping of quarries, mines and tunnels, scene acquisition for virtual reality modeling application and for dimensional measurements of interiors as well as for complex shapes of architecture. Dense data sets and high sampling frequency obtained from TLS also make it suitable for structural monitoring such as structural deformation for risk assessment, change detection and structural model validation. Apart from these many new applications are being targeted. Scanning a building is among the most common and useful application of this technique.

Invariably, in case of a large building several scans are required to capture the geometry of building. The individual scans of a building are referenced onto the coordinate system of the scanner, which varies for each

scan. Integration of different scans is important to generate a complete 3D model, as is required in problem solving. Integration of data points resulting from different scans is carried out through the process of registration, which attempts to bring all data points onto a common reference system. This reference system could be an arbitrary one or the reference system of one of the scans. This paper discusses the significance of 3D models of buildings, scanning procedure using TLS and method of registration adopted. The commercially available CAD software Imageware Surfacar V10.0 has been used for registration purpose in this paper. Finally the error of registration and other relevant points are discussed.

## **2.0 AIM OF THE PAPER**

The aim of this paper is to perform registration of scans taken from different positions which are obtained using the TLS. The different position point cloud scans are required to be stitched together, i.e. registration of scans, so that all scans can be referred onto a single co-ordinate system and can further be used for construction of 3D model. The procedure adopted during registration is discussed in this paper.

## **3.0 SIGNIFICANCE OF 3D BUILDING MODEL**

The TLS can be used for capturing geometry of any structure specially historical and archeological buildings. For many ancient buildings, the building is the only evidence about its existence and history. There are many structures of archeological importance which are on the verge of destruction. 3D scanning can help in archiving their structural details which may be useful for virtual tourism, research and reconstruction in case of damage to the structure.

3D modeling is further equally important for capturing geometry of modern structures. TLS can be used to generate drawings of buildings and other infrastructure on as-it-is basis. Fast data acquisition also helps in assessing the damages to structures, or distribution of debris in case of damage to structure after a disaster.

Thus, for conservation of old historical buildings, archaeological research, reconstruction and visualization of new structures the 3D model can play a significant role. Prior to TLS technique the conventional methods were used for making 3D model. These are discussed in the next section.

## **4.0 CONVENTIONAL METHODS**

The conventional methods used in the past to capture 3D model were theodolite angle intersection, metric photogrammetry, non-metric photogrammetry or close range photogrammetry. The process of creating 3D models from real scenes has some well-known steps viz. data collection, data registration, and modeling (geometry, texture, and lighting). Conventionally, land surveying and terrestrial photography were used for data collection. Land surveying though accurate, fails to capture a dense

point cloud thus missing the fine details of structures. Also, it is cumbersome and error prone. The surveying measurements are imported into CAD software for generating 3D model. In image based methods, photogrammetric bundle adjustment is used for data registration and software like Photo Modeler are employed for preparing the 3D models. Despite the data capture being fast, conversion of photographs into a 3d model is not fully automatic and requires highly skilled human resource and huge processing time.

Invention of TLS technique has eliminated several of limitations of conventional methods and should be ideally suited for capturing accurate and dense 3D data at high speed.

## **5.0 STATE OF ART ON REGISTRATION**

Registration of point clouds from different scans is solved using the classic problem of coordinate transformation. Fundamental to this is computation of transformation parameters i.e. scale, translation, and rotation between two coordinate systems. This is realized by identification of homologous points, e.g. corners in adjacent and overlapping scans or at least three scan ‘targets’ within each scan data. Collection of tie points and search for the homologous points in adjacent scans can be performed automatically using reflecting targets (Bornaz et al., 2002). Since the engineering objects are usually composed of poor reflective materials (clay, soil, stones) reflecting targets are the best option. Researchers have attempted various techniques for registration of scanner point cloud. Besl and McKay (1992) developed one of the most popular methods known as iterative closest point (ICP) algorithm which is accurate and computationally efficient registration of 3-D shapes including free-form curves and surfaces. This method is based on finding the closest point on a geometric entity to a given point. The iterative closest compatible point (ICCP) algorithm has been proposed in order to reduce the search space of the ICP algorithm (Akca, 2003). Roth (1999) proposed a method that exploits the intensity information supplied by the laser scanner. In (Dijkman and van den Heuvel, 2002) a registration method based on parametric model fitting (cylinder and plane) is presented. Akca (2003) presented a full automatic point cloud registration method. He used definite template shape special targets in registration process to transform local point cloud into ground coordinate system. Algorithm is based on cross-correlation matching method on intensity image. For achieving better registration results, Balzani et al. (2002) used laser scanner along with a GPS. The GPS determines the 3D coordinates of the homologous points to georeference scans automatically even if scans are carried out at different times and do not have large overlaps.

The literature reveals that the methods which make use of external targets or GPS measurements on object surface yield better result and can be automatic. However, considering field conditions it is always not possible and also not desirable to place targets on a structure. Further, measurement of control point locations on the structure is also time consuming. In view of

this it is desired to study a method which makes use of overlap area in point cloud for registration. The same is aim of this paper.

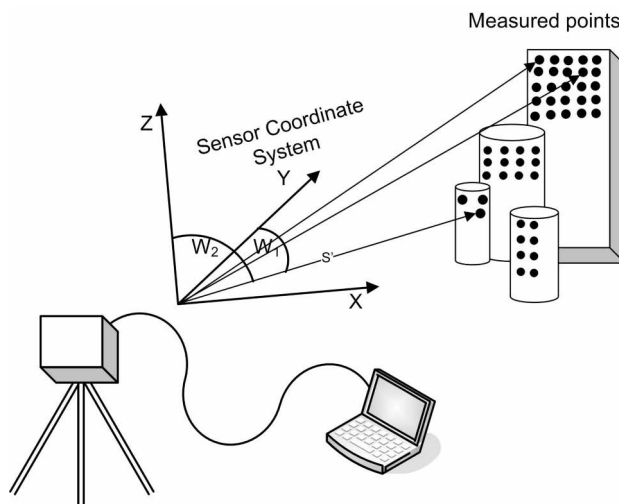


*Figure 1: SIDBI Building, IIT Kanpur*

## 6.0 STUDY SITE AND DATA ACQUISITION

The Sidbi building at IIT Kanpur was chosen for study in view of its typical shape as shown in Figure 1. The building was scanned on May 20<sup>th</sup>, 2003 using Cyrax 2500 TLS. Cyrax is a portable, 3D laser scanning system that captures, visualizes and models complex structures and sites with an unprecedented combination of completeness, speed, accuracy, and safety.

Cyrax 2500 scans the building using time of flight principle. The laser pulse fired from Cyrax is reflected by the object and by measuring the time of flight of laser pulse the laser vector from Cyrax to target point is determined as shown in Figure 2. Combining this vector with the co-ordinates of origin (within Cyrax) results in coordinate of targeted point.



*Figure 2: Mechanism of TLS measurement*



The scanning mechanism of instrument ensures measurement of thousands of points on the surface of object (Figure 2). The specifications of scanner are listed in the Table 1. Since it is not possible to have complete 3D representation from data acquired at a single viewpoint, the scans were carried out from five different positions around the building. The scanning stations were selected such that a part of the building should be present in the overlap area of successive scans. No external targets were used during scanning. Each scan has its own local coordinate system with its origin at the instrument.

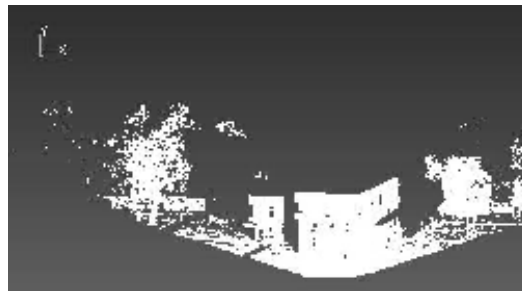
*Table 1: Specification of Cyrax2500*

S.No	Product Quality	Product performance
1	Laser Wavelength (in nm)	532
2	Laser Classification (Class)	2
3	Beam diameter at specified Distance ( $Ymm$ at $Xm$ )	< 6mm from 0 – 50
4	Average Data acquisition Rate ( $pps$ )	1,000
5	Distance Accuracy at Specified Distance ( $Ymm$ at $Xm$ )	$\pm 4mm$ at 50m
6	Position Accuracy at Specified Distance ( $Ymm$ at $Xm$ )	$\pm 4mm$ at 50m
7	Angular accuracy	$\pm 60micro$ – radians
8	Distance Range	1.5m – 100m
9	Field of view ( $H \times V$ )	$40 \times 40$ degrees

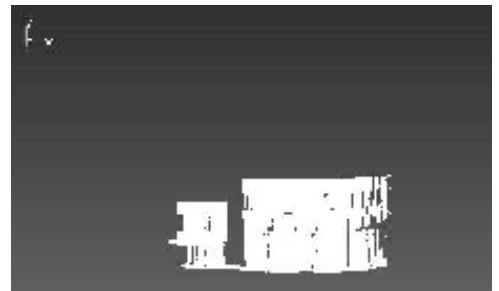
## 7.0 REGISTRATION METHODOLOGY

### 7.1 Data cleaning

Scanning with TLS results in dense data points, which contain unwanted details also. Unwanted details are those which are not related to building. Around each scan there are many objects such as lamp posts, trees and grass which not only increase the size of the file thus creating problem in loading and unloading, but also make moving and visualization of point cloud difficult. Therefore as a first step unwanted point cloud were removed from the scan (Figure 3(a) and 3(b)).



*(a) Total scan taken by TLS*



*(b) Desired portion of point cloud after cutting unwanted details*

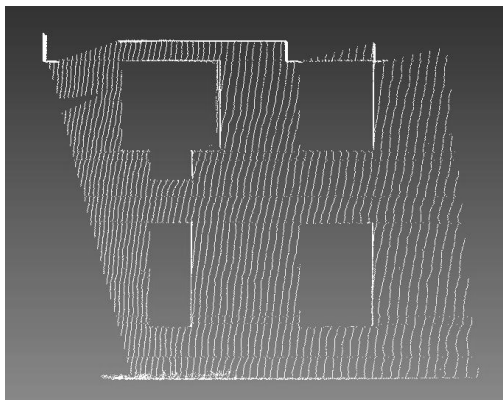
*Figure 3: Cleaning of scans*

The unwanted point cloud is cut using a function “circle-select points” in Imageware Surfacar Software V10.0 and selection mode was chosen as “Points outside (delete inner)”. A selection boundary is created on portion of point cloud and all the points which fall inside this closed boundary are deleted and a new point cloud is generated in which only relevant points are retained which lie outside the boundary. The closed boundary needs to be made carefully so that only unwanted points are removed. This procedure is repeated till all the unwanted portions from all the scans are removed.

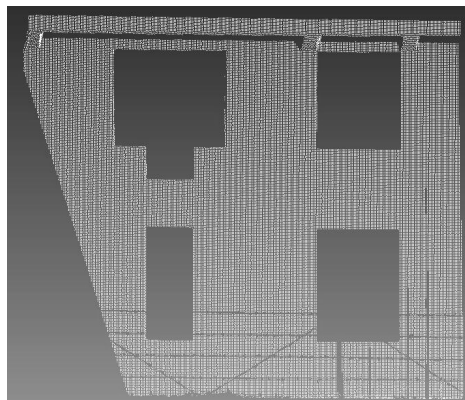
## 7.2 Registration

Since during the scan no external targets were placed on the building, the overlapping area between two scans was considered for registration. Some prominent features in overlapping area were earmarked for registration. Direct registration function of Imageware Surfacar V10.0 is used for registration of five different scans of building. This function aligns a point cloud with a geometric entity in the world coordinate system. Parameters required for the operation are:

- **Mobile Entities:** It is that entity which is to be moved to be registered with the source cloud. It can be picked in the view port, or can also be chosen by selecting its name in the dialog box.
- **Source Entity:** It is the part of mobile entity point cloud and it tries to align itself with the destination entity (Figure 4(a)).
- **Destination Entity:** It is the part of that cloud with respect to which source point cloud tries to align (Figure 4(b)). To register scan 4 to coordinate system of scan 5. Mobile entity is full point cloud scan 4, source entity and destination entity is chosen as a part from scan 4 and 5 respectively (as shown in Figure 4). For getting accurate results, the source cloud entity has to be a subset of the destination entity. The outliers in the entities are deleted before using the function.



(a) Source entity of scan number 4



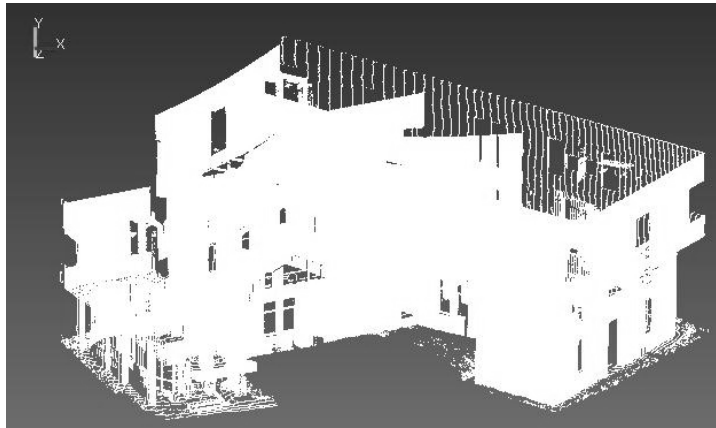
(b) Destination entity of scan number 5

Figure 4: Parameters for direct registration

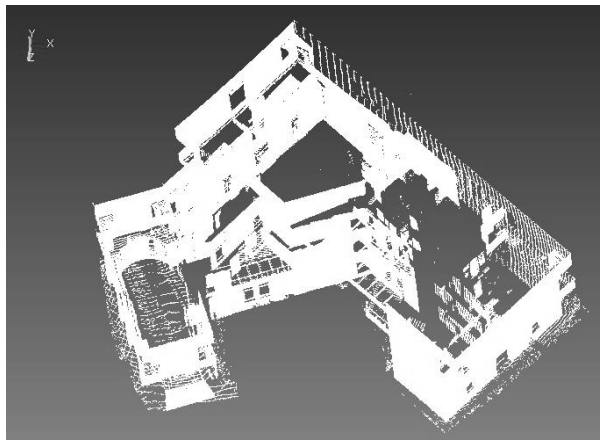
- Tolerance: The tolerance for acceptable registration error is entered as 0.001.
- Registration Option: There are two registration options: Refinement or best possible. Best possible registration option is selected.
- Registration Mode: There are four types of registration modes: No Constraint, Constraint X, Constraint Y, or Constraint Z. No constraint mode is selected. The source point cloud can be rotated and translated in all degrees of freedom.

After inputting all these parameters in direct registration function, the selected source point cloud is rotated and translated so that the mean square distance between the cloud and the destination geometric entity is minimized and is within the specified tolerance, if possible. The registration system works on the assumption that each point in the source cloud has a corresponding point on the destination entity.

All scans were registered with respect to the coordinate system of scan 1. This was realized by registering scan 2 with the scan 1. Then point clouds of scan 1 and 2 are merged into a single registered point cloud using a function “merge point cloud”. The scan 3 is registered with already merged scan 1-2. This results in single point cloud of scans 1-2-3. Separately, scan 4 and scan 5 are registered and merged into a single point cloud. The point cloud 4-5 is then registered with the point cloud 1-2-3 using overlaps between scan 5 and scan 1. This was done to curtail accumulation of registration errors and also the overlap between 3 and 4 was insignificant. Finally all point clouds are merged into one single point cloud with all the scans registered on the co-ordinate system of scan 1. Figure 5 shows the registered point cloud scans.



(a) All scans registered



(b) All scans registered (top view)

Figure 5: Registered point clouds of SIDBI building

### 7.3 Accuracy in registration

Registration was carried out very carefully considering every minute detail in selecting the mobile and destination entity. Also, the spurious points, e.g. unwanted details and outliers were removed prior to registration. The Root Mean Square (RMS) value reported during the registration by software, i.e. the accuracy with which the source entity of one scan translate, rotate and align itself with the destination entity of another scan, are shown in Table 2.

Table 2: RMS error during registration

S.No.	Scan number	Registered RMS error in cm
1	Scan 1 and 2	0.149
2	Registered scan 1-2 and 3	0.192
3	Scan 4 and 5	0.202
4	Registered scan 1-2-3 and registered scan 5-4	0.197

It is important to note that the RMS error as computed by software is the accuracy with which the source point cloud entity gets itself aligned with the destination point cloud entity during the direct registration process. It is not the accuracy of full registration of one point cloud with another point cloud. This RMS error is therefore misleading. This is evident when two full point clouds of scan 1 and scan 2 are visualized after aligning; the edges of balcony and walls are seen at a distance of an average 25.04 cm apart in two scans. Similarly, an average error of 19.00 cm is observed in scan 4 and scan 5. The basis of this latter accuracy determination is measuring distance between two points which represent the same object on the building but belong to two different scans. The average difference in their position is reported by its arithmetic mean for 10-15 points. Selecting the same point in two registered scans is not an easy task unless they appear distinctly separate and are identifiable. Therefore, a better method for determination of accuracy could be by comparing scans with total station measurement of building.

## **8.0 DISCUSSIONS**

With TLS the amount of data obtained is huge. There are more than a lakhs points in each scan, including several redundant data points, which can be used efficiently to make 3D model. The scanner scans everything that comes within its field of view (FOV), including the unwanted details. The unwanted data points cause problem in handling the data files. Since no targets are desirable to be placed while scanning the building, a proper consideration should be given to the overlapping portion between two scans. Improper selection of scan stations results in problem in choosing source entity and destination entity required for registration. Yet another problem is of no data points in some parts of building due to shadows of trees, lamp post and other projected corners of the building. It is unavoidable to get rid of these obstructions. Moreover scanning stations should be chosen in such a way to avoid maximum of these obstructions, which will help in reducing the problem of shadowing.

## **9.0 CONCLUSION AND RECOMMENDATIONS**

For any large and complex building scanning has to be carried out from different viewpoints to get a complete view of the building. In this paper, registration of these different position scans is carried out considering the overlapping regions in between the different scans. Based on the experience of registering the scan it can be concluded that just scanning the building does not solve the problem. The unwanted details and problem of the shadow can be solved by following a proper strategy before scanning. It is recommended to scan in such a way that the effect of projected area on scanning will be least. It would be better to carry out a detail reconnaissance of the area. As the use of targets is not always feasible and desirable during scanning, it is better to have a good overlap between successive scans. Only five scans of a large building, as in the present case, are not sufficient.

Hence, to reduce the time and energy during post processing of data, it is essential to scan following a proper strategy. Else, the time saved during data acquisition will be annihilated in post processing and the desired benefit of time efficiency of this new technique will be no longer be evident.

## ACKNOWLEDGMENT

Elcome Technologies Pvt. Ltd. provided the Cyrax 2500 instrument for scanning and helped in scanning the site. Registration of point clouds was done in CAD laboratory, IIT Kanpur and Mr. Surya Prakash, project associate in CAD lab; IIT Kanpur provided support during learning and registering the scans in Imagerware Surfacar V10.0 software.

## REFERENCES

- Akca, D., September 2003. Full *automatic registration of laser scanner point clouds*. Optical 3-D Measurement Techniques VI, Zurich, 1, 330–337.
- Balzani, M., Pellegrinelli, A., N. Perfetti, P. R., Uccelli, F., Tralli, S., September 2002. *Cyrax tm 2500 laser scanner and g.p.s. operational flexibility: From detailed close range surveying, to urban scale surveying*. ISPRS Commission V, Symposium 2002.
- Besl, P. J., McKay, N. D., February 1992. *A method of registration of 3d shapes*. IEEE Transaction on Pattern Analysis and Machine Intelligence 14 (2), 239–256.
- Boehler, W., Vicent, M. B., Marbs, A., 2003. *Investigating laser scanner accuracy*. XIXth CIPA Symposium.
- Bornaz, L., Lingua, A., Rinaudo, F., September 2002. *Engineering and environmental applications of laser scanner techniques*. ISPRS Commission III, Symposium 2002.
- Colombo, L., Marana, B., May 2002. *3d building models using laser scanning*. GIM International 16 (5), 32–35.
- Dijkman, S., van den Heuvel, F., 2002. *Semi automatic registration of laser scanner data*. IAPRS XXXIV (5).
- Roth, G., 1999. *Registration two Overlapping Range Images* Proc. of second int. conference on 3d digital imaging and modeling, ottawa..
- Schulz, T., Ingensand, H., May 2004. *Terrestrial laser scanning-investigations and applications for high precision scanning*. FIG Working Week 2004.

# **EXTRACTION AND 3D VISUALIZATION OF TREES IN URBAN ENVIRONMENT**

YOSHIFUMI YASUOKA, YOSUKE YAMAGISHI, TAO GUO  
AND TAKAHIRO ENDO

Institute of Industrial Science, University of Tokyo, Japan  
yyasuoka@iis.u-tokyo.ac.jp

## **ABSTRACT**

*Digital city models are required for many applications such as urban microclimate simulation, traffic navigation and landscape planning. The existing 3D digital city models, however, mostly target only on modeling buildings although vegetation plays an important role in the urban environment. This research investigates the 3D digital city model with both of building and trees by extracting individual trees from high resolution IKONOS imagery together with Airborne Laser Scanner (ALS) data and by coupling them with a tree growth model to simulate the growth of trees. Finally, the simulated trees are integrated with the buildings modeled also from IKONOS imagery and ALS data to represent a more realistic 3D urban environment.*

## **1.0 INTRODUCTION**

Urban structure is one of the most essential factors which define the characteristics of urban safety and environment. Land use patterns or distribution of buildings and vegetations are infrastructural information to assess, simulate and predict urban environment and disasters. In particular, three-dimensional information on the distribution of buildings and vegetations, 3D model, plays a key role in microclimate simulation, traffic navigation or landscape planning. It is, however, not easy to model 3D structures in urban area since they are very much complicated. This study investigates the 3D modeling of urban structures with new remote sensing technologies including high spatial resolution observation from satellite and height observation from airborne laser scanner.

There have been several approaches to extract 3D information from remotely sensed data. Aerial photographs were conventionally used in urban 3D modeling. However, it usually needs a lot of human power and processing time. Due to rapid improvement of spatial resolution satellite images have been recently used to produce urban 3D models. For example, Haala and Brenner (1999) integrated multi-spectral imagery and laser altimeter data for the extraction of buildings, trees and grass-covered areas, and for the reconstruction of buildings using laser data and 2D ground plan information. Also Guo and Yasuoka. (2002) combined IKONOS imagery and Airborne Laser Scanner (ALS) data to extract urban 3D information.

The existing 3D city models using remote sensing data, however, mostly focus on modeling of buildings. Although vegetation plays an

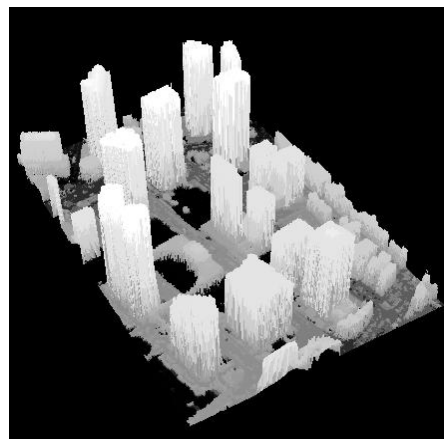
important role in urban environment as well as buildings it has not been modeled properly since vegetation structure is complicated to extract from satellite data and not easy to model. This research develops a method to extract and model 3D structures of trees as well as buildings from remotely sensed data. First trees were extracted from high spatial resolution satellite (IKONOS) image and Airborne Laser Scanning (ALS) data, and then trees in urban environment were modeled in 3D format by integrating the tree data derived from remote sensing data and 3D tree growth model. Finally the modeled trees were integrated with buildings also extracted from IKONOS image and ALS data. The proposed method was applied to Tokyo urban area, and the realistic landscape was demonstrated.

## 2.0 DATA DESCRIPTION AND TEST SITE

Shinjuku area in Tokyo was selected as a test site since the area has very complicated urban structures and it was composed of many different types of buildings and trees. For the test site IKONOS data was used for detail land cover classification including buildings, trees and bare ground, and also ALS data was used for land surface modeling. Table 1 summarizes the data set used in this research. Figure 1 and Figure 2 show IKONOS image and Digital Surface Model (DSM) derived from the ALS data.

*Table 1: Data set*

	IKONOS	ALS
Date	2001.11.4	2000.2.23
Spatial resolution	multispectral:4m/pixel panchromatic:1m/pixel	Around 10cm
Accuracy	—	$\pm 15\text{cm}$ (vertical direction)



*Figure 1: IKONOS panchromatic image    Figure 2: DSM derived from ALS*

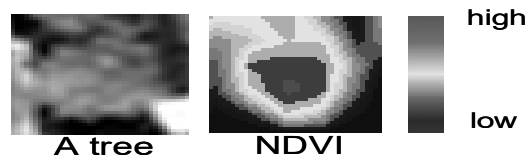


### 3.0 METHODOLOGY

First, Normalized Differential Vegetation Index (NDVI) was calculated from IKONOS image, and the pixel that had large NDVI value was extracted as tree areas. Next, the tree position was detected, and the tree size (age) was evaluated by the detected canopy size. Finally 3D tree model in urban environment was developed using 3D tree growth model. In this research the tree detection scheme assumed the following conditions for the tree structures:

- The tree position is the center of the tree image from the top view.
- NDVI value increases as approaching to the center of a tree.
- Canopy of a tree may be approximated by a circle.

An example of a tree in IKONOS image and the corresponding NDVI is illustrated in Fig. 3.



*Figure 3: the condition of NDVI in a tree*

#### 3.1 Detection of tree positions

A schematic flow for the detection of tree position is shown in Figure 4 and an example of tree position detection is illustrated in Fig. 5. First, NDVI was calculated from IKONOS image to separate vegetation areas and non-vegetation areas. The area of high NDVI value is extracted as vegetation area. Then the ALS data was mask for the vegetation area (high NDVI area) and trees were extracted for high ALS value. That is, the tree is defined as the area of high NDVI and high ALS value area (Figure 5-b).

The position of each tree was detected for the extracted tree area. First, a skeleton of the extracted tree area was calculated based on the assumption that the tree position is the center of the image from the top view. Figure 5-c was obtained by skeletonizing the image in Figure 5-b. Each pixel on the skeleton line was given NDVI value, and Local Maximum Filter (Wulder, et. al., 2000) was applied to the NDVI skeleton image to detect the canopy top (Figure 5-d).

#### 3.2 3D Modeling of trees

Figure 6 shows a flow of modeling of trees in 3D. First, 3D tree model was generated using natFX and 3D modeling software. NatFX was a 3D tree growth model developed based on AMAP (Atelier of Modeling of Architecture of Plants). It can model a lot of types of plants, including

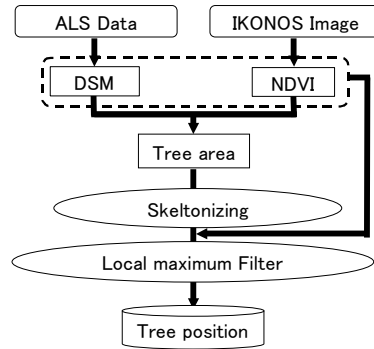
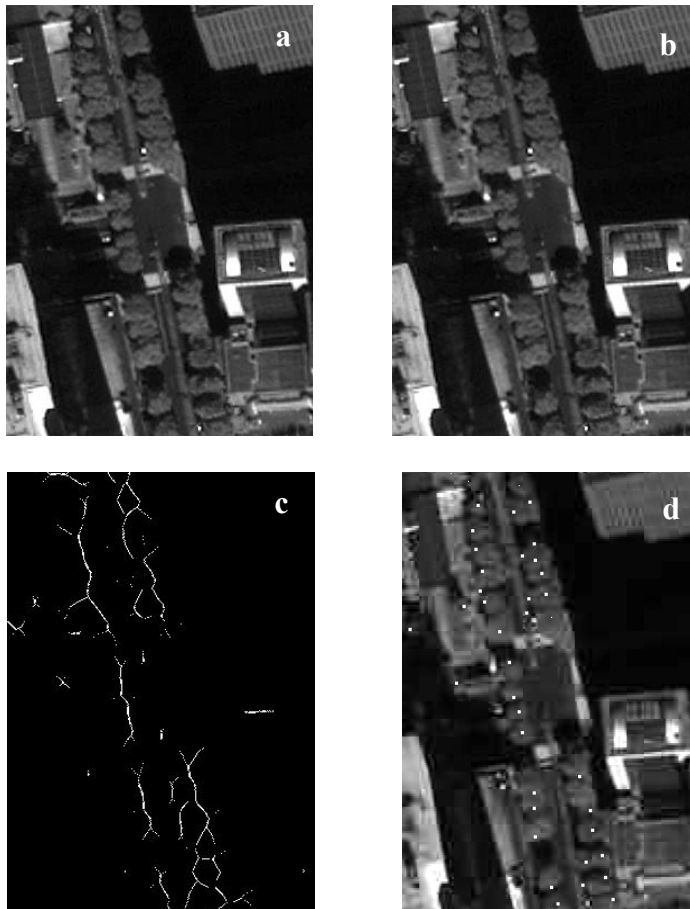


Figure 4: Flow of the detecting tree positions



a: IKONOS panchromatic image      b: the extracted tree area  
c: the skeleton line of the tree area      d: the detected tree positions  
(white points)

Figure 5: The result of tree position detection

flowers, bushes and trees and can generate 3D models of a given plant at different ages and at different seasons (Figure 7). In this model, the tree age was necessary to generate 3D tree model. In this research tree age was estimated from the canopy size of the detected trees.

First, template matching was operated to estimate the diameter of the canopy of the detected tree on the basis of assumption 3. The diameter of

the circle that was best matched to the canopy was defined as a canopy diameter of the tree.

The tree growth was simulated to estimate the age of tree from the diameter of canopy. Figure 8 shows the relation between the diameter of the canopy and the age. The age of tree was estimated from the canopy diameter of the tree.

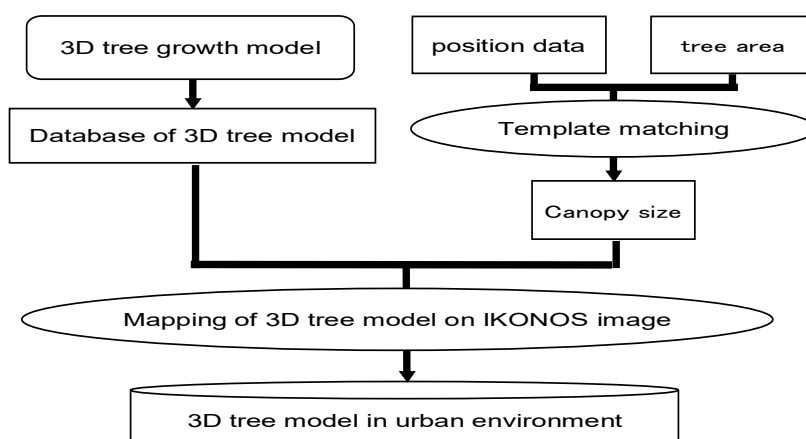


Figure 6: Flow of 3D modeling of trees

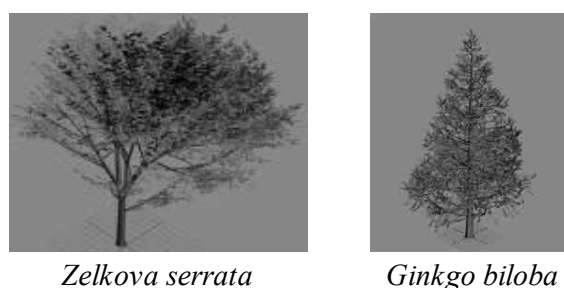


Figure 7: 3D tree model

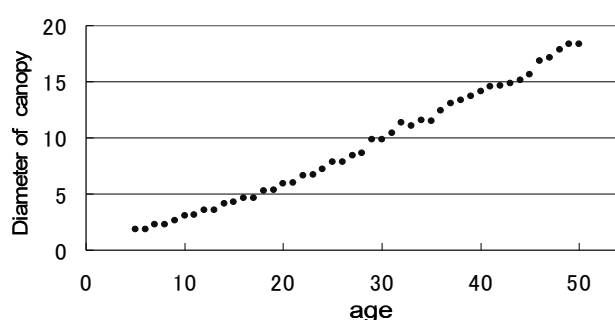


Figure 8: The relation between diameter of canopy and age (zelkova serrata)

Finally 3D tree model for the estimated age was mapped at the detected position in the IKONOS image. The data of tree species were got from the field survey and the ledger of greening roads, which is made by Tokyo Metropolitan Bureau of Construction.

### 3.3 Integration of tree model with 3D building model

3D building model was produced from the same data set following the algorithms developed by Tao, et.al. (2002). The framework of the approach contains the following steps: (1) segmentation of raised objects from ground to generate normalized digital surface model, (2) ortho-rectify images and derive edge etc. clues, (3) building blob detection by multiple height bins, and (4) building contour detection using balloon model. This scheme enables to estimate the building structures with high accuracy, and the estimation error of the 3D buildings was below 1m in average. Figure 10 illustrates an example of the 3D city model integrating building and trees.



*Figure 10: 3D city model including buildings and trees*

### 4.0 CONCLUSION

A method for 3D digital city modeling was developed with remotely sensed data. 3D digital city is one of the key elements to assess and predict environment and disasters. This research may provide an efficient tool to produce more realistic model with buildings and trees.

### REFERENCES

- Haala, N and Brenner C., 1999. *Extraction of building and trees in urban environments*. ISPRS Journal of Photography & Remote Sensing, 54, 130-137.
- Wulder, M., Niemann, K.O and Goodenough D.G, 2000. *Local Maximum Filtering for the Extraction of Tree Locations and Basal Area from High Spatial Resolution Imagery*. Remote sensing of Environment, 73:103-114.
- Tao, G. and Yasuoka Y. 2002. *Data fusion of high-resolution satellite images and airborne laser scanning data for building detection in urban environment*. Proc. of SPIE Conference on Image Processing and Pattern Recognition in Remote Sensing, Vol. 4898, 120-130.

# **GROUND CONTROL FOR THE GEOMETRIC CORRECTION OF REMOTELY SENSED IMAGERY: REQUIREMENTS AND ISSUES IN INDIA**

S. K. KATIYAR<sup>1</sup>, ONKAR DIKSHIT<sup>2</sup> AND KRISHNA KUMAR<sup>3</sup>

<sup>1</sup>Civil Engineering Department, M.A.N.I.T., Bhopal

<sup>2</sup>Civil Engineering Department, I. I. T. Kanpur, Kanpur

<sup>3</sup>M.N.N.I.T., Allahabad

skatiyar7@rediffmail.com

## **ABSTRACT**

*Conventionally ground control (GCPs) are derived from maps, but in the developing countries most of the existing maps are out of date due to large population growth, rapid changes in urban areas and economic development. Global Positioning System (GPS) has emerged as a very powerful tool for the acquisition of GCPs with the desired accuracy. In India full potential of GPS technology could not be utilized by the civilian users for the mapping requirements in Indian datum, due to restriction policies of the Government of India. This research paper presents investigations on the geometric correction accuracy of IRS-1C/D LISS-III and PAN sensor imagery using 1:50,000 and 1:25,000 scale SOI map derived and GPS derived GCP coordinates. Limitations of map derived GCPs and problems in the transformation of GPS coordinates into Indian datum are also investigated.*

## **1.0 INTRODUCTION**

Satellite images are vital tool in various applications like land use and land cover mapping, Geographic Information System (GIS) etc. Remotely sensed images are often considered as maps of the radiometric properties of the earth's surface. However, these are not usually map-like. A variety of factors involved in the process of image acquisition, introduce geometric distortions, which are removed by the process of geometric correction. As technology progresses, the raster picture element (pixel) resolution of digitally acquired remotely sensed imagery continue to become finer in spatial resolution. This dictates the need of ground control points (GCPs) with increased spatial accuracy to geometrically correct remotely sensed data from high resolution satellites like SPOT, IRS-1C/D, RESOURCESAT (IRS-P6) and IKONOS.

The current status of world mapping leaves much to be desired; especially developing countries where most of the existing maps and medium scale maps are out of date. Because of large population growth, rapid change in urban areas and economic development, the topographic maps become rapidly out of date. The data capture using conventional methods (Surveying and Photogrammetry) for topographic mapping and

map updating at small and medium scale takes a long time to complete the tasks involved. The most significant development of the twentieth century for navigators was the development of the Global Positioning System (GPS). GPS has revolutionized positioning concepts on land, at sea, in the air and in space. It has got wide range navigational, geodetic, geophysical, military, marine and social applications. GPS can provide an alternative to the ground control survey methods for the poorly mapped areas, which could not be mapped using conventional methods. Differential mode of GPS (DGPS) has capability of providing very precise coordinates of any point up to centimeter level accuracy.

A major concern in the use of GPS data for various applications is the integration of GPS coordinates with the local datum map coordinates, if the center of Earth spheroid model used for the map preparation has considerable offset from the center of the GPS Earth spheroid model (WGS-84). Because of this coordinates measured on two different ellipsoids will not be same for any position. For various practical applications like map updating and comparison with the existing maps, GPS coordinates are required to be transformed into local datum. In particular, in cadastral and engineering surveys, such transformations are normally the norm rather than the exception.

## **2.0 GCP ACQUISITION SOURCES IN INDIA**

In India the conventional sources of GCPs are Survey of India (SOI) maps. The SOI maps are available to civilian users on two different scales 1:50,000 and 1:25,000. The 1:25,000 scale maps have only about 20% coverage. Thus, 1:50,000 scale maps appear to be ideally suited for deriving GCP coordinates as these are available for the whole country. Also, 1:50,000 scale is the primary surveying scale from which the 1:25,000 scale maps have been compiled (Shiva Kumar, 1998). These SOI maps are based on old-field survey and having coordinates in Indian datum. The new series of maps having coordinate grids in Indian as well as WGS-84 datum has been also announced by SOI. GPS could provide GCPs with the desired accuracy. After the termination of selective availability of GPS signals, even a hand-held GPS could provide sub pixel level accuracy for the geometric correction of Indian Remote Sensing satellite (IRS) images (Katiyar *et al.*, 2002; Katiyar *et al.*, 2003).

## **3.0 ISSUES RELATED TO THE SOI TOPOGRAPHIC MAPS AND INDIAN DATUM**

The SOI maps prepared in Indian Geodetic Datum are based on Everest spheroid which is a local geodetic datum and best fits to certain extent the Indian subcontinent. It is not a geocentric ellipsoid and its origin is far away from the geocentre i.e. center of gravity of the Earth (Agrawal, 1997). The geodetic coordinates based on Everest spheroid differ considerably as compared to WGS-84 and other international ellipsoids. In India, the topographic maps available to a general user are in local geodetic

datum and GPS coordinates of a point observed in WGS-84 datum will differ considerably from the corresponding map coordinates. The main problem with the use of GPS data is that the transformation parameters between WGS-84 and Indian datum which are not available to the civilian users. Recently SOI has announced that the new series of SOI maps will also have WGS-84 coordinates along with the Indian datum coordinates. However we should not ignore the inherent errors of map-making process (Cook and Pinder, 1996; Thapa, 1992). Further, the SOI map sheets are projected individually with Polyconic map projection origin at the center of map sheet. This creates problems in joining different map sheets and rectification of full scenes of remotely sensed images.

GPS is considered to be the best available technique for deriving the precise GCP coordinates for the geometric correction of remotely sensed imagery (Clavet, 1993; Cook and Pinder, 1996; Kardoulas *et al.*, 1996). GPS can prove to be an important tool for GCP data collection in a country like India, where large-scale maps are not available and even 1:25,000 scale Survey of India (SOI) topographic maps have only 20% area coverage (Siva Kumar, 1998). The main problem with the GPS coordinates is the lack of precise transformation parameters between WGS-84 and Indian datum, which is required for the integration of GPS data with the local datum maps. In Indian context various crucial issues related to the GCP acquisition for the high resolution IRS images are as below:

- Accuracy of maps
- Availability of WGS-84 to Indian datum transformation parameters
- Effects of Polyconic map projection

#### **4.0 STUDY SITES AND DATA RESOURCES**

This research work was carried out for three different study sites namely Bhopal, Kanpur and Lucknow. These sites were selected after taking into consideration various aspects like availability of good GCP features and base maps, convenience for GPS field work and GCP coverage for the full scene. The IRS-1C/1D satellite LISS-III and PAN sensor images were used for the investigations. The coordinates of GCPs identified on the maps were also read in the WGS-84 datum, using two different category GPS receivers (DGPS receiver model *SR530* and hand-held stand-alone mode receiver model *GS5* as per specifications given in Table 1.

#### **5.0 METHODOLOGY**

Point pairing techniques was used for the assessment of errors in the GCP determination from the SOI maps. The GCP based geometric correction accuracy was determined in the ILWIS software using GCPs from SOI maps and GPS. Effects of different map projections and datums were also investigated by finding projected distances between widely distributed GCPs in the study sites.

## 6.0 DISCUSSION OF RESULTS

The point pairing analysis results for the different scale SOI maps of different study sites are shown in Table 2. This analysis has shown large variability in the coordinates of derived from maps. The coordinates derived from GPS and SOI maps have large difference and these differences for two different study sites are given in Table 3. Because of the large difference of Indian datum and corresponding WGS-84 coordinates, the transformation of GPS derived coordinates to Indian datum is essential, if used in integration with different maps like cadastral, land use etc. maps. The geometric correction accuracy of IRS, PAN sensor images were investigated by GCPs from different sources and accuracy of each case is given in Table 4. The projected distances on Everest ellipsoid in Polyconic and UTM map projections are given in Table 5. These have shown that different map projections will have different projected distances at full scene level and these are significant in high-resolution images.

*Table 1: Specifications of GPS receivers used in the investigations*

GPS receiver model and type	Available GPS signal channels	Observation mode	Accuracy
Dual frequency DGPS receiver model, SR530 of Leica Geosystems	12 channel dual frequency L1 and L2 of C/A-code and carrier phase	Differential phase Differential code	mm level 30 cm
Hand-held stand alone receiver model, GS5 of Leica Geosystems AG	12 channel L1 C/A-code with parallel automatic selection	Stand-alone mode	3 to 5 m

*Table 2: Distance errors in point-pair analysis for map derived GCP coordinates*

S. No.	Source of map derived GCPs used for point-pair analysis	Range of distance error absolute value (m)
1	1: 50,000 scale SOI maps of Bhopal area	25 to 130
2	1: 50,000 scale SOI maps of Kanpur area	30 to 150
3	1: 50,000 scale SOI maps of Lucknow area	20 to 100
4	1: 25,000 scale SOI maps of Kanpur area	15 to 90
5	1: 25,000 scale SOI maps of Lucknow area	15 to 80



Table 3: Difference between WGS-84 datum and map derived Indian datum planimetric coordinates for the study sites

GCP No.	Bhopal 1:50,000 scale map		Kanpur 1:50,000 scale map		Kanpur 1:25,000 scale map		Lucknow 1:50,000 scale map		Lucknow 1:25,000 scale map	
	$\Delta\phi$ (s)	$\Delta\lambda$ (s)	$\Delta\phi$ (s)	$\Delta\lambda$ (s)	$\Delta\phi$ (s)	$\Delta\lambda$ (s)	$\Delta\phi$ (s)	$\Delta\lambda$ (s)	$\Delta\phi$ (s)	$\Delta\lambda$ (s)
1	-3.54	3.76	-1.41	5.06	-1.31	6.05	-1.26	7.34	-1.54	7.97
2	-2.76	4.03	-2.37	5.87	-1.21	6.58	-0.54	6.61	-0.74	5.11
3	-0.99	5.66	-0.92	7.59	1.67	7.18	-0.50	7.44	-1.09	5.57
4	0.53	3.32	-0.06	6.06	-1.60	7.97	-1.28	7.19	-1.69	5.15
5	-1.67	3.62	-3.93	5.99	-0.90	6.17	-0.57	8.29	-1.33	6.01
6	-0.86	4.54	-3.07	5.88	-0.06	6.11	-1.14	6.90	-0.72	5.14
7	-1.61	3.95	-0.06	6.87	-0.41	4.35	0.04	7.41	-0.32	5.55
8	-0.53	2.49	-0.34	6.14	0.16	6.90	-0.20	7.22	-0.25	5.73
9	-0.49	2.54	-0.68	6.39	-0.98	6.01	-1.07	8.51	-1.63	6.27
10	-0.53	4.64	-1.19	6.41	-0.46	5.16	0.52	6.30	-0.57	4.76
11	-1.27	2.90	-0.15	6.39	-0.74	5.11	0.22	6.99	-0.38	4.88
12	-2.36	3.72	-1.42	6.03	-1.69	6.71	-0.73	7.50	-0.53	5.40
13	-1.23	3.43	-1.36	8.03	-0.12	6.96	-0.57	6.01	-0.09	5.96
14	-1.18	4.01	0.55	6.07	1.13	6.94	-1.77	5.99	-1.98	4.85
15	-1.07	4.55	-1.47	5.37	-1.58	6.79	-0.77	6.93	-1.23	5.98

Table 4: RMS errors in terms of the corresponding image pixels of geometrically corrected LISS-III and PAN images, using GCPs from maps and GPS.

Details of corrected image	1:50, 000 scale map GCPs	1:25, 000 scale map GCPs	Hand-held GPS GCPs	DGPS GCPs
Bhopal PAN image	4.41	NA	0.44	0.54
Kanpur PAN image	5.91	2.87	0.55	0.75
Lucknow PAN image	3.37	2.39	1.14	1.07
Bhopal LISS-III image	1.22	NA	0.30	0.32
Kanpur LISS-III image	1.77	1.34	0.54	0.70
Lucknow LISS-III image	1.10	1.05	0.56	0.65

Table 5: Distances between GCPs, using different map projections and earth ellipsoids

Point pair no.	$d_1$ (m)	$d_2$ (m)	$d_3$ (m)	$(d_1 - d_2)$ (m)	$(d_2 - d_3)$ (m)
1	2495.00	2494.01	2495.86	0.99	-1.85
2	3986.41	3986.83	3988.28	-0.41	-1.45
3	7710.16	7710.81	7714.27	-0.65	-3.46
4	5436.63	5436.88	5439.64	-0.25	-2.76
5	8090.87	8090.30	8094.04	0.57	-3.73
6	3304.32	3305.31	3306.59	-0.99	-1.28
7	8945.02	8943.64	8948.18	1.37	-4.53
8	10380.26	10378.25	10382.28	2.01	-4.04
9	5038.14	5037.04	5039.76	1.10	-2.72
10	8090.87	8090.30	8094.04	0.57	-3.73
11	1805.12	1804.83	1806.01	0.29	-1.17
12	5345.61	5346.72	5348.34	-1.11	-1.61
13	4444.71	4444.48	4446.04	0.23	-1.55
14	13035.40	13036.40	13041.56	-0.99	-5.16
15	20870.69	20871.07	20880.25	-0.38	-9.18
16	26088.75	26087.75	26098.11	0.99	-10.35
17	80904.79	80903.61	80934.07	1.18	-30.46
18	56950.25	56947.68	56970.00	2.57	-22.32
19	47500.49	47500.34	47519.17	0.15	-18.83
20	67840.62	67840.21	67866.53	0.42	-26.33
21	98876.87	98877.15	98915.51	-0.28	-38.36
22	74898.68	74898.93	74926.99	-0.25	-28.07

$d_1$  Distance computed from UTM map projection coordinates in WGS-84 datum

$d_2$  Distance computed from UTM map projection coordinates in Indian datum

$d_3$  Distance computed from Polyconic map projection coordinates in Indian datum, using projection origin at LISS-III scene center

## 7.0 CONCLUSIONS

Based on the investigations of present research work following conclusions can be drawn:

- Map derived GCP coordinates should not be used for the geometric correction of modern age high-resolution images from IRS-1C/1D, IRS-P6 or any other high-resolution sensor. The GCP coordinates collected from hand held GPS receiver would suffice the sub-pixel accuracy requirements even for IRS, PAN sensor images.
- In the use of GPS data, availability of transformation parameters between WGS-84 to Indian datum is a big problem at least for civilian users.

- The declared new series of SOI maps for WGS-84 coordinates will not make any difference for high-resolution image applications. This is due to inherent errors of map-making process.
- Polyconic map projection is not appropriate for the image rectification and India requires appropriate map projection for satellite image applications.
- In view of the developments in satellite geodesy, efforts are needed from SOI for redefinition of Indian datum by selecting geocentric ellipsoid and appropriate map projection for the new series of topographic maps.

## REFERENCES

- Agrawal, N.K., 1997, WGS 84 and GPS. *International Conference on Remote Sensing and GIS/GPS*. June 18-21, Jawaharlal Nehru Technological University, Hyderabad.
- Baveja, S. D., Kapur, R. K., and Mohan, R., 1994. *Transformation Parameters between Indian Datum and World Geodetic Systems (WGS-72 and WGS-84): An Objective Analysis*. Proceedings of 14<sup>th</sup> INCA Congress at Bangalore (India), 28<sup>th</sup> Nov. 1994.
- Clavet, D., Lassere, M. and Pouliot, J., 1993. *GPS control for 1:50,000 – scale topographic mapping from satellite images*. Photogrammetric Engineering and Remote Sensing, Vol. 59, No. 1, pp. 107-111.
- Cook, A. E. and Pinder III, J. E., 1996. *Relative accuracy of rectifications using coordinates determined from maps and the global positioning system*. Photogrammetric Engineering and Remote Sensing, Vol. 62, No. 1, pp. 73-77.
- Kardoulas, N. G., Bird, A. C. and Lawan, A. I., 1996. *Geometric correction of SPOT and Landsat imagery: A comparison of map- and GPS- derived control points*. Photogrammetric Engineering & Remote Sensing, Vol. 62, No. 10, pp. 1173-1177.
- Katiyar, S.K., Dikshit, O. and Kumar, K., 2002. *GPS for the geometric correction of remotely sensed imagery: Possibilities after termination of SA*. Proceedings of The Asian GPS Conference, CSDMS, New Delhi, 24-25 October, 2002., pp.57-62.
- Katiyar, S.K., Dikshit, O. and Kumar, K., 2003. *GPS autonomous mode for satellite imagery geocoding: Benefits of low-cost hand-held GPS*. GIM International, Vol. 17, No. 6, pp. 29-31.
- Shiva Kumar, R., 1998. *An integrated multi-source digital topographic database for India*. Ph.D. thesis, Deptt. Of Civil Engineering, I.I.T. Delhi.
- Singh, S. K., 2002. *Coordinate transformation between Everest and WGS84 datums- A parametric approach*. The Asian GPS Conference, CSDMS, New Delhi, 24-25 October, 2002.
- Thapa, K. and Bossler, J., 1992. *Accuracy of spatial data used in geographic information systems*. Photogrammetric Engineering and Remote Sensing, Vol. 58, No. 6, pp. 835-841.

# **INTERNET GIS BASED MUNICIPAL INFORMATION SYSTEM: A CASE STUDY OF DEHRADUN MUNICIPAL AREA**

<sup>1</sup>SURENDER SINGH AND <sup>2</sup>B. S. SOKHI

<sup>1</sup>M.Tech. Trainee, <sup>2</sup>Head, Human Settlement Analysis Group  
Indian Institute of Remote Sensing, Dehradun, India  
*surenderahlawat@hotmail.com*

## **ABSTRACT**

*The present study has been undertaken to demonstrate the usefulness of Remote Sensing, Internet Geographical Information System (Internet GIS) and Global Positioning System (GPS) techniques for Land use/ Land cover mapping and to locate the facilities and Points of interest of the client, accurately on the base map for further analysis and for the making and development of the website. To attain the goal of this project three tiers of Internet interaction are defined as client, middleware, and server. It will be discussed where Municipal Information System (MIS) components fit within this framework. In the last, GIS based queries are supposed to be provided at the client side Via Internet to provide information with ease and with selection.*

*The broad aim of this study is to apply Remote Sensing, Internet Geographical Information System and Global Positioning System technology. Remote Sensing technology will be applied for the generation of Spatial Data, Internet GIS / Geographical Information System will be used to analyse the data and for providing selected inputs for the formation as well as for the development of website and Global Positioning System will be used to give accurate geographical location of the Facilities / Points of Interest (POI) of the client. In last phase, by using all the technologies, an Internet based Dehradun Municipal Information System (DMIS) will be developed. For this purpose an InternetGIS based conceptual model for Municipal Information Database is discussed in this study.*

## **1.0 INTRODUCTION**

Municipalities are few of the important tiers of local Government. The municipal bodies have a fairly comprehensive range of functional responsibilities and regulatory powers within their boundaries including health, accessibility / transport, primary education, garbage management, water supply, sewerage, planning and development control. Public organizations like municipalities experience a rapidly changing political environment that can cause radical differences in the way public employee's work.

In the last 30 years computers have undergone a marked revolution. Spectacular innovations in new spheres of applications areas are taking

place with the new development of the hardware software technology. Computerisation has marked a new era in human history by these innovations and applications that cover now almost every sphere of human life and his all activities (Quium and Shahidul, 1992)

However, the introduction of GIS technology involved the complex processes of managing municipal functions (Campbell, 1991). The computer system can facilitate Municipal Information System (MIS) to allow easy storage, updating, retrieval and mapping of a wide range of information related to planning and management of municipal functions.

## **2.0 WHAT IS INTERNET GIS?**

Internet GIS is a network-centric GIS tool that uses Internet as a major means to access and transmit distributed data and analysis tool modules, and to conduct analysis and visualization. Internet GIS is a special GIS tool that uses Internet as a means to access and transmit remote data, conduct analysis and make GIS presentation. Internet based geographical data services involve management spatial and non-spatial (attribute) data. Geographic Information System (GIS) has come to be an indispensable tool for analysing and managing spatial data.

Internet has been changing the ways of data access, sharing and dissemination. It is further changing the means of analysis and visualization of Geographic Information Systems (GIS). Internet GIS is rapidly evolving as Internet and Web technologies change. We seriously look at the need for the integration of the Internet and GIS and how its implementation is emerging as the fastest developing application for the web.

Internet GIS is a Geographic Information System (GIS) distributed across a computer network to integrate, disseminate, and communicate geographic information visually on the World Wide Web (Edward, 2000, URL). In performing the GIS analysis tasks, this service is similar to the Client-Server architecture of the Web. The geo-processing breaks down into a server-side and client-side task that make the users will be able to access, manipulate and retrieve the GIS data from their browser without purchasing proprietary GIS software.

Good decisions require good information. The operation level of government (the tax assessors, building inspectors, the meter readers etc.) contains of the people who work with and depend on data, daily to perform their tasks. If the information is inaccurate or out of date then their jobs are difficult to perform. Not all of those data that are created by the operations level of the municipality however are needed at the management level. Managers generally need summary information of the operational data. Instead of house-by-house or parcel-by-parcel data, managers need aggregate information. Even fewer data are needed for policy purposes less detailed but more integration, aggregation and flexibility are needed to meet the ever-changing information needs at the policy level.

Internet-based GIS users can use a Web browser to navigate maps and do basic spatial analysis. A user enters specifications such as location, thematic layers, or searching requests on the web page to set up the environment for mapping or searching. Users can also click buttons to start display commands such as zoom in, zoom out, identify, pan, query, etc. The requests from user will be sent to clients by way of HTML forms. The form is passed to the web server. A gateway at the web server passes the request to a GIS server. For instance, the gateway could pass the request in the form of HTML to an Arc IMS Server. The Arc IMS Server then generates a graphic file that will be converted to a GIF image or JPEG image. The GIF or JPEG image is later sent back to the client and viewed by the users with a standard web browser.

The goal then in developing information system is to design once needed at the operational level of the municipality, but also with the necessary standard and flexibility to allow the data to be integrated with other data in different functions of the organisations and aggregated in summary form for assimilation at the management and policy level. Data processor should strive to develop system that not only improve the municipality, but can also serve the managers and policy makers in improving decision-making, planning and policy analysis. An InternetGIS based Municipal Information System (MIS) can facilitate or satisfy the above-mentioned requirement of the municipality.

### **3.0 PUBLIC PARTICIPATION IN INTERNET MIS**

Increased public involvement in the definition and analysis of questions tied to location and geography is the domain of Internet based Municipal Information System (MIS), which is a type of Public Participation GIS (PPGIS). This approach facilitates the meaningful introduction of appropriate forms of spatial information and related technologies for widening public participation in the Policy making process (NCGIA 1996). This participant driven framework should be capable of representing diverse views without forcing premature resolution of contradictions, inconsistencies and disputed as they arise.

Contexts for introducing PPGIS would include community economic development, environmental dispute resolution, participatory planning, and other activities involving public collaboration. Technologies chosen or developed to support this approach can be designed to document and record the problem resolution process, allowing evolving priorities and problem definitions to be tracked by all participants.

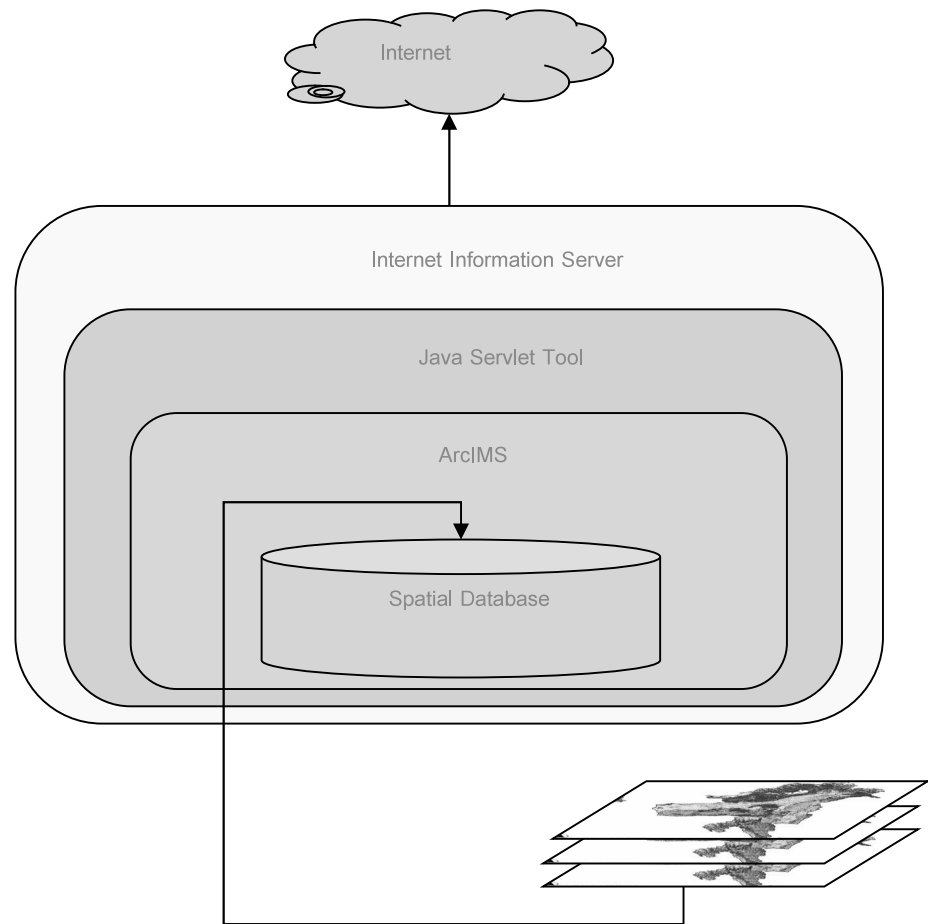
Sandman (1993) has identified nine publics relevant to discussion about community problems. The publics include: neighbors, concerned citizens, technical experts, media, activists, elected officials, business and industry, and local, state and federal government regulators (Nyerges and Barndt, 1997).

A public participation approach would situate GIS analytical tools within an expanded framework of communication and discourse, opening opportunities for public participation across the processes of problem definition and problem resolution (NCGIA, 1996).

#### **4.0 ADVANTAGES OF INTERNET GIS BASED MIS OVER THE PRESENT SYSTEM**

The advantages of InternetGIS based Municipal Information System (IMIS) are manifold. Some of the most important aspects of it are given below:

- Topologically structuring of GIS database can ensure reduction or elimination of data redundancy and only one base map for a municipality. One department develops and maintains the map while all other use it. This procedure makes it easier to produce quality map. Also multiple departments can share the cost for the base map preparation. Time saving is also realized through the interdepartmental cooperation.
- Implementing computerised system can reduce data and time constraints. Electronic field data record improves not only the field data collection process and the efficiency of MIS data acquisition, but it also boosts the efficiency of the collection of Non-MIS related data.
- Data sharing and workload balancing within the departments can be achieved through Internet based MIS. Interdepartmental cooperation can be one of the most prominent advantages. Once the initial resistance is overcome participants in the project would realize the benefits and would be eager to share data and workload.
- Wide array of data and their cumulative presentation helps the manager to foresee the demand and supply situation of a community in the context of community facilities planning. The system also facilitates the decision making process by giving managers more information in a timely manner, thus allowing administrators to be more informed and quicker in decisions making.
- Continuously changing environment requires frequent updating of information. It is relatively easier to update information in a computerised database. Correction and updating of database can be done easily in topologically structured database without any major involvement.
- Decision-makers need data within a short notice to take the decision quickly. As a Decision Support System (DSS), an Internet GIS based municipal information system will provide easy and quick retrieval of information. Maps of selected area / feature and in any scale and size can be produced, in a short notice.



*Figure 1: Conceptual Flow of Internet GIS Software*

#### **4.1 Information shown in DMIS**

As it is discussed that the aim of this study is to develop an InternetGIS based MIS for Dehradun Municipal Area (DMIS). Internet based DMIS has following information with relevant attributes to show and to make query analysis:

- |                                      |  |
|--------------------------------------|--|
| (a) Base Map                         | (m) Post Offices                             |
| (b) Ward Map.                        | (n) Police Stations                          |
| (c) Population Density Map           | (o) Parks and Gardens                        |
| (d) Land use and Land cover Map      | (p) Cinema Halls                             |
| (e) Slum Map                         | (q) Training Centres                         |
| (f) Hydrogeomorphological condition  | (r) Research Centres and National Institutes |
| (g) Railway Line and Railway Station | (s) Hospitals and Dispensaries               |
| (h) Major and Intensive Road Map     | (t) Religious Places                         |
| (i) Hotels                           | (u) Waterbodies.                             |
| (j) Banks and ATMs                   | (v) Physiography of Study Area.              |
| (k) Schools and Colleges             | (w) Bus Stands                               |
| (l) Soil Condition                   |  |



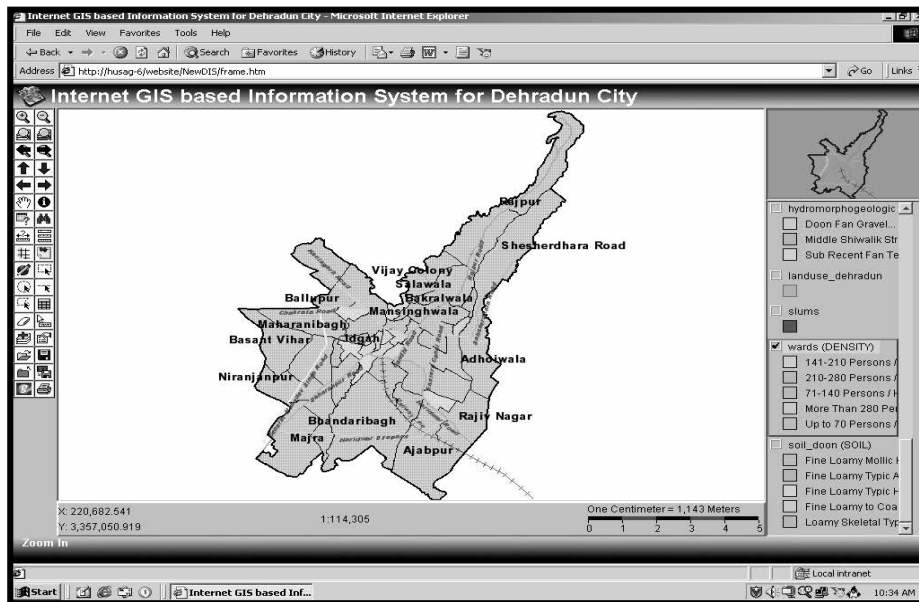


Figure 2: Interface of InternetGIS based website

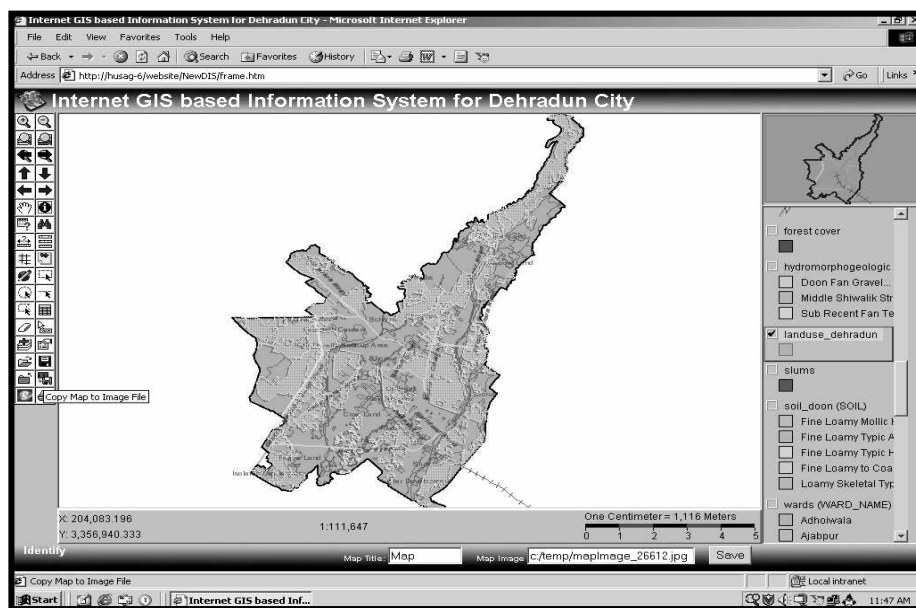


Figure 3: Landuse Information on website

## 5.0 WHY, WHERE AND FOR WHAT INTERNET GIS CAN BE USED

### 5.1 Internet GIS applications in transportation

Internet GIS provides a perfect tool to access, disseminate and visualize transportation data. Any information that can be displayed on a map such as highway and transit traffic levels, construction conditions, weather information and so forth can be transferred using Internet GIS. The US State of California uses “NEVERLOST” – a GIS/GPS application in

their transportation, which gives an exact location of the system and directions and road maps to the desired location from that point.

## **5.2 Application sharing**

Another approach of server-side Internet GIS is to share GIS applications among a group of users. Microsoft has created a freeware software tool that supports collaboration of GIS users over the Internet, called Microsoft NetMeeting. For instance, while one participant in a NetMeeting conference launches Arc View or MapInfo to work on a project. Many people in conference can simultaneously work in the same application.

## **5.3 Integration of data from multiple sources**

Internet GIS provides support for a variety of different data types and a variety of image formats. It can also offer unique and powerful client integration capabilities, making it possible for users to access the data, then quickly and simply integrate it with data from many other Intranet and local sources.

## **5.4 Highly scalable architecture**

Most of the present Internet GIS softwares including ArcIMS are specifically designed to grow with an organization and to provide a completely scalable solution for publishing GIS data, maps and its application. They can be easily scaled to handle the demands of every thing from the smallest Intranet to a high volume Internet site.

## **5.5 Real time information on road conditions and road construction**

Real time information on road conditions and road construction with traffic volume and other related influxes could be studied by Internet GIS within real and no time.

## **5.6 Standards based communication**

Most of the present Internet GIS softwares provide a good communication between clients and servers using computer languages such as Arc IMS uses Arc XML (Standard Extensible Markup Language). This language offers an easy, yet powerful way to customize Arc IMS application. ArcXML also facilitate transfer and exchange of intelligent geographic data between different applications.

## **6.0 GENERAL ANALYSIS**

As a product of this study an Internet GIS based website is generated. It is presently providing spatial information related with facilities or points of interest in following modes at client end:

- Location with respect to base map
- Zoom in and Zoom out function

- Location in terms of X and Y Co-ordinates
- Location in terms of their specific names, *if any*
- Finding any specific point of interest by attributes given (Name, Location etc.)
- Query based Finding Approach for any information
- Finding any land use of any specific place
- Finding any road by name and type of road
- Attaining any desired map or needed map
- Option of saving of the On-screen map is available.
- Option of saving whole project at once is available.
- Direct printout of maps is possible.
- Option of giving and changing Map Tips.
- Option of giving Maps Notes.
- Attributes table is accessible and modifications at client end is possible
- Option of Adding Client's own layers to the site
- Option of adding information by other Websites
- Facility of measuring any line segment or between two points.
- Option of setting scale units of client choice
- Creating buffer around any road segment or any Point / Feature
- Selection of features, points etc falling within buffer area
- Multi-style Selection Possible (By line, point, Rectangle etc.)

Above given options are facilities are available independently and some functions can be used in harmony of each other also. Almost all the GIS based functions are available and can be used at client end with ease.

## 7.0 QUERY BASED ANALYSIS

The main aim behind this study was to provide query-based functions at client end because these are the functions, which are the real functions and characteristics of a true Internet GIS based website. In purposed Internet GIS based website of Dehradun Municipal Area Query function is possible in three modes:

- By Single Entity Selection Approach
- By Finding Approach
- By Multiple Entities Selection Approach

## 8.0 RECOMMENDATIONS

As far as recommendations are concerned, it is suggested that –

- Internet GIS based Municipal Information System can be used as a replacement to paper based information providing system.
- Internet GIS based Information Systems should be client oriented and it should have less technical complexities.

- The authorities handling the paper based information system should be trained so that they can handle Internet GIS based Information System.
- The feedbacks of the clients should be registered properly and weightage should be given to these suggestions whenever upgradation is executed.
- As an experiment, first Internet GIS based Information System can be used at Municipality Level later it can be used at Tehsil or Taluka level, if it meets the requirements and expectation.

## REFERENCES

- George Antonion and Dorthy Deremer, 2001. Computing and Information Technology. World Scientific, New Jersey.
- Robert R. Hoffman and Arthur B. Markman, 2001. Interpreting Satellite Imagery – Human factors. Lewis Publishers, London.
- Environmental Systems Research Institute, Inc., 1997. Using ArcView Internet Map Server: Map Publishing on the Web. Environmental Systems Research Institute, Inc. Redlands (California).
- Harder, Christia, 1998. Serving Maps on the Internet. Environmental Systems Research Institute, Inc., Redlands (California).
- Huxhold, W. 1991. An Introduction to Urban Geographic Information Systems. Oxford University Press, New York, USA.
- Nyerges T. and Barndt M. 1997. Public Participation Geographic Information Systems. Proceedings of Auto Carto 13, Seattle, WA.
- Van Elzakker P.J.M. 2001. Users of Maps on the Internet. Taylor Francis, London.
- Allan Brown and Menno-Jan Kraak 2001. Web Cartography: Developments and Prospectus. Taylor & Francis, London.

# **PREDICTION OF ATMOSPHERIC POLLUTANT DISPERSION IN AN URBAN AREA BY WIND TUNNEL EXPERIMENT AND NUMERICAL SIMULATION**

RYOZO OOKA, SHINSUKE KATO, HONG HUANG  
AND TAKEO TAKAHASHI

Institute of Industrial Science, University of Tokyo  
ooka@iis.u-tokyo.ac.jp

## **ABSTRACT**

*The aim of this study is to predict the concentration distribution of air pollution emitting from the elevated road near the ground level within urban area, when the atmospheric stability is variable. This study consists of wind tunnel experiment and CFD (Computational Fluid Dynamics) analysis. The equation of plume model, which is used in the simplified condition, is applied to the prediction of the characteristics of pollutant dispersion within an urban area, by using data from wind tunnel experiment. This will become the basis of the accurate prediction method of the concentration distribution by each hour. In addition, this data are used for validation of CFD analysis. CFD is conducted using the standard  $k-\varepsilon$  model, and will be used for the real-time prediction of flow and pollutant dispersion in the future.*

## **1.0 INTRODUCTION**

The air quality in urban area becomes worse year by year due to the heavy vehicle traffic and the high density of various urban land uses. Many wind tunnel experiments have been conducted to investigate the phenomena of air pollutant dispersion within the street canyon (e.g. Kennedy and Kent 1977, Wedding 1977, Hoydysh and Dabbert, 1988, 1994). On the other hand, Computational Fluid Dynamics (CFD) method has become employed in order to predict air pollutant dispersion in the street canyon recently.

The purpose of this paper is to study the air pollutant dispersion mechanisms in the street canyons by the wind tunnel experiment and CFD method and develop the prediction method of dispersion in the street canyon by comparing the results of the wind tunnel experiment and CFD.

## **2.0 OUTLINE OF EXPERIMENT**

### **2.1 Objectives**

The area around a crossing road in the street canyon in Ikegami-Shinmachi, Kawasaki-city in Japan was analyzed here. This area is famous for high concentration of NOX from vehicles on the highway and local main road.

## 2.2 Model arrangement and measuring techniques

The wind-field and concentration dispersion were simulated in a boundary layer wind tunnel at the Institute of Industrial Science, University of Tokyo. The size of the test section of this experimental facility is 1.8m (H) × 2.2m(W) and 14m long. The objective area was modeled partially at a scale of 1:600 (see Figure 1). The diameter of the model was about 1.7m. Some of hundred buildings and all the streets within the area were reproduced in the model. There is a fence between piers under the highway in the left hand side from the crossing in Figure 1. For the measurement concentration, a tracer gas (C<sub>2</sub>H<sub>6</sub>) is released from the point source at A ~ E in Figure 1.

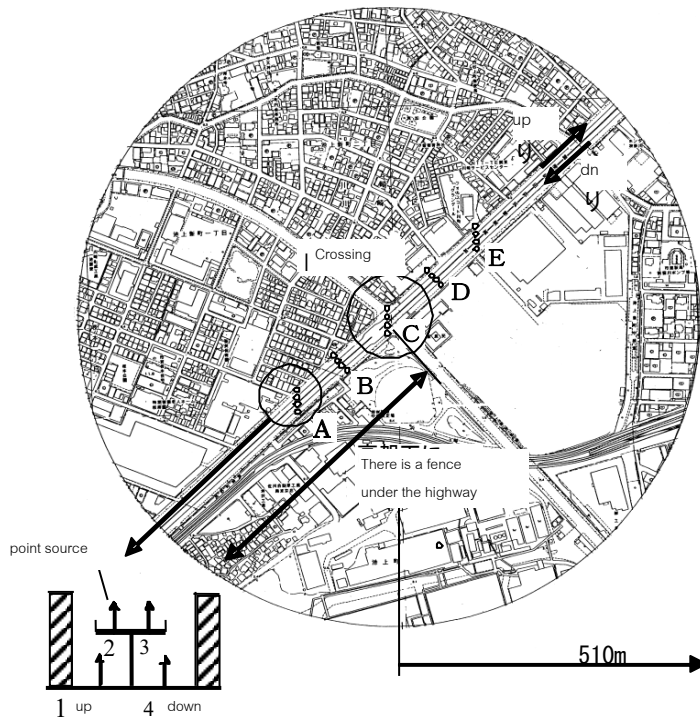


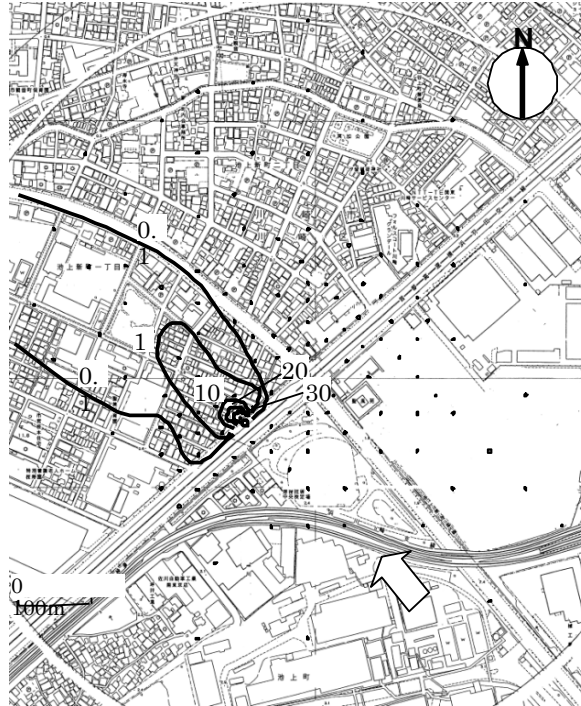
Figure 1: Test area for the wind tunnel experiment

## 3.0 EXPERIMENTAL RESULTS

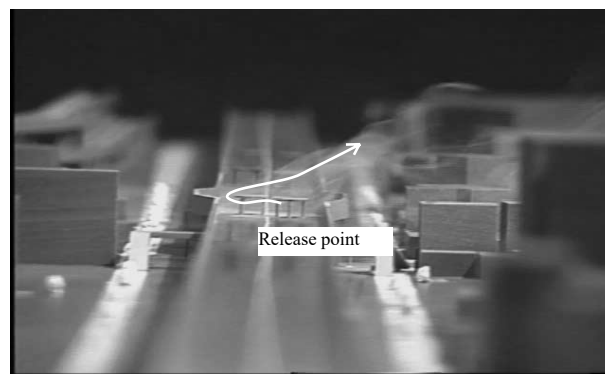
Experimental results of concentration are shown in the non-dimensional value  $C_n = CUH^2/Q$ . Here  $C$  is the dimensional value of concentration,  $H$  is the height of the highway (=1.33cm in model scale =8m in real scale),  $U$  is the inflow velocity at the height of  $H$  and  $Q$  is the release rate of tracer gas(=1cc/s). In this paper, the results under the condition at SE in wind direction and neutral in atmospheric stability are described.

### 3.1 Concentration field

Figure 2 shows the horizontal distribution of gas concentration when gas is released from point A. Gas disperses in the lateral direction along the highway because the building complex intercepts the stream wise wind.  $C_n = 0.06$  at 35m downward. This means rapid decrease of concentration in the stream wise direction.



*Figure 2 Horizontal Distribution of Concentration  
(Wind Direction : SE, Release Point (B1))*



*Photograph 1: Visualization of Dispersion  
(Wind Direction : SE, Release Point(B2))*

### 3.2 Visualization of dispersion

Photograph 1 shows the visualization of dispersion, when the gas is released from point B2 under the condition in SE wind directions. Due to the wake behind the buildings along the highway, the gas flows in the opposite direction to the stream wise.

## 4.0 PREDICTION OF CONCENTRATION FIELD WITH WIND TUNNEL EXPERIMENT AND NUMERICAL SIMULATION

### 4.1 Outline of prediction method with wind tunnel experiment

The Pasquill-Gifford equation is widely used in order to predict concentration field from a point source. Here, the prediction method from a line source which is applicable for traffic pollutant dispersion is proposed by superposing this Pasquill-Gifford equation. The concentration near the ground at x m distance in the stream wise direction from a point source,  $C_{xy}$ , is expressed as follows assuming normal distribution.

$$C_{xy} = C_{x0} * \exp(-y^2 / 2 \sigma_y^2) \quad (1)$$

Where,  $C_{x0}$  is the concentration on the stream wise axis (x axis) through a point source, y is the distance from x axis and is the diffusion width in y direction.

### 4.2 Outline of prediction method with CFD simulation

The standard k-ε model is utilized here for turbulence modeling. Simple method is used for time integration. As to discreteizing scheme, the first order upwind scheme and the second order central difference scheme are employed for convection term and the other terms respectively.

### 4.3 Prediction conditions

The NO<sub>x</sub> distributions at 1.8m high around 9-10 am September 3 are shown in Figure 4. Table 1 shows generation intensity of CO and NO<sub>x</sub>

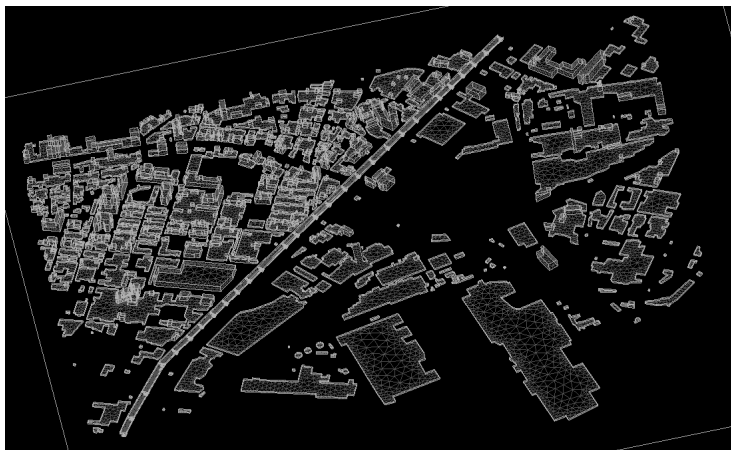


Figure 3: Mesh system of whole computational domain



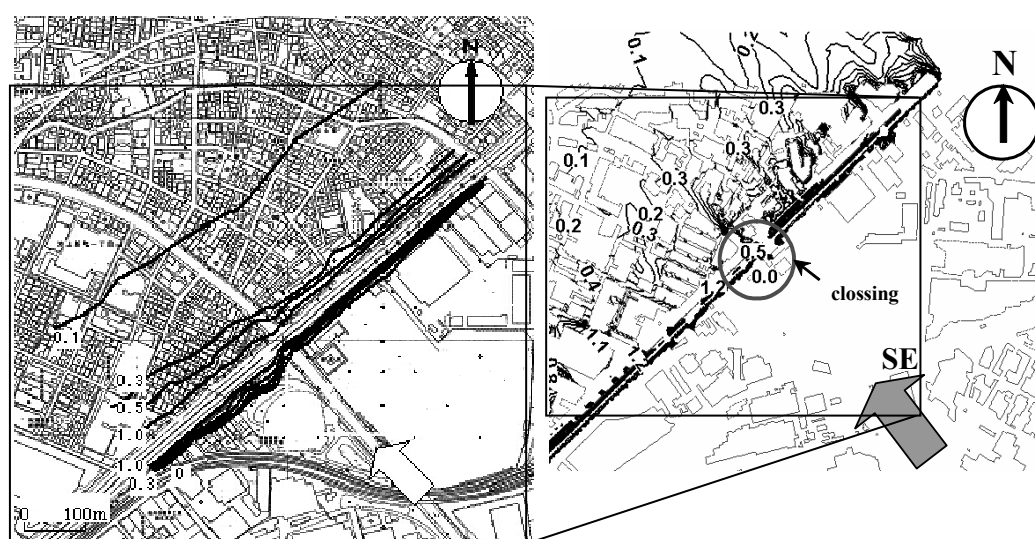
based on the investigation of traffic volume conducted on September 3 in 2003. The weather condition on the same day is also shown in table 1. For three dimensional CFD simulation, the analytical domain is discretized into 1,830,000 unstructured meshes (see Figure 3).

*Table 1: Generation Intensity of NO<sub>x</sub> from Highway and Local Main Road*

September 3 2003	Local Main Load (g . m <sup>-1</sup> . h <sup>-1</sup> )	Highway (g . m <sup>-1</sup> . h <sup>-1</sup> )	Weather Condition	
	NO <sub>x</sub>	NO <sub>x</sub>	Wind Velocity (m/s)	Wind Direction
7to8 am	28.72	23.33	0.80	NNW
8to9 am	32.31	25.51	2.90	SSE
9to10am	35.21	31.83	1.90	SE

#### 4.4 Results

Figure 4 shows the horizontal distribution of NO<sub>x</sub> concentration. The results of both the wind tunnel experiment and numerical simulation shows high concentration about 1.1 ppm around the highway and local main road and low concentration below 0.1 ppm 450m downward (in the north-west direction) from the highway. In the upward region from the highway, the concentration of NO<sub>x</sub> is almost 0 ppm. The comparison between wind tunnel experiment and CFD simulation shows fairly good agreement.



(1) Wind Tunnel Experiment (2) Numerical Simulation  
Figure 3: Horizontal Distribution of NO<sub>x</sub> Concentration (ppm)  
(1.8m high, 9to10am September 3, 2003)

## 5.0 CONCLUSIONS

Wind tunnel experiment and three dimensional numerical simulation are conducted in order to predict pollutant dispersion from highway and local main road in an urban area. The results of CFD simulation correspond well to those of the experiment. Therefore, three dimensional CFD simulation is expected to be powerful tool for urban design because it can predict more detailed concentration distribution.

## REFERENCES

- W.G. Hoydysh and Dabbert W.F. 1988. *Kinematics and dispersion characteristics of flows in asymmetric street canyons*. Atmospheric Environment 22, 2677-2689.
- W.G. Hoydysh and Dabbert W.F. 1994. *Concentration fields at urban intersections: fluid modeling studies*. Atmospheric Environment 28, 1849-1860.
- L.M. Kennedy and Kent J.H. 1977. *Wind tunnel modeling of CO dispersal in city streets*. Atmospheric Environment 11, 541-547.
- J.B. Wedding, Lonbardi D.J. and Cermak J. E. 1977. *A wind tunnel study of gaseous pollutants in city street canyons*. Journal of the Air Pollution Control Association 27, 557-566.

# **AUTOMOBILE TRAFFIC GENERATED ATMOSPHERIC POLLUTION: NEED FOR CONSIDERATION IN URBAN INFRASTRUCTURE PLANNING**

D. MOHAN

Institute of Technology, B.H.U., Varanasi, India.  
devmohan9@yahoo.com

## **ABSTRACT**

*Megacities in Asia have reached alarming levels of atmospheric pollution due to rapid urbanization, enhanced industrial activities and increased emissions from automobiles. Due to severe degradation in air quality, various types of physiological disorders are being noticed in a significant proportion of exposed urban population. Consequently, the expenditure incurred on 'air pollution induced health hazards' has been rising steadily. Automotive traffic also contributes to atmospheric burden of radiatively important trace gases such as carbon dioxide, methane and nitrous oxide. Chlorofluorocarbon emission from automobile air-conditioners has a deep impact on global climate. Light absorbing property of diesel particulate matter affects radiation balance of the planet Earth.*

*In spite of various efforts to curb the menace of automobile traffic generated pollution, improvements achieved in the quality of urban atmospheric environment has remained far from the satisfactory level. In fact, various physiological threats, which may arise, to human health due to this source of pollution are not given appropriate weightage at the time of planning of surface transportation infrastructures in urban areas. This paper draws attention towards the importance of this neglected aspect in urban planning. It also emphasizes that there is an urgent need for inclusion of vehicular traffic generated atmospheric pollution as one of the parameters in planning of surface transportation infrastructures in megacities so that improved level of safety to health of the inhabitants may be ensured.*

## **1.0 INTRODUCTION**

Rapid urbanization coupled with greater demand for transportation for day-to-day activities have created near chaotic traffic conditions in a number of cities and towns in many developing countries of the world. According to certain studies, 50% of the population is expected to live in urban areas in the beginning of the twenty-first century, making the problem of urban transport a challenge to city planners and transport operators (Chandrasekhar, 1994). A large body of data has implicated motor vehicles as a prime contributor to urban air pollution (Ludwig, 1967). Over the years, there has been a substantial increase in air pollution caused by vehicular exhaust emissions due to addition of more and more vehicles on roads to

meet the rising transportation demand (Mayer, 1999; Sharma, 1997; Sharma and Khare, 2001). An economic survey conducted by the Government of India indicated that total number of automotive vehicles (four-wheeler or with more wheels) manufactured in 2000-2001 was 7, 84,000, out of which about 6, 32,000 were cars. Six years ago, the figure was about half of it. The number of two-wheelers manufactured in the same period was staggering 3.75 millions. Over the last few years, the growth in the sale of two-wheelers in India has been compounding at the rate of over 15% every year, at times even touching a whopping 20%. About 35% of total number of two-wheelers are sold in four metropolitan cities (Delhi, Kolkata, Mumbai and Chennai) and 30 'A' class cities with populations exceeding 5 millions in India (Sivaramakrishnan, 2002).

Atmospheric pollution in large urban areas is still on rise worldwide or has shown only marginal reductions at some places. The studies carried out at city of Chile are an appropriate example with respect to various air pollutants (Jorquera, 2002a and 2002b). According to the findings of Global Workshop on Air Pollution, large cities in South Asia have reached alarming levels of air pollution due to rapid urbanization, industrial activities and increasing emissions from automobiles. The expenditure incurred on health-related problems has been estimated to be about U.S. \$ 200 millions per annum for Dhaka, the capital city of Bangladesh (Montague, 2000), which has been found to be highly polluted due to vehicular exhaust in a study carried out continuously for four weeks by Paul and Quader (2002). It was found there that an average concentration of particles with size less than or equal to 10  $\mu\text{m}$  was 422.7  $\mu\text{g}/\text{m}^3$  in ambient air, which is much in excess of the permissible limits set by Department of Environment, Bangladesh or United States Environmental Protection Agency. According to one estimate, the contribution of mobile sources to the total emissions of hydrocarbons ( $\text{C}_2\text{-C}_9$ ) in Korea has been found to be more than 70% (Na, Kim and Moon, 2002). Personal exposure to CO in five European cities of Athens, Basle, Helsinki, Milan and Prague was monitored for 48-hours and for the period shorter than this. It was observed to be pronounced particularly in street traffic, where CO concentration in ambient air became quite high due to inadequate dispersion (Georgoulis *et al.*, 2002). In a recent study on contribution of automobile emissions to air pollution conducted in Beijing and Guangzhou, it was observed that this source contributed more than 80% of CO and 40% of  $\text{NO}_x$  (Fu *et al.*, 2001). Delhi has been found to be the fourth most polluted city in terms of concentration of the suspended particulate matter (SPM) in ambient air (WHO, 1992). Mumbai, the economic capital of India has also been observed to be the fourth highest  $\text{NO}_x$  polluted city in the world (Srinivas, 1999). Table 1 presents the trend of rise in sectoral share of contribution of surface transportation to the pollution of atmospheric environment of Delhi and Table 2 shows estimated quantities of different automotive exhaust pollutants emitted in the atmosphere there.

Table 1: Trend in sectoral share (%) of air pollution in Delhi  
(Srinivas, 1999)

Sector	1970-71	1980-81	1990-91	2000-2001
Industry	56	40	29	20
Transportation	23	42	63	72
Domestic	21	18	8	8

Table 2: Vehicular pollution load in Delhi (PNL, 1997)

Pollutant	Load (thousand tonnes/ year)							
	1991		1996		2000		2005	
	A	B	A	B	A	B	A	B
Carbon monoxide	243	-	373	351	477	406	606	441
Hydrocarbons	82	-	123	113	156	135	198	149
Nitrogen oxides	139	-	208	207	261	250	330	279
Sulfur dioxide	10	-	15	15	18	16	23	18
Lead	0.19	-	0.297	0.259	0.384	0.269	0.489	0.276
Particulate matter	19	-	28	28	35	34	44	41

A-No control measures, B-With enforcement of emission norms and fuel quality

Uniqueness of gasoline consumption in India is that two- and three-wheelers account for about 65% of the total fuel used by all the vehicles. Besides the vast number of two-wheelers, the technology used in their production also ensures this segment of India's vehicular population to remain the largest contributor to load of air pollution in Indian megacities (PNL, 1997). Because of this fact, even a small city like Silchar in the state of Assam in India has been found to have significant level of air pollution due to automotive traffic and it has been reported that a sizeable portion of the urban population was suffering from its adverse effects on human health (Pandey and Pandey, 2003a and b). In a number of studies conducted in different Indian cities, it is found that the quality of air has deteriorated to a perceptible degree due to pollution originating from mobile sources (Mariappan *et al.*, 2000; Pandey *et al.*, 1998; Pandit, 1974; Prakash and Alappat, 1999; Ramamurthy and Thirumaran, 2002; Sivacoumar, 2000; Srinivas, 1999).

CO is one of the most abundant of the gaseous pollutants found in automobile exhaust. It is a colorless, odorless, tasteless but flammable gas, which is a product of incomplete combustion. It accounts for more than 50% of air pollutants pool in USA and also worldwide. More than  $4 \times 10^{12}$  kg of CO is emitted globally every year (Li *et al.*, 2000). In megacities, due to largely obstructed airflow, prolonged periods of stagnation lead to inadequate dispersion and consequently, result in enhancement of ambient concentration of CO in air. Community CO levels vary with proximity to traffic, traffic volume, type of traffic and many meteorological variables. As CO emission increases with decreasing engine speed, traffic congestion enhances ambient CO concentration both by increasing the number of

vehicles on given stretch of road and also, by enhancing the value of emission rate per unit road length travelled by each of the vehicles. CO concentrations in ambient air encountered in heavy traffic is about three times higher in comparison to that in commercial areas and five times higher than the value observed in residential areas. In developed countries, estimations of CO concentration in and around roadways and urban arterials are considered essential (at the stage of environmental impact assessment) to design the layout of different transportation routes (Cooper, 1987; Koushki, 1991; Ward, 1975). Keeping the hazardous nature of CO in view, it has been used as an indicator of air quality for design and operation of tunnel ventilation systems also (Chen *et al.*, 2002).

## 2.0 FACTORS AFFECTING AUTOMOTIVE EXHAUST

Road transport in India poses typical problems because of mixed traffic flow having about 13 different incompatible types of vehicles occupying the same right of way and moving in aggregated flow. This situation causes speed of the traffic movement to go down drastically. This condition results in higher consumption of fuel for relatively less distance travelled and consequently, enhanced quantities of air pollutants are emitted into the exhaust. In general, numerous short low speed trips accompanied by frequent starting, idling, acceleration, deceleration and stopping make for very inefficient and highly polluting automobile operation. In India, operational cost of a vehicle has been estimated to go up by 20-25% on bad roads, in addition to aggravation of the air pollution problem. Due to bad conditions of roads, the fuel of about Rs. 20 millions is wasted everyday, i.e., wastage of about Rs. 7,300 millions every year. In addition, about Rs. 50 millions per day, i.e., approximately Rs. 18,250 millions additional wastage per year has been estimated to be due to expenditure on vehicle maintenance. Average mileage is estimated to be 12 to 30 kmpl in Delhi and average speed on some roads, to be as low as 10 kmph. It has been estimated that by 2011, there may be 6 millions vehicles in Delhi in comparison to 1.2 million cars and 2 millions two-wheelers in the year 2002 (TOI, 2002). These conditions will lead to further worsening of air quality in Delhi, which gives an indication about the air pollution scenario, probably going to emerge in a large number of other Asian megacities.

The exhaust composition depends on many variables like engine type, engine operating conditions, driving mode, type of fuel, vehicle age, make and maintenance conditions, type of emission control system, weight of vehicle and its engine capacity and many other engine variables. Many studies reveal the effects of various operating parameters on exhaust emission from vehicles (Andre *et al.*, 1994; Beaton *et al.*, 1995; Belardini *et al.*, 1993; Bendsten and Thorsen, 1995; Cernuschi *et al.*, 1995; Hansen *et al.*, 1995; Jensen, 1995). Certain parameters related to operation, maintenance and driving behaviours can be modified to a large extent by planning appropriately the surface transportation infrastructures in Asian megacities.

### 3.0 ENVIRONMENTAL IMPACT OF THE AIR POLLUTION

The health effects of the pollution generated by automotive traffic are yet to be fully understood, but increasing incidences of asthma, other respiratory diseases and certain types of cancer have been linked to various exhaust pollutants such as carbon monoxide, oxides of nitrogen and volatile organic compounds (Clifford *et al.*, 1997). One of the studies sponsored by World Bank revealed that about 4.0 millions people were afflicted with ailments caused due to atmospheric pollution in Delhi. In Kolkata, it has been estimated to be around 3.5 millions and in Mumbai, about 2.5 millions. There occurred about 40,000 deaths in India every year, mainly due to adverse physiological effects of air pollution generated by automobiles. In Delhi alone, air pollution related mortality rose to 7,500 deaths per year as the city air received more than 2000 tonnes of air pollutants from automobile exhaust every day (Bhattacharya, 2001; Pandey, 2001). It is shocking to note that about 40 percent of children in Kolkata were found to be suffering from respiratory distress syndrome due to air pollution (Bhattacharya, 2001). Average figure of human morbidity and mortality has risen to about 57,000 everyday in 36 Indian cities, with about 26 million people being hospitalized every year, due to different diseases caused by atmospheric pollution (Pattnaik and Pattnaik, 2000). The estimate of cost (due to biospheric pollution) to India in 1995 was Rs. 3, 68,000 millions out of which an amount of about Rs. 52,400 millions was attributed to adverse health effects of urban air pollution alone (IJE, 1999). There has been conclusive evidence that polluted air of Delhi is responsible for over 40% of the emergency hospital admissions due to breathing or heart problems. The study found an increase of 41% in asthma cases, 39% in chronic bronchitis and 30% in heart attack cases. The emergency ward of All India Institute of Medical Sciences (AIIMS), Delhi has been reported to receive about 150 patients everyday from the geographical area within 10 km of radius (IJE, 1999). The statistics of prevalent diseases in Delhi in recent past shows that there has been a steep rise in the number of patients facing various physiological disorders related to air pollution (Srinivas, 1999).

Automotive emissions not only lead to severe degradation in urban air quality on micro-scale of meteorology, but are also reported to contribute to atmospheric burden of radiatively important trace gases, which have potential to influence the global climate significantly (Deluchi *et al.*, 1987; Unnasch *et al.*, 1989), such as CO<sub>2</sub>, methane and nitrous oxide. Chlorofluorocarbon emission from automobile air-conditioners is found to cause greater impact on global climate than CO<sub>2</sub> emissions from engines using gasoline as fuel (Amann, 1990). Light-absorbing property of diesel particulate matter (DPM) found in exhaust of diesel engines also affects Earth's radiation balance. The transportation sector is responsible for about 26% of the green house gases emissions in United States and due to increasing demand for gasoline and diesel fuels, it has been estimated to be one of the fastest growing sources of such emissions in near future (Transportation and global climate change, 1998).

#### **4.0 TRANSPORTATION INFRASTRUCTURES AND CONTROL OF POLLUTION**

Attempts to control automobile exhaust pollution by adoption of primary and secondary measures have not been successful in light of ever-evolving regulations in connection with concentrations of various pollutants in the exhaust. Therefore, multi-pronged strategy need be adopted for effective abatement of pollution due to automobile exhaust to realize the goal of healthy air environment in Asian megacities. For gasoline powered vehicles, driving at an optimum speed of 30-40 kmph in case of two/three wheelers and 45-55 kmph in case of four wheelers can be possible only after ensuring an appropriate planning and operation of surface transportation routes. This may also help to a large extent in avoiding harsh braking, and frequent acceleration and deceleration while driving, which are highly polluting phases. For diesel-powered automobiles, optimum driving speed should be around 40 kmph. In a study conducted recently in Varanasi city, it was observed that in the vicinity of certain traffic intersections, average speed of two-wheelers was about 12 kmph; that of autorickshaws, around 10 kmph and in case of four wheelers, about 8 kmph. Thus, it is clear that at these speeds, all the automobiles will spew excessively high quantities of exhaust pollutants.

Efforts to abate automobile exhaust generated air pollution without improving transport management will not meet significant success. This type of pollution can be controlled by bringing down the total number of vehicle-kilometres travelled either by reducing the number of vehicles on road and/or the kilometres travelled by each vehicle. According to an estimate, it has been found that if fifty bus passengers travel by two-wheelers, the pollution generated would be about 36 times more; if by cars, it will be 23 times more. The buses in Delhi meet nearly half of the demand for transport, but account for only about 0.7% of total number in the fleet. Introducing bus lanes and priority to buses at traffic intersections can cut down travel time by as much as about 25%. Dedicated bus lanes have been estimated to enhance the carrying capacity of buses by more than 50%. Bus corridors can be identified and also a shuttle service along these routes should be provided. If reliable, comfortable, fast, cheap and easily accessible public transport can be provided and proper infrastructural development is ensured, the number of vehicles on-road will go down drastically.

To achieve lower emissions of automobile exhaust pollutants by ensuring smoother movement of automobile traffic around the least polluting speeds, efforts to develop and apply more and more sophisticated technologies to attain better control of traffic flow have been going on and consequently, many concepts like intelligent vehicle highway system (IVHS) etc. have emerged. IVHS uses the latest technologies to squeeze more transportation from existing capacities of roads, allow the vehicles to move in a more fuel efficient manner and faster, improve highway safety, reduce fuel consumption, ease pressure for new highway construction, make



public transportation system more attractive and also help to reduce quantities of different air pollutants generated by the traffic. Intelligent transportation system (ITS) technologies, if integrated into surface transportation infrastructures and vehicles, traffic flow can be monitored and managed, congestions can be minimized and alternative routes to travellers can be indicated. This will cut down the time of travel and also, reduce the air pollution caused by automobile emissions. Advanced traffic management system can also be applied to monitor the traffic, optimise signal timings on major routes and control the flow of traffic. This will help in mitigation of recurring and non-recurring congestions, leading to reduction in the air pollution. Highway advisory radios may also be used to guide the travellers along less congested routes. These may also provide information about public transit alternatives, traffic conditions along short segments of specific routes and parking availability. Such information may help greatly in bringing down indirectly the quantity of pollutants generated by automobiles.

## 5.0 CONCLUSION

The process of urbanization has progressed at a fast pace in Asia also and so, megacities in this continent have expanded rapidly. Consequently, there has been tremendous rise in number of automobiles to meet the enhanced transportation demand. Due to compulsion of accommodating the increased number of automobiles in existing capacity of roads, average speed of traffic movement has gone down drastically. This has resulted in an alarming rise of air pollution caused by automobile exhaust. Therefore, surface transportation infrastructures need be planned, keeping in view the severity of the threat to public health due to the air pollution.

Properly planned and operated surface transportation infrastructures will help in achieving congestion-free traffic flow along with hindrance-free driving around the least polluting speeds. This will also result in reduction in the probability of formation of street canyons, which tend to retain various air pollutants by restricting wind movement etc.. Thus, urban population will realize improved level of safety to the health and consequently, a huge expenditure on account of 'automobile traffic generated atmospheric pollution induced health hazards' can be brought down significantly along with alleviation of human suffering.

## REFERENCES

- Amann, C. A., 1990. *The Passenger Car and the Green House Effect*. Society of Automotive Engineers, Paper No. 902099, Warrendale, PA.
- Andre, M., Joumard, R., Hickman, A. J. and Hassel, D., 1994. *Actual Car Use and Operating Conditions as Emission Parameters: Derived Urban Driving Cycles*. The Science of the Total Environment 146/147, 225-233.
- Beaton, S. P., Bishop, G. A., Zhang, Y., Asahbaugh, L. L., Lawson, D. R. and Stedman, D. H., 1995 (19 May). *On-Road Vehicle Emissions: Regulations, Costs and Benefits*. Science 2687, 991-993.

- Belardini, P., Bertoli, C., Giacomo, N. D., Iorio, B., 1993. *Combustion and Pollutant Emissions from Light Duty Diesel Engines: The Influence of Mixing Process and Transient Operating Conditions*. The Science of the total Environment 134(1-3), 285-293.
- Bendsten, H. and Thorsen, H., 1995. *A Survey of the Number of Old Vehicles on the Roads*. The Science of the Total Environment 169(1-3), 113-121.
- Bhattacharya, S. K., 2001 (Jan. 13-19). *Protection of Environment and the Role of Law*. Employment News Weekly, New Delhi, 1-2.
- Cernuschi, S., Giugliano, M., Cemin, A. and Giovannini, I., 1995. *Modal Analysis of Vehicle Emission Factor*. The Science of the Total Environment 169(1-3), 175-183.
- Chandrashekhar, B. P., 1994. Abstract Proceedings of Seminar on Technology for a Better Tomorrow, Calcutta, 41-42.
- Chen, K. S., Chung, C. Y. and Wang, S. W., 2002 (March). *Measurement and Three-Dimensional Modeling of Airflow and Pollutant dispersion in an undersea Traffic Tunnel*. Journal of Air & Waste Management Association 52, 349-363.
- Clifford, M. J., Clarke, R. and Riffat, S. B., 1997. *Local Aspects of Vehicular Pollution*. Atmospheric Environment 31(2), 271-276.
- Cooper, D.C., 1987. *Indirect Source Impact Analysis: Carbon Monoxide Modeling*. Journal of Air Pollution Control Association 37 (2), 1308-1313.
- Deluchi, M. A., Johnston, R. A. and Sperling, D., 1987. *Transportation Fuels and the Green House Effect*. University Wide Energy Research Group, UERG California Energy Studies Report No. UER-182, University of California, Davis.
- Fu, L., Hao, J., He, D. and He, K., 2001 (May). *Assessment of Vehicular Pollution in China*. Journal of Air & Waste Management Association 51, 658-668.
- Georgoulis, L. B., Hanninen, O., Samoli, E., Katsouyanni, K., Kunzli, N., Polanska, L., Bruinen de Bruin, Y., Alm, S. and Jantunen, M., 2002. *Personal Carbon Monoxide Exposure in Five European Cities and Its Determinants*. Atmospheric Environment 36, 963-974.
- Hansen, J. Q., Winther, M. and Sorenson, S. C., 1995. *The Influence of Driving Patterns on Petrol Passenger Car Emissions*. The Science of the Total Environment 169(1-3), 129-139.
- IJEP, 1999 (June). *Indian Journal of Environmental Protection* 19(6), 462-470.
- Jensen, S. S., 1995. *Driving Patterns and Emissions from Different Types of Vehicles on Roads*. The Science of the total Environment 169(1-3), 123-128.
- Jorquera, H., 2002a. *Air Quality at Santiago, Chile: A Box Modeling Approach-I: Carbon Monoxide, Nitrogen Oxides and Sulphur Dioxide*. Atmospheric Environment 36, 315-330.

- Jorquera, H., 2002b. *Air Quality at Santiago, Chile: A Box Modeling Approach-II: PM<sub>2.5</sub>, Coarse and PM<sub>10</sub> Particulate Matter Fractions*. Atmospheric Environment 36, 331-344.
- Koushki, P. A., 1991. *Evaluation of Street-Canyon Carbon Monoxide: Dispersion Simulation Model*. Journal of Transportation Engineering (ASCE) 117(4), 444-456.
- Li, X., Yang, L., Lei, Y., Wang, J. and Lu, Y., 2000 (Oct.). *A Method for Removal of CO from Exhaust Gas Using Pulsed Corona Discharge*. Journal of Air & Waste Management Association 50, 1734-1738.
- Ludwig, J. H., 1967 (Aug.). *Progress in Control of Vehicle Emissions*. Journal of Sanitary Engineering Division (ASCE), 73-81.
- Mariappan, G., Rajashekhar, R. V. J. and Muthusubramanian, P., 2000. *Estimation of Automobile Source Strength for Some Air Pollutants in Madurai City*. Indian Journal of Environmental Protection 20(8), 561-565.
- Mayer, H., 1999. *Air Pollution in Cities*. Atmospheric Environment 33, 4029-4037.
- Montague, P., 2000 (July). *Girls are Reaching Puberty Early*. THIMMAKKA'S Resources for Environmental Education 2(1), 5.
- Na, K., Kim, Y. P. and Moon, K. C., 2002. *Seasonal Variations of the C<sub>2</sub>-C<sub>9</sub> Hydrocarbons Concentrations and Compositions Emitted from Motor Vehicles in a Seoul Tunnel*. Atmospheric Environment 36, 1969-1978.
- Pandey, D. K., 2001 (Nov. 17-23). *Effect of Air Pollution on Health*. Employment News Weekly, New Delhi, 1-2.
- Pandey, K. M. and Pandey, A. K., 2003a. *Impact on Health of Usage of Non-Conventional Energy Systems for Controlling Environmental Pollution: A Case Study of Silchar City*. Proceedings of Fourth National Conference on Thermal Systems (FNCTS-2003), Gupta, S. N. and Prakash, O. (editors), Varanasi, 47-59.
- Pandey, K. M. and Pandey, A. K., 2003b. *Usage of Non-Conventional Power Generation for Controlling Environmental Pollution: A Case Study of Silchar City*. Proceedings of Fourth National Conference on Thermal Systems (FNCTS-2003), Gupta, S. N. and Prakash, O. (editors), Varanasi, 39-46.
- Pandey, V., Kumar, A., Pal, A., Singh, N. and Younus, M., 1998. *Status of Ambient Air Quality in Lucknow City*. Indian Journal of Environmental Protection 19(3), 181-184.
- Pandit, V. I., 1974. *Automobile Exhaust: Air Pollution and Its Control*. Indian Journal of Environmental Health 16(4), 344-359.
- Pattnaik, S. and Pattnaik, M., 2000 (Oct. 7-13). *Combating Air Pollution in India*. Employment News Weekly, New Delhi, 1-2.
- Paul, M. K. and Quader, A. K. M. A., 2002. *A Study of the Air Pollution of Dhaka City*. Abstract Proceedings of Indian Chemical Engineering Congress-2002, 54.
- PNL, 1997. *Pollution Control in Problem Areas*. Parivesh News Letter 3 (IV), 1-11.

- Prakash, P. V. S. and Alappat, B. J., 1999. *Control Strategies for Automobile Pollution*. Indian Journal of Environmental Protection 19(3), 185-192.
- Ramamurthy, N. and Thirumaran, M., 2002. *Automobile Exhaust Level of Carbon Monoxide: A Study in Chidambaram Town*. Indian Journal of Environmental Health 44(1), 37-40.
- Sharma, M., 1997 (Nov.-Dec.). *Combating Vehicular Pollution: Options and Approach*. Environmental Pollution Control Journal, 7-10.
- Sharma, P. and Khare, M., 2001. *Modeling of Vehicular Exhaust-A Review*. Transportation Research D6, 179-198.
- Sivacoumar, R., 2000. *Vehicular Pollution near Roadways in Chennai City*. Indian Journal of Environmental Protection 20(8), 592-596.
- Sivaramakrishnan, K. C., 2002. *India's Urban Environment: Growth of New Patterns*. The Hindu Survey of the Environment, 41-46.
- Srinivas, D. S. R. K., 1999. *Spatial Patterns of Air Pollution in Delhi*. Indian Journal of Environmental Protection 19(3), 172-180.
- TOI, 2002 (Feb. 18). *Bad Roads Prove to Be Costly*. *The Times of India*, New Delhi Edition.
- Transportation and Global Climate Change: A Review and Analysis of the Literature (DOT-T-97-03)*, 1998. US Department of Transportation, Office of the Environment and Planning, Washington DC, website: <http://www.fhwa.dot.gov/eee/environment/lit/htm>.
- Unnasch, S., Moyer, C. B., Lowell, D. D. and Jackson, M. D., 1989. *Comparing the Impact of Different Transportation Fuels on the Green House Effect*. California Energy Commission, Sacramento, CA.
- Ward, C. E., 1975. *Air Quality Manual Modifications*. Transportation Laboratory, California Department of Transportation, Sacramento, California.
- WHO, 1992. *Air Quality in Mega Cities of World*. World Health Organization Publication.

# ROAD SAFETY AUDIT - CHENNAI

K.VENKATESAN AND K.P.SUBRAMANAIN

Division of Urban Systems Development, Anna University, Chennai, India

venkatesankanagaraj@yahoo.co.in

## ABSTRACT

*A traffic accident may be taken as a failure of the road or vehicle or driver system to perform one or more operations necessary for completing a trip without damage or injury. Chennai is one of the mega cities in India. The accident rate of Chennai is increasing every year. Efforts are being made to study the traffic accident scene in Chennai in order to take suitable measures to bring down the accident rate.*

## 1.0 INTRODUCTION

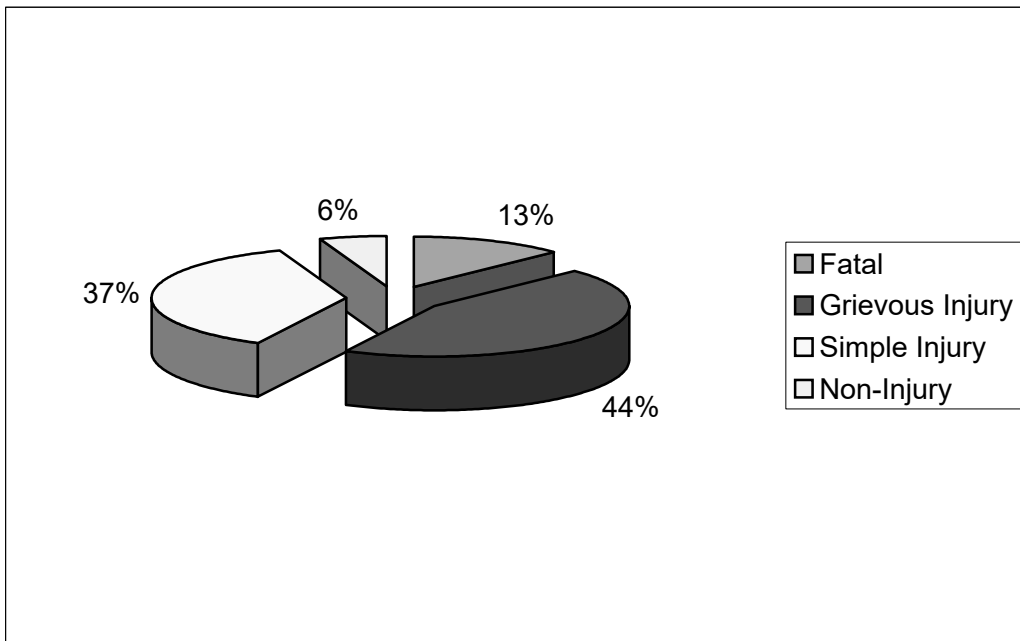
The accident rate of Chennai is increasing every year. So Chennai is taken as a case study for road safety audit. Accident data of 2003 is analyzed and the road safety measures are given.

*Table 1: Trend of accidents in Chennai city during the period 1990 – 2003*

Year	Total no. of accidents
1990	5877
1991	5242
1992	5260
1993	5548
1994	4807
1995	5001
1996	5458
1997	5715
1998	5481
1999	4750
2000	5126
2001	5280
2002	3682
2003	4243

*Source: Office of the Joint Commissioner of Police, Chennai*

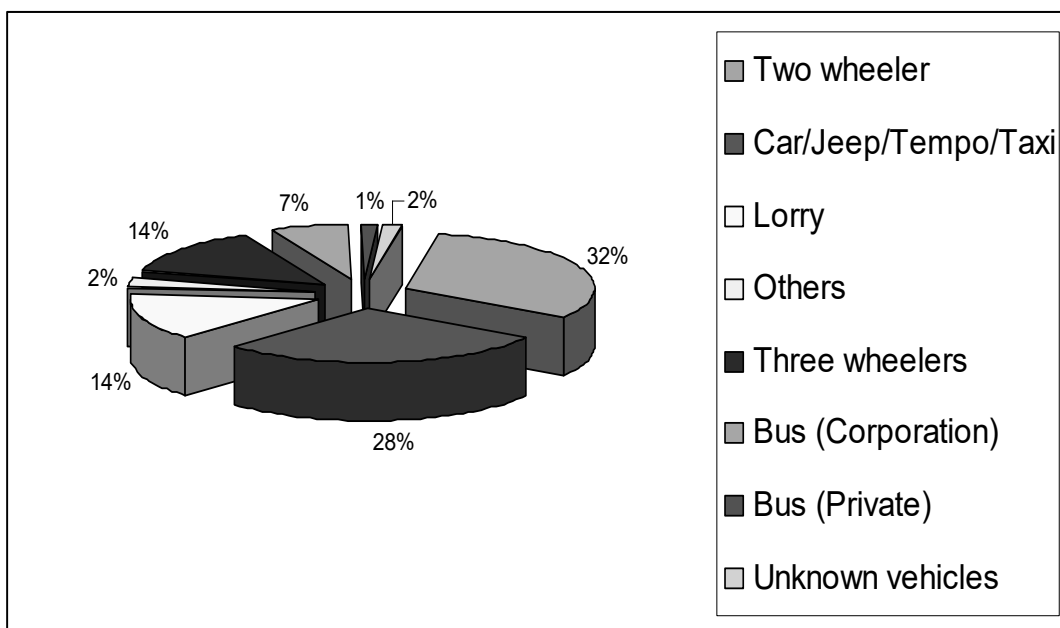
## 2.0 SEVERITY OF ACCIDENTS



*Figure 1: Severity of accidents in Chennai city during the year 2003*

During 2003 in Chennai city grievous injury accidents constitutes 44% and simple injury accidents constitutes 37%. Fatal accidents accounts for 13%.

## 3.0 TYPE OF VEHICLES INVOLVED



*Figure 2: Accidents according to type of vehicles during the year 2003*

From figure 2 it is inferred that two wheelers (32%),Car/Jeep/Tempo/Taxi (28%) are involved in more number of accidents. Lorry and three wheelers constitute 14 % each.

#### 4.0 CAUSES OF ACCIDENTS

Table 2: Number of road accidents in Chennai according to cause of accidents in 2003

Causes	Fatal	Grievous Injury	Minor Injury	Non Injury	Total accidents
Fault of drivers	531	1889	1546	230	4196
Fault on passenger	3	1	3	0	7
Fault of pedestrian	1	1	2	0	4
Mechanical defects	4	6	6	4	20
Bad road condition	1	4	0	0	5
Bad weather	5	3	2	1	11
Total	545	1904	1559	235	4243

Source: Office of Joint Commissioner of Police

From table 2 it is inferred that the fault of drivers is attributed as a major cause for the accidents.

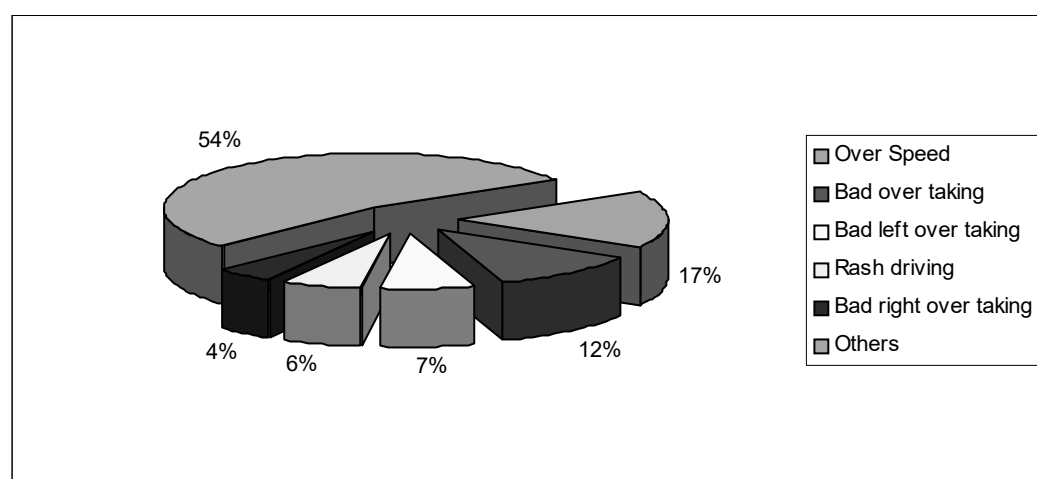


Figure 3: Percentage of accidents according to the type of driver fault during the year 2003

Over speeding is the major type of driver fault which are causing the accidents.Bad overtaking,bad left overtaking,,rash driving and bad right

over taking are other faults of driver. Others include apply sudden brake, careless drive, yellow line violation, followed closely, self fallen etc.

## 5.0 DISTRIBUTION OF ACCIDENTS

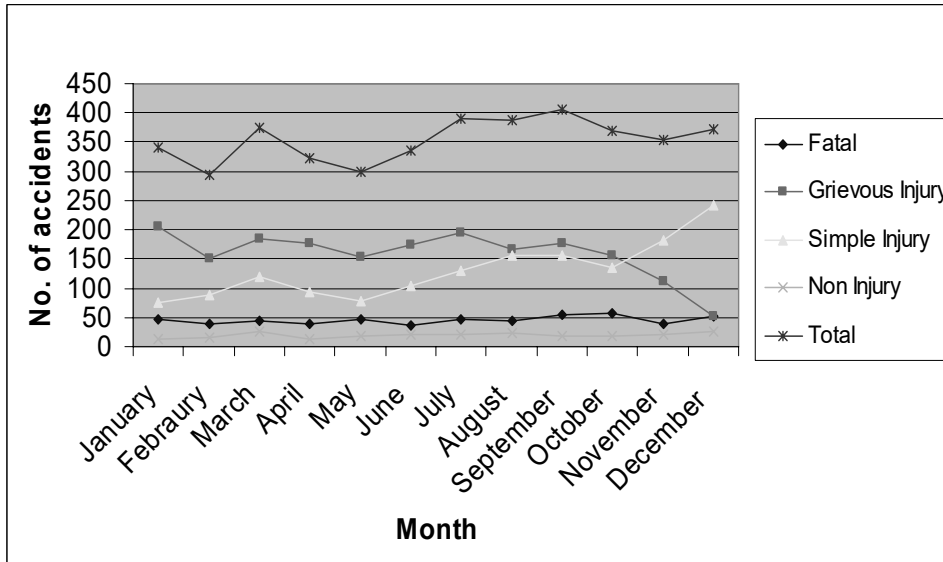


Figure 4: Month wise distribution of different type of vehicles in Chennai during the year 2003

The figure 4 shows that the number of fatal accidents are more in October. The grievous injury and simple injury accidents are more in January and December respectively. In December, the occurrence of non injury accidents are more. During January, the total number of accidents occurred in Chennai is high.

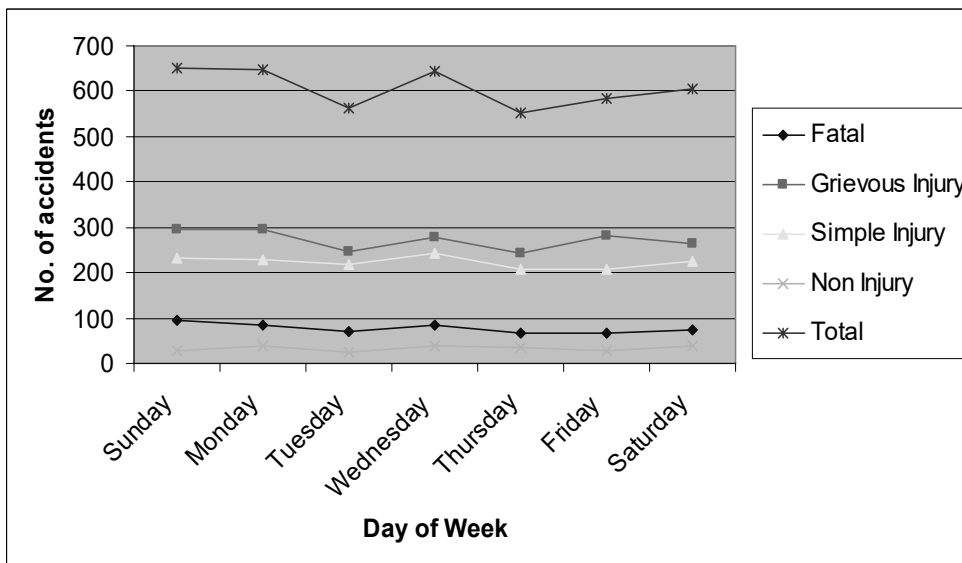


Figure 5: Daywise distribution of accidents in Chennai during the year 2003



The above figure shows that the fatal accidents are occurred high on Sunday. The grievous injury and simple injury accidents are occurred more on Monday and Wednesday respectively. The non injury accidents are more on Saturday.

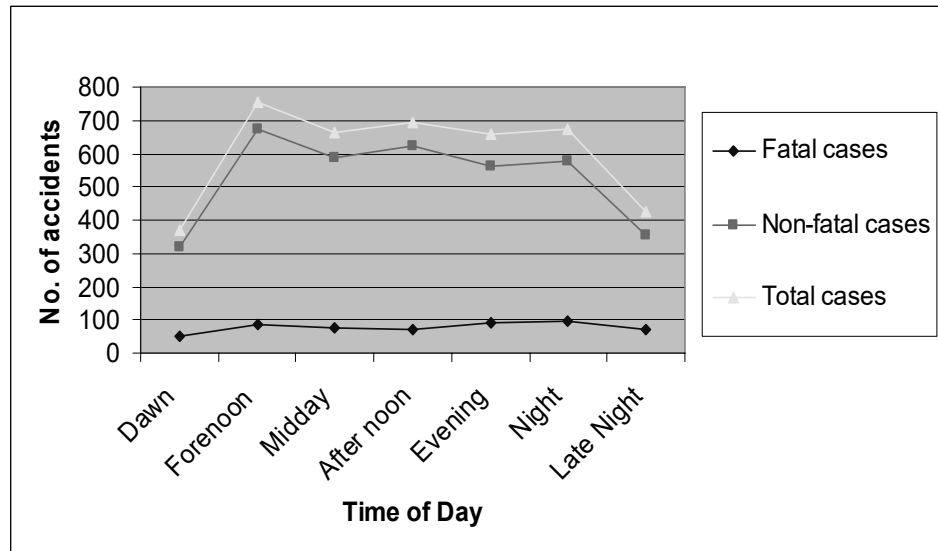


Figure 6: Timewise distribution of accidents in Chennai during the year 2003

The above figure indicates that the fatal cases and non-fatal cases are more in Night and Forenoon period of the day respectively.

## 6.0 ACCIDENTS ON ARTERIAL ROADS

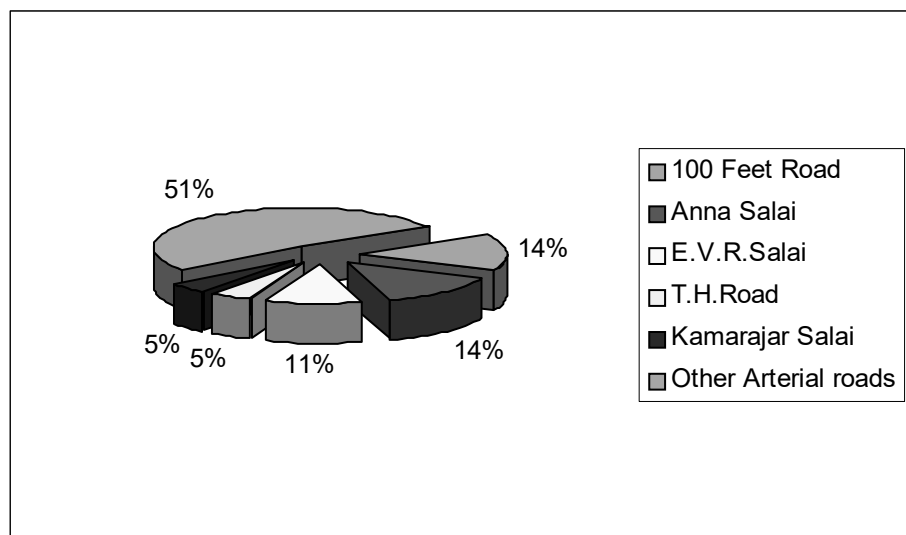


Figure 7: Percentage of accidents on arterial roads in Chennai during the year 2003

The accidents on major arterial roads such as 100 feet road and Anna Salai constitutes 14% each.

## **7.0 REMEDIAL MEASURES**

Keeping in view the type of risks involved the following eleven issues have been identified as thrust areas:

- Road Infrastructure
- Vehicle Safety
- Safer driver
- Safer speed
- Safe motorised two wheelers
- Safety of children
- Safety of pedestrians and cyclists
- Better enforcement
- Emergency Medical service
- Research and HRD for road safety
- Institutional and financial mechanism

### **7.1 Road infrastructure**

The road environment is contributing factor in upto 40 percent of accidents. Safety by design must be an integral part of road infrastructure planning and become a key element in land use development to ensure long term safety benefits for future road users.

#### ***7.1.1 Macro level planning***

Engineering measures are taken at two levels, viz. macro-level and micro-level. In case of macro level, problems are tackled in totality at regional, state and national levels and network planning is carried out as to arrive an optimal solution to the problems. Distribution of traffic among modes, known as inter-modal distribution should be carried out scientifically. Coordinated land use and transport planning needs to be given importance so as to control the demand aspect of the problem.

#### ***7.1.2 Road safety audit***

Road infrastructure design should compensate for the inadequacies of road users and prevent errors of judgement. Safety conscious planning and design of roads and network should be encouraged while undertaking new as well as upgradation and rehabilitation of road schemes through extensive application of road safety audits.

### **7.1.3 Accident black spots**

As high percentage of serious accidents take place on arterial roads, high accident frequency locations on these roads, otherwise known as accident black spots should be selected from scientific studies, improvement plans worked out from detailed studies and implemented on priority basis.

### **7.1.4 Roadside hazards**

Roadside hazards in the form of trees, poles, embankments and other fixed objects contribute significantly to occupant injuries. Such hazards should be identified and treatments known to reduce crash severity such as removal of fixed objects, installation of guard rail and improvement of road shoulder carried out.

### **7.1.5 Ribbon development**

A most serious phenomenon is the ribbon development and encroachments, specially near the urban fringes, where there is lack of access control. At such locations the carriageways are eroded and free flow of traffic is affected resulting in unsafe conditions besides environmental degradation.

## **7.2 Vehicle safety**

The measures such as additional safety features in vehicle design, awareness about regular, preventive and periodic maintenance should be taken. There should be improvement in method, staff and equipment for checking vehicle fitness. Spot inspection of heavy commercial vehicles should be done.

## **7.3 Safer drive**

Safety clinics to be organised for driver of transport vehicles involved in accidents. The standards of driver training schools should be raised and supervision of functioning of driver training schools should be done. The method of driver testing should be improved to cover knowledge of safe driving practices. The licenses should be renewed only after rigorous tests. Enforcement of control drinking and driving should be done.

## **7.4 Safer speed**

Appropriate speed limits needs to be set at the local level within the centrally well planned guidelines to select safe speed. Information system should be created to guide the drivers in the selection of appropriate speed. Enforcement has to be intensified to control over speeding.

### **7.5 Safe motorized two wheelers**

Safety engineering of motorised two wheelers should be improved. Wearing of helmets by riders should be made compulsory. Strict enforcement measures should be taken.

### **7.6 Safety of children**

Training programme for teachers should be conducted and awareness programme for parents is necessary. Road safety should be included in the curriculum. School safety zones should be provided as model projects. School children must involve in road safety activities.

### **7.7 Safety of pedestrians and cyclists**

Land use planning should be directed towards encouraging walking and cycling. Proper infrastructure facilities should be provided for safe and comfortable movement of pedestrians and cyclists. Enforcement should be enhanced to ensure safety of pedestrians and cyclists.

### **7.8 Better traffic enforcement**

Traffic police force should be strengthened and modernised. Well planned and targeted enforcement campaigns should be conducted for achieving greater compliance with traffic laws. Penalties should be more appropriate and proportionate to the seriousness of the offences.

### **7.9 Emergency medical services**

Organized central ambulance services should be there in city. A network of trauma care facilities should be established in the Chennai city. Mass campaigns should be organised to highlight the importance of emergency medical response.

### **7.10 Research and HRD for safety**

The research on priority areas should be encouraged in teaching and research institutions. Suitable institutions for training and research should be established.

### **7.11 Institutional and financial mechanism**

The responsibilities of various stakeholders of road safety should be defined properly. The organisations should be strengthened at appropriate levels. Adequate funds for implementation should be earmarked.

## 8.0 CONCLUSIONS

The accident data of Chennai city for the year 2003 was analysed. The analysis shows that out of the total number of accidents, grievous injury accidents constitutes 44% and simple injury accidents constitutes 37%. Two wheelers (32%), Car/Jeep/Tempo/Taxi (28%) are involved in more number of accidents. The fault of drivers is attributed as a major cause for the accidents in Chennai city during 2003. Over speeding is the major type of driver fault which caused the accidents. The accidents on major arterial roads such as 100 feet road and Anna Salai constitute 14% each.

Based on the analysis road safety audit is done for the Chennai city based on the eleven issues such as Road Infrastructure, Vehicle Safety, Safer driver, Safer speed, Safe motorised two wheelers, Safety of children, Safety of pedestrians and cyclists, Better enforcement, Emergency Medical service, Research and HRD for road safety and Institutional and financial mechanism. The strategy should be evaluated three years and updated depending on the performance, the then prevailing conditions and needs.

## REFERENCES

- Agarwal ,R.C.,1997. *Road accidents in India – Causes and remedial measures*. Indian Highways Journal.
- Deshpande,M.D.,1998. *Study of accidents on N.H.No:8 of Ahmedabad Ajmer section from Kms 388/4 to 481/4*. Indian Highways Journal.
- Srinivasan,N.S., 1987. *Scientific identification and improvement of accident prone locations on N.H.No:47 in Kerala*. Indian Road Congress Journal.
2003. *Studies undertaken to identify critical causes of accidents in the Highways of Tamilnadu*. Indian Highways Journal.

# 2D - EA FOR FACILITY ALLOCATION

RAJIV GUPTA

Birla Institute Of Technology And Science, Pilani, India.

rajiv@bits-pilani.ac.in

## ABSTRACT

*In a world that is rapidly shrinking and where land is at a premium, proper use of land is of utmost importance. This demands that we allocate space to our facilities (residential buildings, commercial houses, recreational and entertainment centers, etc.) effectively. Genetic Algorithms have been used extensively for planning purposes. However, traditional approaches emphasized on the vector or one-dimensional approach.*

*A new algorithm for designing the layout of facilities is presented in this paper. The algorithm uses a 2 - dimensional genetic algorithm (GA), called 2-D Evolution algorithm (2D - EA), which employs GA common operators in 2-dimensional form. The present work makes use of geographical information system software to convert the image/ digital map in two-dimensional matrix that is used as chromosome to apply genetic algorithm. This work deals with the design and implementation of 2D - EA for optimal layout of facilities. Given a set of facilities and the site in which they are to be placed and the distance between each of the facility, the algorithm proposes solutions, which satisfies the distance constraints among the facilities. The algorithm generates an initial population and then calculates the fitness of the individuals of the population and by process of selection and crossover. It generates the next generation of individuals. Various functions which generates the initial population, calculate fitness and perform genetic operations have been implemented using MATLAB. This form is more suitable as compared to vector form of chromosomes due to the nature of the problem that is related to space allocation. Since 2D - EA can be applied directly on the remote sensed images/ scanned maps, the need for compression and possibility of 'dimension crunch' does not arise. The method is demonstrated on a real life problem of campus facilities allotment. The paper concludes with the strength and limitations of proposed algorithm.*

## 1.0 INTRODUCTION

Urban planning involves many functions (general administration, development control, plan making, and strategic planning), scales (whole city, sub-region of a city, a district, a street block, etc.), sectors (land use, transport, housing, land development, environment, etc.) and stages (determination of planning objectives; analysis of existing situations; modeling and projection; development of planning options; selection of planning options; plan implementation; and plan evaluation, monitoring, and feedback). Plan making and non-routine strategic planning are

undertaken much less frequently as compared to General administration and development control (Yeh 1999).

The layout problem is one of the important problems in the planning of service facilities since efficient layout is critical to cost-effective operation of the facilities (Karray et al. 2000). Good facility layout is important to promote safe, efficient, and optimized operations concerned with day-to-days life. Therefore, in the design process of the layout, many objectives are considered (Francis and White 1974; Tompkins et al. 1984). Traditionally, planning a layout is an iterative process till a compromise is reached (Whitehead and Eldars 1965). These trials and error are carried out on maps (2 - D sheet) or now days some computing efficient techniques like Genetic algorithms (Holland 1962) are used. A large amount of work has been reported in the literature to deal with the layout problems. The methods mainly used are Heuristic, Computer-based systems, Artificial Intelligence/ Expert Systems, Artificial Neural Network, Fuzzy Set Theory, Geographical Information system (GIS), and Genetic algorithm (Zouein et al. 2002).

The main weaknesses of the existing methods are their linkage with urban planning model. The present work suggests a model based on EA that can be used as the substitute of this linkage or enhance the efficiency of linkage GIS with planning model. The present work makes use of GIS to convert the images in two-dimensional matrix that are used as chromosomes to apply GA.

### **1.1 Genetic algorithm**

These algorithms perform random searches through a domain of possible solutions, with the aim of finding the best alternative with respect to a given definition of 'goodness'. This goodness is expressed as 'fitness function', a function that evaluates the given solution over the given criteria. The search is performed over a finite set of alternatives. The alternatives or solutions are coded traditionally as a one-dimensional vector, which are called 'chromosomes'. A set of chromosomes is known as a 'gene pool'. The algorithm, in its simplest form can be expressed as:

- Randomly create an initial pool of alternatives (chromosomes).
- Given the 'fitness function', each member of the gene pool is evaluated in terms of this fitness.
- The next generation is selected from the gene pool, by skewing the random selection process in favor of the fitter chromosomes, called 'Natural Selection'.
- The gene pool is modified by performing certain genetics operations, like crossover and mutation and some other special operations like inversion, etc.
- The new population replaces the initial population.
- This process is repeated till the stopping criterion is satisfied.

The proposed EA is a modified form of the generic genetic algorithm. The basic functions of Selection, Crossover, and Extinction are modified. The basic consideration in developing this evolutionary algorithm is to adapt the vector based GA approach to two-dimensional maps/ satellite images. The conversion of images in one-dimensional form leads to a loss of spatial information, and thus could not be used satisfactorily. Here, the attempt is to use the evolutionary approach directly on two-dimensional images.

The basic aim is to get an optimum facility layout such that the proximity among related facilities is as desired. The algorithm can be applied either to optimize the facilities locations in given area or to modify the locations of existing facilities in an area.

## **2.0 TWO-DIMENSIONAL EVOLUTIONARY ALGORITHM (2D - EA)**

The basic steps, which are further described in details, involved in the proposed 2D - EA are as follows:

- Calculation of base values (area, number, and distances) for the original map and for each facility. Here the unit area for a facility is kept constant; and to satisfy the need, number of unit area for the facility is changed.
- Generating a parent pool of two-dimensional matrices, which satisfy the given constraints.
- Calculation of the fitness value for each matrix.
- Generating the gene (child) pool through '*Natural Selection*' process.
- Creation of new matrices through the process of altered crossover.
- Calculation of the fitness value for the child matrix, based on which it is decided whether the matrix to join the child pool or become extinct.
- Repetition of steps 5 to 7, till the specified number of iterations is over.

### **2.1 Calculation of base values**

Base values are the parameters like unit area and number for each facility. These base values for the parameters are created from the map/ images as follows:

- Starting from a processed existing map, the prohibited places (facilities can not be placed due to various reasons) are marked.
- Reading in the processed image into a matrix variable.
- Reading in the processed image for the unit areas into a matrix variable.
- Deciding on a priority for placing each facility. The facilities which occupy maximum space are placed first. Priority is given to



facilities with larger unit areas, and then to facilities with larger total areas but small units.

- Calculating the total area for each facility and the unit area maps. This is done by summing the number of elements in the matrix corresponding to the gray level intensity for the particular facility.
- Dividing the areas in the matrix by the areas in the unit area matrix to get the total number of each facility.

Once the base values are obtained, the next step involves the calculation of the parameters for the generated matrices. The following assumptions have been made to calculate the facilities parameters for the generated matrices:

- The total area available for construction remains constant.
- The area of the unit facility remains same.
- Number of each facility units required is known.
- The increase in facility area is manifested as an increase in facility units.

To optimize the facilities locations in given area, unit area and the total numbers of each unit are decided by the user according to the need. Placing these facilities in random fashion creates a base map, and then algorithm is applied.

## **2.2 Generation of parent pool**

The first step involved in a map creation is to define the areas where facilities cannot be placed. According to the facility priority decided on, a random number is generated for the X and Y coordinates to place the facility unit in the range of map. The area occupied by the prospective facility unit is checked for the presence of any other facility. If the condition is met, place the facility unit by making the values of the elements in the matrix equal to the facility unit number. This process is repeated for all facilities. The numbers stored are in continuous forms, i.e. for 9 facilities with 5 units each, the numbers stored range from 1 to 45. Thus, a separate identification number distinguishes each facility unit placed. The range of facility unit numbers for a particular facility type is stored. The starting point of each facility placed is stored in a separate matrix; this then acts as a reference matrix. This is used to carry out 1-dimensional operations like distance calculations. If it becomes impossible to place a particular facility unit after a specified number of times, then start afresh with a new blank matrix. The process is repeated till the parent population is complete.

## **2.3 The fitness function**

Each chromosome (in the usual GA) or matrix (2D - EA) denotes a particular solution. The higher the fitness value, the better is the solution. Here, proximity is chosen as objective function. Proximity is the shortest edge distance between two entities. In planning of smaller places, proximity

is better indicative of spatial closeness between two entities than center-to-center distance. A facility unit, in case of rectangular shape, is represented by the upper left ( $X_1, Y_1$ ) and lower right ( $X_2, Y_2$ ) coordinates. Here, the proximity between facility unit  $i$  and facility unit  $j$  is expressed as:

$$\text{Min} (\sqrt{(X_l^i - X_m^j)^2 + (Y_l^i - Y_m^j)^2}); l = 1, 2; m = 1, 2 \quad (1)$$

The total proximity for  $n$  facility units is:

$$\sum_{i=1:n} \sum_{j=1:n} \text{Min} \sqrt{(X_l^i - X_m^j)^2 + (Y_l^i - Y_m^j)^2}; l = 1, 2; m = 1, 2 \quad (2)$$

However, the approach described above is not capable of expressing extra spatial relationships. For example, the proximity between a residential area and a shopping complex could be preferably high. The problem is overcome by introducing a Proximity Matrix ( $P_{n \times n}$ : symmetric matrix) for ' $n$ ' facilities, which gives relative weights on the proximity between two facilities. Thus, the  $i^{\text{th}}$  row and the  $j^{\text{th}}$  column will indicate how close the  $i^{\text{th}}$  facility should be to the  $j^{\text{th}}$  facility. The diagonal elements indicate how close the unit areas of the same facility should be to one another. To calculate the diagonal element in the  $i^{\text{th}}$  row and  $i^{\text{th}}$  column, the weight ( $W_{i,i}$ ) attached is:

$$W_{i,i} = \frac{\text{Total number of units of facility } i}{\text{Total number of facilities units in the area}} \quad (3)$$

With this as the diagonal elements, the other weights are given in proportion to this. Hence, the fitness function now becomes:

$$\frac{1}{\sum_{i=1:n} (\sum_{j=1:n} \text{Min} (\sqrt{(X_l^i - X_m^j)^2 + (Y_l^i - Y_m^j)^2}) * W_{i',j'})}; l = 1, 2; m = 1, 2 \quad (4)$$

Here  $W_{i',j'}$  is the weight between the  $i'$  and  $j'$  facilities, with the  $i^{\text{th}}$  unit of  $i'$  facility and the  $j^{\text{th}}$  unit of a  $j'$  facility. This fitness function needs to be maximized for the optimum result. In the proposed method, Natural selection and Crossover functions of prototypal genetic algorithm are modified.

## 2.4 Natural selection

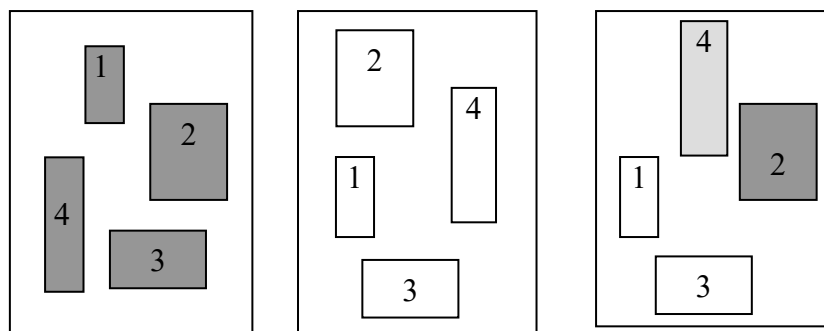
Given a percentage for crossover, the remaining chromosomes (matrices) are generated using natural selection. Thus, for a crossover percentage of 0.4 and population size 100, 60 chromosomes are passed directly to the next generation. The fitness function of each matrix is calculated, which is divided by the sum of fitness to give the relative fitness for each matrix. The values of the relative fitness are summed up in a

stepwise manner, thus yielding a set of continuous intervals, which are larger for matrices with higher fitness. A random number is generated, and checked with the fitness intervals. For the range it falls in, the matrix with the upper bound fitness value is chosen. This process is repeated till the required number of chromosomes is selected.

## 2.5 Crossover

Crossover for 2-D matrices is a rather complicated concept. The regular crossover operation proves to be inefficient in this case. A new crossover mechanism is suggested in this study, which can be viewed as a combination of crossover and random generation. The steps involved are as follows:

- Store the boundary coordinates for each unit of the facility.
- The modified crossover starts with the selection of two parents from the pool. The selection is done using the *natural selection* operation.
- The child matrix will contain each facility on location either from the corresponding facility location in parent 1, or parent 2. The number is randomly generated (either 1 or 2) for each facility unit.
- If the facility cannot be placed according to one parent in the given row and column then try to place it by interchanging the row and the column otherwise try to place it according to other parent. If neither option is possible, then it is randomly placed. As the percentage of random placements to total facilities becomes more than 0.4, the child is discarded and the crossover is repeated.
- The fitness of the child matrix is calculated.



*Chromosome 1* + *Chromosome 2* → *Child Chromosome*

*Figure1: Modified crossover operation*

In this study, a biased random method with respect to the worst fit case of the previous generation is selected to decide on the survival of child chromosome. The user provides a value for the rate of survival. If the matrix generated has fitness less than the least fit of the previous generation, then a random number is generated. If this number is within the survival rate then

the chromosome is allowed to enter the pool or else it is exterminated, and the process is repeated to generate another child matrix.

Using the modified crossover operation, required child matrices are generated. To remove the duplicity, the child chromosome is evaluated and its fitness is compared to the least fit matrix of the previous generation. As per the survival rate, either it joins the population or exterminated. Here too the reference matrix containing the starting points of each facility unit is stored. Finally the fitness is calculated for this generation, and the reference matrix updated. This serves as the parent pool for the next generation, and the process is repeated. For the present study, the mutation operation is not included.

## **2.6 Evaluation of matrices**

Once the parent pool has been created, use the fitness function to get the fitness value for each matrix. Use the reference matrix stored for each chromosome to directly calculate the total weighted-proximity for the whole matrix.

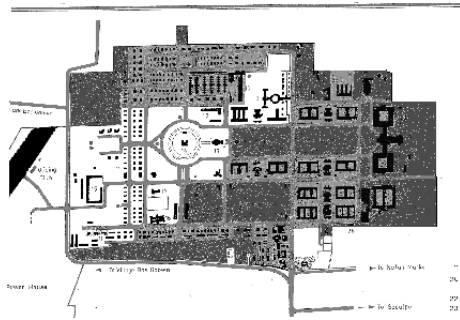
## **3.0 CASE STUDY**

As a case study, the institute campus of Birla Institute of Technology and Science (BITS), Pilani, India is considered (Figure 2).

The campus map obtained for the project was a binary (Blue and White) top view map with proportionate real distances on the ground. Certain modifications were made to the map to use it for analysis. These changes include: Scaling and Resampling of map, Enhancement of scanned image of map, Image classification into separate facility or land-use zones, Conversion of colored map to gray level image (Figure 2), and Conversion map into a two dimensional matrix.

These changes can be achieved using various software platforms. To decide on the total number of facilities, nine facility zones (priority wise) were created: Institute Building, Hostel (boys), Hostel (girls), Staff Quarters, Shopping areas, Telephones exchange, Information Processing Center, Banks, and Miscellaneous.

The second step was to decide on a unit area for each facility. This was decided based on the smallest possible unit that served as a center for that facility. For example, one hostel was considered as a unit. Using the simple 'Cut-Paste' option the areas with a particular facility was filled with rectangles of a particular color equal in size to the unit size of the facility. Each facility was coded with a different color (Figure 3).

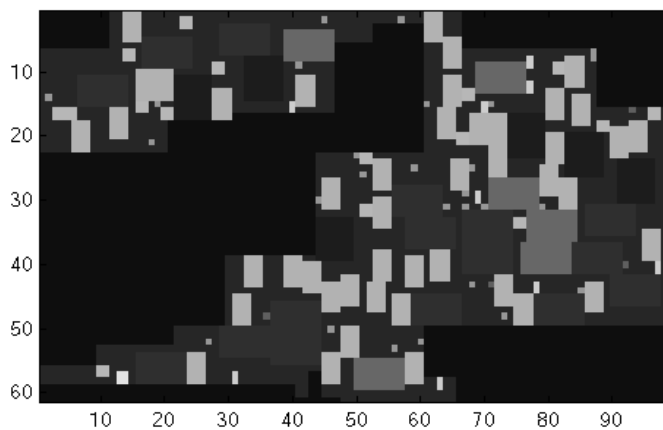


*Figure 2: Base map of BITS campus*



*Figure 3: Map after scaling, reclassification, and gray leveling*

The colors used were shades of gray. The area where construction was not allowed was filled with black, and the free areas were left white. The unit areas were stored in a separate image, which can be used as a reference file, later.



*Figure 4: Output map after implementation of 2D - EA algorithm*

### 3.1 Conversion to a two dimensional matrix

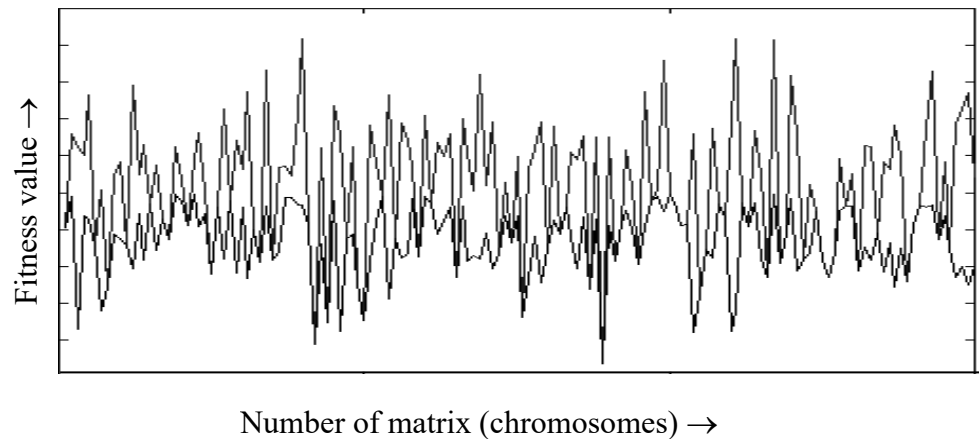
The image thus obtained is read and stored as a 3-dimensional matrix, with the elements in each containing the intensity values for R, G and B layers. For gray level images all these three elements are identical. The Red layer is chosen as a representative, and used for further processing. The original and transformed images are shown in Figure.2 and Figure.3 respectively. Once the gray level image has been read in as a two-dimensional matrix various operations of evolutionary algorithms can be performed on it as it can be treated as an ordinary matrix.

## 4.0 RESULTS

The 2D - EA was developed using MATLAB (MATLAB 1998). The results were stored as the fitness for successive generations. An example of

a sample output map is shown in Figure. 4. The dark blue/black areas indicate the 'no-facility' zones. The output is one of the maps generated after the 2D - EA was implemented. The computation time depends on Size of the image, Number of facility units, Number of iterations specified, and Crossover percentage.

The program was run many times to come up with suitable values for the number of iterations, crossover percentage, and extinction rate. In most of the cases the best results were obtained for crossover percentage less than 50% and close to 40%. The extinction rate was around 99% (implying that 1% of the unfit child vectors would survive without extinction). The output for crossover percentage of 0.45, 150 matrices, and 150 iterations is shown in Figure. 5.



*Figure 5: Output for crossover percentage 0.45, population's size 150, and 150 iterations.*

The graph shown above is for the starting and ending generations. It is clearly visible that the fitness becomes progressively better at the end of the iterations. For the results to converge, it is seen that larger population sizes with large number of iterations should be used. However, in such cases computation time is quite large. Computation time is reduced by increasing the number of iterations, and decreasing the population size and coefficient of crossover. This aspect needs further study, and experimentation.

## 5.0 CONCLUSIONS

The project is an attempt to adapt a traditionally one-dimensional concept to a two-dimensional environment. The results obtained are encouraging. It is observed that two-dimensional approach is more viable than the vector based genetic algorithms followed till now. One of the important application areas that the 2D - EA can be applied is on remote sensed images. Since the 2D - EA can be used directly, the need for compression and possibility of 'dimension crunch' (loss of information suffered when converting images to vectors) does not arise. Another advantage of the method is in process a number of feasible configurations of facilities locations are created that can be used for planning and development purposes. The method is applied with facilities of rectangular

shape. However, it can be applied to the facilities of any shape. The algorithm can be used to incorporate the new facility in existing system or to extend the facilities in near future. The technique is new and needs further study and analysis; this is a step in the paradigm shift from one to two and perhaps three dimensions.

## REFERENCES

- Francis, R.L., and White, J.A. 1974. *Facility Layout and Location*. Englewood Cliffs, NJ: Prentice-Hall.
- Holland, J.H. 1962. *Outline for a logical theory of adaptive systems*. J. Assoc. Comput. Mach., vol. 3, pp. 297-314.
- Karray, F., Zanelidin, E., Hegazy, T, Shabeeb, A.H.M., and Elbeltagi, E. 2000. *Tools of Soft Computing as Applied to the Problem of Facilities Layout Planning*. IEEE Trans. Fuzzy Syst. vol. 8, no. 4, pp. 367-379.
- MATLAB User's Manual*, Version 5.2 1998. The MathWorks, Inc., Natick, MA.
- Tompkins, J.A., and White, J.A. 1984. *Facilities Planning*. New York: Wiley.
- Whitehead, B, and Eldars, M.Z. 1965. *The planning of single-storey layouts*. In Building Sciences. New York: Pergamon, vol. 1, pp. 127-139.
- Yeh A G-O 1999. *Urban Planning and GIS*. In Longley P, Goodchild M, Maguire D, and Rhind D eds Geographical Information Systems: Management Issues and Applications'. John Wiley & Sons, Inc, USA.
- Zouein, P.P, and Tommelien, I.D. 1999. *Dynamic layout planning using a hybrid incremental solution method*. J. Construct. Engrg. Mngmt. ASCE, vol. 119, no. 2, pp. 266-287.

# **PEDESTRIAN SPEED-FLOW MODEL ON ESCALATORS AND STAIRCASES**

FOONG KOK WAI AND CHIN HOONG CHOR

National University of Singapore, Singapore

*cvefkw@nus.edu.sg*

## **ABSTRACT**

*Pedestrian flows in underground rail stations are usually heavy during the peak hours and could result in serious congestion, especially if the escalators, staircases and walkways, are not adequately built to cater to such a demand. During an emergency, it would also be safety hazard to the passengers. Maintenance of good speed and flow conditions in the station is essential to coping with emergencies.*

*This study was conducted to examine pedestrian flow characteristics at underground railway stations in Singapore. Video recordings of pedestrian movements were carried out in Somerset Mass Rapid Transit (MRT) Station in Singapore to collect volumetric flow data of pedestrians on staircases and escalators and their travel times on these facilities. The collected data is then used to calibrate speed-flow relationships for these two facilities. The study shows that the walking speeds at capacity were 23.0 m/min on the staircase and 2.8 m/min on the escalator approach. In addition, the parameters and forms of the relationships differ for working persons, shoppers and the elderly.*

## **1.0 INTRODUCTION**

Escalators and staircases are two of the main pedestrian facilities in an underground railway station, and should be well designed to ensure efficient and safe movement of pedestrians. Although these facilities are provided in Singapore's Mass Rapid Transit (MRT) stations, most of them were designed with referenced to non-local, or out-dated standards. No relevant studies have been conducted on the characteristics of pedestrians on these facilities either prior to, or after the commencement of the rail operation in 1987. Knowledge of the characteristics of pedestrian movements within the MRT stations could help in optimizing space use and result in more efficient and safer designs for pedestrians. Furthermore, with the recent security concerns relating to underground stations, there is an urgent need to evaluate the performance of these stations in times of emergencies. Maintaining an acceptable level of service within the stations during such occurrences would be critical in ensuring safe and efficient evacuation. These two issues have brought about the need to examine the characteristics of pedestrians along walking facilities in underground stations.

In an urban underground railway system characterized by large passenger flows and short train intervals, it is important to accommodate the expected demand so as to ensure the efficient operations of the system.



Fruin (1971) had highlighted a number of problems of using design "standards" in an ad hoc manner, such as using maximum pedestrian capacity, or stated operating capacity of an escalator, as a basis for design. The dense crowding of pedestrians, who need to resort to restricted and uncomfortable locomotion, is a typical result of a lack of understanding of the speed-flow relationships and space requirements of pedestrians. A better knowledge of the relationships can be useful to those involved in the design and operation of pedestrian facilities.

This study examines the relationships between speed and flow of single-directional pedestrian movements, which are the main type of flows in times of an evacuation from an underground station. The work involved includes the collection of pedestrian flow and travel time data on escalators and staircases in an underground MRT station in Singapore, followed by data analysis and model estimation. A number of mathematical relationships have been examined and tested for representation of such flow characteristics.

## **2.0 DATA COLLECTION**

Among the 65 operational MRT stations in Singapore, Somerset MRT station is one where the staircase in the station is relatively more utilized. This is because at this station, the staircase is the nearest facility from the entry gates connecting the concourse to the platform level. Furthermore, it observed that there is negligible pedestrian upward flow along the staircase, since the escalator in the upward direction is located just beside the staircase. The near single-directional flow on the staircase therefore coincides with the objective and scope of the study. The station, which is in the heart of Orchard shopping area, serves mostly working persons, shoppers and tourists.

A survey was carried out in 28 May 2003 during the evening peak hour and pedestrian data were collected on one escalator and one staircase at the station using two video cameras. Information on passenger flow, passenger travel time and the physical dimensions of the facilities were collected at the site. The travel time measurements included queuing time at the approaches as well as the time to travel on the facility, since the congestion at the approach to the escalator and staircase contributes significantly to the delay in travel time. A survey plan for data collection and the location of the cameras at Somerset MRT station is illustrated in Figure 1. Total sample sizes of 676 and 326 pedestrians were collected on the selected staircase and escalator respectively.

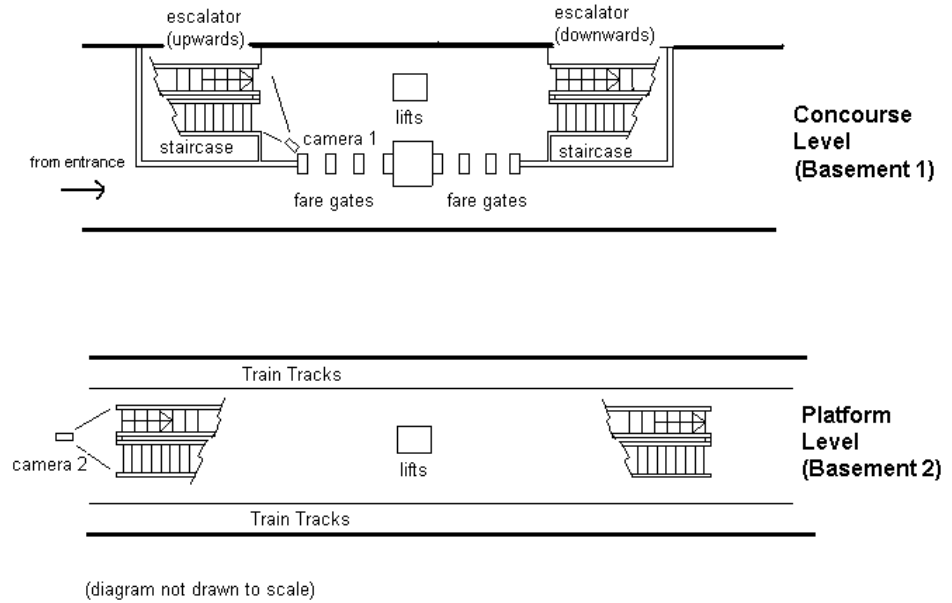


Figure 1: Survey plan of data collection at Somerset station

### 3.0 SURVEY RESULTS

#### 3.1 Observed flow capacity

From the video recordings, pedestrian flow and travel times to traverse the entire staircase or escalator were measured. The flows were measured by counting the number of pedestrian passing the exit of the facility within a 30-second interval. The capacity flow rate, which is assumed to take the value of the maximum flow rate obtained, is shown in Table 1. The travel times at each interval is calculated as the average of all pedestrians passing at that interval. In addition, the operating speed of the escalator is 45 m/min.

Table 1: Dimensions and flow characteristics of facilities.

	Units	Pedestrian Facilities	
		Staircase down)	Escalators (up)
Effective width	m	1.00	1.00
Inclined length	m	8.8	12.0
Approach length	m	2.0	2.0
No. of observations		676	326
Average speed	m/min	30.4	46.4
Observed flow capacity	/m/min	45.8	125.0

#### 3.2 Walking speeds

It was found that the mean speed for descending pedestrians on the staircase was 30.4 m/min. The males generally walked faster than the females on the staircase as their mean walking speeds were 31.3 and

29.3m/min respectively. The differences in walking speeds between the sexes were similarly observed by Tanaboriboon, *et. al.* (1986) and Lam, *et. al.* (1995). In addition, shoppers and the elderly and were found to have much lower walking speeds of 19.9 and 21.1 m/min respectively.

#### 4.0 SPEED-FLOW RELATIONSHIPS

A variety of mathematical relationships were examined to describe the relationships among speed, flow and density of the pedestrian data collected at the station. These functions includes speed-flow-density relationships that have been established for pedestrian flow (Virkler and Elayadath, 1994), as well as capacity-restraint travel-time functions that have been used extensively in vehicular flow, transport modeling and planning purposes.

##### 4.1 Flow-speed functions

Four speed-density functions, namely Greenshields' linear, Underwood's transposed exponential, Greenberg's modified exponential and May's bell-shaped curve, are tested against the pedestrian data. Recognizing that flow can be derived by multiplying speed with density, the corresponding flow-speed relationships for each of these functions can be derived:

$$\text{Greenshields: } V = \alpha S + \beta S^2$$

$$\text{Underwood: } V = \alpha S - \beta (S \ln S)$$

$$\text{Greenberg: } V = \alpha S \exp(-\beta S)$$

$$\text{May : } V^2 = \alpha S^2 \ln(\beta / S)$$

where  $V$  = pedestrian flow (ped/m/min),  $S$  = pedestrian speed (m/min)

##### 4.2 Capacity-restraint functions

Capacity-restraint techniques are based on the observation that as the flow on a facility increases, the speed decreases; and when the flow approaches the capacity of the facility, the rate of reduction in speed increases. They attempt to balance the volume on the facility, the capacity of a facility, and the related speed. There are flow-dependent travel time functions that utilize capacity-restraints, and have been applied in vehicular trip assignment for the prediction of travel times on road networks.

Staircases have similar characteristics as road networks in that their service levels are limited by some capacity-related restraints. For example, the capacity of a staircase is generally governed by its width, and the capacity of the escalator approach is influenced by the speed of the escalator and the boarding times of the pedestrians. It would thus appropriate to

employ capacity-restraint functions to describe the relationship between speed and flow for pedestrian movement.

Several speed-flow curves based on capacity-restraint have been used for the prediction of travel times on road networks. Some of the most used includes the functions by Overgaard (1967), Davidson (1966) and the Bureau of Public Roads, or BPR (1964):

$$\text{Overgaard: } t(V) = t_0 \exp[\beta(V/C)]$$

$$\text{Davidson: } t(V) = t_0 [1 + \beta V/(C-V)]$$

$$\text{BPR: } t(V) = t_0 + \beta(V/C)^n$$

where  $t$  = travel time (min) at flow  $V$ ;  $t_0$  = free-flow travel time (min);  $V$  = pedestrian flow (passenger/m/min);  $C$  = capacity of pedestrian facility (passenger/m/min); while  $\beta$  and  $n$  are parameters to be estimated.

The BPR function, which is probably the most widely used in vehicular flow analysis, was also employed by SATURN assignment model for the London Underground Station Congestion Model (Daly, et. al., 1991), and also by Lam and Cheung (2000) in a study of pedestrian flows in Hong Kong Mass Transit Railway (MTR) stations.

These travel time functions could be converted to speed-flow relationships simply by using the following equation:

$$S = l/t$$

where  $S$  = pedestrian speed (m/min);  $l$  = inclined length of facility (m).

The seven speed-flow functions described above would be tested against the pedestrian data on the staircase and escalator collected in the study. It is recognized that the speed at which a pedestrian moves along the escalator is generally constant. Thus for the case of the escalator, the walking speed at the approach of the escalator, denoted by  $S_A$  in this paper, would instead be modelled using the speed-flow functions.

## 5.0 MODEL RESULTS

Linear regression was used to calibrate the speed-flow models against the collected data. Nonlinear functions were reduced to linear forms, and functions with more than 2 parameters were estimated using sequential programming techniques. The regression results for the functions developed for each facility are discussed in turn.

## 5.1 Staircase

The results for the calibration parameters of the speed-flow functions for staircase in the downwards direction are displayed in Table 2. The field data are shown against the fitted flow models in Figure 2. All seven models satisfied the tests for significance of the regression at 95% level. The coefficient of determination, or  $R^2$ , for the models ranged from 0.28 to 0.54, with the Greenberg model exhibit the highest explanatory power. Using the calibrated Greenberg model, the free flow descending speed on the staircase would be 79.9 m/min, and the speed at capacity is 23.0 m/min.

Table 2: Speed-flow functions of staircases in Somerset MRT station

Model	Regression parameters			
	Equation	$R^2$	$S_e$	$p$ -value ( $F$ -statistic)
<b>Flow-speed functions</b>				
Greenshields	$V = 3.33S + 0.0929 S^2$	0.47	3.20	<0.01
Underwood	$V = 10.4S - 2.92 (S \ln S)$	0.50	0.0978	<0.01
Greenberg	$V = 260 S \exp(-0.21 S)$	0.54	2.99	<0.01
May	$V^2 = 4.23 S^2 \ln(32.5 / S)$	0.31	0.110	<0.01
<b>Capacity-restraint functions</b>				
Overgaard	$S = 35.7 \exp(-0.539 V/C)$	0.37	0.110	<0.01
Davidson	$S = 32.4[1 + 0.162 v/(C-V)]^{-1}$	0.28	0.0329	<0.01
BPR	$S = 8.80[0.174 + 0.191(V/C)^{0.37}]^{-1}$	0.39	0.0303	<0.01

It is noted that the values of the parameters obtained explained only the variability of the data collected in the survey. The parameters for these functions are dependent on factors such as types of pedestrian, time of day, and the design of the staircase. Pedestrians have different trip purposes and the difference would influence how and the speed at which they walk.

To investigate the influence of types of pedestrian on the forms and parameters of the speed-flow function, 3 pedestrian types were identified from the video data. Pedestrians rushing down on the crowded staircase and overtaking slower pedestrians were classified as Type I pedestrians. Type II pedestrians were identified as those who carried heavy bags with them, and those who appeared to be over 60 years old were classified as Type III pedestrians. These two types of pedestrians can also be described as “shoppers” and “elderly” respectively.  $T$ -tests conducted on these three pedestrian types showed significant differences in their walking speeds at 95% level. Table 3 shows the speed-flow functions calibrated for the three types of pedestrians and the calculated speed at free flow for each case.

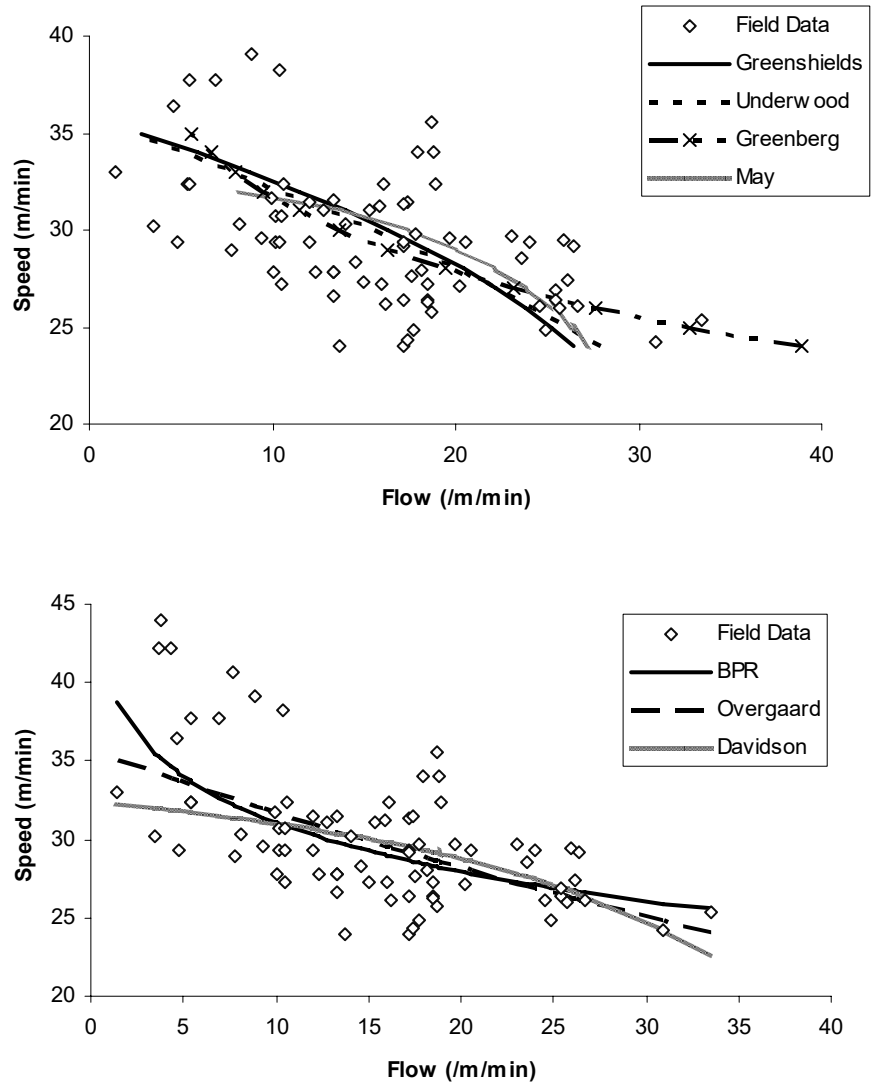


Figure 2: Pedestrian speed-flow plots of flow-speed functions (top) and capacity-restraint functions (bottom) for staircase

Table 3: Speed-flow functions for different types of pedestrian

Types of pedestrian	Best fit function	Speed at capacity (m/min)
All	Greenberg: $V = 260 S \exp(-0.21 S)$	79.9
Type I	Greenberg: $V = 8.25 S \exp(-0.081S)$	180.5
Type II	Greenberg: $V = 413 S \exp(-0.24 S)$	73.6
Type III	Greenshields: $V = 3.89S + 0.124 S^2$	31.3

Type I pedestrians are typically workers going to work in the morning who tend to be in a rush, especially when they notice their trains are standing at the platform. Conversely, Type II pedestrians tend to walk slower as compared to working persons as they usually carry heavy bags with them. They are not restricted by time constraints, or are simply sluggish after sometime of shopping. They also tend to shop during off-peak hours where the shops and the MRT trains are less crowded. Of the three

pedestrian types, only the Type III pedestrian fitted a Greenshields model, which produces relatively lower speeds at low flows. This is typical of the elderly, whose walking speeds are usually limited by their physical capability. The variability in walking speeds of different types of pedestrians has shown to affect the parameters of the speed-flow functions.

In addition, the design of the staircase would also affect walking speeds. Generally, a staircase that is poorly-designed would give rise to lower walking speeds. For example, staircases with high risers (Lam, *et. al.*, 1995), narrow treads, as well as long flight of steps would tend to render walking more difficult and slower. Conversely, the provision of appropriate handrails, intermediate step landings and visible markings on the edge of each step would allow pedestrian to walk easier and faster.

## 5.2 Escalator

Table 4 shows that the speed-flow models of the escalator approach displayed a higher explanatory power as compared to that for the staircase. Similar to the staircase models, the Greenberg model produces the best fit for the escalator approach, with a  $R^2$  value of 0.69. Figure 3 displays the variations of pedestrian speed and flow data for the escalator approach, as well as the fitted speed-flow models. The free flow speed on the escalator approach is calculated to be 24.6 m/min, and the speed at capacity is 2.8 m/min.

Table 4: Speed-flow functions of escalator approach at Somerset MRT station

Model	Regression parameters			
	Equation	$R^2$	$S_e$	$p$ -value ( $F$ -statistic)
<b>Flow-speed functions</b>				
Greenshields	$V = 19.0S + 1.92 S^2$	0.60	1.92	<0.01
Underwood	$V = 31.0S - 13.6 (S \ln S)$	0.63	0.229	<0.01
Greenberg	$V = 272 S \exp(-0.66 S)$	0.69	1.70	<0.01
May	$V^2 = 182 S^2 \ln(8.61 / S)$	0.41	0.258	<0.01
<b>Capacity-restraint functions</b>				
Overgaard	$S = 10.0 \exp(-0.675 V/C)$	0.52	0.278	<0.01
Davidson	$S = 6.49 [1 + 0.0007 V/(C-V)]^{-1}$	0.03	0.121	<0.01
BPR	$S = 2.0[0.223 + 0.183(V/C)^{1.9}]^{-1}$	0.52	0.0828	<0.01

The observed capacity of the escalator of 125 ped/m/min was only 56 per cent of the design operating capacity. The design capacity assumes an occupancy value of 5 ped/m<sup>2</sup> on the escalator, but it was not achieved even during very congested periods as passengers were not occupying gaps on the escalator. This could be because the pedestrian may desire to have a more comfortable personal space and does not want to be too near the other pedestrian in front of him.

As noted earlier, the parameters of the speed-flow function is influenced by the nature of the pedestrians. The earlier assumption of constant speed on the escalator will no longer be valid if a substantial number of pedestrians walk along the escalators. Unlike the staircase, the differences in walking speeds for different types of pedestrian were not significant due to the short length of the escalator approach.

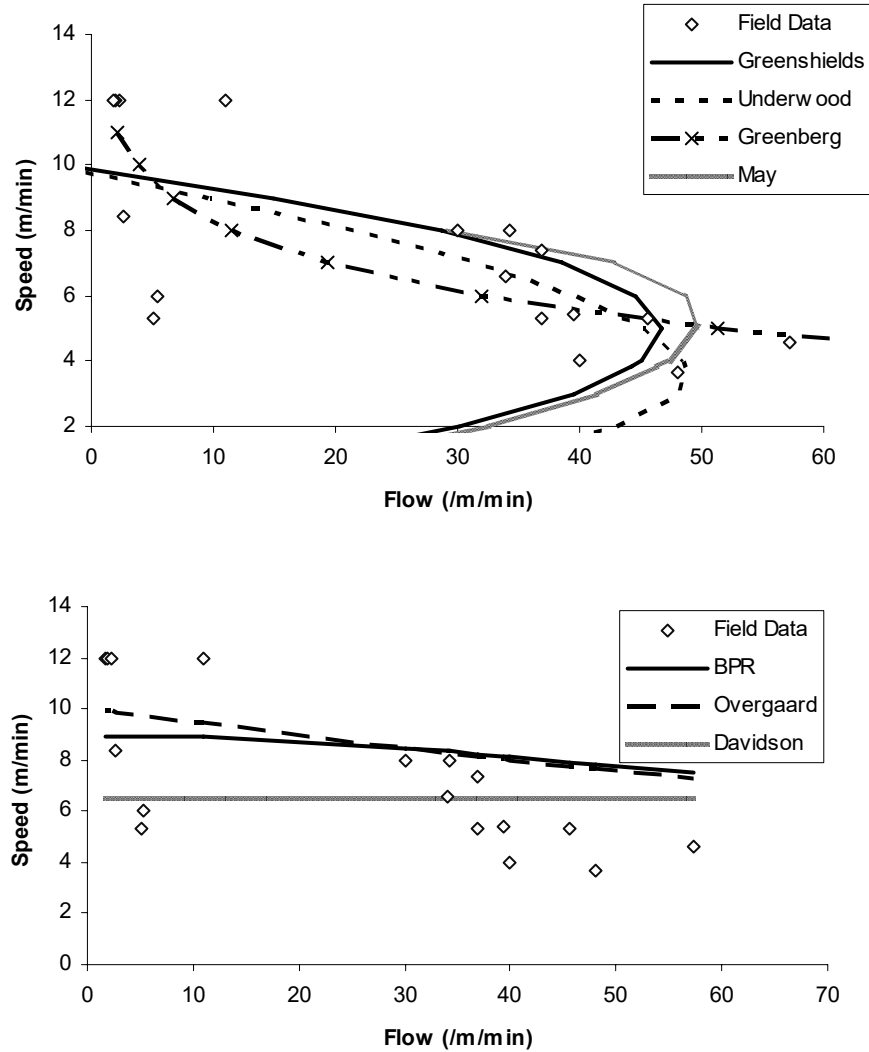


Figure 3: Pedestrian speed-flow plots of flow-speed functions (top) and capacity-restraint functions (bottom) for escalator approach

## 6.0 CONCLUSIONS

This paper has examined the pedestrian flow characteristics along a staircase and an escalator approach in a MRT station in Singapore. Pedestrian flows on both the staircase and the escalator approach are best represented by a Greenberg's speed-flow model. It was found that the free flow walking speeds on the facilities were 79.9 and 24.6 m/min, and the walking speeds at capacity are 23.0 m/min and 2.8 m/min respectively.



It is shown that the parameters of the model are dependent on pedestrian characteristics and facility designs. The fact that no single model is able to fit all pedestrian facilities and types of pedestrians, indicates that there are some areas where further work could be carried out, including more data collection for larger range of flow conditions, as well as estimation of models for other pedestrian facilities such as walkways and junctions. Such works would increase the scope and depth of the research. It is believed that the findings of the paper could provide some insight in pedestrian movements in underground stations that is useful for operational or emergency planning purposes.

## ACKNOWLEDGEMENT

The authors wish to thank SMRT Corporation Limited for its support and cooperation during the survey at Somerset MRT Station.

## REFERENCES

- Bureau of Public Roads (BPR), 1964. *Traffic assignment manual*. Urban Planning Division, U.S. Department of Commerce, Washington, D.C.
- Daly, P.N., McGrath, F. and Annesley, T.J., 1991. *Pedestrian speed/ flow relationships for underground stations*. Traffic Engineering and Control 32, 75-78.
- Davidson, K.B., 1966. *A flow travel time relationship for use in transport planning*. Proceedings Australian Road Research Board 3, 183-194.
- Fruin, J., 1971. *Pedestrian planning and design*. Metropolitan Association of Urban Designer and Environmental Planners, Inc., New York.
- Lam, W.H.K. and Cheung, C.Y., 2000. *Pedestrian speed/ flow relationships for walking facilities in Hong Kong*. Journal of Transportation Engineering 124, 277-285.
- Lam, W.H.K., Morrall, J.F. and Ho, H., 1995. *Pedestrian Flow Characteristics in Hong Kong*. Transportation Research Record 1487. Transportation Research Board, National Research Council, Washington, D.C.
- Overgaard, K.R., 1967. *Urban transportation planning: traffic simulation*. Traffic Quarterly 21, 197-218.
- Tanaboriboon, Y., Sim, S.H. and Chin, H.C., 1986. *Pedestrian characteristics study in Singapore*. Journal of Transportation Engineering 112, 229-235.
- Virkler, M. and Elayadath, S., 1994. *Pedestrian speed-flow-density relationships*. Transportation Research Record 1438. Transportation Research Board, National Research Council, Washington, D.C.

# TELEOPERATED SURVEILLANCE ROBOT

H. JAYARAM, M. VINOTH AND P. RAGHURAM

Department Of Mechanical Engineering  
Amrita Institute of Technology, Coimbatore, India  
*jayvin\_project@yahoo.co.in*

## ABSTRACT

*“Technology makes mistakes and tries to correct them”. Man started the industrial revolution, it resulted in betterment of his life standards in one aspect, but on the other hand it also resulted in hazardous Global warming and Green house effect. Man made weapons of Mass destruction, which threaten the existence of the world itself. The important question is that can we just stop everything and get back to primitive ways of life. The answer would definitely be NO. The thing we can do is reverse Engineer the Problem and try to minimize its impact or find an alternative solution for the problem. The ultimate aim of this project is to find in a small way an alternative solution so that man can evade himself from the effects that he caused for himself.*

*Tele-operated surveillance Robot was designed with keeping in mind to counteract the hazards caused by chemicals. The Robot is a mobile independent unit with toxic gas sensor attached to its end so that it keeps us informed about possible gas hazard. There is a surveillance camera attached to it so that the operator could see around the place. The Robot is controlled by the computer through wireless network. As additional feature the Robot is made Tele-operated, i.e., the operator can control the Robot via the Intranet from a remote location.*

## 1.0 INTRODUCTION

We know that more than half of the total population of the world resides in Mega cities. Most of the major industries are situated in and around big cities of the world. This may be good in socioeconomic point of view but has negative impact on the society as a whole by the advent of pollution and other hazards. Chemical and biological hazards are the newer threats that are poised to mankind. The classic example is that of Bhopal Gas tragedy, a lethal gas (methyl isocyanate) leaked from a chemical factory causing the death for more than 3000 people in the wake of the midnight. The strategy that would have prevented the tragedy was simple; Methyl Isocyanate is highly hygroscopic gas when it comes into contact with water it readily dissolves. Many lives could have been saved by a simple technique of warping wet cloth around the face. The problem was the absence to an alarming device to indicate the leakage of the toxic gas.

The Tele-operated surveillance Robot's main function is to survey an area and warn people the presence of toxic. The use of chemical weaponry in warfare is becoming increasingly common, in such instances this Robot

could be used to inform the soldiers of the possible lethal gas presence. The ultimate aim of the project is surveillance in hazardous environments. The Robots could be Tele-operated so the operator can control the Robot from any place over the Network.

## **2.0 DESIGN ARCHITECTURE FOR THE ROBOT**

The design of the Robot is the most important part project. The performance of the Robot is entirely dependent design of the Robot. The design phase of the Robot can be classified into two sub phases.

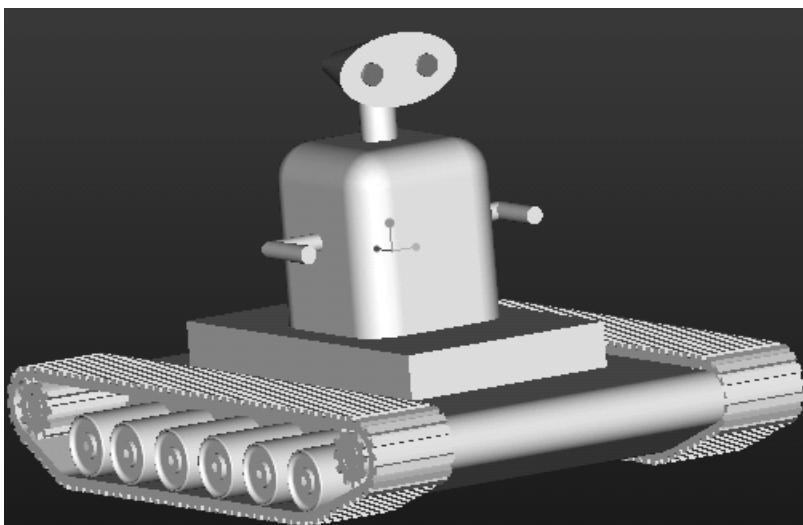
- Navigation system
- Robot body

### **2.1 Navigation system design**

There were certain constraints that were kept in mind while deciding of the navigation system, like movement in rugged uneven terrain's, and harsh environments. There are various options that were available for choosing of navigating the Robot like wheeled Robot, legged Robots, serpentine Robots, and aerial Robots etc. The best-suited navigation system for our application was the wheeled Robots with tracks so that it is gives high traction and capability of moving in rugged terrain. So the base of the Robot was designed in a similar way to military tanks with tracks.

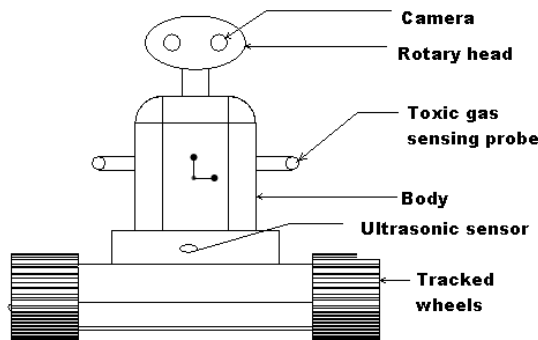
### **2.2 Robot body**

The body for the Robot houses the drive motor circuitry and the sensor circuitry and also the toxic gas-sensing probe. The surveillance camera is mounted on the independent rotary head of the Robot.



*Figure 1: 3D Model of the Robot*

An on-board camera, connected to the server through the video transceiver, is placed on the front-top of the mobile robot in order to give the



*Figure 2: Front View of the Robot*

user a clear view of the environment in front of the robot. The video signal from the camera is transmitted to the host computer through USB port.

The toxic gas sensing probes are attached to the body of the Robot as shown in figure. The body of the Robot also houses the battery for supplying power to the actuators, sensors and also the camera. There are various compartments on which the various circuitries like the WI-Fi circuitry and motor drive circuits are placed.

### **3.0 ACTUATORS**

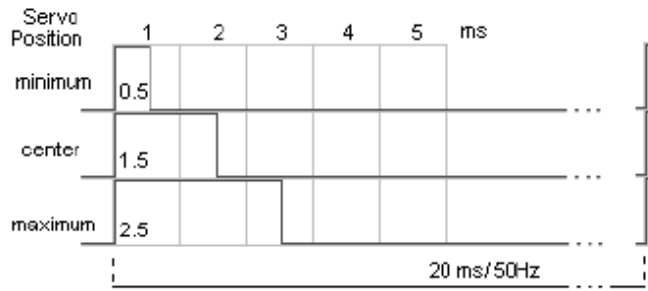
There are many types of actuators that are available for the driving of the motors like the hydraulic actuators, pneumatic actuators etc. The problem with these types of actuators is that they are large, complex and difficult to maintain. Most of the mobile Robots around the world use Electric motors because of the simplicity in installation and control.

In our Robot we have used three hobby servomotors one for the rotary head mountings and the other two are for the independent wheels. The servos has a three wire connection, one for common ground, one for power and the last takes in position commands as encoded PWM (Pulse width modulation- a fixed square wave with variable work factor where a given work factor percentage corresponds to given shaft position). Closed loop position control is in-built in the servo package.

Controlling the position of the actuators is a simple by implementing electronics system whose inputs correspond to suitable square waves in outputs (Fig 3)

#### **3.1 Control electronic for actuators**

The electronics to drive the servomotors are simple and include an voltage regulator (5-15V dc), a power on LED with respective current limiting resistor and the heart of the PWM generating circuit; a PIC16F84A controller from microchip with minimal peripheral electronics (20 MHz



*Figure 3: PMW signals to control the position of Servo motor*

crystal and condensers of the clock signal as well be describe, the use of lower frequency crystals is also possible but this will decrease the position control resolution).

The basics role of the PIC controller is to accept serial data sent by any serial device (typically a computer) and converting that information into PMW position commands for a given (selected) servomotors. Further more the PMW command should be held until another command for the same servo is received.

There are 12 servo outputs available at ports PB0 through PB7 and PA0 through PA3 of the PIC16F84A. The controller needs two bytes of information for each position command, one byte is for the selection of the servomotor (the address byte) and the other specifies the position of the selected servomotor (position byte).

## 4.0 MULTISENSOR SYSTEM

The important factor in Tele-operation is that the Robot must have high degree of local intelligence to deal with the problems caused by low bandwidth and transmission delay of the Intranet. Baseline to achieve the local intelligence desired at the remote site by knowing about the environment; therefore the Robot is equipped with various sensors. The ultrasonic sensors and toxic gas sensors are used on our Robot to attain partial autonomy. The information reported to the operator is mainly of symbolic feature and are indispensable for Tele-operation.

### 4.1 Ultrasonic sensors

Around the base portion of the Robot, array of ultrasonic sensors are placed. The feature of this Ultrasonic sensor system is its flexibility to be operated in different measurement modes. The activation of the sensors can be altered on line. The purpose of mounting this sensor is obstacle avoidance. The obstacle is detected in advance so that the operator can maneuver the Robot to avoid collision.

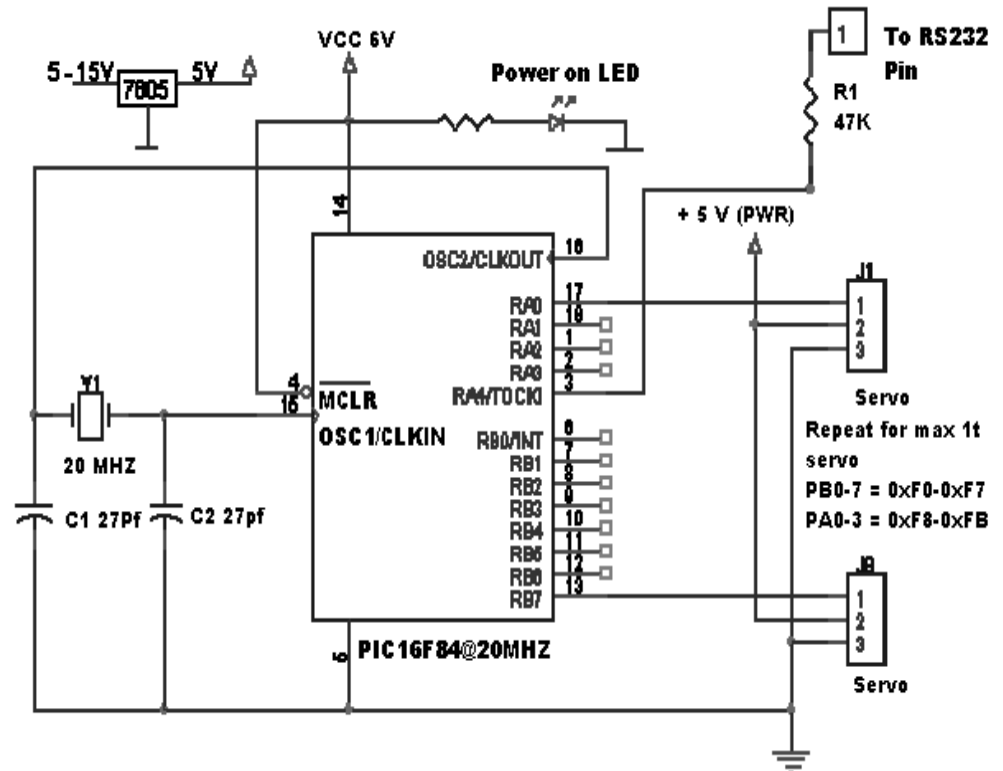


Figure 4: Control electronics for Robot's actuator

## 4.2 Toxic gas sensing

A commercially available toxic gas sensor is mounted on the Robot. The two sensor probes are mounted on each of the arm. The sensors are operated by independent the battery unit. The sensor signals are transmitted to the computer via RS232 serial port.

## 4.3 Active vision system

The visual surveillance of the remote location is brought about with the help of CCTV camera. The camera is mounted on the Rotary head that the operator can control.

## 5.0 HARDWARE ARCHITECTURE

The architecture we follow is client-server wherein the robot is connected to a central server, which can be accessed by the client user from a remote location. The configuration of our current system hardware is shown in Fig. The remote client will be able to control the movement of the Robot as well as receive the sensor input from the ultrasonic sensor and the toxic gas sensor thro' the LAN cable. The interface between the Server computer and the Robot is by wireless serial port so that the Robot will be able to move independently.

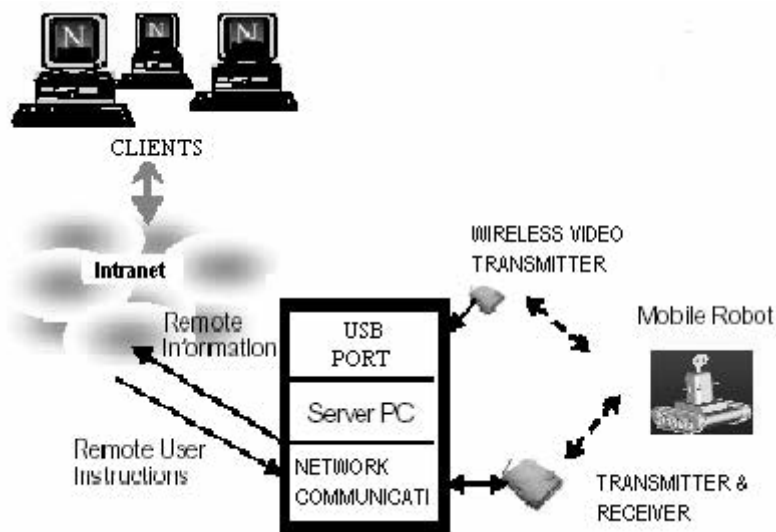


Figure 5: Hardware Architecture

### 5.1 Visual feedback module

The continuous and steady image stream feedback from the robot site is necessary when the client users control the mobile robot at the client site. Moreover, the image quality should be good enough to provide as much information as possible about the remote site for Tele-operation. An on-board camera, connected to the server through the video transceiver, is placed on the front-top of the mobile robot in order to give the user a clear view of the environment in front of the robot. The video signal from the camera is transmitted to the host computer through USB port.

The transmission of video images through the intranet is done by converting the camera image into a stream of still images of JPEG or the GIF format. In the system, the images are captured from the frame grabber based on the bt848 chipset and compressed to JPEG format by software implemented in C++. Then still images are sent at fixed intervals of time and on the client side the reconstruction of the image takes place once the entire frame is received and displayed.

## 6.0 SOFTWARE ARCHITECTURE

As already mentioned, the Robot is computer controlled, the actuation signals to the on-board control a circuit is done by giving signal via the serial port. Software must be developed to control the motion of the Robot and also display the video image and sensor input.

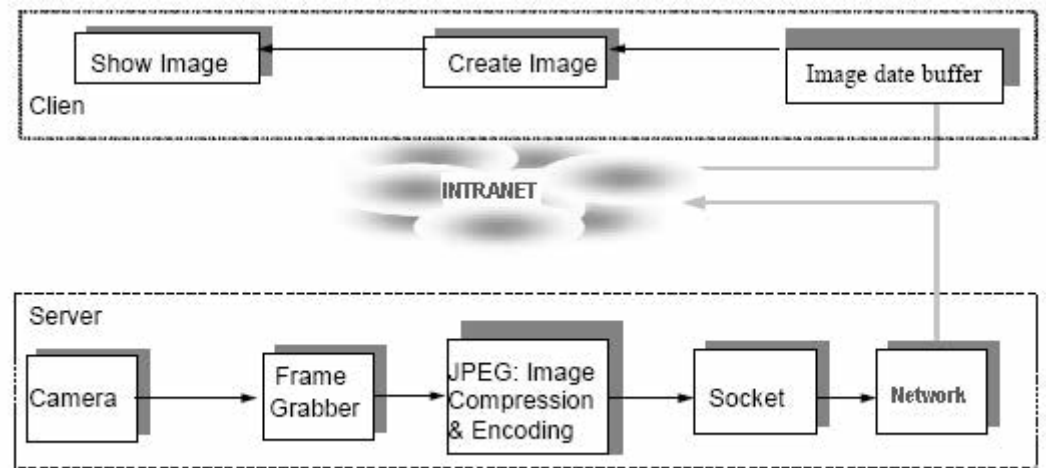


Figure 6: Video Transmission

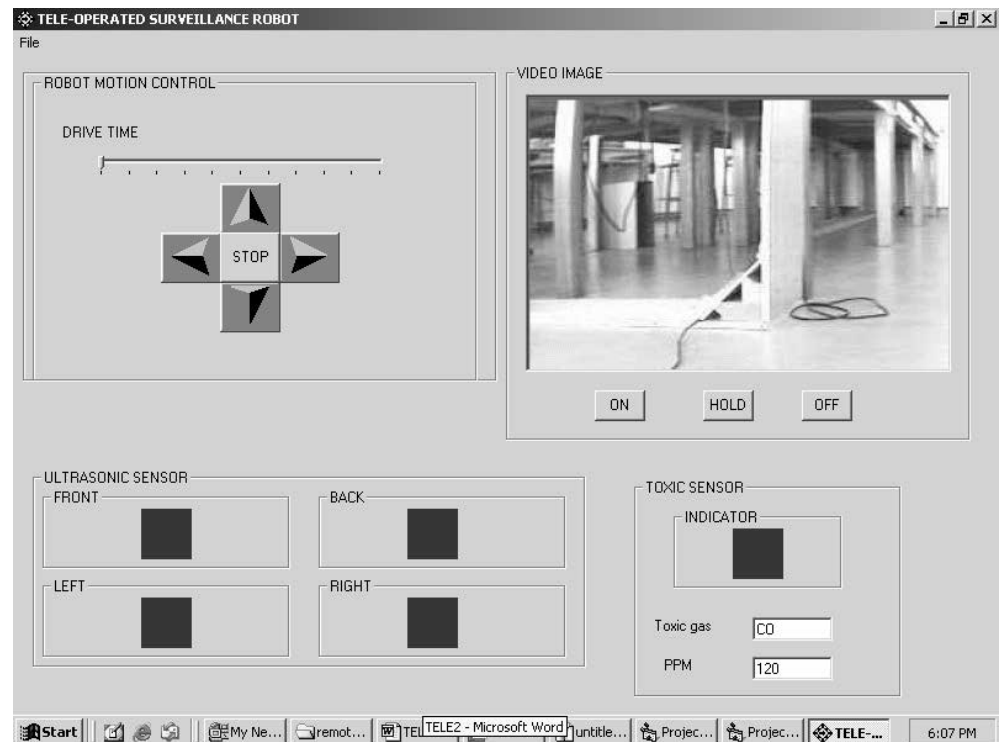


Figure 7: Graphical User Interface

## 6.1 Graphical user interface

Since a Tele-robotic system involves the interaction between humans and robots, a friendly user interface is necessary to assist the human operator. A user friendly GUI was created using Visual Basic which will incorporate, Robot motion control module, Video input and the sensor input.



## 7.0 CONCLUSION

Man cannot work in hazardous environments; in that case it is possible to him to use Robots for doing the intended work. The Tele-operation of Robots means that the controller need not be at the site of the operation, which is dangerous. The application of Robots to in Urban Search and Rescue (USAR) is now quite a common. Similarly this Tele-operated Robot in future will play a vital role in the future for urban safety. The current intended application of toxic gas detection is very vital to prevent mass disasters like that of the Bhopal gas tragedy. The further work involves in making the Robot completely autonomous and multi-purposed such a fire detection, material handling etc. The Robot could be put on the Web so that the operator can control the Robot from any part of the world.

## REFERENCES

- Andreas Birk and Holger Kenn.,2002. RoboGuard, *A Teleoperated Mobile Security Robot, Control Engineering Practice*. Volume 10, no 11, pp.1259-1264, Elsevier.
- Michael Wandel, Udo Weimar, Achim Lilienthal, Andreas Zell.,1998. *Leakage localization with a mobile robot carrying chemical sensors*.
- L. Feng , J. Borenstein , D. Wehe.,1996. *A completely wireless development system for mobile robots*. Proceedings of the ISRAM Conference, Montpellier, France.
- Donny A. Ciccimaro, H.R.Everett,Gillbreath,G.A.,Tran, T.T.,1998. *An Automated Security Response Robot*. SPIE mobile Robots XIII, Boston, MA.
- Ronald Siegwart, Patrick Saucy., 1999. *Interacting mobile robots on the Web*. ICRA'99,Detroit, MI, USA.
- Everett,H.R., 1995. *Sensors for Mobile Robots: Theory and application*. A.K. Peters Ltd., Wellesley, M.A

# **ICUS AND AIT COLLABORATION ON URBAN SAFETY RESEARCH**

DUSHMANTA DUTTA<sup>1,2</sup> AND TAKETO UOMOTO<sup>2</sup>

<sup>1</sup>RNUS, SCE, Asian Institute of Technology, Thailand

<sup>2</sup>ICUS, IIS, University of Tokyo, Japan  
ddutta@ait.ac.th

## **ABSTRACT**

*Over half of the world's population is concentrated in urban areas covering just 4% of the world's surface. Mega cities in particular are characterized by a high population density and tremendous pressure on supporting infrastructure. It is estimated that by 2015, Asia will be host to more than 50% of the mega cities in the world. A phenomenal growth in the number of high-rise buildings and other infrastructure in these cities is clearly foreseen, though a balance is often not ensured with measures for their maintenance.*

*Safety of infrastructure is foremost important for sustainable urbanization and economic development in Asia. With this realization, on October 29, 2002 the International Center for Urban Safety Engineering (ICUS) of the Institute of Industrial Science, the University of Tokyo, Japan and the School of Civil Engineering of the Asian Institute of Technology established a Regional Network Office for Urban Safety (RNUS) to promote and enhance high quality cooperative research in areas related to urban safety in Mega cities of Asia and to nurture scientists of international stature and achievements. This paper presents the collaborative activities initiated by AIT and ICUS through RNUS for urban safety in the South and South-east Asian region.*

## **1.0 INTRODUCTION**

With the rapid economic development in the last few decades, there has been a phenomenal growth of high-rise buildings and other infrastructure in mega cities in Asia. However, this growth in infrastructure is not adequately balanced in appropriate measures for their maintenance and management. This has led to deterioration of urban infrastructures and resulted in urban disasters in many cities. Recently, the issue maintenance of urban buildings and infrastructure in Japan has been sensationalized by mass media after several incidents of falling blocks from concrete structures, such as bridges and tunnels in different parts of Japan (Larimer, T., 2000). The frequency of floods in Asia has doubled in the last 30 years. The rate of increase of urban flood frequency is more prominent in the last 10 years, especially, in the recent three years statistics show rapid increase of floods in Asian cities (Dutta, 2003). Kobe Earthquake disaster of 1995 clearly showed the vulnerability of our cities against earthquake disasters.

The recent developments in various advanced technologies including remote sensing, GIS and other computational tools have generated scope and motivation to focus on devising appropriate methodologies for management and maintenance of urban buildings and infrastructures for sustainable development of the Asian mega cities with adequate safety and security.

The International Center for Urban Safety Engineering (ICUS), a research center located at the Institute of Industrial Science of the University of Tokyo, Japan, focuses on research and developments in the field of urban safety engineering including maintenance and management of infrastructures with new technologies from a global perspective. ICUS emphasizes on collaboration in research with international organizations particularly in Asian region. To strengthen its collaborative research efforts, there have been several activities undertaken by ICUS (Dutta and Uomoto, 2002; Misra and Kato, 2003). One of the most significant steps for expanding its collaborative activities is the establishment of a Regional Network Office for Urban Safety (RNUS) in Thailand. RNUS was established on October 29, 2002 at the School of Civil Engineering (SCE) of the Asian Institute of Technology (AIT) to work in areas of mutual interest of SCE and ICUS for the advancement of urban safety engineering utilizing advanced engineering tools. AIT is a regional international and non-profit institute with the vision of becoming a leading and a unique regional multicultural institution of higher learning, offering state of the art education, research and training in technology, management and societal development. ICUS and AIT signed an agreement towards developing joint research programs and to cooperate in developing strategies for tackling issues related to urban safety through RNUS (Photo 1).



*Photo 1: Opening ceremony of RNUS at SCE/AIT*

RNUS focuses on collaborative research activities with different organizations in Asian countries in areas of urban safety engineering with advanced technology tools such as numerical models, remote sensing, GIS, GPS, etc. for devising appropriate methodologies for management and maintenance of urban buildings, infrastructures, mitigation of urban disasters and environmental problems for sustainable development of Asian cities with adequate safety and security.

## **2.0 OBJECTIVES OF RNUS**

Through RNUS, SCE and ICUS work together for:

- advancement of urban safety engineering utilizing advanced engineering tools,
- establishment of collaborative research activities with other organizations in areas of urban safety engineering in Asian region, and
- establishment of a regional network of researchers for sharing information and resources in the field of urban safety engineering.

## **3.0 FUNCTIONS OF RNUS**

RNUS spearheads initiative of collaborative research projects with researchers from Thailand and other Asian countries and sharing of information through the following activities.

- Fundamental Research
- Collaborative Research Projects
- Information Dissemination  
(Meetings/Seminars/Workshops/Symposia/  
Conference/Publications)
- Network of Researchers
- Exchange of Staff

## **4.0 HIGHLIGHTS OF RECENT ACTIVITIES**

Since its inception, RNUS has undertaken several activities including collaborative research projects with researchers of AIT and other organizations in Asia, seminars and workshops.

### **4.1 Collaborative research projects**

With the support of ICUS, two pilot projects were initiated by RNUS in Bangkok, Thailand immediately after its establishment. In the past year, RNUS has received funding from different international organizations for conducting collaborative research projects. This section briefly introduces the on-going research projects at RNUS.

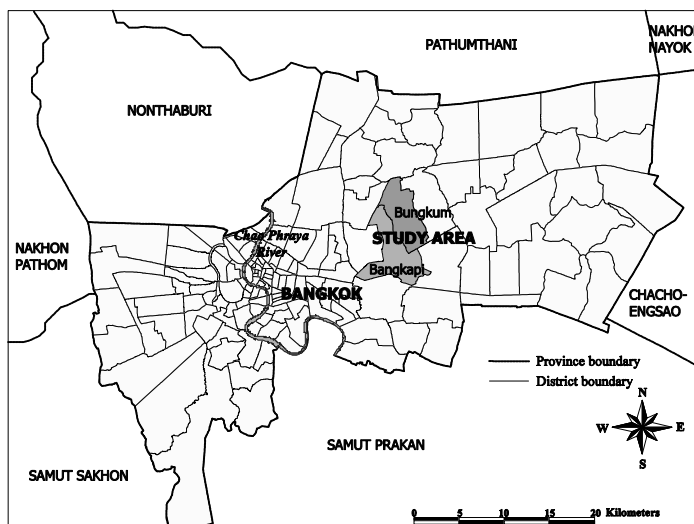
#### ***4.1.1 Development of database for deteriorated concrete bridges***

This is one of the two pilot projects initiated by RNUS in collaboration with the researchers, scientists and engineers of Thailand as a start-up

activity of the center. The participatory organizations in this project are RNUS, ICUS and the Thammasat University, Thailand. Under this project, a database for deteriorated concrete Bridges in Bangkok has been developed. The databased provides detailed information of bridges under the superintending of Bangkok Metropolitan Authority (BMA) including name, location, type of structure, dimension of structure, year of construction, etc., in order to subsequently create GIS of bridges in Bangkok for operation, repair, and maintenance of the structure (Tangtermsirikil, et al., 2003; Kato, et al., 2003).

#### ***4.1.2 Urban flood risk mapping using GIS, RS and mathematical model***

This is the second pilot project initiated by RNUS. The organizations involved in this project are RNUS, ICUS, AIT, Chulalongkorn University, and GISTDA (Geo-Informatics and Space Technology Development Agency, Thailand). Two of the most frequently flood affected districts of the Bangkok Metropolitan area are selected as the study area of this pilot project. The selected districts are Bangkapi (Area: 28.5 km<sup>2</sup>, population: 0.143 million) and Bungkum (Area: 24.3 km<sup>2</sup>; population: 0.137 million), both are adjacent districts located in the eastern side of the Bangkok City (Fig. 1). The project consists of three components; 1) development of flood loss functions for economic loss estimation; ii) development of urban building and infrastructure inventory and iii) flood modeling using a distributed flood model. Flood risk maps can be developed by integrating the outputs of these three components. The first two components of the project have been already completed (Dutta and Tingsanchali, 2003; Dutta and Serker, 2004).



*Figure 1: Location map of the study area*

#### ***4.1.3 Urban flood modeling in mekong river basin***

This is a research project that aims at developing a system for urban flood inundation simulation in the Lower Mekong river basin. The project mainly focuses on physically based surface-river modeling for flood inundation simulation. The system has been developed with the objective of integrating it with airborne and space borne resources and numerical weather prediction models for designing an integrated flood warning system. An existing mathematical model has been modified and improved for flood modeling in the lower Mekong basin. The details of the project are presented by Dutta et al., 2004 in this symposium and included in this proceedings.

#### ***4.1.4 Socio-economic impact assessment of floods in coastal cities under climate change***

RNUS receives an award from the Asian Pacific Network on Global Change (APN) to conduct a research project titled "An Assessment of the Socio-economic Impacts of Floods under Climate Change Conditions in Large Coastal Cities in South and South-east Asia". The project focuses on understanding the flooding characteristics under projected climatic and socio-economic scenarios. It will integrate and analyze existing data, information and results and use existing tools for simulating the flood behavior and impacts. The project scope is limited to selected low-lying large cities of the participating countries: Bangladesh, India, Pakistan, Sri Lanka, Thailand and Vietnam. One city from each country is identified based on their representativeness for the study. The research also focuses on identifying critical gaps in information and policy and a set of recommendations will be made for better decision making to improve the livelihood of the local people. The project duration is one year. Figure 2 shows the approach and possible outcomes of this project.

#### ***4.1.5 Risk analysis due to catastrophic floods in mega cities***

RNUS receives a sponsored research project grant from the United Nations University (UNU) for conducting this research project on "Risk Analysis due to Catastrophic Urban Floods using GIS, Remote Sensing and Surface-River Model". In this project, RNUS will conduct a case study in Bangkok city for risk analysis due to catastrophic urban flooding. The work covers simulation of catastrophic floods due to extreme rainfall events and assessment of its socio-economic impacts using an existing urban flood risk assessment model in a part of the Bangkok city, which is most vulnerable to floods. Risk maps will be prepared using GIS for the simulated catastrophic flood events for existing socio-economic situation. The 15-month long project is started from September 2004.

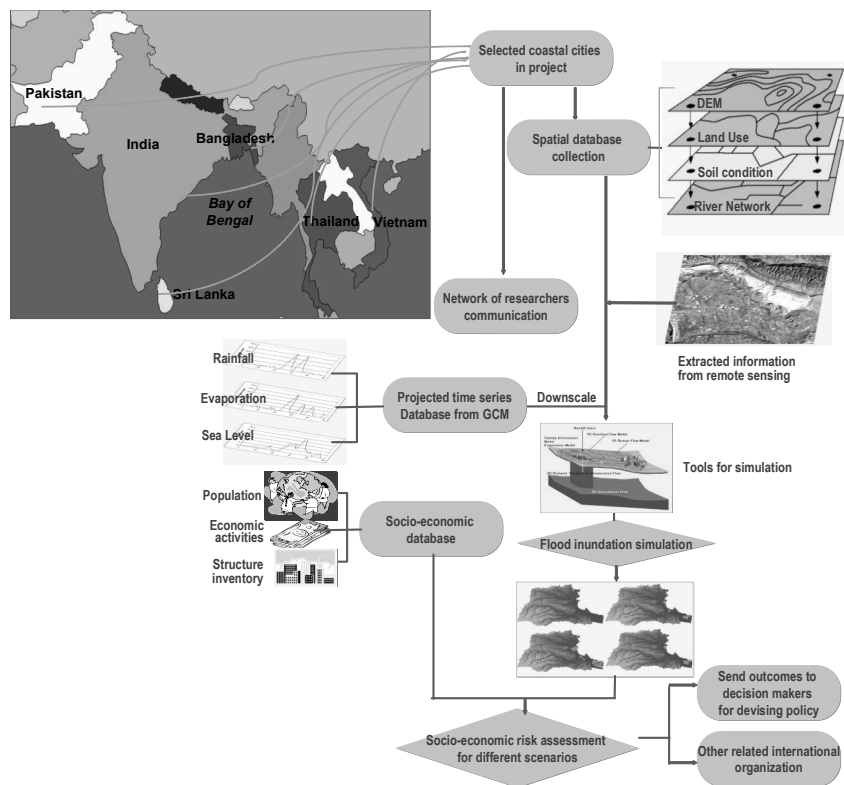


Figure 2: Approach and expected outcomes of APN funded project

#### 4.1.6 Real-time flood forecasting and decision-making system for Chao-Phraya river basin, Thailand

RNUS collaborates with the Water Engineering and Management Field of Study of SCE, AIT for this two-year long period project on "Development of Real-time Flood Forecasting and Decision-Making System of Chao-Phraya River Basin, Thailand" funded by NECTEC, Thailand. In this project, a real-time flood forecasting and decision-making system will be developed for the Chao-Phraya River Basin, Thailand by integrating a physically based distributed hydrological model developed at the University of Tokyo and a hydro-dynamic model for floodplain developed at AIT.

## 4.2 Information dissemination

RNUS has been organizing academic seminars at AIT in regular interval by inviting prominent researchers on various issues related to urban safety. It has also organized two workshops.

### 4.2.1 Seminars

So far, RNUS has organized six seminars on different themes related to urban safety at AIT. Table 1 shows the seminar titles, speakers and dates.

#### **4.2.2 Workshops**

##### ***a) Workshop on collaboration between yamanashi university, japan and research organizations in thailand***

RNUS assisted the University of Yamanashi, Japan in organizing activities of the Workshop on “Collaborative Research and Education Program of the University of Yamanashi COE with Thai Organizations and AIT” that was held on 25 November, 2003 at the Conference Center of AIT. The objective of the workshop was to establish a strong tie for research collaboration between the University of Yamanashi, Japan and various water-related Thai organizations associated with AIT. Several experts from AIT and Thai organizations presented papers on hydrology and water resources in Thailand, water use management, water quality and solid waste management, among other topics.

*Table 1: Seminars organized by RNUS*

No.	Seminar Title	Speakers (Affiliation)	Date
1	Water Resources in the 21st Century under Climate Change Scenarios	Dr. T. Oki, Dr. S. Kanae and Mr. K. Yoshimura (University of Tokyo)	Nov. 14, 2003
2	Applications of Hyperspectral Remote Sensing	Dr. T. Endo (University of Tokyo)	Feb. 24, 2004
3	Remote Sensing from Local to Global Scale: Catering the Need of The 21 <sup>st</sup> Century	Prof. Y. Yasuoka (University of Tokyo) and Dr. D. Dye (Frontier Research System for Global Change, Japan)	Feb. 27, 2004
4	Numerical Models in Fluid and Their Applications	Dr. K. Nakayama (National Institute for Land and Infrastructure Management, Japan)	Mar. 02, 2004
5	Maintenance of Concrete Structures and Retrofitting Promotion System for Low Earthquake-Resistant Structures	Dr. Y. Kato and Ms. M. Yoshimura, (University of Tokyo)	Mar. 12, 2004
6	Catastrophic Disaster Risk Management for Sustainable Urbanization in Asia	Dr. S. Herath (UNU, Tokyo) And Dr. Rajib Shaw (Kyoto University)	Jul. 17, 2004

##### ***b) Third international workshop of WSSI***

RNUS spearheaded the organization of the 3rd International Workshop of the World Seismic Safety Initiative (WSSI) on “Seismic Risk Management for Countries of the Asia Pacific Region” at the Miracle Grand Hotel in Bangkok during 7-8 December, 2003. WSSI is an undertaking of the International Association for Earthquake Engineering (IAEE) in support of the International Decade for Natural Disaster Reduction (IDNDR) of the United Nations. Since its inception in 1992, WSSI has been working with many countries around the world through its programs. To utilize and share the experiences learnt over the past ten or more years, WSSI 2003 was organized to allow participants: 1) to learn from countries where WSSI





*Photo 2: A snapshot during the workshop*

programs have made positive difference in terms of risk mitigation and management; 2) to learn from countries where WSSI programs have not made any major impact in terms of risk mitigation efforts, and 3) to develop a plan in consultation with all the attending countries about what WSSI should do for the next five years and where they should focus their human and financial resources. The workshop was attended by over 55 representatives from 19 countries.

RNUS also spearheaded the editing activities of the final this WSSI workshop (Meguro et al., 2004). The proceedings include country reports from 12 countries, reports on inter-national cooperation of JICA and reports from other International Organizations. The country reports emphasized on the earthquake risk mitigation efforts, strategies, responses and assessment measures initiated in their respective countries. Most of the country reports focused on seismic risk management activities in the last five years, scope for future collaborations in the region for varied resources and further networking and information-sharing with international organizations.



*Photo 3: WSSI workshop participants in a group photo*

## 5.0 CONCLUSIONS

Rapid urbanization is a distinctive feature of Asia in addition to a tremendous rate of population growth. It is estimated that by 2015, more than 50% of the mega-cities of the world are going to be in Asia and their urban development is going to continue in the decades to come. For sustainable urbanization, holistic efforts are needed for urban safety and security. New technologies have inspired us to conduct research for new development in urban safety engineering, which should be integrated with socio-economic and environmental aspects to achieve the sustainable urban development for safer and securer 21<sup>st</sup> century. International collaboration among researchers and other stake holders is needed to target the local and regional problems with shared knowledge and technologies. RNUS is an initiative of ICUS, the University of Tokyo and SCE, AIT in this direction and its success is a demonstrative example to inspire further collaborative efforts in the region. There is still much to do for RNUS to expand its activities of collaboration, which will in turn lead to regional collaboration and networking.

## REFERENCES

- Dutta, D. and T. Uomoto 2002 (ed.). *Urban Safety Engineering 2001*. Proceedings of the Joint Workshop, ICUS/INCEDE Report 1, October.
- Dutta, D. (2003). *Analysis of Urban Flood Disaster trends in Asia*. Watershed Hydrology: Proceedings of the International Conference on Water and Environment, Bhopal, India, December, pp.512-519.
- Dutta, D. and T. Tingsanchali 2003. *Development of Loss Functions for Urban Flood Risk Analysis In Bangkok*. Proceedings of the 2nd International Symposium on New Technologies for Urban Safety of Mega Cities in Asia, ICUS, IIS, The University of Tokyo, October, pp: 229-238.
- Dutta, D. and K. Serker 2004. *Urban Building Inventory from Very High Resolution Remote Sensing data for Bangkok City, Seisan-Kenkyu*. Journal of Institute of Industrial Science, University of Tokyo, Vol. 56, No. 3, pp. 27-30.
- Dutta, D., M. J. Alam and S. Hironaka 2004. *Urban Flood Modeling in Lower Mekong Basin Using a Distributed Surface-River Model*. Proceedings of the 2nd International Symposium on New Technologies for Urban Safety of Mega Cities in Asia, Agra, India, October 18-19.
- Kato, Y., S. Tangtermsirikul and T. Uomoto 2003. *Construction of a Database for Deteriorated Concrete Bridges: Filed Research Report in Company with RNUS*, ICUS/INCEDE Report No. 3, ISBN4-9901475-3-7.
- Meguro, K., D. Dutta and T. Katayama 2004 (ed.). *Seismic Risk Management in the Countries of Asia and Pacific*. Proceedings of the Third WSSI Workshop, ICUS Report 5, The University of Tokyo, Japan, 312 pages, ISBN4-9902067-0-3.
- Misra, S. and Y. Kato (2003) (ed.). *New Technologies for Urban Safety of Mega Cities in Asia*, Proceedings of the International Symposium, ICUS Report 3.

- Tangtermsirikil, S., T. Kaewkhluab and K. Kaewmanee 2003. *Information Acquisition and Structural Health Monitoring of Bridges in Bangkok*, Proceedings of the 2nd International Symposium on New Technologies for Urban Safety of Mega Cities in Asia, ICUS, IIS, The University of Tokyo, October, pp: 133-140.
- Larimer, T. (2000). *The Sky is Falling*. Time Magazine, USA, January 24, 2000.

# **SAFETY ASSESSMENT OF EXISTING ROAD IN THE HIMALAYAS USING GEOGRAPHIC INFORMATION SYSTEM AND SATELLITE IMAGERY**

SHARAD VIMAL OBEROI<sup>1</sup> AND NARINDER KUMAR THAKUR<sup>2</sup>

<sup>1</sup>Institute of Technology, Banaras Hindu University, Varanasi, India

<sup>2</sup>Snow and Avalanche Study Establishment (SASE), Chandigarh, India

*svoberoi11@yahoo.co.in*

## **ABSTRACT**

*Remote sensing has been used to study characteristic properties of ground surface due to the advantages of its broad area observation and periodicity. Geographic Information System (GIS) has also proved to be an ideal tool for hazard modeling owing to its versatility in handling a large set of data, providing an efficient environment for analysis and powerful set of tools for collecting, storing, retrieving, transforming and displaying spatial data. Therefore the integration of GIS with remote sensing data and thematic maps can facilitate greatly the assessment and estimation of regional natural hazards.*

*The present paper explores modern GIS in the routing and alignment of hill road network because of the immense benefits it can offer to planners by identifying the landslide and avalanche prone areas. The roads existing in the Himalayas are subjected to frequent avalanches and landslides, thereby causing fatal casualties and heavy damages to scarce man-made features. The application of remote sensing in transportation has the potential capability to provide information that can reduce the risks involved.*

*It is expected that such risk assessment of the existing infrastructure will help in formulating the necessary precautions to be taken during the planning stage of a project, so as to minimize any possible future human or property losses in case of a calamity.*

## **1.0 INTRODUCTION**

With the rapid growth in population and immense pressure on the existing facilities, today urban growth is extending into hazard prone regions. The result is that the magnitude of the impact of a disaster increases since it is dependent on the susceptibility of the land and the vulnerability of the society (Verstappen, 1995). The vulnerability is also compounded with the increased complexity of interdependent systems (Comfort, 1999).

Natural disasters happen every year and their impact and frequency seem to have greatly increased in recent decades, mostly because of

environmental degradation, such as deforestation, intensified land use, and the increasing population (Vincent, 1997). With today's complexity of society, response and relief from disasters has become a costly concern. Therefore, there is a need to shift to mitigation, which entails activities that strive to reduce the number of hazards and/or their impact before disasters happen (Comfort, 1999).

According to Verstappen (1995), the purposes of using remote sensing include: "to investigate the susceptibility of the land and the vulnerability of the society, to construct hazard zoning maps and potential damage maps, to monitor potential hazards, and to deal with emergency situations after a disaster." Many research studies have been completed that employ remote sensing as the principal information source in the assessment of hazards/disasters. But, not all of the applications are suitable for use in the transportation domain, because of the higher spatial and temporal resolution required for many of the specific applications. Given the importance of transportation in our daily lives, there is a desire to ensure the safety and operation within each of the transportation domains (Gamba et al., 1998). This is another reason why there is a growing interest in using remote sensing to predict, monitor, and assess disasters.

In this study, the authors have attempted to operationalise a working methodology wherein geo-environmental parameters are analyzed to develop models for mapping the hill areas prone to the regional natural disasters (namely avalanches and landslides) using remotely sensed data and Geographic Information System (GIS).

## **2.0 AREA OF STUDY**

The Indian Himalayas stretch from east for about 2500 km across 72° E to 96° E longitude and 26° N to 37° N latitude. The complex folding pattern that they have been subjected to during the upheaval of Himalayas in Pleistocene and subsequent period leading to thrusting of Indian plate with Eurasian plate, has lifted the rock structure to produce a long chain of mountain ranges with deep furrow in between. The interaction of global atmospheric circulation system with the tallest geological feature of the earth has produced diverse climatological, biological and snow climatic zones within the Himalayas. This complex variation is unparalleled in the world (Sharma et al., 2000).

Limited numbers of roads existing in the Himalayas are subjected to frequent avalanches and landslides thereby causing fatal casualties and heavy damages to scarce man-made features. Moreover, the planning and laying out of roads in the mountains is a very slow and cumbersome process, owing to the difficult terrain with ice-fields, snow-covered peaks and very harsh climatic conditions. The Himalayan region of India is normally covered by snow melting during the winter season. The region is cut-off for most part of the year from the rest of the world and the passes only provide the routes of communication. The strategic importance of some of these

areas makes it more important for the roads to be kept open during adverse weather conditions.

The area of study lies along the Manali-Leh Highway from Manali to Darcha for a stretch of about 138 km, which falls in the Lower and Upper Himalayan snow climatic zone. The altitude in this area varies from 1800 to 6200 m. The road is under heavy use by the army and civilians, which underlines its significance in connecting this treacherous landscape to the mainland.

### **3.0 METHODOLOGY OF SAFETY ASSESSMENT**

As the project area is vast and covers heterogeneous terrain the authors have felt that a model addressing the expert knowledge combined with a statistical technique will suffice the need. In this method, expert opinions are employed to determine how each parameter of the terrain and categories within the parameters respond to landslide/avalanche susceptibility. This is subsequently used to classify the area into ranks, which are translated to weightages using the models. Decision space software, Landslide Hazard Zonation and Avalanche Modeller have been used for the generation of the hazard maps.

### **4.0 SAFETY ASSESSMENT WITH RESPECT TO LANDSLIDES**

Landslide is a rapid disaster that usually happens in an unstable slope region, which always includes the falling, sliding or flowing of soil and rock. Every year, landslides cause the death or injury of thousands of people and millions of rupees of property is lost (Raju et al., 1999). Prediction of potential landslide areas has been very difficult because of the complexity of the factors involved and their relationship to each other, which is wide ranging (Yuan et al., 1997). Normally the causes of landslide are determined by carrying out some sampling of the soil, rock, slope inclination, land cover, underground water level, geology, etc. at the site. It is difficult and time-consuming to do this for a large area from time to time and by integrating it with GIS, all the information can be combined, manipulated and analyzed to determine potential landslide areas very quickly and more efficiently.

Among the various methods for landslide hazard zonation, the probability of occurrence of mass movement has been calculated: (a) based on the various terrain parameters and their cumulative influence, and (b) knowledge-based classification (Van Westen, 1994). It is expected that the presence of terrain attributes similar to that of the observed/reported slide elsewhere, is likely to induce slide under the given triggering conditions. Therefore, based on the spatial and temporal distribution of the landslides and their triggering factors, it is possible to identify areas susceptible to similar slide (Nagarajan et al., 1998).

## 4.1 Factors causing landslides

Previous studies have amply demonstrated that landslides are predictable if terrain characteristics are available. The factors generally attributed to cause landslides are lithology, geology, slope-dip (bedding-joint) relation, geomorphology, drainage, slope angle, slope aspect, slope morphology, land use, soil texture, etc. All these have been incorporated in the present study, along with the triggering factors like rainfall, snow ablation, earthquake and anthropogeny. However, it is impossible to exactly predict when and where a landslide will occur because the relationship between the factors mentioned above is complex (Shikada et al., 1997).

## 4.2 Methodology

The methodology was divided into the following steps:

- Selection of area of interest.
- Generation of precision geocoded LISS-III data along the route.
- Preparation of base maps using Survey of India (SOI) toposheet-wise on scale 1 : 50000 with base details.
- Visual interpretation of satellite data for generation of thematic maps.
- Model description with standardization of parameters.
- Ranking i.e. pair-wise comparison in hierarchical approach (based on expert opinions).
- Landslide management map along the area of study and toposheet-wise output.
- Final maps i.e. Landslide Hazard Zonation Maps.

The Landslide Hazard Zonation (LHZ) Maps were classified into various categories based on the parameters described in Table 1.

*Table 1: Assignment of ranks and triggering parameters for landslides*

<b>Landslide Susceptibility</b>	<b>Slope (°)</b>	<b>Land use</b>	<b>Rainfall (mm)</b>	<b>Snow Ablation</b>	<b>Geology</b>	<b>Tectonic Zone</b>
<b>Very High</b>	36-54	Barren land	451-600	↑ 1800 to 4000 m ↓	↑ Youngfold mountains ↓	↑ Seismic Zone- IV ↓
<b>High</b>	18-36	Grasslands/ Pastures	301-450			
<b>Moderate</b>	>54	Forested Area	151-300			
<b>Low</b>	0-18	Settlements	0-150			

## 5.0 SAFETY ASSESSMENT WITH RESPECT TO AVALANCHES

The major avalanche activity in our area of study is along various nallas that drain into Indus and other rivers. The snow cover in this area is likely to evolve under cold climatic conditions. In this context a systematic

study has been carried out to delineate the avalanche-prone areas. The information about the study area was gathered by conducting ground/aerial reconnaissance.

The remote sensing techniques comprising of Digital Elevation Model (DEM) analysis, preparation and visualization of map and satellite data (IRS-1C/1D LISS-III) were carried out using ERDAS Imagine 8.4 software, run under Windows 2000 Professional environment because of its sophisticated procedures for satellite and vector data processing. The avalanche hazard maps offer an effective way to guide and educate the users about the avalanche-prone areas and their possible preventive measures. This technique is user-interactive and offers better visual interpretations that are lacking in conventional techniques, which use toposheets as a visual source of information.

## 5.1 Methods of investigations

The slope, aspect and terrain configurations are derived from DEM using precise geo-referenced topographic digitized data. The terrain configuration has been interpreted using DEM along with the ground data collected during the ground reconnaissance conducted. The ground cover parameters have been derived from the appropriate data selected after the detailed analysis of multi-date IRS-1C/1D LISS III data using image processing techniques. It has been found that the selected data provides up-to-date information for classification of ground cover. The same confirms to the ground data collected during ground recce carried out earlier.

## 5.2 Data type and sources

The data type and sources used for each parameter are discussed in Table 2.

*Table 2: Data used for avalanche hazard zonation mapping*

S.No.	Details	Slope	Aspect	Configuration	Ground cover
01	<b>Data Type</b>	Digital topographic contours	Digital topographic contours	Digital topographic contours/ Satellite imagery	IRS-1C/1D LISS-III
02	<b>Accuracy</b>	+/- 6 m	+/- 6 m	+/- 6 m	-
03	<b>Data Format</b>	Arc Info Generate	Arc Info Generate	Arc Info Generate .img/. pix	.img/.pix (4 bands)
04	<b>Data Collector</b>	SASE	SASE	SASE	SASE
05	<b>Provider</b>	SOI 1972 edition	SOI 1972 edition	SOI /IRS 1972/2000	August 2000



### 5.3 Generation of cartographic model

A cartographic model of data and analytical methodology has been illustrated in Figure 1. LISS-III data has been geo-referenced by using well-defined 25 ground control points, which were established during the ground recce to achieve higher accuracy. The LISS-III data has been then classified for calculating the total area for each class of the ground cover (rocky, barren and grassy).

The DEM gives a realistic view of the area and makes it easy to understand the planar nature of the area. Different terrain features e.g. hills, valleys, gorges and configuration can be identified with ease. For analyzing ground-cover parameter, the LISS-III data is used.

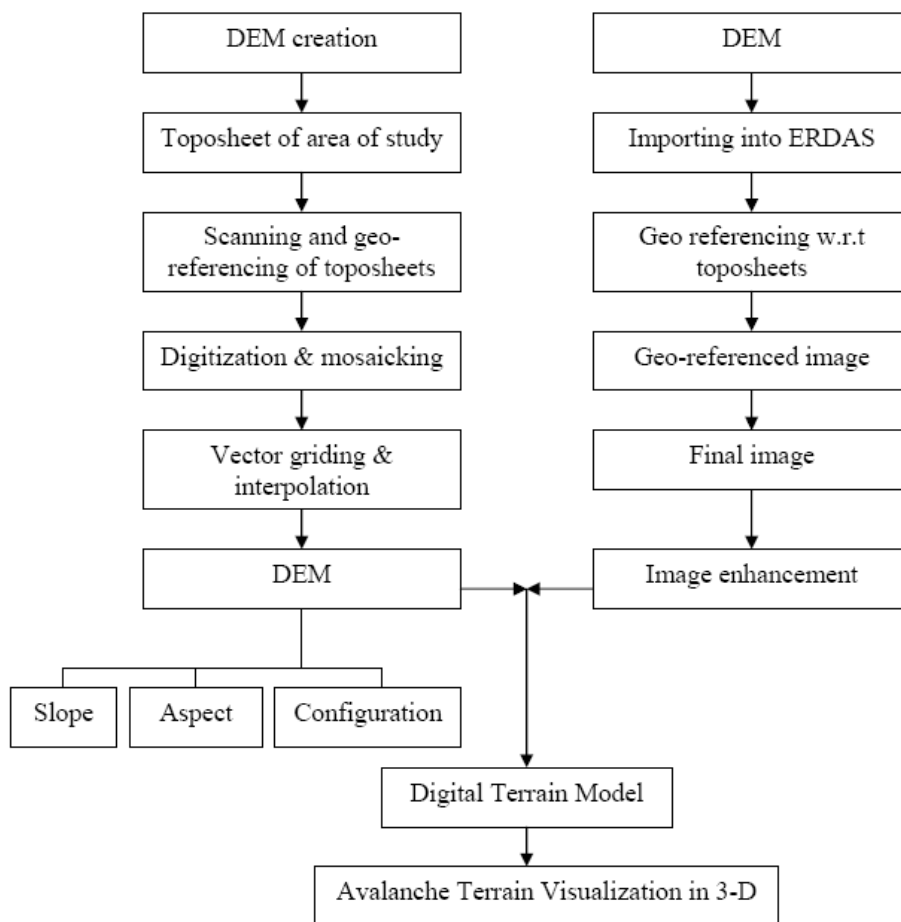


Figure 1: Cartographic Model

## 6.0 RESULTS AND DISCUSSION

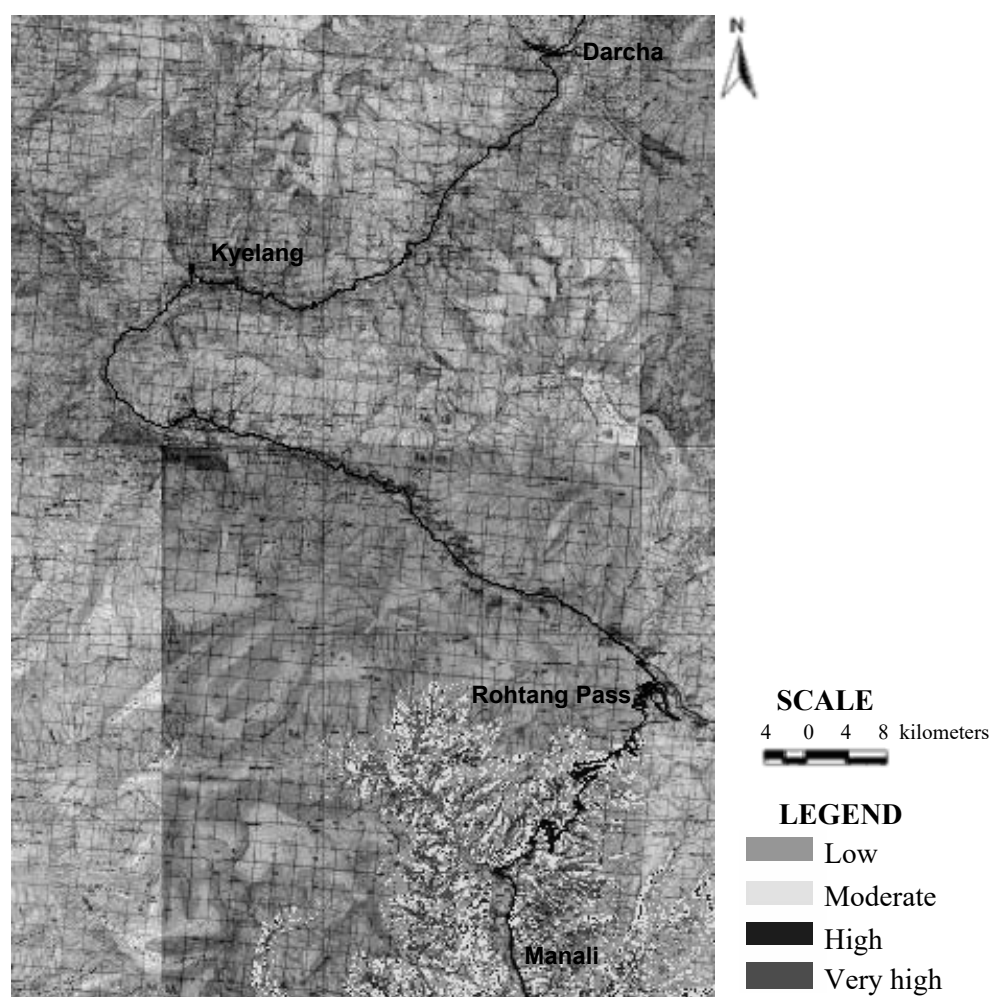
### 6.1 Landslide hazard zonation

Since the study of the meteorological data for the region revealed negligible liquid precipitation in the areas beyond the Rohtang Pass (Lahaul & Spiti), rainfall was assumed to be uniformly distributed for the Kulu

District areas, situated before the Rohtang Pass only. Therefore, the LHZ model gives no results for the region beyond the Rohtang Pass. However, it should be kept in mind that any precipitation that may take place in this mountain desert causes immense havoc, because of the loose soil and boulders present. The percentage of the different risk zones of the study area is given in Table 3 below.

*Table 3: Percentage of different risk zones of the study area*

S. No.	Degree of Susceptibility to Landslides	Percentage of Total Susceptible Area
01	Low	10.32 %
02	Moderate	43.83 %
03	High	44.84 %
04	Very high	1.01 %

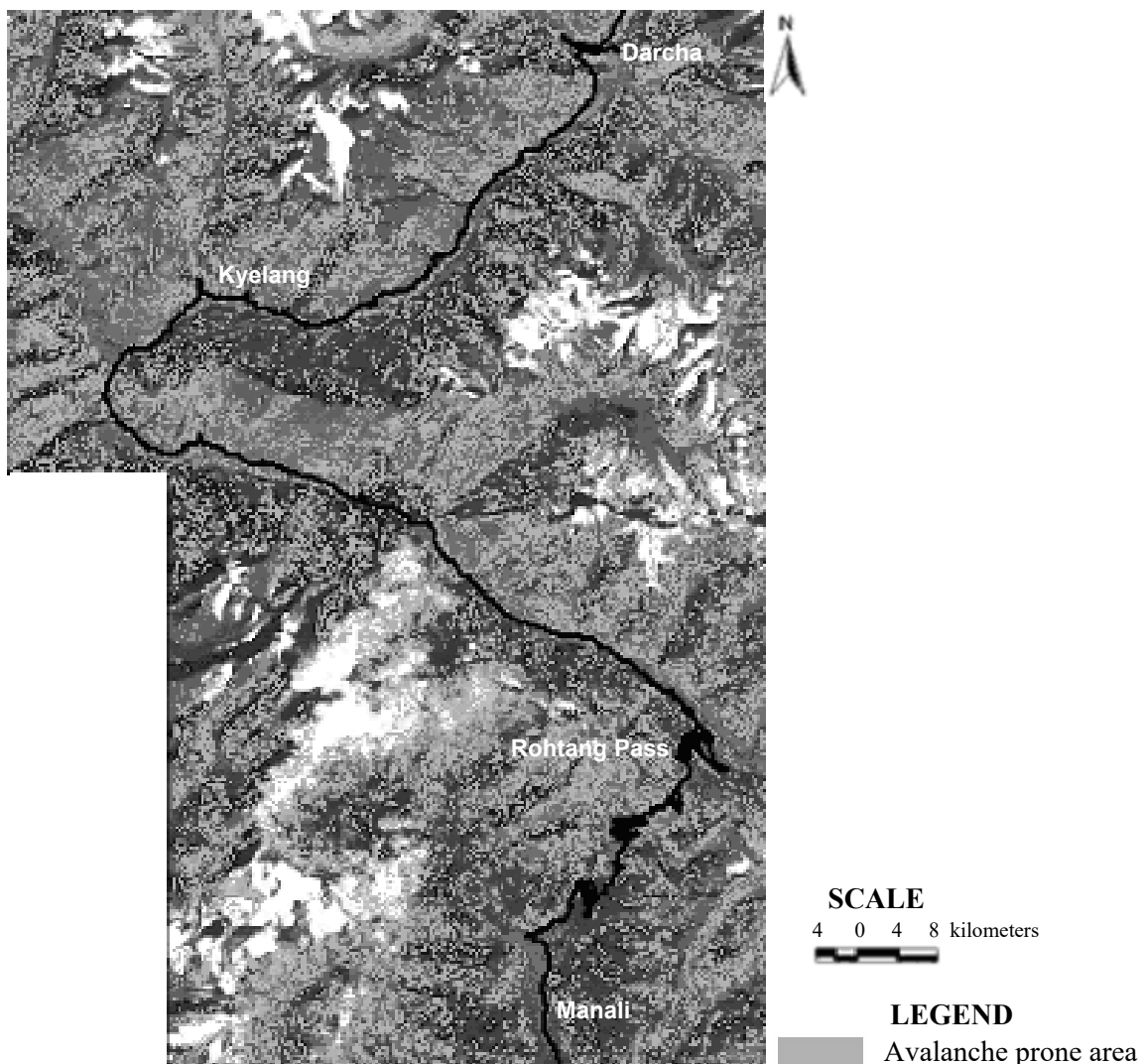


*Figure 2: Landslide hazard zonation map of Manali-Darcha region considering rainfall only up to Rohtang Pass*

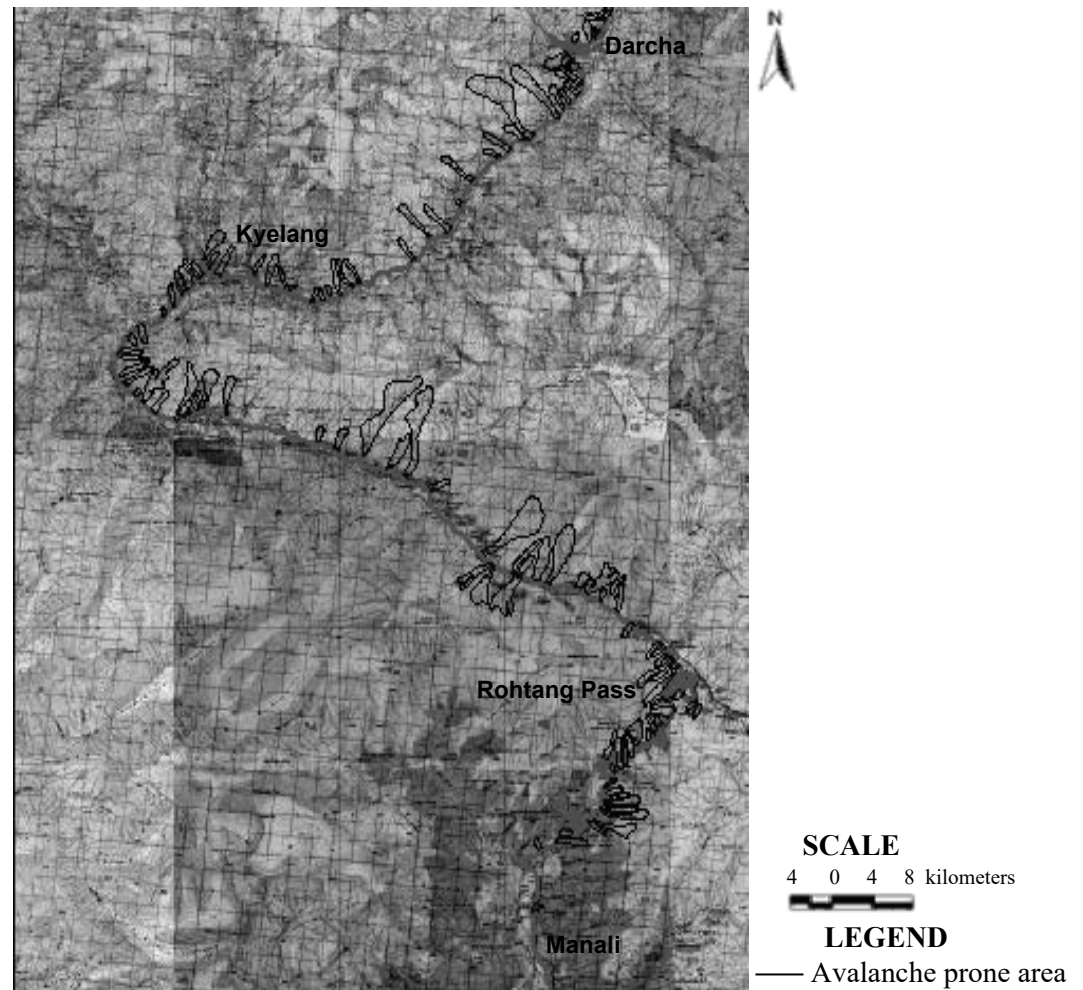
## 6.2 Avalanche hazard investigations

The Avalanche Hazard Zonation Map was prepared to identify the formation zones of avalanches in the hilly terrain based on the DEM, which gives a realistic view of the area and makes it easy to understand the planar nature of the area. Different terrain features like hills, valleys, gorges and configuration were identified and all the thematic layers were overlaid.

A total of 90 avalanche sites have been mapped along the different axes in the Manali-Darcha area as shown in Figure 3. It has been correlated with the ground data collected during reconnaissance surveys, as depicted in Figure 4. This information has significant role for users in the operational areas for visual interpretation of terrain and prediction of avalanche prone areas.



*Figure 3: Avalanche hazard map of Manali-Darcha region draped on IRS-1C LISS-III image*



*Figure 4: Avalanche-prone areas identified by ground recce*

## 7.0 CONCLUSIONS

Today over half of the world's population is concentrated in urban areas covering just 4 % of the world's surface. Mega cities in particular are characterized by a high population density and tremendous pressure on supporting infrastructure, leading to increased vulnerability of the society to natural disasters, if and when they occur. This calls for prior preparation by the authorities and governing agencies by performing the safety assessment of the existing infrastructure. The Landslide Hazard Zonation and Avalanche Modeler as described in this paper are useful tools for the planners and decision makers in analyzing the disaster susceptibility of urban growth extending into hazard prone regions. Nevertheless the accuracy of these estimates can be enhanced by correlating with the ground data collected during reconnaissance surveys.

The implementing of modern GIS technology for developing hazard zonation maps taking into account the spatial variation of mountainous terrain has so far been unexplored in India and hence needs immediate attention.

## ACKNOWLEDGEMENTS

The authors are grateful to Dr. R. N. Sarwade, Director, Snow & Avalanche Study Establishment (SASE), Manali, for granting the permission to publish this paper. Our profound sense of gratitude also to Col. P. Mathur, Deputy Director, SASE and Lt. Col. R. S. Puri, Assistant Director, SASE, for their numerous valuable suggestions and encouragement.

## REFERENCES

- Comfort, L. K., 1999. *The impact of information technology upon disaster mitigation and management*. Proceedings of the Second Conference on the Applications of Remote Sensing and GIS for Disaster Management, Washington D.C., CD-ROM.
- Gamba, P., and Casciati, F., 1998. *GIS and image understanding for near-real-time earthquake damage assessment*. Photogrammetric Engineering & Remote Sensing, Vol. 64, 10, 987-994.
- Nagarajan, R., Mukherjee, A., Roy, A., and Khire, M. V., 1998. *Temporal remote sensing data and GIS application in landslide hazard zonation of part of Western Ghat, India*. International Journal of Remote Sensing, Vol. 19, 4, 573-585.
- Raju, R., and Saibaba, J., 1999. *Landslide hazard zonation mapping using remote sensing and geographic information system*. IEEE 1999 International Geoscience and Remote Sensing Symposium, Hamburg, CD-ROM.
- Sharma, S. S., and Ganju, A., 2000. *Complexities of avalanche forecasting in Western Himalaya: an overview*. Cold Regions Science and Technology, 31 (2000) 95-102, 96-100.
- Shikada, M., Suzuki, Y., Kusaka, T., and Goto, S., 1997. *An application of GIS information and remotely sensed data for extraction of landslide*. IEEE 1997 International Geoscience and Remote Sensing Symposium, Singapore, CD-ROM.
- Van Westen, C. J., 1994. *GIS in landslide hazard zonation: a review with examples from the Andes of Columbia*. In Price, M. F., and Heywood, D. I. (editors), Mountain Environment and Geographic Information Systems, Taylor & Francis, London, 135-166.
- Verstappen, H. T., 1995. *Aerospace technology and natural disaster reduction*. In Singh, R. P., and Furrer, R. (editors), Natural Hazards: Monitoring and Assessment using Remote Sensing Technique, Elsevier Science, Inc., New York, 3-15.
- Vincent, R. K., 1997. *Fundamentals of geological and environmental remote sensing*. Prentice-Hall, Inc., Upper Saddle River, NJ.
- Yuan, R. K. S. and Mohd., M. I. M. (1997). *Integration of remote sensing and GIS techniques for landside applications*. Proceedings of Asian Conference on Remote Sensing (ACRS) 1997. <http://www.gisdevelopment.net/aars/acrs/1997/ps3/ps3006pf.htm>